EMERGING INFECTIOUS DISEASES®

CDC
Centers for Disease Control and Prevention

Mycobacterial Infections

March 2022

Angel (Coin) of the Second Reign (1471–1483) of Edward IV. Gold, 29 mm, 5.1 g, 1473 1477. British Museum, London, UK.

EMERGING INFECTIOUS DISEASES®

Emerging Infectious Diseases is published monthly by the Centers for Disease Control and Prevention, 1600 Clifton Rd NE, Mailstop H16-2, Atlanta, GA 30329-4027, USA. Telephone 404-639-1960; email, eideditor@cdc.gov

EMERGING INFECTIOUS DISEASES®

Mycobacterial Infections **March 2022**

On the Cover

Angel (Coin) of the Second Reign (1471–1483) of Edward IV.
Gold, 29 mm, 5.1 g, 1473–1477. British Museum, London, UK.

About the Cover p. 765

Synopses

Medscape EDUCATION ACTIVITY

Research

Medscape EDUCATION ACTIVITY

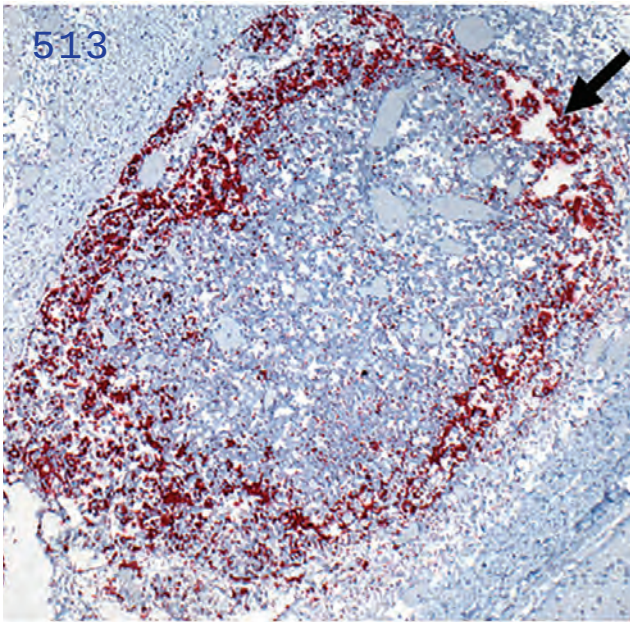

EMERGING INFECTIOUS DISEASES®
March 2022

Dispatches

Photo Quiz

Research Letters

EMERGING INFECTIOUS DISEASES®
March 2022

Comment Letter

About the Cover

Etymologia

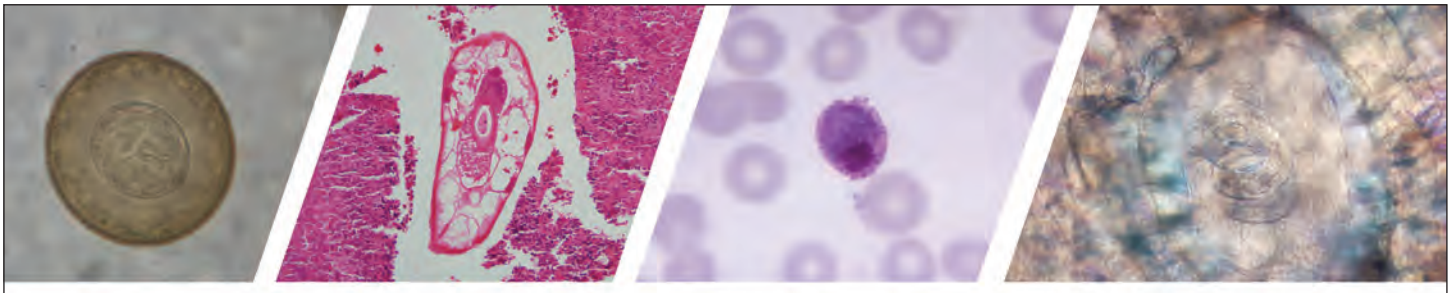

DPDx

Diagnostic Assistance and Training in Laboratory Identification of Parasites

A free service of CDC available to laboratorians, pathologists, and other health professionals in the United States and abroad

- Diagnosis from photographs of worms, histological sections, fecal, blood, and other specimen types
- Expert diagnostic review
- Formal diagnostic laboratory report
- Submission of samples via secure file share

Visit the DPDx website for information on laboratory diagnosis, geographic distribution, clinical features, parasite life cycles, and training via Monthly Case Studies of parasitic diseases.

www.cdc.gov/dpdx
dpdx@cdc.gov

U.S. Department of Health and Human Services
Centers for Disease Control and Prevention

CS272346-DE

Airborne Transmission of SARS-CoV-2 Delta Variant within Tightly Monitored Isolation Facility, New Zealand (Aotearoa)

Andrew Fox-Lewis, Felicity Williamson, Jay Harrower, Xiaoyun Ren, Gerard J.B. Sonder, Andrea McNeill, Joep de Ligt, Jemma L. Geoghegan

In New Zealand, international arrivals are quarantined and undergo severe acute respiratory syndrome coronavirus 2 screening; those who test positive are transferred to a managed isolation facility (MIF). Solo traveler A and person E from a 5-person travel group (BCDEF) tested positive. After transfer to the MIF, person A and group BCDEF occupied rooms >2 meters apart across a corridor. Persons B, C, and D subsequently tested positive; viral sequences matched A and were distinct from E. The MIF was the only shared location of persons A and B, C, and D, and they had no direct contact. Security camera footage revealed 4 brief episodes of simultaneous door opening during person A's infectious period. This public health investigation demonstrates transmission from A to B, C, and D while in the MIF, with airborne transmission the most plausible explanation. These findings are of global importance for coronavirus disease public health interventions and infection control practices.

Coronavirus disease (COVID-19) is a viral respiratory infection caused by severe acute respiratory syndrome coronavirus 2 (SARS-CoV-2) (*1*). Person-to-person transmission primarily occurs when respiratory particles containing SARS-CoV-2 are exhaled by an infected person and subsequently inhaled by others (*2*). Transmission through fomites is also possible but is considered to play a minimal role (*3*). Until recently, the principal route of COVID-19 transmission was thought to be through respiratory droplets (*4*; J.C. Palmer et al., unpub. data, https://www.medrxiv.org/content/10.1101/2021.10.19.21265208v1). Droplets are larger respiratory particles that fall quickly and thus disperse over short distances of generally <2 meters (6 ft) (*2*,*4*). However, evidence is emerging that the dominant route of COVID-19 transmission might in fact be airborne, through respiratory aerosols (*4*). Aerosols are smaller respiratory particles that remain suspended in the air for prolonged periods, and they can thus disperse and result in transmission over distances of >2 meters (*4*; J.C. Palmer et al., unpub. data). Epidemiologic studies are considered the most robust evidence currently available to support the biologic plausibility of airborne transmission of COVID-19 (*5*; J.C. Palmer et al., unpub. data).

To mitigate importation of COVID-19 into New Zealand (Aotearoa), border restrictions have been in place since March 2020; only citizens, permanent residents, and exempted persons have been permitted entry into the country (*6*). Persons entering the country must complete a period of quarantine in one of several government-assigned managed quarantine facilities (MQFs) that form part of the border response (*7*–*9*). While in a MQF, asymptomatic persons undergo mandatory SARS-CoV-2 screening tests by real-time reverse transcription PCR (rRT-PCR) of nasopharyngeal swab samples routinely collected on days 0, 3, and 12 after arrival in New Zealand, or as close to these times as practical (*10*). Symptomatic persons and MQF room companions of SARS-CoV-2–positive persons are tested as soon as possible after symptom onset or case identification (*7*,*10*). Persons who are identified as symptomatic at the border, have had a positive SARS-CoV-2 screening test, or who share the same MQF room as another SARS-CoV-2–positive person are immediately transferred from

Author affiliations: Counties Manukau District Health Board, Auckland, New Zealand (A. Fox-Lewis); Auckland District Health Board, Auckland (F. Williamson, J. Harrower); Institute of Environmental Science and Research, Porirua, New Zealand (X. Ren, G.J.B. Sonder, A. McNeill, J. de Ligt, J.L. Geoghegan); University of Amsterdam, Amsterdam, the Netherlands (G.J.B. Sonder); University of Otago, Dunedin, New Zealand (J.L. Geoghegan)

DOI: https://doi.org/10.3201/eid2803.212318

their respective MQF to a single dedicated managed isolation facility (MIF) for confirmed and suspected COVID-19 cases and close contacts.

Solo traveler A and a 5-person travel group, BCDEF, had traveled on different flights from different countries, arrived in New Zealand on different dates, and been staying in different MQFs. Persons A and E had positive SARS-CoV-2 screening tests, which resulted in the transfer of A and group BCDEF to the MIF, on different dates, where they occupied rooms across the corridor, 2.135 meters (7 ft) apart. Persons B, C, and D subsequently tested positive while in the MIF; viral sequences were linked by whole-genome sequencing (WGS) to person A, not to person E, who was within their travel group. A comprehensive epidemiologic investigation was undertaken by public health to determine whether airborne transmission of SARS-CoV-2 Delta variant had taken place between person A and persons B, C, and D, who were staying in separate, nonadjacent rooms >2 meters apart within the tightly monitored MIF.

Methods

All nasopharyngeal swabs underwent routine rRT-PCR diagnostic testing by using the Cepheid Xpert Xpress SARS-CoV-2 assay (Cepheid, https://www.cepheid.com) or an E gene rRT-PCR laboratory-developed test on the Panther Fusion platform (Hologic, https://www.hologic.com) (*10*,*11*). WGS and phylogenetic analysis was undertaken as previously described (*12*,*13*). In brief, we assigned SARS-CoV-2 genomes from persons A, B, C, D, and E as lineage B.1.617.2 (Delta variant) by using Pangolin (*14*). We then aligned these genomes along with 1,000 Delta variant genomes uniformly sampled at random from GISAID (*15*) samples collected during July 1–14, 2021 using Nextalign (*16*), using the prototype strain Wuhan-Hu-1 (GenBank accession no. NC_045512) as reference. We estimated a maximum-likelihood phylogenetic tree by using IQ-TREE (*17*) using the best fit model and ultrafast bootstrapping for branch support.

COVID-19 is a notifiable disease in New Zealand: all PCR-confirmed cases are reported to Public Health for further investigation. Investigation outcomes of this in-facility transmission event have been communicated to the public by the New Zealand Ministry of Health (*18*,*19*). Because this was a public health investigation, formal ethics approval was not required (*20*). The 6 persons involved are anonymously described here as A–F, and because no identifiable details have been provided, formal written consent was not required. The infectious period was assumed to last up to 10 days after symptom onset or the first positive rRT-PCR test (*21*).

Results

Case Details

Person A arrived in New Zealand from the Philippines on July 16, 2021, and was placed in MQF1. After a positive routine day 1 test result on July 17 (E gene cycle threshold [C_t] value 20.57), person A was transferred to the MIF on July 19 (Figure 1) and placed in block 2, room 277 (Figure 2). Person A remained asymptomatic and had no further tests during the stay in the MIF. Person A was considered infectious up to and including July 27 and was released from the MIF on July 31.

Travel group BCDEF arrived in New Zealand from the United Arab Emirates on July 14 and were quarantined together in MQF2. One member of the group, person E, had a positive routine day 0 test result on July 14 (E/N2 gene C_t values 33.9/37.1). On July 15, the whole group was transferred to the MIF (Figure 1), where they were accommodated in block 2 in adjoining rooms 276 and 278 on the opposite side of the corridor from person A (Figure 2). The distance between the doors to room 277 and room 276 was 2.135 meters. Person E experienced upper respiratory tract infection symptoms on July 16–17 (coryza and subjective fever) and had a further positive SARS-CoV-2 rRT-PCR test on July 16 (E/N2 gene C_t values 15.6/17.3).

Person B experienced upper respiratory tract infection symptoms on July 17–18; on July 18, a rRT-PCR test result was negative for SARS-CoV-2 but positive for rhinovirus/enterovirus. Persons B, C, and D subsequently tested positive for SARS-CoV-2. Persons B and C had positive routine day 13 tests on July 27 (E/N2 gene C_t values 17.6/18.7 for person B and 17.2/18.9 for person C) but were not symptomatic. They had no further SARS-CoV-2 tests during their stay in the MIF. Person D had a negative day 13 test but had a headache on July 29 and tested positive for SARS-CoV-2 by rRT-PCR that day (E/N2 gene C_t values 25.3/27.3). Person D had a further positive test on August 9 (E/N2 gene C_t values 28.7/30.6).

Despite sharing a room with 4 other persons with PCR-confirmed SARS-CoV-2 infection, person F never tested positive for SARS-CoV-2 by rRT-PCR, testing negative on July 14, 18, 21, 27, 29, 31, and August 8, 14, 16, and 23. Person F had received 2 doses of the Pfizer-BioNTech (https://www.pfizer.com) COVID-19 vaccine, but no other members of the travel group had been vaccinated.

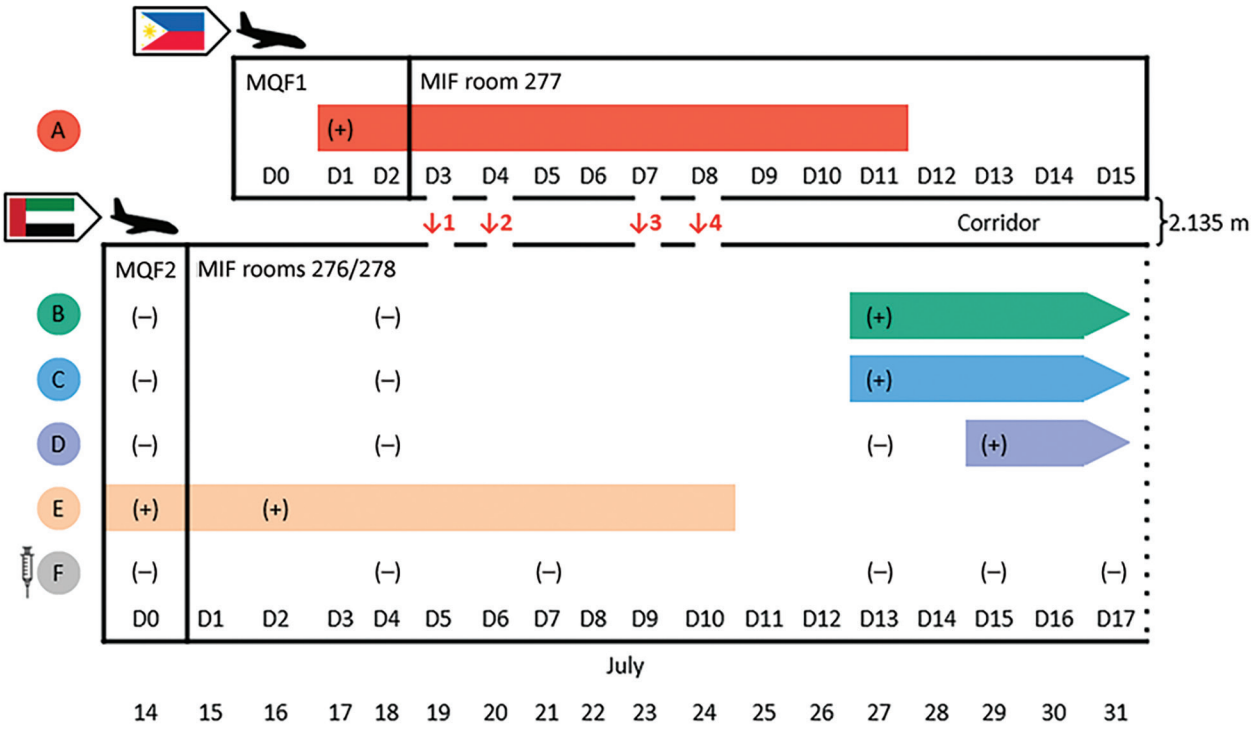

Figure 1. Timeline of infectious periods, test results, and relative locations of persons A–F, implicated in airborne transmission of severe acute respiratory syndrome coronavirus 2 (SARS-CoV-2) Delta variant between separate nonadjacent rooms within a tightly monitored MIF, New Zealand. Colors indicate persons A–F; bars represent each person's infectious period of 10 days after symptom onset or the first positive rRT-PCR test. Syringe symbol indicates person was fully vaccinated against coronavirus disease. Person A occupied room 277 and travel group BCDEF occupied adjoining rooms 276 and 278 on the opposite side of the corridor in block 2 of the MIF. The doors to the rooms were 2.135 m apart. Map-arrow symbols indicate country of origin (Philippines and United Arab Emirates); airplane symbols denote date of arrival in New Zealand. Episodes of simultaneous door-opening between room 277 and rooms 276/278, each lasting 3–5 seconds, are indicated with ↓1 to ↓4. Positive SARS-CoV-2 rRT-PCR test results are indicated by (+); negative rRT-PCR test results are indicated by (–). MIF, managed isolation facility; MQF, managed quarantine facility.

Travel group BCDEF remained together in the MIF until person F had completed the 14-day isolation period after the last SARS-CoV-2 exposure (14 days after August 8, the last day of the infectious period of person D). Travel group BCDEF were released from managed isolation on August 25.

Viral Genomic Data

All samples testing positive for SARS-CoV-2 by rRT-PCR underwent WGS for routine surveillance purposes. Persons A, B, C, D, and E had all been infected with SARS-CoV-2 lineage B.1.617.2 (Delta variant). The viral genome sequence isolated from person A was SARS-CoV-2 sublineage B.1.617.2.7.1 (AY.7.1); the sequence was genetically identical to the sequences isolated from persons B and D and only 1 single-nucleotide polymorphism different from the sequence from person C (Figure 3). However, the viral genomes sequenced from these 4 persons (A, B, C, and D) were genetically distinct (difference of 12–13 single-nucleotide polymorphisms) from the SARS-CoV-2 Delta variant from person E, which was of a different sublineage, B.1.617.2.4 (AY.4). Genomic data for all 5 persons are available on GISAID (accession no. EPI_ISL_3164123 [person A], EPI_ISL_3477087 [person B], EPI_ISL_3477085 [person C], EPI_ISL_3477082 [person D], and EPI_ISL_3164111 [person E]).

Exclusion of Laboratory Error

Initial investigative efforts focused on ruling out laboratory error to exclude a mix-up between samples from persons A and E. The sample from person A and the 2 samples from person E were collected on different dates from different locations, underwent diagnostic rRT-PCR testing at different laboratories, and were sequenced on separate runs at the national reference laboratory. Both samples from person E had already undergone WGS before collection of the positive samples from the subsequent cases in the same travel group (persons B, C, and D). The 2 samples from person E were genomically linked to each other; the July 14 sample (E/N2 gene C_t values 33.9/37.1)

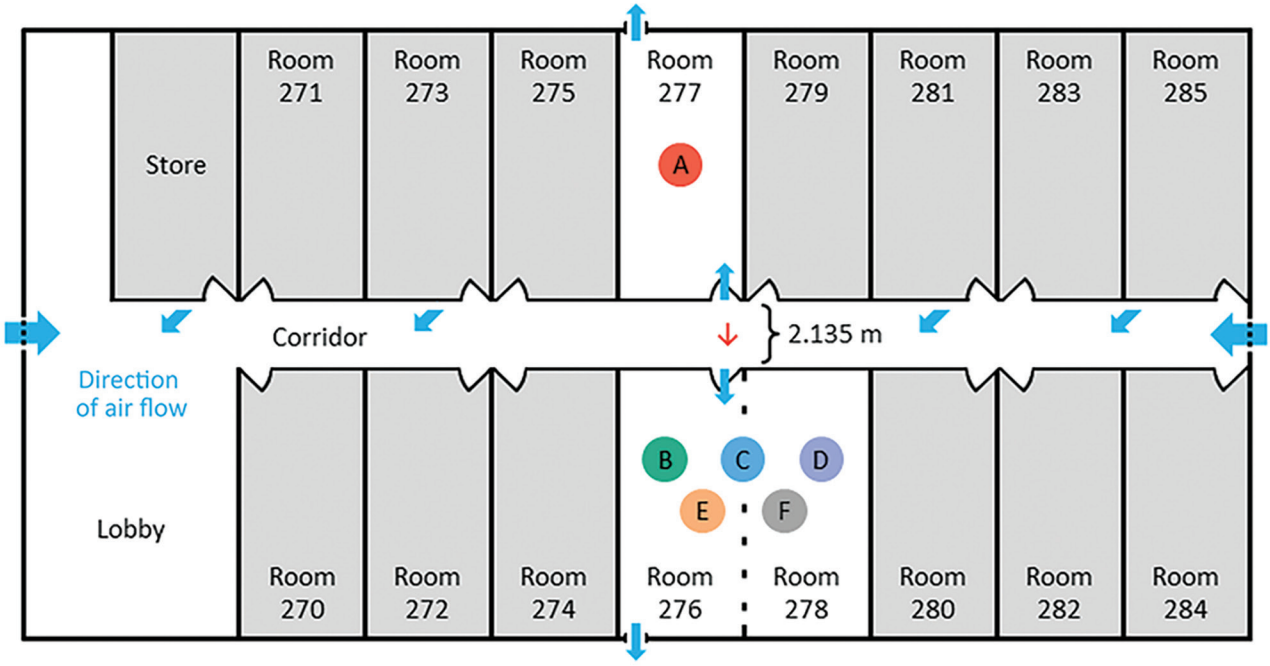

Figure 2. Layout of managed isolation facility block 2, New Zealand, in which airborne transmission of severe acute respiratory syndrome coronavirus 2 Delta variant occurred between separate nonadjacent rooms. Colored circles indicate persons A–F. Person A occupied room 277 and travel group BCDEF occupied adjoining rooms 276 and 278 on the opposite side of the corridor, 2.135 m apart. Red arrow indicates direction of probable airborne transmission of Delta variant from person A to persons B, C, and D. Blue arrows indicate direction of airflow.

yielded a partial genome that matched the sample from July 16 (E/N2 gene C_t values 15.6/17.3), which was sequenced in full. These 2 samples from person E were genomically distinct from the positive samples from persons B, C, and D. These findings exclude a reversal of samples between persons A and E, refuting the hypothesis that person E was linked to subsequent cases in the travel group, rather than these cases being linked to person A, which we determined to be the case.

Security Camera Footage

Review of closed-circuit television security camera footage from the MIF block 2 corridor during the period that person A was deemed to be infectious (July 19–27) revealed 4 separate episodes of simultaneous opening of doors to room 277 and room 276, each of which occurred for intervals of 3–5 seconds. In episode 1, on July 19, person A and a member of group BCDEF opened the respective doors for a food delivery at the same time (timeframe 4.2 s). In episode 2, on July 20, a member of group BCDEF opened the door for a food delivery and talked briefly to the delivering MIF staff member, then person A also opened the door for food, upon which the member of group BCDEF was instructed by the staff member to close that door (timeframe 3 s). In episode 3, on July 23, person A and a member of group BCDEF opened their respective doors for food delivery at the same time (timeframe 3–5 s). In episode 4, on July 24, a MIF nurse conducting a health check initially knocked on the door of room 277; after no answer, the nurse knocked on the door of room 276. However, the door to room 277 was opened first by person A, and then the door to room 276 was opened by a member of group BCDEF. The member of group BCDEF was told by the nurse to close that door while she undertook the health check on person A. After she completed the health check on person A, the door to room 277 was closed. The nurse cleaned equipment and changed gloves, then knocked on the door of room 276, which was opened by a member of group BCDEF (timeframe 4–5 s).

Person A was found to have not left the room at any point during their infectious period at the MIF and only left the room for exercise after the infectious period, from July 28 onward (after persons B and C had already tested positive). During the infectious period of person A, no fire evacuations or other drills at the MIF occurred that would have required guests to leave their rooms. Camera angles meant that security camera footage could not identify which member of group BCDEF opened the doors in the episodes previously described. In addition, security camera footage could not confirm that medical masks were worn

by the persons answering the doors, but wearing of medical masks when opening doors is standard policy in the MIF.

The MIF delivery staff involved in the simultaneous door-opening episodes 1–3 wore medical masks and gloves during these encounters and were positioned >2 meters away from the rooms when the doors were open. The nurse involved in simultaneous door-opening episode 4 was wearing full personal protective equipment, including gloves, gown, goggles, and an N95 particulate respirator. The staff identified as being involved in these interactions had all received 2 Pfizer-BioNTech COVID-19 vaccinations and underwent weekly surveillance rRT-PCR testing; each staff member had ≥3 negative test results after these encounters. No other persons within the facilities had SARS-CoV-2 genomes linked to these cases.

Room and Corridor Air Ventilation

Before this investigation, the negative pressure capabilities of the MIF rooms had been assessed. Within the ensuite bathroom of each room was a continuously operating extractor fan, with an average extraction rate of 36 L/s (128 m^3/h). The extractor fan removed air from the room, venting it to the outside and generating an average negative pressure of approximately −6.6 Pa in each room. The US Centers for Disease Control and Prevention engineering specifications for negative pressure rooms recommend a negative pressure exceeding −2.5 Pa (22). Smoke tests performed

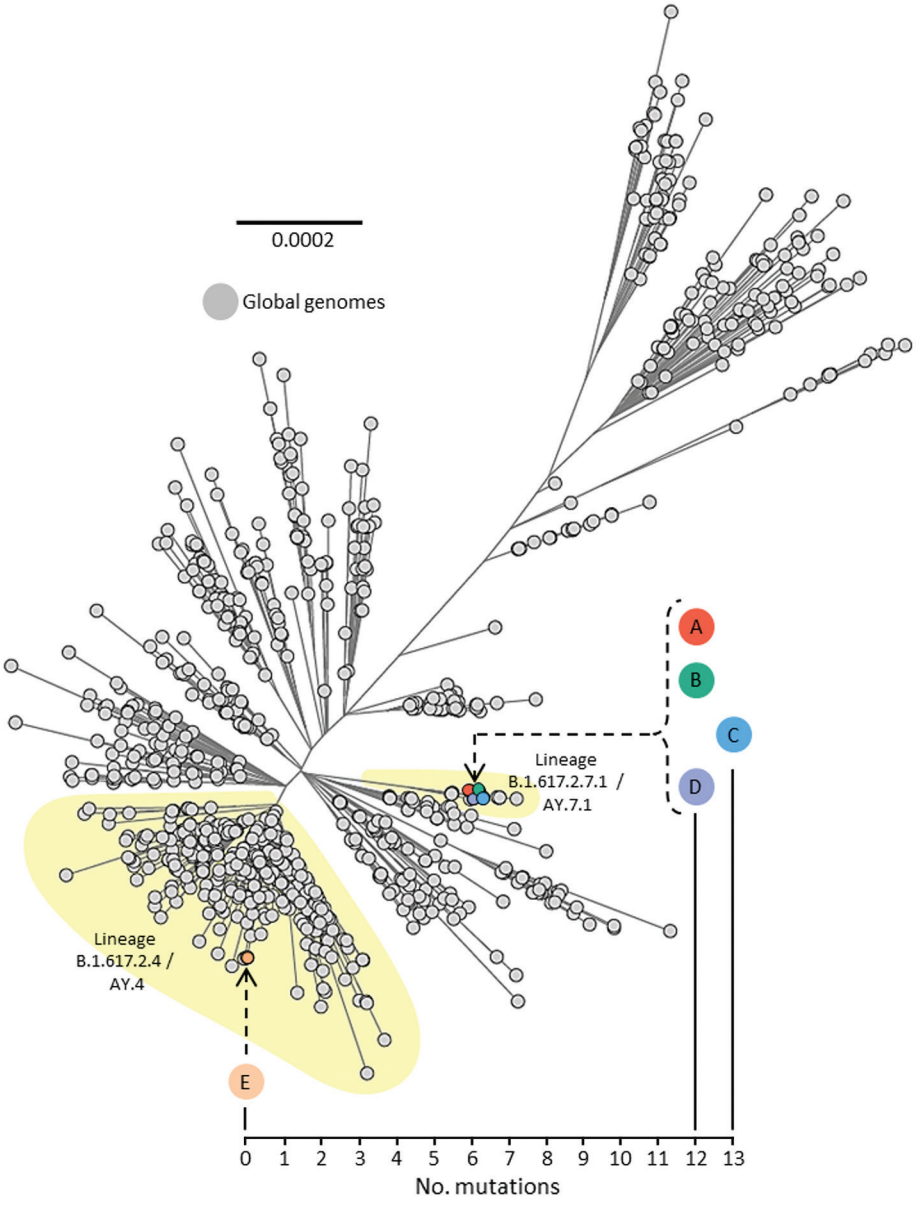

Figure 3. Unrooted maximum-likelihood phylogenetic tree of genomes from severe acute respiratory syndrome coronavirus 2 (SARS-CoV-2) isolated from persons A, B, C, D, and E, implicated in airborne transmission of SARS-CoV-2 Delta variant between separate nonadjacent rooms within a tightly monitored managed isolation facility, New Zealand, set among a background of other lineage B.1.617.2 (Delta variant) genomes sampled from around the world during July 1–14, 2021. Colored circles indicate persons A–E. Person F is not included because they were not infected with SARS-CoV-2 during the timeframe of this investigation. Upper left phylogenetic scale bar indicates number of nucleotide substitutions per site. Lower right scale shows number of mutations (single nucleotide polymorphisms) difference between viral sequences isolated from persons A, B, C, D, and E.

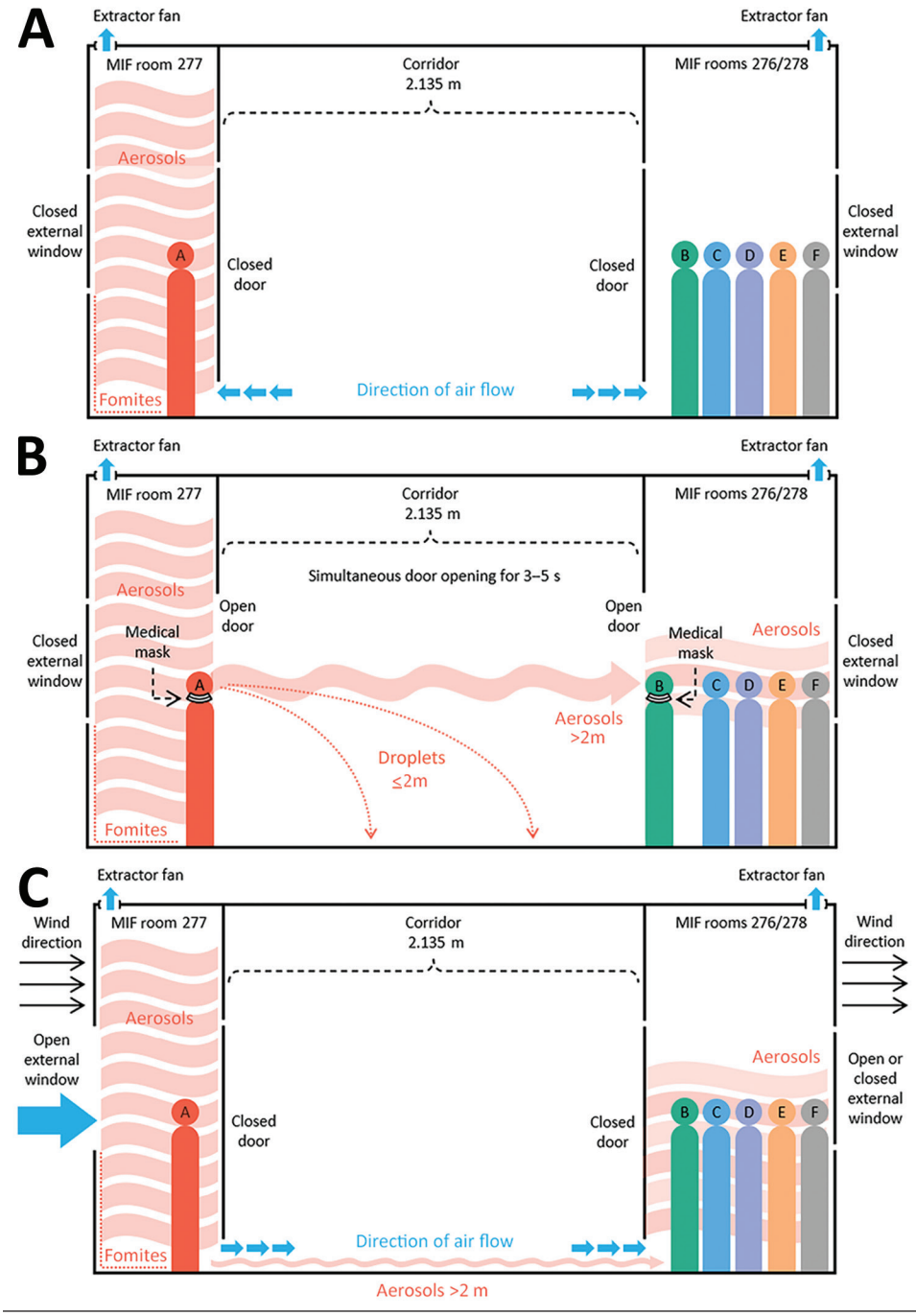

Figure 4. Possible mechanisms of airborne transmission of severe acute respiratory syndrome coronavirus 2 (SARS-CoV-2) Delta variant between separate nonadjacent rooms within a tightly monitored MIF, New Zealand. A) Air flow through rooms when room doors and external windows are closed; rooms are negative pressure and air moves from the corridor into the rooms, exiting by extractor fans. B) Movement of viral aerosols between rooms during episodes of simultaneous door-opening, when negative pressure generated by extractor fans is negated. C) Movement of viral aerosols under room doors, aided by opening of external room windows and outdoor meteorological conditions (wind speed and direction), which can create internal air flows within the building. Colored circles indicate persons A–F. Blue arrows indicate direction of air flow. Different types of infectious particles are annotated in red, with all infectious particles originating from person A. Red arrows indicate direction of movement of infectious particles. Person B is shown opening the door in this example; however, security camera footage could not identify which group member opened the door during the episodes. Security camera footage could not confirm that masks were worn by the persons answering the doors, but wearing of medical masks when opening doors is mandated in the MIF. MIF, managed isolation facility.

in a sample of rooms had confirmed a gradual but definite observed flow toward the closed bathroom door. Each room was equipped with a free-standing high efficiency particulate air (HEPA) filter, which recirculated and filtered air within the room but did not affect air movement into or out of the room. No ventilation systems connected separate rooms. Rooms had external windows that could be freely opened by occupants. External air was pumped into the corridor at either end, which, coupled with the room extractor fans, meant that when room doors and external windows were closed, the direction of air flow was from the corridor into the rooms (Figure 4, panel A).

A total of 4 free-standing HEPA filtration units were present in the MIF block 2 corridor (Figure 2). Investigation of the outward air flow from these units revealed that air exited the units in the horizontal plane at an angle of ≈45 degrees from the wall. The nearest unit to rooms 277 and 276 was mounted on the wall outside room 281, on the same side of the

corridor as room 277. Air flowed out of this unit diagonally from one side of the corridor to the other (i.e., from the door of room 277 to the door of room 276).

Discussion

We concluded that an episode of airborne transmission of SARS-CoV-2 Delta variant occurred between person A, the index case-patient, and persons B, C, and D, the secondary case-patients, who were staying in separate nonadjacent rooms 2.135 meters apart within the MIF. This conclusion is supported by multiple lines of evidence.

First, transmission between person A and persons B, C, and D could only have occurred within the MIF. This facility was the only location where these persons were colocated, because person A and travel group BCDEF had traveled on different flights from different countries, arrived in New Zealand on different dates, stayed in different MQFs, and were transferred to the MIF on different dates. Second, person A and travel group BCDEF were located in relatively close physical proximity within the MIF, in rooms across the corridor from one another. Third, the infectious period of person A preceded infection in persons B, C, and D. Fourth, during the infectious period of person A, several episodes of simultaneous door-opening occurred between the rooms occupied by person A and travel group BCDEF, meaning that for a short time no barriers to the spread of airborne respiratory aerosols between these rooms were in place. Fifth, during the episodes of simultaneous door-opening, person A and the member of travel group BCDEF who opened the door should have been wearing medical masks, as is mandated within the MIF. The wearing of medical masks, short duration of simultaneous door-opening, and separation by >2 meters makes transmission by droplets improbable. Sixth, the risk for fomite transmission of SARS-CoV-2 by shared surfaces is already thought to be low (*3*). Person A and travel group BCDEF had no direct contact with each other or with any shared objects, as corroborated by security camera footage, making transmission by fomites in this case also improbable. Finally, viral genomic data demonstrate that persons A, B, C, and D had genetically identical or closely linked SARS-CoV-2 Delta variant viral genomes and that these were markedly different from the Delta variant genome sequenced from person E. The cumulative evidence of these findings indicates that transmission of SARS-CoV-2 Delta variant took place between person A and persons B, C, and D during their stay in the MIF and that transmission by an airborne route is the most plausible explanation.

Like many such facilities globally, the MIF described here was not built for this function but rather was a commercial hotel complex that had been adapted for use as a MIF in the wake of the COVID-19 pandemic (*9*). Although the rooms did have negative pressure capabilities, they did not have anterooms to maintain negative pressure during entry and exit, and they had external windows that could be freely opened by occupants. Opening either the door to the corridor or the external window could negate the negative pressure within the room, enabling aerosol particles to disperse out of rooms. Person A did not leave the room at any point during their infectious period, likely resulting in a high concentration of viral aerosols accumulating in the room. Our findings support the hypothesis that during episodes of simultaneous door-opening, airborne particles in the room of person A rapidly diffused down a concentration gradient, across the corridor, and into the rooms of group BCDEF (Figure 4, panel B). Air flow from the corridor HEPA filter outside room 281 could have aided in aerosol movement across the corridor (Figure 2). This explanation is more plausible than exhalation and transmigration of viral aerosols only during the brief periods of simultaneous door-opening.

Another potential mechanism for movement of viral aerosols between opposite rooms is air flow under the room doors (Figure 4, panel C). As previously described, continuously operating extractor fans generate negative pressure in the rooms, causing air to flow from the corridor, under closed room doors, and into the rooms. Opening external room windows could negate the negative pressure generated by the extractor fans and permit external weather conditions to influence internal air flow within the building (*23*). Transmission of SARS-CoV-2 during brief periods of simultaneous door-opening or because of subtle internal air flows under room doors highlights the highly infectious nature of the Delta variant, especially in indoor settings. Transmission by an intermediary case, such as a MIF staff member, is highly unlikely given that all MIF staff members are fully vaccinated against COVID-19 and have weekly surveillance SARS-CoV-2 rRT-PCR testing and that no staff members tested positive for SARS-CoV-2 in the weeks surrounding this event.

Locally, the outcome of this investigation effected an immediate change in food delivery and health check protocols at the MIF to eliminate episodes of synchronous door opening. Corridor HEPA filtration units were reoriented so that air exited the units parallel to the wall to mitigate against movement of respiratory aerosols across the corridor. In addition,

depending on occupancy, future room allocation of residents within the MIF will be spread out as much as possible.

Genomic epidemiologic studies such as this one provide the best evidence currently available to support airborne transmission of SARS-CoV-2, the causative agent of COVID-19 (J.C. Palmer et al., unpub. data). The findings of this comprehensive public health investigation describing airborne transmission of SARS-CoV-2 are vital for global public health interventions and infection prevention and control practices relating to COVID-19. The findings are relevant to healthcare settings, managed quarantine and isolation facilities, and other community indoor environments. To date, multiple reports of SARS-CoV-2 transmission over distances incompatible with droplet spread exist (J.C. Palmer et al., unpub. data), including epidemiologic studies from isolation hotels such as the one we describe in this study (*9*,*24*). This study adds key information to the growing body of evidence supporting a primarily airborne route of transmission for COVID-19 (*4*).

Acknowledgments

We would like to thank the persons involved in the investigation and management of this SARS-CoV-2 transmission event and the staff at the managed isolation facility for their full cooperation with this public health investigation.

About the Author

Dr. Fox-Lewis is a clinical microbiology registrar in Auckland, New Zealand. His research interests are public health microbiology and infectious disease epidemiology and diagnostics.

References

1. World Health Organization. Naming the coronavirus disease (COVID-19) and the virus that causes it [cited 2021 Dec 14]. https://www.who.int/emergencies/diseases/novel-coronavirus-2019/technical-guidance/naming-the-coronavirus-disease-(covid-2019)-and-the-virus-that-causes-it
2. Centers for Disease Control and Prevention. How COVID-19 spreads [cited 2021 Dec 14]. https://www.cdc.gov/coronavirus/2019-ncov/prevent-getting-sick/how-covid-spreads.html
3. Centers for Disease Control and Prevention. SARS-CoV-2 and surface (fomite) transmission for indoor community environments [cited 2021 Dec 14]. https://www.cdc.gov/coronavirus/2019-ncov/more/science-and-research/surface-transmission.html
4. Greenhalgh T, Jimenez JL, Prather KA, Tufekci Z, Fisman D, Schooley R. Ten scientific reasons in support of airborne transmission of SARS-CoV-2. Lancet. 2021;397:1603–5. https://doi.org/10.1016/S0140-6736(21)00869-2
5. Jones RM, Brosseau LM. Aerosol transmission of infectious disease. J Occup Environ Med. 2015;57:501–8. https://doi.org/10.1097/JOM.0000000000000448
6. Jefferies S, French N, Gilkison C, Graham G, Hope V, Marshall J, et al. COVID-19 in New Zealand and the impact of the national response: a descriptive epidemiological study. Lancet Public Health. 2020;5:e612–23. https://doi.org/10.1016/S2468-2667(20)30225-5
7. Swadi T, Geoghegan JL, Devine T, McElnay C, Sherwood J, Shoemack P, et al. Genomic evidence of in-flight transmission of SARS-CoV-2 despite predeparture testing. Emerg Infect Dis. 2021;27:687–93. https://doi.org/10.3201/eid2703.204714
8. Managed Isolation and Quarantine. Arriving in New Zealand [cited 2021 Dec 14]. https://www.miq.govt.nz/travel-to-new-zealand/arriving-in-nz/
9. Eichler N, Thornley C, Swadi T, Devine T, McElnay C, Sherwood J, et al. Transmission of severe acute respiratory syndrome coronavirus 2 during border quarantine and air travel, New Zealand (Aotearoa). Emerg Infect Dis. 2021;27:1274–8. https://doi.org/10.3201/eid2705.210514
10. Fox-Lewis S, Fox-Lewis A, Harrower J, Chen R, Wang J, de Ligt J, et al. Lack of N2-gene amplification on the Cepheid Xpert Xpress SARS-CoV-2 assay and potential novel causative mutations: A case series from Auckland, New Zealand. IDCases. 2021;25:e01233. https://doi.org/10.1016/j.idcr.2021.e01233
11. Corman VM, Landt O, Kaiser M, Molenkamp R, Meijer A, Chu DKW, et al. Detection of 2019 novel coronavirus (2019-nCoV) by real-time RT-PCR [Erratum in: Euro Surveill. 2020;25:20200409; 2020;25:2007303; 2021;26:210204e]. Euro Surveill. 2020;25:2000045. https://doi.org/10.2807/1560-7917.ES.2020.25.3.2000045
12. Geoghegan JL, Ren X, Storey M, Hadfield J, Jelley L, Jefferies S, et al. Genomic epidemiology reveals transmission patterns and dynamics of SARS-CoV-2 in Aotearoa New Zealand. Nat Commun. 2020;11:6351. https://doi.org/10.1038/s41467-020-20235-8
13. Geoghegan JL, Douglas J, Ren X, Storey M, Hadfield J, Silander OK, et al. Use of genomics to track coronavirus disease outbreaks, New Zealand. Emerg Infect Dis. 2021;27:1317–22. https://doi.org/10.3201/eid2705.204579
14. O'Toole Á, Scher E, Underwood A, Jackson B, Hill V, McCrone JT, et al. Assignment of epidemiological lineages in an emerging pandemic using the pangolin tool. Virus Evol. 2021;7:veab064.
15. Shu Y, McCauley J. GISAID: Global initiative on sharing all influenza data - from vision to reality. Euro Surveill. 2017;22:30494. https://doi.org/10.2807/1560-7917.ES.2017.22.13.30494
16. Hadfield J, Megill C, Bell SM, Huddleston J, Potter B, Callender C, et al. Nextstrain: real-time tracking of pathogen evolution. Bioinformatics. 2018;34:4121–3. https://doi.org/10.1093/bioinformatics/bty407
17. Nguyen LT, Schmidt HA, von Haeseler A, Minh BQ. IQ-TREE: a fast and effective stochastic algorithm for estimating maximum-likelihood phylogenies. Mol Biol Evol. 2015;32:268–74. https://doi.org/10.1093/molbev/msu300
18. New Zealand Ministry of Health. Low risk in-facility transmission confirmed at Jet Park MIQ facility [cited 2021 Dec 14]. https://www.health.govt.nz/news-media/media-releases/low-risk-facility-transmission-confirmed-jet-park-miq-facility
19. Managed Isolation and Quarantine. Low risk in-facility transmission confirmed at Auckland's Jet Park MIQ facility [cited 2021 Dec 14]. https://www.miq.govt.nz/about/

news/low-risk-in-facility-transmission-confirmed-at-jet-park-auckland-miq-facility
20. New Zealand National Ethics Advisory Committee. National ethical standards for health and disability research and quality improvement [cited 2021 Dec 14]. https://neac.health.govt.nz/publications-and-resources/neac-publications/national-ethical-standards-for-health-and-disability-research-and-quality-improvement/
21. Centers for Disease Control and Prevention. Ending isolation and precautions for people with COVID-19: interim guidance [cited 2021 Dec 14]. https://www.cdc.gov/coronavirus/2019-ncov/hcp/duration-isolation.html
22. Centers for Disease Control and Prevention. Guidelines for environmental infection control in health-care facilities. 2003 [cited 2021 Dec 14]. https://www.cdc.gov/infectioncontrol/guidelines/environmental/background/air.html
23. National Collaborating Centre for Environmental Health. Contextualizing the risks of indirect COVID-19 transmission in multi-unit residential buildings [cited 2021 Dec 14]. https://ncceh.ca/documents/evidence-review/contextualizing-risks-indirect-covid-19-transmission-multi-unit
24. Gu H, Krishnan P, Ng DYM, Chang LDJ, Liu GYZ, Cheng SSM, et al. Probable transmission of SARS-CoV-2 Omicron variant in quarantine hotel, Hong Kong, China, November 2021. Emerg Infect Dis. 2021 Dec 3 [Epub ahead of print].

Address for correspondence: Dr. Andrew Fox-Lewis, Microbiology Department, Main Laboratory, Level 1 Harley Gray Building, Middlemore Hospital, 100 Hospital Rd, Otahuhu, Auckland, 1640, New Zealand; email: afoxlewis@gmail.com

Detection of SARS-CoV-2 in Neonatal Autopsy Tissues and Placenta

Sarah Reagan-Steiner,[1] Julu Bhatnagar,[1] Roosecelis B. Martines, Nicholas S. Milligan, Carly Gisondo, Frank B. Williams, Elizabeth Lee, Lindsey Estetter, Hannah Bullock, Cynthia S. Goldsmith, Pamela Fair, Julie Hand, Gillian Richardson, Kate R. Woodworth, Titilope Oduyebo, Romeo R. Galang, Rebecca Phillips, Elizaveta Belyaeva, Xiao-Ming Yin, Dana Meaney-Delman, Timothy M. Uyeki, Drucilla J. Roberts, Sherif R. Zaki

Severe coronavirus disease in neonates is rare. We analyzed clinical, laboratory, and autopsy findings from a neonate in the United States who was delivered at 25 weeks of gestation and died 4 days after birth; the mother had asymptomatic severe acute respiratory syndrome coronavirus 2 (SARS-CoV-2) infection and preeclampsia. We observed severe diffuse alveolar damage and localized SARS-CoV-2 by immunohistochemistry, in situ hybridization, and electron microscopy of the lungs of the neonate. We localized SARS-CoV-2 RNA in neonatal heart and liver vascular endothelium by using in situ hybridization and detected SARS-CoV-2 RNA in neonatal and placental tissues by using reverse transcription PCR. Subgenomic reverse transcription PCR suggested viral replication in lung/airway, heart, and liver. These findings indicate that in utero SARS-CoV-2 transmission contributed to this neonatal death.

Severe acute respiratory syndrome coronavirus 2 (SARS-CoV-2) infection during pregnancy is associated with severe maternal coronavirus disease (COVID-19) and preterm birth and may increase the risk for other complications of pregnancy (*1*–*5*). Although possible vertical SARS-CoV-2 transmission has been reported (*4*,*6*–*8*), the strength of supportive laboratory evidence varies. Risk for SARS-CoV-2 infection in neonates seems to be low, and severe COVID-19 in neonates seems rare (*2*–*4*,*9*). We describe the detection and localization of SARS-CoV-2 in autopsy tissues from a 25-week neonate who died at 4 days of age with clinical history, laboratory, and pathologic findings consistent with severe COVID-19. Asymptomatic SARS-CoV-2 infection was diagnosed for the infant's mother after universal screening and preeclampsia.

Author affiliations: Centers for Disease Control and Prevention, Atlanta, Georgia, USA (S. Reagan-Steiner, J. Bhatnagar, R.B. Martines, E. Lee, L. Estetter, H. Bullock, C.S. Goldsmith, P. Fair, K.R. Woodworth, T. Oduyebo, R.R. Galang, D. Meaney-Delman, T.M. Uyeki, S.R. Zaki); Tulane University School of Medicine, New Orleans, Louisiana, USA (N.S. Milligan, E. Belyaeva, X.-M. Yin); Oschner Health, New Orleans (C. Gisondo, F.B. Williams, R. Phillips); Oak Ridge Institute for Science and Education, Oak Ridge, Tennessee, USA (E. Lee); Synergy America, Inc., Duluth, Georgia, USA (L. Estetter, H. Bullock); Louisiana Department of Health, Baton Rouge, Louisiana, USA (J. Hand, G. Richardson); Massachusetts General Hospital, Boston, Massachusetts, USA (D.J. Roberts)

DOI: https://doi.org/10.3201/eid2803.211735

Clinical History of the Mother

The mother was a 34-year-old woman in the United States with a history of 3 prior pregnancies that resulted in live births. She was severely obese (prepregnancy body mass index 47.5 kg/m^2) and had chronic hypertension and a history of preeclampsia in 2 prior pregnancies. She was hospitalized at 25 weeks of gestation for preeclampsia management. Other than systolic blood pressure >160 mm Hg and proteinuria, she was otherwise asymptomatic. She received routine prenatal care starting in the first trimester, and her blood pressure was well controlled until 24 weeks of gestation. At the time of hospitalization, she received magnesium sulfate, intravenous antihypertensive medications, and betamethasone for fetal lung maturation. On hospital day 2, a nasopharyngeal swab sample collected for SARS-CoV-2 screening by reverse transcription PCR (RT-PCR) tested positive. The pregnancy had occurred before COVID-19 vaccines were available in the United States. The patient reported no known SARS-CoV-2 exposures, previous SARS-CoV-2 testing, or COVID-19 symptoms. She had completed her antenatal regimen of corticosteroids, and fetal assessment remained reassuring.

[1]These authors contributed equally to this article.

However, on day 5, an urgent cesarean delivery was performed because of preeclampsia with severe features. Delivery and maternal postpartum course were uncomplicated. The patient was discharged on day 9 and did not subsequently experience fever or respiratory symptoms. No subsequent SARS-CoV-2 testing was performed.

Clinical History of the Neonate

The male infant, delivered at 25 weeks and 6 days of gestation, was immediately taken to a radiant warmer without any maternal contact. Apgar scores were 1 at 1 minute, 4 at 5 minutes, and 7 at 10 minutes. He was intubated within 5 minutes of birth. His birth weight was 670 g (16th percentile), length 32.5 cm (33rd percentile), and head circumference 21.5 cm (6th percentile).

In the neonatal intensive care unit, the neonate was immediately placed under airborne, contact, and droplet precautions in a single-patient room. A chest radiograph showed diffuse bilateral granular opacities without focal consolidation. He received oxygen, an intratracheal dose of surfactant, parenteral nutrition, caffeine, and prophylactic fluconazole. A complete blood count revealed a leukocyte count of 3,150 cells/μL (reference range of 9,000–30,000 cells/μL), a hematocrit of 40.7% (reference range 42%–63%), and a platelet count of 114,000/μL (reference range 150,000–350,000 cells/μL).

At 1 day of age, the neonate was extubated and positive-pressure ventilation was administered; however, by 2 days of age, he was reintubated because of worsening respiratory status and consolidative changes on chest radiograph. A second dose of surfactant was given, and a packed red blood cell transfusion was given because of a hematocrit of 29%. A chest radiograph taken ≈12 hours later showed progression of diffuse bilateral lung opacification and air bronchograms in the lung bases. Oxygenation index was 16.2, demonstrating a severe oxygen deficit consistent with severe neonatal acute respiratory distress syndrome (oxygen index ≥16) (*10*).

At 3 days of age, cardiopulmonary resuscitation was initiated for bradycardia; fluids, vasopressors, and hydrocortisone were administered for hypotensive shock. Vancomycin and amikacin were empirically initiated. A complete blood count revealed 850 leukocytes/μL, 85 neutrophils/μL (reference range 1,300–15,000 neutrophils/μL), and platelets 3,000/μL, for which a platelet transfusion was given. Results of SARS-CoV-2 RT-PCRs on nasopharyngeal swab samples collected at 24 and 72 hours after delivery were positive. Bacterial blood and endotracheal aspirate cultures collected at 3 days of age were negative.

When the neonate was 4 days of age, ventilator and vasopressor requirements increased. A chest radiograph showed continued widespread bilateral airspace consolidation, and oxygenation index was 46.7. Phenobarbital was given for possible seizure activity, and cefepime was added. Despite increasing ventilator support, respiratory acidosis worsened, and an acute bradycardic event occurred. Death was pronounced at 4 days of age, and parental consent for autopsy was obtained.

Postmortem and Placenta Examinations

A complete autopsy and placental examination were performed per standard protocol at the clinical institutions. Formalin-fixed, paraffin-embedded (FFPE) neonatal lung, airway, heart, liver, spleen, and kidney tissues and placental tissues were submitted by the clinical institutions to the Infectious Diseases Pathology Branch, Division of High-Consequence Pathogens and Pathology, National Center for Emerging and Zoonotic Infectious Diseases, Centers for Disease Control and Prevention (CDC), for diagnostic consultation along with medical and autopsy records. This activity was reviewed by CDC and conducted consistent with applicable federal law and CDC policy (45 C.F.R. part 46; 21 C.F.R. part 56; 42 U.S.C. §241(d); 5 U.S.C. §552a; 44 U.S.C. §3501 et seq.).

At CDC, we performed routine hematoxylin-eosin staining for histopathologic evaluation and Gram and Grocott methenamine silver staining to evaluate for bacterial and fungal pathogens. We performed immunohistochemistry (IHC) for SARS-CoV-2 viral antigens (nucleocapsid and spike proteins) as previously described (*11*) as well as angiotensin-converting enzyme 2 (ACE2), transmembrane serine protease 2 (TMPRSS2), and CD163 IHC assays. We performed SARS-CoV-2 conventional RT-PCR and sequencing on RNA extracted from FFPE tissues, as previously described (*12*). We also performed subgenomic RNA RT-PCR and in situ hybridization (ISH) on samples positive by conventional RT-PCR (*12*) and selected only areas with abundant IHC or ISH staining for electron microscopy (*11*).

Histopathology and Immunohistochemistry Assays

For SARS-CoV-2 IHC, we used rabbit monoclonal SARS-CoV-2 nucleocapsid HL448 antibody (GTX635686) and mouse monoclonal SARS-CoV-2 spike S1 antibody (GTX635654; both from GeneTex, https://www.genetex.com). We also used ACE2 goat polyclonal antibody (R&D Systems, https://www.rndsystems.com), transmembrane serine protease 2 (TMPRSS2) rabbit polyclonal PA5-76776 (Thermo

Fisher Scientific, https://www.thermofisher.com), and CD163 mouse monoclonal antibody (clone 10D6; Leica Biosystems, https://www.leicabiosystems.com) for IHC. Double-stained IHC assays were performed according to manufacturer guidelines by using the mouse monoclonal SARS-CoV-2 spike S1 antibody and CD163 mouse monoclonal antibody with the TripleStain IHC Kit: M&M&R on human tissue (DAB, AP/Red & HRP/Green, ab183286; abcam, https://www.abcam.com).

RT-PCR, Sequencing, and ISH Assays

We extracted RNA from FFPE autopsy and placental tissues by using the phenol-chloroform extraction protocol, as previously described (*13*) and evaluated all samples by using 2 conventional RT-PCR assays targeting the spike (S) and nucleocapsid (N) genes for SARS-CoV-2. The assays were performed by using the OneStep RT-PCR Kit (QIAGEN, https://www.qiagen.com) and 5 μL of RNA sample. The N-gene (150-bp) and S-gene (162-bp) amplicons positive by PCR were directly sequenced by Sanger sequencing on a GenomeLab GeXP sequencer (AB SCIEX, https://sciex.com). We searched for homologies to known sequences by using the BLAST nucleotide database (http://blast.ncbi.nlm.nih.gov/Blast.cgi). To demonstrate evidence of probable viral replication, we performed subgenomic RNA RT-PCR (*14*). To directly localize SARS-CoV-2 RNA, we performed ISH assays targeting the N and S genes on FFPE tissues that were positive for SARS-CoV-2 by conventional RT-PCR.

Postmortem and Placenta Findings

Neonate

Microscopic examination of lungs from the neonate showed peripheral vascularization consistent with 24–26 weeks of gestation. We observed severe diffuse alveolar damage with hyaline membranes, type II pneumocyte hyperplasia, and mild interstitial mononuclear infiltrate (Figure 1, panel A). We found

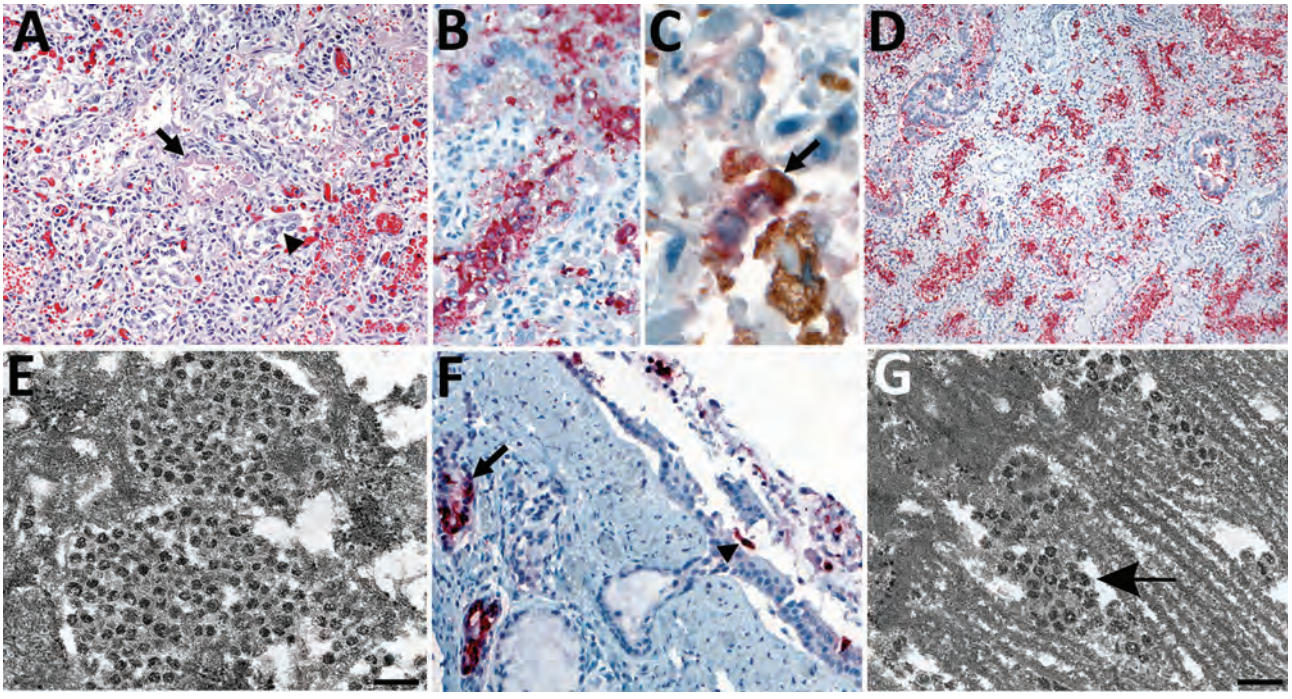

Figure 1. Pulmonary histopathologic, immunohistochemical (IHC), in situ hybridization, and ultrastructural findings in tissues from a neonate in the United States with severe acute respiratory syndrome coronavirus 2 (SARS-CoV-2). A) Lower magnification of the lung showing diffuse alveolar damage, characterized by type II pneumocyte hyperplasia (arrowhead), hyaline membrane (arrow), and interstitial mononuclear infiltrate. Original magnification ×20. B) Extensive intra-alveolar immunostaining by spike protein SARS-CoV-2 IHC assay. Original magnification ×40. C) Double-stain IHC assay showing rare macrophages with SARS-CoV-2/CD-163–positive immunostaining. Red, SARS-CoV-2; brown, CD-163 antibody (arrow). Original magnification ×63. D) Extensive staining of SARS-CoV-2 genomic RNA in pneumocytes by nucleocapsid gene in situ hybridization assay. Original magnification ×10. E) Electron microscopy (EM) image of a pneumocyte containing accumulations of intracellular viral particles. Scale bar indicates 200 nm; viral particles were on average 65 nm in diameter, smaller than commonly observed because of shrinkage during processing. F) Immunostaining of tracheal epithelial cells (arrowhead) and submucosal glands (arrow) by SARS-CoV-2 nucleocapsid IHC assay. Original magnification ×20. G) EM image of a ciliated epithelial cell with extracellular viral particles (arrow) associated with the cilia. Scale bar indicates 200 nm. EM images were collected from 4-μm sections of formalin-fixed, paraffin-embedded tissues affixed to glass slides that were embedded for EM.

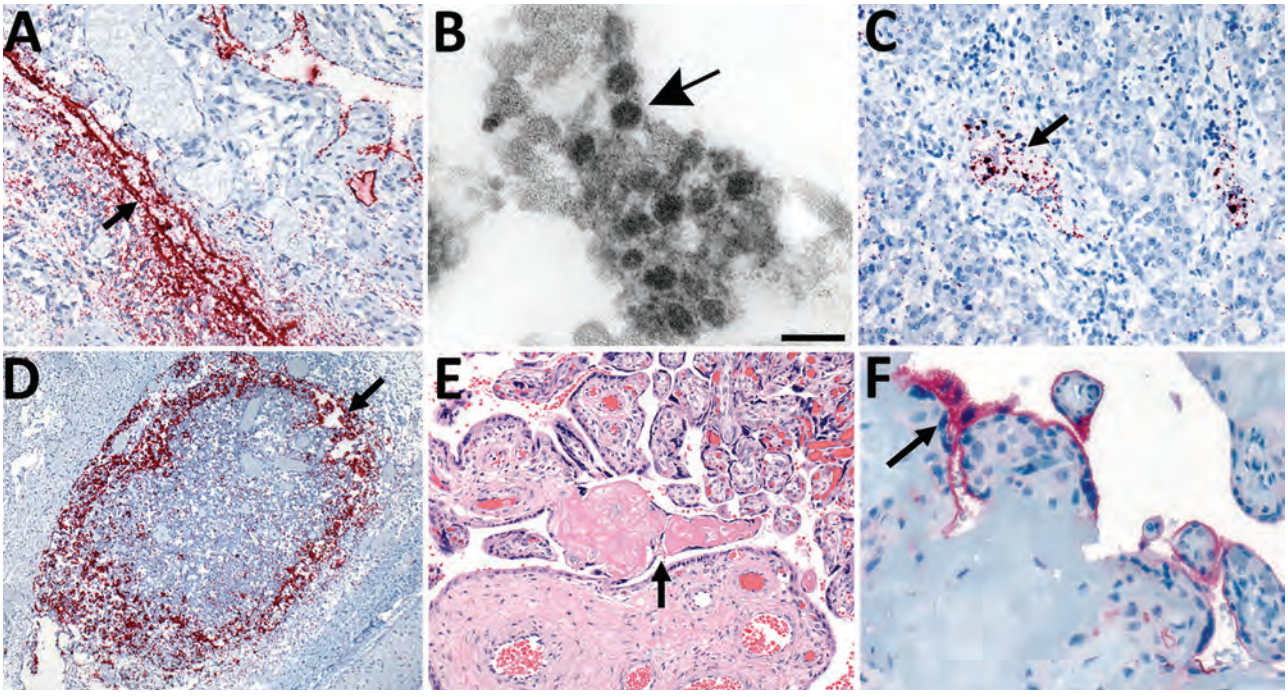

Figure 2. In situ hybridization (ISH) slides demonstrating localization of severe acute respiratory syndrome coronavirus 2 (SARS-CoV-2) genomic RNA in heart, liver, and lymph node tissues and electron microscopic evidence of viral particles in heart tissue from neonate in the United States that died with SARS-CoV-2 infection and placental histopathology and angiotensin-converting enzyme-2 immunohistochemical stain slides. A) SARS-CoV-2 RNA staining by nucleocapsid gene ISH assay in the endothelial cells in myocardium vessel walls (arrow). Original magnification ×20. B) Extracellular virus particles in the connective tissue of the heart (arrow). Scale bar indicates 100 nm. C) Intravascular staining by nucleocapsid gene ISH assay in the liver parenchyma (arrow). Original magnification ×20. D) Extensive nucleocapsid gene ISH staining within macrophages of subcapsular sinus of lymphoid follicle in the submucosa of upper airway (arrow). Original magnification ×10. E) Second trimester placenta with fibrinoid necrosis (arrow). Original magnification ×20. F) Angiotensin-converting enzyme 2 immunostaining in the membrane polarized on the maternal lake side in the syncytiotrophoblast (arrow). Original magnification ×63.

no histopathologic evidence of bronchopneumonia; Gram staining revealed no bacterial pathogens; and Grocott methenamine silver staining revealed no fungal pathogens. We identified SARS-CoV-2 viral antigens in alveolar macrophages, type II pneumocytes (Figure 1, panel B), and hyaline membranes. Rare macrophages demonstrated SARS-CoV-2/CD163 double-staining (Figure 1, panel C). ISH demonstrated viral RNA in alveolar macrophages and pneumocytes (Figure 1, panel D). We observed viral antigens (Figure 1, panel F) and RNA in airway, bronchiolar, and submucosal gland epithelium and in macrophages in prominent airway submucosa lymphoid follicles (Figure 2, panel D).

Although we observed no significant histopathologic findings in extrapulmonary tissues, ISH detected SARS-CoV-2 RNA in vascular endothelial cells in the myocardium (Figure 2, panel A), where viral antigens were also observed, and in the liver (Figure 2, panel C). IHC assays of the liver and IHC and ISH of the spleen and kidney produced negative results.

SARS-CoV-2 RNA was detected in lung, airway, heart, liver, spleen, and kidney tissue by conventional RT-PCR; sequence analysis of PCR amplicons showed 99%–100% nt identity with SARS-CoV-2. Subgenomic RNA, suggesting SARS-CoV-2 replication (*12*), was detected by subgenomic RT-PCR in lung, airway, heart, and liver tissue but not in spleen or kidney tissue.

Electron microscopy revealed coronavirus-like particles in areas corresponding to SARS-CoV-2 IHC and ISH staining in respiratory and myocardial tissues. We found vacuolar accumulations of coronavirus particles within pneumocytes (Figure 1, panel E) and extracellular viral particles in association with cilia of respiratory epithelial cells (Figure 1, panel G) and near collagen in the heart (Figure 2, panel B).

Placenta

The trimmed placenta was 72 g, which was small for gestational age (10th percentile weight for a singleton placenta at 25 weeks gestation would be ≈159 g) (*15*). We found microscopic evidence of maternal vascular malperfusion, including placental

hypoplasia, accelerated villous maturation, and focally increased perivillous fibrin (Figure 2, panel E). We also noted increased villous fibrinoid necrosis, a feature of villous trophoblastic injury. We observed low-grade fetal vascular malperfusion with multifocal avascular villi but no villitis or histiocytic intervillositis. ACE2 was multifocally expressed in the syncytiotrophoblast and cytotrophoblast in the maternal lake side and in the decidua basalis (Figure 2, panel F). Weak TMPRSS2 staining was observed in the syncytiotrophoblast membrane. Placental parenchyma was positive by SARS-CoV-2 conventional RT-PCR, confirmed by sequencing but negative by subgenomic RT-PCR, IHC, and ISH. Trivascular umbilical cord and fetal membranes were unremarkable, and all SARS-CoV-2 assay results for cord and membrane samples were negative.

Discussion

We provide direct evidence of SARS-CoV-2 infection and probable viral replication in multiple autopsy tissues from a premature infant who died with severe COVID-19. Our findings are most consistent with virus acquisition via in utero transmission. We found extensive staining of SARS-CoV-2 antigens and RNA and evidence of plausible virus replication in the lungs, which demonstrated significant pathology. Heart and liver demonstrated vascular endothelial RNA staining and subgenomic RT-PCR positivity, consistent with hematogenous dissemination to the primary targets of fetal circulation and probable virus replication in these organs. Although other mechanisms of vertical transmission cannot be definitively excluded, placental positivity by conventional RT-PCR suggests that SARS-CoV-2 RNA was in the maternal circulation, and transplacental transmission could have occurred only if maternal viremia was present before delivery. Furthermore, although the incubation period after in utero SARS-CoV-2 exposure is unknown, development of advanced pulmonary pathology, including diffuse alveolar damage with extensive staining of viral antigens and RNA, and extrapulmonary dissemination of SARS-CoV-2 would be unlikely if transmission occurred intrapartum or postnatally.

Viral infections during pregnancy and after delivery can lead to infant illness and death (*16*,*17*). Vertical transmission of viruses can occur in 3 ways: 1) in utero (via maternal viremia and either placental cell infection or placental barrier disruption), 2) intrapartum (from maternal body fluids during birth), or 3) postnatally (e.g., from breastfeeding, caregiver exposures) (*16*,*17*). Thus far, reports consistent with in utero SARS-CoV-2 transmission have been rare and include mother–infant pairs with evidence of SARS-CoV-2 in maternal specimens (e.g., placenta) and neonatal specimens (e.g., respiratory swab samples collected <24 hours postnatally) (*18*,*19*). Although a review of 176 neonatal SARS-CoV-2 infections reported in the literature estimated that ≈30% could have resulted from vertical transmission, those data were not based on systematic testing or surveillance activities (*8*).

Vertical transmission of SARS-CoV-2 and severe neonatal COVID-19 seem infrequent; however, risk for medically indicated preterm delivery and stillbirth among women with SARS-CoV-2 infection during pregnancy seems to be elevated (*2*,*3*,*7*,*8*). Although severe respiratory disease in SARS-CoV-2–positive late preterm or term neonates has been reported (*4*–*7*), we detected SARS-CoV-2 and evidence of probable virus replication in autopsy tissues from an extremely preterm neonate. In addition, maternal SARS-CoV-2 infection occurred during the first or second trimester. Most reports of SARS-CoV-2 infection during pregnancy describe infection in the third trimester (*1*–*5*). Additional data on outcomes among women with first or second trimester SARS-CoV-2 infection, including data specifically for preterm infants (*2*–*4*,*9*), are needed.

Given the extreme prematurity of this infant, the relative contributions of neonatal respiratory distress syndrome versus SARS-CoV-2 infection to the observed lung pathology and patient outcome are difficult to disentangle. However, abundant staining of SARS-CoV-2 antigens and RNA in the lungs and evidence of probable virus replication in the context of pathology typical of COVID-19 in adults (*11*,*12*) indicate that SARS-CoV-2 infection played a central role in this case. Furthermore, the neonate's condition did not improve after repeated surfactant administration.

Placental cells express SARS-CoV-2 ACE2 and TMPRSS2 receptors, as in this case, and the genes necessary for viral replication (*20*–*23*). However, receptor density and colocalization vary throughout pregnancy, potentially leading to differential risk for placental infection by trimester (*23*,*24*). In addition, SARS-CoV-2 RNA is rarely detected in the placenta, and electron microscopy has misidentified common subcellular structures as coronavirus particles (*25*–*28*). In this patient, we found neither evidence of placental SARS-CoV-2 infection by ISH or IHC (*29*–*34*) nor evidence of chronic histiocytic intervillositis, which has been identified as a relatively consistent pathologic feature associated with placental SARS-CoV-2infection (*32*–*34*).

Consequently, conventional RT-PCR positivity may represent maternal viremia.

Other case series have described placental SARS-CoV-2 detection in the syncytiotrophoblast, cytotrophoblast, Hofbauer cells, and villous endothelial cells, including in some cases with evidence of in utero SARS-CoV-2 transmission (*18*,*32*–*34*). Although the timing of maternal infection cannot be established in this case, if the infection was acute and viremia was present, it is possible that substantial placenta pathology had not yet developed or may have been missed during placenta sampling. Hematogenous in utero transmission of some viral infections also occurs in the absence of placental infection (*35*). Factors such as hypoperfusion and trophoblast ischemic damage or transient maternal–fetal hemorrhage could have exposed the villus stroma to maternal blood and led to SARS-CoV-2 transfer to fetal circulation without placental cellular infection. The relationship between SARS-CoV-2 infection, preeclampsia, and maternal and infant outcomes is complex. Although the rate of preeclampsia might be elevated among pregnant women with COVID-19 (*2*,*5*), the effect of SARS-CoV-2 infection on its development or severity, particularly in patients with multiple preeclampsia risk factors, is unknown.

The World Health Organization and others have proposed definitions for in utero SARS-CoV-2 transmission (*16*,*17*,*31*). This case would meet World Health Organization criteria for possible in utero SARS-CoV-2 transmission; however, it would not meet the definition of confirmed transmission because virus persistence criteria were not met (i.e., RT-PCR SARS-CoV-2 positivity for a sterile sample at 24–48 hours of life) (*16*). Adding criteria for neonatal autopsy tissue–based molecular evidence of SARS-CoV-2 could be useful, similar to criteria for establishing in utero transmission for a fetal demise.

This case demonstrates that in utero SARS-CoV-2 transmission is possible and can lead to serious outcomes for infants. Further work is needed to provide more information about risk factors for mother-to-child transmission, adverse pregnancy outcomes, and infant outcomes in women with SARS-CoV-2 infection during pregnancy and to inform patient management and testing strategies, prevention, and individual COVID-19 vaccination decision making. COVID-19 vaccination before or during pregnancy is strongly recommended by CDC, the American College of Obstetrics and Gynecology, and the Society for Maternal-Fetal Medicine (*36*–*38*). However, vaccination uptake among pregnant women is currently low in the United States; as of September 27, 2021, only 31% of pregnant women were fully vaccinated before or during pregnancy (*39*). Continued public health surveillance for pregnancy and infant outcomes by trimester of SARS-CoV-2 infection is warranted, including evaluation of placental, fetal, or infant specimens from COVID-19–affected pregnancies when possible and clinically indicated. SARS-CoV-2 testing during pregnancy should be guided by routine assessment for COVID-19–associated signs/symptoms and exposures, presence of complications potentially associated with SARS-CoV-2 infection (e.g., preeclampsia) (*2*,*5*), and level of community transmission. Neonates born to women with suspected or confirmed COVID-19, regardless of neonatal signs/symptoms, should also be tested for SARS-CoV-2 (*40*).

Acknowledgments

We thank Tyler Rorison for histotechnology support, Brooke Leitgeb for coordination and communication activities, and Luciana Flannery for supporting immunohistochemistry double-staining.

Sherif R. Zaki, senior author, died before publication of this article. We are thankful for his leadership.

About the Author

Dr. Reagan-Steiner is a public health physician with the Infectious Diseases Pathology Branch, Division of High-Consequence Pathogens and Pathology, National Center for Emerging and Zoonotic Infectious Diseases, at CDC in Atlanta, Georgia. Her primary research interests are surveillance for and characterization of infectious disease-related deaths. Dr. Bhatnagar is team lead of the Molecular Pathology in the Infectious Diseases Pathology Branch, Division of High-Consequence Pathogens and Pathology, Center for Emerging and Zoonotic Infectious Diseases, at CDC in Atlanta. Her primary research interests include development of tissue-based novel molecular diagnostic assays and techniques for identification of pathogens and study of pathogenesis of emerging infectious diseases.

References

1. Delahoy MJ, Whitaker M, O'Halloran A, Chai SJ, Kirley PD, Alden N, et al.; COVID-NET Surveillance Team. Characteristics and maternal and birth outcomes of hospitalized pregnant women with laboratory-confirmed COVID-19 - COVID-NET, 13 states, March 1–August 22, 2020. MMWR Morb Mortal Wkly Rep. 2020;69:1347–54. https://doi.org/10.15585/mmwr.mm6938e1
2. Villar J, Ariff S, Gunier RB, Thiruvengadam R, Rauch S, Kholin A, et al. Maternal and neonatal morbidity and mortality among pregnant women with and without COVID-19 infection: The INTERCOVID Multinational

Cohort Study. JAMA Pediatr. 2021;175:817–26. https://doi.org/10.1001/jamapediatrics.2021.1050
3. Woodworth KR, Olsen EO, Neelam V, Lewis EL, Galang RR, Oduyebo T, et al.; CDC COVID-19 Response Pregnancy and Infant Linked Outcomes Team; COVID-19 Pregnancy and Infant Linked Outcomes Team (PILOT). Birth and infant outcomes following laboratory-confirmed SARS-CoV-2 infection in pregnancy - SET-NET, 16 jurisdictions, March 29–October 14, 2020. MMWR Morb Mortal Wkly Rep. 2020;69:1635–40. https://doi.org/10.15585/mmwr.mm6944e2
4. Allotey J, Stallings E, Bonet M, Yap M, Chatterjee S, Kew T, et al.; for PregCOV-19 Living Systematic Review Consortium. Clinical manifestations, risk factors, and maternal and perinatal outcomes of coronavirus disease 2019 in pregnancy: living systematic review and meta-analysis. BMJ. 2020;370:m3320. https://doi.org/10.1136/bmj.m3320
5. Wei SQ, Bilodeau-Bertrand M, Liu S, Auger N. The impact of COVID-19 on pregnancy outcomes: a systematic review and meta-analysis. CMAJ. 2021;193:E540–8. https://doi.org/10.1503/cmaj.202604
6. Correia CR, Marçal M, Vieira F, Santos E, Novais C, Maria AT, et al. Congenital SARS-CoV-2 infection in a neonate with severe acute respiratory syndrome. Pediatr Infect Dis J. 2020;39:e439–43. https://doi.org/10.1097/INF.0000000000002941
7. Vivanti AJ, Vauloup-Fellous C, Prevot S, Zupan V, Suffee C, Do Cao J, et al. Transplacental transmission of SARS-CoV-2 infection. Nat Commun. 2020;11:3572. https://doi.org/10.1038/s41467-020-17436-6
8. Raschetti R, Vivanti AJ, Vauloup-Fellous C, Loi B, Benachi A, De Luca D. Synthesis and systematic review of reported neonatal SARS-CoV-2 infections. Nat Commun. 2020;11:5164. https://doi.org/10.1038/s41467-020-18982-9
9. Mullins E, Hudak ML, Banerjee J, Getzlaff T, Townson J, Barnette K, et al.; PAN-COVID investigators and the National Perinatal COVID-19 Registry Study Group. Pregnancy and neonatal outcomes of COVID-19: coreporting of common outcomes from PAN-COVID and AAP-SONPM registries. Ultrasound Obstet Gynecol. 2021;57:573–81. https://doi.org/10.1002/uog.23619
10. De Luca D, van Kaam AH, Tingay DG, Courtney SE, Danhaive O, Carnielli VP, et al. The Montreux definition of neonatal ARDS: biological and clinical background behind the description of a new entity. Lancet Respir Med. 2017;5:657–66. https://doi.org/10.1016/S2213-2600(17)30214-X
11. Martines RB, Ritter JM, Matkovic E, Gary J, Bollweg BC, Bullock H, et al.; COVID-19 Pathology Working Group. Pathology and pathogenesis of SARS-CoV-2 associated with fatal coronavirus disease, United States. Emerg Infect Dis. 2020;26:2005–15. https://doi.org/10.3201/eid2609.202095
12. Bhatnagar J, Gary J, Reagan-Steiner S, Estetter LB, Tong S, Tao Y, et al. Evidence of severe acute respiratory syndrome coronavirus 2 replication and tropism in the lungs, airways, and vascular endothelium of patients with fatal coronavirus disease 2019: an autopsy case series. J Infect Dis. 2021;223:752–64. https://doi.org/10.1093/infdis/jiab039
13. Bhatnagar J, Blau DM, Shieh W-J, Paddock CD, Drew C, Liu L, et al. Molecular detection and typing of dengue viruses from archived tissues of fatal cases by RT-PCR and sequencing: diagnostic and epidemiologic implications. Am J Trop Med Hyg. 2012;86:335–40. https://doi.org/10.4269/ajtmh.2012.11-0346
14. Milewska A, Kula-Pacurar A, Wadas J, Suder A, Szczepanski A, Dabrowska A, et al. Replication of severe acute respiratory syndrome coronavirus 2 in human respiratory epithelium. J Virol. 2020;94:e00957–20. https://doi.org/10.1128/JVI.00957-20
15. Pinar H, Sung CJ, Oyer CE, Singer DB. Reference values for singleton and twin placental weights. Pediatr Pathol Lab Med. 1996;16:901–7. https://doi.org/10.1080/15513819609168713
16. World Health Organization. Definition and categorization of the timing of mother-to-child transmission of SARS-CoV-2 [cited 2021 Oct 6]. https://www.who.int/publications/i/item/WHO-2019-nCoV-mother-to-child-transmission-2021.1
17. Schwartz DA, Morotti D, Beigi B, Moshfegh F, Zafaranloo N, Patanè L. Confirming vertical fetal infection with coronavirus disease 2019: neonatal and pathology criteria for early onset and transplacental transmission of severe acute respiratory syndrome coronavirus 2 from infected pregnant mothers. Arch Pathol Lab Med. 2020;144:1451–6. https://doi.org/10.5858/arpa.2020-0442-SA
18. Schwartz DA, Baldewijns M, Benachi A, Bugatti M, Collins RRJ, De Luca D, et al. Chronic histiocytic intervillositis with trophoblast necrosis is a risk factor associated with placental infection from coronavirus disease 2019 (COVID-19) and intrauterine maternal-fetal severe acute respiratory syndrome coronavirus 2 (SARS-CoV-2) transmission in live-born and stillborn infants. Arch Pathol Lab Med. 2021;145:517–28. https://doi.org/10.5858/arpa.2020-0771-SA
19. Schwartz DA, Baldewijns M, Benachi A, Bugatti M, Bulfamante G, Cheng K, et al. Hofbauer cells and coronavirus disease 2019 (COVID-19) in pregnancy: molecular pathology analysis of villous macrophages, endothelial cells, and placental findings from 22 placentas infected by severe acute respiratory syndrome coronavirus 2 (SARS-CoV-2) with and without fetal transmission. Arch Pathol Lab Med. 2021;145:1328–40. https://doi.org/10.5858/arpa.2021-0296-SA
20. Ashary N, Bhide A, Chakraborty P, Colaco S, Mishra A, Chhabria K, et al. Single-Cell RNA-seq identifies cell subsets in human placenta that highly expresses factors driving pathogenesis of SARS-CoV-2. Front Cell Dev Biol. 2020;8:783. https://doi.org/10.3389/fcell.2020.00783
21. Colaco S, Chhabria K, Singh D, Bhide A, Singh N, Singh A, et al. Expression map of entry receptors and infectivity factors for pan-coronaviruses in preimplantation and implantation stage human embryos. J Assist Reprod Genet. 2021;38:1709–20. https://doi.org/10.1007/s10815-021-02192-3
22. Edlow AG, Li JZ, Collier AY, Atyeo C, James KE, Boatin AA, et al. Assessment of maternal and neonatal SARS-CoV-2 viral load, transplacental antibody transfer, and placental pathology in pregnancies during the COVID-19 pandemic. JAMA Netw Open. 2020;3:e2030455. https://doi.org/10.1001/jamanetworkopen.2020.30455
23. Roberts DJ, Bebell LM, Edlow AG. Placental ACE2 and TMPRSS2 receptor protein expression patterns throughout gestation. J Infect Dis. 2021 Apr 21 [Epub ahead of print]. https://doi.org/10.1093/infdis/jiab164
24. Hecht JL, Quade B, Deshpande V, Mino-Kenudson M, Ting DT, Desai N, et al. SARS-CoV-2 can infect the placenta and is not associated with specific placental histopathology: a series of 19 placentas from COVID-19-positive mothers. Mod Pathol. 2020;33:2092–103. https://doi.org/10.1038/s41379-020-0639-4
25. Algarroba GN, Rekawek P, Vahanian SA, Khullar P, Palaia T, Peltier MR, et al. Visualization of SARS-CoV-2 virus invading the human placenta using electron microscopy. Am J Obstet Gynecol. 2020;13:13.

26. Hosier H, Farhadian SF, Morotti RA, Deshmukh U, Lu-Culligan A, Campbell KH, et al. SARS-CoV-2 infection of the placenta. J Clin Invest. 2020;130:4947–53. https://doi.org/10.1172/JCI139569
27. Sisman J, Jaleel MA, Moreno W, Rajaram V, Collins RRJ, Savani RC, et al. Intrauterine transmission of SARS-COV-2 infection in a preterm infant. Pediatr Infect Dis J. 2020;39 :e265–7. https://doi.org/10.1097/INF.0000000000002815
28. Bullock HA, Goldsmith CS, Zaki SR, Martines RB, Miller SE. Difficulties in differentiating coronaviruses from subcellular structures in human tissues by electron microscopy. Emerg Infect Dis. 2021;27:1023–31. https://doi.org/10.3201/eid2704.204337
29. Schwartz DA, Levitan D. Severe acute respiratory syndrome coronavirus 2 (SARS-CoV-2) infecting pregnant women and the fetus, intrauterine transmission, and placental pathology during the coronavirus disease 2019 (COVID-19) pandemic: it's complicated. Arch Pathol Lab Med. 2021;145:925–8. https://doi.org/10.5858/arpa.2021-0164-ED
30. Schwartz DA, Morotti D. Placental pathology of COVID-19 with and without fetal and neonatal infection: trophoblast necrosis and chronic histiocytic intervillositis as risk factors for transplacental transmission of SARS-CoV-2. Viruses. 2020;12:E1308. https://doi.org/10.3390/v12111308
31. Shah PS, Diambomba Y, Acharya G, Morris SK, Bitnun A. Classification system and case definition for SARS-CoV-2 infection in pregnant women, fetuses, and neonates. Acta Obstet Gynecol Scand. 2020;99:565–8. https://doi.org/10.1111/aogs.13870
32. Roberts DJ, Edlow AG, Romero RJ, Coyne CB, Ting DT, Hornick JL, et al; National Institutes of Health/Eunice Kennedy Shriver National Institute of Child Health and Human Development SARS-CoV-2 Placental Infection Workshop. A standardized definition of placental infection by SARS-CoV-2, a consensus statement from the National Institutes of Health/Eunice Kennedy Shriver National Institute of Child Health and Human Development SARS-CoV-2 Placental Infection Workshop. Am J Obstet Gynecol. 2021 Aug 5 [Epub ahead of print]. https://doi.org/10.1016/j.ajog.2021.07.02
33. Watkins JC, Torous VF, Roberts DJ. Defining severe acute respiratory syndrome coronavirus 2 (SARS-CoV-2) placentitis. Arch Pathol Lab Med. 2021;145:1341–9. https://doi.org/10.5858/arpa.2021-0246-SA
34. Schwartz DA, Bugatti M, Santoro A, Facchetti F. Molecular pathology demonstration of SARS-CoV-2 in cytotrophoblast from placental tissue with chronic histiocytic intervillositis, trophoblast necrosis and COVID-19. J Dev Biol. 2021;9:33. https://doi.org/10.3390/jdb9030033
35. Mahyuddin AP, Kanneganti A, Wong JJL, Dimri PS, Su LL, Biswas A, et al. Mechanisms and evidence of vertical transmission of infections in pregnancy including SARS-CoV-2s. Prenat Diagn. 2020;40:1655–70. https://doi.org/10.1002/pd.5765
36. Centers for Disease Control and Prevention. Interim clinical considerations for use of COVID-19 vaccines currently approved or authorized in the United States [cited 2021 Oct 6]. https://www.cdc.gov/vaccines/covid-19/clinical-considerations/covid-19-vaccines-us.html
37. American College of Obstetricians and Gynecologists. COVID-19 vaccination considerations for obstetric-gynecologic care [cited 2021 Oct 6]. https://www.acog.org/clinical/clinical-guidance/practice-advisory/articles/2020/12/covid-19-vaccination-considerations-for-obstetric-gynecologic-care
38. Society for Maternal-Fetal Medicine. Provider considerations for engaging in COVID-19 vaccine counseling with pregnant and lactating patients [cited 2021 Oct 6]. https://s3.amazonaws.com/cdn.smfm.org/media/3134/Provider_Considerations_for_Engaging_in_COVID_Vaccination_Considerations_10-1-21_%28final%29.pdf
39. Centers for Disease Control and Prevention. COVID-19 vaccination for pregnant people to prevent serious illness, deaths, and adverse pregnancy outcomes from COVID-19. HAN Alert No. 453 [cited 2021 Oct 6]. https://emergency.cdc.gov/han/2021/han00453.asp
40. Centers for Disease Control and Prevention. Evaluation and management considerations for neonates at risk for COVID-19 [cited 2021 Oct 6]. https://www.cdc.gov/coronavirus/2019-ncov/hcp/caring-for-newborns.html

Address for correspondence: Sarah Reagan-Steiner, Centers for Disease Control and Prevention, 1600 Clifton Rd NE, Atlanta, GA 30329-4027, USA; email: sor1@cdc.gov

Association of Healthcare and Aesthetic Procedures with Infections Caused by Nontuberculous Mycobacteria, France, 2012–2020

Côme Daniau, Emmanuel Lecorche, Faiza Mougari, Hanaa Benmansour, Claude Bernet, Hervé Blanchard, Jérôme Robert, Anne Berger-Carbonne, Emmanuelle Cambau

We describe nontuberculous mycobacteria (NTM) infections during 2012–2020 associated with health care and aesthetic procedures in France. We obtained epidemiologic data from the national early warning response system for healtcare-associated infections and data on NTM isolates from the National Reference Center for Mycobacteria. We compared clinical and environmental isolates by using whole-genome sequencing. The 85 original cases were reported after surgery (48, 56%), other invasive procedures (28, 33%) and other procedures (9, 11%). NTM isolates belonged to rapidly growing (73, 86%) and slowly growing (10, 12%) species; in 2 cases, the species was not identified. We performed environmental investigations for 38 (45%) cases; results for 12 (32%) were positive for the same NTM species as for the infection. In 10 cases that had environmental and clinical samples whose genomes were similar, the infection source was probably the water used in the procedures. NTM infections could be preventable by using sterile water in all invasive procedures.

Author affiliations: Santé Publique France, Saint-Maurice, France (C. Daniau, A. Berger-Carbonne); Université de Paris, Paris, France (E. Lecorche, E. Cambau); Assistance Publique Hôpitaux de Paris, Paris (E. Lecorche, F. Mougari, H. Benmansour, H. Blanchard, J. Robert, E. Cambau); Centre National de Référence des Mycobactéries et de la Résistance des Mycobactéries aux Antituberculeux, Paris (E. Lecorche, F. Mougari, H. Benmansour, J. Robert, E. Cambau); Centre d'Appui pour la Prévention des Infections Associées aux Soins en Provence-Alpes-Côte-d'Azur, Lyon, France (C. Bernet); Centre d'Appui pour la Prévention des Infections Associées aux Soins en Île-de-France, Paris (H. Blanchard); Centre d'Immunologie et des Maladies Infectieuses (CIMI), Sorbonne Université, Paris (J. Robert)

DOI: https://doi.org/10.3201/eid2803.211791

Nontuberculous mycobacteria (NTM) are ubiquitous bacteria found in soil, water, and other environments (*1*,*2*). More than 200 NTM species have been described to date. NTM are classified according to their speed of growth in vitro, specifically rapidly growing mycobacteria (such as *Mycobacterium chelonae*, *M. fortuitum* complex, and *M. abscessus*) and slowly growing mycobacteria (such as *M. avium* complex, *M. marinum*, and *M. kansasii*).

NTM infections are usually not transmissible between humans, although outbreaks linked to the same contamination event or from a common water reservoir have been reported. This finding was especially observed for extrapulmonary NTM infections after invasive procedures because of a common source, such as healthcare-associated infections (HAIs) and those related to medical, aesthetic, or cosmetic procedures (*3*–*7*). In particular, NTM HAIs were observed after heart surgery: >100 cases of endocarditis caused by a single clone of *M. chimaera* were found in water tanks of heater-cooler units used for cardiac bypass (*8*). In France, previously reported outbreaks of NTM HAI cases have involved *M. xenopi* in bone and joint infections after orthopedic surgery (*9*) and *M. chelonae* in skin infections after mesotherapy cosmetic procedures (*5*) or in hematopoietic stem cell transplantation (*10*). Endocarditis on bioprosthetic heart valves were also reported to contain *M. wolinskyi* and *M. chelonae* (*11*).

HAI reporting has been mandatory in France since 2001, and reports are collected at the French Public Health Agency. In addition, the National Reference Centre for Mycobacteria and Resistance of Mycobacteria to Anti-Tuberculosis Agents (CNR-MyRMA) regularly receives NTM isolates, including

NTM HAI isolates, from human infections for diagnosis and treatment purposes. A previous case series described an initial cross-database evaluation focusing on NTM infections associated with cosmetic procedures during 2001–2010 (*12*). We describe episodes of extrapulmonary NTM infections associated with surgical, medical, or aesthetic procedures, including cosmetic care, reported in France during 2012–2020, in and outside healthcare facilities (HCFs).

Materials and Methods

Data Sources

We used 2 data sources to include reported cases of NTM infections associated with surgical, medical, or aesthetic procedures during January 2012–June 2020. The first data source was the national early warning response system (EWRS) for HAI diagnosed in HCF, using an electronic reporting process implemented in 2012 (e-SIN), and slightly modified in 2017 (*13*). The second data source was the NTM isolate database of the CNR-MyRMA, which includes microbiological results of clinical isolates, as well as environmental isolates found after epidemiologic investigations. The Regional Support Centre for the Prevention of Healthcare-Associated Infections conducted epidemiologic investigations. We contacted health professionals who reported cases to the national EWRS for HAI and send isolates to CNR-MyRMA to associate isolates with cases. We used this procedure to set up a single database containing epidemiologic and microbiological data.

Case Definition

We included extrapulmonary NTM infections defined as a person who had clinical symptoms compatible with an NTM infection and ≥1 NTM-positive microbiological sample (cases considered as NTM colonization by physicians were excluded); and specific surgical, medical, or aesthetic procedures, including cosmetic care, potentially at the origin of the NTM infection. Pulmonary NTM infections, even hospital-acquired, were excluded. We usually consolidated epidemiologically related cases into a single report.

Data Collection and Analysis

We collected the following information from the 2 data sources: 1) the report itself (the HCF or the laboratory which made the report, date of report); 2) data for infection (date of onset of initial symptoms, symptoms, infection type); 3) the context and suspected cause of the infection (procedure at the origin of the infection, date of contamination or invasive procedure, equipment implicated); 4) epidemic context (number of cases, distribution over time); 5) characteristics of case-patients (age, sex, and immune status); 6) investigation characteristics performed after the NTM infection diagnosis (environmental and professional practices investigations, corrective measures implemented); and 7) microbiological results (name of species and subspecies, whole-genome sequencing [WGS] comparison). We performed a descriptive data analysis by using STATA version 14.2 (https://www.stata.com). We analyzed the rate of NTM infection cases over the study period by using a Poisson regression model.

Genomic Comparison

We performed genotypic analysis by using WGS to compare isolates found in environmental and clinical samples. We extracted DNA by using the DNA Ultraclean Microbial Kit (QIAGEN, https://www.qiagen.com). We prepared DNA libraries by using the Nextera XT Kit (Illumina, https://www.illumina.com) and sequenced them by using the MiSeq System (Illumina) and MiSeq Reagent V2 (2 × 150) Kits (Illumina). We performed WGS comparison by aligning sequencing reads of the isolates to a reference genome. We analyzed sequencing data by using Bionumerics version 7.6 (Applied Maths, https://www.applied-maths.com). We trimmed reads to exclude base calls with a Phred score <15 and then aligned them by using the Trimming and Resequencing analysis options. The single-nucleotide polymorphism (SNP) signature was built by using the Strict filtering (closed SNP set) option, retaining all SNP with a minimum coverage of 5×, at least covered once in both forward and reverse direction and a minimum distance between retained SNP position of 12 bases, removing the nondiscriminatory position. We used the SNP matrix to build a maximum parsimony tree. We defined a cluster in the WGS analysis by isolates sharing ≤10 or fewer SNPs. WGS data are available from the National Center for Biotechnology Information (https://dataview.ncbi.nlm.nih.gov; under BioProject nos. PRJNA597875, PRJNA657124, PRJNA576780, and PRJNA574109).

Results

For the study period, 71 reports of extrapulmonary NTM infections related to HAI surgical, medical, or aesthetic procedures were included to give a total of 85 original cases, a mean of 10 cases/year for complete years (i.e., 2012–2019) (Figure 1). The regression identified an increasing trend of cases

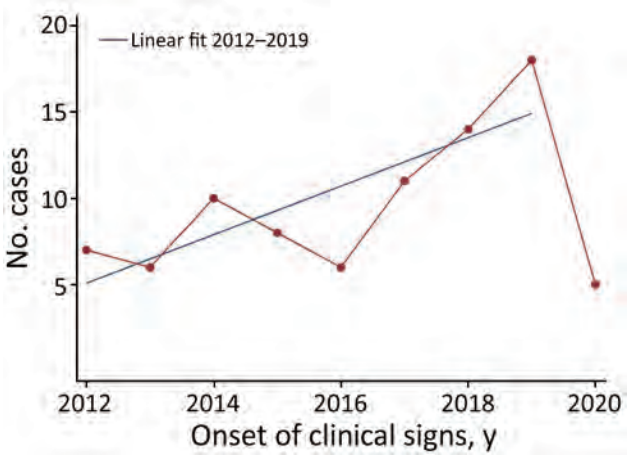

Figure 1. Onset of clinical signs in 85 reported cases of infection with nontuberculous mycobacteria associated with healthcare and aesthetic procedures, by year, France, January 2012–June 2020. Blue line indicates linear fit for 2012–2019 after excluding incomplete year 2020.

per year of onset of clinical signs during the study period after excluding incomplete years ($p<0.01$). This increase was observed particularly during the period 2016–2019 (i.e., after the *M. chimaera* heater–cooler unit [HCU] outbreak) but was caused by addition of these cases because regression analysis without them showed a similar significant trend ($p<0.01$). Among the 85 cases, 36 (42%) were found in the CNR-MyRMA strain database and the e-SIN database. The CNR-MyRMA database contained 30 additional cases, and the e-SIN database contained 19 additional cases.

The reports were received from 46 HCFs throughout France. Twenty-nine of the HCFs sent only 1 report during the study period, and 16 HCFs sent >1 (10 HCFs made 2 reports, 3 HCFs made 3 reports, 2 HCFs made 4 reports, and 1 HCF made 5 reports). Most (90%, 64/71) of the reports concerned an individual case, and 7 reports concerned clusters (2 cases in 4 reports, 3 cases in 1 report, and 5 cases in 2 reports).

For most (69%, 59/85) of cases, the infection was acquired inside the HCF, whereas 26 cases (31%) were acquired outside the reporting HCF. These infections acquired outside the HCF were imported either from another HCF (n = 14) or from a non–hospital-based medical or aesthetic practice (n = 12).

More women than men had cases reported (M:F = 31:46); sex was not reported for 8 case-patients. The median case age was 54 years (range 4–86 years; age was not reported for 12 cases). One third of the cases concerned immunosuppressed patients (33%, 23/70 cases; 15 cases did not report this information). NTM infections resulted from surgical procedures (56%, 48/85 cases), other invasive procedures (33%, 28/85 cases), and noninvasive procedures (11%, 9/85 cases). Cardiovascular surgery (n = 14), orthopedic surgery (n = 11), plastic surgery (e.g., breast surgery, (n = 13), face-lift (n = 2), abdominoplasty (n = 1), or capillary implant (n = 1), and catheter-associated infections (n = 17) comprised most of the surgical and other invasive procedure cases reported. The NTM infections concerned mainly skin and soft tissues (36%, 31/85), intravascular catheters (20%, 17/85), bones and joints (18%, 15/85), and arterial/cardiac (15%, 13/85) (Table 1).

Overall, 14 NTM species were isolated: 10 rapidly growing NTM species and 4 slowly growing NTM species. Rapidly growing NTM were *M. chelonae* (n = 30), *M. fortuitum complex* (n = 24) (17 cases with *M. fortuitum*, 2 with *M. mageritense*, 2 with *M. porcinum*, 1 with *M. senegalense*, and 2 strains for which the exact species could not be determined), *M. abscessus* (n = 14), *M. mucogenicum* (n = 5), *M. neoaurum* (n = 2), *M. fuerthensis* (n = 1), and *M. wolinskyi* (n = 1). Slowly growing NTM species were *M. chimaera* (n = 4), *M. avium* (n = 2), *M. lentiflavum* (n = 1), and *M. marinum* (n = 1). For 2 cases of endocarditis, direct examination of the valve samples identified acid-fast bacilli after Ziehl-Neelsen staining, but culture results were negative.

We determined the hypothesized incubation time (i.e., time between the onset of clinical signs and most probable contamination date, which is most often the date of the procedure) for 50 cases (Table 1). Incubation time was shorter for rapidly growing NTM (median time 34 days, n = 40) than for slowly growing NTM (median time 549 days, n = 5).

We suspected that medical devices were related to the infection for 80% of cases (68/85), but a medical device vigilance report was performed for only 21% of those (14/68 cases). Medical devices comprised implantable devices (e.g., breast prosthesis, artificial heart valve and vascular prosthesis, knee or hip prosthesis) for 50% of case-patients that had a medical device (34/68 cases), invasive devices (e.g., catheter and implantable port, dialysis device, endoscopy device, infiltration device in orthopedic surgery, liposuction cannula, mesotherapy, and tattoo injection equipment) (37%, 25/68 cases), and noninvasive devices (e.g., cardiopulmonary bypass HCU, contact lens) (13%, 9/68 cases).

For nearly half of all reported cases (47%, 40/85 cases; 30 cases did not report this information), there was a specific investigation of professional practices after the NTM infection was diagnosed to assess the level of compliance with hygiene guidelines,

Table 1. Description of 85 reported healthcare and aesthetic-associated NTM infections, France, 2012–2020*

Procedure	Infection type	Sex, M/F	Median age, y (range)	Infection risk factor	Median incubation times, d (range)	Species implicated
Surgical, n = 48						
Cardiovascular surgery, n = 14	Infective endocarditis and aortic infection, n = 13	7/3, NR = 3	69 (47–81); n = 10; NR, n = 3	None, n = 10; NR, n = 3	393 (14–732); n = 11; NR, n = 2	*M. chelonae*, n = 5; *M. chimaera*, n = 3; AFB positive and culture negative, n = 2; *M. wolinskyi*, n = 1; *M. avium*, n = 1; *M. abscessus*,† n = 1; *M. lentiflavum*,† n = 1; *M. fuerthensis*,† n = 1
	SST, n = 1	0/1	69	None	41	*M. fortuitum complex*, n = 1
Breast surgery, n = 13	SST	1/12	42 (31–53); n = 10; NR, n = 3	Breast cancer, n = 2; HIV, n = 1; none, n = 8; NR, n = 2	36 (10–732); n = 12; NR, n = 1	*M. fortuitum*, n = 6; *M. abscessus*, n = 3; *M. senegalense*, n = 1; *M. chelonae*, n = 1; *M. avium*, n = 1; *M. chimaera*, n = 1
Orthopedic surgery, n = 11	Bone and joint	5/2, NR = 4	69 (45–86); n = 7; NR, n = 4	None, n = 6; NR, n = 5	33 (23–183); n = 9, NR, n = 2	*M. fortuitum*, n = 4; *M. abscessus*, n = 3; *M. mageritense*, n = 2; *M. porcinum*, n = 1; *M. chelonae*, n = 1
Skin surgery,‡ n = 7	SST	4/3	65 (42–78); n = 6; NR, n = 1	None, n = 6; NR, n = 1	45 (30–93); n = 6, NR, n = 1	*M. fortuitum*, n = 3; *M. chelonae*, n = 2; *M. abscessus*, n = 1; *M. neoaurum*, n = 1
Other surgery,§ n = 3	Vascular, n = 1	NR	NR	NR	NR	*M. fortuitum*, n = 1
	Urogenital, n = 1	0/1	48	None	NR	*M. fortuitum*, n = 1
	Ocular, n = 1	0/1	83	None	15	*M. chelonae*, n = 1
Invasive, n = 28						
Vascular catheter insertion, n = 17	Intravascular catheter	7/10	58 (4–82); n = 17	Chemotherapy, n = 14; none, n = 2; NR = 1	NR	*M. chelonae*, n = 6; *M. mucogenicum*, n = 5; *M. abscessus*, n = 2; *M. fortuitum*, n = 1; *M. fortuitum complex*, n = 1; *M. porcinum*, n = 1; *M. neoaurum*, n = 1
Infiltration, n = 3	Bone and joint	0/3	52 (52–84); n = 3	Corticosteroid infiltration, n = 3	61 (33–108); n = 3	*M. abscessus*, n = 2; *M. chelonae*, n = 1
Mesotherapy, n = 3	SST	1/2	47 (35–49); n = 3	None, n = 3	30 (15–73); n = 3	*M. chelonae*, n = 2; *M. abscessus*, n = 1
Tattoo, n = 3	SST	3/0	50 (48–56); n = 3	None, n = 3	NR	*M. chelonae*, n = 3
Intestinal endoscopy, n = 2	Abdominal	0/2	68 (60–75); n = 2	Kidney transplant, n = 1; none, n = 1	7 (4–10); n = 2	*M. fortuitum*, n = 1; *M. abscessus*, n = 1
Noninvasive, n = 4						
Eye lens use, n = 3	Ocular	0/3	36 (21–62); n = 3	None, n = 3	NR	*M. chelonae*, n = 3
Balneotherapy, n = 1	SST	0/1	51	Methotrexate plus corticosteroids treatment	20	*M. marinum*, n = 1
Not identified, n = 5						
	SST, n = 3	1/2	44 (28–75); n = 3	Kidney transplant, n = 1; NR = 2	NR	*M. chelonae*, n = 3
	Disseminated, n = 1	1/0	64	Corticosteroids treatment, chronic dialysis	NR	*M. chelonae*, n = 1
	Bone and joint, n = 1	1/0	61	Corticosteroids treatment	NR	*M. chelonae*, n = 1

*AFB, acid-fast bacilli; NR, not reported; NTM, nontuberculous mycobacteria; SST, akin and soft tissue.
†Sample that had several bacteria identified.
‡Skin operations concerning the following diverse procedures: face-lift, n = 2, abdominoplasty, n = 1, capillary implant, n = 1, excision of a basal cell carcinoma, n = 1, wearing a Holter monitor, n = 1 and neurostimulation device, n = 1.
§Lower limb vascular surgery, n = 1, promontofixation, n = 1, eye surgery, n = 1.

sterilization procedures, and treatment procedures. For more than one fourth of these cases (28%, 11/40), the investigations found failure to comply with infection risk prevention recommendations. Corrective measures were implemented for 45% of the reports (17/38 reports; 33 did not report this information), most often involving increased hygiene vigilance and recommendations to improve practices (n = 7). For 32 reports, there was no active case finding; most of them were isolated cases. For 30 reports, this information was not available. Active case finding was conducted after 9 reports (30 did not report this information) for procedures such as breast reconstruction, heart surgery, gastrointestinal endoscopy, mesotherapy, orthopedic surgery, and tattooing sessions.

Environmental investigations were undertaken for 42% (30/71) of the reports. Most (27/30) reports involved water sampling from potential sources of the contamination, such as water supply networks (n = 21), HCU (n = 4), dialysis water (n = 1), and swimming pool water (n = 1). Perioperative surfaces (n = 2) and air samples (n = 1) were rarely sampled. Among the 45% of cases (38/85) involving environmental investigations, mycobacteria samples were positive for 18 (7 were not reported). The same NTM species as in the clinical isolate was found for 12 cases (32%, 12/38) after environmental investigations. For 10 cases, the clinical isolate could not be distinguished from the environmental isolate (Table 2; Figure 2): *M. chimaera* isolates from HCU and heart surgery infection (patient A3) (Figure 2, panel A), isolates from hospital water supply network, *M. fortuitum* breast infection (patient C1) (Figure 2, panel B), *M. chelonae* skin and soft tissue infection (patients D1, E1-E2, E3, and F1) (Figure 2, panel C), *M. marinum* isolates from pool balneotherapy and skin and soft tissue infection (patient I1) (Figure 2, panel D), and *M. mucogenicum* catheter-associated infection (patients J1, J2, and J3) (Figure 2, panel E).

We also performed genomic comparisons for case-patients suspected of being contaminated by a common source. For 8/10 case-patients, studied isolates had the same pattern (Table 2; Figure 2). In report A, 3 clinical isolates of *M. chimaera* endocarditis from 2 patients were clustered (A1-A2 and A3) (Figure 2, panel A). These 2 patients were linked to a worldwide outbreak of HCU contamination, as shown in the section comparing clinical (A3) and environmental (A4-A8) isolates. In report H, which concerned *M. chelonae* catheter-associated infections diagnosed in the same institution (n = 5 cases), clinical isolates were clustered into 2 distinct groups; the first cluster grouped 3 isolates, H1, H4, and H5, from 3 patients, and the second cluster grouped 2 isolates, H2 and H3, from 2 patients (Figure 2, panel C). The presence of 2 clusters in the same HCF suggested that there were 2 sources of contamination, neither of which were found. In report K, the same genotype was found when comparing *M. neoaurum* isolates from blood cultures of 1 patient with the isolate found during microbiological control testing after a peripheral autologous stem cell transplant (n = 1 case) (Figure 2, panel F). The contamination of the stem cell transplant was attributed to colonization of the catheter used for the cell sampling.

Discussion

We describe extrapulmonary NTM infections diagnosed after surgical, medical, or aesthetic procedures in France over an 8-year period (2012–2020). To broaden the spontaneous reporting from medical professionals, we sought 2 information sources: the national EWRS for HAI and the national reference NTM strain database. Because only 85 cases were described in 71 reports over 8 years, we might consider that such NTM infections remain rare. However, most of the cases were related to a medical device, a specific procedure, or lack of hygiene practices and might have been preventable.

Our study highlights a slight increase in reported annual numbers of cases during the study period. This increase, particularly during 2016 (*14*), could be explained by greater global awareness in public health community after invasive infections with *M. chimaera* associated with HCUs used during cardiac surgery (*15*) and other published outbreaks (*6*).

Both infection sites and NTM species isolated from these cases of infections were diverse, emphasizing the opportunistic nature of these pathogens. The most commonly reported infections were skin and soft tissue infections, catheter-related infections, infective endocarditis, and bone and joint infections. When we compared our findings with the major proportion of extrapulmonary NTM infections described in the literature, but not limited to healthcare-associated and aesthetic procedure–associated infections, we found that skin and soft tissue infections were the most commonly reported infection site (*16*,*17*). However, we identified catheter-associated infections, bone and joint infections, or infective endocarditis, which are less described, except for the HCU *M. chimaera* outbreak (*8*).

A wide variety of NTM species were responsible for the infections reported in our study; *M. chelonae*

and *M. fortuitum* were the most common. Isolates of slowly growing NTM species were rare (11%) compared with those found in a review in the United States, in which 50% of all species were in the *M. avium* complex (*16*). One possible explanation for this difference is that rapidly growing NTM cultivated on standard bacteriology diagnostic media might constitute an unexpected etiology diagnosis. We should also consider that these rapidly growing species were regularly found in France in the water networks, one of the sources of infection (*1*).

Most of the cases in our study were linked to surgical, invasive, and noninvasive procedures. In 5 cases, no specific procedures were identified as the cause of infection, even though all patients underwent healthcare procedures such as previous intravenous catheter, or no procedures were identified at all, such as the case of bone and joint infection, which could not have originated from spontaneous infection. As observed in previous reviews, the most commonly reported infections were those associated with aesthetic care (*12*), particularly breast prostheses (*18*).

Table 2. Genomic comparison between clinical versus environmental isolates and comparison of clinical isolates for patients suspected of being contaminated with nontuberculous mycobacteria by a common source, France, 2012–2020

Report	Species involved	Case manifestations	Environmental sample	Result of comparison	Location of information*
A	*M. chimaera*	Endocarditis after cardiac surgery by using contaminated heater-cooler unit (2 patients operated on in 2 hospitals)	Heater-cooler unit water	Clinical isolates from the 2 patients who had *M. chimaera* disseminated disease after open-heart surgery belonged to worldwide epidemic cluster. Environmental isolates, obtained only for 1 of the 2 patients, belonged to the epidemic cluster for 5/10 of them	Figure 2, panel A; Appendix Table 1
B	*M. chimaera*	Prosthesis infection after breast reconstruction (1 patient)	Hospital water supply network	Environmental and clinical isolates did not belong to the same cluster	Figure 2, panel A; Appendix Table 1
C	*M. fortuitum*	Prosthesis infection after breast reconstruction (1 patient)	Hospital water supply network	Environmental and clinical isolates belonged to the same cluster	Figure 2, panel B; Appendix Table 2
D	*M. chelonae*	Skin and soft tissue infection after face lift surgery (1 patient)	Hospital water supply network	Environmental and clinical isolates belonged to the same cluster	Figure 2, panel C; Appendix Table 3
E	*M. chelonae*	Skin and soft tissue infection after tattoo (2 patients tattooed in the same tattoo parlor)	Tattoo parlor water supply network	Environmental and clinical isolates belonged to the same cluster	Figure 2, panel C; Appendix Table 3
F	*M. chelonae*	Skin and soft tissue infection after mesotherapy (1 patient)	Water supply network from doctor's office sink and patient's home	Environmental isolates from doctor's office sink and clinical isolate belonged to the same cluster. Isolates from patient's home were not related	Figure 2, panel C; Appendix Table 3
G	*M. chelonae*	Skin and soft tissue infection after mesotherapy (1 patient)	Water supply network from doctor's office sink and patient's home	Environmental and clinical isolates did not belong to the same cluster	Figure 2, panel C; Appendix Table 3
H	*M. chelonae*	Catheter-associated infection (5 patients from the same institution)	No environmental sample	Two clusters of 2 clinical isolates were identified	Figure 2, panel C; Appendix Table 3
I	*M. marinum*	Skin and soft tissue infection caused by contamination after a bath in a balneotherapy swimming pool (1 patient)	Swimming pool water	Environmental and clinical isolates belong to the same cluster	Figure 2, panel D; Appendix Table 4
J	*M. mucogenicum*	Catheter-associated infection (3 patients from the same institution)	Hospital water supply network	Environmental and clinical isolates belong to the same cluster	Figure 2, panel D; Appendix Table 5
K	*M. neoaurum*	Catheter-associated infection discovered during microbiological control of autologous stem cell transplant (1 patient)	Autologous stem cell transplant; no environmental sample	Environmental and clinical isolates belong to the same cluster	Figure 2, panel E; Appendix Table 6

*Appendix Table 1, https://wwwnc.cdc.gov/EID/article/28/3/21-1791-App1.pdf.

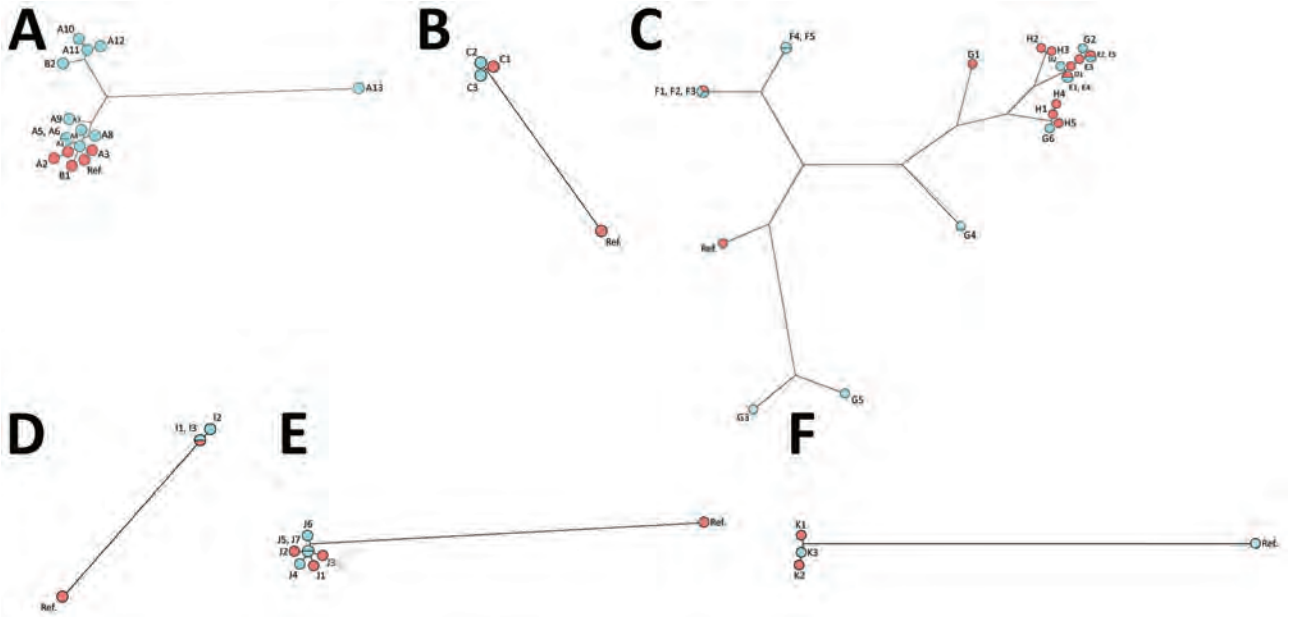

Figure 2. Genomic comparison of nontuberculous mycobacteria isolates by using whole-genome sequencing phylogenetic analysis and maximum parsimony trees. A) *Mycobacterium chimaera*, B) *M. fortuitum*, C) *M. chelonae*, D) *M. marinum*, E) *M. mucogenicum*, F) *M. neoaurum*. Environmental isolates are indicated in blue, and clinical isolates are indicated in red. Additional details on the isolates and their sources are available in an extended figure legend online (https://wwwnc.cdc.gov/EID/article/28/3/21-1791-F2.htm); additional information for the 6 *Mycobacterium* species tested is provided in the Appendix (https://wwwnc.cdc.gov/EID/article/28/3/21-1791-App1.pdf). Ref, referent.

The source of infection was not determined in 9/10 case-patients, despite environmental investigations conducted for ≈50% of the reports. Even when environmental investigations were performed, they occurred months after the suspected contamination because of long incubation times, as in reports B and G (Table 2).

Because a medical device was implicated in most of the NTM infection cases we reported, we believe that these infections can be prevented. The medical device could be contaminated by NTM before its use or can lead to contamination from environmental NTM (*5*,*19*). When an environmental cause is identified, the water system is the major environmental source most frequently considered responsible. Water systems, particularly in hospitals, are frequently identified as NTM reservoirs (*20*,*21*).

Genomic comparison of NTM isolates can be used to rule out or confirm any hypothesis concerning the origin of the contamination. However, careful analysis of genomic sequence comparisons should be conducted because several factors, such as the reference sequence on which the reads are mapped (epidemic strain or unrelated strain), quality of the sequenced data, coverage of the mapping assembly, number of sequences included in the comparison, and use of de novo assembly, influence SNP analysis. WGS appears to be a suitable tool for the molecular investigation of NTM infections, but might need expert rules and standardization to be used further.

The major limitations of this study concern the lack of completeness of the reported data. There is no specific surveillance system for NTM infection in France, and the 2 databases used for this case series are not exhaustive. The purpose of the EWRS for HAI platform is to improve the management of HAI reporting by HCF, and the CNR-MyRMA receives NTM isolates for patient diagnosis and treatment and genotypic comparison in epidemiologically related cases with environmental analyses when necessary. Therefore, underdeclaration of NTM infection cases in France is probable (*22*). However, when combined, the 2 databases provide a useful inventory of extrapulmonary NTM infection cases related to surgical, medical, and aesthetic procedures. The genomic comparison of NTM isolates performed by CNR-MyRMA was able to demonstrate the source when an environmental investigation was conducted and clinical and environmental isolates were available. This comparison provides valuable pointers for the future implementation, improvement, and follow-up of certain preventive measures.

Although data in the current study were not exhaustive, reports of NTM infection cases and subsequent microbiological and workplace practice investigations showed that considerable progress has

been made in understanding contamination mechanisms during healthcare treatment. Water used in the procedures appeared to be the infection source for 10 cases. This finding is particularly true for heart surgery after the alert issued concerning the global outbreak of *M. chimaera* endocarditis as a result of contaminated HCUs (*8*).

Our observations should prompt more stringent recommendations for prompt reporting of NTM infections and provision of clinical and environmental samples for analysis of strains. Better application of these recommendations should improve methods to identify causes of NTM infections and enable their prevention.

Acknowledgments

We thank Sylvain Dagat, Claire Daurel, Marion Duprilot, Pierre Frange, Emmanuelle Gallois, Hélène Guet-Revillet, Frédéric Janvier, Julien Jaubert, Philippe Lanotte, Ludovic Lemée, Alix Pantel, Olivia Peuchant, Catherine Simac, Soumaya Skalli, and Céline Vauterin for their contributions to this study, especially for gathering clinical and biological data; Christine Bisilliat-Gardet, Véronique Charlier, Marie-Emmanuelle Hemet, Isabelle Lacrampe, Patricia Lawson-Body, Marilyne Lemaire, Fabienne Meunier, Marie Monjean, Sylvie Tenza, Odile Vissouarn, and our collaborators Gauthier Pean de Ponfilly and Hervé Jacquier, and all other members of the Lariboisière Bacteriology Laboratory for providing expert technical assistance; and Karine Astruc, Catherine Avril, Karine Blanckaert, France Borgey, Michel Brousse, Jean-Christophe Delaroziere, Nathalie Floret-Bassissi, Jeanne-Marie Germain, Laurence Guet, Bruno Jarrige, Karima Jeblaoui, Catherine Laland, Aba Mahamat, Sophia Mechkour, Nathalie van der Mee-Marquet, Nathalie Passard, Elise Seringe, Loïc Simon, Sophie Vandesteene, lexandra Aubry, Isabelle Bonnet, Vincent Jarlier, Florence Morel, Wladimir Sougakov and Nicolas Veziris for providing support.

This study was supported by the annual grant from French Public Health Agency and the Associate Laboratory of the National Reference Center for Mycobacteria and Antimycobacterial Resistance.

About the Author

Dr. Daniau is an epidemiologic project manager in Infectious Diseases Department of Santé Publique France, Saint-Maurice, France. His primary research interest is coordination at the national level of Point Prevalence Surveys of healthcare-associated infections and antimicrobial drug use in acute care hospitals and long-term care facilities with the European Centre for Disease Prevention and Control.

References

1. Le Dantec C, Duguet JP, Montiel A, Dumoutier N, Dubrou S, Vincent V. Occurrence of mycobacteria in water treatment lines and in water distribution systems. Appl Environ Microbiol. 2002;68:5318–25. https://doi.org/10.1128/AEM.68.11.5318-5325.2002
2. Falkinham JO III. Environmental sources of nontuberculous mycobacteria. Clin Chest Med. 2015;36:35–41. https://doi.org/10.1016/j.ccm.2014.10.003
3. Meyers H, Brown-Elliott BA, Moore D, Curry J, Truong C, Zhang Y, et al. An outbreak of *Mycobacterium chelonae* infection following liposuction. Clin Infect Dis. 2002;34:1500–7. https://doi.org/10.1086/340399
4. Conaglen PD, Laurenson IF, Sergeant A, Thorn SN, Rayner A, Stevenson J. Systematic review of tattoo-associated skin infection with rapidly growing mycobacteria and public health investigation of a cluster in Scotland, 2010. Euro Surveill. 2013;18:20553. https://doi.org/10.2807/1560-7917.ES2013.18.32.20553
5. Carbonne A, Brossier F, Arnaud I, Bougmiza I, Caumes E, Meningaud JP, et al. Outbreak of nontuberculous mycobacterial subcutaneous infections related to multiple mesotherapy injections. J Clin Microbiol. 2009;47:1961–4. https://doi.org/10.1128/JCM.00196-09
6. Leão SC, Viana-Niero C, Matsumoto CK, Lima KV, Lopes ML, Palaci M, et al. Epidemic of surgical-site infections by a single clone of rapidly growing mycobacteria in Brazil. Future Microbiol. 2010;5:971–80. https://doi.org/10.2217/fmb.10.49
7. Mora AD, Giraldo S, Castillo DA, Ferro BE. Clinical behavior of infection and disease caused by non-tuberculous mycobacteria in Latin America: scoping review [in Spanish]. Rev Peru Med Exp Salud Publica. 2021;38:318–25. https://doi.org/10.17843/rpmesp.2021.382.6108
8. van Ingen J, Kohl TA, Kranzer K, Hasse B, Keller PM, Katarzyna Szafrańska A, et al. Global outbreak of severe *Mycobacterium chimaera* disease after cardiac surgery: a molecular epidemiological study. Lancet Infect Dis. 2017;17:1033–41. https://doi.org/10.1016/S1473-3099 (17)30324-9
9. Astagneau P, Desplaces N, Vincent V, Chicheportiche V, Botherel A, Maugat S, et al. *Mycobacterium xenopi* spinal infections after discovertebral surgery: investigation and screening of a large outbreak. Lancet. 2001;358:747–51. https://doi.org/10.1016/S0140-6736(01)05843-3
10. Ferry C, Saussine A, Bouaziz JD, Xhaard A, Peffault de Latour R, Ribaud P, et al. Disseminated cutaneous infection due to *Mycobacterium chelonae* following hematopoietic stem cell transplantation. IDCases. 2014;1:68–9. https://doi.org/10.1016/j.idcr.2014.07.002
11. Yuan SM. Mycobacterial endocarditis: a comprehensive review. Rev Bras Cir Cardiovasc. 2015;30:93–103.
12. Couderc C, Carbonne A, Thiolet JM, Brossier F, Savey A, Bernet C, et al. Non-tuberculous mycobacterial infections related to esthetic care in France, 2001–2010 [in French]. Med Mal Infect. 2011;41:379–83. https://doi.org/10.1016/j.medmal.2011.02.007
13. Ministry of Social Affairs and Health. Decree no. 2017–129 of February 3, 2017 relating to the prevention of healthcare-associated infections, 2017 [in French] [cited 2021 Dec 9]. https://www.legifrance.gouv.fr/jorf/id/JORFTEXT000033982071
14. Rajendran P, Padmapriyadarsini C, Mondal R. Nontuberculous mycobacterium: an emerging pathogen: Indian perspective. Int J Mycobacteriol. 2021;10:217–27.
15. European Center for Disease Prevention and Control. Rapid risk assessment: invasive cardiovascular infection by

Mycobacterium chimaera potentially associated with heater-cooler units used during cardiac surgery, April 30, 2015 [cited 2021 Jun 28]. https://ecdc.europa.eu/en/publications-data/invasive-cardiovascular-infection-mycobacterium-chimaera-potentially-associated
16. Henkle E, Hedberg K, Schafer SD, Winthrop KL. Surveillance of extrapulmonary nontuberculous mycobacteria infections, Oregon, USA, 2007–2012. Emerg Infect Dis. 2017;23:1627–30. https://doi.org/10.3201/eid2310.170845
17. Blanc P, Dutronc H, Peuchant O, Dauchy FA, Cazanave C, Neau D, et al. Nontuberculous mycobacterial infections in a French hospital: a 12-year retrospective study. PLoS One. 2016;11:e0168290. https://doi.org/10.1371/journal.pone.0168290
18. Jaubert J, Mougari F, Picot S, Boukerrou M, Barau G, Ali Ahmed SA, et al. A case of postoperative breast infection by *Mycobacterium fortuitum* associated with the hospital water supply. Am J Infect Control. 2015;43:406–8. https://doi.org/10.1016/j.ajic.2014.12.023
19. Regnier S, Cambau E, Meningaud JP, Guihot A, Deforges L, Carbonne A, et al. Clinical management of rapidly growing mycobacterial cutaneous infections in patients after mesotherapy. Clin Infect Dis. 2009;49:1358–64. https://doi.org/10.1086/606050
20. Donohue MJ, Mistry JH, Donohue JM, O'Connell K, King D, Byran J, et al. Increased frequency of nontuberculous mycobacteria detection at potable water taps within the United States. Environ Sci Technol. 2015;49:6127–33. https://doi.org/10.1021/acs.est.5b00496
21. Li T, Abebe LS, Cronk R, Bartram J. A systematic review of waterborne infections from nontuberculous mycobacteria in health care facility water systems. Int J Hyg Environ Health. 2017;220:611–20. https://doi.org/10.1016/j.ijheh.2016.12.002
22. Regnier S, Caumes E. Non-tuberculous mycobacterial infections related to esthetic care in France, 2001–2010 [in French]. Med Mal Infect. 2011;41:667–8. https://doi.org/10.1016/j.medmal.2011.09.009

Address for correspondence: Côme Daniau, Unité Infections Associées aux Soins et Résistance aux Antibiotiques, Direction de Maladies Infectieuses, Santé Publique France, 12 Rue du Val d'Osne, 94410 Saint-Maurice, France; email: come.daniau@santepubliquefrance.fr

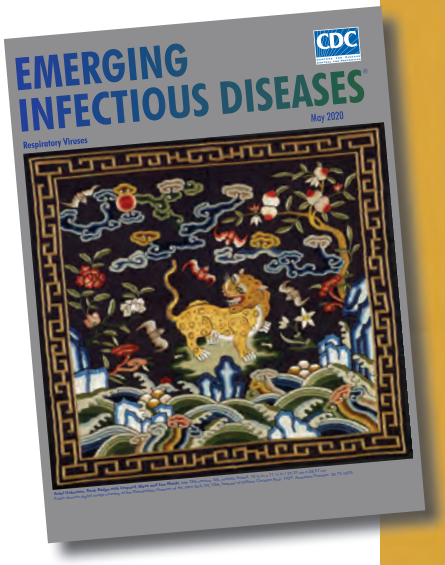

Originally published in May 2020

etymologia revisited

Coronavirus

The first coronavirus, avian infectious bronchitis virus, was discovered in 1937 by Fred Beaudette and Charles Hudson. In 1967, June Almeida and David Tyrrell performed electron microscopy on specimens from cultures of viruses known to cause colds in humans and identified particles that resembled avian infectious bronchitis virus. Almeida coined the term "coronavirus," from the Latin *corona* ("crown"), because the glycoprotein spikes of these viruses created an image similar to a solar corona. Strains that infect humans generally cause mild symptoms. However, more recently, animal coronaviruses have caused outbreaks of severe respiratory disease in humans, including severe acute respiratory syndrome (SARS), Middle East respiratory syndrome (MERS), and 2019 novel coronavirus disease (COVID-19).

Sources:

1. Almeida JD, Tyrrell DA. The morphology of three previously uncharacterized human respiratory viruses that grow in organ culture. J Gen Virol. 1967;1:175–8. https://doi.org/10.1099/0022-1317-1-2-175
2. Beaudette FR, Hudson CB. Cultivation of the virus of infectious bronchitis. J Am Vet Med Assoc. 1937;90:51–8.
3. Estola T. Coronaviruses, a new group of animal RNA viruses. Avian Dis. 1970;14:330–6. https://doi.org/10.2307/1588476
4. Groupe V. Demonstration of an interference phenomenon associated with infectious bronchitis virus of chickens. J Bacteriol. 1949;58:23–32. https://doi.org/10.1128/JB.58.1.23-32.1949

https://wwwnc.cdc.gov/eid/article/26/5/et-2605_article

Rising Incidence of Legionnaires' Disease and Associated Epidemiologic Patterns, United States, 1992–2018

Albert E. Barskey, Gordana Derado, Chris Edens

Medscape ACTIVITY EDUCATION

In support of improving patient care, this activity has been planned and implemented by Medscape, LLC and Emerging Infectious Diseases. Medscape, LLC is jointly accredited by the Accreditation Council for Continuing Medical Education (ACCME), the Accreditation Council for Pharmacy Education (ACPE), and the American Nurses Credentialing Center (ANCC), to provide continuing education for the healthcare team.

Medscape, LLC designates this Journal-based CME activity for a maximum of 1.00 ***AMA PRA Category 1 Credit(s)™***. Physicians should claim only the credit commensurate with the extent of their participation in the activity.

Successful completion of this CME activity, which includes participation in the evaluation component, enables the participant to earn up to 1.0 MOC points in the American Board of Internal Medicine's (ABIM) Maintenance of Certification (MOC) program. Participants will earn MOC points equivalent to the amount of CME credits claimed for the activity. It is the CME activity provider's responsibility to submit participant completion information to ACCME for the purpose of granting ABIM MOC credit.

All other clinicians completing this activity will be issued a certificate of participation. To participate in this journal CME activity: (1) review the learning objectives and author disclosures; (2) study the education content; (3) take the post-test with a 75% minimum passing score and complete the evaluation at http://www.medscape.org/journal/eid; and (4) view/print certificate. For CME questions, see page 769.

Release date: February 17, 2022; Expiration date: February 17, 2023

Learning Objectives

Upon completion of this activity, participants will be able to:

- Analyze trends in the incidence of Legionnaires' disease (LD) according to age
- Assess trends in the incidence of LD according to sex
- Evaluate trends in the incidence of LD according to race
- Distinguish the geographic regions and seasons associated with the highest rates of LD.

CME Editor

Jill Russell, BA, Technical Writer/Editor, Emerging Infectious Diseases. *Disclosure: Jill Russell, BA, has disclosed no relevant financial relationships.*

CME Author

Charles P. Vega, MD, Health Sciences Clinical Professor of Family Medicine, University of California, Irvine School of Medicine, Irvine, California. *Disclosure: Charles P. Vega, MD, has disclosed the following relevant financial relationships: served as an advisor or consultant for GlaxoSmithKline; Johnson & Johnson Pharmaceutical Research & Development, L.L.C.*

Authors

Albert E. Barskey, MPH; Gordana Derado, PhD; *and* ***Chris Edens, PhD.***

Author affiliation: Centers for Disease Control and Prevention, Atlanta, Georgia, USA

DOI: https://doi.org/10.3201/eid2803.211435

Reported Legionnaires' disease (LD) cases began increasing in the United States in 2003 after relatively stable numbers for ≥10 years; reasons for the rise are unclear. We compared epidemiologic patterns associated with cases reported to the Centers for Disease Control and Prevention before and during the rise. The age-standardized average incidence was 0.48 cases/100,000 population during 1992–2002 compared with 2.71 cases/100,000 in 2018. Reported LD incidence increased in nearly every demographic, but increases tended to be larger in demographic groups with higher incidence. During both periods, the largest number of cases occurred among White persons, but the highest incidence was in Black or African American persons. Incidence and increases in incidence were generally largest in the East North Central, Middle Atlantic, and New England divisions. Seasonality was more pronounced during 2003–2018, especially in the Northeast and Midwest. Rising incidence was most notably associated with increasing racial disparities, geographic focus, and seasonality.

Legionnaires' disease (LD) is a severe pneumonia caused by *Legionella* spp. bacteria. Approximately 95% of patients require hospitalization, and 10% die (*1*). Risk factors include older age (>50 years), smoking, a weakened immune system, and chronic lung conditions (*2*). Pontiac fever (a self-limited, influenza-like illness) and extrapulmonary legionellosis (*Legionella* infection with a primary focus outside the lungs) are other less common legionellosis syndromes (*1*).

Legionella is found in most freshwater environments in low numbers. The bacteria can proliferate in built environments, particularly when the water is warm (25°C–45°C), stagnant, and lacking residual disinfectant. Some devices, such as cooling towers, hot tubs, showers, and decorative fountains, can aerosolize water and have frequently been associated with LD outbreaks (*3*). LD can be acquired when aerosolized water containing *Legionella* bacteria is inhaled. A properly designed and implemented water management program (WMP) can reduce the risk for *Legionella* growth and transmission in buildings with complex water systems (*3*–*5*). WMPs were first recommended in 2015 (*4*).

L. pneumophila was discovered in 1977 and recognized as the etiologic agent in an outbreak of severe pneumonia the previous year (*6*,*7*). LD cases reported to the Centers for Disease Control and Prevention (CDC) steadily increased from 235 in 1976 to 1,370 in 1990 (*8*). Reported cases in the United States remained relatively stable during 1990–2002 but began increasing steadily in 2003 (*9*–*11*); however, the reasons are unclear. To explore factors that might have contributed to the increase, we compared epidemiologic patterns associated with the baseline years before the increase (1992–2002) and those associated with the years of increase (2003–2018).

Methods

US jurisdictions (the 50 states plus New York, NY, and Washington, DC) report cases of legionellosis (referred to as LD) (*1*) to CDC through the National Notifiable Diseases Surveillance System (NNDSS). We included data from 1992 (the earliest year of electronically available data) through 2018. Although 2019 data are available, completeness of the data reported by more than one third of US jurisdictions is uncertain because of the coronavirus disease pandemic (*12*). LD was not reportable in Connecticut during 1992–1996 or in Oregon or West Virginia during 1992–2002; we excluded cases and populations from these jurisdictions and years from analyses.

During the study period, the LD case definition changed (in 1997 and 2006); we included cases meeting the case classification criteria for reportable conditions in use at the time the cases occurred (*13*–*15*). All 3 case definitions defined a confirmed case of LD as a clinically compatible illness with isolation of any *Legionella* organism from respiratory secretions, lung tissue, pleural fluid, or other normally sterile fluid; detection of *L. pneumophila* serogroup 1 antigen in urine using validated reagents; or a ≥4-fold rise in specific serum antibody titer to *L. pneumophila* serogroup 1 using validated reagents (*13*–*15*). The 1996 case definition included the detection of *L. pneumophila* serogroup 1 in respiratory secretions, lung tissue, or pleural fluid by direct fluorescent antibody testing, and it required the ≥4-fold rise in antibody titer to reach ≥128. The 1990 case definition included probable cases, defined as a clinically compatible illness with demonstration of a reciprocal antibody titer ≥256 from a single convalescent-phase serum specimen.

Available patient data included age, sex, race, ethnicity, jurisdiction of residence, and date of earliest reported event in case history (event date). We did not analyze ethnicity because data were missing for 30.4% of cases. Cases were associated with the event date rather than the date reported to the health department or CDC. Event dates consisted of onset date (78%), diagnosis date (9%), laboratory result date (6%), date first reported to any public health authority (3%), and date reported to the state health department or CDC (3%); 1% of cases were missing date type.

Jurisdictions were grouped by US Census Bureau regions and divisions (Figure 1). To quantify

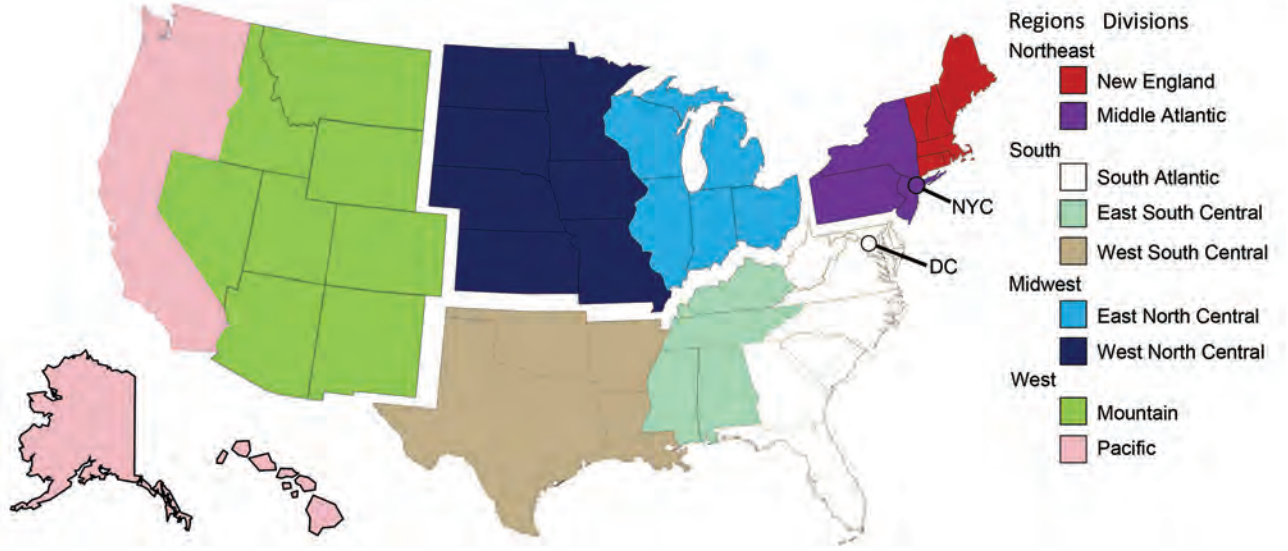

Figure 1. US Census Bureau regions and divisions. Regions: Northeast: Connecticut, Maine, Massachusetts, New Hampshire, New Jersey, New York City, New York State, Pennsylvania, Rhode Island, Vermont; Midwest: Illinois, Indiana, Iowa, Kansas, Michigan, Minnesota, Missouri, Nebraska, North Dakota, Ohio, South Dakota, Wisconsin; South: Alabama, Arkansas, Delaware, District of Columbia, Florida, Georgia, Kentucky, Louisiana, Maryland, Mississippi, North Carolina, Oklahoma, South Carolina, Tennessee, Texas, Virginia, West Virginia; West: Alaska, Arizona, California, Colorado, Hawaii, Idaho, Montana, Nevada, New Mexico, Oregon, Utah, Washington, Wyoming. Divisions: New England: Connecticut, Maine, Massachusetts, New Hampshire, Rhode Island, Vermont; Middle Atlantic: New Jersey, New York City, New York State, Pennsylvania; East North Central: Illinois, Indiana, Michigan, Ohio, Wisconsin; West North Central: Iowa, Kansas, Minnesota, Missouri, Nebraska, North Dakota, South Dakota; South Atlantic: Delaware, District of Columbia, Florida, Georgia, Maryland, North Carolina, South Carolina, Virginia, West Virginia; East South Central: Alabama, Kentucky, Mississippi, Tennessee; West South Central: Arkansas, Louisiana, Oklahoma, Texas; Mountain: Arizona, Colorado, Idaho, Montana, Nevada, New Mexico, Utah, Wyoming; Pacific: Alaska, California, Hawaii, Oregon, Washington.

seasonality, we calculated the annual maximum-to-minimum monthly case ratio by dividing the maximum number of monthly cases by the minimum number of monthly cases within a calendar year. For most analyses, we aggregated data within 2 time periods (baseline years [1992–2002] and increase years [2003–2018]) and then compared them. We selected 2002, the last year before annual cases numbered >2,000, as a breakpoint for our analyses to aid in comparisons with previously published work (*9*–*11*). To quantify the magnitude of increase, we compared the age-standardized incidence in 2018 with the age-standardized average incidence for 1992–2002 (Appendix). We used bridged-race post-censal population estimates to calculate incidence (*16*). Incidence was age-standardized by using the 2005 US standard population as the reference population.

We performed statistical analyses by using SAS (version 9.4; SAS Institute, https://www.sas.com). We performed joinpoint regression analysis, also known as change point regression or segmented regression (Joinpoint software version 4.8.0.1, https://surveillance.cancer.gov/joinpoint) on the age-standardized incidence and mean and median age over time to identify the optimal year when population parameters changed (Appendix).

Results

During 1992–2002, an average of 1,221 (range 1,060–1,547) LD cases were reported annually; during 2003–2018, an average of 4,369 (range 2,082–9,999) cases were reported annually. Crude and age-standardized incidence increased from 0.52 and 0.55 cases/100,000 population in 1992 to 3.06 and 2.71 cases/100,000 population in 2018 (Figure 2). Over the study period, joinpoint analysis selected a model with 1 change point in the trend in age-standardized incidence as the best model (over models with zero or 2 change points). Although joinpoint analysis identified the single optimal change point in the trend in age-standardized incidence ($p<0.05$) as 1999 (95% CI 1996–2002), we retained 2002 as the breakpoint in our analyses to aid in comparisons with previous studies. In addition, the largest relative increase (26%) in a 3-year moving average of age-standardized incidence over the study period occurred in 2003. From 1992 to 2002, no indication of a trend in age-standardized incidence was seen (−0.2%, 95% CI −5.1% to 5.0%); from 2002 to 2018, the average annual increase in age-standardized incidence was 9.3% (95% CI 8.1%–10.4%), of which the largest increase occurred during 2016–2018.

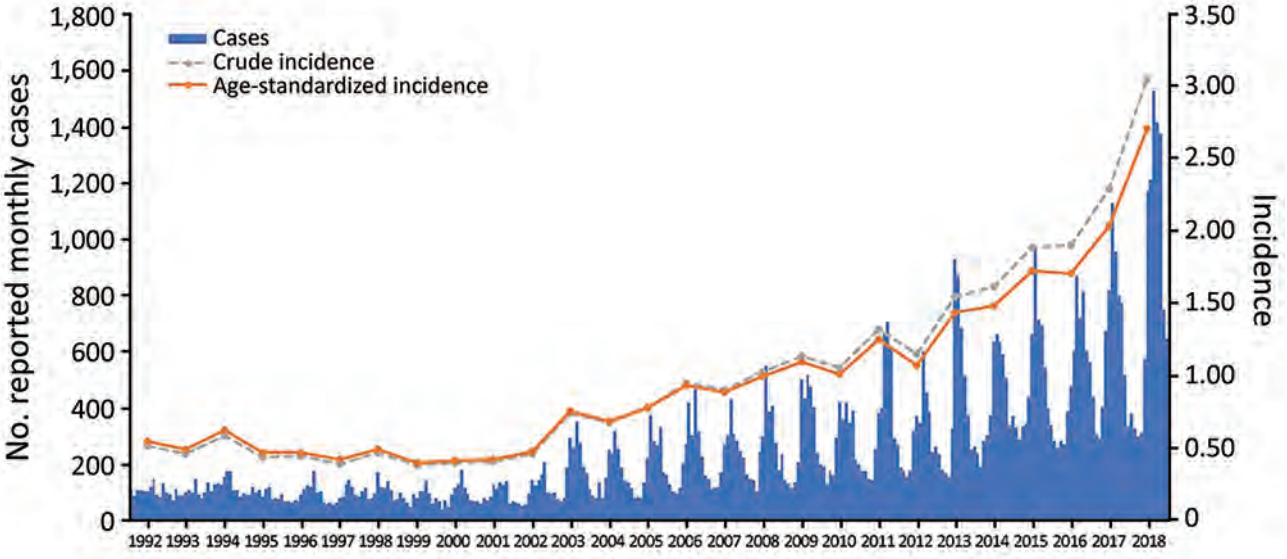

Figure 2. Reported cases of Legionnaires' disease by month and incidence (cases/100,000 population) by year, United States,1992–2018. Monthly cases reported to the Centers for Disease Control and Prevention through the National Notifiable Diseases Surveillance System and the crude and age-standardized annual incidence for 1992–2018 are shown.

Age

Age data were available for 82,649 (99.2%) of the 83,334 cases in the study period. During the baseline years, the largest number of average annual cases (257) was reported in the 65–74-year age group; the average number of cases in the 2 older age groups (75–84 and ≥85 years) was lower than the 2 younger age groups (45–54 and 55–64 years) (Figure 3, panel A). Average age-specific incidence generally increased with age, rising from <0.1 cases/100,000 population in children and young adults (0–24 years) to peak in the 75–84-year age group (1.57 cases/100,000 population) (Appendix Table). During the increase years, the largest number of average annual cases (1,112) was reported in the 55–64-year age group, and the distribution was more symmetric around this peak (Figure 3, panel B) than around the peak for the baseline years. Except for the 0–14-year group, in which incidence remained low (<0.1 cases/100,000 population), average age-specific incidence increased with age through the ≥85 years category (5.52 cases/100,000 population).

Joinpoint analysis identified 2002 as the change point in the trend of median patient age (Figure 4). Median patient age decreased from 62 years in 1992 to 58 years in 2002, then increased to 62 years in 2018. We identified a model with no change points as the best model for the trend in mean patient age over the study period; mean age increased from 58.9 years to 61.7 years.

Sex

During 1992–2002, men accounted for 59.8% of the 13,137 cases for whom sex was reported, compared with 62.8% of 69,226 cases during 2003–2018. The age-standardized average incidence in men was 0.63/100,000 men and in women was 0.35/100,000 women during 1992–2002 (Appendix Table). During 2003–2018,

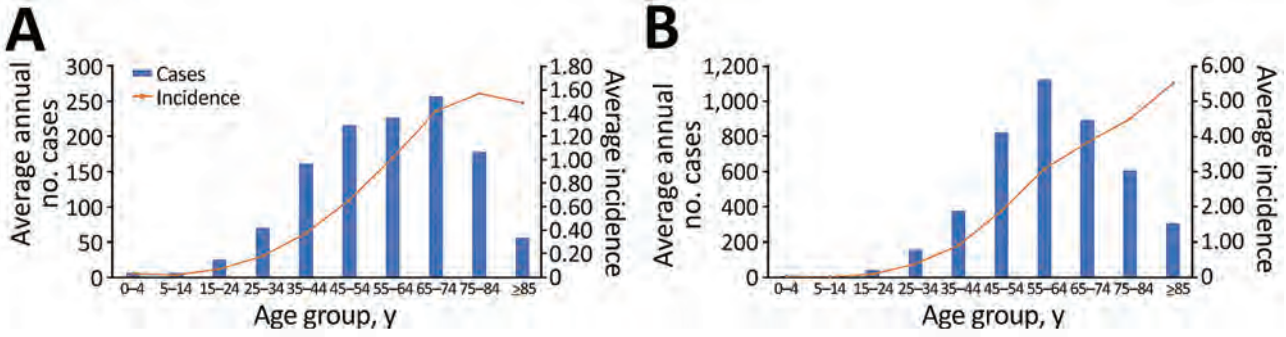

Figure 3. Average annual number of cases of Legionnaires' disease and average incidence (cases/100,000 population), by age group, United States, 1992–2018. A) Reported average number of annual cases and average incidence by age group for 1992–2002. B) Reported average number of annual cases and average incidence by age group for 2003–2018.

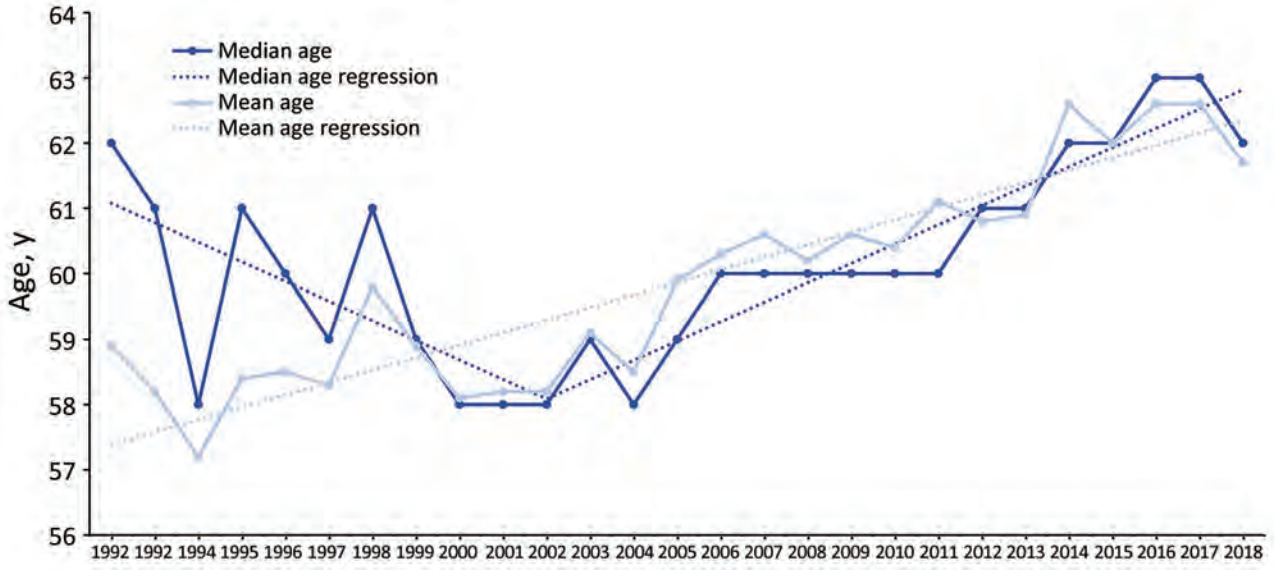

Figure 4. Trends in median and mean age of Legionnaires' disease patients by year, United States, 1992–2018.

the age-standardized average incidence increased to 1.80/100,000 in men and 0.91/100,000 in women.

Race

Race was missing for 18.2% of cases; thus, race-specific case counts and incidences might be slightly higher than measured in this study. During the baseline years, >6 times the number of average annual cases were reported among White persons (813) than Black or African American persons (128), but the age-standardized average incidence was >25% higher among Black or African American persons (0.47/100,000 population) than White persons (0.37/100,000 population) (Figure 5, panel A; Appendix Table). This pattern continued, and racial disparities were more pronounced during the years of increase, when the age-standardized average incidence was twice as high among Black or African American persons (2.15/100,000 population) than among White persons (0.99/100,000 population) (Figure 5, panel B).

Geographic Distribution

During both the baseline years and the years of increase, the age-standardized average incidence was higher in the Northeast (0.68/100,000 population in baseline years; 2.34/100,000 population in years of increase) and Midwest (0.67; 1.67) regions than in the South (0.33; 1.01) and West (0.29; 0.66) regions (Appendix Table). Similarly, the contiguous East North Central (0.77; 2.01), Middle Atlantic (0.71; 2.58), and New England (0.61; 1.64) divisions had the highest age-standardized average incidence during the baseline years and the years of increase. Among the 20 jurisdictions with the highest age-standardized average incidence during 1992–2002, a total of 10 were located within the East North Central, Middle Atlantic, or New England divisions, and 3 others bordered these divisions (Figure 6, panel A). During 2003–2018, 14/20 jurisdictions with the highest age-standardized average incidence were located within these same 3 divisions,

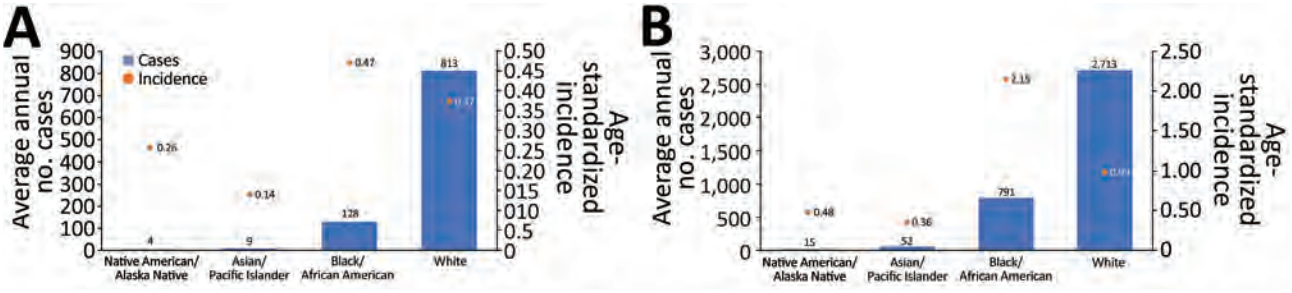

Figure 5. Average annual number of cases of Legionnaires' disease and age-standardized average incidence (cases/100,000 population) by race, United States, 1992–2018. A) Reported average number of annual cases and age-standardized average incidence by race for 1992–2002. B) Reported average number of annual cases and age-standardized average incidence by race for 2003–2018.

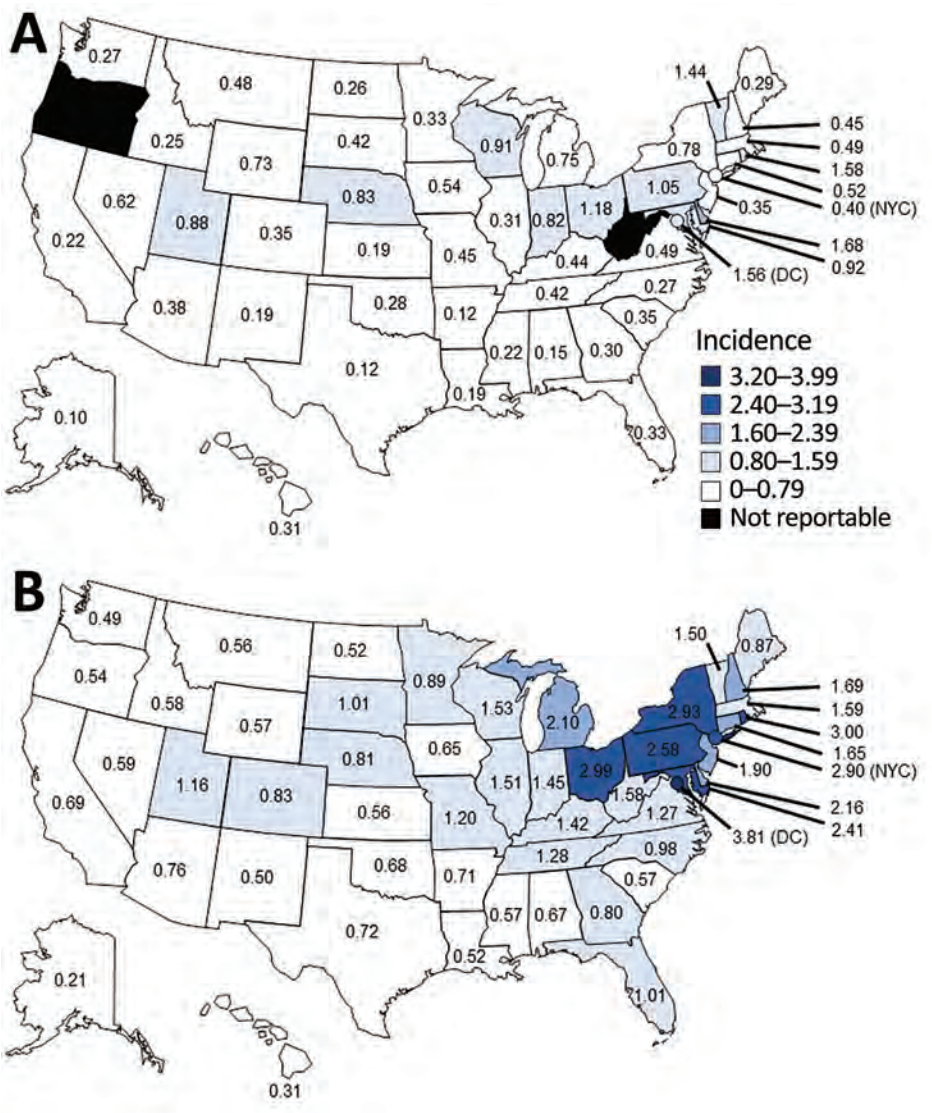

Figure 6. Age-standardized average incidence (cases/100,000 population) of Legionnaires' disease by jurisdiction, United States, 1992–2018. A) Age-standardized average incidence by jurisdiction, 1992–2002. Legionnaires' disease was not reportable in Connecticut during 1992–1996 or in Oregon or West Virginia during 1992–2002. B) Age-standardized average incidence by jurisdiction, 2003–2018.

and 4 additional jurisdictions (of the 20) bordered these divisions (Figure 6, panel B).

Seasonality

Most LD cases occurred during summer or fall months, and this pattern became more extreme after the baseline years (Figure 2). During 1992–2002, an average of 57.8% of annual cases occurred during June–November, increasing to 68.9% during 2003–2018. The average annual maximum-to-minimum monthly cases ratio rose from 2.59 during the baseline years to 4.31 during the years of increase.

By geography, during the baseline years, moderate seasonality was observed in the Northeast region and less so in the Midwest and South regions (Figure 7, panel A). No seasonal pattern was discernible in the West. When cases increased during 2003–2018, seasonality became more prominent in all regions, particularly in the Northeast and Midwest (Figure 7, panel B). A less pronounced but identifiable seasonal pattern was also observed in the West. The LD season began first in the South and maintained a peak in this region from June through October. The LD season began later in the Midwest and Northeast, peaking in July in the Midwest and in August in the Northeast.

Magnitude of Increase

Overall, age-standardized average incidence increased from 0.48/100,000 population during the baseline years (1992–2002) to 2.71/100,000 population in 2018 (incidence risk ratio [RR] 5.67, 95% CI 5.52–5.83) (Table). Relative changes in incidence in the 0–4-year and 5–14-year age groups were not statistically significant (RR 0.16, 95% CI 0.02–1.19 for 0–4 years; RR 0.48, 95% CI 0.15–1.54 for 5–14 years). Incidence increased >5-fold for all age groups above

34 years; the largest relative increases occurred in the ≥85-year (RR 6.50, 95% CI 5.82–7.27), 55–64-year (RR 6.39, 95% CI 6.05–6.75), and 45–54-year (RR 6.28, 95% CI 5.91–6.69) age groups. Age-standardized incidence increased slightly more in men (RR 5.86, 95% CI 5.67–6.05) than in women (RR 5.29, 95% CI 5.06–5.53). The age-standardized incidence increased from 0.47 to 5.21/100,000 population in Black or African American persons (RR 11.04, 95% CI 10.39–11.73) and from 0.37 to 1.99/100,000 population in White persons (RR 5.30, 95% CI 5.12–5.49).

By region, the relative increase in age-standardized incidence was largest in the Northeast (RR 7.04, 95% CI 6.70–7.40), similar in the Midwest (RR 6.13, 95% CI 5.85–6.42) and South (RR 5.97, 95% CI 5.67–6.29), and smallest in the West (RR 3.39, 95% CI 3.11–3.68). By division, the largest relative increase in age-standardized incidence occurred in the West South Central division (RR 9.15, 95% CI 8.10–10.34). The next-largest relative increases were similar among the New England (RR 7.10, 95% CI 6.40–7.87), Middle Atlantic (RR 7.07, 95% CI 6.69–7.48), East North Central (RR 6.48, 95% CI 6.16–6.82), and East South Central (RR 6.40, 95% CI 5.63–7.27) divisions. The smallest relative increase in age-standardized incidence was in the Mountain division (RR 2.47, 95% CI 2.15–2.83). Although the largest relative increase in age-standardized incidence occurred in the West South Central division, the largest absolute increases occurred in the Middle Atlantic, East North Central, and New England divisions.

Discussion

Reported incidence of LD in the United States has been rising since 2003, and the increase appears to be accelerating in recent years. Joinpoint analysis confirmed that a change in trend in age-standardized incidence occurred between 1996 and 2002, inclusively; no trend was identified before the change point, and an increasing trend was identified after. Although 1999 was indicated as the single optimal change point, and age-standardized incidence increased slightly every year after 1999 until 2004, the first substantial increase beyond what was likely the baseline range occurred in 2003. However, the rising incidence was not uniform and affected some demographic groups disproportionately. Increases tended to be larger in demographics with higher incidence. This rise was most strikingly associated with increases in racial disparities, geographic

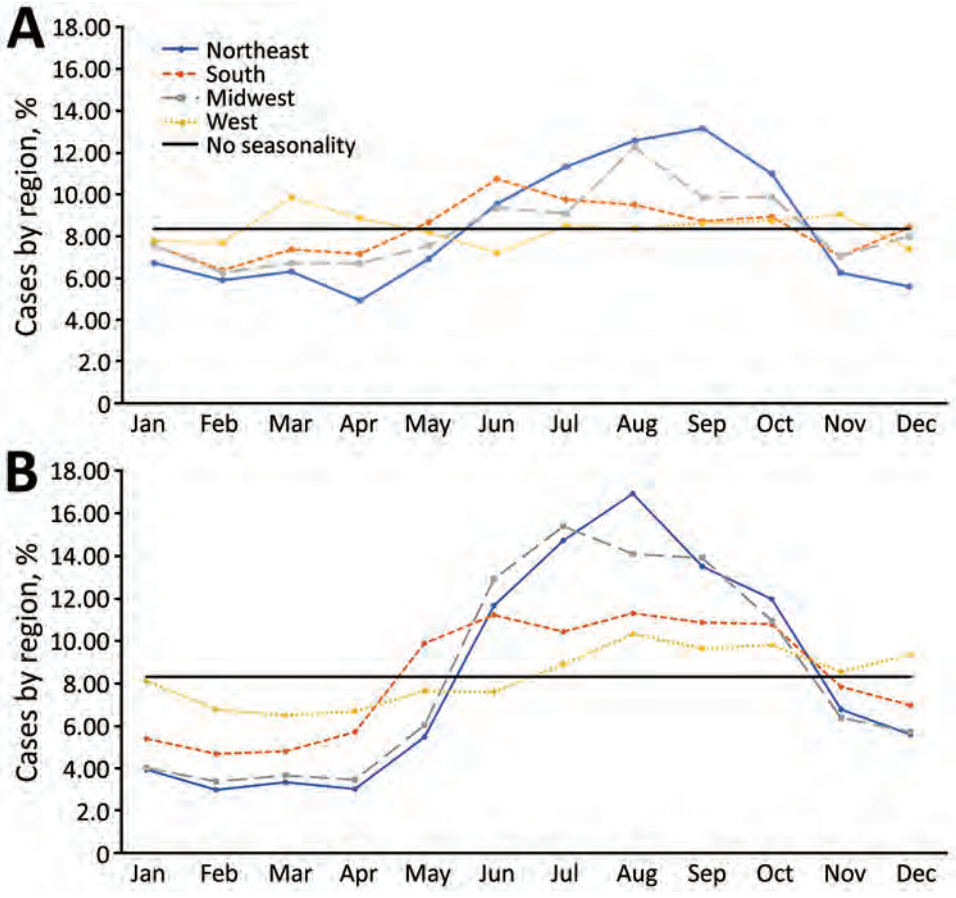

Figure 7. Seasonality of Legionnaires' disease cases by Census Bureau region, United States, 1992–2018. A) Seasonality of cases by US Census Bureau region, 1992–2002. The monthly percentage of each region's cases is shown. If no seasonality existed, approximately the same number of cases would be expected to occur each month (i.e., 1/12 [8.3%] of annual cases would occur each month). B) Seasonality of cases by US Census Bureau region, 2003–2018. The monthly percentage of each region's cases is shown. If no seasonality existed, approximately the same number of cases would be expected to occur each month (i.e., 1/12 [8.3%] of annual cases would occur each month).

Table. Magnitude of increase in age-standardized incidence of Legionnaires' disease, cases/100,000 population, from 1992–2002 (average) through 2018, United States

Demographic	Age-standardized average incidence, 1992–2002	Age-standardized incidence, 2018	Absolute increase in age-standardized incidence	Age-standardized incidence risk ratio, 2018 to 1992–2002 baseline (95% CI)	Increase in age-standardized incidence, %
Age group, y, not standardized					
0–4	0.03	0.01	−0.03	0.16 (0.02–1.19)	−83.52
5–14	0.02	0.01	−0.01	0.48 (0.15–1.54)	−51.61
15–24	0.07	0.19	0.12	2.80 (2.19–3.57)	179.80
25–34	0.18	0.75	0.58	4.30 (3.79–4.88)	330.31
35–44	0.38	1.97	1.59	5.15 (4.74–5.59)	414.89
45–54	0.66	4.12	3.46	6.28 (5.91–6.69)	528.44
55–64	1.02	6.52	5.50	6.39 (6.05–6.75)	539.14
65–74	1.42	7.66	6.24	5.40 (5.11–5.70)	439.63
75–84	1.57	8.52	6.96	5.44 (5.07–5.84)	444.13
≥85	1.49	9.69	8.20	6.50 (5.82–7.27)	550.35
Sex					
M	0.63	3.66	3.04	5.86 (5.67–6.05)	485.55
F	0.35	1.86	1.50	5.29 (5.06–5.53)	429.22
Race*					
Native American or Alaska Native	0.26	1.27	1.01	4.93 (3.51–6.93)	392.94
Asian or Pacific Islander	0.14	0.56	0.42	4.03 (3.19–5.10)	303.18
Black or African American	0.47	5.21	4.74	11.04 (10.39–11.73)	1003.95
White	0.37	1.99	1.61	5.30 (5.12–5.49)	430.15
Region					
Division					
Northeast	0.68	4.82	4.14	7.04 (6.70–7.40)	604.10
New England	0.61	4.33	3.72	7.10 (6.40–7.87)	610.04
Middle Atlantic	0.71	5.00	4.30	7.07 (6.69–7.48)	606.98
South	0.33	1.97	1.64	5.97 (5.67–6.29)	497.23
South Atlantic	0.44	2.29	1.85	5.24 (4.91–5.59)	423.54
East South Central	0.32	2.05	1.73	6.40 (5.63–7.27)	539.66
West South Central	0.15	1.36	1.21	9.15 (8.10–10.34)	815.03
Midwest	0.67	4.10	3.43	6.13 (5.85–6.42)	513.06
East North Central	0.77	5.01	4.24	6.48 (6.16–6.82)	548.02
West North Central	0.42	2.04	1.62	4.81 (4.29–5.40)	381.38
West	0.29	0.99	0.70	3.39 (3.11–3.68)	238.50
Mountain	0.43	1.07	0.64	2.47 (2.15–2.83)	146.55
Pacific	0.23	0.95	0.72	4.13 (3.71–4.59)	312.91
United States	0.48	2.71	2.23	5.67 (5.52–5.83)	467.30

*Ethnicity was not analyzed because data were missing for 30.4% of cases.

focus, and seasonality. We also noted changes in age and sex distributions.

The US population is aging (*16*–*18*); because older age is a risk factor for LD (*2*) and incidence increased with age, the aging population might contribute to the rising national incidence of LD. In this analysis, age-standardized incidence increased less than crude incidence. However, this difference was minor (12% in 2018), and relative increases in incidence from the baseline years to 2018 for all age groups older than 34 years were at least equal to the national average, suggesting that other factors played larger roles in the rising trend.

Although most LD cases occurred among White persons, Black or African American persons were disproportionately affected. Certain underlying conditions, including diabetes, end-stage renal disease, and some cancers, have been associated with an increased risk for LD (*2*), and these conditions are more common among Black or African American persons than White persons (*19*–*22*). Social determinants of health also likely contributed to disparities in incidence (*23*). Black or African American persons had the lowest median household income relative to other races (*24*), and areas of poverty were associated with a higher incidence of LD (*25*,*26*). Residence in areas with more vacant housing, more renter-occupied homes, more homes built before 1970, and lower education levels were also identified as risk factors for LD (*26*). Certain occupations (transportation, repair, protective services, cleaning services, and construction) were found to carry a higher risk for LD, but the associations with race and socioeconomic status were unclear (*25*). The relative increase in LD incidence from baseline years to 2018 was larger among Black or African American persons than any other demographic group, suggesting that the conditions leading to this disparity have been worsening.

Geographically, LD incidence was generally focused around an area extending from Ohio into New

York state and Maryland and decreased with distance from this center. Although incidence rose nationwide, areas with higher incidence tended to have larger increases. These findings indicate that factors shared by geographic areas might have contributed to the rise in cases. Several studies found temperature, precipitation, and humidity to be associated with LD cases, although the mechanics are not completely understood (*27*–*31*). Aging infrastructure might also have played a role, because residing in areas with older homes has been identified as a risk factor for LD (*26*). Median population age varied by jurisdiction; the Northeast region had the highest median population age, followed by the Midwest, South, and West regions (*17*). However, standardizing age across jurisdictions for 2018 did not dramatically alter the jurisdiction-specific incidence from the crude incidence, suggesting that geographic variations in population age did not account for the higher incidence observed in the Middle Atlantic, East North Central, and New England divisions to a large extent.

LD exhibits a summer-through-early-fall seasonality, and this pattern became more pronounced as incidence increased, which could imply that the cyclical factors causing seasonal patterns are becoming more extreme. One likely candidate for a cyclical factor that could cause seasonal patterns in LD cases is weather. From 1990–2020, summer precipitation and the fall mean temperature have been increasing in high-incidence divisions (*32*). Our results and previous findings suggest that the peak of the LD season shifted from late summer to mid-summer, particularly in the Northeast and Midwest regions (*11*). Wetter summers might partly explain this shift, because precipitation and humidity have been associated with increased cases (*27*–*31*). Similarly, temperatures in the South reach *Legionella*-promoting temperatures, which also increase cooling tower use, earlier in the year than in the Northeast or Midwest, which might explain why the LD season begins first in the South (*33*). Furthermore, hurricane-produced rainfall increased during 1998–2016 (*34*), and hurricanes have been associated with elevated concentrations of *Legionella* bacteria in cooling towers and surface water (*35*,*36*). Travel is also a cyclical risk factor for LD but does not appear to influence seasonality; seasonal patterns for travel-associated cases were nearly identical to those for non–travel-associated cases during 2015–2016 (*37*). Furthermore, the percentage of travel-associated cases remained relatively stable over time (*37*).

LD might occur worldwide because *Legionella* is a ubiquitous freshwater bacterium (*38*), but reporting and surveillance vary considerably. Patient demographics and a general rise in incidence were similar in the United States, Europe, Canada, and Australia, but the trajectory of the rising incidence trend was more similar in northern hemisphere locations than Australia (Figure 8) (*39*–*42*). This finding could suggest that factors common to northern regions, such as weather patterns, influenced the increase. In Ontario, Canada, just north of the high-incidence Middle Atlantic and East North Central divisions, LD incidence was generally highest in the southern part of the province, north of Lakes Erie and Ontario

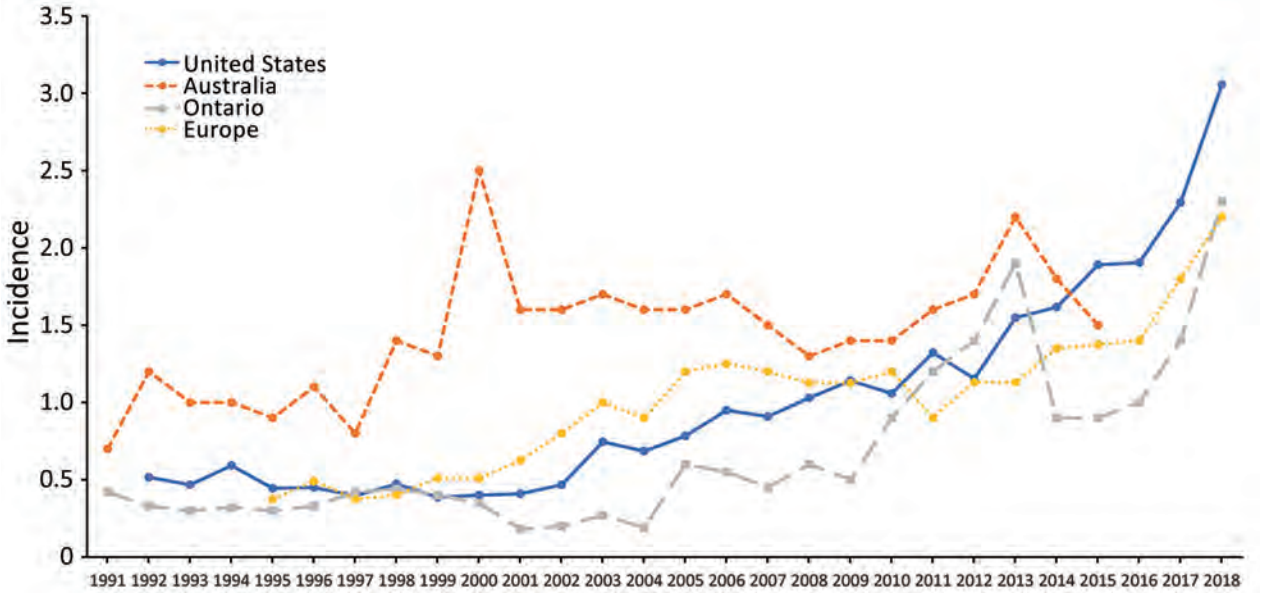

Figure 8. International crude incidence (cases/100,000 population) trends of Legionnaires' disease, United States (National Notifiable Diseases Surveillance System), Europe (*39*), Ontario, Canada (*40*,*41*), and Australia (*42*), 1991–2018.

(*41*). Reasons for the worldwide increase in LD are unclear but might include an aging population, surveillance and reporting improvements, building infrastructure design and maintenance, and weather patterns (*39*,*40*).

The first limitation of our study is that, when evaluating rising incidence, separating the effect of improved surveillance from a true increase in infections is difficult. NNDSS is a passive surveillance system, and incomplete case-reporting is a concern with passive systems; however, a comparison with an active reporting system suggested that nearly all diagnosed LD cases were reported (*43*). LD might be underdiagnosed; studies estimate that 20,000 cases might occur annually (*2*,*44*). Because of the severe acute respiratory syndrome pandemic during 2002–2003 (*45*), practitioners might have increased the thoroughness of testing community-acquired pneumonia (CAP) patients to confirm an alternative diagnosis, thereby increasing the number of LD tests performed (*29*). Although this factor might explain the initial rise in reported LD cases in the United States, it does not explain the continued increase through 2018 or why increases did not occur simultaneously in other areas of the world, particularly Ontario, where severe acute respiratory syndrome cases occurred most outside of Asia (*45*). Although the case definition changed twice during our study period, the differences were small and unlikely to have substantially affected diagnosis or reporting. All case definitions included a positive urinary antigen test, isolation of *Legionella* spp., and a ≥4-fold rise in antibody titer to *L. pneumophila* serogroup 1 as options for confirming a case (*13*–*15*); most cases were confirmed by 1 of these methods (*1*,*46*). Before 2006, the direct fluorescent antibody test was also included, but its use in diagnosis had been declining since the mid-1990s (*46*). At the same time, the urinary antigen test came into widespread use and by 1998 was used in the diagnosis of >70% of reported cases (*46*). Therefore, changes in the case definition or available diagnostic tests are unlikely to account for the rising incidence after 2002.

Despite these limitations, our findings indicate several instructive points. Although professional guidelines recommend testing for *Legionella* in CAP patients associated with certain factors, such as an LD outbreak or recent travel, or in adults with severe CAP (*47*), clinicians might maintain a higher index of suspicion for LD in other CAP patients under certain circumstances because LD cases are rising nationwide and cannot be diagnosed on clinical features alone. Our results showed LD incidence was highest in older persons (particularly ≥55 years of age) and Black or African American persons, but these demographic groups also tended to have the highest rates of pneumonia-associated hospitalizations (*48*). Because LD incidence was highest in the East North Central, Middle Atlantic, and New England divisions, and pneumonia-associated hospitalization incidence was not similarly higher in these divisions (*48*), the likelihood that a CAP case is LD might be elevated in these locations. Similarly, more LD cases occurred during June–November, especially in the Northeast and Midwest, but most pneumonia-associated hospitalizations occurred during December–March (*48*); therefore, a larger percentage of CAP cases during the summer and early fall might be LD. Others have suggested increasing suspicion for LD in CAP patients during warm, humid, rainy weather (*27*).

In conclusion, LD incidence has risen steadily nationwide for >15 years, and the increase was associated with wider racial disparities, intensifying geographic focus, and more pronounced seasonality. The geographic focus and seasonality suggest that deeper investigations into the effects of weather may further elucidate the rising incidence of LD. Although WMPs are recommended for buildings with complex water systems and certain devices (*3*–*5*), uptake might be slow (*49*), and additional prevention methods could be useful. Outbreaks can cause substantial illness and deaths (*50*), but ≈64% of reported LD cases have no known potential exposure and generally lack an identified source (*1*). Improved investigations of sporadic cases and their sources may lead to novel prevention strategies and the identification of previously unrecognized outbreaks.

About the Author

Mr. Barskey is an epidemiologist with the *Legionella* program at the National Center for Immunization and Respiratory Diseases, Centers for Disease Control and Prevention, Atlanta. His primary research interests include infectious disease surveillance and epidemiology.

References

1. Centers for Disease Control and Prevention. Legionnaires' disease surveillance summary report, United States, 2016–2017. February 2020 [cited 2020 August 20]. https://www.cdc.gov/legionella/health-depts/surv-reporting/2016-17-surv-report-508.pdf
2. Marston BJ, Lipman HB, Breiman RF. Surveillance for Legionnaires' disease. Risk factors for morbidity and mortality. Arch Intern Med. 1994;154:2417–22. https://doi.org/10.1001/archinte.1994.00420210049006
3. Garrison LE, Kunz JM, Cooley LA, Moore MR, Lucas C, Schrag S, et al. Vital signs: deficiencies in environmental control identified in outbreaks of Legionnaires' disease—

North America, 2000–2014. MMWR Morb Mortal Wkly Rep. 2016;65:576–84. https://doi.org/10.15585/mmwr.mm6522e1
4. American Society of Heating, Refrigerating and Air-Conditioning Engineers (ASHRAE). ANSI/ASHRAE Standard 188–2015, Legionellosis: risk management for building water systems. 2018 [cited 2020 August 20]. https://www.ashrae.org/technical-resources/bookstore/ansi-ashrae-standard-188-2018-legionellosis-risk-management-for-building-water-systems
5. Centers for Disease Control and Prevention. Toolkit: developing a water management program to reduce *Legionella* growth and spread in buildings. A practical guide to implementing industry standards. 2021 Mar 25 [cited 2021 June 8]. https://www.cdc.gov/legionella/maintenance/wmp-toolkit.html
6. McDade JE, Shepard CC, Fraser DW, Tsai TR, Redus MA, Dowdle WR. Legionnaires' disease: isolation of a bacterium and demonstration of its role in other respiratory disease. N Engl J Med. 1977;297:1197–203. https://doi.org/10.1056/NEJM197712012972202
7. Fraser DW, Tsai TR, Orenstein W, Parkin WE, Beecham HJ, Sharrar RG, et al. Legionnaires' disease: description of an epidemic of pneumonia. N Engl J Med. 1977;297:1189–97. https://doi.org/10.1056/NEJM197712012972201
8. Centers for Disease Control and Prevention. MMWR summary of notifiable diseases, United States, 1993. MMWR Morb Mortal Wkly Rep. 1994;42:1–73.
9. Neil K, Berkelman R. Increasing incidence of legionellosis in the United States, 1990–2005: changing epidemiologic trends Clin Infect Dis. 2008;47:591–9. https://doi.org/10.1086/590557
10. Centers for Disease Control and Prevention (CDC). Legionellosis—United States, 2000–2009. MMWR Morb Mortal Wkly Rep. 2011;60:1083–6.
11. Alarcon Falconi TM, Cruz MS, Naumova EN. The shift in seasonality of legionellosis in the USA. Epidemiol Infect. 2018; 146:1824–33. https://doi.org/10.1017/S0950268818002182
12. Centers for Disease Control and Prevention. Nationally notifiable infectious diseases and conditions, United States: Annual tables. Table 2i. Annual reported cases of notifiable diseases, by region and reporting area, United States and U.S. Territories, excluding non-U.S. residents, 2019 [cited 2021 May 25]. https://wonder.cdc.gov/nndss/static/2019/annual/2019-table2i.html
13. Wharton M, Chorba TL, Vogt RL, Morse DL, Buehler JW. Case definitions for public health surveillance. MMWR Recomm Rep. 1990;39:1–43.
14. Centers for Disease Control and Prevention. Case definitions for infectious conditions under public health surveillance. MMWR Recomm Rep. 1997;46:1–55.
15. Council of State and Territorial Epidemiologists. Strengthening surveillance for travel-associated legionellosis and revised case definitions for legionellosis. Position statement no. 05-ID-01. 2005 Mar 31 [cited 2020 August 20]. https://cdn.ymaws.com/www.cste.org/resource/resmgr/PS/05-ID-01FINAL.pdf
16. Centers for Disease Control and Prevention. Bridged-race population estimates: data files and documentation. 2020 Jul 9 [cited 2020 August 20]. https://www.cdc.gov/nchs/nvss/bridged_race/data_documentation.htm
17. Howden LM, Meyer JA. Age and sex composition: 2010. 2010 Census briefs, C2010BR-03. 2011 May [cited 2021 May 26]. https://www.census.gov/prod/cen2010/briefs/c2010br-03.pdf
18. Roberts AW, Ogunwole SU, Blakeslee L, Rabe MA. The population 65 years and older in the United States: 2016. 2018 Oct [cited 2021 May 26]. https://www.census.gov/content/dam/Census/library/publications/2018/acs/ACS-38.pdf
19. Gaskin DJ, Thorpe RJ Jr, McGinty EE, Bower K, Rohde C, Young JH, et al. Disparities in diabetes: the nexus of race, poverty, and place. Am J Public Health. 2014;104:2147–55. https://doi.org/10.2105/AJPH.2013.301420
20. Bock F, Stewart TG, Robinson-Cohen C, Morse J, Kabagambe EK, Cavanaugh KL, et al. Racial disparities in end-stage renal disease in a high-risk population: the Southern Community Cohort Study. BMC Nephrol. 2019;20:308. https://doi.org/10.1186/s12882-019-1502-z
21 Ryan BM. Lung cancer health disparities. Carcinogenesis. 2018;39:741–51. https://doi.org/10.1093/carcin/bgy047
22. Kirtane K, Lee SJ. Racial and ethnic disparities in hematologic malignancies. Blood. 2017;130:1699–705. https://doi.org/10.1182/blood-2017-04-778225
23. Hunter CM, Salandy SW, Smith JC, Edens C, Hubbard B. Racial disparities in incidence of Legionnaires' disease and social determinants of health: a narrative review. Public Health Rep. 2021 Jun 29 [Epub ahead of print]. https://doi.org/10.1177/00333549211026781
24. Semega J, Kollar M, Creamer J, Mohanty A. Income and poverty in the United States: 2019. 2020 Sep [cited 2021 May 26]. https://www.census.gov/content/dam/Census/library/publications/2020/demo/p60-270.pdf
25. Farnham A, Alleyne L, Cimini D, Balter S. Legionnaires' disease incidence and risk factors, New York, New York, USA, 2002–2011. Emerg Infect Dis. 2014;20:1795–802. https://doi.org/10.3201/eid2011.131872
26. Gleason JA, Ross KM, Greeley RD. Analysis of population-level determinants of legionellosis: spatial and geovisual methods for enhancing classification of high-risk areas. Int J Health Geogr. 2017;16:45. https://doi.org/10.1186/s12942-017-0118-4
27. Simmering JE, Polgreen LA, Hornick DB, Sewell DK, Polgreen PM. Weather-dependent risk for legionnaires' disease, United States. Emerg Infect Dis. 2017;23:1843–51. https://doi.org/10.3201/eid2311.170137
28. Fisman DN, Lim S, Wellenius GA, Johnson C, Britz P, Gaskins M, et al. It's not the heat, it's the humidity: wet weather increases legionellosis risk in the greater Philadelphia metropolitan area. J Infect Dis. 2005;192:2066–73. https://doi.org/10.1086/498248
29. Hicks LA, Rose CE Jr, Fields BS, Drees ML, Engel JP, Jenkins PR, et al. Increased rainfall is associated with increased risk for legionellosis. Epidemiol Infect. 2007;135:811–7. https://doi.org/10.1017/S0950268806007552
30. Beauté J, Sandin S, Uldum SA, Rota MC, Brandsema P, Giesecke J, et al. Short-term effects of atmospheric pressure, temperature, and rainfall on notification rate of community-acquired Legionnaires' disease in four European countries [Erratum in: Epidemiol Infect. 2017;145:3319]. Epidemiol Infect. 2016;144:3483–93. https://doi.org/10.1017/S0950268816001874
31. Passer JK, Danila RN, Laine ES, Como-Sabetti KJ, Tang W, Searle KM. The association between sporadic Legionnaires' disease and weather and environmental factors, Minnesota, 2011–2018. Epidemiol Infect. 2020;148:e156. https://doi.org/10.1017/S0950268820001417
32. National Centers for Environmental Information, National Oceanic and Atmospheric Administration. National trends: temperature, precipitation, and drought [cited 2021 June 8]. https://www.ncdc.noaa.gov/temp-and-precip/us-trends/prcp/sum
33. National Centers for Environmental Information, National Oceanic and Atmospheric Administration. National

temperature and precipitation maps [cited 2021 June 8]. https://www.ncdc.noaa.gov/temp-and-precip/us-maps
34. Guzman O, Jiang H. Global increase in tropical cyclone rain rate. Nat Commun. 2021;12:5344. https://doi.org/10.1038/s41467-021-25685-2
35. Brigmon RL, Turick CE, Knox AS, Burckhalter CE. The impact of storms on *Legionella pneumophila* in cooling tower water, implications for human health. Front Microbiol. 2020;11:543589. https://doi.org/10.3389/fmicb.2020.543589
36. Ulrich N, Rosenberger A, Brislawn C, Wright J, Kessler C, Toole D, et al. Restructuring of the aquatic bacterial community by hydric dynamics associated with superstorm Sandy. Appl Environ Microbiol. 2016;82:3525–36. https://doi.org/10.1128/AEM.00520-16
37. Barskey AE, Lackraj D, Tripathi PS, Lee S, Smith J, Edens C. Travel-associated cases of Legionnaires' disease in the United States, 2015–2016. Travel Med Infect Dis. 2021;40:101943. https://doi.org/10.1016/j.tmaid.2020.101943
38. Graham FF, Hales S, White PS, Baker MG. Review global seroprevalence of legionellosis—a systematic review and meta-analysis. Sci Rep. 2020;10:7337. https://doi.org/10.1038/s41598-020-63740-y
39. European Centre for Disease Prevention and Control. Surveillance reports on Legionnaires' disease [cited 2021 June 8]. https://www.ecdc.europa.eu/en/legionnaires-disease/surveillance-and-disease-data/surveillance
40. Ontario Agency for Health Protection and Promotion (Public Health Ontario). Factors affecting reportable diseases in Ontario (1991–2016) [cited 2020 August 20]. https://www.publichealthontario.ca/-/media/documents/f/2018/factors-reportable-diseases-ontario-1991-2016.pdf
41. Public Health Ontario. Infectious disease trends in Ontario: Legionellosis [cited 2021 June 8]. https://www.publichealthontario.ca/en/data-and-analysis/infectious-disease/reportable-disease-trends-annually#/31
42. Australian Government Department of Health. National notifiable diseases: Australia's notifiable diseases status: annual report of the National Notifiable Diseases Surveillance System. 2019 Mar [cited 2020 August 20]. https://www1.health.gov.au/internet/main/publishing.nsf/Content/cda-pubs-annlrpt-nndssar.htm
43. Dooling KL, Toews KA, Hicks LA, Garrison LE, Bachaus B, Zansky S, et al. Active Bacterial Core surveillance for legionellosis—United States, 2011–2013. MMWR Morb Mortal Wkly Rep. 2015;64:1190–3. https://doi.org/10.15585/mmwr.mm6442a2
44. Collier SA, Deng L, Adam EA, Benedict KM, Beshearse EM, Blackstock AJ, et al. Estimate of burden and direct healthcare cost of infectious waterborne disease in the United States. Emerg Infect Dis. 2021;27:140–9. https://doi.org/10.3201/eid2701.190676
45. Hui DSC, Zumla A. Severe Acute Respiratory Syndrome: historical, epidemiologic, and clinical features. Infect Dis Clin North Am. 2019;33:869–89. https://doi.org/10.1016/j.idc.2019.07.001
46. Benin AL, Benson RF, Besser RE. Trends in legionnaires disease, 1980–1998: declining mortality and new patterns of diagnosis. Clin Infect Dis. 2002;35:1039–46. https://doi.org/10.1086/342903
47. Metlay JP, Waterer GW, Long AC, Anzueto A, Brozek J, Crothers K, et al. Diagnosis and treatment of adults with community-acquired pneumonia: an official clinical practice guideline of the American Thoracic Society and Infectious Diseases Society of America. Am J Respir Crit Care Med. 2019;200:e45–67. https://doi.org/10.1164/rccm.201908-1581ST
48. Hayes BH, Haberling DL, Kennedy JL, Varma JK, Fry AM, Vora NM. Burden of pneumonia-associated hospitalizations: United States, 2001–2014. Chest. 2018;153:427–37. https://doi.org/10.1016/j.chest.2017.09.041
49. Leftwich B, Opoku S, Yin J, Adhikari A. Assessing hotel employee knowledge on risk factors and risk management procedures for microbial contamination of hotel water distribution systems. Int J Environ Res Public Health. 2021;18:3539. https://doi.org/10.3390/ijerph18073539
50. Lapierre P, Nazarian E, Zhu Y, Wroblewski D, Saylors A, Passaretti T, et al. Legionnaires' disease outbreak caused by endemic strain of *Legionella pneumophila*, New York, New York, USA, 2015. Emerg Infect Dis. 2017;23:1784–91. https://doi.org/10.3201/eid2311.170308

Address for correspondence: Albert E. Barskey, Centers for Disease Control and Prevention, 1600 Clifton Rd NE, Mailstop H24-6, Atlanta, GA 30329, USA; email: abarskey@cdc.gov

Neutralizing Enterovirus D68 Antibodies in Children after 2014 Outbreak, Kansas City, Missouri, USA

Robyn A. Livingston,[1] Christopher J. Harrison,[1] Rangaraj Selvarangan[1]

Medscape ACTIVITY EDUCATION

In support of improving patient care, this activity has been planned and implemented by Medscape, LLC and Emerging Infectious Diseases. Medscape, LLC is jointly accredited by the Accreditation Council for Continuing Medical Education (ACCME), the Accreditation Council for Pharmacy Education (ACPE), and the American Nurses Credentialing Center (ANCC), to provide continuing education for the healthcare team.

Medscape, LLC designates this Journal-based CME activity for a maximum of 1.00 ***AMA PRA Category 1 Credit(s)™***. Physicians should claim only the credit commensurate with the extent of their participation in the activity.

Successful completion of this CME activity, which includes participation in the evaluation component, enables the participant to earn up to 1.0 MOC points in the American Board of Internal Medicine's (ABIM) Maintenance of Certification (MOC) program. Participants will earn MOC points equivalent to the amount of CME credits claimed for the activity. It is the CME activity provider's responsibility to submit participant completion information to ACCME for the purpose of granting ABIM MOC credit.

All other clinicians completing this activity will be issued a certificate of participation. To participate in this journal CME activity: (1) review the learning objectives and author disclosures; (2) study the education content; (3) take the post-test with a 75% minimum passing score and complete the evaluation at http://www.medscape.org/journal/eid; and (4) view/print certificate. For CME questions, see page 770.

Release date: February 17, 2022; Expiration date: February 17, 2023

Learning Objectives

Upon completion of this activity, participants will be able to:

- Describe neutralizing EV-D68 antibodies to the 2014 B1, 2014 B2, and 2014 D clade virus in pediatric sera salvaged during 2017 in patients aged 6 months to 18 years, including persons born after the 2014 outbreak, according to a serologic study in Kansas City, Missouri
- Determine associations of neutralizing EV-D68 antibody titers with demographic and medical history factors, according to a serologic study in Kansas City, Missouri
- Identify clinical and public health implications of neutralizing EV-D68 antibodies to the 2014 B1, 2014 B2, and 2014 D clade virus in pediatric sera salvaged during 2017 from patients aged 6 months to 18 years, including persons born after the 2014 outbreak, and of associations of antibody titers with demographic and medical history factors, according to a serologic study in Kansas City, Missouri

CME Editor

P. Lynne Stockton Taylor, VMD, MS, ELS(D), Technical Writer/Editor, Emerging Infectious Diseases. *Disclosure: P. Lynne Stockton Taylor, VMD, MS, ELS(D), has disclosed no relevant financial relationships.*

CME Author

Laurie Barclay, MD, freelance writer and reviewer, Medscape, LLC. *Disclosure: Laurie Barclay, MD, has disclosed the following relevant financial relationships: owns stock, stock options, or bonds from the following ineligible company(ies): AbbVie Inc. (former).*

Authors

Robyn A. Livingston, MD, MPH; Christopher J. Harrison, MD; *and* ***Rangaraj Selvarangan, BVSc, PhD.***

Author affiliations: Children's Mercy Hospital Kansas City, Kansas City, Missouri, USA; University of Missouri, Kansas City

DOI: https://doi.org/10.3201/eid2803.211467

[1]All authors contributed equally to this article.

Enterovirus D68 (EV-D68) causes severe respiratory illness outbreaks among children, particularly those with asthma. We previously detected neutralizing antibodies against the predominant EV-D68 B1 clade in the 2014 outbreak in serum collected before the outbreak (2012–2013) from persons 24 months to 85 years of age. We recently detected neutralizing antibodies to the 2014 B1, B2, and D clade viruses in serum collected after the 2014 outbreak (April–May 2017) from 300 children 6 months to 18 years of age. B1 virus neutralizing antibodies were found in 100% of patients, even children born after 2014; B2 in 84.6%, and D in 99.6%. In 2017, titers increased with patient age and were higher than titers in 2012–2013 from comparably aged children. Rate of seronegativity was highest (15.3%) for B2 virus. Multivariate analysis revealed an association between asthma and higher titers against B2 and D viruses. EV-D68 seems to have circulated during 2014–2017.

Enterovirus D68 (EV-D68) rose to prominence because of its association with acute flaccid myelitis (AFM) (*1*,*2*) and the US outbreak of severe respiratory disease among children in 2014 (381 cases in Kansas City, Missouri, USA; 1,153 confirmed cases nationally). Severe disease affected children with a history of atopic disease, asthma, or reactive airway disease (*3*–*6*). Although the 2014 EV-D68 outbreak in the United States was caused predominantly by a clade B1 virus, 2 less frequent viruses, clades B2 and D (previously A2), were also detected. In the United States, EV-D68 activity varies year to year and regionally; some areas show a biennial pattern and others do not (*7*), yet EV-D68 seems to be seasonal (primarily late summer through fall).

Before 2014, sporadic small regional/local EV-D68 outbreaks were reported in the United States (*8*) and globally. However, during 2014–2016, EV-D68 was the most frequently reported enterovirus in the United States (*9*). Prevalence of nonoutbreak cases is unclear; however, new B clade viruses emerged in 2012 and 2013 (*10*–*12*), and new B subclade and D clade viruses emerged in 2016–2019 (*12*). In contrast to other US regions, activity in Kansas City was minimal in 2015 (*7*), 2016, and 2017 (R. Selvarangan, unpub. data).

Prospective EV-D68 surveillance has recently been undertaken by the New Vaccine Surveillance Network (NVSN, https://www.cdc.gov/surveillance/nvsn/index.html), which includes Kansas City. NVSN reported an uptick in activity in July and October 2018 (*13*) in not only Missouri (54 detections in Kansas City, clade B3 [*14*]) but also Ohio, Tennessee, Pennsylvania, Texas, Washington, and New York. Clade B3 virus in Kansas City was similar to the virus that caused a 2016 outbreak associated with AFM in nonmidwestern US areas. Nevertheless, increased worldwide attention has led to seroprevalence and genotyping reports from multiple countries (*15*–*20*).

EV-D68 community circulation remains underrecognized because clinically used multiplex respiratory PCR assays do not specifically identify EV-D68. We previously evaluated EV-D68 neutralizing antibodies in serum collected in Kansas City during 2012–2013 from persons 2–85 years of age (*21*). Despite no prior documented EV-D68 outbreaks or outbreaks of EV-D68 compatible illnesses in Kansas City, all samples had neutralizing antibodies to the B1 virus, suggesting EV-D68 circulation before the major outbreak in 2014.

Our goals with this study were to use the same assay that we used previously to evaluate neutralizing EV-D68 antibodies to the 2014 clade B1, B2, and D viruses in serum collected during 2017 from children 6 months to 18 years of age, including those born after 2014, and to examine associations of antibody titers with demographic and medical history factors. This study was approved by the institutional review board at Children's Mercy Hospital Kansas City.

Methods

We examined deidentified serum from 300 nonimmunocompromised children 6 months to 18 years of age in Kansas City for EV-D68 neutralizing antibodies. Samples were taken from excess serum after standard-care phlebotomy during April–May 2017 (Appendix, https://wwwnc.cdc.gov/EID/article/28/3/21-1467-App1.pdf). We matched age, sex, and race distributions with those from 2016 Kansas City pediatric census data (*10*). We used the following age groups: 6–35 months of age (n = 76) born after September 2014 (post-outbreak), 36–71 months (n = 51), 72 months–10 years (n = 70), 11–15 years (n = 69), and >15 years (n = 34). We excluded serum from children younger than 6 months because of confounding transplacentally acquired maternal EV-D68 antibodies. We used electronic medical records to document patient age, sex, race, family size, underlying conditions, and number of both hospitalizations and of chest radiographs in the prior 3 years.

The Centers for Disease Control and Prevention (CDC; Atlanta, Georgia, USA) performed serologic testing for this study, using the same microneutralization assay as in our previous study, adapted from a standardized polio antibody assay (*22*,*23*). Three phylogenetically distinct EV-D68 viruses were used: 2014 Missouri 14-18949 (clade B1, GenBank accession no. KM851227); and 2 non-Missouri 2014 strains 14-18952 (clade B2, GenBank accession no. KM851230)

and 14-18953 (clade D, formerly A2, GenBank accession no. KM851231). The 2014 detection frequency among US patients was >91% for B1, 7.4% for B2, and <2% for D viruses (*10*).

This EV-D68 microneutralization assay performed at CDC was previously published (*21*,*24*,*25*). In brief, 2-fold serum dilutions, 1:8 to 1:1,024, were combined with 100 cell culture 50% infectious doses of EV-D68 to enable antibody to bind to virus. After 3 hours of incubation, each virus–serum mixture was inoculated onto rhabdomyosarcoma (CCL-136; American Type Culture Collection, https://www.atcc.org) cell monolayers. CDC tested each serum dilution in triplicate against each virus. Each run had known positive control serum (horse antibodies against the Fermon prototype EV-D68 virus); multiple (≥4) positive control replicates were distributed across each run. When >7 serum samples were tested in the same run, sample position was randomized via a balanced block randomization scheme. Each run included 2 control plates with no serum or control antibodies; rhabdomyosarcoma cells alone served as a no-virus control. A back-titration virus–control plate was used for each of the 3 EV-D68 strains to confirm the amount of antigen used in each run. A luminescent cell viability kit (ATPlite; Perkin Elmer, http://www.perkinelmer.com) was used to evaluate neutralization, and samples with luminescent activity at a titer of >3 $\log_2$ (1:8 dilution) were considered to be positive for neutralizing antibodies (*21*,*24*,*25*).

We performed statistical analyses by using Sigmaplot version 12.2 (http://www.sigmaplot.co.uk) for univariate and multivariate analyses; we considered $p<0.05$ to be significant. We assigned a value of $\log_2$ 2.5 to seronegative samples. We did not analyze ethnicity and daycare attendance because of incomplete data. Categorical values were analyzed by using the χ^2 test. We analyzed antibody titers by using the Kruskal-Wallis rank-sum test to determine if overall distributions' medians significantly differed among groups, and we performed subset comparisons by using the Kolmogorov-Smirnov test. We assessed differences between viruses in each age group by using nonparametric analysis of variance and adjusted for multiple comparisons by using Tukey-Kramer comparisons. To determine whether responses differed between children born after the outbreak and in the year of the outbreak, we used a subset analysis of variance to compare titers for children born in 2014, 2015, and 2016.

We presented comparisons of antibody titer distributions as reverse cumulative distributions (RCD; Appendix). We compared areas under the curve (AUCs) of the RCD curves for each age group among viruses and for each virus among age groups, to represent overall population neutralizing antibody responses by age group (Figure) and by virus (Appendix Figure).

For univariate analysis of demographic and underlying condition data, we used the Mann-Whitney rank sum or the Kruskal-Wallis test, as appropriate. We then used multivariable logistic regression based on binary outcome of high versus low titer to analyze factors significant by univariate analyses.

Results

Samples were from 300 patients with a median age of 6.0 years (range 0.5–17.9 years), and 152 (51%) patients were male. Self-reported race/ethnicity from medical records indicated that 200 (66.6%) patients were White, 49 (16.3%) Black, 45 (15.0%) mixed/other, 6 (2%) Asian, 6 (2.0%) Native American, and 1 Micronesian. In total, 33 patients self-reported as Hispanic/Latino and 8 were listed as non-Hispanic/Latino; ethnicity was not available in the medical records for 259 (86.3%) patients. Families can opt out of reporting ethnicity when registering at our institution. Family size averaged 4.4 ± 1.1 members. Overall, the mean number of hospital admissions in the previous 3 years was 1.4 ± 1.1 (range 0–6). Underlying conditions were reported for 130 (43.3%): asthma, 39 (13.0%); neurologic disease, 25 (8.3%); diabetes mellitus, 16 (5.3%); cardiac disease, 15 (5%); renal disease, 13 (4.3%); other lung conditions, 6 (2.0%); blood disorder not cancer, 6 (2.0%); and other disease (hepatic, metabolic, other endocrine), 10 (3.3%).

In all 300 samples, neutralizing antibodies against B1 virus were detected (i.e., ≥3 $\log_2$, 1:8 titer) (Table 1). Seropositive rates were lower for B2 (254/300, 84.7%) than for B1 (100%) or D virus 296/300 (98.7%; $p<0.001$ for each).

More samples were seronegative for B2 (n = 76) than for D virus (n = 6). Male patients were overrepresented among those seronegative for B2 virus, 65% (30/46) compared with the overall sample set, for which 48% (122/254) were male (odds ratio 2.029, 95% CI 1.054–3.905; p = 0.03). For the B2 virus, the seronegative rate was higher (25/76, 32.9%) among patients 6–35 months of age (all born after the 2014 outbreak) than among those ≥36 months of age (21/224, 9.4%) and born before the 2014 outbreak. Two patients 6–35 months of age were seronegative for both B2 and D viruses. Seronegative rates did not differ by race (data not shown).

Median neutralizing titers rose with advancing age ($p<0.001$; Table 1), but titers among patients 11–15 years of age were similar to those among patients >15

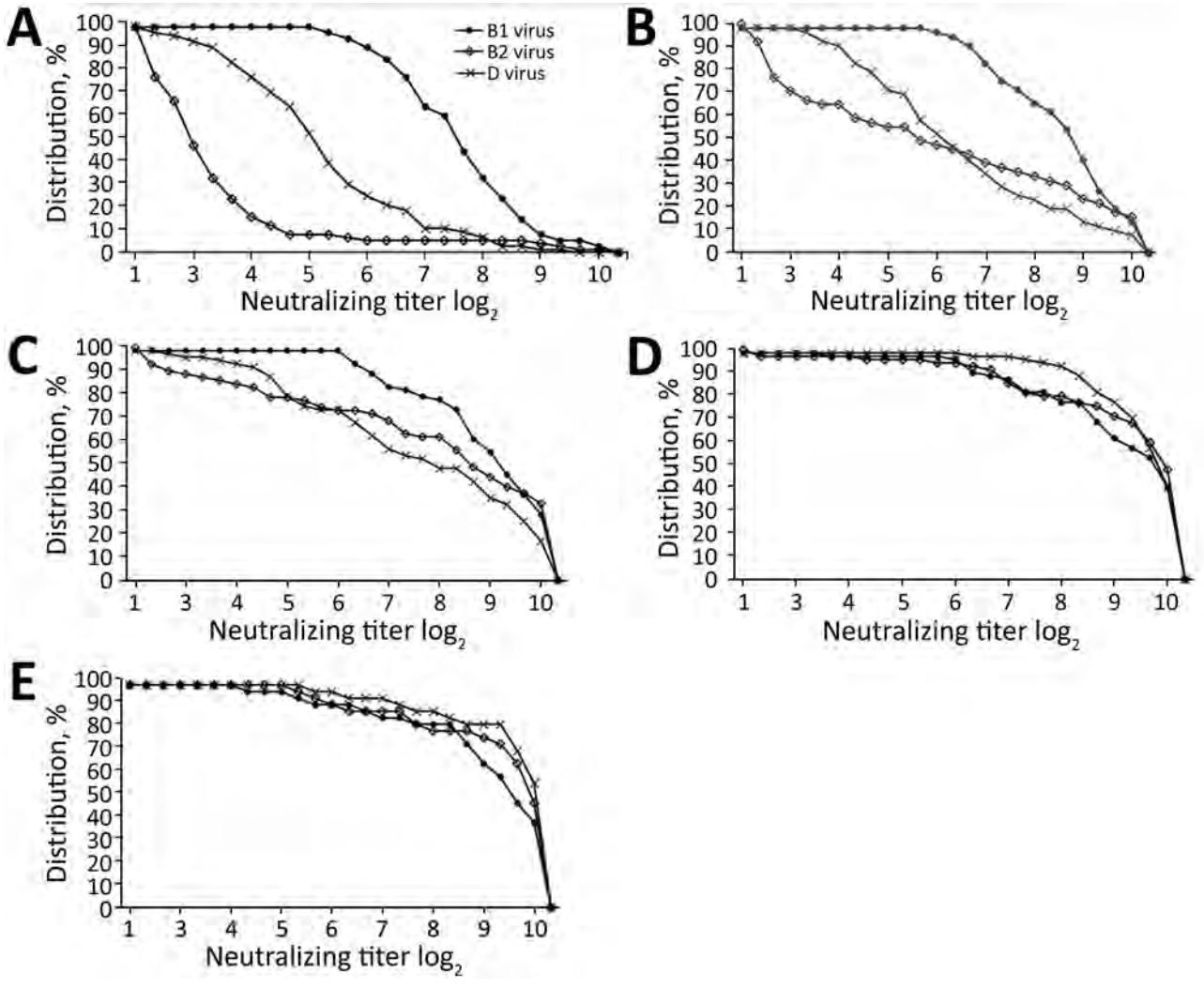

Figure. Reverse cumulative distribution (RCD) curves of enterovirus D68 (EV-D68) representing the distribution of neutralizing antibody titers against 3 EV-D68 viruses (clades B1, B2, and D) in serum samples obtained in 2017 from children <18 years of age in Kansas City, Missouri, USA, by patient age group. A) 6–35 months of age; B) 36–71 months of age; C) 72 months–10 years of age; D) 11–15 years of age; E) 16–18 years of age. A titer >3.0 $\log_2$ was considered positive for neutralizing antibodies. RCDs are curves for which each data point is the proportion of the population with a titer at least as high as the value on the x-axis. The calculated values for each area under curve (AUC) enable comparison of overall immune responses among age groups. Each panel shows 3 RCDs (1 for each virus). Panel A shows that the widest divergence of curves occurred among patients 6–35 months of age, who were born after the 2014 outbreak, suggesting less cross-neutralization among the 3 related viruses in this age group. RCDs become more convergent with each increasing age group. The largest AUCs in each age group are for the B1 predominant 2014 outbreak virus.

years of age. The overall median titer was highest for B1 viruses (9.17 $\log_2$, range 5.5–10.5 $\log_2$) and lowest for D viruses (7.5 $\log_2$, range 2.5–10.5 $\log_2$; p<0.001). We found no significant differences in median titers for any of the 3 viruses between children born in 2014, 2015, or 2016 (data not shown). Overall, neutralizing titers did not differ by sex, race, or family size (data not shown).

Patients 8–13 years of age, whose samples were obtained in 2017, would have been 5–10 years of age (the age group previously documented to have had the most severe disease) in 2014 (*21*). The median B1 virus titer for those 8–13 years of age in 2017 is higher (9.83, interquartile range [IQR] 9.5–10.5) than titers for those who were either 8–13 (8.17, IQR 5.83–9.83) or 5–10 (7.83, IQR 4.17–10.5) years of age in 2012–2013 (*21*). Likewise, low titers were more frequent in serum collected in 2012 than in 2017 (Table 2).

RCD curves show differences in the distribution of 5 age groups of patients (Figure); titers of neutralizing antibodies against the 3 viruses targeted in the neutralization assays are expressed along

Table 1. Serum neutralizing antibody positivity and titers for enterovirus D68 clades B1, B2, and D, by patient age group, Kansas City, Missouri, USA, 2017

Age group	No. patients	% Neutralizing antibody positive, median (range) neutralizing antibody titer*		
		B1 clade virus	B2 clade virus	D clade virus
6–35 mo	76	100, 7.83 (5.50–10.5)	76.9, 3.17 (2.5–10.5)	98.1, 5.5 (2.5–9.83)
36–71 mo	51	100, 9.17 (6.17–10.5)	89.8, 6.00 (2.5–10.5)	100, 6.5 (3.5–10.5)
72 mo−10 y	70	100, 9.50 (6.50–10.5)	96.7, 8.83 (2.5–10.5)	99.5, 8.17 (2.83–10.5)
11–15 y	69	100, 10.17 (6.5–10.5)	99.3, 10.17 (2.5–10.5)	100, 10.17 (3.83–10.5)
>15 y	34	100, 10.5 (5.83–10.5)	100, 10.50 (5.5–10.5)	100, 10.5 (4.5–10.5)
Total	300	100, 9.17 (5.5–10.5)	84.6, 7.83 (2.5–10.5)	99.6, 7.50 (2.5–10.5)

*Antibody titers were measured by using the cell viability kit ATPlite (Perkin Elmer, http://www.perkinelmer.com); the titers shown are the $\log_2$ inverse dilution of the lowest antibody concentration with luminescent activity. Seronegative patients are included.

the x-axis. We calculated AUCs and used them for comparative analyses.

The RCDs for the 3 viruses became less divergent with advancing age group. RCD curve AUCs for B1 were larger than those for B2 or for D viruses in the 3 younger age groups, ($p<0.001$ for each). Within the 2 older age groups, RCD profiles did not differ significantly.

When we evaluated the RCDs for each of the 3 viruses (Appendix Figure) for the 5 age groups, overall RCDs were larger for B1 than for B2 or D viruses ($p<0.01$). RCD AUCs for each virus became larger with advancing age groups (i.e., smallest for those 6–36 months of age and largest for those >15 years of age). For each virus, RCD differences were most notable for the 3 youngest age groups. Indeed, RCD curves for the 11-15–year age group and the >15 years age group were larger than curves for the 3 younger age groups ($p<0.001$ for each virus; Appendix Figure).

We performed univariate analysis for associations by using median titer differences. We noted significant differences for patients with asthma (higher median titer 10.17 [IQR 9.17–10.5] vs. 9.17 [IQR 7.83–10.17]; $p = 0.001$) by univariate analysis (Table 3). Median titers were higher for those who had been hospitalized during the previous 3 years ($p = 0.036$) but not for the subset admitted specifically for respiratory illness. Other associated factors, but with lower median titers, were chronic nonasthma lung disease (lower median titer 7.17 [IQR 6.75–8.83] vs. 9.5 [IQR 8.09–10.17]; $p = 0.01$), congenital heart disease (lower median titer 8.17 [IQR 7.17–8.5] vs. 9.5 [IQR 8.17–10.5]; $p = 0.02$), and a chest radiograph performed in the previous 3 years ($p<0.001$). Two factors, daycare attendance and ethnicity, were not analyzed because of insufficient patient numbers with data documented in the medical record. For analyzed underlying conditions, no differences were associated with diabetes mellitus, other endocrine disorders, hematologic illness (immune-compromising conditions were excluded), neurologic, renal, hepatic, or metabolic diseases (data not shown)

Multivariate analysis based on binary categorization (high vs. low titer) and using variables that were significant in univariate analyses revealed persistent significance for a history of asthma (higher titers). However, when we excluded children <24 months of age from the analysis (given that titers are associated with age and no patient in the asthma group was <24 months of age), significantly higher titers persisted for B2 and D viruses only (Appendix Table).

Discussion

All samples, even from children born after the 2014 outbreak and as young as 6 months, contained EV-D68 neutralizing antibodies to the 2014 outbreak B1 virus. This finding indicates that the outbreak virus, or a closely related EV-D68 strain, circulated in Kansas City from 2014 through 2017. EV-D68 was not detected in the clinical or research laboratory at Children's Mercy Hospital Kansas City during 2015 or 2017 from research surveillance or clinical samples obtained from children receiving medical care at that hospital. Yet EV-D68 activity in Kansas

Table 2. Low versus high neutralizing antibody titers for enterovirus D68 clades B1, B2, and D in serum collected in 2017 compared with titers previously reported from 2012–2013, from patients <18 years of age, Kansas City, Missouri, USA*

Group	Total	No. (%) patients		
		B1 clade virus	B2 clade virus	D clade virus
Serum obtained in 2017	300			
Low titer†		0	110 (36.7)	66 (22.0)
High titer		300 (100)	190 (63.3)	234 (78.0)
Serum obtained in 2012–2013 (*18*)	273			
Low titer†		54 (19.8)	117 (42.9)	133 (48.7)
High titer		219 (80.2)	156 (57.1)	140 (51.3)

*Antibody titers were measured by using the cell viability kit ATPlite (Perkin Elmer, http://www.perkinelmer.com). Seronegative patients are included.
†Low neutralizing titer defined as <6 $\log_2$ (<1:64 titer).

Table 3. Neutralizing antibody titers for enterovirus D68 clades B1, B2 and D, in patients >24 months of age with and without a clinical diagnosis of asthma, Kansas City, Missouri, USA, 2017

Group	No. patients	Neutralizing antibody, median (range)*		
		B1	B2	D
Asthma†	39	9.83 (5.50–10.50)	9.17 (2.50–10.50)	9.17 (3.17–10.50)
No asthma	214	9.50 (5.83–10.50)	8.83 (2.50–10.50)	8.17 (2.50–10.50)
Total	253	9.50 (5.50–10.50)	9.17 (2.50–10.50)	8.83 (2.50–10.50)

*Antibody titers were measured by using the cell viability kit ATPlite (Perkin Elmer, http://www.perkinelmer.com); the titers shown are the $\log_2$ inverse dilution of the lowest antibody concentration with luminescent activity. Includes seronegative patients.
†Asthma as noted by clinician diagnosis in electronic medical record. Because no patients had an asthma diagnosis at <24 mo of age, to balance the age distributions of the nonasthma group with the asthma age group, we excluded nonasthma patients <24 mo of age from this analysis.

City after, and presumably during, 2014 may have contributed to the higher titers in samples collected in spring 2017 compared with titers in samples collected in 2012 from children of comparable ages. EV-D68 was detected in 11 routine clinical samples in 2016 and in 255 NVSN research samples collected in 2018 (*13*), but the 2018 detections were all later than the April 2017 date of the samples in our study. Furthermore, excess hospital admissions for severe respiratory disease, particularly intensive care unit admissions, such as had been noted in 2014, were infrequent among children seeking care at our Kansas City institution during 2015–2017 (C.J. Harrison, unpub. data). The only outbreak detected in Kansas City after the 2014 outbreak was caused by a B3 virus in 2018 (*13*) (a national EV-D68 outbreak occurred in 2018 and was associated with increased reports of AFM and emergency department visits/hospitalizations for EV-D68 respiratory illnesses) (*13*).

Our data also confirm age-associated higher titers (e.g., generally increasing median titers and larger RCD curves for the B1 2014 outbreak virus with each increasing age group), the highest being from those in the 2 oldest age groups. Indeed, data for children ≥11 years of age were remarkably similar to our previously reported data for children of these same ages and to our previous data for adults and elderly persons (*21*). Titers increasing with patient age suggest EV-D68 exposures during nonoutbreak interval years without detected EV-D68 illnesses. If there had been only a single exposure, one might expect antibody titers to peak within 6 months and then decline unless re-exposure occurs (*26*). Nevertheless, higher titers with age could also result in part from increasing EV-D68 antibody specificity over time after initial infection.

Although overall B1 virus titers were lowest for those in the youngest age group (6–35 months), titers were universally ≥5.0 $\log_2$ (≈1:64) even in children born since 2014, also suggesting B1 virus circulation sometime during 2015–2017. Alternatively, antibodies elicited by exposure to undetected but related non-B1 viruses may cross-neutralize the targeted viruses (e.g., B1, B2, and D). However cross-neutralization activity may be variable, as suggested by overall differences in titers against B1 virus compared with B2 and D and age-associated differences for each virus. Of note, B2 and D viruses were not detected in Kansas City in 2014 (*8*,*10*). Indeed, the low rates of seronegativity to both B2 and the 2014 D virus in our current and prior studies suggest that antibodies induced by the 2014 B1 virus cross-neutralize B2 and D viruses. Such cross-neutralization seems reasonable given the close relatedness of the B1 and B2 viruses and the less but still relatively close relatedness of the D virus (*27*).

Comparing our data with data from other serosurveys shows similarities and differences. We confirmed our prior data and those of others (i.e., higher overall titers in serosurveys performed soon after outbreak years). A 2011 study from China showed higher neutralizing titers to locally circulating Beijing/2008/01 EV-D68 in postoutbreak 2011 samples compared with preoutbreak 2004 samples, despite few reported EV-D68 illnesses in the Beijing area during 2009–2011 (*16*). Likewise, more recent data from China, Taiwan, the Netherlands, and the United Kingdom show the same pattern of higher neutralization titers in years soon after outbreaks (*20*,*28*).

Similarly, the age-dependent increases in neutralizing titers in this and our previous study (*21*) parallel prior data (*15*,*18*–*20*,*28*,*29*) regardless of any temporal relation to outbreak years. Nevertheless, it was somewhat surprising that titers from 2017 in Kansas City, even in patients born after the 2014 outbreak, were uniformly ≥1:64 against the 2014 B1 virus outbreak strain. Furthermore, low neutralizing titers (defined as <5 $\log_2$ or <1:32) were less common in serum collected in 2017 than in our previously reported samples collected from children during 2012–2013 (*21*) against the 2014 major B1 virus (0/300 vs. 54/273 [19.8%]), against B2 virus (110/300 [36.7%] vs. 117/273 [42.9%]), and against D virus (66/300 [22.0%] vs. 133/273 [48.7%]).

Although differences in the assays used by other investigators (e.g., target virus) make comparing

absolute titers challenging, our seropositivity rates for patients 6–35 months of age were also higher than those found in other studies before and after the 2014 outbreak (*15*,*17*,*18*,*28*,*29*). It is possible that the modest EV-D68 activity detected in Kansas City in 2016 led to mild or asymptomatic infections in younger children and boosted titers in older children.

We also detected higher titers associated with a history of asthma, but after excluding children too young to have an asthma diagnosis, we found significantly higher titers for only the B2 and D viruses. Nevertheless, asthma was the only underlying condition associated with high titers in multivariate analysis. In 2014, severe EV-D68 respiratory disease occurred in children up to 10 years of age and in populations with atopic disease, asthma, or reactive airway disease, despite what seems to have been the universal presence of neutralizing antibodies, at least in Kansas City children (*8*,*21*). This finding suggests that the mere presence of neutralizing antibodies at a $\log_2$ titer $\geq$3.0 may not be protective against disease, at least in some populations. Protection may occur only if sufficient serum neutralizing antibodies are available. For example, severe respiratory tract disease or AFM is unusual or nonexistent among those in age groups with the highest overall neutralizing titers: adolescents, adults, or the elderly (most with titers >1:256 [i.e., $\log_2 \geq 8$] in our current and prior studies [*21*]).

Of note, in our current study, neutralizing activity against the non-B1 viruses was higher in children who had asthma as an underlying condition, suggesting an altered response to infection resulting from genetic factors or perhaps to asthma itself (*4*). For example, asthma is associated with enhanced tight junction injury from rhinovirus infection (*30*). Alternatively, immunopathologic responses may play a role, as can be seen in the influenza cotton rat model (*31*). Serum neutralizing antibodies also may not correlate best with protection. For example, T-cell activity or mucosal antibodies may be more protective than serum antibodies (*32*), or perhaps antibodies to certain epitopes are crucial, as suggested in an EV-D68 mouse model in which monoclonal antibodies were more effective than convalescent polyclonal antibodies in intravenous immunoglobulin preparations (*33*).

Unlike one previous study (*29*), we did not find family size to be associated with seropositivity. We could not evaluate our prior observation of lower titers in Hispanic patients (*21*) because of low numbers of self-reports of ethnicity (41/300). Similarly, we could not analyze effects of daycare (data available for only 36/300).

Limitations of our study include a study design that used salvaged samples and a retrospective chart review. Because we tested for neutralizing antibodies against only 3 EV-D68 strains, patterns of neutralizing activity against other EV-D68 strains could differ. However, we did test for the 2014 B1 clade strain known to have circulated in Kansas City as well as B2 and D viruses. EV-D68 activity in Kansas City during 2016 and 2020 (D) was low but could have boosted titers. Indeed, we also noted EV-D68 activity in 2018 (B3) and 2020 (clade unknown). Age ranges for our pediatric groups could be considered arbitrary; the age groups we used were similar to those used in our previous study, except we added children 6–35 months of age, paralleling other reports (*3*). The racial and age distributions of our population matched those of Kansas City census data and, therefore, might not be generalizable to other geographic areas. That said, these distributions closely mirrored those of the United States as a whole during 2015–2017. Last, the numbers of patients with each underlying condition were relatively small, so we may not have had the power to detect associations (e.g., higher titers to B1 virus in those with asthma).

In conclusion, we detected neutralizing antibodies to the dominant 2014 B1 clade EV-D68 virus at titers $\geq$1:64 for all 300 serum samples from children in 2017, a time frame with little documented EV-D68 activity since the 2014 outbreak. In the same samples, overall titers to the less frequently detected B2 and D viruses were lower. Titers increased with increasing age. Titers against B2 and D virus were higher in those with asthma. Our findings support the concepts that an unusual host–virus interaction of EV-D68 occurs in children with asthma and that EV-D68 can cause disease despite the presence of at least some neutralizing antibodies.

Acknowledgments

We thank Yiting Zhang, Deborah Moore, Sharla McDonald, Will Hendley, Mario Nicolas, and Patricia Mitchell for EV-D68 serology testing. We also thank William C. Weldon and M. Steven Oberste for project advice and overseeing the serology work at CDC. We thank the Medical Writing Center at Children's Mercy Hospital Kansas City for editing this manuscript.

About the Author

Dr. Livingston is an associate professor of pediatrics at the University of Missouri at Kansas City and medical director of Infection Prevention and Control at Children's Mercy Hospital Kansas City, Kansas City, Missouri, USA.

References

1. Aliabadi N, Messacar K, Pastula DM, Robinson CC, Leshem E, Sejvar JJ, et al. Enterovirus D68 infection in children with acute flaccid myelitis, Colorado, USA, 2014. Emerg Infect Dis. 2016;22:1387–94. https://doi.org/10.3201/eid2208.151949
2. Greninger AL, Naccache SN, Messacar K, Clayton A, Yu G, Somasekar S, et al. A novel outbreak enterovirus D68 strain associated with acute flaccid myelitis cases in the USA (2012–14): a retrospective cohort study. Lancet Infect Dis. 2015;15:671–82. https://doi.org/10.1016/S1473-3099 (15)70093-9
3. Khetsuriani N, Lamonte-Fowlkes A, Oberst S, Pallansch MA; Centers for Disease Control and Prevention. Enterovirus surveillance—United States, 1970–2005. MMWR Surveill Summ. 2006;55:1–20.
4. Schuster JE, Miller JO, Selvarangan R, Weddle G, Thompson MT, Hassan F, et al. Severe enterovirus 68 respiratory illness in children requiring intensive care management. J Clin Virol. 2015;70:77–82. https://doi.org/10.1016/j.jcv.2015.07.298
5. Wang H, Diaz A, Moyer K, Mele-Casas M, Ara-Montojo MF, Torrus I, et al. Molecular and clinical comparison of enterovirus D68 outbreaks among hospitalized children, Ohio, USA, 2014 and 2018. Emerg Infect Dis. 2019;25:2055–63. https://doi.org/10.3201/eid2511.190973
6. Oermann CM, Schuster JE, Conners GP, Newland JG, Selvarangan R, Jackson MA. Enterovirus D68. A focused review and clinical highlights from the 2014 U.S. outbreak. Ann Am Thorac Soc. 2015;12:775–81. https://doi.org/10.1513/AnnalsATS.201412-592FR
7. Park SW, Pons-Salort M, Messacar K, Cook C, Meyers L, Farrar J, et al. Epidemiological dynamics of enterovirus D68 in the United States and implications for acute flaccid myelitis. Sci Transl Med. 2021;13:eabd2400. https://doi.org/10.1126/scitranslmed.abd2400
8. Midgley CM, Watson JT, Nix WA, Curns AT, Rogers SL, Brown BA, et al.; EV-D68 Working Group. Severe respiratory illness associated with a nationwide outbreak of enterovirus D68 in the USA (2014): a descriptive epidemiological investigation. Lancet Respir Med. 2015;3:879–87. https://doi.org/10.1016/S2213-2600(15)00335-5
9. Abedi GR, Watson JT, Nix WA, Oberste MS, Gerber SI. Enterovirus and parechovirus surveillance—United States, 2014–2016. MMWR Morb Mortal Wkly Rep. 2018;67:515–8. https://doi.org/10.15585/mmwr.mm6718a2
10. Huang W, Wang G, Zhuge J, Nolan SM, Dimitrova N, Fallon JT. Whole-genome sequence analysis reveals the enterovirus D68 isolates during the United States 2014 outbreak mainly belong to a novel clade. Sci Rep. 2015;5:15223. https://doi.org/10.1038/srep15223
11. Tan Y, Hassan F, Schuster JE, Simenauer A, Selvarangan R, Halpin RA, et al. Molecular evolution and intraclade recombination of enterovirus D68 during the 2014 outbreak in the United States. J Virol. 2015;90:1997–2007. https://doi.org/10.1128/JVI.02418-15
12. Eshaghi A, Duvvuri VR, Isabel S, Banh P, Li A, Peci A, et al. Global distribution and evolutionary history of enterovirus D68, with emphasis on the 2014 outbreak in Ontario, Canada. Front Microbiol. 2017;8:257. https://doi.org/10.3389/fmicb.2017.00257
13. Kujawski SA, Midgley CM, Rha B, Lively JY, Nix WA, Curns AT, et al. Enterovirus D68–associated acute respiratory illness—New Vaccine Surveillance Network, United States, July–October, 2017 and 2018. MMWR Morb Mortal Wkly Rep. 2019;68:277–80. https://doi.org/10.15585/mmwr.mm6812a1
14. Pakala SB, Tan Y, Hassan F, Mai A, Markowitz RH, Shilts MH, et al. Nearly complete genome sequences of 17 enterovirus D68 strains from Kansas City, Missouri, 2018. Microbiol Resour Announc. 2019;8:e00388-19. https://doi.org/10.1128/MRA.00388-19
15. Sun S, Gao F, Hu Y, Bian L, Wu X, Su Y, et al. A cross-sectional seroepidemiology study of EV-D68 in China. Emerg Microbes Infect. 2018;7:99. https://doi.org/10.1038/s41426-018-0103-4
16. Xiang Z, Li L, Ren L, Guo L, Xie Z, Liu C, et al. Seroepidemiology of enterovirus D68 infection in China. Emerg Microbes Infect. 2017;6:e32. https://doi.org/10.1038/emi.2017.14
17. Sun SY, Gao F, Hu YL, Bian LL, Mao QY, Wu X, et al. Seroepidemiology of enterovirus D68 infection in infants and children in Jiangsu, China. J Infect. 2018;76:563–9. https://doi.org/10.1016/j.jinf.2018.02.003
18. Liu Y, Gong C, Luo M, Zhang T, Li M, Shen L, et al. Seroepidemiology of enterovirus D68 in a healthy population in Beijing, China, between 2012 and 2017: a retrospective study. J Med Virol. 2020.
19. Hu YL, Huang LM, Lu CY, Fang TY, Cheng AL, Chang LY. Manifestations of enterovirus D68 and high seroconversion among children attending a kindergarten. J Microbiol Immunol Infect. 2019;52:858–64. https://doi.org/10.1016/j.jmii.2019.04.010
20. Karelehto E, Koen G, Benschop K, van der Klis F, Pajkrt D, Wolthers K. Enterovirus D68 serosurvey: evidence for endemic circulation in the Netherlands, 2006 to 2016. Euro Surveill. 2019;24. https://doi.org/10.2807/1560-7917.ES.2019.24.35.1800671
21. Harrison CJ, Weldon WC, Pahud BA, Jackson MA, Oberste MS, Selvarangan R. Neutralizing antibody against enterovirus D68 in children and adults before 2014 outbreak, Kansas City, Missouri, USA. Emerg Infect Dis. 2019;25:585–8. https://doi.org/10.3201/eid2503.180960
22. Wallace GS, Pahud BA, Weldon WC, Curns AT, Oberste MS, Harrison CJ. Seroprevalence of poliovirus antibodies in the Kansas City metropolitan area, 2012–2013. Hum Vaccin Immunother. 2017;13:776–83. https://doi.org/10.1080/21645515.2016.1255386
23. Weldon WC, Oberste MS, Pallansch MA. Standardized methods for detection of poliovirus antibodies. In: Walker JM, editor. Methods in Molecular Biology. New York: Humana Press; 2016. p. 145–76.
24. Schieble JH, Fox VL, Lennette EH. A probable new human picornavirus associated with respiratory diseases. Am J Epidemiol. 1967;85:297–310. https://doi.org/10.1093/oxfordjournals.aje.a120693
25. Oberste MS, Maher K, Schnurr D, Flemister MR, Lovchik JC, Peters H, et al. Enterovirus 68 is associated with respiratory illness and shares biological features with both the enteroviruses and the rhinoviruses. J Gen Virol. 2004;85:2577–84. https://doi.org/10.1099/vir.0.79925-0
26. Kadji FMN, Nishimura H, Okamoto M, Sato K, Ohmiya S, Ito H, et al. Fluctuations in antibody titers against enterovirus D68 in pediatric sera collected in a community before, during, and after a possible outbreak. Jpn J Infect Dis. 2020;73:55–7. https://doi.org/10.7883/yoken.JJID.2019.056
27. Freeman MC, Wells AI, Ciomperlik-Patton J, Myerburg MM, Yang L, Konopka-Anstadt J, et al. Respiratory and intestinal epithelial cells exhibit differential susceptibility and innate immune responses to contemporary EV-D68 isolates. eLife. 2021;10:10. https://doi.org/10.7554/eLife.66687
28. Kamau E, Harvala H, Blomqvist S, Nguyen D, Horby P, Pebody R, et al. Increase in enterovirus D68 infections in

young children, United Kingdom, 2006–2016. Emerg Infect Dis. 2019;25:1200–3. https://doi.org/10.3201/eid2506.181759
29. Lee JT, Shih WL, Yen TY, Cheng AL, Lu CY, Chang LY, et al. Enterovirus D68 seroepidemiology in Taiwan, a cross sectional study from 2017. PLoS One. 2020;15:e0230180. https://doi.org/10.1371/journal.pone.0230180
30. Looi K, Buckley AG, Rigby PJ, Garratt LW, Iosifidis T, Zosky GR, et al. Effects of human rhinovirus on epithelial barrier integrity and function in children with asthma. Clin Exp Allergy. 2018;48:513–24. https://doi.org/10.1111/cea.13097
31. Blanco JC, Pletneva LM, Wan H, Araya Y, Angel M, Oue RO, et al. Receptor characterization and susceptibility of cotton rats to avian and 2009 pandemic influenza virus strains. J Virol. 2013;87:2036–45. https://doi.org/10.1128/JVI.00638-12
32. Wang SM, Liu CC. Update of enterovirus 71 infection: epidemiology, pathogenesis and vaccine. Expert Rev Anti Infect Ther. 2014;12:447–56. https://doi.org/10.1586/14787210.2014.895666
33. Vogt MR, Fu J, Kose N, Williamson LE, Bombardi R, Setliff I, et al. Human antibodies neutralize enterovirus D68 and protect against infection and paralytic disease. Sci Immunol. 2020;5:eaba4902. https://doi.org/10.1126/sciimmunol.aba4902

Address for correspondence: Christopher J. Harrison, Pediatric Infectious Diseases Division, Department of Pediatrics, Children's Mercy Hospital Kansas City, 2401 Gillham Rd, Kansas City, MO 64108, USA; email: cjharrison@cmh.edu

High-Dose Convalescent Plasma for Treatment of Severe COVID-19

Gil C. De Santis, Luciana Correa Oliveira, Pedro M.M. Garibaldi, Carlos E.L. Almado, Julio Croda, Ghislaine G.A. Arcanjo, Érika A.F. Oliveira, Adriana C. Tonacio, Dante M. Langhi Jr., José O. Bordin, Renato N. Gilio, Leonardo C. Palma, Elaine V. Santos, Simone K. Haddad, Benedito P.A. Prado Jr., Marjorie Cornejo Pontelli, Rogério Gomes, Carlos H. Miranda, Maria Auxiliadora Martins, Dimas T. Covas, Eurico Arruda, Benedito A.L. Fonseca, Rodrigo T. Calado

To assess whether high-dose coronavirus disease (COVID-19) convalescent plasma (CCP) transfusion may benefit patients with severe COVID-19, we conducted a multicenter randomized trial in Brazil. Patients with severe COVID-19 who were within 10 days of initial symptom onset were eligible. Patients in the CCP group received 3 daily doses of CCP (600 mL/d) in addition to standard treatment; control patients received standard treatment only. Primary outcomes were death rates at days 30 and 60 of study randomization. Secondary outcomes were ventilator-free days and hospital-free days. We enrolled 107 patients: 36 CCP and 71 control. At day 30, death rates were 22% for CCP and 25% for the control group; at day 60, rates were 31% for CCP and 35% for control. Needs for invasive mechanical ventilation and durations of hospital stay were similar between groups. We conclude that high-dose CCP transfused within 10 days of symptom onset provided no benefit for patients with severe COVID-19.

Author affiliations: University of São Paulo, São Paulo, Brazil (G.C. De Santis, L.C. Oliveira, E.V. Santos, S.K. Haddad, B.P.A. Prado Jr., D.T. Covas, R.T. Calado); Hospital Estadual de Serrana, Serrana, Brazil (P.M.M. Garibaldi, C.E.L. Almado); Hospital Regional do Mato Grosso do Sul, Campo Grande, Brazil (J. Croda); Fundação Oswaldo Cruz, Campo Grande (J. Croda); Universidade do Mato Grosso do Sul, Campo Grande (J. Croda, G.G.A. Arcanjo); Hospital São Camilo, São Paulo (É.A.F. Oliveira, A.C. Tonacio, D.M. Langhi Jr.); Universidade Federal de São Paulo, São Paulo (D.M. Langhi Jr., J.O. Bordin); Hospital Estadual de Américo Brasiliense, Américo Brasiliense, Brazil (R.N. Gilio); Hospital das Clínicas da Faculdade de Medicina de Ribeirão Preto, Ribeirão Preto, Brazil (L.C. Palma); Faculdade de Medicina de Ribeirão Preto da Universidade de São Paulo, São Paulo (M.C. Pontelli, R. Gomes, C.H. Miranda, M.A. Martins, E. Arruda, B.A.L. Fonseca)

DOI: https://doi.org/10.3201/eid2803.212299

Clinical signs and symptoms of coronavirus disease (COVID-19) are pleomorphic, varying from none (asymptomatic) to life-threatening. Typical signs/symptoms are fever, dry cough, dyspnea, fatigue, myalgia, anosmia, and ageusia (*1*). Radiography or computed tomography of the chest usually reveals bilateral pulmonary ground-glass opacifications, mainly in posterior and peripheral areas of the lungs (*2*). The most common laboratory test alterations are lymphopenia and elevated serum concentrations of inflammatory biomarkers and D-dimers (*3*). Risk factors for unfavorable outcomes are older age, concurrent conditions, and perhaps but of lesser importance, blood type A (*4*,*5*). Thus far, there is no consensual agreement about specific therapy for this disease, despite several attempts to develop one (*3*,*6*). More recently, antiviral agents such as MK-4482/EIDD-2801 and PF-07321332 seem to be promising (*7*,*8*).

In the past, passive antibody transfer by plasma or serum transfusion has been used clinically to treat other infectious diseases, including Ebola, influenza A, severe acute respiratory syndrome, and Middle East respiratory syndrome, as well as COVID-19 (*9*–*13*). The presence of antiviral antibodies, in patient serum or in COVID-19 convalescent plasma (CCP), has been associated with more favorable clinical outcomes (*14*). Thus, CCP seems to be an attractive therapy because it is a potential source of neutralizing antibodies (*15*,*16*).

The first case series reported from China suggested favorable outcomes for 5 patients receiving undergoing mechanical ventilation who received CCP on days 10–22 after hospital admission (*17*). Also in China, 10 critically ill patients received 200 mL of CCP with a neutralizing antibody titer of >640, which resulted in undetectable viral load and clinical improvement for 7 of the 10 patients (*18*). In a nonrandomized

observational study that evaluated 3,082 CCP recipients, transfusion was associated with reduced mortality rates among patients who received CCP that had a higher titer against severe acute respiratory syndrome coronavirus 2 (SARS-CoV-2). Mortality rates within 30 days after CCP transfusion were 22.3% for the high-titer group, 27.4% for the medium-titer group, and 29.6% for the low-titer group. The relative risk for death was lower among patients who were not undergoing mechanical ventilation before transfusion (*19*). A prospective multicenter study in China that involved 103 patients with severe COVID-19 was stopped early, but initial findings suggested that CCP transfusion was associated with a higher percentage of patients being negative for SARS-CoV-2 by reverse transcription PCR (RT-PCR) at 72 hours (87.2%) than for controls (37.5%) (*20*).

Clinical improvement has been observed for Ebola patients with severe manifestations but not for those with life-threatening disease (*9*). Recently, a randomized trial in Argentina involving 228 patients who received CCP (median titer 3,200) and 105 who received placebo found that CCP transfusion did not reduce mortality rates at day 30 after randomization (10.96% for transfused and 11.43% for nontransfused groups) (*21*). A recent systematic review concluded that CCP transfusion makes little or no difference, at least for patients who needed mechanical ventilation (*22*).

To evaluate the efficacy and safety of high-dose CCP transfusion to treat severe COVID-19, we conducted an open-label multicenter randomized controlled trial. This study was approved by the national review board (Comissão Nacional de Ética em Pesquisa, CONEP; CAAE number 30509920.0.1001.0008). Written informed consent was obtained from all patients or legal representatives. The trial was performed in accordance with the principles of the Declaration of Helsinki and the International Conference on Harmonization–Good Clinical Practice guidelines. The trial was registered at the Brazilian Registry of Clinical Trials (http://www.ensaiosclinicos.gov.br, no. RBR-7f4mt9f).

Materials and Methods

Study Design

We conducted our investigator-initiated multicenter open-label randomized controlled trial in 5 hospitals: 4 in the state of São Paulo (Hospital das Clínicas da Faculdade de Medicina de Ribeirão Preto da Universidade de São Paulo, Hospital Estadual de Américo Brasiliense, Hospital São Camilo, and Hospital São Paulo); and 1 in Campo Grande, state of Mato Grosso do Sul (Hospital Regional de Mato Grosso do Sul). The 5 inclusion criteria were 1) diagnosis of COVID-19 based on RT-PCR results; 2) respiratory distress (oxygen saturation at room air ≤93%, or arterial partial pressure of oxygen/fraction of inspired oxygen ≤300, or requiring mechanical ventilation) resulting from pneumonia; 3) being within 10 days of initial symptoms; 4) age 18–80 years; and 5) signed written informed consent by the patient or legal representative. The 7 exclusion criteria were 1) history of previous severe allergy to plasma transfusion, 2) severe congestive heart failure, 3) terminal renal failure, 4) hepatic cirrhosis, 5) any severe illness expected to confer a short life expectancy, 6) participation in any other clinical trial with therapeutic intervention, and 7) immunosuppression. All included participants most likely had COVID-19 caused by the parental virus lineages (during the first wave), before emergence of the Gamma and Delta variants.

We enrolled 120 patients (40 in the CCP group and 80 in the control group), considering predicted death rates of 30% for the CCP group and 50%–60% for the control group. Computer-generated random numbering randomly assigned patients to receive either standard treatment (control) or CCP transfusion added to the standard treatment at a ratio of 2(control):1(CCP). For most patients, CCP transfusion was performed the day of or the day after randomization; only 2 patients received CCP 2 days after randomization. Patients and physicians were not blinded to treatment assignments. Placebo was not administered to control patients because we considered that the infused volume of saline or nonconvalescent plasma could harm the patients, especially those less tolerant to intravenous volume overload (i.e., those who were elderly, had acute kidney injury, or had other concurrent conditions). In addition, we considered it would be impossible to blind infusion of such a large volume of plasma to CCP patients. At the time of randomization, SARS-CoV-2 IgM/IgA was detected in all 65 patients who were tested and IgG was detected in 53 (81.5%).

Convalescent Plasma Procurement and Transfusion

To prevent transfusion-associated lung injury, we limited CCP donor candidates to adult men or nulliparous women (*23*). According to regulation in Brazil, convalescent candidates may donate plasma after 15 days have passed since symptom resolution. Donor screening was similar to that used for conventional blood donation, including clinical evaluation for COVID-19 and access to peripheral veins. Plasma

collection was performed by using a TRIMA ACCEL automated blood collection system (Terumo BCT, Inc., https://www.terumobct.com). We determined neutralizing antibody titers as described elsewhere (*24*). For both groups, transfused CCP median neutralizing antibody titer against SARS-CoV-2 was 128 (minimum titer of 64 in just 1 plasma unit). CCP units did not undergo pathogen reduction.

The total transfusion dose of CCP per patient was 1,800 mL (minimum dose 1,200 mL), divided into 3 daily doses of 600 mL for 3 days. The 600 mL volumes were divided into 2 subunits of 300 mL or 200 and 400 mL. All patients were randomized during days 7–10 after symptom onset, and the first CCP transfusion was administered on day 9 (range 8–10) for both groups. The first CCP transfusion had to be given by day 10 of initial symptoms.

We performed neutralizing assays for serum samples obtained from each plasma unit. In brief, we conducted virus neutralization testing with SARS-CoV-2 in 96-well plates containing 5×10^4 cells/mL of Vero cells (CCL-81). Serum samples were initially inactivated for 30 min at 56°C. We used 11 serial dilutions (1:2 to 1:2,048). Subsequently, we mixed serum and virus (vol/vol) and preincubated the mixture at 37°C for 2 h for neutralization. We transferred the serum/virus mixture onto the confluent cell monolayer and incubated at 37°C at 5% CO_2. After 3 days, we analyzed the plates by using light microscopy to determine presence/absence of cytopathic effect. Neutralizing antibody titer is described as the highest serum dilution that impeded cytopathic effect.

The primary clinical outcome was death rate at days 30 and 60 from the day of randomization. Secondary outcomes were ventilator-free days and hospital-free days on days 30 and 60 after randomization and adverse reactions to plasma transfusion. Adverse events were graded according to the Common Terminology Criteria for Adverse Events version 5.0.

Patient Serologic Testing and Measurement of C-Reactive Protein and Interleukin-6

Using ELISA, we tested serum samples at randomization for the presence of SARS-CoV-2 IgM plus IgA (Vircell, https://www.vircell.com) and IgG (Euroimmun, https://www.euroimmun.com). We measured C-reactive protein (CRP) and interleukin 6 (IL-6) on days 0 and day 7 after randomization.

Statistical Analyses

Results were expressed as mean ± SD or median (range) and proportions according to distribution characteristics. When comparing 2 groups, we used a 2-sided unpaired Student *t*-test (parametric data) or a Mann-Whitney test (nonparametric data). For statistical comparisons of categorical variables between groups, we used the χ^2 test. We generated overall survival estimates by using the Kaplan-Meier method and assessed differences between the groups by using the log-rank test. We considered results to be statistically different when the p value was <0.05 (by 2-tailed testing). We used GraphPAD Prism version 8.4.3 (https://www.graphpad.com) for statistical analyses.

Results

During April–November 2020, we enrolled 110 patients at 5 centers. Because recruiting became more difficult as the number of new cases substantially decreased, we halted recruitment early, before reaching 120 participants. Of the 110, we excluded 3 participants from analysis: 1 in the CCP group did not receive plasma transfusion; 1 in the control group withdrew consent; and 1 in the control group was intubated and underwent invasive mechanical ventilation for neurologic reasons, not pneumonia, a prerequisite for inclusion in this study (Figure 1). The median duration of symptoms before randomization was 8 (range 7–10) days. The median age at randomization was 60 (range 24–80) years; male:female ratio was 1.7:1.0 (Table 1). All patients had severe COVID-19 (≥6 points according to the World Health Organization severity ordinal scale (https://www.who.int/docs/default-source/documents/emergencies/minimalcoreoutcomemeasure.pdf).

Because of low body weight (50 kg), 2 patients received a total of 1,200 mL of CCP. For 2 other patients, CCP doses were divided over 4 days, as allowed by protocol. No participant was unable to be reached during follow-up.

Death Rates

A total of 36 (34%) of the 107 enrolled patients died during hospitalization, 10 after day 30 (median 45.5, range 31–50 days); 3 were in the CCP group and 7 were in the control group (p = 1.00). At randomization day 30, death rates were 22% for the CCP group and 25% for the control group (odds ratio [OR] 0.84, 95% CI 0.32–2.25; p = 0.81). At day 60, death rates were 31% for the CCP group and 35% for the control group (OR 0.81, 95% CI, 0.35–1.86; p = 0.67) (Table 2). We performed a nonscheduled analysis of death rates on day 21 after randomization because at that point it seemed that there could be a difference between the groups, as suggested by the survival curve (Figure 2). We determined that on day 21, there had been a total

of 3/36 (8.33%) deaths in the CCP group and 14/71 (19.7%) deaths in the control group (OR 0.37, 95% CI 0.11–1.3; p = 0.17).

Duration of Mechanical Ventilation and Hospitalization

At randomization day 30, the number of days free of invasive mechanical ventilation was 12.5 (range 0–30) for the CCP group and 12 (range 0–30) for the control group (p = 0.82); at day 60, the number of days was 42.5 (0–60) for the CCP group and 39 (0–60) for the control group (p = 0.80) (Table 2). We did not observe differences in hospital stay duration at days 30 and 60. At day 30, hospital-free days were 3 (0–24) days for the CCP group and 0 (0–28) days for the control group (p = 0.27); at day 60, hospital-free days were 30.5 (0–53) days for the CCP group and 21.0 (0–58) days for the control group (p = 0.43) (Table 2).

Inflammatory Biomarkers

CRP concentrations were elevated at the time of randomization (day 0) and decreased significantly by day 7 in a similar fashion in both groups. The medians (interquartile ranges [IQRs]) on day 0 were 11.4 (3.31–20.55) mg/dL for the CCP group and 12.82 (5.05–24.40) mg/dL for the control group (p = 0.55). On day 7, medians (IQRs) were 2.53 (0.72–6.17) mg/dL for the CCP group and 2.75 (1.19–6.15) mg/dL for the control group (p = 0.52) (Figure 3, panel A). IL-6 concentrations were elevated on days 0 and 7 and, likewise, did not differ significantly between groups. IL-6 medians (IQRs) were 15.20 (6.99–26.00) pg/mL on day 0 and 13.80 (7.95–37.95) pg/mL on day 7 (p = 0.88) for the CCP group and 16.00 (6.61–30.40) pg/mL on day 0 and 18.65 (6.40–54.85) pg/mL on day 7 (p = 0.72) for the control group (Figure 3, panel B).

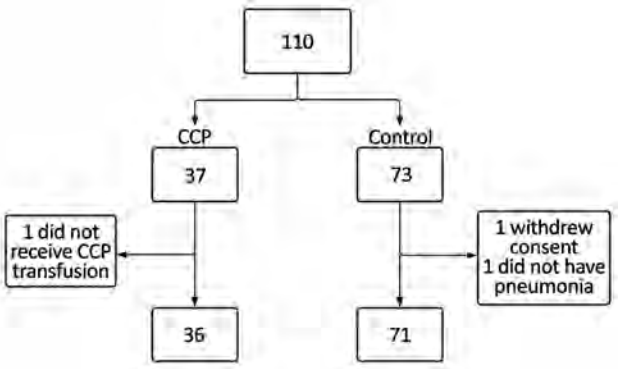

Figure 1. Enrollment and randomization process for study of high-dose CCP for treatment of severe COVID-19, Brazil. COVID-19, coronavirus disease; CCP, COVID-19 convalescent plasma.

Safety

No serious adverse reactions attributable to CCP transfusion were observed during study follow-up. We considered severe reactions to be greater than grade 3 according to the Common Terminology Criteria for Adverse Events version 5.0 (https://ctep.cancer.gov).

Discussion

In this randomized clinical trial, transfusion of high-dose CCP did not reduce death rates, hospitalization durations, or number of days receiving mechanical ventilation for patients with very severe COVID-19.

Table 1. Baseline demographics and clinical characteristics of participants in study of high-dose convalescent plasma for treatment of severe COVID-19, Brazil*

Variable	CCP, n = 36	Control, n = 71	p value
Demographic			
Age, mean ± SD, y	56.11 ± 15.15	59.25 ± 12.35	0.25
Sex, no. (%)			
M,	23 (63.89)	44 (64.79)	1.0
F	13 (36.11)	27 (35.21)	
Body mass index, median (range), kg/m^2	29.75 (18.37–58.00)	29.41 (20.31–74.22)	0.88
Weight, median (range), kg	85 (50–156)	85 (50–190)	0.95
Underlying conditions			
Hypertension, no. (%)	19 (52.78)	41 (57.75)	0.68
Diabetes mellitus, no. (%)	12 (33.33)	29 (40.85)	0.53
Renal replacement therapy, no. (%)	13 (36.11)	27 (38.03)	1.0
SAPS-3 score, median (range)†	56 (37–94)	68 (39–100)	0.15
SOFA score, median (range)	7.5 (1.0–14.0)	9.0 (2.0–14.0)	0.17
Clinical characteristic			
Mechanical ventilation, no. (%)	32 (88.88)	58 (81.69)	0.41
D-dimer, median (range), μg/mL‡	1.02 (0.27–10.00)	1.65 (0.39–20.00)	0.12
Blood type O/A§	13/18	31/27	0.38
Blood type, rH positive/negative§	33/3	67/3	0.41

*CCP, COVID-19 convalescent plasma; COVID-19, coronavirus disease; CRP: C-reactive protein; SAPS-3 score, Simplified Acute Physiology Score 3 at admission to intensive care unit; SOFA score, Sequential Organ Failure Assessment (on day of randomization) for 20 CCP and 41 control patients.
†31 CCP and 57 control patients.
‡23 CCP and 39 control patients on day of randomization.
§106 patients.

Table 2. Clinical outcomes for participants in study of high-dose convalescent plasma for treatment of severe COVID-19, Brazil*

Outcome	CCP, n = 36	Control, n = 71	p value
Death at HD 30, no. (%)	8 (22.22)	18 (25.35)	0.81
Death at HD 60, no. (%)	11 (30.55)	25 (35.21)	0.67
Ventilator-free days at HD 30†	12.5 (0–30)	12.0 (0–30)	0.82
Ventilator-free days at HD 60‡	42.5 (0–60)	39.0 (0–60)	0.80
Hospital-free days at HD 30†	3 (0–24)	0 (0–28)	0.27
Hospital-free days at HD 60§	30.5 (0–53)	21.0 (0–58)	0.45

*CCP, COVID-19 convalescent plasma; COVID-19, coronavirus disease; HD, hospitalization day.
†35 CCP and 70 control samples.
‡33 CCP and 67 control samples.
§33 CCP and 69 control samples.

We detected a slightly reduced death rate, but it did not reach statistical significance. Serum inflammatory biomarkers were also reduced, but CCP transfusion did not influence the reduction. All enrolled patients experienced severe respiratory failure resulting from viral pneumonia, and most of them were undergoing invasive mechanical ventilation. Most patients had ≥1 concurrent condition, which increases mortality rates (*25*). More than one third of the enrolled patients needed kidney replacement therapy (hemodialysis). These characteristics emphasize the extreme severity of COVID-19 in the patients in our cohort. Participants received CCP as soon as possible, always within 10 days of symptom onset. This transfusion window was considered adequate at the time of the study planning and execution, especially when compared with other studies, in which transfusion occurred as late as day 39 (*9*). Of note, we observed that most trials evaluated the death rate at days 28 or 30 of randomization, but we observed that more than one fourth of the deaths in our study occurred during days 30–60.

Our results challenge those of nonrandomized studies previously conducted at the beginning of the pandemic (*17*), as well as those of a large nonrandomized study involving >3,000 US patients, which suggested that CCP could be an efficacious treatment for COVID-19 (*19*). In our study, mortality rate on day 30 was lower among patients who received CCP with higher titers of SARS-CoV-2 antibodies (22.3%) than among those who received CCP with medium (27.4%) or low (29.6%) titers. We observed a lower mortality rate for the high-titer group than for the low-titer group among patients who had not received mechanical ventilation before transfusion (relative risk 0.66, 95% CI 0.48–0.91) but not among patients who had received mechanical ventilation (relative risk 1.02, 95% CI 0.78–1.32) (*19*).

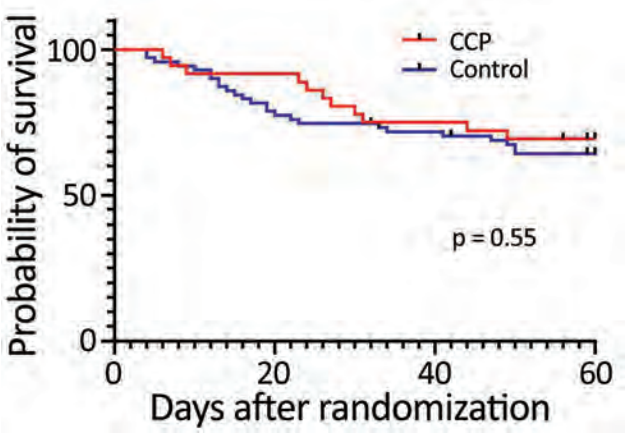

Figure 2. Probability of survival after randomization for study of high-dose CCP for treatment of severe COVID-19. COVID-19, coronavirus disease; CCP, COVID-19 convalescent plasma.

Our findings contrast with those of a previous multicenter randomized trial involving 103 participants (52 received CCP, 51 received standard treatment alone), which showed clinical improvement within 28 days in the subgroup of patients with severe disease who received CCP but not in the subgroup with life-threatening disease (*9*). In that study, CCP transfusion resulted in a higher rate of conversion to negative viral PCR results at 72 hours, suggesting potential benefit. In our study, most patients had life-threatening disease, which may explain, at least in part, the different outcomes. It is possible that patients with less severe disease may benefit from CCP. Nevertheless, in our study, an interim nonplanned analysis of death rates on day 21 suggested a possible benefit of CCP, similar to that observed by others (*26–28*), which was not confirmed by subsequent analyses. This finding raises the questions whether CCP provided a temporary benefit that was lost during the disease course and, if so, whether CCP should be transfused for a longer period during the disease.

Our study findings are in accordance with those of a randomized study in Argentina involving 228 patients who received CCP and 105 who received placebo, which did not show any survival benefits among patients receiving CCP (*21*). Of note, patient profiles for that study indicated less severe disease than did profiles for patients in our study. In the Argentina study, patients receiving mechanical ventilation were excluded, conflicting with the hypothesis that patients with less severe disease may benefit from CCP. The difference in disease severity also

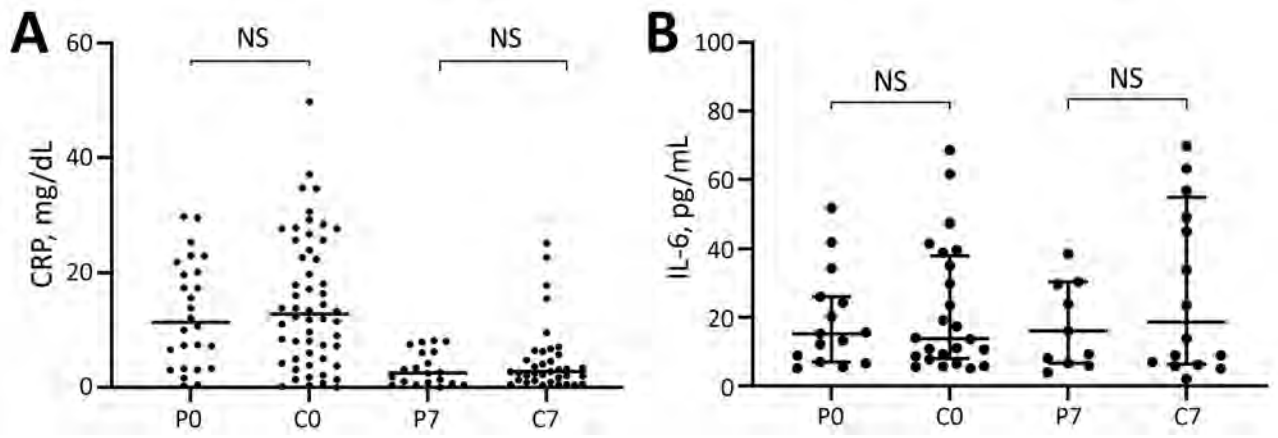

Figure 3. Scatter plots of inflammatory biomarker levels among participants in study of high-dose convalescent plasma for treatment of severe COVID-19, Brazil. A) C-reactive protein (CRP); total 80 patients (26 CCP, 54 control) on day 0 and 56 (20 CCP, 36 control) on day 7. B) Interleukin-6 (IL-6); total 39 patients (15 CCP, 24 control) on day 0 and 27 (11 CCP, 16 control) on day 7. Horizontal bars indicate medians. C0, control group day 0; C7, control group day 7; COVID-19, coronavirus disease; CCP, COVID-19 convalescent plasma; NS, not significant; P0, convalescent plasma group day 0; P7, convalescent plasma group day 7

may explain the higher mortality rate observed in our study (33.64%) compared with that in the Argentina trial (10.96%). A study in Brazil also did not find clinical improvement in the group that received CCP (*29*). Our results are in agreement with those obtained in another randomized study, in which 464 participants with moderate COVID-19 were assigned to receive 2 doses of 200 mL CCP (n = 235) or standard treatment (n = 229) (*30*). The authors of that study evaluated the composite outcomes of progression to severe disease and observed that CCP transfusion was not associated with clinical benefit. A recent randomized clinical trial with >16,000 enrolled patients showed that CCP transfusion did not improve survival rates (*31*). In that trial, the 28-day mortality rate was 24% for both groups (1,399 of 5,795 vs. 1,408 of 5,763; p = 0.95). Also, CCP transfusion had no significant effect on the proportion of patients discharged from the hospital. In that trial, only 5% of the patients in each group were receiving invasive mechanical ventilation; however, this percent value meant that administration of CCP to >550 patients did not influence outcomes in that subgroup of patients. Last, a recently published multicenter randomized trial (patients hospitalized with moderate disease up to day 12 from symptom onset) also found that CCP did not reduce the risk for intubation or death at day 30 in hospitalized patients with moderate disease (*32*).

The first strength of our study is the randomized design, which provided homogeneity and adequate comparison between groups with similar characteristics and disease severity. Second, we used only CCP with adequate neutralizing antibody titers. Third, the transfused CCP volume was high, making it less likely that the lack of response could be attributable to a low dose of neutralizing antibodies. Fourth, the patients received CCP transfusion up to day 10 after symptom onset, which was relatively early in comparison with other studies (*9*,*17*). However, one may hypothesize that up to 10 days for CCP transfusion may be too late for those with the most severe disease. It is possible that by day 9–10 after symptom onset, most patients would have endogenous antibodies, which was determined for patients in our study and has been shown by others (A. Gharbharan et al., unpub. data, http://medrxiv.org/lookup/doi/10.1101/2020.07.01.20139857). Perhaps it would be more effective to administer CCP earlier in disease, especially for patients considered to be at higher risk for unfavorable outcome. Libster et al. recently demonstrated that early CCP transfusion (within 72 hours of symptom onset) in older patients with mild COVID-19 reduced progression to severe respiratory disease by 48% (*33*). Another group also demonstrated reduced hospitalizations for those who received early CCP transfusion with high titers of neutralizing antibodies (D.J. Sullivan, unpub. data, https://www.medrxiv.org/content/10.1101/2021.12.10.21267485v1). These results seem logical because a more effective clinical response with early CCP transfusion, before the spontaneous appearance of antibodies, would be expected.

Among the limitations of our study, the number of patients enrolled was relatively small. However, because we anticipated difficulties obtaining the necessary amount of CCP to be administered to each patient, we decided to assign the participants at a ratio of 2 control to 1 CCP. Another weakness

was that the study was not blinded. However, infusion of a high volume of intravenous placebo could have been harmful to recipients. Patients in the control group should not be exposed to additional risk as a consequence of their participation in a clinical trial. Another limitation was that our patients already had SARS-CoV-2 antibodies when they received CCP transfusion, which could explain the absence of response to this therapy.

In conclusion, our study found that high-dose convalescent plasma transfusion provided no benefits for patients with severe COVID-19. Transfusions did not reduce death rates at days 30 and 60 from randomization, time receiving mechanical ventilation, or length of hospital stay for patients with severe COVID-19.

Acknowledgments

We thank Nathália Cristine André and Tatiane Marazia for their assistance.

This work was supported by Fundação de Amparo à Pesquisa do Estado de São Paulo (grant no. 20/05367-3).

About the Author

Dr. De Santis is a clinical hematologist at the University of São Paulo. His research interests include blood transfusion and cellular therapy, such as laboratory support for hematopoietic stem cell transplantation.

References

1. Izda V, Jeffries MA, Sawalha AH. COVID-19: a review of therapeutic strategies and vaccine candidates. Clin Immunol. 2021;222:108634. https://doi.org/10.1016/j.clim.2020.108634
2. Chung M, Bernheim A, Mei X, Zhang N, Huang M, Zeng X, et al. CT imaging features of 2019 novel coronavirus (2019-nCoV). Radiology. 2020;295:202–7. https://doi.org/10.1148/radiol.2020200230
3. Wang Y, Zhang D, Du G, Du R, Zhao J, Jin Y, et al. Remdesivir in adults with severe COVID-19: a randomised, double-blind, placebo-controlled, multicentre trial. Lancet. 2020;395:1569–78. https://doi.org/10.1016/S0140-6736(20)31022-9
4. Garibaldi PMM, Oliveira LC, Fonseca BA, Auxiliadora–Martins M, Miranda CH, Almado CEL, et al. Histo-blood group A is a risk factor for severe COVID-19. Transfus Med. 2021 Jun 3; [Epub ahead of print]. https://doi.org/10.1111/tme.12796
5. Zhou F, Yu T, Du R, Fan G, Liu Y, Liu Z, et al. Clinical course and risk factors for mortality of adult inpatients with COVID-19 in Wuhan, China: a retrospective cohort study. Lancet. 2020;395:1054–62. https://doi.org/10.1016/S0140-6736(20)30566-3
6. Horby P, Lim WS, Emberson JR, Mafham M, Bell JL, Linsell L, et al.; RECOVERY Collaborative Group. Dexamethasone in hospitalized patients with Covid-19. N Engl J Med. 2021;384:693–704. https://doi.org/10.1056/NEJMoa2021436
7. Cox RM, Wolf JD, Plemper RK. Therapeutically administered ribonucleoside analogue MK-4482/EIDD-2801 blocks SARS-CoV-2 transmission in ferrets. Nat Microbiol. 2021;6:11–8. https://doi.org/10.1038/s41564-020-00835-2
8. Owen DR, Allerton CMN, Anderson AS, Aschenbrenner L, Avery M, Berritt S, et al. An oral SARS-CoV-2 M^{pro} inhibitor clinical candidate for the treatment of COVID-19. Science. 2021;374:1586–93. https://doi.org/10.1126/science.abl4784
9. Lee JS, Adhikari NKJ, Kwon HY, Teo K, Siemieniuk R, Lamontagne F, et al. Anti-Ebola therapy for patients with Ebola virus disease: a systematic review. BMC Infect Dis. 2019;19:376. https://doi.org/10.1186/s12879-019-3980-9
10. Casadevall A, Scharff MD. Serum therapy revisited: animal models of infection and development of passive antibody therapy. Antimicrob Agents Chemother. 1994;38:1695–702. https://doi.org/10.1128/AAC.38.8.1695
11. Hung IF, To KK, Lee C-K, Lee K-L, Chan K, Yan W-W, et al. Convalescent plasma treatment reduced mortality in patients with severe pandemic influenza A (H1N1) 2009 virus infection. Clin Infect Dis. 2011;52:447–56. https://doi.org/10.1093/cid/ciq106
12. Arabi YM, Hajeer AH, Luke T, Raviprakash K, Balkhy H, Johani S, et al. Feasibility of using convalescent plasma immunotherapy for MERS-CoV infection, Saudi Arabia. Emerg Infect Dis. 2016;22:1554–61. https://doi.org/10.3201/eid2209.151164
13. Roback JD, Guarner J. Convalescent plasma to treat COVID-19: possibilities and challenges. JAMA. 2020;323:1561–2. https://doi.org/10.1001/jama.2020.4940
14. Yokoyama APH, Wendel S, Bonet-Bub C, Fachini RM, Dametto APF, Blumm F, et al. COVID-19 convalescent plasma cohort study: evaluation of the association between both donor and recipient neutralizing antibody titers and patient outcomes. Transfusion. 2021;61:2295–306. https://doi.org/10.1111/trf.16573
15. Bloch EM, Shoham S, Casadevall A, Sachais BS, Shaz B, Winters JL, et al. Deployment of convalescent plasma for the prevention and treatment of COVID-19. J Clin Invest. 2020;130:2757–65. https://doi.org/10.1172/JCI138745
16. Stadlbauer D, Amanat F, Chromikova V, Jiang K, Strohmeier S, Arunkumar GA, et al. SARS-CoV-2 seroconversion in humans: a detailed protocol for a serological assay, antigen production, and test setup. Curr Protoc Microbiol. 2020;57:e100. https://doi.org/10.1002/cpmc.100
17. Shen C, Wang Z, Zhao F, Yang Y, Li J, Yuan J, et al. Treatment of 5 critically ill patients with COVID-19 with convalescent plasma. JAMA. 2020;323:1582–9. https://doi.org/10.1001/jama.2020.4783
18. Duan K, Liu B, Li C, Zhang H, Yu T, Qu J, et al. Effectiveness of convalescent plasma therapy in severe COVID-19 patients. Proc Natl Acad Sci U S A. 2020;117:9490–6. https://doi.org/10.1073/pnas.2004168117
19. Joyner MJ, Carter RE, Senefeld JW, Klassen SA, Mills JR, Johnson PW, et al. Convalescent plasma antibody levels and the risk of death from COVID-19. N Engl J Med. 2021;384:1015–27. https://doi.org/10.1056/NEJMoa2031893
20. Li L, Zhang W, Hu Y, Tong X, Zheng S, Yang J, et al. Effect of convalescent plasma therapy on time to clinical improvement in patients with severe and life-threatening COVID-19: a randomized clinical trial. JAMA. 2020;324:460–70. https://doi.org/10.1001/jama.2020.10044
21. Simonovich VA, Burgos Pratx LD, Scibona P, Beruto MV, Vallone MG, Vázquez C, et al.; PlasmAr Study Group. A randomized trial of convalescent plasma in COVID-19 severe pneumonia. N Engl J Med. 2021;384:619–29. https://doi.org/10.1056/NEJMoa2031304
22. Piechotta V, Iannizzi C, Chai KL, Valk SJ, Kimber C, Dorando E, et al. Convalescent plasma or hyperimmune

immunoglobulin for people with COVID-19: a living systematic review [cited 2021 Dec 3]. https://www.cochranelibrary.com/cdsr/doi/10.1002/14651858.CD013600.pub4/full
23. Roubinian N. TACO and TRALI: biology, risk factors, and prevention strategies. Hematology (Am Soc Hematol Educ Program). 2018;2018:585–94. https://doi.org/10.1182/asheducation-2018.1.585
24. Wendel S, Kutner JM, Machado R, Fontão-Wendel R, Bub C, Fachini R, et al. Screening for SARS-CoV-2 antibodies in convalescent plasma in Brazil: preliminary lessons from a voluntary convalescent donor program. Transfusion. 2020;60:2938–51. https://doi.org/10.1111/trf.16065
25. Rosenthal N, Cao Z, Gundrum J, Sianis J, Safo S. Risk factors associated with in-hospital mortality in a us national sample of patients with COVID-19. JAMA Netw Open. 2020;3:e2029058. https://doi.org/10.1001/jamanetworkopen.2020.29058
26. Avendaño-Solá C, Ramos-Martínez A, Muñez-Rubio E, Ruiz-Antorán B, Malo de Molina R, Torres F, et al. ConPlas-19 Study Group. A multicenter randomized open-label clinical trial for convalescent plasma in patients hospitalized with COVID-19 pneumonia. J Clin Invest. 2021;131:e152740. https://doi.org/10.1172/JCI152740
27. O'Donnell MR, Grinsztejn B, Cummings MJ, Justman JE, Lamb MR, Eckhardt CM, et al. A randomized double-blind controlled trial of convalescent plasma in adults with severe COVID-19. J Clin Invest. 2021;131:150646. https://doi.org/10.1172/JCI150646
28. Körper S, Weiss M, Zickler D, Wiesmann T, Zacharowski K, Corman VM, et al.; CAPSID Clinical Trial Group. Results of the CAPSID randomized trial for high-dose convalescent plasma in patients with severe COVID-19. J Clin Invest. 2021;131:e152264. https://doi.org/10.1172/JCI152264
29. Sekine L, Arns B, Fabro BR, Cipolatt MM, Machado RRG, Durigon EL, et al.; PLACOVID Study Group. Convalescent plasma for COVID-19 in hospitalised patients: an open-label, randomised clinical trial. Eur Respir J. 2021 Aug 12 [Epub ahead of print]. https://doi.org/10.1183/13993003.01471-2021
30. Agarwal A, Mukherjee A, Kumar G, Chatterjee P, Bhatnagar T, Malhotra P; PLACID Trial Collaborators. Convalescent plasma in the management of moderate COVID-19 in adults in India: open label phase II multicentre randomised controlled trial (PLACID Trial). BMJ. 2020;371:m3939. https://doi.org/10.1136/bmj.m3939
31. Abani O, Abbas A, Abbas F, Abbas M, Abbasi S, Abbass H, et al.; RECOVERY Collaborative Group. Convalescent plasma in patients admitted to hospital with COVID-19 (RECOVERY): a randomised controlled, open-label, platform trial. Lancet. 2021;397:2049–59. https://doi.org/10.1016/S0140-6736(21)00897-7
32. Bégin P, Callum J, Jamula E, Cook R, Heddle NM, Tinmouth A, et al.; CONCOR-1 Study Group. Convalescent plasma for hospitalized patients with COVID-19: an open-label, randomized controlled trial. Nat Med. 2021;27:2012–24. https://doi.org/10.1038/s41591-021-01488-2
33. Libster R, Pérez Marc G, Wappner D, Coviello S, Bianchi A, Braem V, et al.; Fundación INFANT–COVID-19 Group. Early high-titer plasma therapy to prevent severe COVID-19 in older adults. N Engl J Med. 2021;384:610–8. https://doi.org/10.1056/NEJMoa2033700

Address for correspondence: Gil C. De Santis, Rua Tenente Catão Roxo, 2501 Ribeirão Preto, 14051-140 SP, Brazil; email: gil@hemocentro.fmrp.usp.br

SARS-CoV-2 Period Seroprevalence and Related Factors, Hillsborough County, Florida, USA, October 2020–March 2021

Anna R. Giuliano, Shari Pilon-Thomas, Michael J. Schell, Martha Abrahamsen, Jessica Y. Islam, Kimberly Isaacs-Soriano, Kayoko Kennedy, Christopher W. Dukes, Junmin Whiting, Julie Rathwell, Jonathan A. Hensel, Leslie N. Mangual, Ernst Schonbrunn, Melissa Bikowitz, Dylan Grassie, Yan Yang

Estimating the actual extent of the severe acute respiratory syndrome coronavirus 2 (SARS-CoV-2) pandemic is challenging because virus test positivity data undercount the actual number and proportion of persons infected. SARS-CoV-2 seroprevalence is a marker of past SARS-CoV-2 infection regardless of presence or severity of symptoms and therefore is a robust biomarker of infection period prevalence. We estimated SARS-CoV-2 seroprevalence among residents of Hillsborough County, Florida, USA, to determine factors independently associated with SARS-CoV-2 antibody status overall and among asymptomatic antibody-positive persons. Among 867 participants, SARS-CoV-2 period prevalence (October 2020–March 2021) was 19.5% (asymptomatic seroprevalence was 8%). Seroprevalence was 2-fold higher than reported SARS-CoV-2 virus test positivity. Factors related to social distancing (e.g., essential worker status, not practicing social distancing, contact with a virus-positive person, and length of contact exposure time) were consistently associated with seroprevalence but did not differ by time since suspected or known infection (<6 months vs. ≥6 months).

In late 2019, severe acute respiratory syndrome coronavirus 2 (SARS-CoV-2) emerged in China, ultimately leading to a global pandemic (*1*). Since January 2020, the United States has observed a dramatic rise in the incidence of SARS-CoV-2 infection, for which no endogenous immunity exists (*2*), leading to >70.6 million cases of SARS-CoV-2 and ≈860,000 deaths in the United States (*3*). Although these data provide an estimate of the infection burden, challenges exist in estimating the actual extent of the pandemic. US public health data record the number of residents that test positive for SARS-CoV-2 RNA, rates of hospitalizations, and deaths from coronavirus disease (COVID-19) among those who undergo viral testing. Missing is the proportion of the population that was ever positive for SARS-CoV-2, including those who were symptomatic but did not undergo testing and those with no or mild symptoms, where the person did not recognize COVID-19 symptoms and therefore did not undergo testing (*4*–*6*). Complicating the estimate of SARS-CoV-2 prevalence is the fact that early in the pandemic in the United States, the availability of test reagents varied on any given day at any location and recommendations for testing eligibility changed. Test positivity data likely undercounted the actual number and proportion of persons who were infected with SARS-CoV-2 (*7*,*8*). As such, the period prevalence of SARS-CoV-2 remains unknown for most communities.

Antibodies to SARS-CoV-2 begin to be detected 7 days after symptom onset (*9*) and IgG antibodies are detectable within 2 weeks after onset of infection (*10*). SARS-CoV-2 seroprevalence is a marker of past SARS-CoV-2 infection regardless of presence or severity of symptoms and therefore is a robust biomarker of infection period prevalence.

As of June 1, 2021, Florida had the third-highest number of confirmed SARS-CoV-2 cases in the United States, 2,283,315 cases (10.6% of residents), resulting in 95,210 hospitalizations and 36,869 deaths (*11*). Hillsborough County (≈1.47 million residents), where the city of Tampa is located, is one of the most

Author affiliations: Moffitt Cancer Center, Tampa, Florida, USA (A.R. Giuliano, S. Pilon-Thomas, M.J. Schell, M. Abrahamsen, J.Y. Islam, K. Isaacs-Soriano, K. Kennedy, C.W. Dukes, J. Whiting, J. Rathwell, J.A. Hensel, L.N. Mangual, E. Schonbrunn, D. Grassie, Y. Yang); University of South Florida Morsani College of Medicine, Tampa (M. Bikowitz)

DOI: https://doi.org/10.3201/eid2803.211495

populous counties in Florida. As of June 1, 2021, a total of 142,013 test-confirmed SARS-CoV-2 cases had occurred among Hillsborough County residents (9.7% of the population). The goals of this study were to estimate SARS-CoV-2 seroprevalence among Hillsborough County residents and to determine the demographic and behavioral factors independently associated with SARS-CoV-2 antibody status overall and among asymptomatic antibody-positive persons.

Study Design

We conducted a cross-sectional study of adults residing in Hillsborough County during October 2020–March 2021. The study was approved by the Advarra Institutional Review Board and Moffitt Cancer Center's Scientific Review Committee. The University of Florida's Bureau of Economic and Business Research drew the study population from the greater Hillsborough County by using randomly selected mailing addresses. Adults ≥18 years of age who were free of fever at the time of interview were eligible for the study. To ensure an adequate sample size of residents across the lifespan, we aimed to enroll relatively equal numbers of persons (balanced on sex) in each of 4 age groups: 18–34, 35–54, 55–64, and ≥65 years. We contacted potential participants by mail and email to inform them of the study. If they agreed to participate, they were scheduled for an in-person blood draw after completion of a web-based eligibility criteria checklist and informed consent form and a short questionnaire that captured demographic information, SARS-CoV-2 exposure history, underlying conditions, immunosuppression status, and use of immunosuppressive medications. Participants received a $25 gift card after completing the blood draw.

Selection of Hillsborough County Residents for Study

The Bureau of Economic and Business Research created a random representative sample of Hillsborough County residents by using the address-based sample method, a probability-based frame of street addresses that relies on the US Postal Service Computerized Delivery Sequence File. Because this file contains >147 million residential addresses, the address-based sample frame covers nearly 100% of all households in the country. We sent letters and postcards to potential participants inviting them to go to the study website and complete a brief form to indicate their interest in participating. In addition, emails were sent to a randomly selected population by eTargetMedia (https://www.etargetmedia.com), a multichannel marketing company with a detailed database of email addresses.

The study webpage described the study rationale and assessed eligibility criteria, which included residency in Hillsborough County and age of ≥18 years. At the time of the scheduled clinic visit, eligibility for the blood draw also included not currently experiencing COVID-19 symptoms (e.g., being free of fever [body temperature <100.4°F, as assessed using a noncontact infrared thermometer], cough, and shortness of breath). Eligible potential participants were then directed to an online informed consent form to review and sign and a brief questionnaire to complete before scheduling a date and time for the blood draw.

Forty thousand letters or postcards and 10,000 emails were sent to Hillsborough County addresses. A total of 1,621 residents completed the eligibility questionnaire, and 1,571 were eligible to participate. Of those eligible, 1,135 electronically signed a consent form, 1,038 completed the online questionnaire, and 922 completed the study visit and blood draw. Fifty-five of the study participants had received ≥1 COVID-19 vaccine doses and were excluded from the analyses, resulting in a final sample size of 867.

Study Procedures

Data Acquisition and Management

Persons who were contacted through postal mail were provided a link to a website that enabled authentication using a unique identifier they were assigned. After authenticating, persons were shown a webpage with a brief description of the study. Those who chose to proceed were asked to electronically sign the informed consent form. Participants were then asked to complete a short questionnaire and contact the research clinic to schedule an appointment for a blood draw. If participants did not contact the research clinic within 3 days of completing the online questionnaire, the research staff contacted the person to schedule an appointment. The questionnaire collected information related to sociodemographic information, SARS-CoV-2 exposure history (self-reported in exposure hours per day), past COVID-19 symptoms, underlying conditions associated with increased infection and disease risk, immunosuppression status, and use of immunosuppressive medications.

Clinic Procedures

After we verifying participants' identities and their completion of the required forms, participants attended an in-person clinic visit at Moffitt Cancer Center's Research Clinic. All staff and study participants were required to wear facemasks at all times, no-touch temperature screening was used, and questions

regarding respiratory illness were asked. One tiger top tube of blood was drawn per participant. We processed blood by letting it stand for 20–60 min to clot and then spun it for 20 min at 3,200 rpm, and placed it in a refrigerator until couriered to the laboratory. We aliquoted and then maintained serum samples at –80°C until antibody analysis. Before antibody testing, we heat-inactivated all serum samples in a 56°C water bath for 1 h.

SARS-CoV-2 IgG Antibody Assay

To evaluate serostatus, we performed a 2-step ELISA adapted from the Krammer (Icahn School of Medicine at Mount Sinai) protocol, which measured IgG responses against the receptor-binding domain and spike protein (*12*,*13*). In brief, a high-throughput screening of samples against receptor-binding domain was followed by a second step in which positive samples underwent a confirmatory ELISA against the full-length spike protein. We diluted presumptive positives 1:100, 1:300, 1:900, 1:2,700, and 1:8,100, and used goat anti–human horseradish peroxidase–conjugated antibody (diluted 1:5,000) as the secondary antibody. We designated as positive the samples having 2 consecutive dilutions with optical density values >3 × SD of the mean of the negative controls. Negative controls included serum pools collected before 2020. Positive controls included convalescent serum from SARS-CoV-2–positive patients or monoclonal antibodies against SARS-CoV-2 proteins (L. Pinto, Frederick Laboratories, National Institutes of Health, pers. comm., emails, April and October 2020). Assay sensitivity was 96.8%, and specificity was 94.1% (Appendix, https://wwwnc.cdc.gov/EID/article/28/3/21-1495-App1.pdf).

Data Analyses

We summarized sociodemographic and behavioral characteristics by using descriptive statistics. We compared SARS-CoV-2 antibody positivity across participant sociodemographic and behavioral characteristics by using bivariate analyses, specifically Fisher exact test or χ^2 test as appropriate. We evaluated associations between SARS-CoV-2 antibody positivity with potential predictors by using univariate logistic regression analyses. We developed the fully adjusted model by using a backward elimination approach; specifically, we removed variables with p values >0.25 from the final model. We included the following variables in the backward selection model: age, sex, race, ethnicity, marital status, smoking status, living with chronic disease, lung problem, work environment during pandemic, practiced mask use since start of pandemic, practiced social distancing since start of pandemic, mean hours/week interacting with virus-positive contact, traveled out of state after February 2020, relationship to virus-positive contact, avoid groups of people, only going outside the home for essential trips, and ever had COVID-19 symptoms. We performed all analyses by using SAS 9.4 (https://www.sas.com) and RStudio 4.0.2 (https://www.rstudio.com).

Results

Among 867 COVID vaccine-naive Hillsborough County residents, 19.5% (95% CI 16.9%–22.3%) tested antibody-positive (Appendix Table); adjusted prevalence of 15% did not differ significantly from the crude estimate. The median age of study participants was 50 years (interquartile range 38–61 years), and 65.7% were women. Most participants were White (82.7%), non-Hispanic (83.2%), never smokers (74.2%), and immunocompetent (91.8%). Eighteen percent reported essential worker status (i.e., employed in either a hospital, clinic, grocery store, or in a public services industry). Approximately 60% had either never been exposed to a SARS-CoV-2–positive person or were not sure if they had been exposed. Nearly all respondents (99.5%) indicated they had changed their behavior since the pandemic started (data not shown); 96.1% reported wearing a mask outside of the home fairly often or often, and 89% reported keeping ≥6 feet away from other persons since the start of the pandemic. Approximately 30% (30.2%) reported ever having COVID-19 symptoms, although 14.5% reported testing virus positive. Only 7 participants had been hospitalized because of COVID-19.

We observed no differences in SARS-CoV-2 seroprevalence by sex, age group, race, or ethnicity (Appendix Table). Seroprevalence was higher among those living with lung disease (27.2%), especially persons who reported having asthma (28.1%), and lower among those living with an autoimmune disease (9.9%). Reported exposure to virus-positive persons was significantly associated with higher seroprevalence; 35.8% of those reporting contact with a documented positive person and 36.7% reporting contact with a presumed positive person were antibody-positive. In addition, 44.9% seroprevalence occurred among those whose virus-positive contact was a family member. More than 96% of those who tested positive for SARS-CoV-2 RNA (97% for those infected <6 months ago and 96.2% if positive ≥6 months ago) were antibody-positive. Forty-five percent of those who reported having COVID-19 symptoms were antibody-positive, and 8.3% of those who reported

never having COVID-19 symptoms were antibody-positive, which we refer to as asymptomatic infection. Seroprevalence did not significantly differ by reported social-distancing or mask-wearing practices. We noted the relationship between hours per week exposed to a virus-positive person and antibody-positivity (Figure). The percentage testing antibody-positive increased with increasing exposure time but plateaued at ≈50% seroprevalence at ≥48 hours of exposure per week.

We noted factors independently associated with testing positive for SARS-CoV-2 antibodies (Table 1). Potential exposure to a virus-infected person increased the odds of testing antibody-positive, including essential workers employed in a hospital, clinic, grocery store or other public services industry (adjusted odds ratio [aOR] 2.40 [95% CI 1.42–4.07]), contact with a virus-positive family member (aOR 4.62 [95% CI 2.49–8.58]) or friend (aOR 4.22 [95% CI 2.44–7.30]), not avoiding groups of people (aOR 1.71 [95% CI 1.06–2.76]), and mean hours per week exposed to the virus-positive person (adjusted continuous odds ratio 1.01 [95% CI 1.00–1.01]). Odds of testing antibody-positive were high among those who reported ever experiencing COVID-19 symptoms (aOR 9.14 [95% CI 5.93–14.08]). We observed significantly lower odds of testing antibody-positive among divorced, separated, or widowed persons (aOR 0.40 [95% CI 0.20–0.77]) and those living with a chronic illness (aOR 0.56 [95% CI 0.34–0.93]).

Among 605 participants who reported never having COVID symptoms, 50 tested antibody-positive and are referred to as having asymptomatic infection (Appendix Table). Essential worker status (aOR 2.28 [95% CI 1.13–4.60]), interacting with a virus-positive friend (aOR 3.72 [95% CI 1.71–8.11]), and not avoiding groups of people (aOR 2.90 [95% CI 1.53–5.50]) were independently associated with having asymptomatic infection (Table 2).

Discussion

Overall, ≈20% of study participants in this single Florida county had evidence of past infection with SARS-CoV-2, approximately 2-fold higher than the period prevalence of confirmed SARS-CoV-2 infections reported by the Florida Department of Health (10.6% through June 1, 2021) (*11*). This finding is not surprising given that molecular testing was not widely available early in the pandemic and, when it was available, not all persons with symptoms sought testing, and some never experienced symptoms; thus, many who were infected were undercounted in public health databases. A key finding of this study is that nearly 100% of persons who had confirmed or suspected infection were antibody-positive and remained antibody-positive even if the infection occurred ≥6 months before antibody testing. A question that remains unanswered by our analysis and other studies is the duration of the antibody response among those who experienced infection with SARS-CoV-2.

The seroprevalence estimated in our study demonstrates that, by March 2021, 1 in 5 adults residing in Hillsborough County may have been previously infected with SARS-CoV-2. This seroprevalence is higher than that found in other studies conducted during a similar timeframe of the COVID-19 pandemic; however, differences in SARS-CoV-2 seroprevalence are highly influenced by geographic location and the

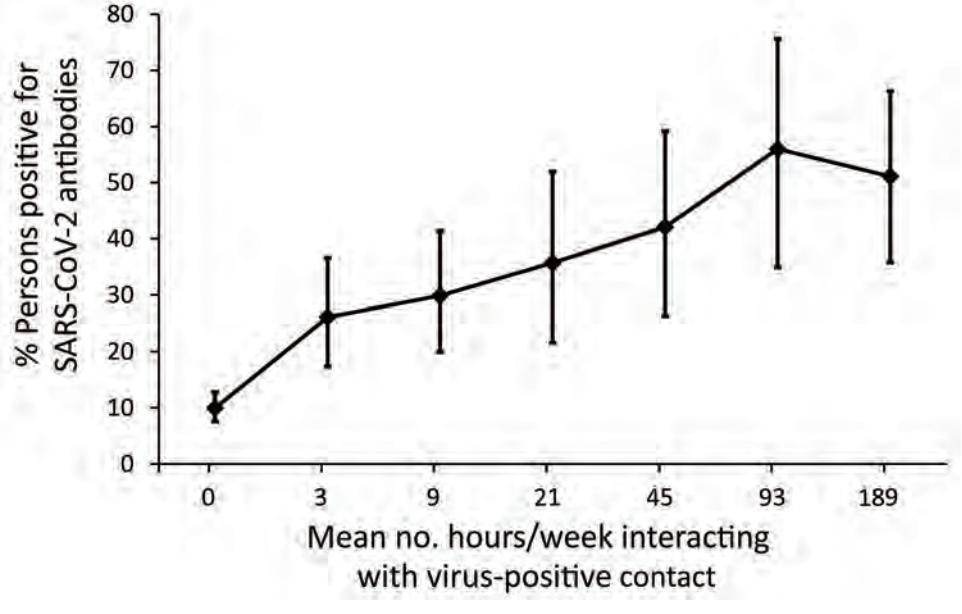

Figure. Relationship between mean number of hours per week exposed to a SARS-CoV-2–positive person and antibody positivity among residents, Hillsborough County, Florida, USA, October 2020–March 2021. Error bars indicate 95% CIs. SARS-CoV-2, severe acute respiratory syndrome coronavirus 2.

Table 1. Factors associated with severe acute respiratory syndrome coronavirus 2 antibody prevalence among residents, univariate and multivariable models, Hillsborough County, Florida, USA, October 2020–March 2021*

Characteristic	Unadjusted OR (95% CI)	Adjusted OR† (95% CI)
Age group, y		
18–44	Referent	Referent
45–54	0.88 (0.56–1.37)	1.13 (0.64–1.98)
55–64	0.71 (0.46–1.12)	0.86 (0.48–1.55)
≥65	0.71 (0.43–1.18)	1.64 (0.80–3.35)
Sex		
M	Referent	Referent
F	0.95 (0.67–1.35)	0.88 (0.57–1.38)
Marital status		
Married or living together	Referent	Referent
Single, never married	0.91 (0.60–1.37)	1.05 (0.61–1.80)
Divorced, separated , or widowed	0.49 (0.28–0.86)	0.40 (0.20–0.77)
Living with chronic disease‡	0.88 (0.61–1.28)	0.56 (0.34–0.93)
Essential worker status		
Not essential worker	Referent	Referent
Hospital, clinic, grocery store, public services	1.89 (1.26–2.84)	2.40 (1.42–4.07)
Financial services, banking, or other	0.91 (0.55–1.52)	0.70 (0.37–1.31)
Mean hours/week interacting with virus-positive contact	1.02 (1.01–1.02)	1.01 (1.001–1.01)
Relationship to virus-positive contact		
No known contact with virus-positive person	Referent	Referent
Family member	8.79 (5.62–13.77)	4.62 (2.49–8.58)
Friend or other	5.52 (3.43–8.90)	4.22 (2.44–7.30)
Co-worker	2.89 (1.51–5.53)	2.04 (0.95–4.40)
Does not avoid groups of people	1.65 (1.12–2.43)	1.71 (1.06–2.76)
Ever had coronavirus disease symptoms	9.24 (6.33–13.48)	9.14 (5.93–14.08)

*Based on a 863-person sample size. The following variables were included in the backward selection modeling approach: age, sex, race, ethnicity, marital status, smoking status, living with chronic disease, lung problem, work environment during pandemic, practiced mask use since start of pandemic, practiced social distancing since start of pandemic, mean hours/week interacting with virus-positive contact, traveled out of state after February 2020, relationship to virus-positive contact, avoid groups of people, only going outside the home for essential trips, and ever had coronavirus disease symptoms. OR, odds ratio.
†Results from the full model, which included all variables, listed in Appendix Table (https://wwwnc.cdc.gov/EID/article/28/3/21-1495-App1.pdf).
‡Including cancer, heart disease, diabetes, autoimmune disease, kidney disease, liver disease, and being immunosuppressed.

populations included in the study. For example, a seroprevalence study conducted in Virginia during June–August 2020 found that, although the overall prevalence estimated was low at 2.4%, the range by ZIP code varied from 0% to 20% (*7*). Similar to our study, the seroprevalence of 2.4% in Virginia was 2.8 times higher than the confirmed case counts. This ratio is relatively low compared with previous studies conducted in the United States, which have shown 6–53 times more infections than those ascertained by confirmed case counts (*8*,*14*,*15*). Differences in underascertainment across studies evaluating seroprevalence may be attributed to differences in the population included, timing of the epidemic across regions, and differences in test characteristics of assays used.

A nationwide study conducted by the Centers for Disease Control and Prevention that examined residual clinical samples from inpatients and outpatients found seroprevalence ranged from 0% in South Dakota (August 10–27, 2020) to 23% in New York State (July 27–August 13, 2020) (*16*). This analysis, which used commercial assays, found a seroprevalence of 8.5% for the state of Florida in September 2020. A prior Florida seroprevalence study of >5,500 healthcare workers and first responders tested in early summer of 2020 observed a seroprevalence of 4.1% (range 2.6%–8.7%) (*17*). However, considerable heterogeneity in SARS-CoV-2 antibody prevalence among first responders and healthcare workers was observed; those residing in Miami–Dade County and adult members of racial and ethnic minority populations, including Haitian, Creole, non-Hispanic Black, and Hispanic or Latino, were more likely to be seropositive (*17*). Similarly, a nationwide study of adults who had never had COVID-19 diagnosed found a seroprevalence of 4.6%; higher prevalence was found among adults living in early outbreak locations, Black adults, Hispanic adults, and adults residing in urban areas (*18*). Although our study did not demonstrate racial disparities, we observed that essential workers, including those working in grocery stores, had higher odds of SARS-CoV-2 antibody positivity. Because persons in minority communities are more likely to hold such occupations (*19*), our results contribute to the literature demonstrating the disproportionate burden of COVID-19 in the United States among vulnerable populations such as racial and ethnic minorities.

In our study, mask wearing was not associated with antibody status. This lack of an association is

likely attributable to several factors. Nearly 100% of respondents reported mask usage, so social desirability likely influenced responses to this question. In addition, we did not assess detailed information regarding mask use, such as type of mask, situations in which mask wearing occurred, and consistency of proper mask usage, so our study cannot adequately assess the protection conferred by mask usage. In contrast, social-distancing behaviors consistently emerged as a factor associated with risk for infection, despite 11% of participants reporting that they never, rarely, or almost never practiced social distancing. This behavior included not avoiding crowds and interacting with a known or suspected virus-positive family member, co-worker, or friend. The percentage seropositive increased with increasing hours per week exposed to an infected person. We did not ask participants to report the physical distance they maintained, so we cannot assess what distance in feet was associated with protection.

Throughout the pandemic, much discussion has occurred about the dangers of infection for those with autoimmune disease and their greater susceptibility to illness. Study participants with autoimmune disease or on immunosuppressant medication had lower rates of antibody positivity, roughly half that of the overall study population. This finding is likely attributable to extra precautions taken to avoid infection as opposed to a reflection of actual susceptibility to illness.

Despite some study participants reporting a large number of hours per week exposed to a person with COVID-19 symptoms, only ≈50% became infected themselves. Infection rates among adults with high exposure to COVID-19 is likely multifactorial and varies from population to population on the basis of contextual factors, which can be demonstrated by seroprevalence studies conducted in large healthcare systems of healthcare workers with high exposure to COVID-19. For example, the seroprevalence of healthcare personnel tested during June–August 2020 throughout all Mayo Clinic facilities was only 0.6%, and areas undergoing greater community disease transmission and burden were associated with higher seroprevalence among healthcare providers (*20*). Notably, the Mayo Clinic in Florida had a seroprevalence of 0.8%. In contrast, the seroprevalence of healthcare workers in New York City during the same period was 13.7% (*21*). The marked difference in seroprevalence among these highly exposed adults may be caused by differences in hotspots or outbreaks of SARS-CoV-2 infection in the regions each health system is located, as well as differences in access to personal protective equipment and adherence to precautions including wearing masks. Similarly, differences we observed in our study may be caused by variability in adherence to preventive behaviors, such as prompt isolation from persons with COVID-19, or the household setting and environment. We observed that the odds of SARS-CoV-2 seroprevalence was highest among those with a family member as a known virus-positive contact. In shared family spaces where social distancing may not be possible,

Table 2. Factors associated with severe acute respiratory syndrome coronavirus 2 antibody prevalence among asymptomatic participants, univariate and multivariable models, Hillsborough County, Florida, USA, October 2020–March 2021*

Characteristic	Unadjusted OR (95% CI)	Adjusted OR (95% CI)†
Age group, y		
18–44	Referent	Referent
45–54	0.95 (0.47–1.92)	1.04 (0.49–2.21)
55–64	0.48 (0.21–1.11)	0.57 (0.23–1.38)
≥65	0.43 (0.16–1.18)	0.69 (0.24–2.03)
Sex		
M	Referent	Referent
F	1.11 (0.60–2.06)	0.91 (0.47–1.78)
Essential worker status		
Not essential worker	Referent	Referent
Hospital, clinic, grocery store, public services	2.44 (1.28–4.65)	2.28 (1.13–4.60)
Financial services, banking, or other	0.76 (0.28–2.02)	0.55 (0.19–1.58)
Mean hours/week interacting with virus-positive contact	1.01 (1.01–1.02)	1.01 (1.00–1.02)
Relationship to virus-positive contact		
No known contact with virus-positive person	Referent	Referent
Family member	4.23 (1.95–9.16)	2.67 (0.94–7.59)
Co-worker	2.32 (0.83 −6.52)	1.89 (0.62–5.73)
Friend or other	4.40 (2.10–9.21)	3.72 (1.71–8.11)
Does not avoid groups of people	3.03 (1.66–5.56)	2.90 (1.53–5.50)

*Based on a 602-person sample size. The following variables were included in the backward selection modeling approach: age, sex, race, ethnicity, marital status, smoking status, living with chronic disease, lung problem, work environment during pandemic, practiced mask use since start of pandemic, practiced social distancing since start of pandemic, mean hours/week interacting with virus-positive contact, traveled out of state after February 2020, relationship to virus-positive contact, avoid groups of people, only going outside the home for essential trips, and ever had coronavirus disease symptoms. OR, odds ratio.
†Results from the full model, which included all variables, listed in Appendix Table (https://wwwnc.cdc.gov/EID/article/28/3/21-1495-App1.pdf).

risk for household transmission is high (22). Asymptomatic transmission before the onset of symptoms in a household is also highly probable.

A low percentage of antibody-positive persons never had COVID-19 symptoms, what we refer to as the asymptomatic infection prevalence. Surprisingly, this percentage was relatively low (≈8%) and was not associated with age. The only factors significantly associated with asymptomatic infection were those related to social distancing, whether that was not avoiding crowds, contact with a friend who was virus-positive, or repeated contact with community members as an essential worker.

A strength of this study is the relatively large sample size and inclusion of a broad range of ages. We captured participant information regarding factors that may be associated with susceptibility to infection, protective behaviors practiced, and exposure and length of exposure to SARS-COV-2–infected persons. Although invitations were sent at random to county residents, a small rate of participation resulted from this recruitment method. Some residents may have received multiple invitations (i.e., email and letter, or email and postcard). Because of the low rate of participation, we were not able to obtain a representative sample of the underlying county population. However, the study enrolled persons from 53 (96%) of the 55 ZIP codes associated with Hillsborough County. The final study sample included a higher proportion of women than men, and participants were predominantly non-Hispanic White. Many reported exposure to an infected person, so the seroprevalence we report may be an overestimate of the actual period prevalence. Hillsborough County includes the city of Tampa as well as both rural and suburban communities. Although the area is relatively densely populated, few residents use public transportation; this county is less densely populated than other urban counties in Florida, such as Miami–Dade County. Therefore, the period seroprevalence we have reported may be lower than what would be observed in city centers.

The estimates of seroprevalence from our study demonstrate that the cumulative case numbers confirmed through molecular RNA–based testing likely underrepresent the actual number of cases of SARS-CoV-2 infection in the United States and Florida. Frequency of contact with family or friends with confirmed COVID-19 diagnoses was strongly associated with being SARS-CoV-2 antibody–positive, indicating the importance of social distancing, particularly from friends or family with confirmed COVID-19. The availability of vaccination should help alleviate disparities in SARS-CoV-2 positivity observed for higher risk groups because of structural and occupational factors, such as among essential workers and those with frequent contact with persons with confirmed COVID-19. This analysis should inform the broader ongoing policy in the United States regarding the relative benefits of recommended mitigation strategies against the spread of SARS-CoV-2.

Acknowledgments

We thank Ligia Pinto for the methods to measure IgG responses against the receptor-binding domain and spike proteins of SARS-CoV-2. We also thank the Krammer Laboratory at the Icahn School of Medicine at Mount Sinai for providing receptor-binding domain and spike expression vectors.

This work was supported in part by the Chemical Biology Core; the Participant Research, Interventions, and Measurement Core; and the Biostatistics and Bioinformatics Shared Resource Core at Moffitt Cancer Center, a comprehensive cancer center designated by the National Cancer Institute and funded in part by Moffitt's Cancer Center Support Grant (grant no. P30CA076292). A private donation to the Moffitt Foundation supported study infrastructure and start-up. This work has also been supported in part by a research grant from the Investigator-Initiated Studies Program of Merck Sharp & Dohme Corp. The opinions expressed in this paper are those of the authors and do not necessarily represent those of Merck Sharp & Dohme Corp. Development of SARS-CoV-2 reagents was partially supported by the Centers of Excellence for Influenza Research and Surveillance at the National Institutes of Health's National Institute of Allergy and Infectious Diseases (contract no. HHSN272201400008C).

About the Author

Dr. Giuliano is a cancer epidemiologist and the founding director of the Center for Immunization and Infection Research in Cancer at the Moffitt Cancer Center in Tampa, Florida. Her primary research interest is the use of preventive and therapeutic vaccines to eliminate cancers caused by human papillomavirus.

References

1. Sohrabi C, Alsafi Z, O'Neill N, Khan M, Kerwan A, Al-Jabir A, et al. World Health Organization declares global emergency: a review of the 2019 novel coronavirus (COVID-19). Int J Surg. 2020;76:71–6. https://doi.org/10.1016/j.ijsu.2020.02.034
2. Miller IF, Becker AD, Grenfell BT, Metcalf CJE. Disease and healthcare burden of COVID-19 in the United States. Nat Med. 2020;26:1212–7. https://doi.org/10.1038/s41591-020-0952-y

3. Centers for Disease Control and Prevention. COVID data tracker [cited 2021 Jun 15]. https://covid.cdc.gov/covid-data-tracker/#datatracker-home
4. Sakurai A, Sasaki T, Kato S, Hayashi M, Tsuzuki S-I, Ishihara T, et al. Natural history of asymptomatic SARS-CoV-2 infection. N Engl J Med. 2020;383:885–6. https://doi.org/10.1056/NEJMc2013020
5. Payne DC, Smith-Jeffcoat SE, Nowak G, Chukwuma U, Geibe JR, Hawkins RJ, et al.; CDC COVID-19 Surge Laboratory Group. SARS-CoV-2 infections and serologic responses from a sample of U.S. Navy service members—USS Theodore Roosevelt, April 2020. MMWR Morb Mortal Wkly Rep. 2020;69:714–21. https://doi.org/10.15585/mmwr.mm6923e4
6. Yousaf AR, Duca LM, Chu V, Reses HE, Fajans M, Rabold EM, et al. A prospective cohort study in non-hospitalized household contacts with SARS-CoV-2 infection: symptom profiles and symptom change over time. Clin Infect Dis. 2021;73:e1841–9. https://doi.org/10.1093/cid/ciaa1072
7. Rogawski McQuade ET, Guertin KA, Becker L, Operario D, Gratz J, Guan D, et al. Assessment of seroprevalence of SARS-CoV-2 and risk factors associated with COVID-19 infection among outpatients in Virginia. JAMA Netw Open. 2021;4:e2035234. https://doi.org/10.1001/jamanetworkopen.2020.35234
8. Havers FP, Reed C, Lim T, Montgomery JM, Klena JD, Hall AJ, et al. Seroprevalence of antibodies to SARS-CoV-2 in 10 sites in the United States, March 23–May 12, 2020. JAMA Intern Med. 2020 Jul 21 [Epub ahead of print].
9. Thevarajan I, Nguyen THO, Koutsakos M, Druce J, Caly L, van de Sandt CE, et al. Breadth of concomitant immune responses prior to patient recovery: a case report of non-severe COVID-19. Nat Med. 2020;26:453–5. https://doi.org/10.1038/s41591-020-0819-2
10. Okba NMA, Müller MA, Li W, Wang C, GeurtsvanKessel CH, Corman VM, et al. Severe acute respiratory syndrome coronavirus 2–specific antibody responses in coronavirus disease patients. Emerg Infect Dis. 2020;26:1478–88. https://doi.org/10.3201/eid2607.200841
11. Florida Department of Health. Florida COVID-19 response [cited 2021 Jun 2]. https://floridahealthcovid19.gov
12. Amanat F, Stadlbauer D, Strohmeier S, Nguyen THO, Chromikova V, McMahon M, et al. A serological assay to detect SARS-CoV-2 seroconversion in humans. Nat Med. 2020;26:1033–6. https://doi.org/10.1038/s41591-020-0913-5
13. Stadlbauer D, Amanat F, Chromikova V, Jiang K, Strohmeier S, Arunkumar GA, et al. SARS-CoV-2 seroconversion in humans: a detailed protocol for a serological assay, antigen production, and test setup. Curr Protoc Microbiol. 2020;57:e100. https://doi.org/10.1002/cpmc.100
14. Bendavid E, Mulaney B, Sood N, Shah S, Bromley-Dulfano R, Lai C, et al. COVID-19 antibody seroprevalence in Santa Clara County, California. Int J Epidemiol. 2021;50:410–9. https://doi.org/10.1093/ije/dyab010
15. Bruckner TA, Parker DM, Bartell SM, Vieira VM, Khan S, Noymer A, et al. Estimated seroprevalence of SARS-CoV-2 antibodies among adults in Orange County, California. Sci Rep. 2021;11:3081. https://doi.org/10.1038/s41598-021-82662-x
16. Bajema KL, Wiegand RE, Cuffe K, Patel SV, Iachan R, Lim T, et al. Estimated SARS-CoV-2 Seroprevalence in the US as of September 2020. JAMA Intern Med. 2021;181:450–60. https://doi.org/10.1001/jamainternmed.2020.7976
17. Matthias J, Spencer EC, Michniewicz M, Bendle TM, Wilson C, Scheppke KA, et al. SARS-CoV-2 antibody prevalence among healthcare workers and first responders, Florida, May–June 2020. Fla Public Health Rev. 2021;18:1–10.
18. Kalish H, Klumpp-Thomas C, Hunsberger S, Baus HA, Fay MP, Siripong N, et al. Undiagnosed SARS-CoV-2 seropositivity during the first 6 months of the COVID-19 pandemic in the United States. Sci Transl Med. 2021;13:eabh3826. https://doi.org/10.1126/scitranslmed.abh3826
19. Centers for Disease Control and Prevention. Health equity considerations and racial and ethnic minority groups [cited 2021 Jun 16]. https://www.cdc.gov/coronavirus/2019-ncov/community/health-equity/race-ethnicity.html
20. Carter RE, Theel ES, Breeher LE, Swift MD, Van Brunt NA, Smith WR, et al.; Mayo Clinic Serology Screening Program Operations Team. Prevalence of SARS-CoV-2 antibodies in a multistate academic medical center. Mayo Clin Proc. 2021;96:1165–74. https://doi.org/10.1016/j.mayocp.2021.03.015
21. Moscola J, Sembajwe G, Jarrett M, Farber B, Chang T, McGinn T, et al.; Northwell Health COVID-19 Research Consortium. Prevalence of SARS-CoV-2 antibodies in health care personnel in the New York City area. JAMA. 2020;324:893–5. https://doi.org/10.1001/jama.2020.14765
22. Grijalva CG, Rolfes MA, Zhu Y, McLean HQ, Hanson KE, Belongia EA, et al. Transmission of SARS-COV-2 infections in households—Tennessee and Wisconsin, April–September 2020. MMWR Morb Mortal Wkly Rep. 2020;69:1631–4. https://doi.org/10.15585/mmwr.mm6944e1

Address for correspondence: Anna Giuliano, H. Lee Moffitt Cancer Center and Research Institute, 12902 USF Magnolia Dr, Tampa, FL 33612, USA; email: anna.giuliano@moffitt.org

Nowcasting (Short-Term Forecasting) of COVID-19 Hospitalizations Using Syndromic Healthcare Data, Sweden, 2020

Armin Spreco, Anna Jöud, Olle Eriksson, Kristian Soltesz, Reidar Källström, Örjan Dahlström, Henrik Eriksson, Joakim Ekberg, Carl-Oscar Jonson, Carl-Johan Fraenkel, Torbjörn Lundh, Philip Gerlee, Fredrik Gustafsson, Toomas Timpka

We report on local nowcasting (short-term forecasting) of coronavirus disease (COVID-19) hospitalizations based on syndromic (symptom) data recorded in regular healthcare routines in Östergötland County (population ≈465,000), Sweden, early in the pandemic, when broad laboratory testing was unavailable. Daily nowcasts were supplied to the local healthcare management based on analyses of the time lag between telenursing calls with the chief complaints (cough by adult or fever by adult) and COVID-19 hospitalization. The complaint cough by adult showed satisfactory performance (Pearson correlation coefficient r>0.80; mean absolute percentage error <20%) in nowcasting the incidence of daily COVID-19 hospitalizations 14 days in advance until the incidence decreased to <1.5/100,000 population, whereas the corresponding performance for fever by adult was unsatisfactory. Our results support local nowcasting of hospitalizations on the basis of symptom data recorded in routine healthcare during the initial stage of a pandemic.

During the initial stage of the coronavirus disease (COVID-19) pandemic, large variations in virus dissemination within countries often led to lack of sufficiently specific information for local authorities to make accurate decisions about health service adjustments (*1*,*2*). The situation was further worsened by heterogeneity in virus testing strategies, usually a result of local differences in laboratory capacities (*3*), leading to a need for local-scale COVID-19 forecasting methods based on resources available in the existing healthcare infrastructure (*4*). In particular, experts called for short-term forecasts of incident hospitalizations to plan staff reallocation and creation of temporary facilities for intensive or subintensive care with ventilators (*5*).

We have previously developed a local influenza nowcasting (short-term forecasting) method whereby syndromic healthcare data are used to nowcast later diagnostic events (*6*). The method has shown satisfactory performance in prospective evaluations (*7*,*8*). We used this experience during the initial stage of the pandemic in 2020 to nowcast local cases of patients hospitalized with COVID-19 by modeling associations with data from Swedish Healthcare Direct's 24-hour telenursing service (telephone number 1177) (*9*). Telenursing services are available in numerous countries for health counseling and evaluation of clinical service needs in the general population (*10*–*12*). In Sweden, the chief complaint for each call is recorded in an administrative database (*13*). During the 2009 influenza pandemic, records of telenursing chief complaints were used to forecast variations in local healthcare load, although less accurately than during regular influenza seasons (*14*).

The purpose of our study was to examine the performance of syndromic healthcare data in nowcasting local hospital admissions during the initial stage of the COVID-19 pandemic, when resources for diagnostic laboratory testing were limited. The specific aim was to investigate the prospective performance of symptoms recorded during telenursing calls in

Author affiliations: Linköping University, Linköping, Sweden (A. Spreco, O. Eriksson, R. Källström, Ö. Dahlström, H. Eriksson J. Ekberg, C.-O. Jonson, F. Gustafsson, T. Timpka); Region Östergötland, Linköping (A. Spreco, R. Källström, J. Ekberg, C.-O. Jonson, T. Timpka); Lund University, Lund, Sweden (A. Jöud, K. Soltesz); Skåne University Hospital, Lund (A. Jöud. C.-J. Fraenkel); Chalmers University of Technology, Gothenburg, Sweden (T. Lundh, P. Gerlee); Gothenburg University, Gothenburg (T. Lundh, P. Gerlee)

DOI: https://doi.org/10.3201/eid2803.210267

nowcasting daily cases of patients hospitalized with COVID-19 during March–June 2020 in Östergötland County, Sweden (population ≈465,000). The Swedish Ethical Review Authority (dnr. 2020-03183) approved the study design. Because COVID-19 and influenza share characteristic symptoms, we interpreted the performance of the COVID-19 nowcasting using syndromic symptom data, taking into consideration parallel winter influenza activity in the county.

Methods

We used prospective evaluation design; that is, we defined the COVID-19 nowcasting procedure and the evaluation protocol before beginning to collect evaluation data. The management of Region Östergötland, the public (tax-financed) healthcare provider serving Östergötland County, used the daily nowcasts we created for planning resource allocation. Nowcasting of COVID-19 hospitalizations was based on the time lag from telenursing calls with selected chief complaints (Appendix, https://wwwnc.cdc.gov/EID/article/28/3/21-0267-App1.pdf); we retrieved nowcasting data from the countywide health information system managed by the healthcare provider (*15*). Because the COVID-19 pandemic reached the study county during an ongoing influenza season, we describe the progress of both local epidemics for comparison.

Data Sources

Syndromic data were recorded from telenursing calls made by county residents to Swedish Healthcare Direct. Daily numbers of calls with chief complaints possibly associated with COVID-19 were retrieved from Hälsoläge, the national database, using the fixed-field terminology register service (*16*). The diagnostic data were collected from patients hospitalized with the International Classification of Diseases, 10th Revision (ICD-10), code U07.1 (COVID-19, virus identified). All patients hospitalized with suspected COVID-19 were given a PCR test for virus identification and diagnosis.

We retrieved daily numbers of patients diagnosed with laboratory-confirmed influenza (inpatient and outpatient) for February 20–June 30, 2020. For comparison, we also retrieved corresponding influenza and telenursing chief complaint data for the same period for each year during 2015–2019.

Nowcasting Procedure

We began developing the local COVID-19 nowcasting procedure on February 20, 2020. During March 2–6, we examined peer-reviewed scientific reports on COVID-19 symptoms to select telenursing chief complaints for the nowcasting, (*17*–*19*). The largest study retrieved, involving 1,099 patients from 30 provinces in China, reported fever (89%) and cough (68%) to be the most common symptoms, followed by fatigue (38%), shortness of breath (19%), and sore throat (14%) (*17*). The study also reported that hospitalized patients were almost exclusively adults. In the selection of corresponding telenursing chief complaints for use in nowcasting, we excluded unspecific symptoms of upper respiratory tract infection (fatigue and sore throat) and complaints expected to lead to a recommendation for immediate physical examination (shortness of breath). We chose the remaining telenursing chief complaints, cough by adult and fever by adult, as syndromic variables for use in the nowcasting of COVID-19 hospitalizations. We finalized the procedure on March 20.

Definition of Time Lag

After consultations with local healthcare managers, we found that we needed short-term forecasts in the interval of 14–21 days for implementing adjustments of hospital resources. To select the time lag in the interval with the highest correlation (i.e. the highest Pearson correlation coefficient, r) between syndromic and hospital admission data, we performed analyses of time series data from the previous 4 weeks for each of the 2 syndromic variables, leading to 16 possible outcomes: 8 time lags of 14–21 days for each variable. To eliminate weekday effects, we smoothed all series by calculating a 7-day moving average. If correlations for time lags were equal, we chose the longest. To adjust for the higher daily numbers of telenursing calls compared with hospitalization cases, we multiplied the level for each of the 2 chief telenursing complaints by a ratio calculated by dividing the sum of hospitalizations during a 14-day period by the sum of telenursing calls (separately for each syndromic variable) over a previous 14-day interval at a time distance, chosen depending on the resulting best time lag. The length of the interval should be a multiple of 7 days to level out weekday effects and be about the same as the time lag. Therefore, we chose an interval of 14 days.

Hospital Admission Nowcasting

We created daily nowcasts and forwarded them to the healthcare management at Region Östergötland beginning March 22, 2020. We performed a new calculation of the correlation coefficient each nowcasting day and chose the time lag with the highest correlation for each of the 2 chief complaints for nowcasts.

We performed daily nowcasts of forthcoming hospitalizations for the period covered by the time lag between COVID-19 hospitalizations and telenursing calls for cough by adult and fever by adult throughout the study period (Appendix).

Descriptive Analyses

Because COVID-19 and influenza share symptoms (telenursing chief complaints), we examined the daily numbers of COVID-19 hospitalizations and cases of laboratory-confirmed influenza in Östergötland County (primary and hospital care) for the period February 20–June 30, 2020. We also descriptively analyzed the annual trends for this period in 2015–2019 for cases of laboratory-confirmed influenza and for the telenursing chief complaints cough by adult and fever by adult.

Evaluation Procedure was defined

We evaluated the nowcasting performance during March 22–June 30, 2020. We defined the evaluation protocol on March 20 and followed it without alteration throughout the evaluation period. We evaluated performance by calculating the correlation between trends in the selected telenursing calls and trends in later hospitalizations, and by determining the accuracy of the nowcasted incidence of daily hospitalizations. The outcome measures were the Pearson correlation coefficient between the telenursing and hospitalization data from the nowcasting date through the period covered by the time lag (denoted as r^{FND}) and the mean absolute percentage error (MAPE) of the nowcasted hospitalization incidence. r^{FND} can vary between −1 and 1 (where −1 is perfect negative correlation and 1 is perfect positive correlation). The lower limit for MAPE is 0; an upper limit does not exist. Before beginning data collection, we defined the limits for satisfactory nowcasting performance as r^{FND} >0.80 and MAPE <20%.We derived the limit for r^{FND} from previous nowcasting studies (*20*) and determined the MAPE limit, following discussions with health service managers, on the basis of hospital resources in Sweden, which were overextended before the COVID-19 pandemic (on average, 103 patients occupied 100 administrative hospital bed units [*21*]).

Results

COVID-19 Pandemic

Calls by Östergötland county residents to Swedish Healthcare Direct with the chief complaint of cough by adult peaked on March 21 (Figure 1, panel A). On the same day, calls for the complaint fever by adult reached a plateau that lasted for ≈2 weeks (until April 3) (Figure 1, panel A).

The first hospitalization in Östergötland County for COVID-19 occurred on March 8, 2020. At the start of the evaluation period on March 22, the daily hospitalization incidence was 1.8 patients/100,000 population; peak incidence (4.9 patients/day/100,000 population) was reached on April 2 (Table; Figure 1, panel B). In mid-May, the daily incidence had declined to <1.5 hospitalizations/100,000 population; it was 0.6 hospitalizations/100,000 population on June 30, the end of the study period.

Influenza Season

The daily incidence of patients with laboratory-confirmed influenza peaked on March 10 (Figure 1, panel C). The recorded incidence decreased thereafter to a level that was notably below the 5-year historical trend. Calls to Swedish Healthcare Direct for the chief complaints cough by adult and fever by adult did not show a corresponding decrease in March 2020 (Figure 1, panel A). The comparative display of the historical trends from the previous 5-year period for these chief complaints showed that the levels usually increased throughout the month of March (Figure 1, panels D, E).

Nowcasting Performance

The selected optimal time lag for both the cough by adult and fever by adult variables was 14 days throughout the study period, except for cough by adult during March 26–28, when the time lag was 15 or 16 days (Video, https://wwwnc.cdc.gov/EID/article/23/3/21-0267-V1.htm). During the ascending stage of the first wave of the pandemic (March 22–April 4), as hospitalizations increased (Figure 2, panel A), r^{FND} for the Swedish Healthcare Direct chief complaint cough by adult was satisfactory (0.86–0.98), and MAPE decreased rapidly to a satisfactory level (from 28% to 3%) (Table; Figure 2, panels B, C; Video). r^{FND} for the chief complaint fever by adult decreased during this period to −0.63, and MAPE was mostly unsatisfactory (14%–47%). At the peak of the wave, with a daily hospitalization incidence >2.5/100,000 population (April 5–25), r^{FND} (0.74–0.97) and MAPE (4%−9%) remained satisfactory for cough by adult. For fever by adult, r^{FND} (−0.63 to 0.95) and MAPE (14%–52%) stayed at unsatisfactory levels. During the descending stage, r^{FND} and MAPE for cough by adult remained satisfactory until hospitalizations declined. When the daily hospitalizations decreased to <1.5/100,000 population in mid-May, r^{FND} and MAPE

indicated unsatisfactory performances for both syndromic indicators (Table; Figure 2).

Discussion

This study examined the performance of syndromic healthcare data (symptoms reported during telenursing calls) in nowcasting local hospital loads during the initial stage of the COVID-19 pandemic when resources for diagnostic laboratory testing were limited. We found that the telenursing chief complaint cough by adult accurately (r^{FND} 0.74–0.98; MAPE <10%) nowcasted local hospital loads ≥14 days in advance during periods with intense local dissemination of COVID-19 (corresponding to >2.5 hospitalizations/day/100,000 population) and continued to provide reliable nowcasts until the intensity decreased to <1.5 hospitalizations/day/100,000 population.

Although fever is a characteristic COVID-19 symptom, the performance of the Swedish Healthcare Direct chief complaint fever by adult in nowcasting was less satisfactory. This observation could be cause by the co-circulation of influenza virus strains and severe acute respiratory syndrome coronavirus 2 (SARS-CoV-2); fever by adult was recorded as a chief complaint from telenursing calls resulting from both influenza infection and COVID-19 (*22*). Even though cough was also a representative symptom for influenza, it appeared to be more uniquely recorded as the chief complaint from telenursing calls for COVID-19. We also observed that the incidence of patients with a laboratory-confirmed diagnosis of influenza peaked on March 10, just before the COVID-19 pandemic reached Östergötland County, and thereafter decreased to a level notably below the 5-year historical trend. It is unclear whether this decrease in the recorded incidence of influenza represents a true decline in infections or due to changes in healthcare-seeking behaviors (*23*). These observations suggest that COVID-19 nowcasting based on symptom data should be performed with caution during periods in which SARS-CoV-2 is co-circulating with influenza and other respiratory viruses.

Poor forecasting reliability during the first wave of the COVID-19 pandemic led to demands on investments in developing task-specific models and quality data collection (*24*,*25*). One explanation for the satisfactory local nowcasting performance we observed is the rapid and stable access to syndromic and diagnostic data throughout the emerging first wave of the pandemic. Most methods for COVID-19 nowcasting have used diagnostic data to model the near-future progress (typically 2–6 days) of the corresponding events (*26*); A. Altmejd, et al., unpub. data, https://arxiv.org/pdf/2006.06840.pdf). In contrast to such autoregressive models, we used a separate syndromic data source to nowcast COVID-19 hospitalizations 14–21 days in advance. This time lag to hospitalizations was needed to rearrange the local healthcare organization to care for patients with COVID-19 while minimizing collateral effects on other patient groups. We collected the syndromic and diagnostic data used for the nowcasting from a regular health information system (*15*) and

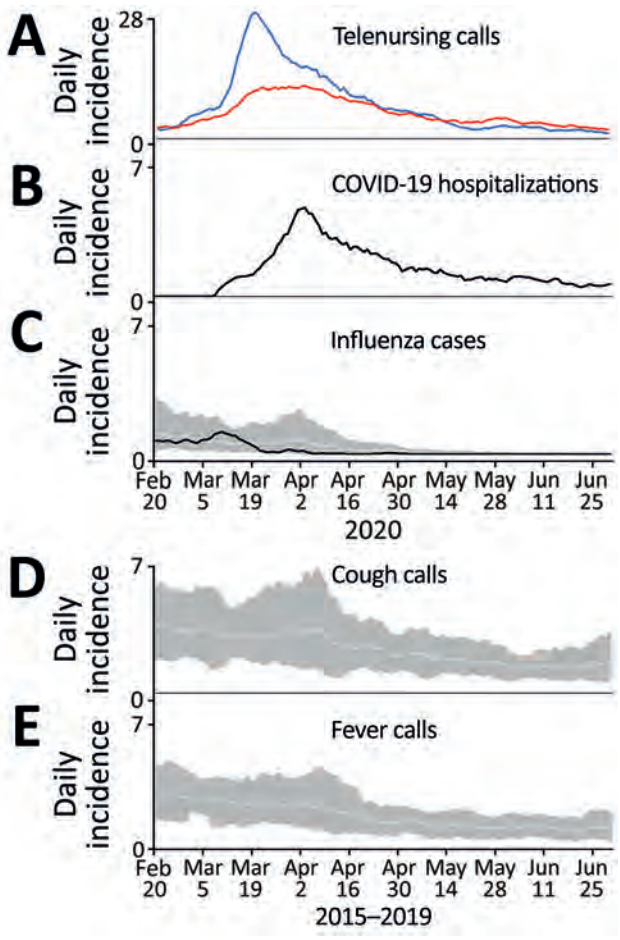

Figure 1. Daily incidence of telenursing calls for 2 chief complaints, COVID-19 hospitalizations, and laboratory-confirmed influenza plus reference data from before the COVID-19 pandemic, Östergötland County, Sweden. A) Telenursing calls per 100,000 population for chief complaints of cough by adult (blue line) and fever by adult (red line), February 20–June 30, 2020. B) COVID-19 hospitalizations per 100,000 population, February 20–June 30, 2020. C) Cases of laboratory-confirmed influenza per 100,000 population February 20–June 30, 2020 (black line). Light gray line indicates the average for cases of laboratory-confirmed influenza in 2015–2019; dark gray shaded area is the corresponding range. D) Telenursing calls per 100,000 population for the chief complaint cough by adult in 2015–2019 (light grey line) with corresponding range (dark grey shaded area). E) Telenursing calls per 100,000 population for the chief complaint fever by adult in 2015–2019 (light grey line) with corresponding range (dark grey shaded area).

Table. Weekly nowcasting performance for 2 syndromic variables in the first wave of the coronavirus pandemic, Östergötland County, Sweden, 2020*

Nowcasting dates	Hospitalizations/day/ 100,000 population	Cough by adult		Fever by adult	
		r^{FND}	MAPE	r^{FND}	MAPE
Week 1 (Mar 22–28)	1.8–3.4	0.86–0.97	9 –28	0.01–0.99	14–20
Week 2 (Mar 29–Apr 4)	3.4–4.9	0.93–0.98	3–5	−0.63 to −0.32	17–47
Week 3 (Apr 5–11)†	3.2–4.5	0.89–0.95	4–6	−0.20 to 0.79	39–52
Week 4 (Apr 12–18)	2.6–3.2	0.92–0.97	4–6	0.87–0.95	16–45
Week 5 (Apr 19–25)	2.1–2.6	0.74–0.94	6–9	0.70–0.93	15–21
Week 6 (Apr 26–May 2)	1.4–2.1	0.46–0.73	10–13	0.58–0.73	9–13
Week 7 (May 3–9)	1.4–1.6	0.64–0.91	7–13	0.65–0.82	8–11
Week 8 (May 10–16)	1.1–1.5	0.53–0.74	8–17	0.45–0.65	9–11
Week 9 (May 17–23)	0.9–1.1	−0.28 to 0.57	19–41	−0.08 to 0.44	9–14
Week 10 (May 24–30)	0.9–1.1	−0.87 to −0.46	38–47	−0.57 to −0.16	14–18
Week 11 (May 31–Jun 6)	0.8–1.1	−0.86 to −0.26	19–32	−0.90 to 0.63	17–28
Week 12 (Jun 7–13)	0.8–1.0	−0.03 to 0.48	29–55	0.74–0.78	21–34
Week 13 (Jun 14–20)	0.6–1.0	−0.41 to 0.36	17–48	−0.53 to 0.60	12–32
Week 14 (Jun 21–27)	0.5–0.7	−0.20 to 0.58	15–28	0.13–0.78	10–23
Week 15 (Jun 28–30)‡	0.6–0.7	0.42 to 0.50	24 to 25	0.66 to 0.70	20–22

*MAPE, mean absolute percentage error; r^{FND}, Pearson correlation coefficient between the telenursing and hospitalization data from the nowcasting date through the period covered by the time lag.
†Includes local peak of the first pandemic wave.
‡Only 3 days because it is the end of the study period.

analyzed the data using experiences from nowcasting the 2009 influenza pandemic and subsequent winter influenza seasons (*6*,*14*,*27*). The syndromic data were recorded by telenurses specially trained in assessment of adults and children who experienced infectious-disease symptoms (*13*). At the time of the outbreak of COVID-19 in Sweden (February 2020), telenursing had evolved from a triage practice within primary care (*28*–*31*) into a key resource in healthcare provision staffed by experienced nursing professionals (*9*). The diagnostic data we used for the nowcasting in this study were recorded using standardized coding routines (*32*) by physicians with clinical responsibility for patients hospitalized with COVID-19.

Syndromic symptom data have been used for several purposes in the early response to the COVID-19 pandemic. Using web-based data collection from the general public, the EPICOVID19 study in Italy found a strong association between olfactory and taste symptoms and laboratory-confirmed COVID-19 (*33*). Loss of smell and taste have also been reported as a characteristic COVID-19 symptom from similar research in

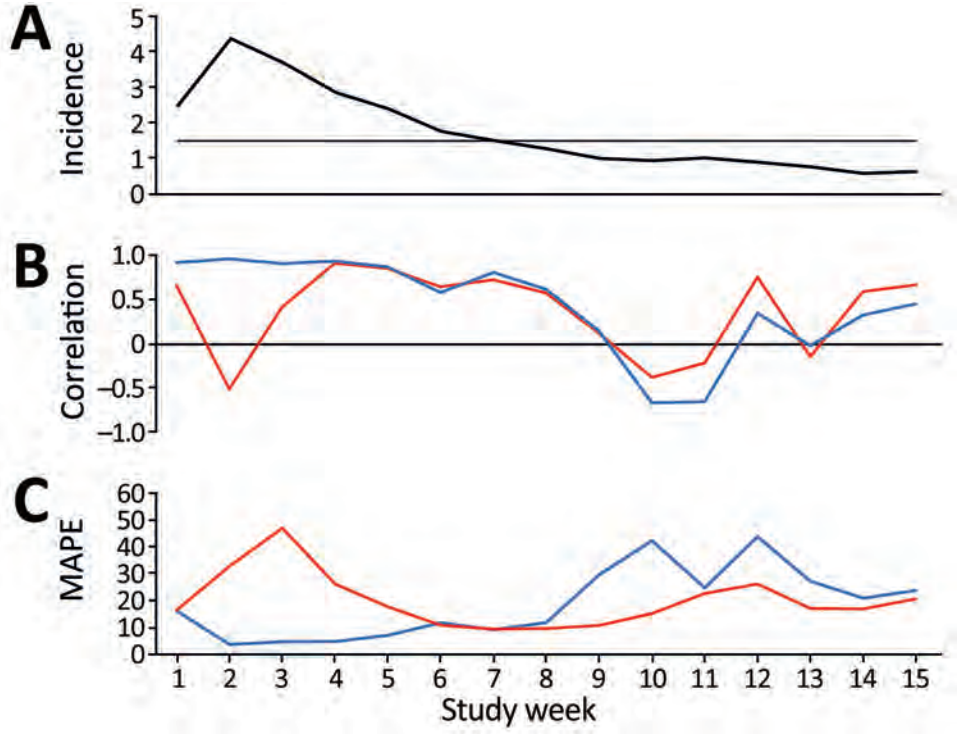

Figure 2. Local nowcasting performance in Östergötland County, Sweden, during the first wave of coronavirus disease (COVID-19), March 22–June 30, 2020. A) Weekly average of daily incidence of COVID-19, hospitalizations/week/100,000 population. The horizontal line indicates lowest incidence for reliable predictions (1.5 daily hospitalizations/100,000 population). B) Weekly average of daily correlation between telenursing data and COVID-19 hospitalizations from the nowcasting date through the period covered by the time lag for cough by adult (blue line) and fever by adult (red line). C) Weekly average of daily MAPE per week for cough by adult (blue line) and fever by adult (red line). MAPE, mean absolute percentage error.

the United Kingdom and the United States (*34*), Italy (*35*), and France (*36*). These symptom-tracking studies have provided important insights into the spectrum of COVID-19 symptoms, the rate of these symptoms in nonhospitalized persons, and the natural history of the infection. Nonetheless, for local nowcasting of hospital admissions during the early stages of a pandemic, rapid initiation of data collection and representative population coverage are required. Studies conducted in April and May 2020 showed that willingness to use a mobile application to support COVID-19 surveillance was 55%–70% in countries such as the United States, Switzerland, and Italy (*37*). However, by November 2020, the use of such mobile applications was still limited in nations where governments had promoted their development and dissemination; for example, 26% in Australia, 13% in Italy, and 2% in France (*38*). These proportions indicate that achievement of representative population coverage and continuity in data collection are challenging for COVID-19 forecasting using mobile applications. One reason for the low use of mobile applications is that legal and confidentiality issues have not been resolved for data collection from personal Internet devices in public health practice (*39*). Our nowcasting approach used trends in routinely recorded healthcare data for short-term forecasts of hospitalization cases. The approach did not require data normally unavailable for local healthcare providers and did thereby allow early initiation of nowcasting to support the local healthcare managers in their decision making.

The aim of this study was to assess hospital admission nowcasting during the early pandemic stage when broad laboratory testing still was unavailable. The syndromic variables (telenursing chief complaint codes) were thus determined in mid-March 2020 based on the information available. A limitation of the study is that it is possible that later selection of codes would have influenced the nowcasting outcomes. Also, use of individual-level telenursing data and sociodemographic data may have enabled detailed detection of municipality-level clusters during the initial stage of a pandemic. However, reports of variations in telenursing outreach and use across geographic areas and population groups, for example, among immigrants and the elderly (*12*,*40*), imply that further studies are needed to establish whether a more detailed version of our nowcasting procedure would be suitable for more specific early detection. Moreover, the outcome measures used in the study may not cover all aspects of healthcare load during pandemics. The coefficient r^{FND} shows correspondences between the nowcasted and observed series of hospitalization incidences over time, and MAPE displays how much the nowcasted incidences deviated as a percentage from the observed incidences. In future studies of COVID-19 hospitalizations, nowcasting the prevalence of hospitalized patients can be considered, which will require considering the length of hospital stay for different categories of COVID-19 patients. Moreover, the study did not use accuracy metrics such as uncertainty bounds around the point predictions because the public health practitioners did not request such bounds. It would have been possible to change the evaluation metrics afterwards, but doing so would have neutralized the prospective evaluation design. In the future, the nowcasting method can be further developed by including uncertainty bounds or probability estimates (*41*). The current approach has at least 2 uncertainties that can be quantified; uncertainty about how many persons with symptoms call the telenursing service, and uncertainty about the proportion of calls for a specific chief complaint that is constituted by COVID-19 cases. Finally, the nowcasting method was intended for use during the initial stage of a pandemic when broad laboratory testing is unavailable. The results are mainly generalizable to other early pandemic settings in which comparable infrastructural resources are available. Generalization of our results and application of the nowcasting method to later pandemic phases, when population-level laboratory testing is available, warrants more research.

We conclude that symptom data regularly recorded in healthcare can be used for local nowcasting of hospital loads during the initial stage of a pandemic when broad laboratory testing still is unavailable. The telenursing chief complaint cough by adult displayed satisfactory nowcasting performance during initial pandemic periods with high community dissemination of COVID-19 (>1.5 hospitalization cases/day/100,000 population). The study also indicates that symptom data should be used with caution for pandemic nowcasting when the novel virus is co-circulating with competing viruses. Our results support local nowcasting of hospitalizations on the basis of regularly recorded syndromic data during the initial stage of a pandemic.

This study was supported by grants from the Swedish Civil Contingencies Agency (grant no. 2010-2788), the Swedish Research Council (grant no. 2021-05608), ALF grants from Region Östergötland (dnr. 936190), and by grants from the Research Council of Southeast Sweden (grant no. FORSS-940915). The funders had no role in the study design, data collection and analysis, decision to publish, or preparation of the manuscript.

Authors' contributions: A.S., A.J., O.E., Ö.D., and T.T conceived and designed the study. A.S. and O.E. analyzed the data. O.E., K.S., and F.G. verified the results. A.S. and T.T. wrote the article. A.J., O.E., R.K., K.S., Ö.D., H.E., J.E., C.O.J., C.J.F., T.L., P.G., and F.G. revised the article and provided intellectual content. A.J., O.E., R.K., Ö.D., H.E., J.E., C.O.J., C.J.F., K.S., T.L., P.G., and F.G. gave final approval of the version to be published. T.T. is the guarantor of the content.

About the Author

Dr. Spreco is a researcher in the field of syndromic infectious disease surveillance at Linköping University, and Region Östergötland, Sweden. His main research focus is on evaluation and development of algorithms for local detection and prediction of infectious diseases. During the 2020 pandemic, he provided local forecasts of COVID-19 hospitalizations and healthcare capacity needs to Swedish healthcare regions.

References

1. Paul R, Arif AA, Adeyemi O, Ghosh S, Han D. Progression of COVID-19 from urban to rural areas in the United States: a spatiotemporal analysis of prevalence rates. J Rural Health. 2020;36:591-601. https://doi.org/10.1111/jrh.12486
2. García-Basteiro AL, Chaccour C, Guinovart C, Llupià A, Brew J, Trilla A, et al. Monitoring the COVID-19 epidemic in the context of widespread local transmission. Lancet Respir Med. 2020;8:440–2. https://doi.org/10.1016/S2213-2600(20)30162-4
3. Gill M, Sridhar D, Godlee F. Lessons from Leicester: a COVID-19 testing system that's not fit for purpose. BMJ. 2020;370:m2690. https://doi.org/10.1136/bmj.m2690
4. Chiolero A. Predicting COVID-19 resurgence: do it locally. BMJ. 2020;370:m2731. https://doi.org/10.1136/bmj.m2731
5. Grasselli G, Pesenti A, Cecconi M. Critical care utilization for the COVID-19 outbreak in Lombardy, Italy: early experience and forecast during an emergency response. JAMA. 2020;323:1545–6. https://doi.org/10.1001/jama.2020.4031
6. Spreco A, Eriksson O, Dahlström Ö, Cowling BJ, Timpka T. Integrated detection and prediction of influenza activity for real-time surveillance: algorithm design. J Med Internet Res. 2017;19:e211. https://doi.org/10.2196/jmir.7101
7. Spreco A, Eriksson O, Dahlström Ö, Cowling BJ, Timpka T. Evaluation of nowcasting for detecting and predicting local influenza epidemics, Sweden, 2009–2014. Emerg Infect Dis. 2018;24:1868–73. https://doi.org/10.3201/eid2410.171940
8. Spreco A, Eriksson O, Dahlström Ö, Cowling BJ, Biggerstaff M, Ljunggren G, et al. Nowcasting (short-term forecasting) of influenza epidemics in local settings, Sweden, 2008–2019. Emerg Infect Dis. 2020;26:2669–77. https://doi.org/10.3201/eid2611.200448
9. Online counselling support [in Swedish]. 2020 [cited 2020 Mar 10]. https://www.1177.se/om-1177-vardguiden/om-1177-vardguiden/radgivningsstodet-webb%2D%2Dett-stod-i-din-verksamhet
10. Kvedar J, Coye MJ, Everett W. Connected health: a review of technologies and strategies to improve patient care with telemedicine and telehealth. Health Aff (Millwood). 2014;33:194–9. https://doi.org/10.1377/hlthaff.2013.0992
11. Cunningham PN, Grant-Pearce C, Green L, Miles ID, Rigby J, Uyarra E. In sickness, in health, and in innovation: NHS DIRECT—a health sector innovation study. Presented at: Breaking New Ground: Innovation in the Public Sector International Conference; September 22–23, 2005; University College, Cork, Ireland.
12. Blakoe M, Gamst-Jensen H, von Euler-Chelpin M, Collatz Christensen H, Møller T. Sociodemographic and health-related determinants for making repeated calls to a medical helpline: a prospective cohort study. BMJ Open. 2019;9:e030173. https://doi.org/10.1136/bmjopen-2019-030173
13. Kaminsky E, Aurin IE, Hedin K, Andersson L, André M. Registered nurses' views on telephone nursing for patients with respiratory tract infections in primary healthcare—a qualitative interview study. BMC Nurs. 2020;19:65. https://doi.org/10.1186/s12912-020-00459-1
14. Timpka T, Spreco A, Eriksson O, Dahlström Ö, Gursky EA, Strömgren M, et al. Predictive performance of telenursing complaints in influenza surveillance: a prospective cohort study in Sweden. Euro Surveill. 2014;19:20966. https://doi.org/10.2807/1560-7917.ES2014.19.46.20966
15. Timpka T, Eriksson H, Gursky EA, Strömgren M, Holm E, Ekberg J, et al. Requirements and design of the PROSPER protocol for implementation of information infrastructures supporting pandemic response: a Nominal Group study. PLoS One. 2011;6:e17941. https://doi.org/10.1371/journal.pone.0017941
16. Folkhälsomyndigheten. Syndrome monitoring [in Swedish] [cited 2020 Mar 15]. https://www.folkhalsomyndigheten.se/smittskydd-beredskap/overvakning-och-rapportering/syndromovervakning
17. Guan WJ, Ni ZY, Hu Y, Liang WH, Ou CQ, He JX, et al.; China Medical Treatment Expert Group for COVID-19. Clinical characteristics of coronavirus disease 2019 in China. N Engl J Med. 2020;382:1708–20. https://doi.org/10.1056/NEJMoa2002032
18. Wu Z, McGoogan JM. Characteristics of and important lessons from the coronavirus disease 2019 (COVID-19) outbreak in China: summary of a report of 72,314 cases from the Chinese Center for Disease Control and Prevention. JAMA. 2020;323:1239–42. https://doi.org/10.1001/jama.2020.2648
19. Chen N, Zhou M, Dong X, Qu J, Gong F, Han Y, et al. Epidemiological and clinical characteristics of 99 cases of 2019 novel coronavirus pneumonia in Wuhan, China: a descriptive study. Lancet. 2020;395:507–13. https://doi.org/10.1016/S0140-6736(20)30211-7
20. Spreco A, Eriksson O, Dahlström Ö, Timpka T. Influenza detection and prediction algorithms: comparative accuracy trial in Östergötland county, Sweden, 2008–2012. Epidemiol Infect. 2017;145:2166–75. https://doi.org/10.1017/S0950268817001005
21. Sveriges Kommuner och landsting (SKL). No one unnecessarily at hospital [in Swedish]. 2016 [cited 2021 Oct 10]. https://webbutik.skr.se/bilder/artiklar/pdf/7585-421-2.pdf
22. US Centers for Disease Control and Prevention. Flu symptoms and complications. 2020 [cited 2020 Oct 19]. https://www.cdc.gov/flu/symptoms/symptoms.htm
23. Melidou A, Pereyaslov D, Hungnes O, Prosenc K, Alm E, Adlhoch C, et al.; World Health Organization European Region Influenza Surveillance Network. Virological surveillance of influenza viruses in the WHO European Region in 2019/20—impact of the COVID-19 pandemic. Euro Surveill. 2020;25:2001822. https://doi.org/10.2807/1560-7917.ES.2020.25.46.2001822

24. Chin V, Samia NI, Marchant R, Rosen O, Ioannidis JPA, Tanner MA, et al. A case study in model failure? COVID-19 daily deaths and ICU bed utilization predictions in New York state. Eur J Epidemiol. 2020;35:733–42. https://doi.org/10.1007/s10654-020-00669-6
25. Press WH, Levin RC. Modeling, post COVID-19. Science. 2020;370:1015. https://doi.org/10.1126/science.abf7914
26. Guenther F, Bender A, Katz K, Kuechenhoff H, Höhle M. Nowcasting the COVID-19 pandemic in Bavaria. Biom J. 2021;63:490–502 https://doi.org/10.1002/bimj.202000112
27. Timpka T, Spreco A, Dahlström Ö, Eriksson O, Gursky E, Ekberg J, et al. Performance of eHealth data sources in local influenza surveillance: a 5-year open cohort study. J Med Internet Res. 2014;16:e116. https://doi.org/10.2196/jmir.3099
28. Timpka T, Arborelius E. The primary-care nurse's dilemmas: a study of knowledge use and need during telephone consultations. J Adv Nurs. 1990;15:1457–65. https://doi.org/10.1111/j.1365-2648.1990.tb01789.x
29. Marklund B, Bengtsson C, Blomkvist S, Furunes B, Gäcke-Herbst R, Silfverhielm B, et al. Evaluation of the telephone advisory activity at Swedish primary health care centres. Fam Pract. 1990;7:184–9. https://doi.org/10.1093/fampra/7.3.184
30. Marklund B, Koritz P, Bjorkander E, Bengtsson C. How well do nurse-run telephone consultations and consultations in the surgery agree? Experience in Swedish primary health care. Br J Gen Pract. 1991;41:462–5.
31. Timpka T. The patient and the primary care team: a small-scale critical theory. J Adv Nurs. 2000;31:558–64. https://doi.org/10.1046/j.1365-2648.2000.01310.x
32. Socialstyrelsen. Coding of COVID-19 [in Swedish]. 2020 [cited 2021 Jan 1]. https://www.socialstyrelsen.se/globalassets/sharepoint-dokument/dokument-webb/klassifikationer-och-koder/kodning-av-covid-19.pdf
33. Adorni F, Prinelli F, Bianchi F, Giacomelli A, Pagani G, Bernacchia D, et al. Self-reported symptoms of SARS-CoV-2 infection in a nonhospitalized population in Italy: cross-sectional study of the EPICOVID19 web-based survey. JMIR Public Health Surveill. 2020;6:e21866. https://doi.org/10.2196/21866
34. Menni C, Valdes AM, Freidin MB, Sudre CH, Nguyen LH, Drew DA, et al. Real-time tracking of self-reported symptoms to predict potential COVID-19. Nat Med. 2020;26:1037–40. https://doi.org/10.1038/s41591-020-0916-2
35. Popovic M, Moccia C, Isaevska E, Moirano G, Pizzi C, Zugna D. COVID-19-like symptoms and their relation to SARS-CoV-2 epidemic in children and adults of the Italian birth cohort. Research Square. 2020. https://doi.org/10.21203/rs.3.rs-34027/v1
36. Denis F, Galmiche S, Dinh A, Fontanet A, Scherpereel A, Benezit F, et al. Epidemiological observations on the association between anosmia and COVID-19 infection: analysis of data from a self-assessment web application. J Med Internet Res. 2020;22:e19855. https://doi.org/10.2196/19855
37. Hargittai E, Redmiles E. Will Americans be willing to install COVID-19 tracking apps? Sci Am. 2020 Apr 28 [cited 2022 Jan 4]. https://blogs.scientificamerican.com/observations/will-americans-be-willing-to-install-covid-19-tracking-apps
38. Blasimme A, Vayena E. What's next for COVID-19 apps? Governance and oversight. Science. 2020;370:760–2. https://doi.org/10.1126/science.abd9006
39. Bernard R, Bowsher G, Sullivan R. COVID-19 and the rise of participatory SIGINT: an examination of the rise in government surveillance through mobile applications. Am J Public Health. 2020;110:1780–5. https://doi.org/10.2105/AJPH.2020.305912
40. Cook EJ, Sharp C, Randhawa G, Guppy A, Gangotra R, Cox J. Who uses NHS health checks? Investigating the impact of ethnicity and gender and method of invitation on uptake of NHS health checks. Int J Equity Health. 2016;15:13. https://doi.org/10.1186/s12939-016-0303-2
41. Gneiting T, Balabdaoui F, Raftery AE. Probabilistic forecasts, calibration and sharpness. J R Stat Soc Series B Stat Methodol. 2007;69:243–68. https://doi.org/10.1111/j.1467-9868.2007.00587.x

Address for correspondence: Armin Spreco, Department of Health, Medicine and Caring Sciences, Linköping University, s-581 83 Linköping, Sweden; email: armin.spreco@liu.se

Infection Control Measures and Prevalence of SARS-CoV-2 IgG among 4,554 University Hospital Employees, Munich, Germany

Johanna Erber, Verena Kappler, Bernhard Haller, Hrvoje Mijočević, Ana Galhoz, Clarissa Prazeres da Costa, Friedemann Gebhardt, Natalia Graf, Dieter Hoffmann, Markus Thaler, Elke Lorenz, Hedwig Roggendorf, Florian Kohlmayer, Andreas Henkel, Michael P. Menden, Jürgen Ruland, Christoph D. Spinner, Ulrike Protzer,[1] Percy Knolle,[1] Paul Lingor,[1] on behalf of the SeCoMRI Study Group[2]

Hospital staff are at high risk for severe acute respiratory syndrome coronavirus 2 (SARS-CoV-2) infection during the coronavirus disease (COVID-19) pandemic. This cross-sectional study aimed to determine the prevalence of SARS-CoV-2 infection in hospital staff at the University Hospital rechts der Isar in Munich, Germany, and identify modulating factors. Overall seroprevalence of SARS-CoV-2-IgG in 4,554 participants was 2.4%. Staff engaged in direct patient care, including those working in COVID-19 units, had a similar probability of being seropositive as non–patient-facing staff. Increased probability of infection was observed in staff reporting interactions with SARS-CoV-2–infected coworkers or private contacts or exposure to COVID-19 patients without appropriate personal protective equipment. Analysis of spatiotemporal trajectories identified that distinct hotspots for SARS-CoV-2–positive staff and patients only partially overlap. Patient-facing work in a healthcare facility during the SARS-CoV-2 pandemic might be safe as long as adequate personal protective equipment is used and infection prevention practices are followed inside and outside the hospital

Author affiliations: University Hospital rechts der Isar, Munich, Germany (J. Erber, V. Kappler, B. Haller, H. Mijočević, C. Prazeres da Costa, F. Gebhardt, N. Graf, D. Hoffmann, M. Thaler, H. Roggendorf, F. Kohlmayer, A. Henkel, J. Ruland, C.D. Spinner, U. Protzer, P. Knolle, P. Lingor); German Center for Infection Research, Munich (J. Erber, D. Hoffmann, J. Ruland, U. Protzer, C.D. Spinner); Helmholtz Zentrum München-German, Neuherberg, Germany (A. Galhoz, M.P. Menden); Ludwig-Maximilians University Munich, Martinsried, Germany (A. Galhoz, M.P. Menden); German Center for Diabetes Research, Neuherberg (M.P. Menden); Technical University of Munich, Munich (M.P. Menden)

DOI: https://doi.org/10.3201/eid2803.204436

Healthcare workers (HCWs) are exposed to severe acute respiratory syndrome coronavirus 2 (SARS-CoV-2) in the private context, as well as professionally with varying exposure risk depending on their workplace. Prevalence rates have been measured as high as 13.7% in the New York, NY, USA, area, 10.2% in a nationwide study in Spain, 7.5% for 580 HCWs in a hospital in Spain, 6.4% for >3,000 HCWs in a tertiary hospital in Belgium, 4.0% for >2,8790 HCWs in Denmark, and 0.4%–3.8% for hospitals in China (*1*–*6*). Working in coronavirus disease (COVID-19)–designated units has been reported to carry an increased risk for infection (*4*,*7*).

The greater Munich area in Germany became the epicenter of a SARS-CoV-2 outbreak after a confirmed case was reported on January 27, 2020. A rapid and massive increase in SARS-CoV-2 infections occurred during March 2020, when infected persons returned from skiing resorts, such as Ischgl, Austria, where the spread of infection was dramatic (*8*). The University Hospital Munich rechts der Isar faced the challenge of rapidly increasing numbers of COVID-19 patients, combined with an increasing number of staff in quarantine. To reduce the spread of infections, guidelines for the use of personal protective equipment (PPE) for staff and patients were introduced, including the obligation to wear face masks in all areas of the hospital (Figure 1). In addition, a telephone hotline was established to provide staff with guidance for reverse transcription PCR (RT-PCR) testing and quarantine policies.

[1]These authors contributed equally to this article.

[2]Members of the SeCOMRI study group are listed at the end of this article..

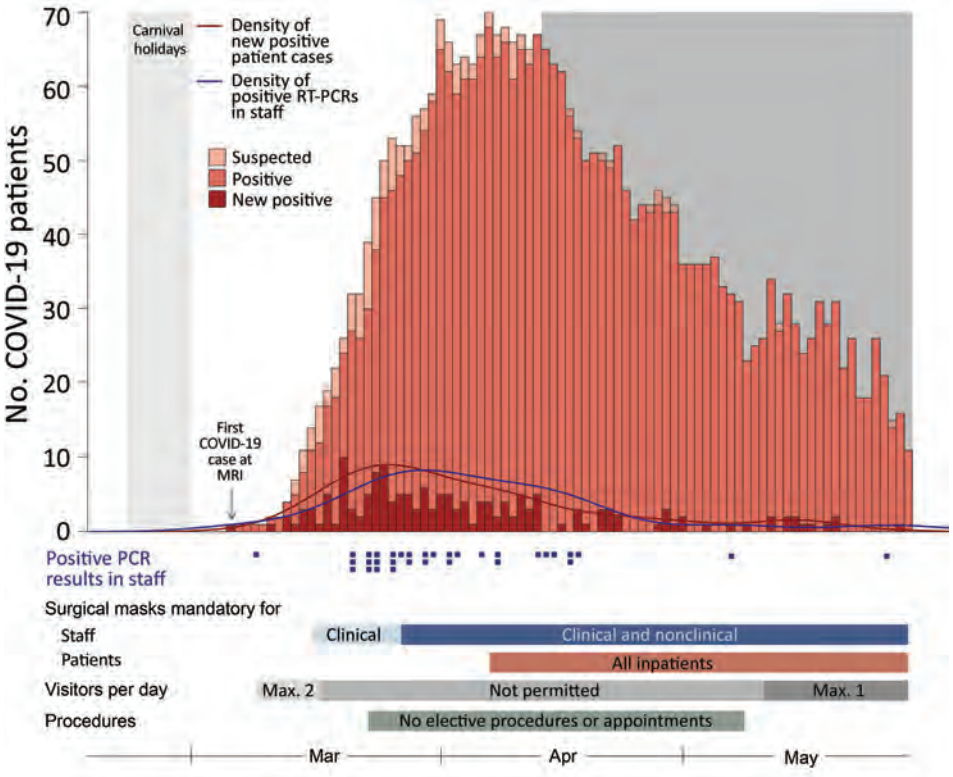

Figure 1. Prevalence and distribution of severe acute respiratory syndrome coronavirus 2 (SARS-CoV-2) infections in patients and staff at a university hospital in Munich, Germany. Shown is the number of all COVID-19 patients admitted to the hospital; the first COVID-19 patient was admitted on March 6, 2020. Light gray shading indicates dates of carnival holidays (February 22–March 1, 2020); dark gray shading indicates dates of seroprevalence study (April 14–May 29, 2020). Blue squares below graph indicate positive RT-PCR test results for SARS-CoV-2 RNA in university hospital staff. Bars below graph indicate densities of positive RT-PCR test results in staff (blue), new COVID-19 cases in patients (red), and limitations on number of visitors allowed and elective procedures and appointments (gray). COVID-19, coronavirus disease; Max., maximum; MRI, University Hospital Munich Rechts der Isar; RT-PCR, reverse transcription PCR.

To determine the epidemiology and immune response to SARS-CoV-2 and to identify best-practice approaches protecting staff and patients, we initiated a prospective, observational cohort study. The purpose of this study was to assess risk factors and evidence for infection, including clinical symptoms, and to determine the seroprevalence of SARS-CoV-2 antibodies.

Materials and Methods

Study Design and Participants

During April 14–May 29, 2020, all clinical and nonclinical Munich rechts der Isar staff ≥18 years of age (n = 6,305) and medical students at the Technical University of Munich (n = 1,699) were invited to participate in this prospective, monocentric, observational study (Appendix Figure 1, https://wwwnc.cdc.gov/EID/article/27/3/20-4436-App1.pdf). Previous positive SARS-CoV-2 antibody tests results was not an exclusion criterion. Upon receiving written informed consent, we obtained demographic data; chronic medical conditions; occupation; work location; use of PPE; exposure to SARS-CoV-2–positive patients, co-workers, or private contacts; symptom history; previous PCR testing for SARS-CoV-2; and outcome by using a standardized electronic questionnaire (Appendix) before the blood test result was known. We defined endoscopy, bronchoscopy, tracheal intubation, noninvasive ventilation, and transesophageal echocardiography as aerosol-generating medical procedures (AGPs).

We collected serum samples and subjected them to SARS-CoV-2 IgG and IgM testing (primary outcome). We tested for IgM in all persons until May 4, 2020 (n = 1,620), and thereafter only if IgG was positive or typical symptoms of COVID-19 were reported (n = 88) (Appendix Figure 2). Staff reporting symptoms or testing positive for IgM were recommended to undergo testing of nasopharyngeal swab specimens for SARS-CoV-2 by RT-PCR to exclude persistent infection. We stored personal data in a pseudonymized manner by using the open-source electronic case form system m4 DIS (BitCare GmbH, https://www.bitcare.de) (*9*). The study was approved by the Ethics Committee of the Technical University of Munich School of Medicine (approval no. 216/20S).

Since March 2020, a continuous infection surveillance program for all staff has been implemented at the University Hospital rechts der Isar in Munich, including an employee testing center and staff counselling (Corona Hotline), which is available 7 days per week. Persons who have symptoms compatible with COVID-19 or previous risk contacts are scheduled for testing for SARS-CoV-2 by RT-PCR from combined oropharyngeal and nasopharyngeal swab specimens.

We included RT-PCR results of staff testing in the analysis if the study participants consented.

Laboratory Analysis

We detected serum IgM and IgG against SARS-CoV-2 spike 1 protein or nucleocapsid protein by using a paramagnetic particle chemiluminescent immunoassay on an iFlash 1800 Immunoassay Analyzer (Shenzhen Yhlo Biotech Co., http://en.szyhlo.com). We subjected all serum samples that were positive for IgM or IgG (≥10 AU/mL), all serum samples that had 5–10 AU/mL of IgG, and all serum samples from SARS-CoV-2 RT-PCR–positive persons to confirmatory testing. For confirmation, we determined total antibodies against SARS-CoV-2 nucleocapsid by using an electrochemiluminescent immunoassay on a Cobas e411 Analyzer (Roche Diagnostics, https://www.roche.com). For all samples that had incongruent results, we determined IgG against SARS-CoV-2 spike 1 protein by using an ELISA (Euroimmun, https://www.euroimmun.com) and used immunoblotting to differentiate antibodies against nucleocapsid protein, spike 1 protein 1, and the receptor-binding domain of SARS-CoV-2 from those against seasonal coronaviruses (Mikrogen, https://www.mikrogen.de) (Appendix).

We extracted nucleic acids from nasopharyngeal swab specimens by using the mSample Preparation System DNA Kit identical to the Promega Maxwell Viral Total Nucleic Acid Extraction Kit (Promega, https://www.promega.com) according to a standard protocol on an m2000sp Device for RNA and DNA Extraction (Abbott, https://www.abbott.com). SARS-CoV-2 RT-PCR was performed by using SARS-CoV-2_N1 and SARS-CoV-2_N2 primer and probe sets for amplification on an ABI 7500 Device (Thermofisher Scientific, https://www.thermofisher.com) according to the protocol of the Centers for Disease Control and Prevention (Atlanta, GA, USA), as approved by the US Food and Drug Administration.

Analysis of Patient and Staff Trajectories

We extracted anonymized patient mobility trajectory data from our hospital information system. COVID-19 was diagnosed when patients either showed typical clinical symptoms or had COVID-19–typical findings in low-dose lung computed tomography scans and tested positive for SARS-CoV-2 by RT-PCR or for SARS-CoV-2 IgM or IgG (*10*). For spatiotemporal analysis of patient data, we used all trajectories available during December 30, 2019–May 29, 2020, for each admitted COVID-19 patient because we could not determine the exact interval when the patients were contagious. We obtained trajectories of SARS-CoV-2 IgG seropositive staff from our questionnaire data if available (February 1–May 29, 2020).

On the basis of the spatiotemporal trajectories of patients and staff, we created 2 types of representations: static representations over all timeframes and dynamically animated representations. The static representation is based on the relative proportion of patients or staff members at each hospital location normalized by all locations of the available trajectory time. For the dynamic representation, we illustrated 2 different relative proportions normalized by all time frames: the relative proportion of individual patients in each hospital location and the relative proportion of staff members mapped to their past locations for 14 days before they tested positive for SARS-CoV-2 IgG or were quarantined.

To analyze patient mobility within the hospital during the pandemic, we compared the spatial trajectories of COVID-19 patients to all patients given a diagnosis of any non–COVID-19 pneumonia (viral or bacterial) during December 1, 2019–June 10, 2020 (Appendix Figure 3). We performed all analyses by using R software version 3.6.0 (R Foundation for Statistical Computing, https://www.r-project.org) and made the source code available on GitHub (https://github.com/AnaGalhoz37/SeCOMRI).

Statistical Analysis

Absolute and relative frequencies of positive test results for SARS-CoV-2 IgG and IgM (Chemiluminescence Immunoassay, Shenzhen Yhlo Biotech Co.) are given for all study participants and relevant subgroups, along with exact 95% CIs for the estimated seroprevalence. To evaluate the association with potential risk factors, we estimated odds ratios (ORs) and corresponding exact 95% CIs (mid-p intervals). The distributions of antibody titers are visualized by boxplots or dot plots and are described by medians and quartiles. We used the Spearman rank correlation coefficient to evaluate the association between the time of IgG testing and the IgG titer. We did not adjust the 95% CI widths for multiplicity. Missing data were not imputed, and the number of missing values is presented for each variable. We conducted statistical analyses by using R software version 4.0.2 (R Foundation for Statistical Computing).

Results

Seroprevalence of SARS-CoV-2 IgG for 4,554 Hospital Employees

The study participation rate was 63.5% (4,001/6,305) for employees and 35.5% (603/1,699) for medical

students; complete data for 4,554 persons were available for primary analysis (Appendix Figure 1). The mean age of the study participants was 38.5 years; 3,207 (70.4%) were women and 1,342 (29.5%) were men (Appendix Figure 4). Positive results for SARS-CoV-2 IgG were found for 108/4,554 study participants. For 102 persons, additional assays confirmed the SARS-CoV-2 IgG screening result (Appendix Table 1). Two additional persons who had a positive PCR result seroconverted during follow-up. Four persons who had IgG titers of 5–10 AU/mL in the screening assay, which is below the cutoff, were found to be positive in ≥2 other assays (Appendix Tables 1, 2). For 5 persons, the screening result could not be confirmed by the other assays used; for 1 person, there was insufficient material available to complete testing (Appendix Tables 3, 4). When we considered all 108 study participants who were positive for SARS-CoV-2 IgG in ≥2 different assays, we determined a seroprevalence of 2.4% (95% CI 1.9%–2.9%) (primary endpoint).

Individual and Occupational Risk Factors for SARS-CoV-2 Infection

The first patient who had PCR-confirmed COVID-19 was admitted to our university hospital on March 6, 2020, and 163 COVID-19 patients were hospitalized during March 6–May 29 (Figure 1). Infection prevention measures, such as the obligation to wear surgical masks, physical distancing measures, visitor rules, or policies for nonurgent procedures, were dynamically adjusted according to the prevalent pandemic situation (Figure 1). Risk factors for infection of staff were identified through correlation of self-reported survey data with seropositivity for SARS-CoV-2 IgG (Table 1). We found an association between seropositivity and male sex (OR 1.54, 95% CI 1.03–2.27) or age; the highest frequency was observed for persons 51–60 years of age (OR 1.75, 95% CI 1.06–2.85, compared with persons ≤30 years of age) (Table 1; Appendix Figures 4, 5). We found a higher relative frequency of seropositivity for persons who had diabetes mellitus (OR 2.96, 95% CI 1.01–6.81) but observed no major differences in staff who had preexisting pulmonary or cardiovascular disease (Table 2; Appendix Figure 5). Seropositivity was decreased for smokers (OR 0.52, 95% CI 0.26–0.94) (Table 2); relevant difference in seropositivity was observed between HCWs involved in direct patient care, including care of COVID-19 patients, and HCWs working in intensive care units or the emergency department compared with staff members not working in these units and not performing patient-associated tasks (Table 2; Figure 2, panel A; Appendix Figure 5).

Conversely, we found that seropositivity was particularly high for administrative staff who did not have any direct patient contact (OR 2.36, 95% CI 1.19–4.80) (Table 1; Figure 2, panel B; Appendix Figure 5). Nonclinical staff were not obliged to wear masks at work at the beginning of the pandemic (Figure 1). Seropositivity was also markedly increased in staff who reported exposure to co-workers (OR 1.74, 95% CI 1.11–2.65) or private contacts with persons who had SARS-CoV-2 infections (OR 5.56, 95% CI 3.32–8.94) (Table 2; Figure 2, panel A; Appendix Figure 5). Self-reported unprotected contact with COVID-19 patients (no surgical mask, <1.5-m distance, or AGP without

Table 1. Seroprevalence of SARS-CoV-2 infections in patients and staff, by general characteristics and occupation, at a university hospital, Munich, Germany*

Characteristic	SARS-CoV-2 IgG, no. (%)		Odds ratio (95% CI)
	Negative	Positive	
Age group, y			
18–30, n = 1,622	1,585 (97.7)	37 (2.3)	Referent
31–40, n = 1,134	1,115 (98.3)	19 (1.7)	0.73 (0.41–1.27)
41–50, n = 758	740 (97.6)	18 (2.4)	1.05 (0.58–1.83)
51–60, n = 766	736 (96.1)	30 (3.9)	1.75 (1.06–2.85)
>60, n = 274	270 (98.5)	4 (1.5)	0.66 (0.19–1.66)
Sex			
F, n = 3,207	3,141 (97.9)	66 (2.1)	Referent
M, n = 1,342	1,300 (96.9)	42 (3.1)	1.54 (1.03–2.27)
Unreported, n = 5	5 (100)	0	
Profession			
Nurses, n = 958	934 (97.5)	24 (2.5)	1.55 (0.80–3.10)
Physicians, n = 860	846 (98.4)	14 (1.6)	Referent
Clinical ancillary staff, n = 383	374 (97.7)	9 (2.3)	1.46 (0.60–3.39)
Nonclinical ancillary staff, n = 120	118 (98.3)	2 (1.7)	1.09 (0.16–4.02)
Scientists/laboratory workers, n = 635	627 (98.7)	8 (1.3)	0.78 (0.31–1.84)
Administrative staff, n = 557	536 (96.2)	21 (3.8)	2.36 (1.19–4.80)
Other, n = 424	412 (97.2)	12 (2.8)	1.76 (0.79–3.88)
Students, n = 603	586 (97.2)	17 (2.8)	1.75 (0.85–3.65)

*SARS-CoV-2, severe acute respiratory syndrome coronavirus 2.

Table 2. SARS-CoV-2 seroprevalence for healthcare workers, by self-reported risk factors and symptoms, at a university hospital, Munich, Germany*

Characteristic	No. SARS-CoV-2 IgG positive/no. with data available (%)		Odds ratio (95%CI)	No. SARS-CoV-2 IgG positive/no. with data missing
	True	False		
Individual risk factors				
Pulmonary disease	8/317 (2.5)	99/4,212 (2.4)	1.1 (0.48–2.14)	1/25
Cardiovascular disease	5/329 (1.5)	102/4,200 (2.4)	0.64 (0.22–1.43)	1/25
Diabetes mellitus	5/79 (6.3)	102/4,451 (2.3)	2.96 (1.01–6.81)	1/24
Immunodeficiency	0/92 (0.0)	107/4,434 (2.4)		1/28
Immunosuppressive therapy	1/69 (1.4)	105/4,461 (2.4)	0.7 (0.03–3.15)	2/24
Smoking	11/817 (1.3)	96/3,718 (2.6)	0.52 (0.26–0.94)	1/19
Exposure				
Patient facing role	55/2559 (2.1)	50/1,934 (2.6)	0.83 (0.56–1.22)	3/61
AGPs	9/712 (1.3)	96/3,794 (2.5)	0.50 (0.23–0.94)	3/48
COVID-19 assigned unit	21/712 (2.9)	85/3,803 (2.2)	1.34 (0.80–2.13)	2/39
Emergency department	11/515 (2.1)	95/3,999 (2.4)	0.91 (0.46–1.64)	2/40
Ward	43/1633 (2.6)	63/2,882 (2.2)	1.21 (0.81–1.79)	2/39
Intensive care unit	16/690 (2.3)	89/3,824 (2.3)	1.00 (0.56–1.67)	3/40
Contact with SARS-CoV-2–positive person				
Patient	31/1028 (3.0)	74/3436 (2.2)	1.42 (0.91–2.15)	3/90
Co-worker	29/816 (3.6)	76/3644 (2.1)	1.74 (1.11–2.65)	3/94
Private contact	22/220 (10.0)	83/4218 (2.0)	5.56 (3.32–8.94)	3/116
Unprotected contact	34/435 (7.8)	70/3997 (1.8)	4.77 (3.09–7.22)	4/122
Protected contact	32/1230 (2.6)	73/3237 (2.3)	1.16 (0.75–1.75)	3/87
Personal protective equipment				
Use of PPE	104/4458 (2.3)	2/75 (2.7)	0.81 (0.25–5.35)	2/21
Surgical mask	104/4437 (2.3)	2/95 (2.1)	1.04 (0.32–6.83)	2/22
FFP2/N95-mask	32/1497 (2.1)	74/3011 (2.5)	0.87 (0.56–1.31)	2/46
FFP3-mask	8/325 (2.5)	96/4163 (2.3)	1.09 (0.48–2.13)	4/66
Protective clothing	34/1677 (2.0)	72/2835 (2.5)	0.8 (0.52–1.19)	2/42
Eye protection or face shield	29/1580 (1.8)	77/2934 (2.6)	0.7 (0.45–1.06)	2/40
Symptoms				
Experienced symptoms	79/1272 (6.2)	28/3263 (0.9)	7.62 (4.98–12.00)	1/19
Exhaustion	54/771 (7.0)	53/3763 (1.4)	5.27 (3.57–7.78)	1/20
Fatigue	67/795 (8.4)	40/3738 (1.1)	8.49 (5.72–12.77)	1/21
Cough	50/668 (7.5)	57/3861 (1.5)	5.40 (3.65–7.97)	1/25
Shortness of breath	19/307 (6.2)	88/4222 (2.1)	3.12 (1.82–5.08)	1/25
Rhinitis	47/689 (6.8)	60/3843 (1.6)	4.62 (3.11–6.82)	1/22
Loss of smell	36/144 (25.0)	71/4384 (1.6)	20.23 (12.87–31.41)	1/26
Loss of taste	39/124 (31.5)	67/4402 (1.5)	29.62 (18.79–46.38)	2/28
Sore throat	30/740 (4.1)	77/3792 (2.0)	2.05 (1.31–3.11)	1/22
Headache	46/766 (6.0)	61/3766 (1.6)	3.88 (2.61–5.73)	1/22
Limb pain	36/403 (8.9)	71/4129 (1.7)	5.61 (3.67–8.45)	1/22
Shivering	36/442 (8.1)	71/4092 (1.7)	5.03 (3.29–7.56)	1/20
Diarrhea	20/316 (6.3)	87/4214 (2.1)	3.22 (1.90–5.21)	1/24
Increased temperature	46/491 (9.4)	61/4032 (1.5)	6.73 (4.51–9.98)	1/31
Fever, temperature >38°C	29/233 (12.4)	77/4288 (1.8)	7.79 (4.90–12.1)	2/33

*AGP, aerosol-generating procedure, COVID-19, coronavirus disease; FFP, filtering face piece; PPE¸ personal protective equipment, SARS-CoV-2, severe acute respiratory syndrome coronavirus 2.

filtering masks with either filtering face piece or N95 standard or eye protection or face shields) was associated with higher seroprevalence (OR 4.77, 95% CI 3.09–7.22) (Table 2; Appendix Figure 5). For staff reporting to perform AGPs we observed an even lower rate of seropositivity (OR 0.50, 95% CI 0.23–0.94) (Table 2; Figure 2, panel A; Appendix Figure 5).

Symptoms and SARS-CoV-2 IgG Titers for Hospital Staff

In our cohort, 1,272 (27.9%) persons reported current or recent (within 8 weeks before testing) presence of ≥1 symptom indicative of COVID-19 (Table 2; Appendix Figure 5), 79 (6.2%) of whom were seropositive for SARS-CoV-2 IgG (Table 2; Appendix Figure 5). Loss of smell (36 [25.0%] seropositive of 144 persons who had reported loss of smell) and loss of taste (39 [31.5%] of 124 persons) had the highest positive predictive value (Table 2; Appendix Figure 5), and seropositivity was associated with a higher number of symptoms reported (Table 3; Appendix Figure 5).

For seropositive persons, we found no major differences in SARS-CoV-2 IgG titers for different age groups, sex, comorbidities, or exposure profiles (Appendix Figure 6). However, SARS-CoV-2

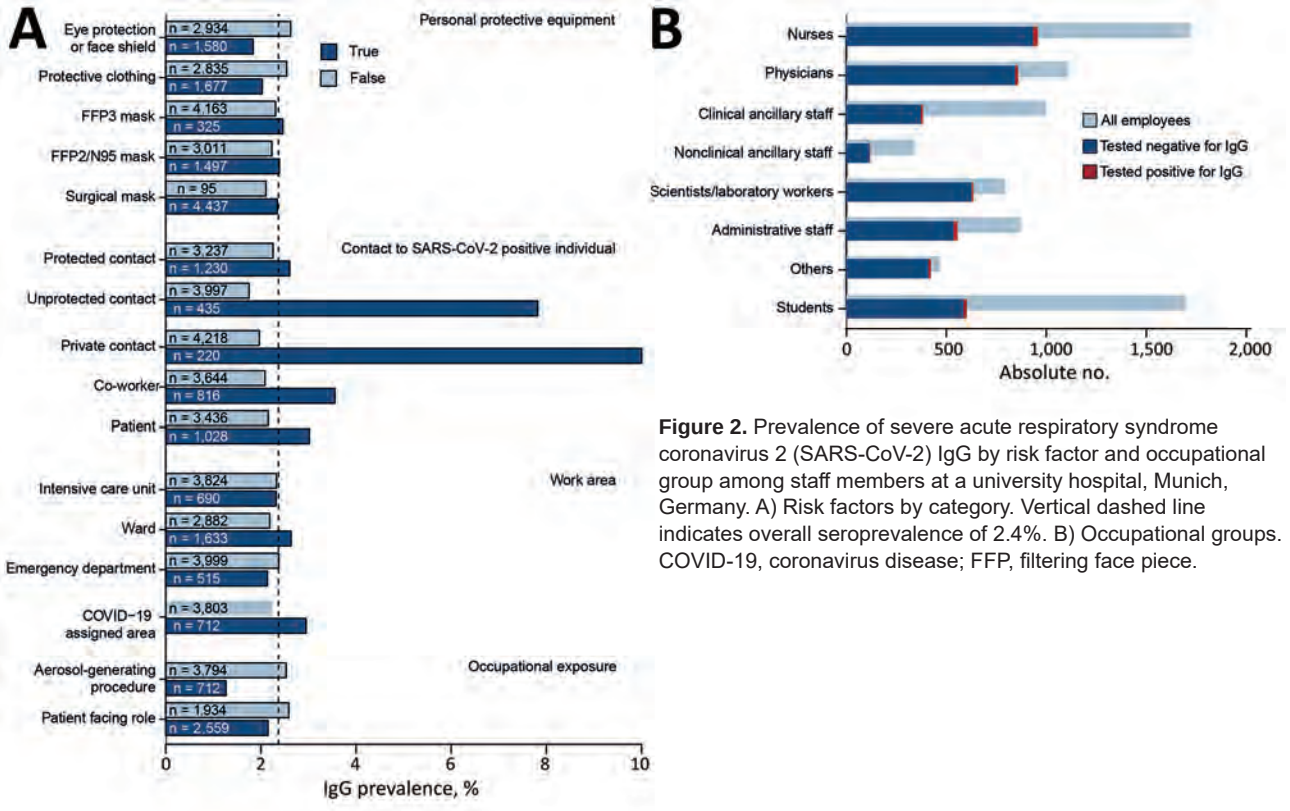

Figure 2. Prevalence of severe acute respiratory syndrome coronavirus 2 (SARS-CoV-2) IgG by risk factor and occupational group among staff members at a university hospital, Munich, Germany. A) Risk factors by category. Vertical dashed line indicates overall seroprevalence of 2.4%. B) Occupational groups. COVID-19, coronavirus disease; FFP, filtering face piece.

IgG levels were higher for staff who reported more COVID-19-related symptoms (Appendix Figure 7). We observed the highest titers for those persons who reported diarrhea, fever, increased temperature, shivering, limb pain, and headache (Appendix Figure 7).

Value of Symptom-Based RT-PCR Testing

We initiated symptom-based RT-PCR testing of material obtained from nasopharyngeal swab specimens early during the pandemic through a dedicated COVID-19 telephone hotline. The first hospital employee with SARS-CoV-2 infection was identified on March 9, 2020, and 28 persons who had SARS-CoV-2 infections detected by RT-PCR before participating in this study were positive for SARS-CoV-2 IgG (Figure 1; Appendix Figure 8). Ten seropositive persons had a positive PCR result; 1 positive antibody testing result was obtained at another facility. However, 68 (63%) of 108 SARS-CoV-2 infections had not been diagnosed previously; data on previous testing was missing for 1 person. Among these 68 seropositive persons, 28 did not report any COVID-19-typical symptoms in the initial survey (25.9% of all seropositive staff), indicating that symptom-based testing can miss SARS-CoV-2 infection.

Table 3. Seroprevalence of SARS-CoV-2 IgG in patients and staff, by symptom onset and frequency, at a university hospital, Munich, Germany*

Characteristic	SARS-CoV-2IgG, no. (%)		Odds ratio (95% CI)
	Negative	Positive	
Symptom onset			
Not applicable, n = 3,373	3,336 (98.9)	37 (1.1)	Referent
Past 14 days, n = 219	209 (95.4)	10 (4.6)	4.36 (2.02–8.59)
Past 3–8 weeks, n = 943	883 (93.6)	60 (6.4)	6.11 (4.05–9.35)
Unknown, n = 19	18	1	
Symptom frequency, p<0.001			
0, n = 3,273	3,245 (99.1)	28 (0.9)	Referent
1–4, n = 548	529 (96.5)	19 (3.5)	4.17 (2.27–7.50)
5–8, n = 491	454 (92.5)	37 (7.5)	9.42 (5.72–15.70)
9–14, n = 223	200 (89.7)	23 (10.3)	13.32 (7.45–23.58)
Unknown, n = 19	18	1	

*SARS-CoV-2, severe acute respiratory syndrome coronavirus 2.

Analysis of Spatiotemporal Trajectories

To identify and localize potential hotspots of infection, we systematically analyzed contact between staff and COVID-19 patients by using the cumulative data for serologic analysis for staff and the patient registry. Thus, we plotted available spatial and temporal information on the presence of COVID-19 patients and SARS-CoV-2 IgG–positive staff with daily resolution on a hospital map. Visualization of these spatiotemporal mobility trajectories showed only a slight overlap between the distinct spatial and temporal hotspots of COVID-19 patients and SARS-CoV-2 IgG–positive staff (Figure 3; Videos 1–3, https://wwwnc.cdc.gov/EID/article/28/3/20-4436-V1.htm, https://wwwnc.cdc.gov/EID/article/28/3/20-4436-V2.htm, https://wwwnc.cdc.gov/EID/article/28/3/20-4436-V3.htm).

Discussion

Despite the high overall number of patients in our hospital who had COVID-19 disease, the seroprevalence of 2.4% for SARS-CoV-2 IgG among university hospital staff after the first wave in Germany is lower than that reported in previous studies (*11*,*12*). This difference might be attributed to differences in cohort composition, fast implementation of protective measures, or frequency of exposure.

Hospital staff have an increased occupational risk for contact with SARS-CoV-2–infected patients, and a high level of SARS-CoV-2 infection among HCWs involved in the care of COVID-19 patients has been reported (*7*,*13*). Consistent with these findings, the seropositivity in a population-based prospective cohort study performed in Munich in parallel with our study was 1.8% and thus lower than for this HCW cohort study (*14*). We did not observe higher seroprevalences in staff who reported direct patient contact, including those working in COVID-19–designated units. We also observed lower seroprevalence in staff who reported performing AGPs, possibly reflecting increased awareness and use of particularly rigorous infection prevention practices at work and in private life in this subgroup. Furthermore, the type of PPE used was not associated with seroprevalence, but 98% of staff reported routinely using surgical masks, which was required by internal hospital policy for staff involved in patient care starting on March 16, 2020, and for all staff starting

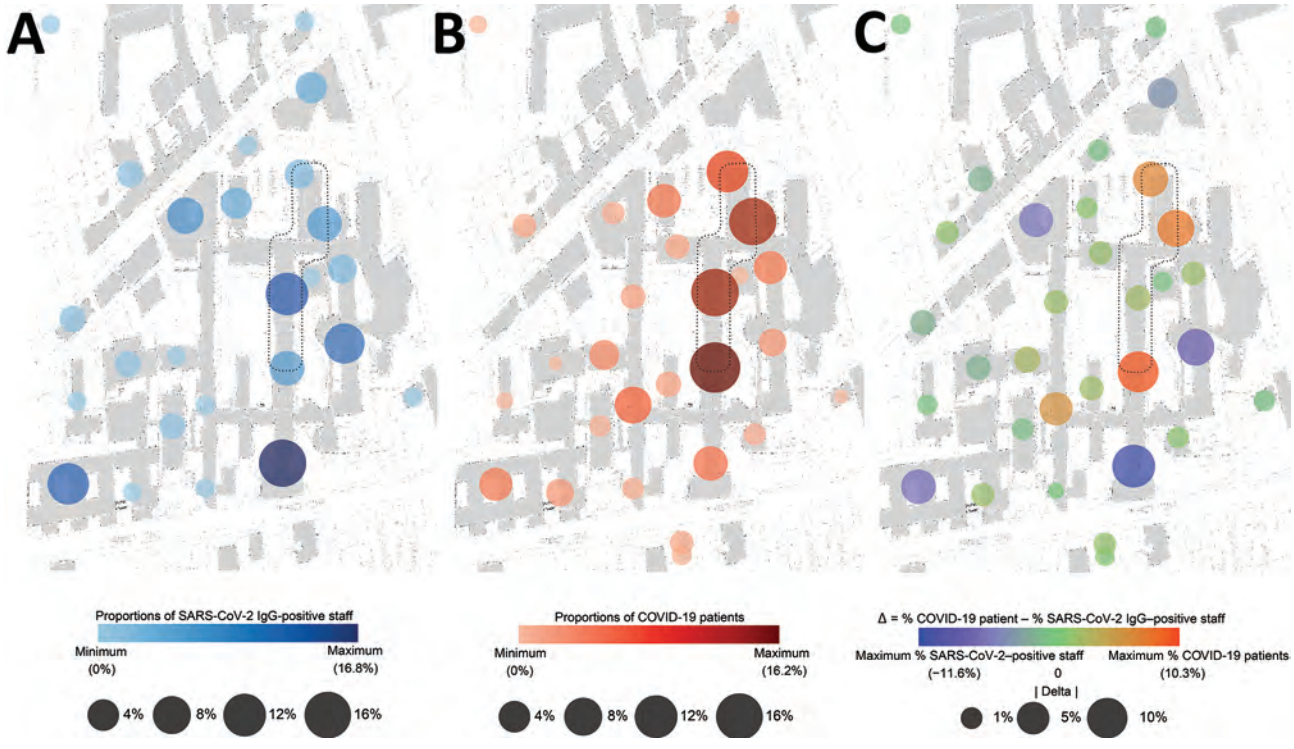

Figure 3. Spatiotemporal trajectories of severe acute respiratory syndrome coronavirus 2–infected patients and staff mobility in university hospital, Munich, Germany. A) Cumulative representation of proportions of seropositive staff. B) Cumulative representation of proportions of COVID-19-patients. C) Differences (Δ) for staff and patients between different hospital areas. Difference are indicated by dot plots and assigned to distinct hospital areas. For purposes of discretion of data from study participants, the graphic representation of spatial information is partially distorted. Dashed lines indicate COVID-19–designated areas in the hospital.

on March 27. The almost parallel increase in SARS-CoV-2 infection cases in staff and patients is suggestive of extrinsic infection causes in both groups, such as simultaneous return from high-risk holiday areas. Consistently, exposure to SARS-CoV-2-infected private contacts or co-workers was the most critical risk factor for SARS-CoV-2 infection in our cohort. This finding underscores the need for adherence to protective measures during private, professional staff, and professional patient contacts.

Male staff in our study cohort showed a higher seroprevalence. A recent study reporting lower perceived infection risk for men than for women found that adherence to hygiene guidelines and social distancing measures might have been lower in male staff (*15*,*16*). Smokers showed a lower seroprevalence, which is in contrast to that reported in previous studies (*2*,*6*,*15*,*17*). Because smokers are more susceptible to respiratory tract infections and smoking involves hand-to-mouth contact and frequent social interactions, the lower seroprevalence is unexpected but consistent with those of other reports (*18*–*21*). Staff who had diabetes mellitus had a higher seroprevalence than staff who did not have this disease. Previously, diabetes mellitus reportedly correlated with severity of COVID-19 and associated deaths, but no increase in susceptibility to SARS-CoV-2 infection has been reported to date (*22*).

Serologic assessment confirmed infection in most persons who reported positive test results for SARS-CoV-2 by PCR. However, repeated testing over >4 weeks with ≥2 separate assays each did not detect antibodies in 6 persons (2 who had positive in-house and 4 who had reported positive external RT-PCR test results) (Appendix Figure 8). This finding might be explained by false-positive PCR results or by the failure to develop antibody responses after low-symptom infection, which might occur in ≤10% of convalescent-phase patients after SARS-CoV-2 infection (*25*).

The IgG immunoassay used for screening had a specificity of 99.89% in our study; it uses 2 SARS-CoV-2 antigens (nucleocapsid and spike 1) for detection and has an estimated sensitivity of 96.30% (Appendix Table 5). We retested all IgM-positive or IgG-positive serum samples and all serum samples that had titers of 5–10 AU/mL, which is below the cutoff, by a second assay with particularly high specificity (99.90%) that uses recombinant nucleocapsid protein as antigen. If required, additional assays were performed: either an ELISA using recombinant spike 1 protein as capture antigen, or immunoblotting that tested for antibodies against 3 different SARS-CoV-2 antigens. Serum was only considered positive if ≥2 antibody assay results were positive (Appendix). However, the requirement of such extensive confirmatory testing strengthens the notion that each test for SARS-CoV-2 antibodies requires critical evaluation.

Our study also showed that approximately two thirds of the seropositive staff had a previously undetected infection. These infections might have been oligosymptomatic or asymptomatic without even alarming medically trained personnel. Furthermore, 25 SARS-CoV-2 IgG–positive persons had not been PCR tested, despite reporting ≥1 COVID-19–compatible symptom. A total of 1,183 staff members tested seronegative despite reporting ≥1 symptom related to COVID-19. The focus on symptoms with the strongest association with seropositivity, such as loss of smell, loss of taste, fatigue, fever, and cough, might therefore be helpful in developing more accurate and economical screening algorithms. Our results highlight that symptom-based testing might miss infections in hospital staff. All 28 asymptomatic seropositive persons remained undiagnosed before the study, emphasizing the need for rigorous implementation of systematic infection prevention practices in pandemic situations. Transmission by asymptomatic and presymptomatic staff might occur at any time and will not be prevented by random testing. These results strongly support the continuous use of at least surgical masks as a simple and efficient measure for employee and patient protection.

To identify infection hotspots and putative patient/staff overlaps, we visualized the temporospatial mobility trajectories of patients and staff to monitor the infection dynamics. Real-time use of such trajectory mapping at high resolution might yield additional information that enables the reaction to procced more quickly and intuitively to infection foci. Continuous evaluation of mobility trajectory mappings might highlight areas of recurrent infections and thus identify previously unattended needs that should be addressed for future waves of the pandemic.

Our study's first limitation is that because this was a voluntary assessment, participation was incomplete and might have biased the results. We cannot exclude the possibility that staff members with a higher perceived risk for infection were more likely to participate. Second, symptoms and exposures were retrospectively assessed and self-reported and thus subject to a recall bias in participants knowing of their SARS-CoV-2 infection. Third, we did not assess individual adherence of mask wearing in our questionnaire, especially regarding specific, potentially

hazardous situations (e.g., during breaks, in locker rooms). Consequently, this approach does not enable us to pinpoint risk for work-related infection to specific situations.

In addition, because it was not obligatory to indicate in our questionnaire the periods during which masks were worn, the analysis reflects the protective effect of masks over the entire period. Furthermore, although we attempted a cross-sectional analysis, our data document average seroprevalence during the entire testing period. Thus, seroconversions occurring during this period might have been missed. Finally, RT-PCR testing results were available only for persons who consented to their use (4,373/4,554), limiting the possibility of cross-validating PCR-testing results with seroprevalence.

Our findings have several major implications. The infection rate for HCWs was not markedly increased, and infections occurred in parallel to the general population. We did not observe a relevant increase in SARS-CoV-2 IgG seropositivity in HCWs (including those working with COVID-19 patients) compared with staff who were not directly involved in patient care, as long as PPE was used, suggesting that PPE and other infection control practices successfully prevented transmission from SARS-CoV-2–infected patients. Interaction with SARS-CoV-2–infected co-workers or private contacts was a major risk factor for infection. The infection rate among HCWs seemed to decrease when wearing surgical face masks became obligatory in all areas of the hospital. Thus, obligatory wearing of certified surgical masks by all employees, no matter when in contact with patients, relatives, or colleagues, and, whenever tolerated, also by patients, might minimize virus transmission risks. However, it was not possible to formally separate that effect from that of minimizing personal contacts imposed by the general lock-down and a concomitant decrease in COVID-19 incidence.

In summary, the value of SARS-CoV-2 antibodies for protective immunity and their sustainability in infected persons remains unclear. Longitudinal studies with combined testing for virus-specific antibodies and their infection-neutralizing ability, as well as virus-specific T-cell immunity, are needed to estimate the longevity and protective value of SARS-CoV-2 IgG responses in hospital staff. However, our results show that patient-facing healthcare work during the SARS-CoV-2 pandemic might be safe as long as adequate PPE is used and infection prevention practices are followed, both inside and outside the hospital.

Members of the SeCoMRI Study Group: Balqees Al Darweesh, Clara Balzer, Felix Bauerdorf, Alexander Böhner, Dirk Busch, Lisena Cala, Ana Cirac, Adam Chaker, Anaïs Marie Theresa Doll, Johanna Erber, Manon Feuchtinger, Ana Galhoz, Friedemann Gebhardt, Marisa Geisberger, Markus Gerhard, Oliver Goldhardt, Katharina Gresset-Kaliebe, Natalia Graf, Florian Groß, Roman Günthner, Martin Halle, Bernhard Haller, Joachim Hellemann, Andreas Henkel, Maximilian Hinz, Dieter Hoffmann, Klaus-Peter Janssen, Robert Kaczmarczyk, Verena Kappler, Percy Knolle, Florian Kohlmayer, Susanne Kossatz, Klaus Kuhn, Zsuzsanna Kurgyis, Vincent Lallinger, Judith Lammer, Paul Lingor, Elke Lorenz, Felix Mayr, Michael M. Menden, Hrvoje Mijočević, Caroline Sandra Moesta, Ruth Neuhauser, Andrea Pagani, Anna Caroline Pilz, Clarissa Prazeres da Costa, Sarah Preis, Ulrike Protzer, Michael Quante, Hedwig Roggendorf, Jürgen Ruland, Cora Scheerer, Roland M. Schmid, Paul Schmidle, Christine Schönmann, Florian Schraml, Christoph D. Spinner, Annette Susanne Steimle-Grauer, Christian Stöß, Pavel Stupakov, Markus Thaler, Dolores Thum, Dirk Tomsitz, Wolfgang Weber, Angelika Werner, and Christof Winter.

Acknowledgments

We thank the study participants for consenting to have their data published; clinical and administrative staff at our hospital for providing contributions involved in enrollment and obtaining informed consent of study participants; technical staff of the Institute of Virology and the Institute of Clinical Chemistry for performing diagnostic tests; Yhlo (Shenzhen, China) and Mikrogen (Neuried, Germany), for providing some of the test kits for free; and the hospital board of directors for providing financial and organizational support.

About the Author

Dr. Erber is a clinician scientist in the Medical Department II of the University Hospital Munich rechts der Isar (Technical University Munich), Munich, Germany. Her primary research interests are infection control measures, and epidemiology and diagnostics of COVID-19 and other infectious diseases.

References

1. Moscola J, Sembajwe G, Jarrett M, Farber B, Chang T, McGinn T, et al.; Northwell Health COVID-19 Research Consortium. Prevalence of SARS-CoV-2 antibodies in health care personnel in the New York City Area. JAMA. 2020;324:893–5. https://doi.org/10.1001/jama.2020.14765
2. Pollán M, Pérez-Gómez B, Pastor-Barriuso R, Oteo J, Hernán MA, Pérez-Olmeda M, et al.; ENE-COVID Study Group. Prevalence of SARS-CoV-2 in Spain (ENE-COVID): a

nationwide, population-based seroepidemiological study. Lancet. 2020;396:535–44. https://doi.org/10.1016/S0140-6736(20)31483-5
3. Xu X, Sun J, Nie S, Li H, Kong Y, Liang M, et al. Seroprevalence of immunoglobulin M and G antibodies against SARS-CoV-2 in China. Nat Med. 2020;26:1193–5. https://doi.org/10.1038/s41591-020-0949-6
4. Iversen K, Bundgaard H, Hasselbalch RB, Kristensen JH, Nielsen PB, Pries-Heje M, et al. Risk of COVID-19 in health-care workers in Denmark: an observational cohort study. Lancet Infect Dis. 2020;20:1401–8. https://doi.org/10.1016/S1473-3099(20)30589-2
5. Steensels D, Oris E, Coninx L, Nuyens D, Delforge ML, Vermeersch P, et al. Hospital-wide SARS-CoV-2 antibody screening in 3,056 staff in a tertiary center in Belgium. JAMA. 2020;324:195–7. https://doi.org/10.1001/jama.2020.11160
6. Garcia-Basteiro AL, Moncunill G, Tortajada M, Vidal M, Guinovart C, Jiménez A, et al. Seroprevalence of antibodies against SARS-CoV-2 among health care workers in a large Spanish reference hospital. Nat Commun. 2020;11:3500. https://doi.org/10.1038/s41467-020-17318-x
7. Poulikakos D, Sinha S, Kalra PA. SARS-CoV-2 antibody screening in healthcare workers in a tertiary centre in North West England. J Clin Virol. 2020;129:104545. https://doi.org/10.1016/j.jcv.2020.104545
8. Medical University of Innsbruck. Ischgl study: 42.4 percent are antibody-positive [in German] [cited 2020 Aug 10]. https://www.i-med.ac.at/mypoint/news/746359.html
9. Prasser F, Kohlbacher O, Mansmann U, Bauer B, Kuhn KA. Data integration for future medicine (DIFUTURE). Methods Inf Med. 2018;57(S 01):e57–e65.
10. Burian E, Jungmann F, Kaissis GA, Lohöfer FK, Spinner CD, Lahmer T, et al. Intensive care risk estimation in COVID-19 pneumonia based on clinical and imaging parameters: experiences from the Munich cohort. J Clin Med. 2020;9:E1514. https://doi.org/10.3390/jcm9051514
11. World Health Organization. Coronavirus disease (COVID-19) outbreak situation [cited 2020 Aug 10]. https://www.who.int/emergencies/diseases/novel-coronavirus-2019
12. Wei XS, Wang XR, Zhang JC, Yang WB, Ma WL, Yang BH, et al. A cluster of health care workers with COVID-19 pneumonia caused by SARS-CoV-2. J Microbiol Immunol Infect. 2020.
13. Chou R, Dana T, Buckley DI, Selph S, Fu R, Totten AM. Epidemiology of and risk factors for coronavirus infection in health care workers. Ann Intern Med. 2020;173:120–36. https://doi.org/10.7326/M20-1632
14. Pritsch M, Radon K, Bakuli A, Le Gleut R, Olbrich L, Guggenbüehl Noller JM, et al.; on behalf of the KoCo Study Group. Prevalence and risk factors of infection in the representative COVID-19 cohort Munich. Int J Environ Res Public Health. 2021;18:3572. https://doi.org/10.3390/ijerph18073572
15. Stringhini S, Wisniak A, Piumatti G, Azman AS, Lauer SA, Baysson H, et al. Seroprevalence of anti-SARS-CoV-2 IgG antibodies in Geneva, Switzerland (SEROCoV-POP): a population-based study. Lancet. 2020;396:313–9. https://doi.org/10.1016/S0140-6736(20)31304-0
16. Behrens GM, Cossmann A, Stankov MV, Witte T, Ernst D, Happle C, et al. Perceived versus proven SARS-CoV-2-specific immune responses in health-care professionals. Infection. 2020;48:631–4. https://doi.org/10.1007/s15010-020-01461-0
17. Xu X, Sun J, Nie S, Li H, Kong Y, Liang M, et al. Seroprevalence of immunoglobulin M and G antibodies against SARS-CoV-2 in China. Nat Med. 2020;26:1193–5. https://doi.org/10.1038/s41591-020-0949-6
18. Grundy EJ, Suddek T, Filippidis FT, Majeed A, Coronini-Cronberg S. Smoking, SARS-CoV-2 and COVID-19: a review of reviews considering implications for public health policy and practice. Tob Induc Dis. 2020;18:58. https://doi.org/10.18332/tid/124788
19. Millett ER, De Stavola BL, Quint JK, Smeeth L, Thomas SL. Risk factors for hospital admission in the 28 days following a community-acquired pneumonia diagnosis in older adults, and their contribution to increasing hospitalisation rates over time: a cohort study. BMJ Open. 2015;5:e008737. https://doi.org/10.1136/bmjopen-2015-008737
20. Almirall J, Serra-Prat M, Bolíbar I, Balasso V. Risk factors for community-acquired pneumonia in adults: a systematic review of observational studies. Respiration. 2017;94:299–311. https://doi.org/10.1159/000479089
21. Farsalinos K, Niaura R, Le Houezec J, Barbouni A, Tsatsakis A, Kouretas D, et al. Editorial: nicotine and SARS-CoV-2: COVID-19 may be a disease of the nicotinic cholinergic system. Toxicol Rep. 2020;7:658–63. https://doi.org/10.1016/j.toxrep.2020.04.012
22. Mazucanti CH, Egan JM. SARS-CoV-2 disease severity and diabetes: why the connection and what is to be done? Immun Ageing. 2020;17:21. https://doi.org/10.1186/s12979-020-00192-y
23. Long QX, Tang XJ, Shi QL, Li Q, Deng HJ, Yuan J, et al. Clinical and immunological assessment of asymptomatic SARS-CoV-2 infections. Nat Med. 2020;26:1200–4. https://doi.org/10.1038/s41591-020-0965-6

Address for correspondence: Paul Lingor, Department of Neurology, University Hospital rechts der Isar, Technical University of Munich, Germany, Ismaningerstrasse 22, 81675 Munich, Germany; paul.lingor@tum.de

Overseas Treatment of Latent Tuberculosis Infection in US–Bound Immigrants

Amera Khan, Christina R. Phares, Hoang Lan Phuong, Dang Thi Kieu Trinh, Ha Phan, Cindy Merrifield, Phan Thi Hong Le, Quach Thi Kim Lien, Sooc Ngoc Lan, Phan Thi Kim Thoa, Le Tran Minh Thu, Tiffany Tran, Cuc Tran, Lucy Platt, Susan A. Maloney, Nguyen Viet Nhung, Payam Nahid, John E. Oeltmann

Seventy percent of tuberculosis (TB) cases in the United States occur among non–US-born persons; cases usually result from reactivation of latent TB infection (LTBI) likely acquired before the person's US arrival. We conducted a prospective study among US immigrant visa applicants undergoing the required overseas medical examination in Vietnam. Consenting applicants ≥15 years of age were offered an interferon-γ release assay (IGRA); those 12–14 years of age received an IGRA as part of the required examination. Eligible participants were offered LTBI treatment with 12 doses of weekly isoniazid and rifapentine. Of 5,311 immigrant visa applicants recruited, 2,438 (46%) consented to participate; 2,276 had an IGRA processed, and 484 (21%) tested positive. Among 452 participants eligible for treatment, 304 (67%) initiated treatment, and 268 (88%) completed treatment. We demonstrated that using the overseas medical examination to provide voluntary LTBI testing and treatment should be considered to advance US TB elimination efforts.

In 1989, the US Advisory Council on the Elimination of Tuberculosis declared a goal to eliminate tuberculosis (TB) in the United States by 2010 (*1*). TB elimination is defined as <1 case/1 million population; in 2018, the United States reported 28 TB cases/1 million population (*1*). Although US TB incidence has been declining for the past 20 years, with an all-time low of ≈9,000 reported cases in 2018, TB elimination is still far from reality (*2*).

US TB epidemiology can be summarized as a dwindling overall incidence with an increasing proportion of cases diagnosed among non–US-born persons. In 2018, 70.2% of TB cases were diagnosed among non–US-born persons (*2*). Molecular studies suggest most TB cases occurring among non–US-born persons are caused by reactivation of latent TB infection (LTBI), likely acquired before the person's US arrival because of higher risk for TB exposure overseas (*3*,*4*). LTBI treatment has been demonstrated to substantially reduce the risk for progression to TB disease (*5*). Modeling studies suggest progression toward TB elimination requires strengthening efforts for diagnosing and treating LTBI among non–US-born persons (*6*,*7*). However, postarrival stateside strategies to address LTBI have had suboptimal results (*8*). A recent analysis of data on newly arriving immigrants and refugees at risk for TB found that 35.5% did not complete a US postarrival evaluation for TB and LTBI. Among those who did and were recommended for LTBI treatment, 69.0% initiated treatment and 40.0% completed treatment (*8*).

Immigrant visa applicants abroad are required to undergo a medical examination before US arrival, conducted by panel physicians who are under agreement with the US Department of State. The purpose of the overseas medical examination is to screen for communicable diseases of public health importance as required by the US Immigration and Nationality Act (8 US Code 1182 and 1222) and the Public Health Service Act (US Code 252). Because TB is transmissible, screening and treatment for TB disease are essential components of the examination and are performed in accordance with the Centers for Disease

Author affiliations: Stop TB Partnership, Geneva, Switzerland (A. Khan); London School of Hygiene and Tropical Medicine, London, UK (A. Khan, L. Platt); Centers for Disease Control and Prevention, Atlanta, Georgia, USA (C.R. Phares, C. Tran, S.A. Maloney, J.E. Oeltmann); Cho Ray Hospital Visa Medical Clinic, Ho Chi Minh City, Vietnam (H.L. Phuong, D.T.K. Trinh, P.T.H. Le, Q.T.K. Lien, S.N. Lan, P.T.K. Thoa, L.T.M. Thu); Vietnam National TB Program/University of California–San Francisco Research Collaboration, Hanoi, Vietnam (H. Phan, C. Merrifield, T. Tran, N.V. Nhung, P. Nahid); University of California–San Francisco, San Francisco, California, USA (H. Phan, C. Merrifield, P. Nahid); Vietnam National TB Program, Hanoi (N.V. Nhung)

DOI: https://doi.org/10.3201/eid2803.212131

Control and Prevention (CDC) Technical Instructions for Tuberculosis Screening and Treatment Using Cultures and Directly Observed Therapy 2019 (*9*). Improvements in TB screening and treatment in the overseas medical examination have been associated with a temporal decline in TB cases among non–US-born persons in the United States since 2007 (*10*).

One potential strategy to improve the uptake and completion of LTBI treatment among non–US-born persons is to expand the overseas medical examination to include the use of IGRAs to identify persons with TB infection, and to offer a voluntary 3-month regimen of isoniazid and rifapentine given once weekly (3HP) treatment to applicants who had LTBI diagnosed before immigration (*11*). To date, empirical evidence on the feasibility, acceptability, and effectiveness of predeparture testing and treatment approach is scarce. Therefore, we conducted a prospective study to assess voluntary uptake of LTBI testing and 3HP treatment initiation and completion among US-bound immigrant visa applicants in Vietnam while following them through the LTBI cascade of care.

Methods

Vietnam is in the top 5 countries of birth for non–US-born persons with TB in the United States (*2*). According to the World Health Organization, Vietnam has a high TB burden, with an incidence of 182 cases/100,000 population (95% CI 116–263 cases/100,000 population) (*12*). Approximately one third of the adult population in Vietnam has LTBI (*13*). The Cho Ray Hospital Visa Medical Department (CRH VMD) in Ho Chi Minh City, the main panel physician site, screens ≈1,500 US-bound immigrant visa applicants per month and was selected as the study site.

During September 2018–October 2019, we conducted a prospective study, the Preventing Tuberculosis Overseas Pilot Study (PTOPS), at CRH VMD. Our aim was to assess voluntary uptake of LTBI testing and treatment initiation and completion by US-bound immigrant visa applicants.

Study Eligibility Criteria

Study eligibility included US-bound immigrant visa applicants attending their required medical examination who were ≥12 years of age, not pregnant or breastfeeding, and living in the area of Ho Chi Minh City Province. If during the medical examination or study participants were found to have any of the following conditions, they were excluded from participation: signs or symptoms of TB disease, HIV infection, close-contact with someone with isoniazid- or rifampin-resistant TB; previous treatment for TB disease or LTBI; substance-related disorders or mental disorders; sensitivity to isoniazid or rifamycins; or hepatitis B or C. Participants were also excluded from the study if they had a baseline serum alanine aminotransferase (serum glutamic pyruvic transaminase) >5× the upper limit of normal. Those with known liver disease were excluded if they had a baseline alanine aminotransferase >3× the upper limit of normal or total bilirubin >2× the upper limit of normal.

Study Process

Ethical approvals were obtained by CDC, London School of Hygiene and Tropical Medicine, University of California–San Francisco, and the Vietnam National Lung Hospital. During recruitment, eligible immigrant visa applicants were provided study information in Vietnamese and an opportunity to ask questions (Figure 1). Applicants were informed that participation was voluntary and accepting or declining to participate would not impact their visa application. They were also informed that LTBI testing and treatment are available in the United States after arrival, if they preferred. For insight into losses in the LTBI care cascade, those who declined to participate were asked if they would be willing to provide their reasons for nonparticipation. Immigrant visa applicants who consented to participate were enrolled (Table 1). Participants ≥15 years of age were administered an IGRA, the QuantiFERON Gold in Tube Test (QIAGEN, https://www.qiagen.com) to test for TB infection free of charge as part of the study. Participants 12–14 years of age were already required to receive an IGRA as part of the medical examination. Additional laboratory tests for participants included liver function tests, hepatitis B and C serologic test, and pregnancy tests, if indicated. All laboratory tests were processed unless participants withdrew from the study or were determined to be ineligible because of an abnormal chest radiograph or any other signs or symptoms of TB disease discovered.

For IGRA-negative participants and for IGRA-positive participants who were also hepatitis B- or C-positive, pregnant, or otherwise ineligible, no further participation in the study was requested. However, as part of the immigration process, these IGRA-positive participants were categorized with a class B2 TB, LTBI evaluation classification, which alerts US health departments through CDC's Electronic Disease Notification (EDN) system of the arrival of persons with LTBI (*14*). The classification comes with the recommendation for immigrants to complete a postarrival

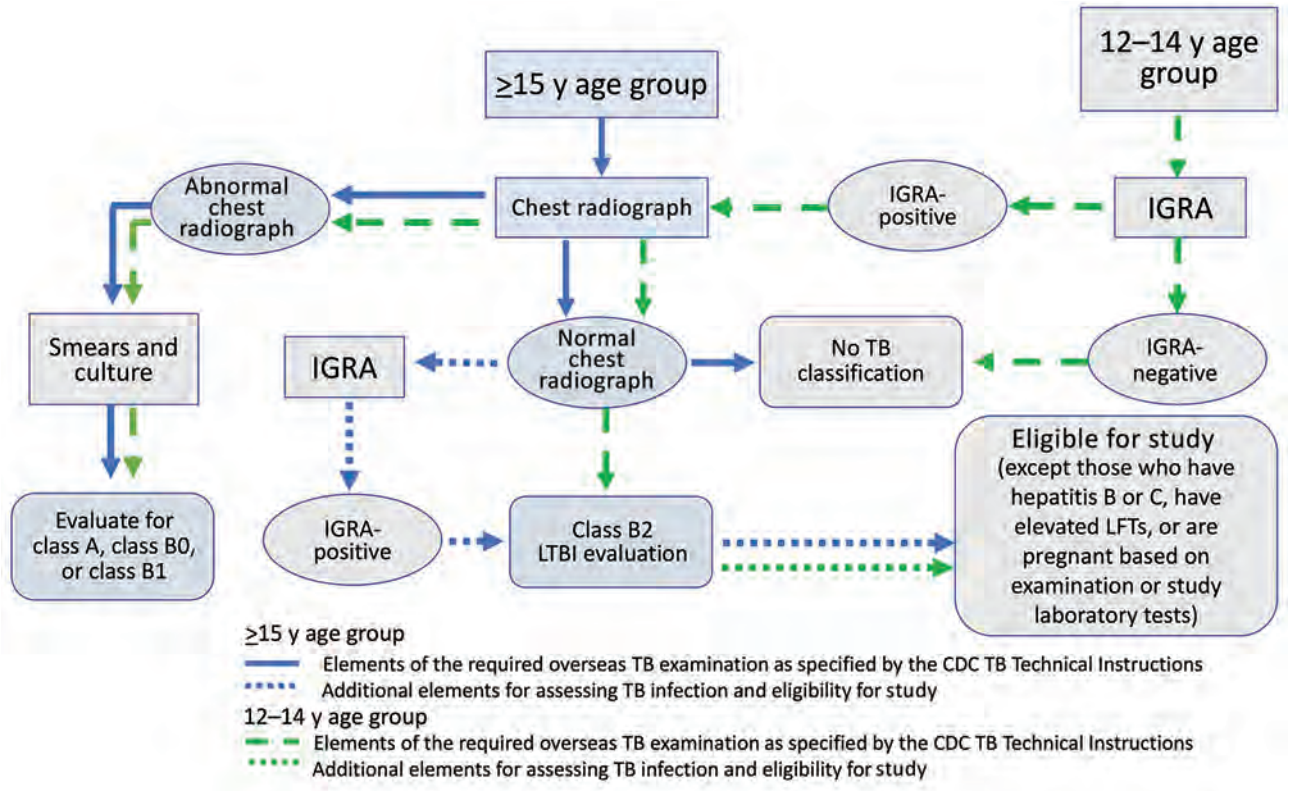

Figure 1. Overseas TB medical examination pathway and TB classifications for US immigrant visa applicants and modifications for the Preventing Tuberculosis Overseas Pilot Study, Vietnam, 2018–2019. TB classifications for overseas medical examination outcomes: No TB classification, no TB disease or infection; class A, TB disease (treatment completion required); class B0, completed treatment for TB disease by directly observed therapy supervised by panel physician; class B1, clinical signs, symptoms, or chest radiograph suggestive of TB or known HIV infection but negative sputum smears and culture; class B2, LTBI evaluation. CDC, Centers for Disease Control and Prevention; IGRA, interferon-γ release assay; LFTs, liver function tests; LTBI, latent tuberculosis infection; TB, tuberculosis.

follow-up evaluation at a US health department where LTBI treatment can be provided if indicated.

The remaining IGRA-positive participants were offered 3HP (12 weekly doses) by directly observed therapy (DOT) at CRH VMD free of charge as part of the study. For those emigrating to the United States before treatment completion, an option was provided for completing ≥8 doses of DOT at CRH VMD and taking the remaining ≤4 doses by self-administration therapy (SAT) in the United States. Thus, a minimum of 8 weeks' stay in Vietnam before immigration was required for participation in the treatment portion of the study. IGRA-positive participants who declined treatment were asked to provide their reasons for declining and were educated about the signs and symptoms of TB. They received a B2 classification with the recommendation to complete a postarrival follow-up in the United States. Participants who accepted treatment were given 3HP weekly by DOT for at least the first 8 doses at CRH VMD. At these DOT visits, participants were assessed for treatment side effects. Those who took the last ≤4 doses by SAT in the United States received a weekly follow-up call by a US-based, Vietnamese-speaking study coordinator to document whether treatment was taken and to assess for any adverse events. We defined treatment completion as taking ≥11 of the 12 doses of 3HP within 16 weeks (*15*).

Results

Study Flow and LTBI Cascade of Care

Of 5,311 eligible US-bound immigrant visa applicants, 2,438 (46%) consented to participate in the study and receive an IGRA to test for LTBI (including 143 applicants 12–14 years of age for whom an IGRA was a required component of their immigrant medical examination) (Figure 2). Among those who consented, 2,276 (93%) received an IGRA and additional study laboratory tests; the remaining 7% who had consented either withdrew from the study or were found to be ineligible during the medical examination before the processing of the IGRA. Among participants who received an IGRA, 484 (21%) were positive and 452

were eligible for 3HP. Of those who were eligible, 304 (67%) initiated treatment and 268 (88%) successfully completed treatment; 192 (72%) persons completed treatment in Vietnam and 76 (28%) by SAT within the United States.

Losses along the LTBI Cascade of Care

Each point along the LTBI cascade of care saw losses in participation (Tables 2–4); 2,873 (54%) immigrant visa applicants approached for participation in PTOPS declined. Among eligible visa applicants who declined to participate, 881 (31%) noted they were too busy or stressed because of their impending move, 723 (25%) noted that either the study or the IGRA (or both) were not requirements for the medical examination, 641 (22%) noted their belief that they were not infected with *Mycobacterium tuberculosis*, 407 (14%) reported that family advised against enrollment, 178 (6%) reported concerns about blood draws, 37 (1%) noted concerns around delaying or otherwise affecting the visa process, and 27 (1%) noted their belief that prior Bacille Calmette-Guérin (BCG) vaccination would protect them against TB disease.

Of those who consented, 162 (7%) did not have their IGRA processed for study exclusions identified during the medical examination: 119 (73%) had an abnormal chest radiograph or another condition requiring further TB disease screening, 25 (15%) reported having hepatitis B, 3 (2%) had a prior history of extrapulmonary TB, 2 (<1%) were applying for a visa type that was not included in the study, 1 (<1%) previously completed LTBI treatment, 1 (<1%) was breastfeeding, and 1 (<1%) recently received a live-virus vaccine. For 10 (6%) persons, consent was withdrawn or the reason was not specified.

Of the 484 participants who were IGRA-positive, 32 (7%) were excluded on the basis of additional screening or laboratory results. Eighteen (56%) had hepatitis B, 5 (16%) had hepatitis C, 3 (9%) previously received LTBI treatment, 1 (3%) had liver disease, 1 (3%) had a substance addiction, 1 (3%) was planning to get pregnant in the next 4 months, 1 (3%) had an abnormal chest radiograph, and 2 (6%) participants did not specify the reason.

Of the 452 participants who were IGRA-positive and eligible for treatment, 148 (33%) declined treatment. Of those, 99 (67%) reported not having enough time for treatment because they were immigrating within 2 months, 23 (16%) preferred taking treatment in the United States, 22 (15%) thought weekly DOT at CRH VMD was inconvenient because of time or distance, 7 (5%) were concerned about adverse events, and 3 (2%) did not feel sick and therefore believed they did not need treatment.

Thirty-six (12%) persons who initiated treatment did not complete treatment. Eighteen (50%) did not want to continue because of a grade 1 or 2 adverse event, 5 (14%) suffered a serious adverse event or a grade 3 event resulting in treatment discontinuation, 5 (14%) were too busy to continue treatment or had to move earlier than anticipated, 5 (14%) were identified as contacts to persons with multidrug-resistant or isoniazid-resistant TB or were diagnosed with extrapulmonary TB after initiating LTBI treatment, and 3 (8%) were not available for follow-up after US arrival.

Discussion

Our study suggests overseas (prearrival) LTBI testing and voluntary 3HP treatment during the required visa medical examination should be considered as a strategy to further US TB elimination efforts. Approximately 21% of all participants were IGRA-positive, and the proportion positive increased with age (24% of all adults); expanding IGRAs to adults could identify a high proportion of immigrants who have LTBI in Vietnam. We were able to achieve similar results

Table 1. Characteristics of study participants in the Preventing Tuberculosis Overseas Pilot Study of US immigrant visa applicants, Vietnam, 2018–2019*

Characteristic	No. (%) participants						
	Recruited	Enrolled	IGRA processed	IGRA-positive	3HP-eligible	Initiated 3HP	Completed 3HP
Total	5,311	2,438	2,276	484	452	304	268
Sex							
F	2,888 (54)	1,350 (55)	1,304 (57)	272 (56)	259 (57)	170 (56)	152 (57)
M	2,423 (46)	1,088 (45)	972 (43)	212 (44)	193 (43)	134 (44)	116 (43)
Age group, y							
12–14	298 (6)	143 (6)	142 (6)†	9 (2)	9 (2)	4 (1)	4 (1)
15–17	431 (8)	226 (9)	223 (10)	19 (4)	18 (4)	14 (5)	13 (5)
18–35	1,527 (29)	773 (32)	749 (33)	114 (24)	109 (24)	69 (23)	62 (23)
36–65	2,909 (55)	1,254 (51)	1,128 (50)	333 (69)	307 (68)	211 (69)	184 (69)
≥66	146 (3)	42 (2)	34 (1)	9 (2)	9 (2)	6 (2)	5 (2)

*IGRA, interferon-γ release assay; 3HP, 3-mo regimen of isoniazid and rifapentine.
†IGRA required as part of medical examination for participants 12–14 y of age; 1 participant's IGRA was not processed for the study because of recent measles, mumps, and rubella vaccination.

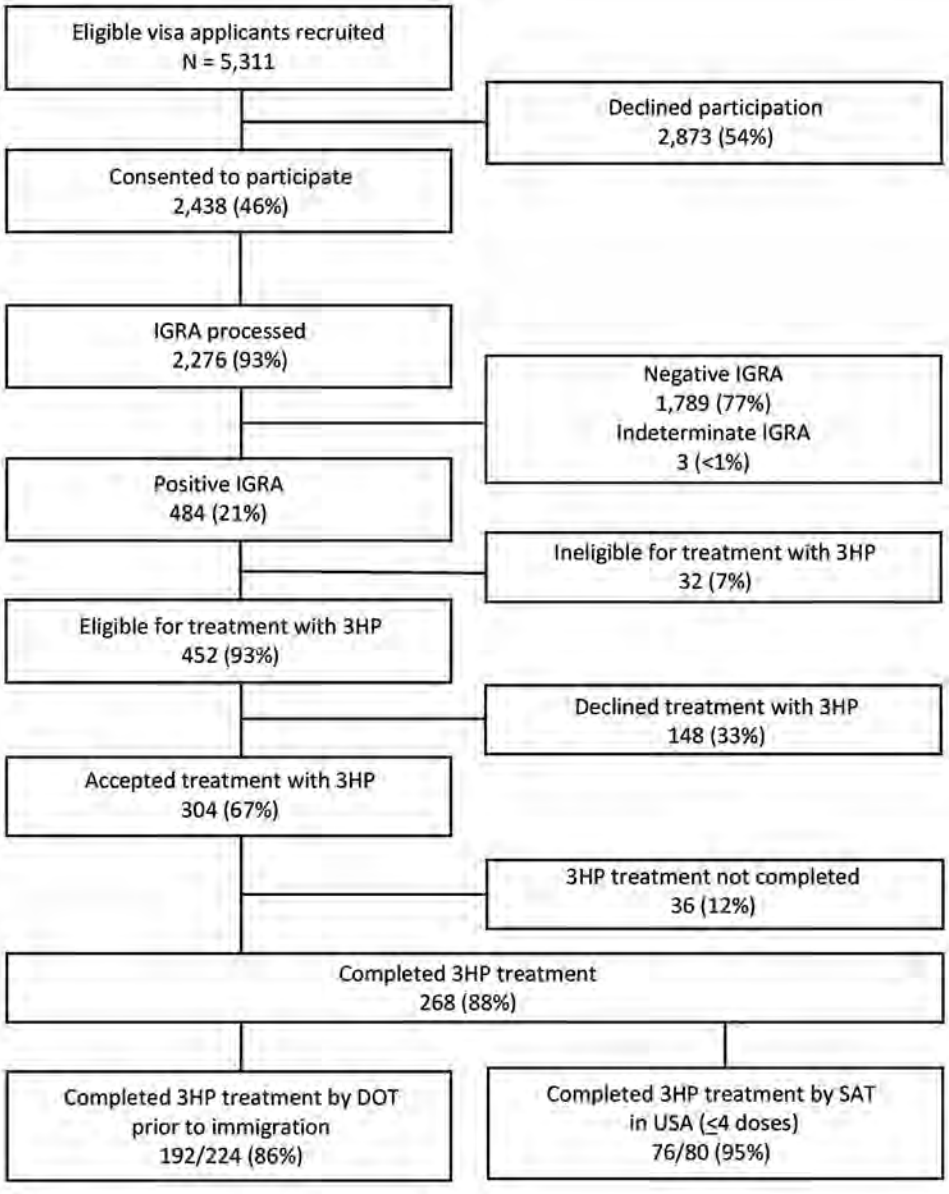

Figure 2. Flowchart of US immigrant visa applicants who consented to participate, initiated treatment, and completed treatment along the latent TB infection cascade of care in the Preventing Tuberculosis Overseas Pilot Study, Vietnam, 2018–2019. Participants who completed ≥8 doses of 3HP by DOT in Vietnam were given the option of taking the remaining ≤4 doses by SAT after arrival in the United States. DOT, directly observed therapy; IGRA, interferon-γ release assay; LTBI, latent tuberculosis infection; SAT, self-administered therapy; TB, tuberculosis; 3HP, 3-month regimen of isoniazid and rifapentine.

for the proportion initiating LTBI treatment and a higher proportion for completion compared with current US postarrival efforts. In our study, 67% of eligible IGRA-positive participants initiated treatment, and 88% of those completed treatment, resulting in 59% of all eligible participants completing treatment. These results can be compared with a recent assessment of the recommended US postarrival evaluation for immigrants at risk for TB (2013–2016), in which 35.5% of immigrants and refugees at risk for TB did not complete a US postarrival evaluation for TB and LTBI; among those who did and were recommended for LTBI treatment, 69% initiated treatment and 40% completed treatment (*8*).

Currently, most low-incidence countries, similar to the United States, focus on postarrival strategies to address LTBI in immigrant populations (*16*,*17*). Although a few countries provide LTBI testing prearrival (*16*), our study evaluates offering voluntary LTBI testing and treatment to immigrants prearrival. A major challenge with postarrival screening for newly arriving immigrants and refugees is the lack of resources needed to follow up with recent arrivals to initiate and complete LTBI treatment (*18*). Proportions of postarrival follow-up have ranged from 60% to 75% over the years despite improvements, including the EDN system that alerts health departments to immigrants with a TB condition arriving in

their jurisdictions (*14*,*19*). Further, because immune response tests, such as an IGRA, are not routinely required during the overseas examination for immigrants ≥15 years of age, those with LTBI are currently missed, and health departments therefore receive no alert from the EDN system of their arrival. However, expansion of just IGRA testing overseas, without also offering treatment overseas, would result in additional workload for already challenged health departments to follow-up and care for arriving adolescent and adult immigrants with LTBI. Moreover, immigrants themselves may experience challenges seeking care postarrival because of language barriers, transportation issues, and competing priorities with employment and educational commitments (*20*). These challenges and limitations underscore the need to maximize the use of the overseas process to improve LTBI testing and treatment among US-bound immigrants and refugees.

Our prearrival intervention demonstrated a high proportion of treatment completion, but for this approach to reach maximum effectiveness, 3 points along the cascade must be improved. First, participation and IGRA testing was low at 46%. Reported reasons for nonparticipation suggest that this low level was attributable to the perceived time commitment to participate in a study during a stressful time preparing for immigration to the United States (31%). Moreover, this project was conducted as a research study, coupled with a lengthy consent process, and whether this process itself deterred participation is unclear. Many visa applicants who declined to participate reported doing so because neither the study nor the IGRA was a requirement for immigration (25%). Thus, a decline for an IGRA was not necessarily caused by lack of interest in knowing one's LTBI status. Currently, an IGRA is not a required element in the overseas medical examination for visa applicants ≥15 years of age and is not offered routinely to this age group. A prearrival IGRA would enhance the diagnostic workup for TB disease; routinely offering or requiring a prearrival IGRA for this group would have the added benefit of apprising immigrants of their TB infection status, giving them the opportunity to make an informed decision about LTBI treatment. Second, among those who learned they were IGRA-positive, treatment acceptance was 67%. Although this figure is similar to the proportion initiating treatment observed in the postarrival evaluation of immigrants and refugees with a B2 classification (mostly children) (*8*) in the United States and other studies evaluating 3HP (*21*), this proportion could be improved. Of participants who declined 3HP, 67% did so because they felt they did not have enough time to complete treatment before immigration. PTOPS participation required a minimum of 8 weekly DOT doses, meaning participants needed to remain in Vietnam for at least 2 months before immigrating to the United States. An additional 15% of participants declined treatment because of distance and time required to travel to CRH VMD for DOT. Third, although the proportion completing treatment was relatively high, 36 (12%) persons did discontinue treatment. Fifty percent of discontinuations were attributable to minor adverse events, and 28% were attributable to severe adverse events or other medical conditions resulting in treatment suspension. Fourteen percent of participants who discontinued treatment did so because they were too busy with their move to continue DOT. These data underscore the need for a strategy for LTBI testing and treatment that is person-centered,

Table 2. Self-reported reasons for declining to participate in the Preventing Tuberculosis Overseas Pilot Study of US immigrant visa applicants, Vietnam, 2018–2019*

Reason†	No. (%) respondents
Total	2,873 (100)
Too busy or too much stress currently	881 (31)
Study or IGRA not required for medical examination	723 (25)
Did not believe infected	641 (22)
Family advised against enrollment	407 (14)
Worried about blood draw	178 (6)
Worried that participation could delay immigration process	37 (1)
Believed BCG vaccination would protect them from TB	27 (1)
Worried about enrolling in research	11 (<1)
Worried that IGRA results may affect immigration status	7 (<1)
Concerned about taking medication	6 (<1)
Worried about stigma	5 (<1)
Inconvenient to return to CRH VMD	5 (<1)
Did not understand study	1 (<1)
Undecided	1 (<1)

*BCG, Bacille Calmette-Guérin; CRH VMD, Cho Ray Hospital Visa Medical Department; IGRA, interferon-γ release assay; TB, tuberculosis.
†A total of 2,940 reasons were given (>1 reason could be provided by respondents).

Table 3. Reasons IGRA not processed or 3HP not offered to participants in the Preventing Tuberculosis Overseas Pilot Study of US immigrant visa applicants, Vietnam, 2018–2019*

Reason	No. (%) participants
IGRA not processed for participants who consented to be tested	162 (100)
Previous TB or abnormality on chest radiograph	119 (73)
Hepatitis B	25 (15)
History of extrapulmonary TB	3 (2)
Previous treatment	1 (1)
Breastfeeding	1 (1)
Applying for visa type not included in study	2 (1)
Recent receipt of live virus vaccine	1 (1)
Unknown; may have withdrawn consent	10 (7)
3HP not offered to IGRA-positive participants	32 (100)
Hepatitis B	18 (56)
Hepatitis C	5 (16)
Previous TB or abnormality on chest radiograph	1 (3)
Liver disease	1 (3)
Planning to get pregnant in next 4 mo	1 (3)
Substance addiction	1 (3)
Previous LTBI treatment	3 (9)
Unknown	2 (6)

*IGRA, interferon-γ release assay; LTBI, latent tuberculosis infection; TB, tuberculosis; 3HP, 3-mo regimen of isoniazid and rifapentine.

convenient, and not perceived by immigrants as interfering with their immigration plans.

Reducing the number of required DOT visits could theoretically increase treatment initiation and completion. This study included a minimum requirement of 8 weekly doses for DOT because, at the time, CDC recommended administration of 3HP by DOT. Now the World Health Organization and CDC have revised recommendations to support SAT for 3HP (*22*,*23*), enabling a reduction in the number of DOT visits. In addition, this course may be the least burdensome option for both staff and participants in terms of time and financial costs. However, although a SAT-only approach may increase treatment acceptance and completion for some persons, it may also result in more early treatment discontinuations because of concerns over minor side effects without the benefit of further support and education from healthcare workers during DOT visits. Because high rates of LTBI treatment completion are needed to be effective toward elimination (*24*) and missed appointments early in the course of treatment have been associated with completion failure (*25*), an approach worth considering is providing the first month of doses as DOT, using of digital adherence tools, or both, to allow participants to take their medicine and be supported without having to visit the clinic (*26*).

Recommendations for expanding overseas LTBI testing and treatment have been suggested previously (*11*); however, empirical evidence of how this approach would work has not been available. Until recently, diagnosis of LTBI relied upon the tuberculin skin test, which cross-reacts with BCG antigens. Thus, concerns existed about testing for infection because of the potential for false-positives in BCG-vaccinated populations. In addition, until recently, the standard LTBI treatment regimen was 9 months of isoniazid, a lengthy regimen prone to adverse events. The PTOPS approach relies on an IGRA, which is more specific than the tuberculin skin test, for diagnosis, reducing the potential for false-positive results (*27*). Moreover, PTOPS relies on voluntary acceptance of 3HP

Table 4. Reasons for declining to initiate 3HP and discontinuing treatment among participants in the Preventing Tuberculosis Overseas Pilot Study of US immigrant visa applicants, Vietnam, 2018–2019*

Reason	No. (%) participants
Declined to initiate 3HP	148 (100)
Not enough time; planned to depart for United States immediately after receiving visa	99 (67)
Preferred to take medicine in United States	23 (16)
Inconvenient to go to hospital for treatment: distance, time, or both	22 (15)
Concerned about adverse events from medicine	7 (5)
Did not feel sick	3 (2)
Treatment discontinued	36 (100)
Participant decided on own to stop because of grade 1 or 2 adverse events	18 (50)
Participant decided on own because too busy or moving to United States earlier	5 (14)
Identified as contact to a person with MDR or isoniazid-resistant TB or had extrapulmonary TB diagnosed after treatment initiation	5 (14)
Serious adverse event: grade 3 event, elevated liver function test, or both	5 (14)
Lost to follow-up in United States	3 (8)

*MDR, multidrug-resistant; TB, tuberculosis; 3HP, 3-mo regimen of isoniazid and rifapentine.

treatment. Although concerns exist that visa applicants may feel the need to comply with testing and treatment for immigration purposes, our data suggest that visa applicants understood that testing (for those ≥15 years of age) and treatment were voluntary and that declining had no effect on immigration status (54% of applicants declined participation, and 33% of participants declined treatment). For the immigrant visa applicants, the PTOPS approach can be advantageous because it enables testing and treatment in a familiar environment and language and does not require participants to navigate the unfamiliar US healthcare system upon arrival.

The overseas medical examination is an opportunity to prevent importation of TB and contribute to elimination. This process has proven to be a high-yield intervention for identifying and treating TB disease in US-bound immigrants and refugees. Moreover, the successful implementation of the TB technical instructions (which included the addition of mycobacterial cultures and DOT for TB diagnosis and treatment) at the overseas panel physician sites (*10*) suggests that panel site personnel can acquire the necessary expertise to provide testing for TB infection and voluntary LTBI treatment (*28*). A cost-benefit analysis modeling implementation of LTBI testing and treatment at overseas refugees panel sites hypothesized that this approach could save millions of dollars compared with the current strategy of relying on post-arrival follow-up at health departments and could lead to a reduction of TB cases in the United States (*29*); however, a detailed evaluation of the actual costs and the benefits of this approach is needed. In addition, further studies should be conducted at other panel sites while also ensuring that visa applicants do not experience delays in migration.

Our study demonstrated that using the overseas medical examination to provide voluntary testing and treatment of LTBI in a high-burden country yields high initiation and completion of treatment and should be considered to address LTBI in US-bound immigrants and to advance TB elimination efforts. This strategy should be further evaluated as an addition to or replacement for post-arrival testing and treatment for LTBI and as a complement to other domestic strategies to address LTBI in immigrant populations.

More than 30 years have passed since the declaration of the US TB elimination goal and 20 years since the Institutes of Medicine published its report Ending Neglect: The Elimination of Tuberculosis in the United States. However, the basic question put forth in the report still remains: "[Will] the renewed opportunity that now presents itself to move toward the elimination of tuberculosis be seized or [will] tuberculosis be subject to another period of neglect until the next resurgence?" (*11*).

Acknowledgments

We thank Drew Posey, Nina Marano, Le Dieu Hien, Nguyen Thi My Loc, Alyssa Finlay, Jessica Webster, Nam Pham Thanh, Hanh Nguyen, Richard Coker, and Carla Winston.

This study was supported by Cooperative Agreement U50/CCU 200-2016-92351 from the Centers for Disease Control and Prevention. Its contents are solely the responsibility of the authors and do not necessarily represent the official views of the Centers for Disease Control and Prevention, the US Department of Health and Human Services, or the US government.

The rifapentine was donated by Sanofi, the manufacturer. However, the company had no role in the study design, implementation, analysis, or reporting.

About the Author

Dr. Khan serves as a technical officer for the TB REACH Initiative at the Stop TB Partnership, where she works on innovative tools and strategies to further the fight against tuberculosis. Prior to that, she was a team lead at the Division of Tuberculosis Elimination in the National Center for HIV/AIDS, Viral Hepatitis, STD, and TB Prevention, Centers for Disease Control and Prevention. This study served as the basis of her doctoral thesis work at the London School of Hygiene and Tropical Medicine.

References

1. Dowdle WR; Centers for Disease Control (CDC). A strategic plan for the elimination of tuberculosis in the United States. MMWR Suppl. 1989;38:1–25.
2. Talwar A, Tsang CA, Price SF, Pratt RH, Walker WL, Schmit KM, et al. Tuberculosis—United States, 2018. MMWR Morb Mortal Wkly Rep. 2019;68:257–62. https://doi.org/10.15585/mmwr.mm6811a2
3. Yuen CM, Kammerer JS, Marks K, Navin TR, France AM. Recent transmission of tuberculosis—United States, 2011–2014. PLoS One. 2016;11:e0153728. https://doi.org/10.1371/journal.pone.0153728
4. Ricks PM, Cain KP, Oeltmann JE, Kammerer JS, Moonan PK. Estimating the burden of tuberculosis among foreign-born persons acquired prior to entering the U.S., 2005-2009. PLoS One. 2011;6:e27405. https://doi.org/10.1371/journal.pone.0027405
5. Sterling TR, Njie G, Zenner D, Cohn DL, Reves R, Ahmed A, et al. Guidelines for the treatment of latent tuberculosis infection: recommendations from the National Tuberculosis Controllers Association and CDC, 2020. MMWR Recomm Rep. 2020;69:1–11. https://doi.org/10.15585/mmwr.rr6901a1

6. Menzies NA, Hill AN, Cohen T, Salomon JA. The impact of migration on tuberculosis in the United States. Int J Tuberc Lung Dis. 2018;22:1392–403. https://doi.org/10.5588/ijtld.17.0185
7. Hill AN, Becerra J, Castro KG. Modelling tuberculosis trends in the USA. Epidemiol Infect. 2012;140:1862–72. https://doi.org/10.1017/S095026881100286X
8. Liu Y, Phares CR, Posey DL, Maloney SA, Cain KP, Weinberg MS, et al. Tuberculosis among newly arrived immigrants and refugees in the United States. Ann Am Thorac Soc. 2020;17:1401–12. https://doi.org/10.1513/AnnalsATS.201908-623OC
9. Centers for Disease Control and Prevention. Tuberculosis technical instructions for panel physicians. 2019 [cited 2020 Jun 21]. https://www.cdc.gov/immigrantrefugeehealth/panel-physicians/tuberculosis.html
10. Liu Y, Posey DL, Cetron MS, Painter JA. Effect of a culture-based screening algorithm on tuberculosis incidence in immigrants and refugees bound for the United States: a population-based cross-sectional study. Ann Intern Med. 2015;162:420–8. https://doi.org/10.7326/M14-2082
11. Waterman S, Moser K. Ending neglect: the elimination of tuberculosis in the United States. Am J Prev Med. 2002; 22:134–5. https://doi.org/10.1016/S0749-3797(01)00416-0
12. World Health Organization. Global tuberculosis report 2019 [cited 2020 Jul 22]. https://www.who.int/publications/i/item/9789241565714
13. Marks GB, Nhung NV, Nguyen TA, Hoa NB, Khoa TH, Son NV, et al. Prevalence of latent tuberculous infection among adults in the general population of Ca Mau, Viet Nam. Int J Tuberc Lung Dis. 2018;22:246–51. https://doi.org/10.5588/ijtld.17.0550
14. Lee D, Philen R, Wang Z, McSpadden P, Posey DL, Ortega LS, et al.; Centers for Disease Control and Prevention. Disease surveillance among newly arriving refugees and immigrants—Electronic Disease Notification System, United States, 2009. MMWR Surveill Summ. 2013;62:1–20.
15. Sterling TR, Villarino ME, Borisov AS, Shang N, Gordin F, Bliven-Sizemore E, et al.; TB Trials Consortium PREVENT TB Study Team. Three months of rifapentine and isoniazid for latent tuberculosis infection. N Engl J Med. 2011;365:2155–66. https://doi.org/10.1056/NEJMoa1104875
16. Pareek M, Baussano I, Abubakar I, Dye C, Lalvani A. Evaluation of immigrant tuberculosis screening in industrialized countries. Emerg Infect Dis. 2012;18:1422–9. https://doi.org/10.3201/eid1809.120128
17. Zenner D, Hafezi H, Potter J, Capone S, Matteelli A. Effectiveness and cost-effectiveness of screening migrants for active tuberculosis and latent tuberculous infection. Int J Tuberc Lung Dis. 2017;21:965–76. https://doi.org/10.5588/ijtld.16.0935
18. Campbell J, Marra F, Cook V, Johnston J. Screening immigrants for latent tuberculosis: do we have the resources? CMAJ. 2014;186:246–7. https://doi.org/10.1503/cmaj.131025
19. Taylor EM, Painter J, Posey DL, Zhou W, Shetty S. Latent tuberculosis infection among immigrant and refugee children arriving in the United States: 2010. J Immigr Minor Health. 2016;18:966–70. https://doi.org/10.1007/s10903-015-0273-2
20. Wieland ML, Weis JA, Yawn BP, Sullivan SM, Millington KL, Smith CM, et al. Perceptions of tuberculosis among immigrants and refugees at an adult education center: a community-based participatory research approach. J Immigr Minor Health. 2012;14:14–22. https://doi.org/10.1007/s10903-010-9391-z
21. Stennis NL, Burzynski JN, Herbert C, Nilsen D, Macaraig M. Treatment for tuberculosis infection with 3 months of isoniazid and rifapentine in New York City Health Department Clinics. Clin Infect Dis. 2016;62:53–9. https://doi.org/10.1093/cid/civ766
22. Borisov AS, Bamrah Morris S, Njie GJ, Winston CA, Burton D, Goldberg S, et al. Update of recommendations for use of once-weekly isoniazid-rifapentine regimen to treat latent *Mycobacterium tuberculosis* infection. MMWR Morb Mortal Wkly Rep. 2018;67:723–6. https://doi.org/10.15585/mmwr.mm6725a5
23. World Health Organization. Latent tuberculosis infection: updated and consolidated guidelines for programmatic management. 2018 [cited 2020 Jul 22]. https://apps.who.int/iris/handle/10665/260233
24. World Health Organization. End TB strategy. 2014 [cited 2020 Jul 22]. https://www.who.int/tb/strategy/End_TB_Strategy.pdf
25. Menzies D, Dion MJ, Francis D, Parisien I, Rocher I, Mannix S, et al. In closely monitored patients, adherence in the first month predicts completion of therapy for latent tuberculosis infection. Int J Tuberc Lung Dis. 2005;9:1343–8.
26. Lam CK, McGinnis Pilote K, Haque A, Burzynski J, Chuck C, Macaraig M. Using video technology to increase treatment completion for patients with latent tuberculosis infection on 3-month isoniazid and rifapentine: an implementation study. J Med Internet Res. 2018;20:e287. https://doi.org/10.2196/jmir.9825
27. Centers for Disease Control and Prevention. Updated guidelines for using interferon gamma release assays to detect *Mycobacterium tuberculosis* infection—United States, 2010. MMWR Morb Mort Wkly Rep. 2010;59(5).
28. Liu Y, Weinberg MS, Ortega LS, Painter JA, Maloney SA. Overseas screening for tuberculosis in U.S.-bound immigrants and refugees. N Engl J Med. 2009;360:2406–15. https://doi.org/10.1056/NEJMoa0809497
29. Wingate LT, Coleman MS, de la Motte Hurst C, Semple M, Zhou W, Cetron MS, et al. A cost-benefit analysis of a proposed overseas refugee latent tuberculosis infection screening and treatment program. BMC Public Health. 2015;15:1201. https://doi.org/10.1186/s12889-015-2530-7

Address for correspondence: Amera Khan, Stop TB Partnership, Chemin du Pommier 40, 1218 Le Grand-Saconnex, Geneva, Switzerland; email: amerak@stoptb.org

Effectiveness of 3 COVID-19 Vaccines in Preventing SARS-CoV-2 Infections, January–May 2021, Aragon, Spain

Alicia del Cura-Bilbao, Héctor López-Mendoza, Armando Chaure-Pardos, Alberto Vergara-Ugarriza, Joaquín Guimbao-Bescós

Reducing severe acute respiratory syndrome coronavirus 2 (SARS-CoV-2) transmission is a worldwide challenge; widespread vaccination could be one strategy for control. We conducted a prospective, population-based cohort study of 964,258 residents of Aragon, Spain, during December 2020–May 2021. We used the Cox proportional-hazards model with vaccination status as the exposure condition to estimate the effectiveness of 3 coronavirus disease vaccines in preventing SARS-CoV-2 infection. Pfizer-BioNTech had 20.8% (95% CI 11.6%–29.0%) vaccine effectiveness (VE) against infection after 1 dose and 70.0% (95% CI 65.3%–74.1%) after 2 doses, Moderna had 52.8% (95% CI 30.7%–67.8%) VE after 1 dose and 70.3% (95% CI 52.2%–81.5%) after 2 doses, and Oxford-AstraZeneca had 40.3% (95% CI 31.8%–47.7%) VE after 1 dose. All estimates were lower than those from previous studies. Results imply that, although high vaccination coverage remains critical to protect people from disease, it will be difficult to effectively minimize transmission opportunities.

Since the beginning of the coronavirus disease (COVID-19) pandemic, one of the main challenges countries have experienced is finding effective ways to reduce illness and death from the disease. Nonpharmaceutical measures have been used extensively, and vaccines were added to the resources of the European Union beginning in December 2020. Results from phase 3 and phase 4 studies have found the vaccines to be highly effective (*1*–*12*). Studies assessing the effectiveness of vaccines in real-world settings among elderly populations (*13*,*14*) have also shown a high effectiveness from a single dose.

Spain has had one of the world's highest rates of illness and death from COVID-19 (*15*). The Aragon region, in the northeast of the country, has one of Spain's largest elderly populations; 22% of people among a total population of 1.3 million people are ≥65 years of age (*16*). Through May 31, 2021, the region had reported 125,465 COVID-19 cases, 3,522 deaths (*17*), and a fatality rate of 2.8%. Vaccination programs have proven to be the most effective measure to control the pandemic (*18*) and have been used in conjunction with hygiene and social distancing measures.

The European Union vaccination program started on December 27, 2020. Pfizer-BioNTech (BNT162b2; https://www.pfizer.com), Moderna (mRNA-1273; https://www.modernatx.com), Oxford-AstraZeneca (hAdOx1-S-AZD1222; https://www.astrazeneca.com), and Janssen (https://www.janssen.com) COVID-19 vaccines are currently authorized by the European Medicines Agency (EMA; https://www.ema.europa.eu) for administration in the European Union (*19*). The Pfizer-BioNTech, Moderna, and Oxford-AstraZeneca vaccines have been widely used in Spain and Aragon in accord with the vaccination strategy (*20*,*21*). The Janssen vaccine was added to the vaccination plan later. As of May 31, 2021, 44% of the population of Aragon ≥18 years of age had been vaccinated with ≥1 dose of vaccine, and 24.5% had been fully vaccinated (*22*).

The context of coexisting vaccinated and unvaccinated persons and periods of high infection rates among the general population lends urgency to performing vaccine effectiveness (VE) studies. We

Author affiliations: Miguel Servet University Hospital, Zaragoza, Spain (A. del Cura-Bilbao); Aragon Department of Health, Zaragoza (A. del Cura-Bilbao, H. López-Mendoza, A. Chaure-Pardos, A. Vergara-Ugarriza, J. Guimbao-Bescós); University of Zaragoza CASSETEM Research Group, Zaragoza (H. López-Mendoza); Lozano Blesa University Hospital, Zaragoza (H. López-Mendoza, A. Chaure-Pardos); GRISSA Research Group, Zaragoza (A. Chaure-Pardos); Aragon Health Research Institute Foundation (IIS Aragon), Zaragoza (A. Chaure-Pardos)

DOI: https://doi.org/10.3201/eid2803.212027

carried out a cohort study to estimate the effectiveness of vaccination in preventing severe acute respiratory syndrome coronavirus 2 (SARS-CoV-2) infection, in which we compared the Pfizer-BioNTech, Moderna, and Oxford-AstraZeneca COVID-19 vaccines.

Institutional Review Board Statement

The authors declare that they have complied with the provisions of Spanish Organic Law 3/2018 of December 5 on Personal Data Protection and Digital Rights Guarantee and with the provisions of Regulation (EU) 2016/679 of the European Parliament and of the Council of 27 April 2016 on the protection of natural persons with regard to the processing of personal data and on the free movement of such data, and repealing Directive 95/46/EC (General Data Protection Regulation). Approval for this research was obtained from the Aragon Research Ethics Committee (no. 2021/141).

Methods

We conducted a prospective, population-based cohort study of residents in the region of Aragon, Spain. Participants were all of the users of the Aragon Health Service, ≥16 years old of age, who had no evidence of previous SARS-CoV-2 infection, confirmed by reverse transcription PCR (RT-PCR), antigen test, or immunoglobulin G test for SARS-CoV-2 infection at any time before December 27, 2020. We included all residents registered in the Aragon Healthcare System Users Registry (AHSUR) who met the eligibility criteria as of December 31, 2020. AHSUR consists of periodically updated basic demographic data from users of the Aragon Healthcare Service, the public healthcare provider in Aragon. AHSUR contains data from 89% of Aragon inhabitants. We based the study on data collected during December 28, 2020–May 31, 2021.

Vaccination Program

The goal of COVID-19 vaccination strategy in Spain and Aragon (*20*,*21*) was to protect vulnerable and exposed populations and to achieve full vaccination in as much of the population as possible. Some priority groups were targeted for earlier vaccination during December 2020–February 2021: residents of care (nursing) or residential homes for elderly or disabled people, frontline healthcare workers, caregivers and residential home workers, second-line healthcare workers, and disabled persons not residing in a nursing or residential home. In Aragon, from February 2021 the rollout was expanded to all adults ≥80 years of age and essential workers—civil protection staff, firefighters, security forces, and educational center staff. In April 2021, the rollout was extended to all adults 60–79 years of age; persons with high-risk conditions and younger age groups have been progressively incorporated into the rollout schedule (*23*).

Specific vaccines were incorporated into the vaccination plan at different times. In Aragon, the Pfizer-BioNTech vaccine was administered beginning December 27, 2020, the Moderna vaccine beginning January 13, 2021, and the Oxford-AstraZeneca vaccine beginning February 7, 2021 (*21*). Because of the stoppage in Oxford-AstraZeneca vaccination in people <60 years of age, those participants receiving that vaccine who we tracked in follow-up had received only 1 dose at the time of the analysis. Because only 8,727 doses of the single-dose Janssen vaccine had been administered since its initiation on April 21, 2021 (*21*), we excluded data on that vaccine from the analysis.

Exposure Definition (Vaccination Status)

The exposure condition was vaccination status. On each exposure condition, we followed participants, grouped by vaccination status, until that status changed because of SARS-CoV-2 infection, death, loss to follow-up, or end of the study period, whichever occurred first. For first dose vaccination, participants were defined as exposed from 12 days after 1 dose of the Pfizer-BioNTech vaccine, 14 days after 1 dose of the Moderna vaccine, and 21 days after 1 dose of the Oxford-AstraZeneca vaccine according to previous studies. For second dose vaccination, we defined participants as exposed beginning 7 days after 2 doses of the Pfizer-BioNTech vaccine, and 14 days after 2 doses of the Moderna vaccine (*1*–*3*). We defined unvaccinated participants as unexposed.

Outcome Definition

We considered a participant to be SARS-CoV-2 infected if confirmed by RT-PCR or rapid antigen detection test according to World Health Organization definitions (*24*). Following COVID-19 detection and surveillance guidelines in Spain and Aragon (*25*,*26*), criteria to test for SARS-CoV-2 were having symptoms compatible with COVID-19 or close contact with a person with a laboratory-confirmed SARS-CoV-2 infection diagnosis. We extracted vaccination registry and laboratory testing data from the electronic medical record system of health-related information. The electronic medical record system was automatically updated with those data.

Patient Characteristics and Confounders

We studied cohort population characteristics to determine if they could potentially act as confounders. These characteristics included age, sex, work or residence in nursing or residential homes, weekly cumulative incidence (WCI) of SARS-CoV-2 infection in each primary care service area, and number of SARS-CoV-2 tests administered in the previous 6 months. We defined SARS-CoV-2 infection WCI as the total number of newly confirmed SARS-CoV-2 infections per 100,000 inhabitants in each primary care service area within the previous 7 days. We extracted data on age, sex, and the primary care service areas from AHSUR. We extracted specific information on nursing and residential homes residents and workers from the Aragon nursing and residential homes information system, an information system to manage care, prevention, and control measures for residents and workers at nursing and residential homes in the context of the COVID-19 pandemic. We used formal tests to compare data between participants lost to follow-up and the studied cohort: $\chi 2$ tests for all the variables except follow-up time, for which we used Student t-tests, resulting in statistically significant ($p<0.01$) differences for all the variables.

Statistical Analysis

We defined the incidence rate (IR) of SARS-CoV-2 infection as the number of confirmed SARS-CoV-2 infections divided by the sum of exposure times for each participant. We computed unadjusted estimators using a Cox proportional-hazards model in which only vaccination status was included, and unadjusted VE against SARS-CoV-2 infection as 1 – hazard ratio. We computed adjusted estimators using a Cox proportional-hazards model and included baseline data on age, sex, and being a resident or worker in a nursing or residential home as categorical covariates in the models. We included WCI from each primary care service area and the number of SARS-CoV-2 tests administered in the previous 6 months as time-variable terms. To introduce the time-variable terms, we split individual follow-up times into weekly intervals. Therefore, we assigned each interval the immediately previous week's WCI and introduced all intervals into the model as individual observations. We split age and WCI into 4 categories based on percentiles 0–10, 11–50, 51–90, and 91–100. We calculated adjusted VE against SARS-CoV-2 infection as 1 – hazard ratio.

Results

We prospectively followed a cohort of 964,258 people ≥16 years of age from the general population, corresponding to 72.5% of the population of Aragon; the size and exposure status of the cohort evolved across the study period (Figure 1). We stratified participants' vaccination exposure by their demographic characteristics (Table 1). As of May 31, 2021, among the participants, 242,142 had been vaccinated with ≥1 dose of the Pfizer-BioNTech vaccine and 212,419 with 2 doses; 32,522 participants had been vaccinated with at least 1 dose of the Moderna vaccine and 15,660 of them with 2 doses; and 97,492 participants had been vaccinated with 1 dose of the Oxford-AstraZeneca vaccine; 592,102 participants had not yet been vaccinated. We observed differences in the number of Pfizer-BioNTech, Moderna, and Oxford-AstraZeneca vaccines doses administered over the study period, which occurred because of different EMA approval times, vaccine doses available over time, and prioritizing of groups considered for earlier vaccination, specifically persons ≥75 years old and residents and workers in nursing and residential homes (Table 1). Over the study period, 11,557 (1.2%) participants dropped out of the study; we recorded lost participants by demographic characteristics and causes of withdrawal (Tables 1, 2).

The 592,102 unvaccinated participants had 25,767 SARS-CoV-2 infections and an IR of 1.41/1,000 person-weeks. The 242,142 participants vaccinated with 1 dose of the Pfizer-BioNTech vaccine had 463 infections (IR 0.86) and the 212,419 with 2 doses had 280 infections (IR 0.23). The 32,522 participants vaccinated with 1 dose of the Moderna vaccine had 28 infections (IR 0.31) and the 15,660 with 2 doses had 18 infections (IR 0.21). The 97,492 participants vaccinated with 1 dose of the Oxford-AstraZeneca vaccine had 230 infections (IR 0.55).

Unadjusted Vaccine Effectiveness against SARS-CoV-2 Infection

The Pfizer-BioNTech vaccine had 23.5% (95% CI 16.0%–30.3%) unadjusted VE against SARS-CoV-2 infection after 1 dose and 76.1% (95% CI 73.1%–78.8%) after 2 doses. The Moderna vaccine had 69.2% (95% CI 55.4%–78.8%) unadjusted VE after 1 dose and 78.4% (95% CI 65.6%–86.4%) after 2 doses. The Oxford-AstraZeneca vaccine had 43.7% (95% CI 35.7%–50.7%) unadjusted VE after 1 dose (Table 3).

Adjusted Vaccine Effectiveness against SARS-CoV-2 Infection

After adjusting for age, sex, work or residence in a nursing or residential home, WCI in each primary care service area, and number of SARS-CoV-2 tests administered in the previous 6 months, we found that the

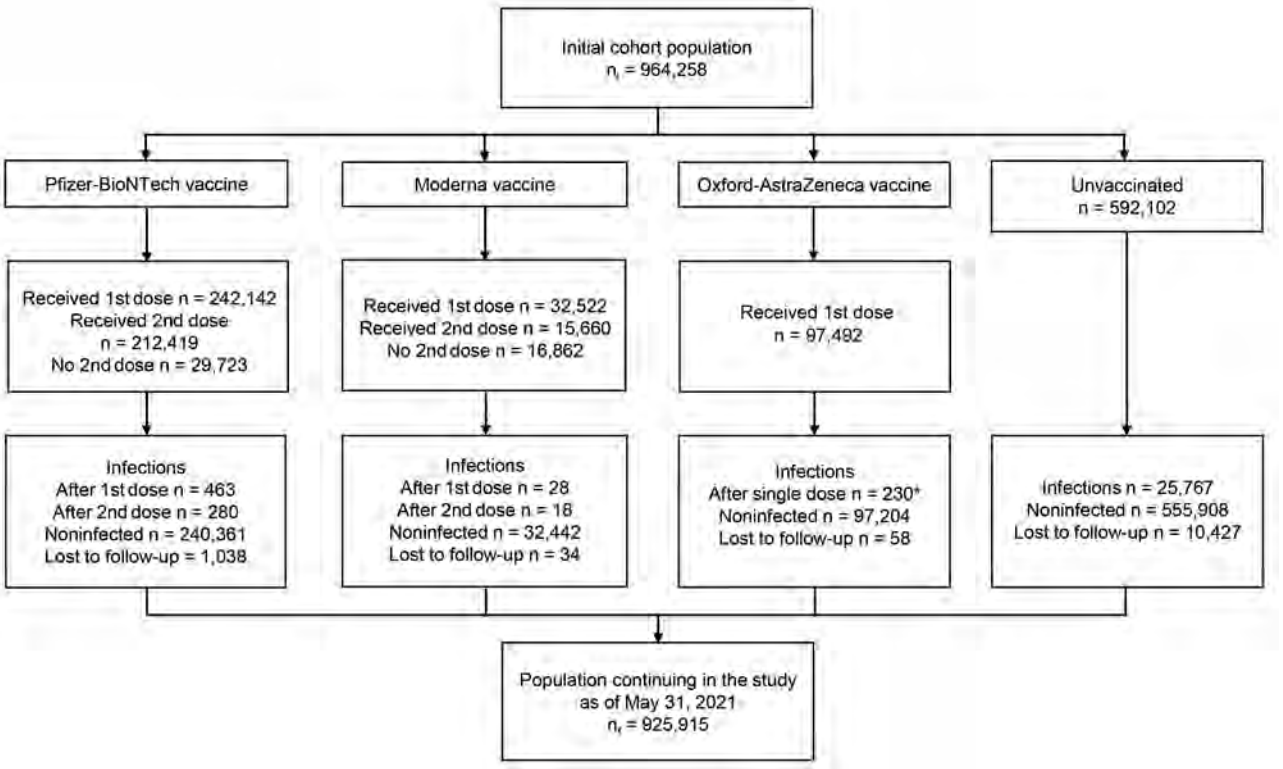

Figure 1. Flowchart of cohort evolution for study of coronavirus disease vaccines in preventing confirmed severe acute respiratory syndrome coronavirus 2 infection, Aragon, Spain, January–May 2021. *Participants vaccinated with the AZ vaccine had all received only 1 dose as of May 31, 2021.

Pfizer-BioNTech vaccine had 20.8% (95% CI 11.6%–29.0%) adjusted VE after 1 dose and 70.0% (95% CI 65.3%–74.1%) after 2 doses. The Moderna vaccine had 52.8% (95% CI 30.7%–67.8%) adjusted VE after 1 dose and 70.3% (95% CI 52.2%–81.5%) after 2 doses; and the Oxford-AstraZeneca vaccine had 40.3% (95% CI 31.8%–47.7%) adjusted VE after 1 dose (Table 3).

SARS-CoV-2 Infection Cumulative Risk Curves

For unvaccinated participants, the risk for SARS-CoV-2 infection rose to 2% at day 44 and to 4% at day 154 of follow-up. For participants who received 1 dose of the Pfizer-BioNTech vaccine, the risk rose to 1% at day 40 of follow-up, but remained <1% during the entire follow-up period (120 days) for those with 2 doses (Figure 2, panel A). For participants who received 1 dose of the Moderna vaccine, risk remained <0.5% during the entire follow-up time (120 days) and for participants vaccinated with 2 doses, the risk rose from 0% to 0.5% during days 30–71, then remained at 0.5% until the end of follow-up (day 90; Figure 2, panel B). For participants who received 1 dose of the Oxford-AstraZeneca vaccine, risk rose to 0.9% after 80 days of follow-up (Figure 2, panel C).

Discussion

In the general population, our findings showed an effectiveness of 3 different vaccines against SARS-CoV-2 infection, but with lower efficacy estimates than from clinical trials and other VE studies. We found 20.8% VE after 1 dose of the Pfizer-BioNTech vaccine and 70.0% after 2 doses; for the Moderna vaccine, these numbers were 52.8% VE after 1 dose and 70.3% VE after 2 doses, and for the Oxford-AstraZeneca vaccine, 40.3% after 1 dose.

For the Pfizer-BioNTech and Moderna vaccines, these values were lower than those in other observational studies, which had ranges of 61.9%–80% VE after 1 dose and 90%–96% VE ≥7 days after 2 doses (*8*,*9*,*27*–*29*). These differences could possibly be explained by the population-wide design of our study, which included a higher percentage of elderly persons in the Pfizer-BioNTech–vaccinated group than in the other studies. In contrast, our results showed a higher VE after 2 doses of the Pfizer-BioNTech vaccine than the 65% VE found in another study (*30*), probably because they used a different approach for estimating VE that included only close contacts of positive cases and assigned every person in the cohort the same observation period and as a result vaccinated and

Table 1. Characteristics of participants according to vaccination status at endpoint, Aragon, Spain, January–May 2021*

Characteristic	Initial cohort population	PBNT 1st dose	PBNT 2nd dose	MOD 1st dose	MOD 2nd dose	AZ single dose	Unvaccinated	Lost to follow-up
Age group, y								
<25	92,287 (9.6)	1,745 (0.7)	1,489 (0.7)	338 (1.0)	155 (1.0)	3,440 (3.5)	86,764 (14.7)	1,392 (12.0)
25–49	372,525 (38.6)	19,702 (8.1)	16,957 (8.0)	4,230 (13.0)	2,509 (16.0)	19,079 (19.6)	329,514 (55.7)	3,942 (34.1)
50–74	364,754 (37.8)	110,824 (45.8)	86,764 (40.8)	15,541 (47.8)	2,480 (15.8)	74,939 (76.9)	163,45 (27.6)	2,497 (21.6)
≥75	134,692 (14.0)	109,871 (45.4)	107,209 (50.5)	12,413 (38.2)	10,516 (67.2)	34 (0.0)	12,374 (2.1)	3,726 (32.2)
Sex								
F	485,237 (50.3)	143,950 (59.4)	128,280 (60.4)	18,277 (56.2)	10,212 (65.2)	54,132 (55.5)	268,878 (45.4)	5,986 (51.8)
M	479,021 (49.7)	98,192 (40.6)	84,139 (39.6)	14,245 (43.8)	5,448 (34.8)	43,360 (44.5)	323,224 (54.6)	5,571 (48.2)
Site								
Rural	354,418 (36.8)	93,723 (38.7)	82,281 (38.7)	5,154 (15.8)	1,373 (8.8)	35,387 (36.3)	220,154 (37.2)	4,741 (41.0)
Urban	609,840 (63.2)	148,419 (61.3)	130,138 (61.3)	27,368 (84.2)	14,287 (91.2)	62,105 (63.7)	371,948 (62.8)	6,816 (59.0)
Nursing and residential homes								
Residents	11,447 (1.2)	10,847 (4.5)	10,431 (4.9)	11 (0.0)	10 (0.1)	7 (0.0)	582 (0.1)	507 (4.4)
Workers	10,174 (1.1)	8,734 (3.6)	8,570 (4.0)	46 (0.1)	6 (0.0)	155 (0.2)	1,239 (0.2)	33 (0.3)
Follow-up, mean d (SD)	133 (34.9)	15.5 (5.1)	41 (35.3)	19.5 (10.4)	37.9 (23.7)	30.1 (21.7)	148.1 (25.2)	60.1 (33.1)
Total	964,258 (100)	242,142 (100)	212,419 (100)	32,522 (100)	15,660 (100)	97,492 (100)	592,102 (100)	11,557 (100)

*Values are no. (%) participants except as indicated. AZ, Oxford-Astra-Zeneca; MOD, Moderna; PBNT, Pfizer-BioNTech.

unvaccinated participants most likely experienced similar exposure to SARS-CoV-2.

Our findings indicated a higher VE (52.8%) after 1 dose of the Moderna vaccine than after 1 dose of either the Pfizer-BioNTech or Oxford-AstraZeneca vaccines and similar VEs after 2 doses of both the Moderna and Pfizer-BioNTech vaccines. However, our results did not reach the VE estimates of 83% after 1 dose and 82% after 2 doses of Moderna vaccine found in another study (*28*). The small sample size in that study, which only included healthcare personnel and other essential workers, might explain these differences in VE. However, as in that study (*28*), VE after 1 and 2 doses of the Moderna vaccine were also very close.

Safety concerns resulted in the suspension of the Oxford-AstraZeneca vaccine before anyone in our cohort received a second dose, and therefore we estimated VE only after 1 dose (40.3%), similar to the 44% VE after 1 dose of the Oxford-AstraZeneca vaccine in another article (*30*). In contrast, another study found a VE of 60% against symptomatic disease after a single dose of the Oxford-AstraZeneca vaccine in adults ≥70 years of age, as expected because of the study's more severe outcome measures and exclusively elderly population (*14*).

Cumulative risk curves of SARS-CoV-2 infection show that the cumulative risk of infection in unvaccinated participants rose to 4% at day 154 of follow-up whereas the risk remained <1% during the entire follow-up period (120 days) in fully Pfizer-BioNTech–vaccinated participants, results consistent with those from a nationwide study (*8*). Risk remained <0.5% in participants vaccinated with 1 dose of the Moderna vaccine during the entire follow-up time (120 days) and <1% during the entire follow-up time (90 days) in fully vaccinated participants. In the participants with 2 doses of the Moderna vaccine, the slight increase in risk from day 30 onwards might be explained by the relatively small number of participants from our cohort who

Table 2. Causes of loss to follow-up during the study period, Aragon, Spain, January–May 2021

Causes	No. patients
Expiration of service*	3,328
Death	2,903
Change of residence to another region of Spain	2,020
Loss of entitlement†	250
Change of residence to another country	15
Duplicate user‡	2
Unknown	3,039

*Aragon Health Service healthcare ended for administrative reasons. Most common were expiration of temporary service for persons who moved from another self-governing region of Spain for a specific period of time (maximum 6 months), subject to renewal; and for foreign citizens with no residence license who had not applied for renewal of Aragon Health Service–provided healthcare in 2 years.
†Loss of entitlement to Aragon Health Service–provided healthcare when person begins working unless they renounce mutual insurance company–provided healthcare (applies to a few public workers in Spain whose healthcare provider is a mutual insurance company).
‡Health record of participant was duplicated in the Healthcare System Users Registry.

Table 3. Effectiveness of Pfizer-BioNTech, Moderna, and Oxford-AstraZeneca coronavirus disease vaccines in preventing confirmed SARS-CoV-2 infection, Aragon, Spain, January–May 2021*

Vaccination status	Person-days, total (average)	Population	SARS-CoV-2 infections	IR†	Unadj HR‡	Adj HR‡	Unadj VE,§ % (95% CI)	Adj VE, § % (95% CI)
Pfizer-BioNTech								
1 dose	3,750,582 (15.5)	242,142	463	0.86	0.77	0.79	23.5 (16.0–30.3)	20.8 (11.6–29.0)
2 doses	8,705,040 (41.0)	212,419	280	0.23	0.24	0.30	76.1 (73.1–78.8)	70.0 (65.3–74.1)
Moderna								
1 dose	633,821 (19.5)	32,522	28	0.31	0.31	0.47	69.2 (55.4–78.8)	52.8 (30.7–67.8)
2 doses	592,877 (37.9)	15,660	18	0.21	0.22	0.30	78.4 (65.6–86.4)	70.3 (52.2–81.5)
Oxford-AstraZeneca								
1 dose	2,932,610 (30.1)	97,492	230	0.55	0.56	0.60	43.7 (35.7–50.7)	40.3 (31.8–47.7)
Unvaccinated	128,261,888 (133.0)	592,102	25,767	1.41	1.00	1.00	NA	NA

*Adj, adjusted; HR, hazard ratio; IR, incidence rate; NA, not applicable; SARS-CoV-2, severe acute respiratory syndrome coronavirus; unadj, unadjusted; VE, vaccine effectiveness.
†Incidence rate of SARS-CoV-2 infection was measured in 1,000 person-weeks (not person-days) to make it to read the table (estimates expressed with ≤2 decimals).
‡HR was adjusted by age, sex, work, or residence in nursing or residential homes, weekly cumulative incidence in each primary care service area, and number of SARS-CoV-2 tests administered in the previous 6 months.
§Vaccine effectiveness against SARS-CoV-2 infection was calculated as 1 – HR.

were vaccinated with the second dose and reached long follow-up times (≥50 days), which can cause instability of estimates for prolonged follow-up times. For the Oxford-AstraZeneca vaccine, the difference in risk between unvaccinated participants and those vaccinated with 1 dose (2.5% vs. 0.9% at day 80 of follow-up) highlights the VE after 1 dose of the Oxford-AstraZeneca vaccine.

One limitation of our study was losses to follow-up because of administrative leaves from AHSUR. Participants lost to follow-up were statistically different from the studied cohort. Nevertheless, they represent only 1.2% of the initial population, which limited the magnitude of this bias. Timing of vaccine rollout also varied between priority groups, targeted for earlier vaccination, and the general population. This difference may have affected the results by adding more variability, particularly because Pfizer-BioNTech was mostly used in population ≥75 years of age, who were vaccinated earlier, whereas Oxford-AstraZeneca was mostly used in general population, who were vaccinated at a later time.

Research has documented that the proportion of symptomatic infections in vaccinated persons is lower than in unvaccinated ones because vaccination prevents symptoms (*28*). Therefore, studies based on symptomatic persons (*1–7*,*11*,*13*,*14*) underestimate the total infection rate in vaccinated persons to a greater extent than in unvaccinated ones and consequently overestimate VE. Our study included all confirmed symptomatic and asymptomatic SARS-CoV-2 infections, and thus it would be expected that VE

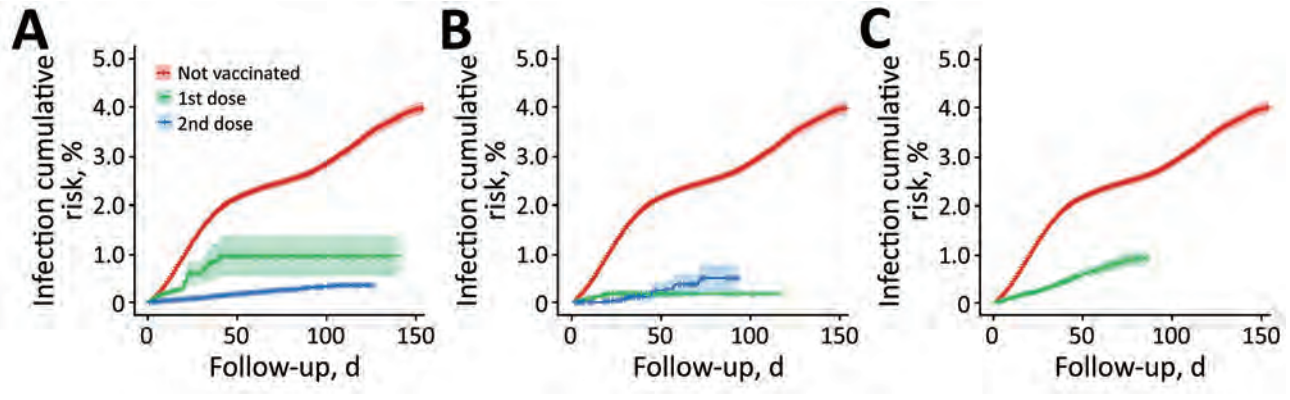

Figure 2. Cumulative risk curves (1 minus the Kaplan-Meier risk) of severe acute respiratory syndrome coronavirus 2 (SARS-CoV-2) infection for 3 coronavirus disease vaccines, Aragon, Spain, January–May 2021. A) BioNTech-Pfizer BNT162b2 mRNA, B) Moderna mRNA-1273, and C) Oxford-AstraZeneca ChAdOx1-S-AZD1222. Shadows across lines represent 95% CI. For unvaccinated participants, 95% CI at day 90 of follow-up was 2.6%–2.8%. For participants who went on to receive the BioNTech-Pfizer vaccine, 95% CI at day 90 of follow-up was 0.5%–1.4% (1 dose) and 0.3%–0.4% (2 doses). For the Moderna vaccine, 95% CI at day 90 of follow-up was 0.1%–0.2% (1 dose), and 0.2%–0.8% (2 doses). For Oxford-AstraZeneca, 95% CI at day 90 of follow-up was 0.7%–1.0% (1 dose). Cumulative risk curves of SARS-CoV-2 infection start from the day after vaccination when full protection against SARS-CoV-2 infection is thought to begin, according to previous studies (*1–3*). The hairs on both sides of the lines represent participants lost to follow-up; gaps represent periods of time between losses.

would be lower than in studies only including symptomatic disease and our VE estimates more relevant to transmission control, because in real-world conditions, symptomatic and asymptomatic infections coexist and both contribute to transmission.

Similarly, according to COVID-19 detection and surveillance guidelines in Spain and Aragon (*25*,*26*), tests were administered less frequently to asymptomatic than to symptomatic persons, resulting in underdetection of asymptomatic infections. This bias was reduced because underdetection occurred in both vaccinated and unvaccinated persons but could still lead to overestimating VE. On the other hand, also following the detection program guidelines, tests were administered to close contacts regardless of their vaccination status, which reduced the chance of detection bias in our study. However, routine screenings carried out in nursing and residential homes could have altered our findings if there were more screenings in vaccinated than in unvaccinated participants. The role of dominant variants of concern in the transmission was unknown at the time of our data analyses. The rapid circulation of these variants may have introduced confounding, but it was minimized by including weekly variability, and therefore calculated VE estimates represent a summarized measure against all variants, adjusted by incidence. Practical factors such as hygiene and social distance measures might also have affected the estimates of VE.

Our study shows great strength in statistical power because of the large population cohort and use of a refined methodology. Risk of infection differed between participants according not only to vaccination status but also to the evolution of the epidemic curve. For this reason, we used an approach of weekly repeated measures, adjusted by WCI in each primary care service area.

In conclusion, we found effectiveness against SARS-CoV-2 infection for Pfizer-BioNTech, Moderna, and Oxford-AstraZeneca vaccines to be lower than efficacy estimates from clinical trials and other VE studies. Even if high vaccination coverages are reached in the general population (*31*,*32*), effectively minimizing transmission opportunities might be limited, because age groups of persons <12 years of age were not being immunized at the time of our data gathering. Even so, reaching high vaccination coverage is important to decrease SARS-CoV-2 transmission in the general population.

Acknowledgments

The authors thank the anonymous reviewers and editors for their helpful suggestions.

About the Author

Ms. del Cura is currently working as a preventive medicine and public health specialist in the Population-based Screening Coordination Unit at the Aragon Department of Health, Zaragoza, Spain. Her primary research interests include public health issues such as vaccination effectiveness, epidemiology of communicable and noncommunicable diseases, and health promotion.

References

1. Baden LR, El Sahly HM, Essink B, Kotloff K, Frey S, Novak R, et al.; COVE Study Group. Efficacy and safety of the mRNA-1273 SARS-CoV-2 vaccine. N Engl J Med. 2021;384:403–16. https://doi.org/10.1056/NEJMoa2035389
2. Polack FP, Thomas SJ, Kitchin N, Absalon J, Gurtman A, Lockhart S, et al.; C4591001 Clinical Trial Group. Safety and efficacy of the BNT162b2 mRNA Covid-19 vaccine. N Engl J Med. 2020;383:2603–15. https://doi.org/10.1056/NEJMoa2034577
3. Voysey M, Costa Clemens SA, Madhi SA, Weckx LY, Folegatti PM, Aley PK, et al.; Oxford COVID Vaccine Trial Group. Single-dose administration and the influence of the timing of the booster dose on immunogenicity and efficacy of ChAdOx1 nCoV-19 (AZD1222) vaccine: a pooled analysis of four randomised trials. [Erratum in: Lancet. 2021;397:880]. Lancet. 2021;397:881–91. https://doi.org/10.1016/S0140-6736(21)00432-3
4. Sadoff J, Gray G, Vandebosch A, Cárdenas V, Shukarev G, Grinsztejn B, et al.; ENSEMBLE Study Group. Safety and efficacy of single-dose Ad26.COV2.S vaccine against Covid-19. N Engl J Med. 2021;384:2187–201. https://doi.org/10.1056/NEJMoa2101544
5. Logunov DY, Dolzhikova IV, Shcheblyakov DV, Tukhvatulin AI, Zubkova OV, Dzharullaeva AS, et al.; Gam-COVID-Vac Vaccine Trial Group. Safety and efficacy of an rAd26 and rAd5 vector-based heterologous prime-boost COVID-19 vaccine: an interim analysis of a randomised controlled phase 3 trial in Russia. Lancet. 2021;397:671–81. https://doi.org/10.1016/S0140-6736(21)00234-8
6. Al Kaabi N, Zhang Y, Xia S, Yang Y, Al Qahtani MM, Abdulrazzaq N, et al. Effect of 2 inactivated SARS-CoV-2 vaccines on symptomatic COVID-19 infection in adults: a randomized clinical trial. JAMA. 2021;326:35–45. https://doi.org/10.1001/jama.2021.8565
7. Shinde V, Bhikha S, Hoosain Z, Archary M, Bhorat Q, Fairlie L, et al.; 2019nCoV-501 Study Group. 2019nCoV-501 Study Group. 2019nCoV-501 Study Group. Efficacy of NVX-CoV2373 Covid-19 vaccine against the B.1.351 variant. N Engl J Med. 2021;384:1899–909. https://doi.org/10.1056/NEJMoa2103055
8. Dagan N, Barda N, Kepten E, Miron O, Perchik S, Katz MA, et al. BNT162b2 mRNA Covid-19 vaccine in a nationwide mass vaccination setting. N Engl J Med. 2021;384:1412–23. https://doi.org/10.1056/NEJMoa2101765
9. Haas EJ, Angulo FJ, McLaughlin JM, Anis E, Singer SR, Khan F, et al. Impact and effectiveness of mRNA BNT162b2 vaccine against SARS-CoV-2 infections and COVID-19 cases, hospitalisations, and deaths following a nationwide vaccination campaign in Israel: an observational study using national surveillance data. Lancet. 2021;397:1819–29. https://doi.org/10.1016/S0140-6736(21)00947-8
10. McDonald I, Murray SM, Reynolds CJ, Altmann DM, Boyton RJ. Comparative systematic review and meta-analysis

of reactogenicity, immunogenicity and efficacy of vaccines against SARS-CoV-2. NPJ Vaccines. 2021;6:74. https://doi.org/10.1038/s41541-021-00336-1
11. Vasileiou E, Simpson CR, Shi T, Kerr S, Agrawal U, Akbari A, et al. Interim findings from first-dose mass COVID-19 vaccination roll-out and COVID-19 hospital admissions in Scotland: a national prospective cohort study. Lancet. 2021;397:1646–57. https://doi.org/10.1016/S0140-6736(21)00677-2
12. Hall VJ, Foulkes S, Saei A, Andrews N, Oguti B, Charlett A, et al.; SIREN Study Group. COVID-19 vaccine coverage in health-care workers in England and effectiveness of BNT162b2 mRNA vaccine against infection (SIREN): a prospective, multicentre, cohort study. Lancet. 2021; 397:1725–35. https://doi.org/10.1016/S0140-6736(21)00790-X
13. Hyams C, Marlow R, Maseko Z, King J, Ward L, Fox K, et al. Effectiveness of BNT162b2 and ChAdOx1 nCoV-19 COVID-19 vaccination at preventing hospitalisations in people aged at least 80 years: a test-negative, case-control study. [Erratum in Lancet Infect Dis. 2021;21:e208]. Lancet Infect Dis. 2021;21:1539–48. https://doi.org/10.1016/S1473-3099(21)00330-3
14. Lopez Bernal J, Andrews N, Gower C, Robertson C, Stowe J, Tessier E, et al. Effectiveness of the Pfizer-BioNTech and Oxford-AstraZeneca vaccines on covid-19 related symptoms, hospital admissions, and mortality in older adults in England: test negative case-control study. BMJ. 2021;373:n1088. https://doi.org/10.1136/bmj.n1088
15. Johns Hopkins University. Coronavirus resource center. [cited 2021 Aug 1] https://coronavirus.jhu.edu/map.html
16. Government of Aragon (Spain). Aragon population register. Population pyramids [in Spanish]. [cited 2021 Aug 1] https://www.aragon.es/-/piramides-de-poblacion.-aragon
17. Aragon Department of Health. Aragonese COVID-19 epidemiological report [in Spanish], Zaragoza, Spain [cited 2021 Jul 31] https://datacovid.salud.aragon.es/covid
18. García-Montero C, Fraile-Martínez O, Bravo C, Torres-Carranza D, Sanchez-Trujillo L, Gómez-Lahoz AM, et al. An updated review of SARS-CoV-2 vaccines and the importance of effective vaccination programs in pandemic times. Vaccines (Basel). 2021;9:433. https://doi.org/10.3390/vaccines9050433
19. European Medicines Agency. COVID-19 vaccines authorized: vaccines authorised in the European Union (EU) to prevent COVID-19, following evaluation by the European Medicines Agency (EMA) [cited 2021 Jun 9]. https://www.ema.europa.eu/en/human-regulatory/overview/public-health-threats/coronavirus-disease-covid-19/treatments-vaccines/vaccines-covid-19/covid-19-vaccines-authorised
20. Interterritorial Board of the Spanish National Health System. COVID-19 vaccination strategy in Spain, 8th update [in Spanish]. 2021 Jun 22 [cited 2021 Aug 1]. https://www.mscbs.gob.es/profesionales/saludPublica/prevPromocion/vacunaciones/covid19/docs/COVID-19_Actualizacion8_EstrategiaVacunacion.pdf
21. Aragon Department of Health. Action plan for COVID-19 vaccination in Aragon, updated 2021 May 3 [in Spanish] [cited 2021 Aug 1]. https://www.aragon.es/documents/20127/1650151/Plan_Operativo_Vacunacion_Covid19_Aragon_20210503.pdf
22. Aragon Department of Health. Aragon weekly epidemiologic bulletin, week 20 (2021 May 17–23) [in Spanish] [cited 2021 Aug 1] https://www.aragon.es/documents/20127/1650151/BEsA_202021.pdf
23. Aragon Department of Health. Aragon weekly epidemiologic bulletin, week 29 (2021 July 19–25) [in Spanish] [cited 2021 Aug 1] https://www.aragon.es/documents/20127/1650151/BEsA_292021.pdf
24. World Health Organization. Public health surveillance for COVID-19: interim guidance. 2020 Dec 16 [cited 2021 Aug 1]. https://www.who.int/publications/i/item/who-2019-nCoV-surveillanceguidance-2020.8
25. Spanish Directorate-General of Public Health, Spanish Department of Health. Strategy for early detection, surveillance and control of COVID-19, updated 2021 Jul 23 [in Spanish] [cited 2021 Aug 1] https://www.mscbs.gob.es/profesionales/saludPublica/ccayes/alertasActual/nCov/documentos/COVID19_Estrategia_vigilancia_y_control_e_indicadores.pdf
26. Aragon Department of Health. General procedure for COVID-19 healthcare in Aragon, updated 2021 Jun 29 [in Spanish] [cited 2021 Aug 1]. https://www.aragon.es/documents/20127/1650151/20210629_Procedimiento_COVID_19_Aragon.pdf
27. Bianchi FP, Germinario CA, Migliore G, Vimercati L, Martinelli A, Lobifaro A, et al.; Control Room Working Group. BNT162b2 mRNA Covid-19 vaccine effectiveness in the prevention of SARS-CoV-2 infection: a preliminary report. J Infect Dis. 2021;224:431–4. https://doi.org/10.1093/infdis/jiab262
28. Thompson MG, Burgess JL, Naleway AL, Tyner HL, Yoon SK, Meece J, et al. Interim estimates of vaccine effectiveness of BNT162b2 and mRNA-1273 COVID-19 vaccines in preventing SARS-CoV-2 infection among health care personnel, first responders, and other essential and frontline workers—eight U.S. locations, December 2020–March 2021. MMWR Morb Mortal Wkly Rep. 2021;70:495–500. https://doi.org/10.15585/mmwr.mm7013e3
29. Chodick G, Tene L, Rotem RS, Patalon T, Gazit S, Ben-Tov A, et al. The effectiveness of the two-dose BNT162b2 vaccine: analysis of real-world data. Clin Infect Dis. 2021 May 17 [Epub ahead of print]. https://doi.org/10.1093/cid/ciab438
30. Martínez-Baz I, Miqueleiz A, Casado I, Navascués A, Trobajo-Sanmartín C, Burgui C, et al.; Working Group for the Study of COVID-19 in Navarra. Effectiveness of COVID-19 vaccines in preventing SARS-CoV-2 infection and hospitalisation, Navarre, Spain, January to April 2021. Euro Surveill. 2021;26:2100438. https://doi.org/10.2807/1560-7917.ES.2021.26.21.2100438
31. Frederiksen LSF, Zhang Y, Foged C, Thakur A. The long road toward COVID-19 herd immunity: vaccine platform technologies and mass immunization strategies. Front Immunol. 2020;11:1817. https://doi.org/10.3389/fimmu.2020.01817
32. Randolph HE, Barreiro LB. Herd Immunity: Understanding COVID-19. Immunity. 2020;52:737–41. https://doi.org/10.1016/j.immuni.2020.04.012

Address for correspondence: Alicia del Cura-Bilbao, Aragon Department of Health, 36 Vía Univérsitas, 50017 Zaragoza, Spain; email: adelcura@salud.aragon.es

Case–Control Study of *Clostridium innocuum* Infection, Taiwan

Yi-Ching Chen,[1] Yi-Chun Kuo,[1] Mi-Chi Chen, Young-Da Zhang, Chyi-Liang Chen, Puo-Hsien Le, Cheng-Hsun Chiu

Vancomycin-resistant *Clostridium innocuum* was recently identified as an etiologic agent for antibiotic-associated diarrhea in humans. We conducted a case–control study involving 152 *C. innocuum*-infected patients during 2014–2019 in Taiwan, using 304 cases of *Clostridioides difficile* infection (CDI) matched by diagnosis year, age (±2 years), and sex as controls. The baseline characteristics were similar between the 2 groups. *C. innocuum*–infected patients experienced more extraintestinal clostridial infection and gastrointestinal tract–related complications than did patients with CDI. The 30-day mortality rate among *C. innocuum*–infected patients was 14.5%, and the overall rate was 23.0%. Chronic kidney disease, solid tumor, intensive care unit admission, and shock status were 4 independent risk factors for death. *C. innocuum* identified from clinical specimens should be recognized as a pathogen requiring treatment, and because of its intrinsic vancomycin resistance, precise identification is necessary to guide appropriate and timely antimicrobial therapy.

Clostridium species are obligate anaerobic, endospore-forming bacilli that usually colonize in the gastrointestinal tracts of humans. Of the ≥200 species of *Clostridium*, ≥30 are potential pathogens in humans, such as *C. perfringens* and *Clostridioides difficile.* However, *C. innocuum* has rarely been described as associated with human disease.

C. innocuum was first identified in the 1960s among 8 patients in the United States; the name, innocuum, described its lack of virulence (*1*,*2*). It was challenging to distinguish *C. innocuum* from other *Clostridium* species (especially *C. ramosum* and *C. clostridioforme*, together called the RIC group) because of their similar phenotypes of atypical clostridial colonial morphology, rare spore-forming features, and fatty acid pattern (*3*–*5*). Identifying *C. innocuum* has become faster and more accurate after the introduction of molecular techniques such as 16S RNA sequencing and matrix-associated laser desorption/ionization time-of-flight (MALDI-TOF) mass spectrometry (*6*).

In 1995, Cutrona et al. reported the first case of endocarditis caused by *C. innocuum* (*7*). Although the bacterium was considered less pathogenic and seldom caused infections previously, more and more clinical evidence has emerged since 2000s, suggesting *C. innocuum* might be a potential cause of antibiotic-associated diarrhea and of extraintestinal clostridial infection (EICI), such as bacteremia, intra-abdominal infection, and endocarditis (*8*–*10*). However, we are not aware of a study of *C. innocuum* infection with a large enough cohort of patients to describe its clinical characteristics.

Precise diagnosis of *C. innocuum* is necessary because of its unique intrinsic resistance to vancomycin, presumably caused by the presence of 2 chromosomal genes that enable the synthesis of a peptidoglycan precursor terminating in serine with low vancomycin affinity (*9*,*11*). Although vancomycin is one of the recommended antimicrobial drugs to treat infections caused by *Clostridium* species, especially *C. difficile*, intrinsic resistance to vancomycin in *C. innocuum* poses the risk for inappropriate treatment for patients who acquire *C. innocuum* infection (*12*). *C. difficile* is one of the most representative clostridial species to cause human disease and has been well investigated. In the United States, ≈500,000 infections were identified annually, and 15,000–30,000 deaths were associated with *C. difficile* infection (CDI) (*12*–*14*)

In previous studies, we demonstrated *C. innocuum* as a potential invasive pathogen causing severe colitis and EICI in a small case series and proved its cellular toxicity in vitro (*8*,*9*). Herein, we conducted a retrospective case–control study to describe and

Author affiliations: Chang Gung University, Taoyuan, Taiwan (Y.-C. Chen, Y.-C. Kuo, C.-H. Chiu); Chang Gung Memorial Hospital, Taoyuan (Y.-C. Chen, M.-C. Chen, Y.-D. Zhang, C.-L. Chen, P.-H. Le, C.-H. Chiu)

DOI: https://doi.org/10.3201/eid2803.204421

[1]These authors contributed equally to this article.

evaluate the clinical characteristics and outcomes of infections caused by *C. innocuum*. To this end, we selected case-patients with CDI as the control group.

Institute Review Boards in Chang Gung Memorial Hospital (CGMH; Taoyuan, Taiwan) approved the study, allowing review of the medical data of the patients (IRB#201900906B0). A waiver of consent was granted given the retrospective nature of the project and anonymous analysis of the clinical information of patients.

Methods

Study Design, Clinical Setting, and Case Enrollment

We conducted a retrospective case–control study at CGMH during 2014–2019. CGMH is a tertiary medical center accommodating 3,700 patient beds. We selected *C. difficile* as the control to better illustrate the clinical features of *C. innocuum* infection. The case and control groups were assigned in a 1:2 ratio and matched in the diagnosed year, age ±2 years, and sex.

We identified cases with *C. innocuum* and *C. difficile* infections using the rapid ID 32A system (bioMérieux, https://www.biomerieux.com) and MALDI-TOF mass spectrometry Biotyper (Bruker Daltonik GmbH, https://www.bruker.com) (*15*–*17*). MALDI-TOF mass spectrometry was introduced in 2009 in the clinical microbiology laboratory of CGMH, but *C. innocuum* was not reported routinely because it was considered a clinically insignificant microorganism. To trace the cases infected with *C. innocuum*, we reviewed the original reporting database from the MALDI-TOF mass spectrometry system directly and identified the samples reporting *C. innocuum*. Our definition of a microbiologically confirmed *C. innocuum* infection was that the original report from the MALDI-TOF mass spectrometry database revealed *C. innocuum* in the strongest 2 signals and had signal scores >2.00. We defined *C. difficile* infections by the same rationale.

We reviewed baseline information of each patient and enlisted all patients with *C. innocuum* infection in the study. We defined *C. difficile* infection as a positive PCR-based toxin assay with presence of clinical symptoms compatible with the infection, or a positive culture of *C. difficile* with compatible clinical symptoms (e.g., documented diarrhea or radiologic features of toxic megacolon). We excluded cases with concomitant *C. innocuum* and *C. difficile* isolated from the same clinical sample from the study. For the case-control matching, 3 authors (Y.-C. Chen, Y.-C. Kuo, and M.-C. Chen) reviewed baseline information of all cases with *C. innocuum* and *C. difficile* infection. We randomly selected 2 controls for each case, matched by diagnostic year, age (±2 years), and sex of the index case. If no controls were eligible from these 3 matching variables, then we dropped the sex criterium, followed by the age criterium if necessary. After the matching process, we further reviewed the clinical information of these patients.

Clinical Data Resources, Variables, and Definition

We collected demographic data, clinical manifestations, laboratory testing results, images, and microbiology reports through an electronic medical record system (EMR). Demographic data were age, sex, race, underlying systemic diseases, and acquisition modality (community vs. hospital). We defined hospital-acquired infection as the symptoms that occurred >48 hours after admission, or <4 weeks after discharge from a healthcare facility; otherwise, it was classified as a community-acquired infection (*18*). We calculated the Charlson Comorbidity Index score for each patient to represent the baseline physiologic condition affected by underlying disease. The index is composed of 19 underlying conditions in 4 categories. Each category had a weighted score based on the risk for 1- and 10-year mortality rate (*19*).

We recorded clinical symptoms such as diarrhea, fever, bloody stool, abdominal pain, vomiting, and abdominal distension. We also reviewed disease-related complications, including toxic megacolon, ileus, bowel perforation, and shock. Recurrent infection was defined if the patient had a repeated microbiological culture from the same specimen source within 8 weeks of initial documented symptoms resolution (*20*,*21*). Outcome assessment included 30-day, 90-day, and overall deaths after the infection. We reviewed previous antibiotic exposures according to each class: penicillins, cephalosporins, carbapenems, fluoroquinolones, aminoglycosides, macrolides, tetracyclines, glycopeptides, oxazolids, polymyxins, lincosamides, and metronidazole. We defined antibiotic exposure rates as the percentage of patients who received any drugs ≤30 days before *C. innocuum* or *C. difficile* infection and duration of antibiotic exposure as total days of any antimicrobial drug use in a patient ≤30 days before the event of *C. innocuum* or *C. difficile* infection.

Bacterial Isolation and Identification

We performed anaerobic bacterial cultures in the clinical microbiology laboratory, as described

Table 1. Baseline characteristics and clinical diagnoses in 2 groups of patients by the infecting *Clostridium* species in case–control study of *C. innocuum* infection, Taiwan*

Variable	Total, N = 456	*C. innocuum*, n = 152	*Clostridioides difficile*, n = 304	OR (95% CI)	p value
Age, mean (SD)†	66.7 (18.2)	66.6 (18.3)	66.7 (18.1)	NA	0.978
Sex					
M	266 (58.3)	97 (63.8)	169 (55.6)	1.41 (0.94–2.10)	0.094
F	190 (41.7)	55 (36.2)	135 (44.4)	0.71 (0.48–1.06)	0.094
Hospitalization	439 (96.2)	142 (93.4)	297 (97.7)	0.34 (0.13–0.90)	0.03
No. days, median (IQR, range)‡	22 (36, 0–492)	14 (33, 0–492)	26 (36, 0–409)	NA	<0.001
Charlson Comorbidity Index, mean (SD)†	6.1 (3.2)	5.7 (3.2)	6.2 (3.3)	NA	0.100
Diabetes mellitus	135 (29.6)	52 (34.2)	83 (27.3)	1.39 (0.91–2.11)	0.128
Chronic kidney disease	122 (26.8)	28 (18.4)	94 (30.9)	0.50 (0.31–0.81)	0.005
Congestive heart failure	45 (9.9)	12 (7.9)	33 (10.9)	0.70 (0.35–1.40)	0.315
AIDS	4 (0.9)	1 (0.7)	3 (1.0)	0.66 (0.07–6.44)	0.724
Solid tumor	138 (30.3)	42 (27.6)	96 (31.6)	0.83 (0.54–1.27)	0.387
Initial ICU admission	65 (14.3)	36 (23.7)	29 (9.5)	2.94 (1.72–5.03)	<0.001
Acquisition of infection					
Hospital acquired	354 (77.6)	101 (66.4)	253 (83.2)	0.40 (0.25–0.63)	<0.001
Community acquired	102 (22.4)	51 (33.6)	51 (16.8)	2.50 (1.60–3.93)	<0.001
Clinical diagnosis					
Clostridium-associated diarrhea	375 (82.2)	96 (63.2)	279 (91.8)	0.15 (0.09–0.26)	<0.001
Extraintestinal clostridial infection	81 (17.8)	56 (36.8)	25 (8.2)	6.51 (3.85–11.01)	<0.001
Bacteremia	8 (1.8)	7 (4.6)	1 (0.3)	14.63 (1.78–120.00)	0.012
Intra-abdominal infection	31 (6.8)	21 (13.8)	10 (3.2)	4.71 (2.16–10.23)	<0.001
Biliary tract infection	4 (0.9)	3 (2.0)	1 (0.3)	6.10 (0.63–59.15)	0.119
Recurrent infection	15 (3.3)	0 (0)	15 (4.9)	NA	NA
Skin and soft tissue infection	36 (7.9)	23 (15.1)	13 (4.3)	3.99 (1.96–8.13)	<0.001
Genital tract infection§	2 (0.4)	2 (1.3)	0 (0)	NA	NA
Complication					
Ileus	34 (7.5)	17 (11.2)	17 (5.6)	2.12 (1.05–4.29)	0.035
Bowel perforation	14 (3.0)	11 (7.2)	3 (1.0)	7.83 (2.15–28.50)	0.002
Hypovolemic or septic shock	43 (9.4)	22 (14.5)	21 (6.9)	2.28 (1.21–4.30)	0.011
Mortality					
30-day mortality	81 (17.7)	22 (14.5)	59 (19.4)	0.70 (0.41–1.20)	0.195
90-day mortality	97 (21.3)	24 (15.8)	73 (24.0)	0.59 (0.36–0.99)	0.045
Overall mortality	122 (26.7)	35 (23.0)	87 (28.6)	0.77 (0.49–1.21)	0.264

*Values are no (%) except as indicated. p value of ORs was analyzed by univariate logistic regression. ICU, intensive care unit; IQR, interquartile range; NA, not applicable for continuous variables or too few events (<5) to calculate a stable OR; OR, odds ratio.
†By independent *t* test.
‡By Mann-Whitney test.
§Two cases were diagnosed as pyospermia and bacterial vaginitis.

previously (*9*). We streaked all the anaerobic samples onto the selective agar plate, including CDC-ANA-BAP (anaerobic blood agar plate), CDC-ANA-PEA (anaerobic phenylethyl alcohol blood agar plate), and BBE/KVLB (Bacteroides bile esculin and laked kanamycin) bi-plate. We incubated agar plates in anaerobic conditions (90% N_2/10% CO_2) at 37°C for 5 days. We grossly reviewed the growing colonies on

Table 2. Antibiotic exposure before *Clostridium* infection in case–control study of *C. innocuum* infection*

Antibiotic exposure	*C. innocuum*, n = 152	*Clostridioides difficile*, n = 304	Odds ratio (95% CI)	p value
Any antibiotic exposure	121 (79.6)	289 (95.1)	0.20 (0.11–0.39)	<0.001
Mean duration of antibiotic exposure, d (SD)†	13.7 (8.6)	15.6 (8.3)	NA	0.039
Antibiotic exposure rate by drug class				
Penicillins	36 (23.7)	107 (35.2)	0.57 (0.37–0.89)	0.013
Cephalosporins	81 (53.3)	206 (67.8)	0.54 (0.36–0.81)	0.003
Carbapenems	36 (23.7)	102 (33.6)	0.62 (0.40–0.96)	0.031
Fluoroquinolones	31 (20.4)	108 (35.5)	0.47 (0.29–0.74)	0.001
Aminoglycosides	13 (8.6)	20 (6.6)	1.33 (0.64–2.75)	0.444
Macrolides	3 (2.0)	8 (2.6)	0.75 (0.20–2.85)	0.667
Tetracyclines	6 (3.9)	5 (1.6)	2.46 (0.74–8.19)	0.143
Glycopeptides	52 (34.2)	92 (30.3)	1.20 (0.79–1.81)	0.393
Oxazolids	0 (0)	2 (0.7)	NA	NA
Polymyxins	6 (3.9)	11 (3.6)	1.10 (0.40–3.02)	0.861
Lincosamides	6 (13.9)	21 (6.9)	0.55 (0.22–1.40)	0.213
Metronidazole	16 (10.5)	33 (10.9)	0.97 (0.51–1.81)	0.915

*Data are presented as no (%) unless otherwise indicated. NA, not applicable for continuous variables or too few events (<5) to calculate a stable odds ratio.
†By independent student *t* test. The p value of odds ratio was analyzed by univariate logistic regression.

Table 3. Clinical and laboratory characteristics by the infecting *Clostridium* species in case–control study of *C. innocuum* infection, Taiwan*

Characteristic	*C. innocuum*, n = 152	*Clostridioides difficile*, n = 304	p value
Clinical symptoms			
Diarrhea	56 (36.8)	217 (71.4)	<0.001
Fever	29 (19.1)	92 (30.3)	0.011
Abdominal pain	37 (24.3)	54 (17.8)	0.098
Vomiting	13 (8.6)	29 (9.5)	0.731
Abdominal distension	25 (16.4)	41 (13.5)	0.391
Blood testing			
Leukocytes, cells/μL†	10,454 (6,773)	11,005 (6,788)	0.783
Hemoglobin, g/dL†	10.7 (2.4)	9.8 (2.0)	<0.001
Platelet count × 1,000/μL†	243 (110.4)	231 (135.0)	0.134
CRP, mg/L, median (IQR)‡	55.7 (104.7)	55.7 (97.2)	0.108
Stool routine, no. positive/total (%)			
Occult blood	53/73 (72.6)	175/216 (81.0)	0.128
Mucus	9/70 (12.8)	39/205 (19.0)	0.241
Pus cells	8/70 (11.4)	30/205 (14.6)	0.502
Sample site			
Stool	96 (63.2)	279 (91.8)	<0.001
Blood	7 (4.6)	1 (0.3)	0.001
Ascites	13 (8.5)	8 (2.7)	0.002
Bile§	2 (1.3)	1 (0.3)	0.219
Pus/abscess§	16 (10.5)	3 (1.0)	<0.001
Wound/deep tissue§	16 (10.5)	12 (3.6)	0.006
Endocervix§	1 (0.7)	0	0.592
Semen§	1 (0.7)	0	0.592
Antimicrobial susceptibility#			
Metronidazole	20/20 (100)	53/53 (100)	1.000
Clindamycin§	30/44 (68.2)	17/20 (85.0)	0.158
Penicillin§	35/44 (79.5)	12/20 (60.0)	0.101
Ampicillin/sulbactam	21/21 (100)	44/44 (100)	1.000

*Values are no. (%) patients except as indicated. Among patients with *C. difficile* (CD)–associated diarrhea, the CD toxin assay positive rate was 65%. χ^2 tests were used to compare all the categorical variables listed in the table except as noted. CRP, C-reactive protein; IQR, interquartile range.
†By independent *t* test.
‡By Mann-Whitney test.
§By Fisher exact test.
#Data are expressed as susceptible isolate number/total isolate number (%).

plate and analyzed 1 representative colony for each agar plate by the rapid ID 32A system (bioMérieux) for identification of the microorganisms.

Antimicrobial Susceptibility Testing

We tested antimicrobial susceptibilities to clindamycin, metronidazole, penicillin, piperacillin, and ampicillin/sulbactam by the break-point agar dilution method according to Clinical and Laboratory Standards Institute criteria (document M11-A8) for anaerobic bacteria (*22*). We used interpretive criteria in document M100S to determine susceptibility (*22*).

Statistical Analysis

We performed statistical analysis by SPSS Statistics 24.0 (SPSS Inc., https://www.ibm.com/products/spss-statistics). For continuous variables, we determined significance by using the independent t test or Mann-Whitney U test as appropriate. If the continuous variable had outliers and did not fit the normal distribution, variables were shown as median (interquartile range, range). We analyzed the categorical variables by χ^2 test and considered $p<0.05$ statistically significant. We obtained odds ratios (ORs) from cross-tabulation and analyzed the p value of ORs by univariate logistic regression. We estimated mortality rate at 30 days and 90 days after the positive culture and analyzed by Kaplan-Meier survival analysis using methods described previously (*23*). In addition, we examined risk factors associated with 30- and 90-day mortality in both groups by logistic regression.

Results

Participants and Demographic Information

By the MALDI-TOF mass spectrometry system, 180 samples yielded the growth of *C. innocuum*. We excluded 22 of those from further analysis because of lack of access to clinical information and 6 because of concomitant isolation of *C. innocuum* and *C. difficile* from the same sample (CI group). We matched the control group with *C. innocuum* samples in accordance with the study criteria. From 1,134 *C. difficile* cases during the study period, we enrolled 304 cases as controls (CD group). All control cases were

matched precisely on diagnostic year and age (±2 years); 25 controls were not matched on sex. The mean patient age for the 456 cases was 66.7 years, and 58.3% of patients were male (Table 1). Both groups were similar regarding age, sex, and Charlson Comorbidity Index score (5.7 ± 3.2 for CI and 6.2 ± 3.3 for CD). Subgroup analysis of each age group (<50, 50–60, 60–70, 70–80, and >80 years) also revealed no statistical difference. Overall, 8 pediatric patients were recruited, 3 in the CI group and 5 in the CD group. Regarding underlying systemic diseases, the CD group showed more patients with chronic kidney disease (18.4% vs. 30.9%; p = 0.005) (Table 1). Of note, more patients acquired the infection in the community in the CI group (33.6% vs. 16.8%; odds ratio [OR] 2.5, 95% CI 1.6–3.9; p<0.001) (Table 1).

Disease Characteristics and Severity

We observed notable differences in disease characteristics between the 2 groups. Those in the CI group had a 6.5 times higher risk of developing EICI, including bacteremia, intra-abdominal infection, biliary tract infection, skin and soft tissue infection, pyospermia, and bacterial vaginitis (36.8% for CI vs. 8.2% for CD; OR 6.5, 95% CI 3.9 –11.0; p<0.001) (Table 1). On the contrary, most disease manifestation in the CD group was confined to the intestine and colon, mainly *C. difficile*–associated diarrhea. Most patient had antibiotic exposure 30 days before the CI or CD infection event. CD group showed higher 30-day antibiotic exposure rate (95.1%) than CI group (79.6%; p<0.001) (Table 2) and longer duration (mean 15.6 days, SD 8.3) than CI group (mean 13.7 days, SD 8.6; p<0.001). Patients in CD group received more penicillins, cephalosporins, carbapenems, and fluroquinolones (Table 2).

Regarding disease severity, most of the patients in both groups required hospitalization (93.4% in the CI group and 97.7% in the CD group; p = 0.03) (Table 1). Although most patients in CD group had intestinal infections, gastrointestinal tract–related complications of ileus, bowel perforation, clinical sepsis, and shock occurred more frequently in the CI group (26.3%) than CD group (11.2%; OR 2.8, 95% CI 1.7–4.7; p<0.001). CI group also showed a higher rate of intensive care unit (ICU) admission (23.6% vs. 9.5%; OR 2.9, 95% CI 1.7–5.0; p<0.001) (Table 1). All the data indicated that the disease severity at the acute stage was more severe and invasive in the *C. innocuum*–infected patients. Furthermore, we saw no recurrence of infection in CI group but recurrence of infection in 4.9% of CD group (p = 0.005).

We observed no statistically significant differences in clinical presentations, but patients with *C. innocuum* infection had fewer diarrheal symptoms

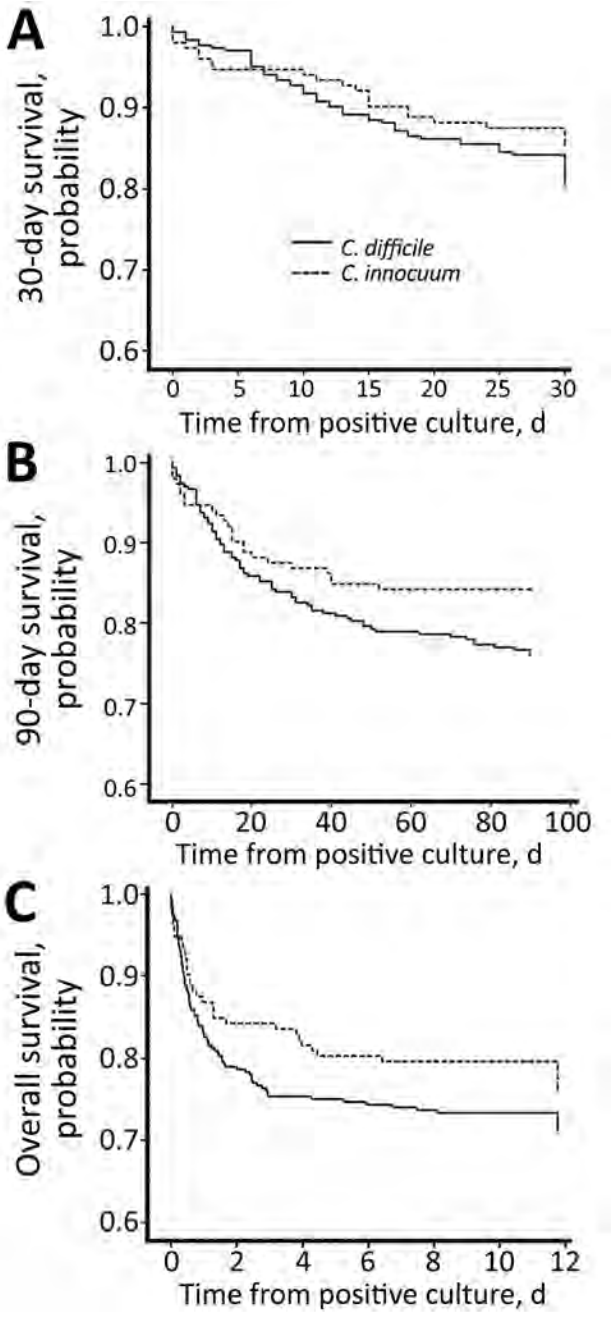

Figure. Kaplan-Meier curve of 30-day (A), 90-day (B), and overall (C) survival rates of patients with *Clostridioides difficile* and *Clostridium innocuum*, Taiwan. In the *C. innocuum* group, the 30-day survival rate was 85.5%, 90-day survival rate 84.2%, and overall survival rate 77.0%. The 90-day survival rate was slightly higher than the *C. difficile group* (p value of log rank test = 0.05), whereas the 30-day and overall survival rates did not show a significant difference between the 2 groups.

Table 4. Reported cases of extraintestinal *Clostridium innocuum* infection, 2000–2020, Taiwan*

Characteristic	Castiglioni et al. (*10*)	Crum-Cianflone et al. (*29*)	Hung et al. (*30*)	Mutoh et al. (*31*)	Aroca-Ferri et al. (*32*)
Year and country	2003 United States	2009 United States	2014 Taiwan	2015 Japan	2019 Spain
Age, y/sex	38/F	38/M	85/M	32/M	44/F
Underlying conditions	Chronic HCV, interstitial nephritis after renal transplant	AIDS	DM with CDAD and CMV colitis	ALL	Takayasu arteritis, ESRD under PD
Isolation site	Blood	Blood	Blood	Blood, BM	Peritoneal fluid
Vancomycin MIC	16 μg/mL	NA	>32 μg/mL	8 μg/mL	8 μg/mL
Diagnosis	Bacteremia secondary to infectious hematoma	Bacteremia	Bacteremia	Pelvic osteomyelitis complicated with iliac muscle abscess	PD peritonitis complicated with sigmoid colon perforation
Treatment	IV TZP, IV CLI	IV DAP, PO MTZ	IV TZP	IV TZP, IV MTZ, IV CLI	IV CTX, IP AMP, IP CLI
Duration	11 days and surgery	NA	2 weeks	8 weeks	15 days
Outcome	Recovered	Recovered	Recovered	Recovered	Died

*ALL, acute lymphoblastic leukemia; AMP, ampicillin; BM, bone marrow; CDAD, *C. difficile*–associated diarrhea; CLI, clindamycin; CMV, cytomegalovirus; CTX, cefotaxime; DAP, daptomycin; ERY, erythromycin; ESRD, end stage renal disease; HCV, hepatitis C virus; IP, intraperitoneal route; IV, intravenous route; MIC, minimum inhibitory concentration; MTZ, metronidazole; NA, not available; PD, peritoneal dialysis; PO, oral route; TZP, piperacillin/tazobactam.

and less fever. In the laboratory testing results, patients experienced anemia more commonly in the CD group than CI group; hemoglobin counts were 9.8 (2.0) g/dL in CD and 10.7 (2.4) g/dL in CI (p<0.001) (Table 3). We observed no difference in other systemic inflammatory markers. A limited number of patients received colonoscopy examination, and we found no pseudomembranous colitis in the CI group.

Outcome and Risk Factor for Mortality Rate

The 30-day mortality rate in the CI group was 14.5%; the 90-day rate, 15.8%, and the overall rate, 23.0%. Although the 90-day mortality rate was slightly higher in the CD group with a significant difference (p value of log rank test = 0.05) in Kaplan-Meier survival analysis, the overall mortality rate did not show a statistically significant difference between the 2 groups (Figure). Using logistic regression, we identified chronic kidney disease (OR 8.6, 95% CI 2.6–28.4; p<0.001), solid tumor (OR 3.5, 95% CI 1.0–12.0; p = 0.051), ICU admission (OR 7.3, 95% CI 2.4–21.9; p<0.001), and shock status (odds ratio 8.0, 95% CI 2.4–27.2; p<0.001) as 4 independent risk factors for both 30-day and overall mortality rates in the patients with *C. innocuum* infection. We identified 7 bacteremias caused by *C. innocuum* in this study. Two of those patients experienced septic shock, and 1 needed ICU hospitalization. The 30-day mortality rate for the 7 patients was 42.9% (3/7) and 90-day was 57.1% (4/7).

Microbiologic Result and Antimicrobial Susceptibility

Among the 152 *C. innocuum* isolates, we recovered 96 (63.2%) isolates from stool specimens; the rest were from the blood (*7*), ascites (*13*), pus/abscess (*16*), wound/deep tissue (*16*), bile juice (*2*), endocervix (*1*), and semen (*1*). We detected 18 polymicrobial infections in the CI group, most of which were from ascites and pus/abscess samples. More *C. innocuum* isolates (36.8%) than *C. difficile* isolates (8.2%) were from extraintestinal specimens (p<0.001) (Table 3), which is compatible with our clinical observation. We performed antimicrobial susceptibility testing on limited isolates. In the *C. innocuum* isolates, we observed the highest susceptibility rate for metronidazole (20/20, 100%) and ampicillin/sulbactam (21/21, 100%), followed by penicillin (35/44, 79.5%) and clindamycin 30/44 (68.2%).

Discussion

Genus *Clostridium* is large and heterogeneous; it includes ≤200 species. Accurate species identification has been difficult. In recent years, several new species have been recognized and others reclassified using newer molecular diagnostic methods, such as 16S rRNA gene sequencing (*24*). Among the medically important *Clostridium* spp., *C. perfringens* is the predominant species isolated from cases of bacteremia. The severity of EICI varies; for bacteremia, the mortality rate was found to be 48%–52% by different studies (*25*–*27*). The risk factors for disease acquisition and death were related to an underlying immunocompromised condition such as hemodialysis, malignancy, immunosuppressant use, and Crohn's disease (*25*). The main portal of entry is the hepatobiliary and gastrointestinal tract. We believe this is also the case in *C. innocuum* because stool was a common source for the *C. innocuum* isolates and gastrointestinal tract–related complications were not uncommon in *C. innocuum*–infected patients.

A recent study by Ha et al. (*28*) also found that *C. innocuum* is one of the most common bacteria that could translocate from intestine to mesenteric tissue in patients with Crohn's disease and further induce adipogenesis and local fibrosis, known together as creeping fat.

We found that among anaerobic clostridial species, *C. innocuum* has long been overlooked as a human pathogen. Our study is to date the most comprehensive observational study to depict the clinical manifestations and outcome of *C. innocuum* infection; not only it is more invasive than most *Clostridium* species, but it can cause more gastrointestinal tract complications following intestinal infection. Case reports of EICI related to *C. innocuum* infection have been published from the United States, Spain, Japan, and Taiwan (*10*,*29*–*32*) (Table 4). Bacteremia and intraabdominal infection were the most common manifestations, which is compatible with our observations. All the infections occurred in patients with underlying conditions; prolonged antimicrobial therapy was required to treat these patients, whose mortality rate (20%) was similar to that observed in our study (23%). Compared to *C. difficile*, which is known to be a nosocomial pathogen, nearly one third of the *C. innocuum* infections occurred in the community. This observation indicates that *C. innocuum* could be more virulent and competitive than *C. difficile*.

Among the EICI, bacteremia is the most severe form of infection. In a recent study by Morel et al. (*33*), non–*C. difficile Clostridium* bacteremia requiring ICU hospitalization showed an aggressive clinical course and was usually life-threatening. The 28-day mortality rate was 55% and the 90-day mortality rate was 71% (*33*). This report is compatible with our findings of 30-day (42.9%) and 90-day (57.1%) mortality rates in the CI bacteremic patients.

Identifying *C. innocuum* infection is important because the microorganism expresses intrinsic resistance to vancomycin, because of the synthesis of peptidoglycan precursors with low affinity for vancomycin (MIC 4–16 mg/L) (*8*,*26*). Moreover, highly vancomycin-resistant strains (MIC >16 mg/L) could develop if the bacteria were previously exposed to vancomycin (*34*). Because oral vancomycin has been recommended as the first-line therapy for *C. difficile* infection, distinguishing *C. innocuum* from other clostridial species becomes essential to avoid treatment failure caused by inappropriate antimicrobial use. Metronidazole and clindamycin appear to be appropriate choices for treating *C. innocuum* infection, according to our antimicrobial susceptibility testing results.

The main limitation of our study is the retrospective study design and the inevitable missing data. The lack of standardized medical record format prevented us from precisely defining every case-patient's diagnosis, especially antibiotic-associated diarrhea and acute colitis, which have similar clinical descriptions in the medical records. Some objective data were not available, which may potentially compromise the accuracy of the estimated rates of presentations and diagnoses among the patients. However, the proportion of missing data appeared small and should not significantly affect the results of the study. Second, not all the *C. innocuum* isolates from the enrolled patients were tested for antimicrobial susceptibility, and that testing did not include vancomycin. Third, the study does not advance our understanding on virulence mechanism of *C. innocuum*. It is possible that *C. innocuum* possesses a unique virulence mechanism to cause gastrointestinal as well as extraintestinal infections, such as the lipopolysaccharide-like structure we described in our previous study (*9*). *C. difficile* also contains surface lipocarbohydrate, which has a similar biologic activity to the lipopolysaccharide in gram-negative bacteria (*35*); this hypothesis needs further experimental verification.

In conclusion, *C. innocuum* should be considered an important *Clostridium* species causing EICI and gastrointestinal infection that has a risk for severe complications and a high mortality rate in immunocompromised patients; physicians should recognize it as a pathogen to treat clinically. More studies are needed to understand the virulence mechanism of *C. innocuum*. Precise identification of *C. innocuum* will guide appropriate and timely antimicrobial therapy for patients because of its intrinsic vancomycin resistance.

The study was financially supported by grants (CIRPG3H0031-2 and CIRPG3H0041-2) from Chang Gung Memorial Hospital, Taiwan, and the Maintenance Project of the Center for Big Data Analytics and Statistics at Chang Gung Memorial Hospital (grant CLRPG3D0048) for statistical consultation and data analysis.

About the Author

Dr. Chen is an infectious disease specialist at Chang Gung Memorial Hospital, Chang Gung University, Taoyuan, Taiwan. Her research interests are epidemiology, pathogenesis, and resistance mechanisms of enteric bacterial infection.

References

1. Smith LD, King E. *Clostridium innocuum*, sp. n., a sporeforming anaerobe isolated from human infections. J Bacteriol. 1962;83:938–9. https://doi.org/10.1128/jb.83.4.938-939.1962
2. Alexander CJ, Citron DM, Brazier JS, Goldstein EJ. Identification and antimicrobial resistance patterns of clinical isolates of *Clostridium clostridioforme*, *Clostridium innocuum*, and *Clostridium ramosum* compared with those of clinical isolates of *Clostridium perfringens*. J Clin Microbiol. 1995;33:3209–15. https://doi.org/10.1128/jcm.33.12.3209-3215.1995
3. Stokes NA, Hylemon PB. Characterization of delta 4-3-ketosteroid-5 beta-reductase and 3 beta-hydroxysteroid dehydrogenase in cell extracts of *Clostridium innocuum*. Biochim Biophys Acta. 1985;836:255–61. https://doi.org/10.1016/0005-2760(85)90073-6
4. Carlier JP, Sellier N. Identification by gas chromatography-mass spectrometry of short-chain hydroxy acids produced by *Fusobacterium* species and *Clostridium innocuum*. J Chromatogr A. 1987;420:121–8. https://doi.org/10.1016/0378-4347(87)80161-5
5. Johnston NC, Goldfine H, Fischer W. Novel polar lipid composition of *Clostridium innocuum* as the basis for an assessment of its taxonomic status. Microbiology (Reading). 1994;140:105–11. https://doi.org/10.1099/13500872-140-1-105
6. Li Y, Shan M, Zhu Z, Mao X, Yan M, Chen Y, et al. Application of MALDI-TOF MS to rapid identification of anaerobic bacteria. BMC Infect Dis. 2019;19:941. https://doi.org/10.1186/s12879-019-4584-0
7. Cutrona AF, Watanakunakorn C, Schaub CR, Jagetia A. *Clostridium innocuum* endocarditis. Clin Infect Dis. 1995;21:1306–7. https://doi.org/10.1093/clinids/21.5.1306
8. Chia JH, Wu TS, Wu TL, Chen CL, Chuang CH, Su LH, et al. *Clostridium innocuum* is a vancomycin-resistant pathogen that may cause antibiotic-associated diarrhoea. Clin Microbiol Infect. 2018;24:1195–9. https://doi.org/10.1016/j.cmi.2018.02.015
9. Chia JH, Feng Y, Su LH, Wu TL, Chen CL, Liang YH, et al. *Clostridium innocuum* is a significant vancomycin-resistant pathogen for extraintestinal clostridial infection. Clin Microbiol Infect. 2017;23:560–6. https://doi.org/10.1016/j.cmi.2017.02.025
10. Castiglioni B, Gautam A, Citron DM, Pasculle W, Goldstein EJC, Strollo D, et al. *Clostridium innocuum* bacteremia secondary to infected hematoma with gas formation in a kidney transplant recipient. Transpl Infect Dis. 2003;5:199–202. https://doi.org/10.1111/j.1399-3062.2003.00037.x
11. David V, Bozdogan B, Mainardi JL, Legrand R, Gutmann L, Leclercq R. Mechanism of intrinsic resistance to vancomycin in *Clostridium innocuum* NCIB 10674. J Bacteriol. 2004;186:3415–22. https://doi.org/10.1128/JB.186.11.3415-3422.2004
12. Peng Z, Ling L, Stratton CW, Li C, Polage CR, Wu B, et al. Advances in the diagnosis and treatment of *Clostridium difficile* infections. Emerg Microbes Infect. 2018;7:15. https://doi.org/10.1038/s41426-017-0019-4
13. Jewkes J, Larson HE, Price AB, Sanderson PJ, Davies HA. Aetiology of acute diarrhoea in adults. Gut. 1981;22:388–92. https://doi.org/10.1136/gut.22.5.388
14. McDonald LC, Gerding DN, Johnson S, Bakken JS, Carroll KC, Coffin SE, et al. Clinical Practice guidelines for *Clostridium difficile* infection in adults and children: 2017 update by the Infectious Diseases Society of America (IDSA) and Society for Healthcare Epidemiology of America (SHEA). Clin Infect Dis. 2018;66:987–94. https://doi.org/10.1093/cid/ciy149
15. Shannon S, Kronemann D, Patel R, Schuetz AN. Routine use of MALDI-TOF MS for anaerobic bacterial identification in clinical microbiology. Anaerobe. 2018;54:191–6. https://doi.org/10.1016/j.anaerobe.2018.07.001
16. Veloo AC, de Vries ED, Jean-Pierre H, Justesen US, Morris T, Urban E, et al.; ENRIA workgroup. The optimization and validation of the Biotyper MALDI-TOF MS database for the identification of Gram-positive anaerobic cocci. Clin Microbiol Infect. 2016;22:793–8. https://doi.org/10.1016/j.cmi.2016.06.016
17. Li Y, Shan M, Zhu Z, Mao X, Yan M, Chen Y, et al. Application of MALDI-TOF MS to rapid identification of anaerobic bacteria. BMC Infect Dis. 2019;19:941. https://doi.org/10.1186/s12879-019-4584-0
18. Khanna S, Pardi DS, Aronson SL, Kammer PP, Orenstein R, St Sauver JL, et al. The epidemiology of community-acquired *Clostridium difficile* infection: a population-based study. Am J Gastroenterol. 2012;107:89–95. https://doi.org/10.1038/ajg.2011.398
19. Charlson ME, Pompei P, Ales KL, MacKenzie CR. A new method of classifying prognostic comorbidity in longitudinal studies: development and validation. J Chronic Dis. 1987;40:373–83. https://doi.org/10.1016/0021-9681(87)90171-8
20. Pepin J, Alary ME, Valiquette L, Raiche E, Ruel J, Fulop K, et al. Increasing risk of relapse after treatment of *Clostridium difficile* colitis in Quebec, Canada. Clin Infect Dis. 2005;40:1591–7. https://doi.org/10.1086/430315
21. Lee HY, Hsiao HL, Chia CY, Cheng CW, Tsai TC, Deng ST, et al. Risk factors and outcomes of *Clostridium difficile* infection in hospitalized patients. Biomed J. 2019;42:99–106. https://doi.org/10.1016/j.bj.2018.12.002
22. Clinical and Laboratory Standards Institute (CLSI). Performance standards for antimicrobial susceptibility testing: 27th edition (M100–S27). Wayne (PA): The Institute; 2017.
23. Van Daele E, Van de Putte D, Ceelen W, Van Nieuwenhove Y, Pattyn P. Risk factors and consequences of anastomotic leakage after Ivor Lewis oesophagectomy. Interact Cardiovasc Thorac Surg. 2016;22:32–7. https://doi.org/10.1093/icvts/ivv276
24. Finegold SM, Song Y, Liu C, Hecht DW, Summanen P, Könönen E, et al. *Clostridium clostridioforme*: a mixture of three clinically important species. Eur J Clin Microbiol Infect Dis. 2005;24:319–24. https://doi.org/10.1007/s10096-005-1334-6
25. Leal J, Gregson DB, Ross T, Church DL, Laupland KB. Epidemiology of *Clostridium* species bacteremia in Calgary, Canada, 2000–2006. J Infect. 2008;57:198–203. https://doi.org/10.1016/j.jinf.2008.06.018
26. Bodey GP, Rodriguez S, Fainstein V, Elting LS. Clostridial bacteremia in cancer patients. A 12-year experience. Cancer. 1991;67:1928–42. https://doi.org/10.1002/1097-0142(19910401)67:7<1928::AID-CNCR2820670718>3.0.CO;2-9
27. Shah M, Bishburg E, Baran DA, Chan T. Epidemiology and outcomes of clostridial bacteremia at a tertiary-care institution. ScientificWorldJournal. 2009;9:144–8. https://doi.org/10.1100/tsw.2009.21
28. Ha CWY, Martin A, Sepich-Poore GD, Shi B, Wang Y, Gouin K, et al. Translocation of viable gut microbiota to mesenteric adipose drives formation of creeping fat in humans. Cell. 2020;183:666–83. https://doi.org/10.1016/j.cell.2020.09.009
29. Crum-Cianflone N. *Clostridium innocuum* bacteremia in a patient with acquired immunodeficiency syndrome. Am J Med Sci. 2009;337:480–2. https://doi.org/10.1097/MAJ.0b013e31819f1e95

30. Hung YP, Lin HJ, Wu CJ, Chen PL, Lee JC, Liu HC, et al. Vancomycin-resistant *Clostridium innocuum* bacteremia following oral vancomycin for *Clostridium difficile* infection. Anaerobe. 2014;30:24–6. https://doi.org/10.1016/j.anaerobe.2014.07.009
31. Mutoh Y, Hirai R, Tanimura A, Matono T, Morino E, Kutsuna S, et al. Osteomyelitis due to *Clostridium innocuum* in a patient with acute lymphoblastic leukemia: case report and literature review. Springerplus. 2015;4:385. https://doi.org/10.1186/s40064-015-1176-3
32. Aroca-Ferri M, Suárez-Hormiga L, Bosch-Benitez-Parodi E, Bolaños-Rivero M. Peritonitis by *Clostridium innocuum* associated to peritoneal dialysis [in Spanish]. Rev Esp Quimioter. 2019;32:192–3.
33. Morel G, Mulier G, Ghrenassia E, Abdel Nabey M, Tandjaoui Y, Kouatchet A, et al. Non–*C. difficile Clostridioides* bacteremia in intensive care patients, France. Emerg Infect Dis. 2021;27:1840–9. https://doi.org/10.3201/eid2707.203471
34. Cherny KE, Ozer EA, Kochan TJ, Johnson S, Kociolek LK. Complete genome sequence of *Clostridium innocuum* strain LC–LUMC-CI-001, isolated from a patient with recurrent antibiotic-associated diarrhea. Microbiol Resour AnnounC. 2020;9:e00365–20. https://doi.org/10.1128/MRA.00365-20
35. Sánchez-Hurtado K, Poxton IR. Enhancement of the cytotoxic activity of *Clostridium difficile* toxin A by surface-associated antigens. J Med Microbiol. 2008;57:739–44. https://doi.org/10.1099/jmm.0.47678-0

Address for correspondence: Cheng-Hsun Chiu, Chang Gung Children's Hospital—Department of Pediatrics, 5 Fu-Hsin St, Kweishan Taoyuan County 333, Taiwan; email: chchiu@adm.cgmh.org.tw

Plasmodium falciparum pfhrp2 and *pfhrp3* Gene Deletions from Persons with Symptomatic Malaria Infection in Ethiopia, Kenya, Madagascar, and Rwanda

Eric Rogier, Jessica N. McCaffery, Doug Nace, Samaly Souza Svigel, Ashenafi Assefa, Jimee Hwang, Simon Kariuki, Aaron M. Samuels, Nelli Westercamp, Arsène Ratsimbasoa, Milijaona Randrianarivelojosia, Aline Uwimana, Venkatachalam Udhayakumar, Eric S. Halsey

Histidine-rich protein 2 (HRP2)–based rapid diagnostic tests detect *Plasmodium falciparum* malaria and are used throughout sub-Saharan Africa. However, deletions in the *pfhrp2* and related *pfhrp3* (*pfhrp2/3*) genes threaten use of these tests. Therapeutic efficacy studies (TESs) enroll persons with symptomatic *P. falciparum* infection. We screened TES samples collected during 2016–2018 in Ethiopia, Kenya, Rwanda, and Madagascar for HRP2/3, pan-*Plasmodium* lactate dehydrogenase, and pan-*Plasmodium* aldolase antigen levels and selected samples with low levels of HRP2/3 for *pfhrp2/3* genotyping. We observed deletion of *pfhrp3* in samples from all countries except Kenya. Single-gene deletions in *pfhrp2* were observed in 1.4% (95% CI 0.2%–4.8%) of Ethiopia samples and in 0.6% (95% CI 0.2%–1.6%) of Madagascar samples, and dual *pfhrp2/3* deletions were noted in 2.0% (95% CI 0.4%–5.9%) of Ethiopia samples. Although this study was not powered for precise prevalence estimates, evaluating TES samples revealed a low prevalence of *pfhrp2/3* deletions in most sites.

Author affiliations: Centers for Disease Control and Prevention, Atlanta, Georgia, USA (E. Rogier, J.N. McCaffery, D. Nace, S.S. Svigel, A.M. Samuels, N. Westercamp, V. Udhayakumar); Ethiopia Public Health Institute, Addis Ababa, Ethiopia (A. Assefa); Centers for Disease Control and Prevention, Atlanta, Georgia, USA (J. Hwang, E.S. Halsey); Centre for Global Health Research, Kenya Medical Research Institute, Kisumu, Kenya (S. Kariuki); Centers for Disease Control and Prevention, Kisumu (A.M. Samuels); Madagascar National Malaria Control Program, Antananarivo, Madagascar (A. Ratsimbasoa); Institut Pasteur de Madagascar, Antananarivo (M. Randrianarivelojosia); Université de Toliara, Toliara, Madagascar (M. Randrianarivelojosia); Rwanda Biomedical Center, Kigali, Rwanda (A. Uwimana)

DOI: https://doi.org/10.3201/eid2803.211499

The World Health Organization (WHO) estimates there were 228 million cases of malaria in 2019, which resulted in 409,000 deaths; >90% of these deaths occurred in sub-Saharan Africa (*1*). Although all 4 human malaria *Plasmodium* species are present in Africa, *Plasmodium falciparum* accounts for most symptomatic infections (*1*). After the WHO recommended confirming *Plasmodium* infection before initiating treatment (*2*), malaria rapid diagnostic tests (RDTs) have been widely deployed because of their ease of use and high diagnostic sensitivity for symptomatic infection (*3*–*5*). The histidine-rich protein 2 (HRP2) antigen is produced exclusively by *P. falciparum* parasites, and RDTs detecting this antigen provide a practical tool for diagnosis in both healthcare and community settings (*1*,*3*,*6*) and have revolutionized the diagnosis of malaria throughout Africa.

HRP2-based RDTs are an accurate diagnostic tool because HRP2 is abundantly expressed during the erythrocytic stage of *P. falciparum* infection (*6*). The *pfhrp3* gene is paralogous to *pfhrp2* and has a high level of similarity in both gene sequence and the expressed histidine-rich protein 3 (HRP3) antigen, although the HRP3 antigen is substantially shorter in length (*7*,*8*). However, because of common epitopes on both antigens, they jointly contribute to an overall HRP2-based RDT positive result or laboratory assay signal (*6*,*9*). In many areas of the world, *P. falciparum* variants have been identified with loss-of-function mutations or complete deletions of the *pfhrp2* and *pfhrp3* (*pfhrp2/3*) genes, which lead to false-negative RDT results (*6*,*10*). Multiple countries in sub-Saharan Africa have reported the presence of *P. falciparum* with deletions in these genes (*9*,*11*–*16*), although only Eritrea and Djibouti

have reported a prevalence of >5% among isolates from symptomatic infections (*17*,*18*).

WHO recommends routine therapeutic efficacy studies (TESs) approximately every 2 years in malaria-endemic countries to assess antimalarial drug efficacy, and US President's Malaria Initiative funding ensures these studies routinely occur in many countries throughout sub-Saharan Africa (*19*). According to established WHO protocol (*20*), symptomatic patients with uncomplicated *P. falciparum* malaria are enrolled in healthcare facilities after infection is verified by light microscopy examination of a blood smear. In addition, on the day of enrollment and subsequent follow-up days, a blood sample from a finger prick is dried on filter paper to form a dried blood spot (DBS) to monitor chemotherapeutic efficacy and test for putative drug resistance genetic markers (*19*). TESs are often implemented at multiple sites in a country because efficacy might vary depending on local endemicity, *P. falciparum* haplotypes, and antimalarial use.

We investigated deletions in *pfhrp2/3* genes by using samples from TESs in Ethiopia (2017), Kenya (2016–2017), Madagascar (2018), and Rwanda (2018). DBS samples from day of enrollment were subjected to multiplex antigen detection and subsequent PCR assays if *pfhrp2/3* genotyping was warranted on the basis of the antigen profile.

Materials and Methods

Therapeutic Efficacy Studies

This study focuses on TESs in 4 countries: Ethiopia (enrollment during September–December 2017) (*21*), Kenya (enrollment during June 2016–March 2017) (*22*), Madagascar (enrollment during May–September 2018) (*23*), and Rwanda (enrollment during May–December 2018) (*24*). Specific site information and enrollment criteria are provided for each TES by the indicated reference. Of note, enrollment criteria in the Madagascar TES included a positive HRP2-based RDT result. CDC human subjects review for laboratory analyses for all TES samples were determined independently for each study: Ethiopia as engaged research (#6892.0), Rwanda as program evaluation (#2018-060), Madagascar as nonengaged research (#2018-435), and Kenya as engaged research (#6696.0).

Bead-Based Multiplex Assay for Malaria Antigen Detection

All DBS samples were processed and analyzed within 1 year of creation. We performed elution of whole blood from DBS samples and the bead-based multiplex assay for malaria antigen detection as described previously (*25*) (Appendix, https://wwwnc.cdc.gov/EID/article/28/3/21-1499-App1.pdf). Differences among parasite densities or antigen levels were assessed by Student t test for unequal variances using the log-transformed data.

Selection of Samples for Further Genetic Assays

Using the strategy reported previously (*26*,*27*), we selected samples for further genetic assays on the basis of the relationship between the 2 pan-*Plasmodium* antigens (aldolase and lactate dehydrogenase [LDH]) and the HRP2/3 signal. Samples were selected if they completely lacked an assay signal for HRP2/3 or if the assay signal for HRP2/3 was atypically lower compared with the level of pAldolase or pLDH antigens.

We extracted total genomic DNA from 6-mm punches of selected DBS samples by using the QIAGEN DNA extraction kit (QIAGEN, https://www.qiagen.com) following the manufacturer's instructions for blood dried on filter paper. The DNA was eluted in 150 μL of elution buffer, aliquoted, and stored at −20°C until further use.

Photo-Induced Electron Transfer PCR and Genotyping for *pfmsp1*, *pfmsp2*, *pfhrp2*, *and pfhrp3*

After DNA extraction, we performed photo-induced electron transfer PCR as described previously (*28*) to ensure presence of *P. falciparum* DNA. We used nested PCR to genotype *pfmsp1, pfmsp2,* and *pfhrp3* as described previously (*29*). For *pfhrp2* genotyping, we performed PCR on these samples under conditions described previously (*30*). Results for *pfhrp2/3* genotyping were only reported if both *pfmsp1* and *pfmsp2* (both single-copy genes in the *P. falciparum* genome) were successfully amplified for a DNA sample (*31*).

Results

The Kenya 2016–2017 TES had the fewest number of sites at 1, followed by the Ethiopia 2017 TES at 2, the Rwanda 2018 TES at 3, and the Madagascar 2018 TES at 5 (Figure 1). The number of participants providing DBS samples from each site at enrollment varied for each of the 4 countries and ranged from a low of 15 participants at the Arba Minch, Ethiopia, site to a high of 332 participants at the Siaya, Kenya, site (Table 1). Reflecting the different enrollment criteria for each TES, the median and range of participant ages were unique to each TES; median age was 18.0 years in Ethiopia, 2.7 years in Kenya, 7.0 years in Madagascar, and 3.3 years in Rwanda. Enrollment by sex was mostly equal for the Kenya, Madagascar, and Rwanda

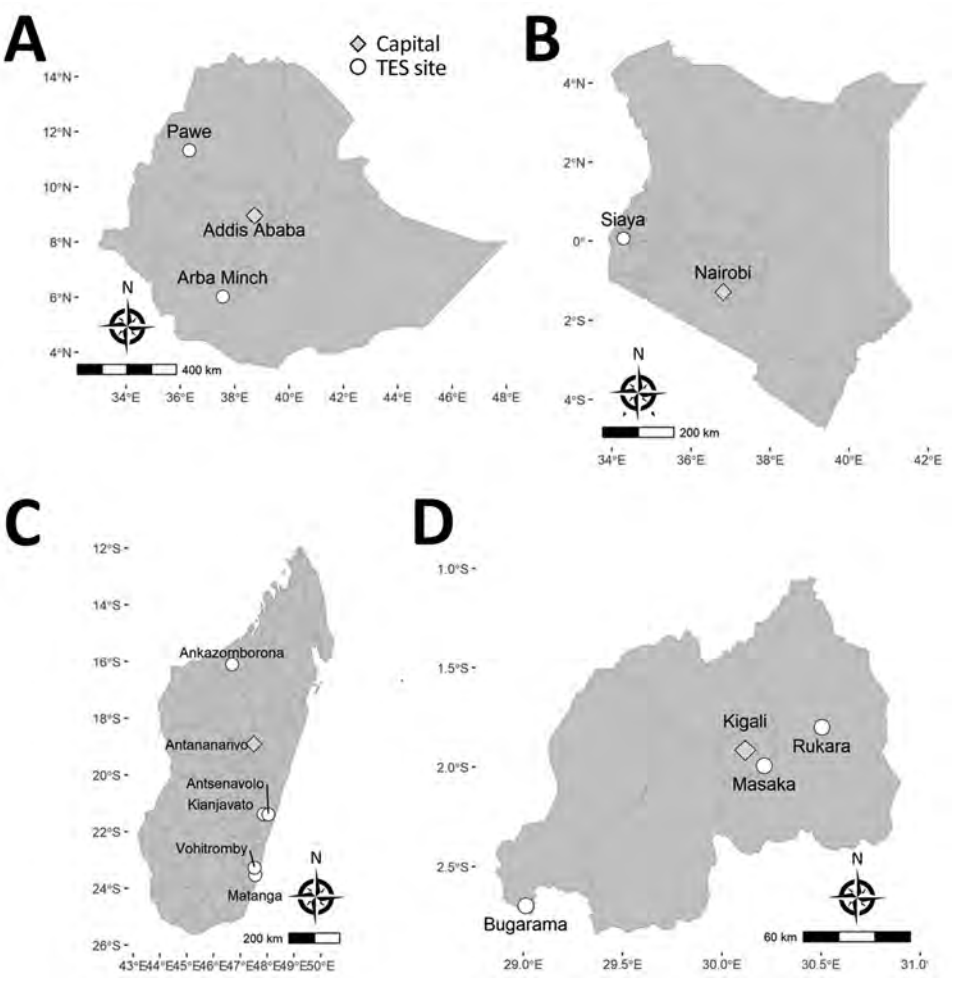

Figure 1. Location of TES sites where *Plasmodium falciparum* malaria-infected participants were enrolled, Ethiopia, Kenya, Madagascar, and Rwanda, 2016–2018. A) Ethiopia, B) Kenya, C) Madagascar, D) Rwanda. Circles indciate study sites and diamonds the country capitals. Scale bars are unique to each map. TES, therapeutic efficacy study.

TESs; 48.8% (Kenya), 47.1% (Madagascar), and 50.9% (Rwanda) of participants providing DBS samples in these studies were women. Enrollment of women in the Ethiopia TES was notably lower at 32.9%.

The antigen screening methodology provided phenotypic rationale for categorizing the infecting *P. falciparum* as a high producer of HRP2/3 antigens or a HRP2/3 low-producer requiring subsequent characterization though genetic assays (*25*,*26*). Correlation of antigen assay signal with parasite density (as determined by microscopy during enrollment for each TES) (Appendix Figure 1) showed that the 2 pan-*Plasmodium* antigens displayed a moderate correlation with microscopy-estimated *P. falciparum* parasite density, whereas the HRP2 antigen showed higher variability, as seen previously (*25*). We compared the pAldolase and pLDH assay signal to the HRP2 assay signal for all samples from each of the 4 countries and chose select samples for DNA extraction (Table 2; Appendix Figures 2–5). Ethiopia had the highest percentage (n = 21, 14.3% of all DBS samples) of samples selected for DNA extraction and PCR genotyping, followed by Rwanda (n = 16, 7.3%), Madagascar (n = 25, 4.0%), and Kenya (n = 7, 2.1%).

After initial sample selection for genotyping, we evaluated DNA quantity and quality appropriate for genotyping by amplification of both *pfmsp1* and *pfmsp2* genes. Final *pfhrp2/3* genotyping results were evaluated for amplification of (+) or failure to amplify (–) these 2 different gene targets (Figure 2). Only samples from which both the single-copy *pfmsp1* and *pfmsp2* genes were successfully amplified had *pfhrp2/3* genotype reported (*31*); from all selected samples, only 1 sample from Ethiopia and 4 samples from Rwanda were unsuccessfully amplified for these control genes. Most selected samples (76.6%) showed a wild-type genotype of *pfhrp2*+/*pfhrp3*+. Single gene deletions were observed in samples from 3 countries: single gene *pfhrp2* deletions from Ethiopia and Madagascar, and single gene *pfhrp3* deletions from Ethiopia, Madagascar, and Rwanda (Table 3). The *pfhrp2*–/*pfhrp3*– double deletion genotype was observed only

in Ethiopia; 3 of the 20 samples selected, all from the Pawe site, showed this genotype. Because the *pfhrp3* nested PCR includes a reaction for an exon 1-to-2 spanning primer and a separate reaction for an exon 2 primer, a nested PCR reaction could have amplified one of these targets and not the other if the gene was not fully deleted from the genome. For 9 samples classified as negative for the *pfhrp3* gene, both of these nested PCR targets failed to amplify in all, with the exception of a single sample from Ethiopia (exon 1–2 target did not amplify and exon 2 target did; the sample was positive for the *pfhrp2* gene).

In an exploratory analysis of the 64 samples that were successfully genotyped, different *pfhrp2/3* genotype combinations showed significant differences in microscopy-estimated parasite densities (Figure 3, panel A). In comparison to wild-type parasites, significantly lower parasite densities were observed in infections with *P. falciparum* lacking the *pfhrp3* gene alone. Parasites lacking the *pfhrp2* gene alone showed significantly higher mean parasite densities when compared with the *pfhrp3* single-deleted infections. To link the phenotypic data of antigen expression with the *pfhrp2/3* genotypic data, we plotted the antigen detection assay signal by genotype for the 64 total samples that underwent successful genotyping. Assay signals for pan-*Plasmodium* aldolase, pan-*Plasmodium* LDH, and HRP2/3 by the 4 potential combinations of *pfhrp2/3* genotypes are given (Figure 3, panel B). With loss of either of the *pfhrp2* or *pfhrp3* genes and loss of both, no overall trend was observed for changes in pAldolase or pLDH signal, although the numbers of each of these genotypes were small. However, we observed a lower HRP2/3 assay signal with either the loss of the *pfhrp3* gene or the *pfhrp2* gene; the lowest mean HRP2/3 assay signal occurred when both genes were absent.

Table 1. Countries and study sites for each therapeutic efficacy study enrolling *Plasmodium falciparum* malaria–infected participants, 2016–2018

Country and study site	No. specimens at enrollment	Median age (range), y	Sex, % F
Ethiopia	147	18.0 (1–65)	32.9
Arba Minch	15	19.5 (10–54)	50.0
Pawe	132	18.0 (1–65)	31.3
Kenya			
Siaya	332	2.7 (0.5–4.9)	48.8
Madagascar	620	7.0 (0.2–15)	47.1
Ankazomborona	168	8.3 (1.5–15)	41.7
Antsenavolo	54	6.0 (0.2–14)	53.7
Kianjavato	116	9.0 (0.3–15)	46.6
Matanga	172	5.0 (0.3–15)	48.3
Vohitromby	110	7.0 (1–15)	50.9
Rwanda	218	3.3 (0.7–4.8)	50.9
Bugarama	88	3.3 (0.8–4.8)	52.3
Masaka	42	3.3 (0.8–4.0)	54.8
Rukara	88	3.1 (0.7–4.8)	46.6

Discussion

Deletion of the *pfhrp2* and *pfhrp3* genes poses a threat to the accuracy of HRP2-based RDT diagnosis of *P. falciparum* malaria, and parasites with deletions in one or both these genes have now been found in numerous countries (*6*,*10*). By far, most malaria cases in Africa are caused by *P. falciparum*, and the presence of these deletion genotypes in many countries throughout the continent poses an additional challenge to malaria control because of false-negative diagnostic results (*1*). Most countries in Africa have adopted the HRP2-based RDT as a pragmatic and sensitive diagnostic tool and the only *P. falciparum*-specific diagnostic test available in many settings. Loss of this tool would be a substantial setback to accurate monitoring of malaria case incidence within a country and to achieving the goal of universal confirmation of malaria infection before administrating antimalarials (*3*).

In this study, we sought to identify the presence of deletions in either the *pfhrp2* or *pfhrp3* genes from

Table 2. *Plasmodium falciparum* malaria–infected participant DBS samples with atypical HRP2 levels selected for further genomic assays, Ethiopia, Kenya, Madagascar, and Rwanda*

Country and study site	No. specimens at enrollment	No. specimens selected for genetic assays (%)	No. selected on pAldolase ratio only	No. selected on pLDH ratio only	No. selected on ratio to both
Ethiopia	147	21 (14.3)	4	7	10
Arba Minch	15	2 (13.3)	1	1	0
Pawe	132	19 (14.4)	3	6	10
Kenya					
Siaya	332	7 (2.1)	1	1	5
Madagascar	620	25 (4.0)	7	10	8
Ankazomborona	168	11 (6.5)	4	2	5
Antsenavolo	54	6 (11.1)	2	4	0
Kianjavato	116	1 (0.9)	0	1	0
Matanga	172	3 (1.7)	0	2	1
Vohitromby	110	4 (3.6)	1	1	2
Rwanda	218	16 (7.3)	5	6	5
Bugarama	88	9 (10.2)	2	4	3
Masaka	42	2 (4.8)	0	1	1
Rukara	88	5 (5.6)	3	1	1

*DBS, dried blood spot; HRP2, histidine-rich protein 2; pAldolase, pan-*Plasmodium* aldolase; pLDH, pan-*Plasmodium* lactate dehydrogenase.

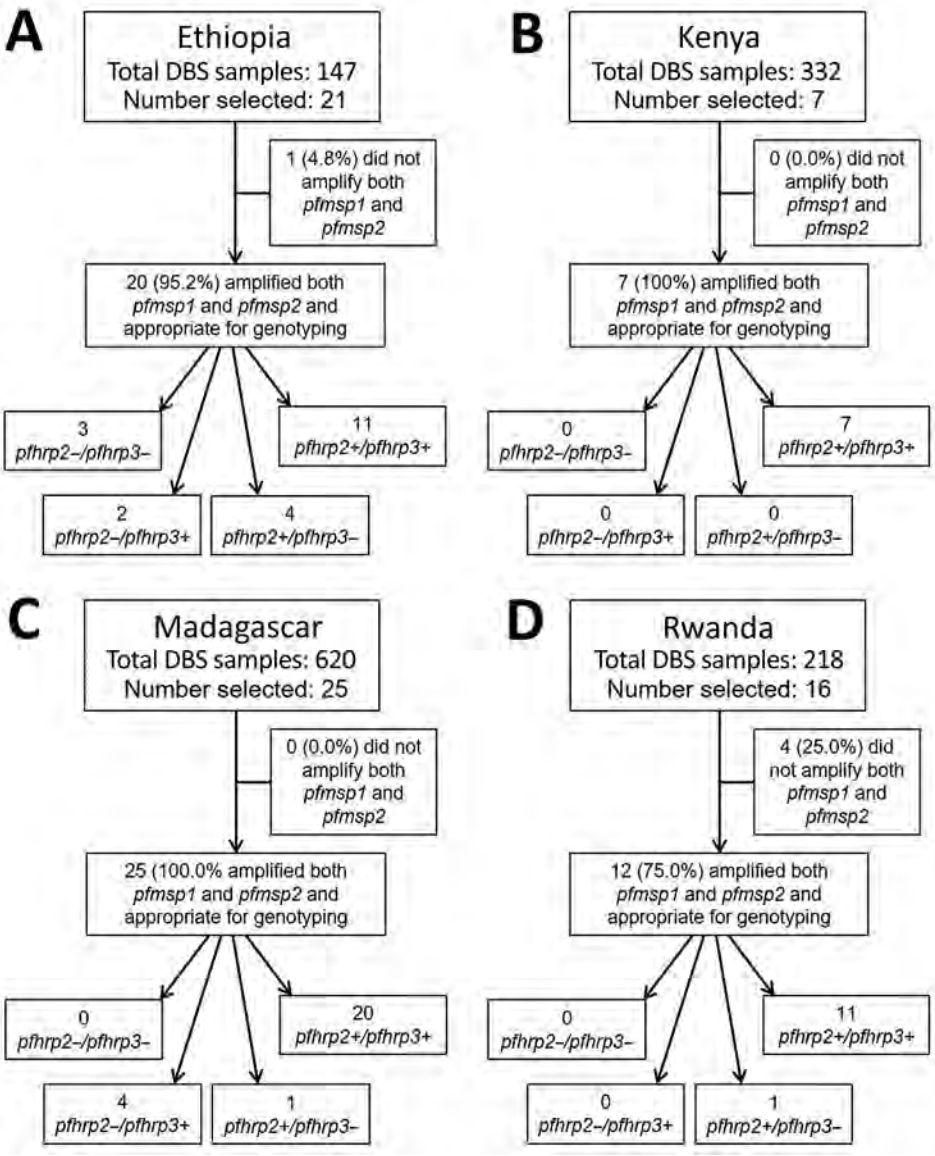

Figure 2. Results for *pfhrp2* and *pfhrp3* genotyping for DBSs from *Plasmodium falciparum* malaria-infected participants, Ethopia, Kenya, Madagascar, and Rwanda, 2016–2018. A) Ethiopia, B) Kenya, C) Madagascar, D) Rwanda. Each flowchart outlines how many specimens were selected for genotyping, how many were appropriate for genotyping (by amplification of both *pfmsp1* and *pfmsp2*), and genotyping results for presence (+) or absence (–) of the *pfhrp2* and *pfhrp3* genes. DBS, dried blood sample.

samples collected during routine TESs that enroll participants with microscopically confirmed *P. falciparum* infection. The primary objective of a TES is to assess in vivo efficacy of antimalarials, and some studies have also investigated the presence of *P. falciparum* drug resistance genetic markers (*19*). Because DBS samples are collected for many of these TESs, residual patient samples represent a convenience sampling of known *P. falciparum* infections with estimated parasite densities, and enrollment at healthcare facilities conforms to the WHO *pfhrp2* deletion guidance to sample symptomatic patients (*32*). Quantitative detection of malaria antigens in these DBS samples not only enables the confirmation of the presence or absence of HRP2, HRP3, or both in the patient's blood sample, it also enables the simultaneous detection of other *Plasmodium* antigens for comparison. For these 4 TESs, a total of 1,317 DBS samples were available, and performing genetic characterization for all these samples would have required a large time and financial commitment. However, by initially employing a low-cost, high-throughput antigen screening step, fewer samples can be carefully selected for more definitive investigation into production of these RDT targets (*25*–*27*). This strategy of phenotypic screening and genetic confirmation is not unique for the TES sampling design and has also been used for healthcare facility (*25*,*27*) and community (*26*) surveys. Further exploration of this strategy with large datasets is needed throughout global *P. falciparum* populations to determine the overall accuracy of this

methodology and its ability to generalize antigen levels with deletions of *pfhrp2* and *pfhrp3*.

Many TESs seek to enroll participants at multiple sites throughout a country to gain a more geographically representative sampling of *P. falciparum* for in vivo efficacy estimates. Of the data presented in this study, 3 of the 4 countries had multiple enrollment sites; only Kenya enrolled persons from just 1 site. Ultimately, high global variation has been observed in *pfhrp2* gene sequences (*7*,*33*,*34*), and deletions in the *pfhrp2* and *pfhrp3* genes can arise de novo in a *P. falciparum* population (*18*,*35*). Therefore, presence (or absence) of these gene deletions could not be accurately ascertained for an entire country by sampling a limited number of sites. Recent WHO guidance recommended enrolling from ≥10 health facilities per province to estimate whether *pfhrp2* deletions exceed 5% of all *P. falciparum* infections for a country (*32*). Because TESs do not enroll at many study sites, the data presented in this study do not provide country-representative or even precise local estimates of gene deletion prevalence, but they generate a data signal to point toward the presence of deletions at a site of a previous TES. Troublesome data signals generated from TES samples could be followed up with a more thorough study, such as the WHO-recommended approach of enrolling from a minimum of 10 health facilities per province to estimate whether *pfhrp2* deletions exceed 5% of all *P. falciparum* infections for a country. A benefit of this sampling design is that TESs are routinely performed in countries that receive support from the US President's Malaria Initiativeevery 2–3 years (*19*); consistently collecting quantitative antigen data from these sample sets will provide a longitudinal approach to better identify emerging deletion genotypes in a country.

Samples with an absence of both the *pfhrp2* and *pfhrp3* are of greatest concern because these 2 genes express the only antigen targets recognized by an HRP2-based RDT. For the 69 samples selected for genotyping on the basis of antigen profile, only 3 double-deletions were noted, all arising from the Pawe study site in the Benishangul-Gumuz region in northeastern Ethiopia. As an external evaluation activity, persons enrolling in the Ethiopia TES were also tested by HRP2-based RDTs, and of the 3 persons with double-deleted *P. falciparum* infections, 2 tested negative by the HRP2 band on the RDT. These same 2 persons had a complete absence of HRP2/3 antigens by the bead-based assay, whereas the third double-deleted infection had an HRP2/3 antigen concentration in blood of 27.5 ng/mL. An additional 2 samples from Pawe were also found to be deleted for the *pfhrp2* gene alone (both of these persons were HRP2-RDT positive), meaning of the 132 total *P. falciparum* isolates available from Pawe, 3.8% (95% CI 1.2%–8.6%) showed a deletion of the *pfhrp2* gene. Multiple recent reports have uncovered the presence of *pfhrp2/3* deletions in central (*36*) and northern (*37*,*38*) Ethiopia at levels above the 5% WHO recommendation to reevaluate national RDT selection (*32*). The data presented in this study do not attempt to provide a prevalence estimate of single- or double-deletion *P. falciparum* genotypes in Ethiopia, but they add to the growing evidence of the pervasiveness of these parasites lacking *pfhrp2* in the country by demonstrating their presence in 2017.

Deletions in *pfhrp2* were also observed in samples from Madagascar, a country with numerous haplotypes circulating according to previous studies (*39*,*40*). Even with the identification of *pfhrp2* deletions in Madagascar, these cases represent a very

Table 3. Deletion genotypes by individual therapeutic efficacy study sites, Ethiopia, Kenya, Madagascar, and Rwanda

Country and study site	No. specimens at enrollment*	No. (%) specimens detected with *pfhrp2–/pfhrp3–*	No. (%) specimens detected with *pfhrp2–/pfhrp3+*	No. (%) specimens detected with *pfhrp2+/pfhrp3–*
Ethiopia				
Arba Minch	15	0	0	2 (13.3)
Pawe	132	3 (2.3)	2 (1.5)	2 (1.5)
Kenya				
Siaya	332	0	0	0
Madagascar				
Ankazomborona	168	0	3 (1.8)	1 (0.6)
Antsenavolo	54	0	0	0
Kianjavato	116	0	0	0
Matanga	172	0	0	0
Vohitromby	110	0	1 (0.9)	0
Rwanda				
Bugarama	88	0	0	1 (1.1)
Masaka	42	0	0	0
Rukara	88	0	0	0

*Percentages may underestimate the actual amount of deleted parasites because not all samples were genotyped, rather only those found to initially have depressed histidine-rich protein 2 levels. All samples with high histidine-rich protein 2 signal assumed to be from wild-type infections.

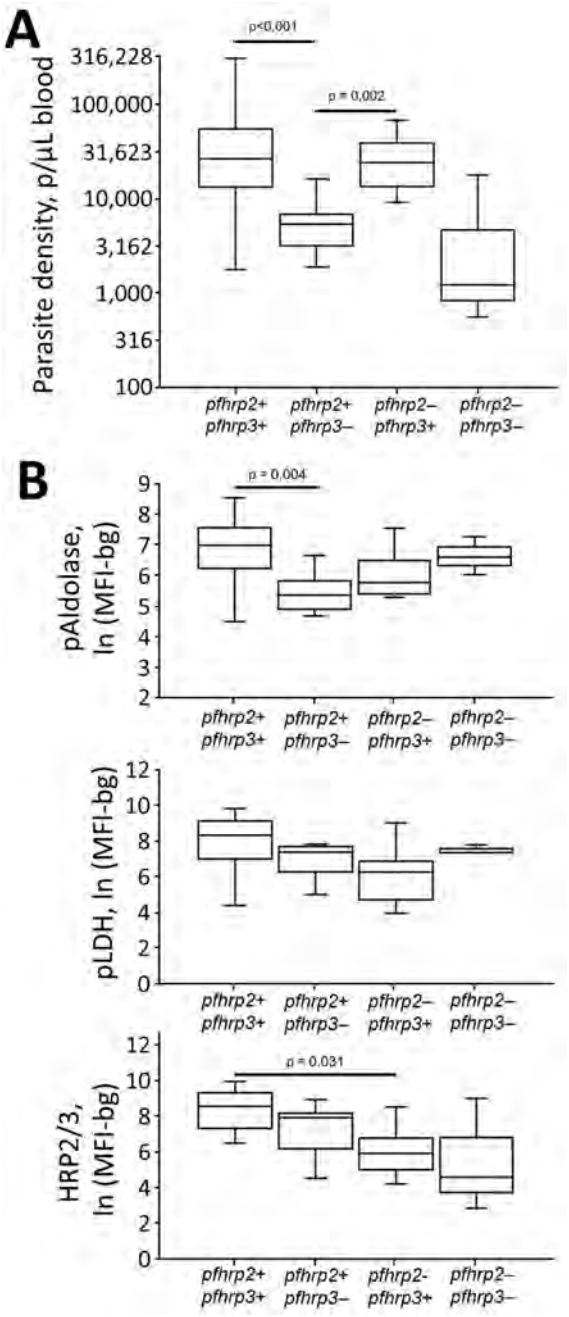

Figure 3. *Plasmodium falciparum* parasite density and antigen levels by *pfhrp2/3* genotype in study of *Plasmodium falciparum* malaria-infected participants, Ethopia, Kenya, Madagascar, and Rwanda, 2016–2018. A) Peripheral blood parasite density as determined by light microscopy. B) Log-transformed assay signal to pAldolase, pLDH, and HRP2/3 antigens. Boxes display interquartile range, horizontal lines within boxes indicate medians, and whiskers indicate 1.5× interquartile range. Significant differences in means are indicated with corresponding p values. Within each plot, all other differences among genotypes did not reach statistical significance at α = 0.05. HRP2/3, histidine-rich protein 2/3; ln (MFI-bg), log-transformed median fluorescence intensity minus background value; pAldolase, pan-*Plasmodium* aldolase; pLDH, pan-*Plasmodium* lactate dehydrogenase.

small proportion (4 of 620, 0.6%) of all *P. falciparum*–infected children providing DBS samples for this study. Three of the 4 *pfhrp2*-deleted samples came from the Ankazomborona study site in the northern part of the country, which could provide rationale for further investigation of deletions in this part of Madagascar. Of note, the Madagascar TES had enrollment criteria of positivity to both microscopy and HRP2-based RDT. Because infections in persons with double-deleted parasites would likely have been excluded from enrollment, these data should be taken in that context.

Separate investigations have (*9*) and have not (*7*) detected *pfhrp2* and *pfhrp3* deletions in Kenya. From the 332 DBS samples available from the 2016–2017 Kenya TES, most *P. falciparum* infections produced high amounts of HRP2/3 antigens, and no phenotypic or genotypic evidence was seen for gene deletions of these targets. A single report from Rwanda also identified nonamplification of the *pfhrp2* gene from microscopically positive *P. falciparum* infections, although the primers were only targeting the exon 2 of the gene (*13*), which is not crucial for antigen expression. In this study, no deletions of the *pfhrp2* gene were identified in Rwanda, and only 1 *P. falciparum* isolate was found with a *pfhrp3* deletion.

Existence of HRP2/3 antigens in a blood sample does not necessarily indicate that the currently infecting *P. falciparum* parasite possesses functioning *pfhrp2/3* genes. The bead assay limit of detection is ≈10 pg/mL, and HRP2 antigen can remain in blood for months after successful treatment of a *P. falciparum* infection (*6*,*41*). A person could therefore be actively infected with a deleted strain but have HRP2 antigen in their blood from a previous infection (although the levels would be expected to be atypically low in this scenario). Because of the phenotypic selection criteria outlined in this study, infections with high levels of HRP2/3 would not be selected for genotyping but might still harbor parasites with deletions of the *pfhrp2/3* genes and would not be captured, although this possibility is likely low. If deleted parasites were more likely to induce asymptomatic or less symptomatic infections, this enrollment criteria in healthcare facilities would lead to underestimating actual deletion prevalence in a population, although data have not demonstrated this effect. Simultaneous infection with multiple *P. falciparum* haplotypes was also not investigated in this study, so the presence of deleted parasites could be masked by the presence of wild-type parasites in the same host (*42*). These 2 scenarios would be more probable in a higher-transmission setting,

where the likelihood for residual HRP2/3, as well as higher multiplicity of infection and more frequent infections, would be more common. In addition, the genetic assays used in this study attempted to simply amplify a region of DNA and do not provide information regarding potential loss-of-function point mutations or other genetic scenarios which would cause these 2 antigens not to be expressed. Because antigen degradation might occur in DBS samples over time, quantitative antigen detection should occur as soon as possible.

In conclusion, with appropriate patient consent, screening samples that were previously collected for routine TESs for *pfhrp2* and *pfhrp3* deletions represent a useful convenience sampling of persons with symptomatic and microscopically confirmed *P. falciparum* infection. These phenotypic and genotypic data provide information for a country to evaluate whether these genotypes exist and promote a basis for more targeted future surveys to obtain precise point estimates of prevalence.

Acknowledgments

We thank Veronika Laird for her help with creating the maps in Figure 1.

This study was funded by the US President's Malaria Initiative. J.H., J.M., S.S.S., and E.S.H. receive salary support from the US President's Malaria Initiative.

The findings and conclusions in this report are those of the author(s) and do not necessarily represent the official position of the Centers for Disease Control and Prevention or US President's Malaria Initiative. The manuscript was published with the permission of the Director, KEMRI.

About the Author

Dr. Rogier is a microbiologist in the Malaria Branch, Division of Parasitic Diseases and Malaria, Center for Global Health, Centers for Disease Control and Prevention. His current research interests focus on multiplex IgG and antigen detection assays for malaria surveillance purposes and integrated disease serosurveys.

References

1. World Health Organization. World malaria report 2020. Geneva: The Organization; 2020.
2. World Health Organization. Guidelines for the treatment of malaria: 2nd edition. Geneva: The Organization; 2010.
3. World Health Organization. Universal access to malaria diagnostic testing: an operational manual. Geneva: The Organization; 2011.
4. Harvey SA, Bell D. How to use a rapid diagnostic test (Generic Pf): a guide for training at the village and clinic level. Geneva: World Health Organization; 2008.
5. Plucinski M, Dimbu R, Candrinho B, Colborn J, Badiane A, Ndiaye D, et al. Malaria surveys using rapid diagnostic tests and validation of results using post hoc quantification of *Plasmodium falciparum* histidine-rich protein 2. Malar J. 2017;16:451. https://doi.org/10.1186/s12936-017-2101-8
6. Poti KE, Sullivan DJ, Dondorp AM, Woodrow CJ. HRP2: transforming malaria diagnosis, but with caveats. Trends Parasitol. 2020;36:112–26. https://doi.org/10.1016/j.pt.2019.12.004
7. Nderu D, Kimani F, Thiong'o K, Karanja E, Akinyi M, Too E, et al. *Plasmodium falciparum* histidine-rich protein (PfHRP2 and 3) diversity in Western and Coastal Kenya. Sci Rep. 2019;9:1709. https://doi.org/10.1038/s41598-018-38175-1
8. Fontecha G, Pinto A, Escobar D, Matamoros G, Ortiz B. Genetic variability of *Plasmodium falciparum* histidine-rich proteins 2 and 3 in Central America. Malar J. 2019;18:31. https://doi.org/10.1186/s12936-019-2668-3
9. Beshir KB, Sepúlveda N, Bharmal J, Robinson A, Mwanguzi J, Busula AO, et al. *Plasmodium falciparum parasites* with histidine-rich protein 2 (*pfhrp2*) and *pfhrp3* gene deletions in two endemic regions of Kenya. Sci Rep. 2017;7:14718. https://doi.org/10.1038/s41598-017-15031-2
10. Thomson R, Parr JB, Cheng Q, Chenet S, Perkins M, Cunningham J. Prevalence of *Plasmodium falciparum* lacking histidine-rich proteins 2 and 3: a systematic review. Bull World Health Organ. 2020;98:558–568F. https://doi.org/10.2471/BLT.20.250621
11. Koita OA, Doumbo OK, Ouattara A, Tall LK, Konaré A, Diakité M, et al. False-negative rapid diagnostic tests for malaria and deletion of the histidine-rich repeat region of the hrp2 gene. Am J Trop Med Hyg. 2012;86:194–8. https://doi.org/10.4269/ajtmh.2012.10-0665
12. Wurtz N, Fall B, Bui K, Pascual A, Fall M, Camara C, et al. *Pfhrp2* and *pfhrp3* polymorphisms in *Plasmodium falciparum* isolates from Dakar, Senegal: impact on rapid malaria diagnostic tests. Malar J. 2013;12:34. https://doi.org/10.1186/1475-2875-12-34
13. Kozycki CT, Umulisa N, Rulisa S, Mwikarago EI, Musabyimana JP, Habimana JP, et al. False-negative malaria rapid diagnostic tests in Rwanda: impact of *Plasmodium falciparum* isolates lacking *hrp2* and declining malaria transmission. Malar J. 2017;16:123. https://doi.org/10.1186/s12936-017-1768-1
14. Funwei R, Nderu D, Nguetse CN, Thomas BN, Falade CO, Velavan TP, et al. Molecular surveillance of *pfhrp2* and *pfhrp3* genes deletion in *Plasmodium falciparum* isolates and the implications for rapid diagnostic tests in Nigeria. Acta Trop. 2019;196:121–5. https://doi.org/10.1016/j.actatropica.2019.05.016
15. Parr JB, Verity R, Doctor SM, Janko M, Carey-Ewend K, Turman BJ, et al. *Pfhrp2*-deleted *Plasmodium falciparum* parasites in the Democratic Republic of the Congo: a national cross-sectional survey. J Infect Dis. 2017;216:36–44.
16. Thomson R, Beshir KB, Cunningham J, Baiden F, Bharmal J, Bruxvoort KJ, et al. *pfhrp2* and *pfhrp3* gene deletions that affect malaria rapid diagnostic tests for *Plasmodium falciparum*: analysis of archived blood samples from 3 African countries. J Infect Dis. 2019;220:1444–52. https://doi.org/10.1093/infdis/jiz335
17. Iriart X, Menard S, Chauvin P, Mohamed HS, Charpentier E, Mohamed MA, et al. Misdiagnosis of imported *falciparum* malaria from African areas due to an increased prevalence of *pfhrp2/pfhrp3* gene deletion: the Djibouti case. Emerg Microbes Infect. 2020;9:1984–7. https://doi.org/10.1080/22221751.2020.1815590

18. Berhane A, Anderson K, Mihreteab S, Gresty K, Rogier E, Mohamed S, et al. Major threat to malaria control programs by *Plasmodium falciparum* lacking histidine-rich protein 2, Eritrea. Emerg Infect Dis. 2018;24:462–70. https://doi.org/10.3201/eid2403.171723
19. Halsey ES, Venkatesan M, Plucinski MM, Talundzic E, Lucchi NW, Zhou Z, et al. Capacity development through the US President's Malaria Initiative–supported Antimalarial Resistance Monitoring in Africa Network. Emerg Infect Dis. 2017;23:23. https://doi.org/10.3201/eid2313.170366
20. World Health Organization. Methods for surveillance of antimalarial drug efficacy. Geneva: The Organization; 2009.
21. Leonard CM, Mohammed H, Tadesse M, McCaffery JN, Nace D, Halsey ES, et al. Missed *Plasmodium falciparum* and *Plasmodium vivax* mixed infections in Ethiopia threaten malaria elimination. Am J Top Med Hyg. 2021 Nov 30 [Epub ahead of print].
22. Chebore W, Zhou Z, Westercamp N, Otieno K, Shi YP, Sergent SB, et al. Assessment of molecular markers of anti-malarial drug resistance among children participating in a therapeutic efficacy study in western Kenya. Malar J. 2020;19:291. https://doi.org/10.1186/s12936-020-03358-7
23. Dentinger CM, Rakotomanga TA, Rakotondrandriana A, Rakotoarisoa A, Rason MA, Moriarty LF, et al. Efficacy of artesunate-amodiaquine and artemether-lumefantrine for uncomplicated *Plasmodium falciparum* malaria in Madagascar, 2018. Malar J. 2021;20:432. https://doi.org/10.1186/s12936-021-03935-4
24. Uwimana A, Umulisa N, Venkatesan M, Svigel SS, Zhou Z, Munyaneza T, et al. Association of *Plasmodium falciparum kelch13* R561H genotypes with delayed parasite clearance in Rwanda: an open-label, single-arm, multicentre, therapeutic efficacy study. Lancet Infect Dis. 2021;21:1120–8. https://doi.org/10.1016/S1473-3099(21)00142-0
25. Plucinski MM, Herman C, Jones S, Dimbu R, Fortes F, Ljolje D, et al. Screening for *Pfhrp2/3*-deleted *Plasmodium falciparum*, non-*falciparum*, and low-density malaria infections by a multiplex antigen assay. J Infect Dis. 2019;219:437–47. https://doi.org/10.1093/infdis/jiy525
26. Bakari C, Jones S, Subramaniam G, Mandara CI, Chiduo MG, Rumisha S, et al. Community-based surveys for *Plasmodium falciparum pfhrp2* and *pfhrp3* gene deletions in selected regions of mainland Tanzania. Malar J. 2020;19:391. https://doi.org/10.1186/s12936-020-03459-3
27. Herman C, Huber CS, Jones S, Steinhardt L, Plucinski MM, Lemoine JF, et al. Multiplex malaria antigen detection by bead-based assay and molecular confirmation by PCR shows no evidence of *Pfhrp2* and *Pfhrp3* deletion in Haiti. Malar J. 2019;18:380. https://doi.org/10.1186/s12936-019-3010-9
28. Lucchi NW, Narayanan J, Karell MA, Xayavong M, Kariuki S, DaSilva AJ, et al. Molecular diagnosis of malaria by photo-induced electron transfer fluorogenic primers: PET-PCR. PLoS One. 2013;8:e56677. https://doi.org/10.1371/journal.pone.0056677
29. Abdallah JF, Okoth SA, Fontecha GA, Torres RE, Banegas EI, Matute ML, et al. Prevalence of *pfhrp2* and *pfhrp3* gene deletions in Puerto Lempira, Honduras. Malar J. 2015;14:19. https://doi.org/10.1186/s12936-014-0537-7
30. Jones S, Subramaniam G, Plucinski MM, Patel D, Padilla J, Aidoo M, et al. One-step PCR: a novel protocol for determination of *pfhrp2* deletion status in *Plasmodium falciparum*. PLoS One. 2020;15:e0236369. https://doi.org/10.1371/journal.pone.0236369
31. Cheng Q, Gatton ML, Barnwell J, Chiodini P, McCarthy J, Bell D, et al. *Plasmodium falciparum* parasites lacking histidine-rich protein 2 and 3: a review and recommendations for accurate reporting. Malar J. 2014;13:283. https://doi.org/10.1186/1475-2875-13-283
32. World Health Organization. Response plan to *pfhrp2* gene deletions. Geneva: The Organization; 2019.
33. Lee N, Baker J, Andrews KT, Gatton ML, Bell D, Cheng Q, et al. Effect of sequence variation in *Plasmodium falciparum* histidine-rich protein 2 on binding of specific monoclonal antibodies: Implications for rapid diagnostic tests for malaria. J Clin Microbiol. 2006;44:2773–8. https://doi.org/10.1128/JCM.02557-05
34. Lee N, Gatton ML, Pelecanos A, Bubb M, Gonzalez I, Bell D, et al. Identification of optimal epitopes for *Plasmodium falciparum* rapid diagnostic tests that target histidine-rich proteins 2 and 3. J Clin Microbiol. 2012;50:1397–405. https://doi.org/10.1128/JCM.06533-11
35. Gamboa D, Ho MF, Bendezu J, Torres K, Chiodini PL, Barnwell JW, et al. A large proportion of *P. falciparum* isolates in the Amazon region of Peru lack *pfhrp2* and *pfhrp3*: implications for malaria rapid diagnostic tests. PLoS One. 2010;5:e8091. https://doi.org/10.1371/journal.pone.0008091
36. Golassa L, Messele A, Amambua-Ngwa A, Swedberg G. High prevalence and extended deletions in *Plasmodium falciparum hrp2/3* genomic loci in Ethiopia. PLoS One. 2020;15:e0241807. https://doi.org/10.1371/journal.pone.0241807
37. Alemayehu GS, Blackburn K, Lopez K, Cambel Dieng C, Lo E, Janies D, et al. Detection of high prevalence of *Plasmodium falciparum* histidine-rich protein 2/3 gene deletions in Assosa zone, Ethiopia: implication for malaria diagnosis. Malar J. 2021;20:109. https://doi.org/10.1186/s12936-021-03629-x
38. Girma S, Cheaveau J, Mohon AN, Marasinghe D, Legese R, Balasingam N, et al. Prevalence and epidemiological characteristics of asymptomatic malaria based on ultrasensitive diagnostics: a cross-sectional study. Clin Infect Dis. 2019;69:1003–10. https://doi.org/10.1093/cid/ciy1005
39. Willie N, Mehlotra RK, Howes RE, Rakotomanga TA, Ramboarina S, Ratsimbasoa AC, et al. Insights into the performance of SD Bioline Malaria Ag P.f/Pan rapid diagnostic test and *Plasmodium falciparum* histidine-rich protein 2 gene variation in Madagascar. Am J Trop Med Hyg. 2018;98:1683–91. https://doi.org/10.4269/ajtmh.17-0845
40. Baker J, Ho MF, Pelecanos A, Gatton M, Chen N, Abdullah S, et al. Global sequence variation in the histidine-rich proteins 2 and 3 of *Plasmodium falciparum*: implications for the performance of malaria rapid diagnostic tests. Malar J. 2010;9:129. https://doi.org/10.1186/1475-2875-9-129
41. Plucinski MM, Dimbu PR, Fortes F, Abdulla S, Ahmed S, Gutman J, et al. Posttreatment HRP2 clearance in patients with uncomplicated *Plasmodium falciparum* malaria. J Infect Dis. 2018;217:685–92. https://doi.org/10.1093/infdis/jix622
42. Koita OA, Doumbo OK, Ouattara A, Tall LK, Konaré A, Diakité M, et al. False-negative rapid diagnostic tests for malaria and deletion of the histidine-rich repeat region of the *hrp2* gene. Am J Trop Med Hyg. 2012;86:194–8. https://doi.org/10.4269/ajtmh.2012.10-0665

Address for correspondence: Eric Rogier, Centers for Disease Control and Prevention, 1600 Clifton Rd NE, Mailstop D-67, Atlanta, GA, 30029-4027, USA; email: erogier@cdc.gov

Genomic and Phenotypic Insights for Toxigenic Clinical *Vibrio cholerae* O141

Yaovi M.G. Hounmanou, Brandon Sit, Bolutife Fakoya, Matthew K. Waldor, Anders Dalsgaard

Vibrio cholerae remains a major public health threat worldwide, causing millions of cholera cases each year. Although much is known about the evolution and pathogenicity of the O1/O139 serogroups of *V. cholerae*, information is lacking on the molecular epidemiology of non–O1/O139 strains isolated from patients who have diarrheal illnesses. We performed whole-genome sequence analysis and in vivo infections to investigate characteristics of *V. cholerae* O141 isolated from sporadic diarrheal cases in 4 countries. The strains formed a distinct phylogenetic clade distinguishable from other serogroups and a unique multilocus sequence type 42, but interstrain variation suggests that O141 isolates are not clonal. These isolates encode virulence factors including cholera toxin and the toxin-coregulated pilus, as well as a type 3 secretion system. They had widely variable capacities for intestinal colonization in the infant mouse model. We propose that O141 isolates comprise a distinct clade of *V. cholerae* non–O1/O139, and their continued surveillance is warranted.

There are an estimated 3–4 million cases of cholera globally each year, driving marked interest in understanding the genomic diversity and evolution of the causative pathogen (*1*,*2*). Of the >200 known *Vibrio cholerae* serogroups distinguished by unique O-antigen structures, only O1 and O139 have been recognized as being capable of causing sustained epidemics. The O139 serogroup, which caused large epidemics on the Indian subcontinent during 1992–1994, arose from *V. cholerae* O1 by exchange of the O139 gene cluster encoding O-antigen biosynthesis for the O1 cluster (*3*). The 2 biotypes of *V. cholerae* serogroup O1 have been the causes of the previous 6 (classical) and ongoing seventh cholera pandemic (El Tor) (*4*,*5*). Decades of study of *V. cholerae* O1 have showed that cholera pathogenesis is largely driven by the activity of the secreted cholera toxin (Ctx), a potent AB_5 toxin that targets intestinal epithelial cells and causes secretory diarrhea in infected hosts. *V. cholerae* intestinal colonization depends on the toxin-coregulated pilus (Tcp), which is coordinately expressed with Ctx (*6*).

Compared with information available on *V. cholerae* O1, relatively little knowledge is available on the pathogenesis and genomic diversity of *V. cholerae* isolates from other serogroups, such as O37, O75, and O141 (collectively termed non–O1/O139). These serogroups have been isolated from patients who had diarrheal illness, as well as from aquatic environmental sources (*7*–*10*). In the United States, for instance, toxigenic *V. cholerae* O141 has occasionally been associated with diarrhea and bloodstream infections (*11*,*12*). Although non–O1/O139 strains can encode Ctx and Tcp, they may be underreported as a cause of diarrheal illness because routine laboratory testing in cholera-endemic settings only includes testing for O1 and O139 serogroups (*13*). Surveillance of non–O1/O139 serogroups in the United States over the past 30 years has reported diarrheal illness associated with *V. cholerae* O75 and O141 infection from consumption of seafood or exposure to water in lakes and rivers (*8*,*9*).

Previous studies showed that *V. cholerae* O141 isolates can encode Ctx and Tcp (*10*,*14*). In this study, we investigated the genomics and in vivo colonization ability of *V. cholerae* O141 strains isolated from diarrheal cases from 4 different countries during 1984–1994. The strains were isolated from sporadic cases of diarrhea without any documented epidemiologic association.

Materials and Methods

Strain Collection, DNA Extraction, and Whole-Genome Sequencing

We obtained *V. cholerae* O141 isolates sequenced in the present study from a strain collection initially reported by Dalsgaard et al. (*10*,*15*). The strains were

Author affiliations: University of Copenhagen, Frederiksberg, Denmark (Y.M.G. Hounmanou, A. Dalsgaard); Brigham & Women's Hospital, Boston, Massachusetts, USA (B. Sit, B. Fakoya, M.K. Waldor); Harvard Medical School, Boston (B. Sit, B. Fakoya, M.K. Waldor)

DOI: https://doi.org/10.3201/eid2803.210715

isolated from sporadic cases of diarrhea, which did not appear to be epidemiologically related. Information about whether stool samples were cultured for major enteric pathogens other than *V. cholerae* was not available for the strains studied.

We obtained strains from the Center for Disease Control and Prevention (Atlanta, GA, USA) and the Japanese National Institute of Infectious Diseases (Tokyo, Japan). We stored strains in 10% glycerol at −80°C, and revived them by streaking onto blood agar plates. We extracted genomic DNA from overnight liquid cultures of the isolates by using the Maxwell RSC Cultured Cells DNA kit following the manufacturer's protocol and the automated Maxwell RSC Machine (both from Promega, https://www.promega.com). We sequenced genomic DNA samples by using the MiSeq System (Illumina, https://www.illumina.com) as described (*16*). The coverage of the sequenced genomes ranged from 50× to 75× (Table). We submitted the sequence reads to the European Nucleotide Archive (accession no. PRJEB42289).

Read Processing and Genome Assembly

We trimmed raw sequence reads by using with bbduk2 (*17*) (from BBmap version 6.49) and a cutoff score of 20. We evaluated read quality by using FastQC version 0.11.5 (https://guix.gnu.org) before and after trimming. We assembled trimmed reads by using Spades version 3.13.0 (*18*), error correction, a coverage cutoff of 2, and kmer sizes 21, 33, 55, 77, 99 and 127. We discarded contigs <200 bases and assessed the quality of the de novo assembled contigs by using Quast version 4.5 (*19*). We then analyzed the assembled genomes for species identification and *V. cholerae*–specific genome annotation (biotype, serogroup, and *Vibrio* pathogenicity island conservation) by using the CholeraeFinder tool (https://cge.cbs.dtu.dk/services/CholeraeFinder). We identified resistance genes by using ResFinder (20) and plasmid replicons by using PlasmidFinder (*21*).

Phylogenetic Analysis

We used the generated *V. cholerae* O141 genomes for phylogenetic analysis with publicly available genomes representing the other Ctx-positive *V. cholerae* serogroups. Representative clinical nontoxigenic and non–O1/O139 genomes from strains isolated in Germany were also included in the analysis (*22*). We analyzed 23 additional *ctxA*-positive *V. cholerae* and 7 *ctx*A-negative non–O1/0139 reference genomes and compared them with the 8 genomes we had (total = 38). These genomes included the only whole genomes sequences of *V. cholerae* O141 available before this study (strain V51 and 234–93), all publicly available genomes of *V. cholerae* O75 and O37 (all *ctxA*+ non–O1/O139 serogroups), the representative O139 strain MO10, and a variety of historical and contemporary O1 strains with differing *ctxB* alleles, which were selected to capture the genomic variation of pandemic *V. cholerae* O1. These historical and contemporary O1 strains included strains O395 (classical, *ctx*B1), N16961 (El Tor, *ctx*B3), CTMA1422 (El Tor variant, *ctx*B1), L254 (El Tor variant, *ctx*B1) and ZB6 (El Tor variant, *ctx*B7). We provide details and accession numbers of these genomes, including the nontoxigenic non–O1/O139 strains (Appendix Table 1, https://wwwnc.cdc.gov/EID/article/28/3/21-0715-App1.xlsx).

We called single-nucleotide variants by using Snippy version 4.6.0 (https://github.com/tseemann/snippy) under the following parameters: mapping quality of 60, a minimum base quality of 13, a minimum read coverage of 4, and a 75% concordance at a locus. We aligned core genome single-nucleotide variants by using Snippy version 4.1.0 for phylogeny inference. We detected masked putative recombinogenic regions by using Gubbins version 2.4.1 (*23*). We built a maximum-likelihood phylogenetic tree by using RAxML version/8.2.12 and the generalized time-reversible model with 100 bootstraps (*24*). We rooted the final tree on the V51 genome and visualized it with iTOL version 3 (*25*). We provide pairwise single-nucleotide polymorphism (SNP) data for the 38 strains (Appendix Table

Table. Characteristics of whole-genome sequences of *Vibrio cholerae* O141 strains*

Strain	GC, %	No. contigs	Length, bp	N50 of contigs	Place and year of isolation	cgMLST†
AD3_609–84	47.5	136	3,959,387	195,630	USA, 1984	479
AD4_2454–85	47.44	145	4,110,364	104,771	USA, 1985	479
AD5_2466–85	47.42	134	4,096,622	111,701	USA, 1985	479
AD6_2527–87	47.52	140	4,073,408	111,688	USA, 1987	479
AD7_2533–86	47.41	150	4,056,508	157,587	USA, 1986	479
AD8_F2031	47.43	101	3,976,610	187,293	Spain, 1994	246
AD9_234–93	47.5	130	4,046,144	185,481	India, 1993	479
AD10_1178–96	47.41	118	4,082,579	101,628	Taiwan, 1993	479

*cgMLST, core genome multilocus sequence type; N50, shortest contig length covering 50% of the genome.
†The conventional 7-gene MLST profile is ST42 for all.

2). The alignment length from all analyzed genomes was 3,464,958 and represented 82.3% of the reference *V. cholerae* strain V51 used.

Comparative Genomics

We annotated all genomes used for phylogenetic analysis by using Prokka version 1.14.5 (*26*), and used resulting general feature format 3 files as inputs to the Roary version 3.7.0 (*27*) pangenome analysis tool. We then used the binary presence/absence data of the accessory genome produced in Roary to calculate associations between all genes in the accessory genome and serogroups by using Scoary version 1.6.11 (*28*). We depicted a heatmap of the genes present or absent in the core genome, along with the accessory genome, in phandango (*29*) to enable the identification and extraction of the unique coding sequence (CDS) blocks observed for the O141 serogroup by applying the query_pan_genome function of Roary. After a BLAST Atlas analysis from the GView server (https://server.gview.ca), we mapped the multi-FASTA files of the O141-specific CDS block to the reference V51 to localize the block in the genome.

To understand how O141-specific CDS could play a role in intestinal colonization, we analyzed the extracted multi-FASTA file by using the VRprofile pipeline (*30*), which detects virulence and colonization determinants within bacterial genomes. We customized this analysis to focus on the gene clusters encoding Tcp, T3SS2 a *Vibrio* type III secretion system that is found in clinical *V. parahaemolyticus* isolates and in some *V. cholerae* non–O1/O139, and other accessory colonization factors known to promote *V. cholerae* intestinal colonization (*31*–*34*). In addition, we individually investigated genes/open reading frames located in these clusters by using local blastn and blastp (https://blast.ncbi.nlm.nih.gov/Blast.cgi) searches against our query genomes with intentionally low 60% query cover and 30% identity thresholds to avoid false-negative gene, absence outcomes that might be caused by recombination.

Infant Mouse Intestinal Colonization Assay

We orally inoculated 5-day-old, infant CD-1 mice (Charles River Laboratories https://www.criver.com) with *V. cholerae* as described (*35*). We used frozen stocks of each strain to inoculate lysogeny broth that did not contain antimicrobial dugs and incubated the broth overnight with shaking at 250 rpm at 37°C. We diluted cultures 1:1,000 in lysogeny broth and mixed the cultures with 4 μL/mL of green food coloring to track the inoculum. We removed pups from their dams 1 hour preinoculation and orally inoculated them with 50 μL of diluted culture (≈2–4 $\times 10^5$ CFU/pup). We combined and randomly assigned pups from multiple litters to inoculation groups to reduce the effect of litter effects on *V. cholerae* colonization. We housed inoculated pups in a warmed box with nest material for 20 hours in the dark apart from their dams, at which point they were euthanized with isoflurane inhalation followed by decapitation. We dissected and mechanically homogenized small intestines by using a Tissue Tearor (BioSpec, https://biospec.com), followed by serial dilution and bead plating onto thiosulfate-citrate-bile salt (TCBS) agar plates that did not contain antimicrobial drugs. We incubated plates at 37°C overnight for counting. No non-*Vibrio* (non-yellow) colonies were detected on the TCBS agar plates. Animal work in this study was approved by the Brigham and Women's Hospital Institutional Animal Care and Use Committee under Protocol #2016N000416.

Results

Genomic Characterization and Phylogenetic Analysis

To investigate the genomic diversity of clinical isolates of *V. cholerae* O141, we sequenced and annotated the genomes of 8 serotype-confirmed O141 strains collected from stool samples of gastroenteritis patients in the United States, Spain, Taiwan, and India over a 10-year period during 1984–1994 (*10*) (Table). These strains had been characterized by using ribotyping, PCRs for *ctx*A and *tcp*A, and antimicrobial drug susceptibility testing, but little was known about their genomic characteristics (*10*,*15*). All 8 isolates had gene sequences in the O-antigen lipopolysaccharide region and gene rearrangements between *gmh*D and *wbf*Y, consistent with known O141-specific lipopolysaccharide changes (Appendix Table 3) (*9*,*36*). Sequence typing also placed all 8 isolates in the same multilocus sequence type (MLST), MLST42, as the known O141 isolate V51 (Table). On the basis of concordance in the 7-gene MLST profile, these observations suggest that ST42 might be specific to the serogroup O14, and could serve as a serogroup-specific marker for genomic studies because no other *V. cholerae* serogroups have been associated with this MSLT (*2*,*16*,*37*).

The core genome MLST, which is based on the entire core genome rather than the 7 housekeeping genes used for conventional MLST, was cgST-479 for all except the strains AD8 (cgST-246) and V51 (cgST-248). This variation was further reflected in the whole-genome phylogenetic analysis, in which O141 strains, although distinct from other serogroups, were not internally clonal, differing in up to 261 SNPs (Figure 1).

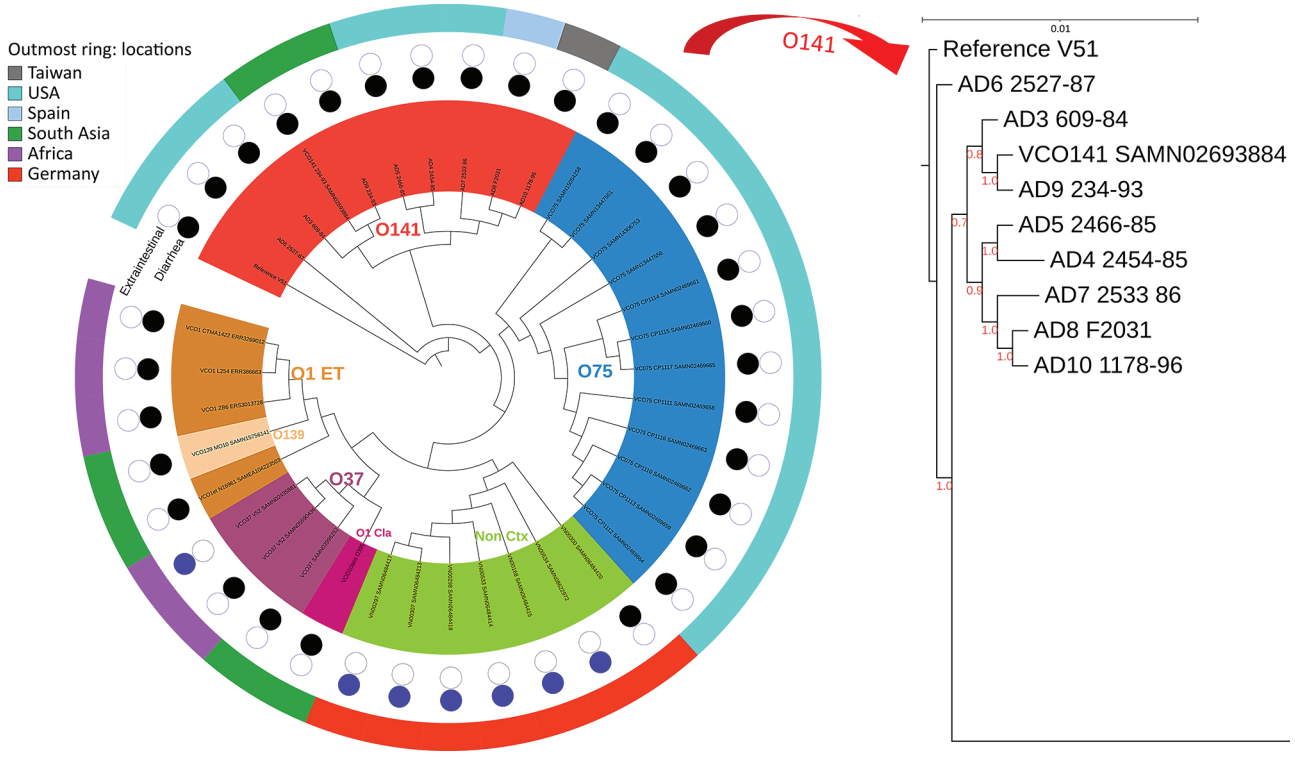

Figure 1. Maximum-likelihood phylogenetic tree for *Vibrio cholerae* O141 in a global context for 38 isolates from Ctx-positive *V. cholerae* and Ctx-negative serogroups. Numbers along branches are bootstrap values. Scale bar indicates nucleotide substitutions per site. Ctx, cholera toxin.

Despite their diverse sites and years of isolation, all 8 O141 strains encoded a CTX prophage similar to the classical CTX prophage with the *ctxB1* allele and the classical rstR as indicated (*38*). The presence of the classical CTX prophage in all 8 strains suggests that the presence of this sequence along with the alleles that constitute MLST42 might be characteristic of serogroup O141. In addition to *ctxAB*, the genes encoding the signature virulence factor of *V. cholerae*, these strains also encoded cholix toxin, an accessory toxin that is found in *V. cholerae* non–O1/O139 (*39*). Although these strains harbored a classical CTX prophage, they all also contained an El Tor type *tcpA*, which encodes the major subunit of the Tcp pilus, the CTXϕ receptor, and a critical determinant of intestinal colonization *V. cholerae* O1 (*40*). Although most strains also contained genes in the *tcp* operon needed for Tcp biogenesis (encoded in the *Vibrio* pathogenicity island VPI-I), they generally lacked an intact *tcpJ*, which encodes a prepilin peptidase required for processing of TcpA (*41*). All sequenced strains also appeared to encode a type III secretion system (T3SS) known as T3SS2, that is a critical colonization and virulence determinant of *V. parahaemolyticus* and is also found in V51 (*34*,*42*). The co-occurrence of the TCP and T3SS2 pathogenicity islands in *V. cholerae* O141 strains suggests that *V. cholerae* O141 might rely on diverse mechanisms for pathogenicity, potentially deploying these distinct virulence mechanisms in different hosts.

The O141 strains did not contain detectable antimicrobial resistance genes, supporting prior phenotypic antimicrobial drug susceptibility findings in which all strains were susceptible to a panel of 12 antimicrobial drugs, except for colistin (to which all non–O1 *V. cholerae* naturally show resistance) (*10*). In addition, none of the analyzed *V. cholerae* O141 genomes contained plasmid replicons, consistent with the absence of plasmids, as shown by previous plasmid extraction analysis of these isolates (*10*).

Despite the observed homogeneity in MLST profile and conservation of major virulence genes in *V. cholerae* O141 strains, there were substantial variations in the O141 genomes (up to 261 SNPs), regardless of country of origin (Figure 1; Appendix Table 2), most of which occurred in noncoding regions. This finding suggests that the strains are epidemiologically unrelated, consistent with the idea that infections caused by *V. cholerae* O141 are sporadic. All

the O141 serogroup strains, including V51, formed a separate clade distinguishable from the other serogroups, all strains from serogroup O75 also grouped into a distinct clade (Figure 1). The observed genetic variations between the serogroups indicates that *V. cholerae* O141 and O75 are not phylogenetically related, contrary to a previous proposal (*8*). The phylogeny also suggests that serogroup O37 is closely related to the classical O1 strain O395. As expected, serogroup O139 represented by the reference strain MO10 was localized to the O1 El Tor subclade, consistent with the idea that this serogroup arose from an O1 El Tor seventh pandemic strain (*3*,*21*,*37*). Moreover, the nontoxigenic non–O1/O139 clinical strains formed a separate clade on the phylogenetic tree that is unrelated to the other known toxigenic, as well as nontoxigenic serogroups.

Intestinal Colonization of Infant Mice by *V. cholerae* Serogroup O141

The presence of canonical pandemic *V. cholerae* colonization factors such as Tcp in their genomes led us to hypothesize that O141 strains, like their pandemic O1 counterparts, might colonize the small intestine. To test this idea, we used the well-characterized infant mouse model of *V. cholerae* small intestinal colonization. Infant mice orally inoculated with 2–4 × 10^5 CFU of selected O141 strains that grew well on TCBS agar plates (AD3, AD5, AD8, AD9, and AD10) showed marked variation in their colonization capacity (Figure 2). In comparison to a *V. cholerae* O1 isolate from the recent cholera epidemic in Haiti, which robustly colonizes the small intestine (*43*), strains AD8 and AD5 had similar numbers of CFU recovered in intestinal homogenates as the strain from Haiti (Figure 2). In contrast, the other 3 strains had from ≈1,000-fold (AD9) to ≈10,000-fold (AD3 and AD10) lower numbers of recoverable bacteria, indicating that although they can all colonize the small intestine, there are considerable strain-specific differences in the capacities of these O141 isolates to colonize the mammalian small intestine.

Differential genomic conservation of virulence or colonization determinants could underlie the variable colonization phenotypes. To evaluate strain-level conservation of accessory genetic features, we next performed pangenome analysis of genomes from only the toxigenic strains used in the phylogenetic analysis. This analysis identified an accessory genome made of shell and cloud genes of 2,598 coding sequences (CDS) in a total pangenome size of 5,627 CDS (Figure 3, https://wwwnc.cdc.gov/EID/article/28/3/21-0715-F3.htm; Appendix Table 4). A targeted analysis of the accessory genome showed strain-specific gene absences in the in vivo–tested O141 strains (Figure 4,). For example, AD3, which had the lowest intestinal colonization among the strains tested, lacked *toxT*, the master transcription activator of *V. cholerae* virulence genes (*44*) (Figure 4). The accessory genomes of AD3, AD9, and AD10, which did not colonize as well as the robustly colonizing strains AD5 and AD8, all lacked T3SS2 genes *vcrS2* and *vopB2* (Figure 4, panel A). AD3 also lacked the known T3SS effectors *vop*F and *sse*J (Figure 4, panel A). All analyzed strains, including V51, contained protein sequences corresponding to VopV and VopZ, 2 T3SS2-associated genes known to be critical for intestinal colonization by *V. parahaemolyticus* (*34*,*42*).

Discussion

Our findings show that *V. cholerae* O141 clinical isolates form a genetically distinct clade that is distinguishable from pandemic and nonpandemic *V. cholerae* serogroups. The observation that all tested isolates encoded known virulence factors and were capable of colonizing the infant mouse intestine, albeit in a highly variable manner, supports the idea that *V. cholerae* O141 could be an underestimated source of cholera-like diarrhea. Currently, O141 cases would be grouped under the umbrella of non–O1/O139 cases because of a lack of widely available serogroup-specific antiserum for O141. Nevertheless, from this study, the ST42 that appears to be specific/unique to the serogroup O141 might be used for diagnostic purposes as an alternative to O141 antiserum, which is not widely available.

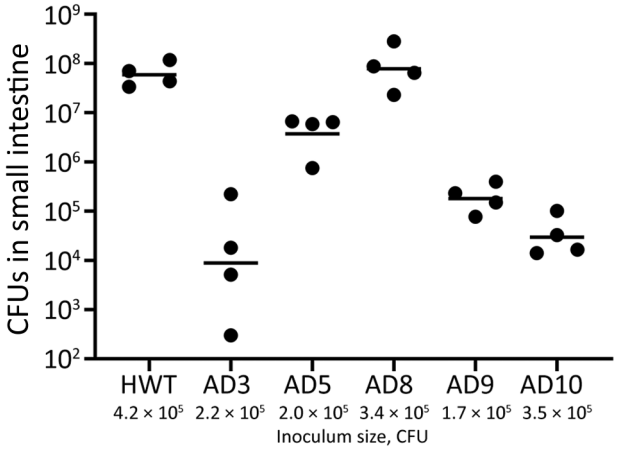

Figure 2. Intestinal colonization of 5-day-old infant mice by *Vibrio cholerae* O141. Pups were orally inoculated with the indicated amount of the indicated strain, and CFUs in the small intestine were enumerated at 20 hours postinoculation. Dots indicate individual animals, and horizontal bars indicate geometric means of each group. HWT, *V. cholerae* O1 isolate from the recent cholera epidemic in Haiti used as a positive control; AD, *V. cholerae* O141 strains analyzed in this study.

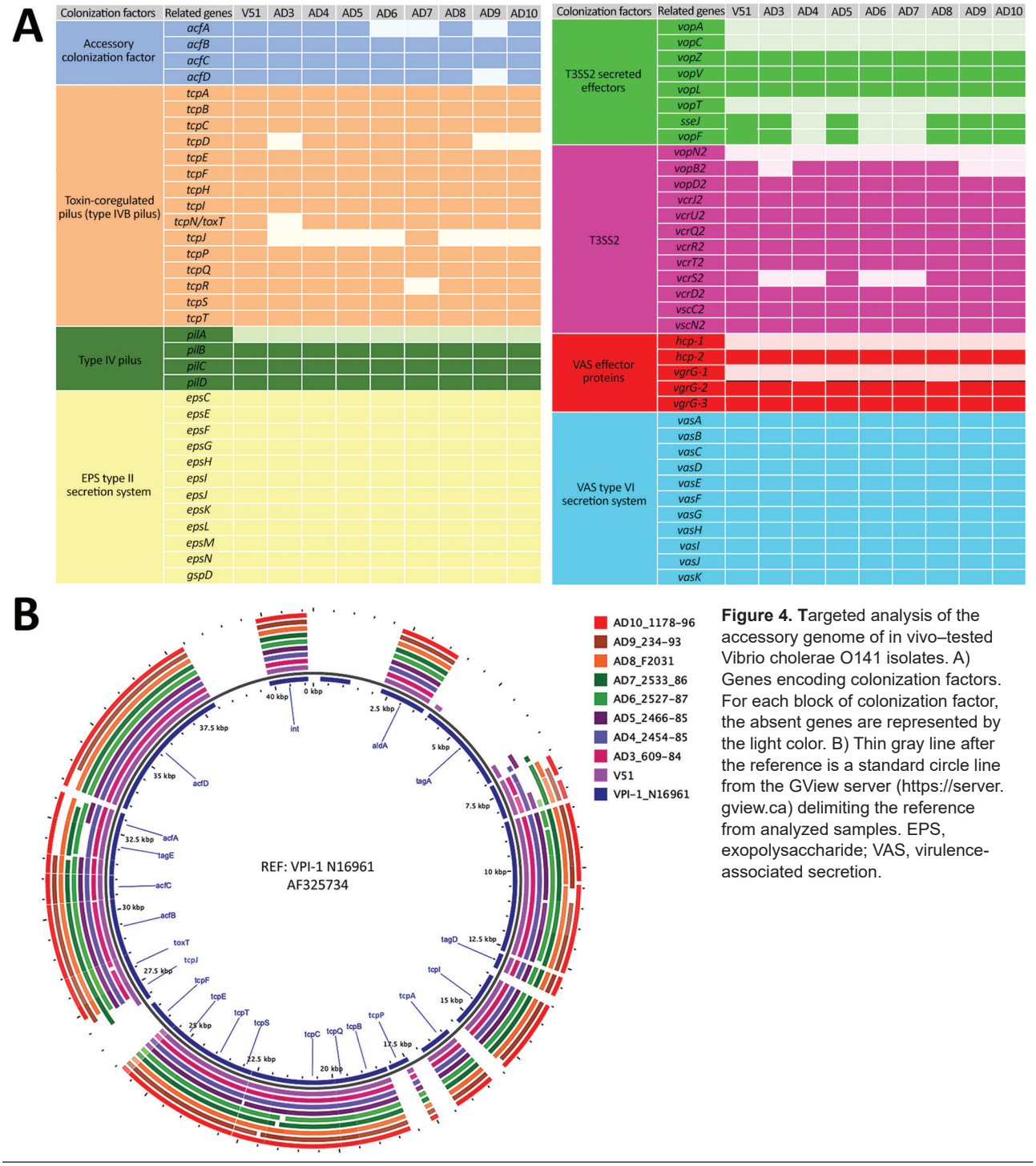

Figure 4. Targeted analysis of the accessory genome of in vivo–tested Vibrio cholerae O141 isolates. A) Genes encoding colonization factors. For each block of colonization factor, the absent genes are represented by the light color. B) Thin gray line after the reference is a standard circle line from the GView server (https://server.gview.ca) delimiting the reference from analyzed samples. EPS, exopolysaccharide; VAS, virulence-associated secretion.

Our findings show that some O141 strains are capable of robust colonization. These strains encode at least 2 potential mechanisms, Tcp and T3SS2, that could enable intestinal colonization. Variable colonization among O141 strains could be explained by differential conservation of T3SS components/effectors or other colonization factors. Deciphering the colonization requirements of different O141 isolates will be a useful endeavor.

The factors that have limited *V. cholerae* O141 from causing sustained cholera epidemics remain to be elucidated. It is possible that *V. cholerae* O141 is not as well adapted as *V. cholerae* O1 to the aquatic environment, which is thought to be a key feature of the

lifecycle of *V. cholerae*. Although we did not assess the aquatic fitness of the O141 serogroup, *V. cholerae* O141 has been detected in environmental reservoirs, such as oysters, clams, and freshwater in lakes and rivers in the United States, suggesting an environmental defect is unlikely to fully explain the low frequency of these strains in the clinic (*8*,*9*). These discrepancies call for further genomic and experimental studies on environmental, as well as additional clinical *V. cholerae* O141 isolates. Additional techniques, such as multilocus sequence typing, could overcome challenges related to the identification of *V. cholerae* non–O1/O139 serogroups.

Overall, *V. cholerae* O141 strains constitute a distinct phylogenetic clade that includes shared and unique genomic elements. In addition, we found that *V. cholerae* O141 clinical isolates showed marked variation in intestinal colonization capacity in the infant mouse model. These findings shed light on a little-known *V. cholerae* serogroup associated with diarrheal illness.

This study was supported by the University of Copenhagen. M.K.W. was supported by the National Institutes of Health (grant AI-042347) and the Howard Hughes Medical Institute.

About the Author

Dr. Hounmanou is a postdoctoral fellow at the Department of Veterinary and Animal Sciences, University of Copenhagen, Frederiksberg, Denmark. His primary research interests are One Health; microbial genomics; human bacterial pathogens that arise from animals and the aquatic environment; and the ecology and routes of transmission between animals, humans, and waterbodies, with a specific focus on V. cholerae.

References

1. Ali M, Nelson AR, Lopez AL, Sack DA. Updated global burden of cholera in endemic countries. PLoS Negl Trop Dis. 2015;9:e0003832. https://doi.org/10.1371/journal.pntd.0003832
2. Weill F-X, Domman D, Njamkepo E, Almesbahi AA, Naji M, Nasher SS, et al. Genomic insights into the 2016–2017 cholera epidemic in Yemen. Nature. 2019;565:230–3. https://doi.org/10.1038/s41586-018-0818-3
3. Faruque SM, Sack DA, Sack RB, Colwell RR, Takeda Y, Nair GB. Emergence and evolution of Vibrio cholerae O139. Proc Natl Acad Sci U S A. 2003;100:1304–9. https://doi.org/10.1073/pnas.0337468100
4. Mutreja A, Kim DW, Thomson NR, Connor TR, Lee JH, Kariuki S, et al. Evidence for several waves of global transmission in the seventh cholera pandemic. Nature. 2011;477:462–5. https://doi.org/10.1038/nature10392
5. Grad YH, Waldor MK. Deciphering the origins and tracking the evolution of cholera epidemics with whole-genome-based molecular epidemiology. MBio. 2013;4:e00670–13. https://doi.org/10.1128/mBio.00670-13
6. Faruque SM, Albert MJ, Mekalanos JJ. Epidemiology, genetics, and ecology of toxigenic Vibrio cholerae. Microbiol Mol Biol Rev. 1998;62:1301–14. https://doi.org/10.1128/MMBR.62.4.1301-1314.1998
7. Fang L, Ginn AM, Harper J, Kane AS, Wright AC. Survey and genetic characterization of Vibrio cholerae in Apalachicola Bay, Florida (2012–2014). J Appl Microbiol. 2019;126:1265–77. https://doi.org/10.1111/jam.14199
8. Crowe SJ, Newton AE, Gould LH, Parsons MB, Stroika S, Bopp CA, et al. Vibriosis, not cholera: toxigenic Vibrio cholerae non-O1, non-O139 infections in the United States, 1984–2014. Epidemiol Infect. 2016;144:3335–41. https://doi.org/10.1017/S0950268816001783
9. Haley BJ, Choi SY, Grim CJ, Onifade TJ, Cinar HN, Tall BD, et al. Genomic and phenotypic characterization of Vibrio cholerae non-O1 isolates from a US Gulf Coast cholera outbreak. PLoS One. 2014;9:e86264. https://doi.org/10.1371/journal.pone.0086264
10. Dalsgaard A, Serichantalergs O, Forslund A, Lin W, Mekalanos J, Mintz E, et al. Clinical and environmental isolates of Vibrio cholerae serogroup O141 carry the CTX phage and the genes encoding the toxin-coregulated pili. J Clin Microbiol. 2001;39:4086–92. https://doi.org/10.1128/JCM.39.11.4086-4092.2001
11. Crump JA, Bopp CA, Greene KD, Kubota KA, Middendorf RL, Wells JG, et al. Toxigenic Vibrio cholerae serogroup O141-associated cholera-like diarrhea and bloodstream infection in the United States. J Infect Dis. 2003;187:866–8. https://doi.org/10.1086/368330
12. Loeck BK, Roberts A, Craney AR, King S, Im MS, Safranek TJ, et al. Notes from the field: toxigenic Vibrio cholerae O141 in a traveler to Florida—Nebraska, 2017. MMWR Morb Mortal Wkly Rep. 2018;67:838–9. https://doi.org/10.15585/mmwr.mm6730a7
13. Chen M, Guo D, Wong HC, Zhang X, Liu F, Chen H, et al. Development of O-serogroup specific PCR assay for detection and identification of Vibrio parahaemolyticus. Int J Food Microbiol. 2012;159:122–9. https://doi.org/10.1016/j.ijfoodmicro.2012.08.012
14. Udden SM, Zahid MS, Biswas K, Ahmad QS, Cravioto A, Nair GB, et al. Acquisition of classical CTX prophage from Vibrio cholerae O141 by El Tor strains aided by lytic phages and chitin-induced competence. Proc Natl Acad Sci U S A. 2008;105:11951–6. https://doi.org/10.1073/pnas.0805560105
15. Dalsgaard A, Forslund A, Mortensen HF, Shimada T. Ribotypes of clinical Vibrio cholerae non-O1 non-O139 strains in relation to O-serotypes. Epidemiol Infect. 1998;121:535–45. https://doi.org/10.1017/S0950268898001654
16. Hounmanou YM, Leekitcharoenphon P, Kudirkiene E, Mdegela RH, Hendriksen RS, Olsen JE, et al. Genomic insights into Vibrio cholerae O1 responsible for cholera epidemics in Tanzania between 1993 and 2017. PLoS Negl Trop Dis. 2019;13:e0007934. https://doi.org/10.1371/journal.pntd.0007934
17. Bushnell B, Rood J, Singer E. BBMerge: accurate paired shotgun read merging via overlap. PLoS One. 2017;12:e0185056. https://doi.org/10.1371/journal.pone.0185056
18. Bankevich A, Nurk S, Antipov D, Gurevich AA, Dvorkin M, Kulikov AS, et al. SPAdes: a new genome assembly algorithm and its applications to single-cell sequencing. J Comput Biol. 2012;19:455–77. https://doi.org/10.1089/cmb.2012.0021
19. Gurevich A, Saveliev V, Vyahhi N, Tesler G. QUAST: quality assessment tool for genome assemblies.

Bioinformatics. 2013;29:1072–5. https://doi.org/10.1093/bioinformatics/btt086
20. Bortolaia V, Kaas RS, Ruppe E, Roberts MC, Schwarz S, Cattoir V, et al. ResFinder 4.0 for predictions of phenotypes from genotypes. J Antimicrob Chemother. 2020;75:3491–500. https://doi.org/10.1093/jac/dkaa345
21. Siriphap A, Leekitcharoenphon P, Kaas RS, Theethakaew C, Aarestrup FM, Sutheinkul O, et al. Characterization and genetic variation of Vibrio cholerae isolated from clinical and environmental sources in Thailand. PLoS One. 2017;12:e0169324. https://doi.org/10.1371/journal.pone.0169324
22. Schwartz K, Hammerl JA, Göllner C, Strauch E. Environmental and clinical strains of Vibrio cholerae non-O1, non-O139 from Germany possess similar virulence gene profiles. Front Microbiol. 2019;10:733. https://doi.org/10.3389/fmicb.2019.00733
23. Croucher NJ, Page AJ, Connor TR, Delaney AJ, Keane JA, Bentley SD, et al. Rapid phylogenetic analysis of large samples of recombinant bacterial whole genome sequences using Gubbins. Nucleic Acids Res. 2015;43:e15–15. https://doi.org/10.1093/nar/gku1196
24. Stamatakis A. RAxML version 8: a tool for phylogenetic analysis and post-analysis of large phylogenies. Bioinformatics. 2014;30:1312–3. https://doi.org/10.1093/bioinformatics/btu033
25. Letunic I, Bork P. Interactive tree of life (iTOL) v3: an online tool for the display and annotation of phylogenetic and other trees. Nucleic Acids Res. 2016;44(W1):W242–5. https://doi.org/10.1093/nar/gkw290
26. Seemann T. Prokka: rapid prokaryotic genome annotation. Bioinformatics. 2014;30:2068–9. https://doi.org/10.1093/bioinformatics/btu153
27. Page AJ, Cummins CA, Hunt M, Wong VK, Reuter S, Holden MT, et al. Roary: rapid large-scale prokaryote pan genome analysis. Bioinformatics. 2015;31:3691–3. https://doi.org/10.1093/bioinformatics/btv421
28. Brynildsrud O, Bohlin J, Scheffer L, Eldholm V. Rapid scoring of genes in microbial pan-genome-wide association studies with Scoary. Genome Biol. 2016;17:238. https://doi.org/10.1186/s13059-016-1108-8
29. Hadfield J, Croucher NJ, Goater RJ, Abudahab K, Aanensen DM, Harris SR. Phandango: an interactive viewer for bacterial population genomics. Bioinformatics. 2018;34:292–3. https://doi.org/10.1093/bioinformatics/btx610
30. Li J, Tai C, Deng Z, Zhong W, He Y, Ou H-Y. VRprofile: gene-cluster-detection-based profiling of virulence and antibiotic resistance traits encoded within genome sequences of pathogenic bacteria. Brief Bioinform. 2018;19:566–74.
31. Shakhnovich EA, Sturtevant D, Mekalanos JJ. Molecular mechanisms of virstatin resistance by non-O1/non-O139 strains of Vibrio cholerae. Mol Microbiol. 2007;66:1331–41. https://doi.org/10.1111/j.1365-2958.2007.05984.x
32. Shin OS, Tam VC, Suzuki M, Ritchie JM, Bronson RT, Waldor MK, et al. Type III secretion is essential for the rapidly fatal diarrheal disease caused by non-O1, non-O139 Vibrio cholerae. MBio. 2011;2:e00106–11. https://doi.org/10.1128/mBio.00106-11
33. Zhou X, Gewurz BE, Ritchie JM, Takasaki K, Greenfeld H, Kieff E, et al. A Vibrio parahaemolyticus T3SS effector mediates pathogenesis by independently enabling intestinal colonization and inhibiting TAK1 activation. Cell Rep. 2013;3:1690–702. https://doi.org/10.1016/j.celrep.2013.03.039
34. Hiyoshi H, Kodama T, Saito K, Gotoh K, Matsuda S, Akeda Y, et al. VopV, an F-actin-binding type III secretion effector, is required for Vibrio parahaemolyticus-induced enterotoxicity. Cell Host Microbe. 2011;10:401–9. https://doi.org/10.1016/j.chom.2011.08.014
35. Fleurie A, Zoued A, Alvarez L, Hines KM, Cava F, Xu L, et al. A Vibrio cholerae BolA-like protein is required for proper cell shape and cell envelope integrity. MBio. 2019;10:10. https://doi.org/10.1128/mBio.00790-19
36. Aydanian A, Tang L, Morris JG, Johnson JA, Stine OC. Genetic diversity of O-antigen biosynthesis regions in Vibrio cholerae. Appl Environ Microbiol. 2011;77:2247–53. https://doi.org/10.1128/AEM.01663-10
37. Mutreja A, Dougan G. Molecular epidemiology and intercontinental spread of cholera. Vaccine. 2020;38 Suppl 1:A46–51. https://doi.org/10.1016/j.vaccine.2019.07.038
38. Davis BM, Kimsey HH, Kane AV, Waldor MK. A satellite phage-encoded antirepressor induces repressor aggregation and cholera toxin gene transfer. EMBO J. 2002;21:4240–9. https://doi.org/10.1093/emboj/cdf427
39. Awasthi SP, Asakura M, Chowdhury N, Neogi SB, Hinenoya A, Golbar HM, et al. Novel cholix toxin variants, ADP-ribosylating toxins in Vibrio cholerae non-O1/non-O139 strains, and their pathogenicity. Infect Immun. 2013;81:531–41. https://doi.org/10.1128/IAI.00982-12
40. Clemens JD, Nair GB, Ahmed T, Qadri F, Holmgren J. Cholera. Lancet. 2017;390:1539–49. https://doi.org/10.1016/S0140-6736(17)30559-7
41. Kaufman MR, Seyer JM, Taylor RK. Processing of TCP pilin by TcpJ typifies a common step intrinsic to a newly recognized pathway of extracellular protein secretion by gram-negative bacteria. Genes Dev. 1991;5:1834–46. https://doi.org/10.1101/gad.5.10.1834
42. Zhou X, Massol RH, Nakamura F, Chen X, Gewurz BE, Davis BM, et al. Remodeling of the intestinal brush border underlies adhesion and virulence of an enteric pathogen. MBio. 2014;5:5. https://doi.org/10.1128/mBio.01639-14
43. Sit B, Zhang T, Fakoya B, Akter A, Biswas R, Ryan ET, et al. Oral immunization with a probiotic cholera vaccine induces broad protective immunity against Vibrio cholerae colonization and disease in mice. PLoS Negl Trop Dis. 2019;13:e0007417. https://doi.org/10.1371/journal.pntd.0007417
44. Matson JS, Withey JH, DiRita VJ. Regulatory networks controlling Vibrio cholerae virulence gene expression. Infect Immun. 2007;75:5542–9. https://doi.org/10.1128/IAI.01094-07

Address for correspondence: Yaovi M.G. Hounmanou, Department of Veterinary and Animal Sciences, University of Copenhagen, 1870 Frederiksberg, Denmark; email: gil@sund.ku.dk

Development and Evaluation of Statewide Prospective Spatiotemporal Legionellosis Cluster Surveillance, New Jersey, USA

Jessie A. Gleason,[1] Kathleen M. Ross[1]

Incidence of Legionnaires' disease is increasing, particularly in the Mid-Atlantic states in the United States; since 2015, New Jersey has documented ≈250–350 legionellosis cases per year. We used SaTScan software to develop a semiautomated surveillance tool for prospectively detecting legionellosis clusters in New Jersey. We varied temporal window size and baseline period to evaluate optimal parameter selections. The surveillance system detected 3 community clusters of Legionnaires' disease that were subsequently investigated. Other, smaller clusters were detected, but standard epidemiologic data did not identify common sources or new cases. The semiautomated processing is straightforward and replicable in other jurisdictions, likely by persons with even basic programming skills.

Legionellosis, a bacterial disease caused by *Legionella*, can manifest as either Legionnaires' disease or Pontiac fever. Legionnaires' disease causes severe pneumonia, often requiring hospitalization, and has a fatality rate of 10%–25%, whereas Pontiac fever is generally milder and resolves on its own. In extremely rare cases, *Legionella* can cause extrapulmonary infections, such as endocarditis or wound infections.

Legionella bacteria are found naturally in freshwater environments, such as lakes and streams, but if the bacteria enter human-made water systems with conditions favorable to growth, such as hot tubs, cooling towers, and plumbing systems, *Legionella* can become a health concern. People develop Legionnaires' disease or Pontiac fever primarily by inhaling aerosolized water droplets containing the bacteria. Any source of aerosolized water is a potential mode of transmission: shower heads, faucets, hot tub jets, decorative fountains, medical devices. Less commonly, aspiration of contaminated drinking water can transmit the bacteria. Extrapulmonary infections result from direct inoculation or secondary hematogenous spread from the lung. Since 2000, the incidence of Legionnaires' disease has been on the rise, particularly in the Mid-Atlantic states in the United States (*1*).

In accordance with communicable disease reporting regulations detailed in the New Jersey Administrative Code, healthcare providers must report diagnosed cases of legionellosis within 24 hours of laboratory confirmation to the health department local to where the case-patient resides. Local health departments are responsible for investigating all cases of legionellosis occurring within their jurisdictions that are reported to the New Jersey Communicable Disease Reporting and Surveillance System (CDRSS). Investigations include interviewing each case-patient using a standardized questionnaire to gather additional information about possible exposures to *Legionella* during the incubation period, such as spending a night away from home, visiting a healthcare facility, or being near a hot tub. These data are used to identify epidemiologic links between cases and determine the need for outbreak investigations, which are critical for detecting transmission sources and implementing control measures. These outbreaks, or clusters, are easily identified when ≥2 persons with diagnosed legionellosis report the same exposure location during their incubation periods within a 12-month period. Since 2015, New Jersey has documented ≈250–350 legionellosis cases per year. However, outbreaks

Author affiliation: New Jersey Department of Health, Trenton, New Jersey, USA

DOI: https://doi.org/10.3201/eid2803.211147

[1]These authors contributed equally to this article.

account for <10% of reported legionellosis cases in New Jersey; remaining cases are classified as sporadic occurrences, defined as isolated events with no known epidemiologic link to other reported cases or confirmed outbreak sources.

Sporadic cases might share a common source of exposure in the community, such as cooling towers (*2*,*3*), underlying issues with a water utility (*4*,*5*), decorative fountains (*6*), or a wide variety of other sources (*3*). Despite exhaustively reviewing epidemiologic, environmental, and microbiological information collected during case investigations, identifying common sources or even linking multiple cases with spatiotemporal associations can be difficult (*7*). Without a reported common source location, such as a specific building, or a sudden unexplained increase in reported cases, clusters might go undetected because cases manifested in an unusual geographic or temporal pattern that may be caused, for example, by an intermittently operated cooling tower or because disease baselines are very high (*8*,*9*).

In addition to using standard surveillance practices, some jurisdictions have developed systems to enhance prospective detection of legionellosis clusters using SaTScan software (https://www.satscan.org). SaTScan is a free software program that can be used to identify disease clusters across both space and time by calculating a space-time scan statistic for every possible combination of geographic extent and length of time within specified ranges. The test statistics indicate an unusual disease cluster if the number of observed cases within each spatiotemporal window exceeds the number of expected cases (*10*,*11*). SaTScan users have to specify parameter settings to determine which clusters will be detected (*12*). Local health departments, such as the New York City (NYC) Department of Health and Mental Hygiene (DOHMH) (*10*,*13*) and the Allegheny County (Pennsylvania) Health Department (*9*), have developed automated programs to run SaTScan to detect legionellosis clusters in real time. NYC DOHMH's automated prospective cluster detection system detected a large outbreak of legionellosis associated with a cooling tower before it was identified using traditional methods (*9*,*13*).

Given the challenges in finding epidemiologic links and spatiotemporal associations among cases, we used SaTScan to develop and evaluate a semiautomated system that was successful in prospectively identifying active clusters. Here, we document the methods used to create the system and provide a technical guide and a description of the detected clusters (Tables 1, 2; Appendix, https://wwwnc.cdc.gov/EID/article/28/3/21-1147-App1.pdf).

Methods

Data Sources

SaTScan scans require a case file and coordinate file. The case file includes 1 record for each case, including their geocoded census tracts and event dates (earliest among date of illness onset, specimen collection, or report). The coordinates file includes geographic coordinates for the centroid of each census tract, identified by a unique location identification. Census blocks, counties, postal codes, or geographic units can alternatively be used as the geographic unit for coordinate files. The US Census Bureau provides geographic state census tract layers, which can be projected and displayed in ArcGIS (https://www.arcgis.com).

SaTScan Parameter Selections

SaTScan requires users to select parameters for analyses being conducted. The SaTScan user guide provides guidance on selecting parameter files (*14*). In brief, we created 4 parameter files using the SaTScan user interface and saved them in .prm format files to be used for weekly analyses. Parameter files locate the case and coordinates file names and file paths. We selected the prospective analysis and the space-time permutation model options. Prospective analysis is used to detect disease outbreaks early when analyses are conducted on a routine basis (e.g., daily, weekly). We searched only for alive clusters, defined as active clusters that must reach the study period end date.

For prospective analyses, SaTScan users can adjust analysis parameters, including the duration of study period baselines, temporal windows, time aggregation, and maximum spatial cluster sizes to optimize detecting clusters. Given the potential effects of parameter selections on results, we evaluated 4 different combinations of analysis parameters. Because of increasing legionellosis incidence in New Jersey, we conducted analyses using both 2- and 5-year study periods to establish a stable baseline. To adjust the length of baseline periods, users can define start dates. We further adjusted the temporal window size to account for clusters of varying time lengths. We conducted analyses using both 30-day (acute) and 90-day (prolonged) window sizes. We used the default maximum spatial cluster size of 50% for all analyses, to enable detection of both small and large clusters.

Finally, spatiotemporal analyses can be very computer intensive. To reduce computing time, case data can be aggregated into time intervals. For all 4 of our parameter files, we chose to aggregate data into 7-day windows to reduce data size and ease processing

Table 1. Summary of results for different parameter file selections across 3 detected and investigated community clusters, New Jersey, USA, 2019*

Cluster	County	Duration of SaTScan signal	Cluster radius size, km	Cases, no.	First RI/max RI
1	Mercer	2 weeks	2.78	3	130 d/175 d
2	Union†	6–13 weeks	6.77–6.96	8–22	184 d/8,130 y
3	Morris	4 weeks	4.59	7	3.3 y

*RI, recurrence interval.
†Because this outbreak was prolonged and geographically large and results varied based on parameter files and timing of the scan, ranges are indicated.

time. Early test runs of the different parameter files found these settings resulted in both reasonable processing times and sensitivity for detecting clusters.

Automation Process

To automate the process (Appendix), we prepared case files in SAS version 9.4 (*15*). We exported legionellosis data from CDRSS using SAS/ACCESS Interface to Oracle and used the SAS GEOCODE procedure to assign each case to a census tract of residence using a street address. We then exported a case file and used it to replace the previous week's case file of exactly the same file name. The SAS program calls open a command prompt window and points to the directory where SaTScan is located and launches it in batch mode with the 4 parameter files. Weekly analyses require that the start and end dates be changed each week relative to the current date. Although these dates can be adjusted manually in the SaTScan interface on a weekly basis, we automated this process by defining the new dates on the command prompt which overrides the start and end dates specified in the parameter file. After SaTScan completes scanning for clusters, it creates results files and saves them in standard text-based format to a file path defined within the parameter file. The SAS program generates and sends emails to users with results files attached for review.

Signal Detection and Public Health Response

Results files contain information about the detected clusters, including the location and size of the cluster, number of cases, expected number of cases, p values, and recurrence intervals. We evaluated all clusters with a recurrence interval ≥100 days, the equivalent of 1 expected false positive every 100 days, the value used by the NYC daily prospective cluster detection system (*13*). Recurrence intervals, a reciprocal of p values, are a measure of how often an observed cluster would be of that size or larger by chance (*14*). Public health departments can use recurrence intervals to minimize the number of false signals generated during a selected time period (*11*).

When a cluster with a recurrence interval ≥100 days was identified, disease investigators closely reviewed the cluster results (cluster radius, recurrence interval, and number of cases). Some clusters with short recurrence intervals (e.g., <365 days), small numbers of cases (e.g., 2 or 3), or large radii were closely monitored in subsequent weekly analyses to evaluate any changes to the cluster and other case details. Other cluster signals with longer recurrence intervals, larger numbers of cases, or smaller geographic radii spurred investigators to take immediate additional action, including reviewing details from each case investigation to determine any common exposures. If no common exposures were identified, case-patients associated with the suspected cluster were reinterviewed using the New Jersey cluster hypothesis generating questionnaire. Based on information gathered from these interviews, we considered whether further investigation and an environmental assessment were needed.

If the investigation confirmed a likely outbreak source, we removed the cases associated with the cluster from future analyses, at a time decided on a case-by-case basis; however, a general guideline was 4 weeks, roughly 2 incubation periods, after the cluster was no longer statistically significant. The cases

Table 2. Comparison of results based on parameter selection using performance measures for legionellosis clusters prospectively detected with recurrence intervals ≥100 d, New Jersey, USA, 2019*

			5-y baseline		2-y baseline	
Cluster	County	Performance measure	90-d window, parameter 1	30-d window, parameter 2	90-d window, parameter 3	30-d window, parameter 4
1	Mercer	Detected earliest		✓†		
		Longest RI		✓		
2	Union	Detected earliest	✓	✓	✓	✓†
		Longest RI	✓			
3	Morris	Detected earliest	✓			
		Longest RI	✓			

*Check marks (✓) indicate parameter files that satisfied the performance measure; blank cells indicate parameter files that did not satisfy performance measure. RI, recurrence interval.
†Smaller cluster of cases was detected 2 weeks before the other scans detected it with a RI of 184 d. RI was ≥100 d in the next weekly scan but was detected in the following weekly scan.

were removed from the case file to ensure future clusters in the same location would not be missed.

Results

We ran the SAS/SaTScan program for each week of 2018 starting January 1, and identified 3 clusters. We compared the 4 weekly results files created to assess how differences in the analysis parameters selected affected the detection of signals.

Cluster 1

The first analysis on January 1, 2019 detected a cluster with 3 cases and a recurrence interval of 130 days in Mercer County. The following week, the cluster's recurrence interval increased to 175 days (cluster 1, Table 1). Public health officials interviewed case-patients associated with the cluster but identified no common exposure among the case-patients or additional cases in the following weeks. Because of the short recurrence interval, this signal possibly represented a false positive.

Cluster 2

An analysis performed on April 17, 2019, detected a cluster of 10 cases in Union County with a recurrence interval as long as 15 years, depending on the parameter file. New Jersey Department of Health (NJDOH) requested that local health departments reinterview the case-patients using the New Jersey cluster hypothesis generating questionnaire. The interviews identified no common sources of exposure, but additional cases associated with the cluster continued to be reported. At its peak on May 15, 2019, the recurrence interval increased to 8,130 years. Ongoing weekly SaTScan analyses identified additional clusters, which were further investigated to determine whether they were part of the larger, primary cluster.

Investigators at NJDOH were able to present the SaTScan results to public health management as evidence that there was an ongoing, unexplained statistically significant increase in disease above the baseline that warranted additional public health resources. Subsequently, NJDOH requested Epi-Aid rapid epidemiologic assistance from the Centers for Disease Control and Prevention to help guide an epidemiologic and environmental investigation to determine the extent of disease and identify and mitigate any risks of continued exposure.

We identified 21 cases with illness onset dates during March 8–13, 2019; median patient age was 72 years (range 46–95 years). All patients were hospitalized, and 5 died. The investigative team identified several outdoor aerosol-generating devices determined to be conducive for *Legionella* growth. Devices identified as at-risk were required to undergo remediation to eliminate the risk of *Legionella* growth and transmission. Although we identified no definitive links, no additional cases were reported after the conclusion of the Epi-Aid.

This cluster investigation and its findings were unique. The cases occurred over a span of 11 weeks, with 0–3 cases occurring per week. The case-patients resided across 15 different municipalities, many with their own local health department. Local health departments only have access to reports of disease occurring in their jurisdiction and are therefore not aware of cases occurring in neighboring jurisdictions. SaTScan was useful for linking cases in space and time across several jurisdictions.

Cluster 3

An analysis performed on June 26, 2019, detected a cluster of 7 cases with a recurrence interval of 3.3 years in Morris County. The initial interview of the case-patients did not identify a common source of exposure. In response to the suspected cluster, case-patients were reinterviewed using the New Jersey cluster hypothesis generating questionnaire. The investigation identified 6 case-patients with illness onset during April 28–June 25, 2019, all of whom reported visiting the same hardware store during their incubation periods.

Investigators visited the hardware store to identify any potential sources of aerosolized water and discovered that a filled hot tub had been on display and operating from January through June 22, 2019. Hot tubs not appropriately treated and maintained can become contaminated with *Legionella* and are a known source of outbreaks. During the visit, investigators identified notable concerns about the operation of the hot tub including no written records to indicate what test parameters were being measured, no implementation of a draining or cleaning schedule, no written maintenance protocols, and no clear understanding by staff of the potential risk of *Legionella* growth.

Signal Detection and Parameter Comparison

Different parameter selections produced different results. Two performance measures, early detection and length of recurrence intervals, were compared across the 4 analysis parameter combinations (Table 2). Whereas shorter 30-day maximum temporal windows (which we used for parameter files 2 and 4) detected clusters earlier, longer 90-day windows captured more cases with longer recurrence intervals. For prolonged clusters, using the longer maximum temporal windows maintained statistical significance in subsequent weekly scans. In the Union County and

Morris County clusters, cases occurred over 30-day periods, suggesting ongoing but intermittent sources of exposure, likely better detected using longer temporal windows and longer baseline parameters.

Discussion

We identified 3 suspected community clusters of Legionnaires' disease in New Jersey using a semiautomated prospective cluster detection surveillance tool developed using SaTScan software. Although public health departments would possibly have detected the 3 community clusters using standard surveillance practices, they might not have been alerted to them as soon or been as promptly reactive without the strong recurrence interval signals from SaTScan. SaTScan also identified additional potential cases in clusters that were not associated by public health investigators alone. Cluster detection validated disease investigators' suspicions of a possible increase in cases in space and time and provided additional statistical support for taking resource-intensive action.

Users should select parameters on the basis of their jurisdiction's needs because those choices can meaningfully vary results (*16*). No one model will be most effective for the surveillance needs of all urban or rural, or city, county, or state jurisdictions, so investigators would benefit from piloting and exploring a variety of different options and performing continued surveillance using different parameters, baseline periods, and geographic units. NJDOH will continue to use the results from the 4 different sets of SaTScan parameters to identify possible disease clusters because they have different abilities in different contexts. It is notable that SaTScan does not adjust the recurrence interval when making multiple comparisons running different sets of SaTScan parameters simultaneously.

Allegheny County demonstrated the ability of the modified NYC program to detect simulated outbreaks except when fewer cases occurred over a longer timeframe (*9*). The slowly occurring outbreak that Allegheny County simulated was based on information from a published description of a suspected outbreak in New Jersey associated with an area of a community water system, confirmed through retrospective cluster surveillance using SaTScan (*4*). This outbreak was thought to occur over 5 years, not 163 days as simulated. Allegheny County used 1- and 2-year baseline periods, possibly not long enough to detect the cluster. Results from New Jersey when using a 5-year baseline demonstrate the ability of scans with longer baselines to detect clusters with longer recurrence interval signals, suggesting that longer baselines should be considered more often. However, using baselines >1 year long increases the risk for population shift bias, which occurs when the background population increases or decreases faster in some areas than in others, which in turn can produce biased p values.

A multistate analysis of data from SaTScan scans to detect prospective clusters missed certain cluster types, such as travel-associated clusters or those with prolonged times between cases (*8*). SaTScan is not likely to improve detection of small clusters (e.g., ≤2 cases associated with a single facility) (*8*); however, current public health surveillance methods sufficiently detect these most common types. Incorporating SaTScan-generated prospective cluster analyses as part of the New Jersey Legionnaires' disease surveillance system has enabled us to identify geographically larger clusters crossing multiple local health jurisdictions that usually require additional public health surveillance tools to verify.

Our outbreak case removal practice differed from the NYC cluster surveillance system, which removes all cases identified during the cluster period from the baseline, regardless of evidence linking them to the cluster (*13*). Although the population of NYC is similar to that of the entire state of New Jersey, the geographic coverage area is much smaller. Removing all cases statewide, even those clearly not associated with a cluster during an outbreak period, might restrict our ability to detect future prolonged clusters in other locations. However, removing all cases in an outbreak area might inadvertently remove cases unrelated to the outbreak and artificially lower the true baseline of disease, which could lead to false cluster detection in future analyses.

Legionnaires' disease diagnosis in the United States relies largely on the *Legionella* urinary antigen test (UAT), which provides rapid results for diagnosing Legionnaires' disease. However, UATs only identify infections caused by *L. pneumophila* serogroup 1, and because other *Legionella* spp. are also pathogenic, public health surveillance systems may be underdiagnosing and underreporting cases (*17*). Healthcare providers, concurrent with UAT testing of a patient, should consider collecting a respiratory specimen for *Legionella* culture or PCR tests that can identify other *Legionella* species and serogroups.

Some jurisdictions may find it practical to adapt an existing system for their surveillance needs. NYC DOHMH created a SAS program to automate daily spatiotemporal cluster detection for reportable communicable diseases (*13*), which Allegheny County modified for use in its own jurisdiction (*9*). New Jersey has a population of just under 9 million and comprises 21 counties of varying population densities—most largely urban, but some rural. Our statewide setting could provide a template to assist other states, regions,

and countries in developing their own tools to prospectively detect spatiotemporal legionellosis clusters across multiple jurisdictions. The semiautomated process developed in New Jersey (Appendix) may similarly be replicable for other jurisdictions, even by basic SAS users, without the need to include macros.

In conclusion, our prospective cluster detection system identified 3 community outbreaks of Legionnaires' disease that led to public health investigations. Prospective cluster detection can be used in conjunction with standard epidemiologic methods, which are successful at identifying environmental sources such as premise plumbing in a single facility. Using the strategies together has provided better public health response in New Jersey.

Acknowledgments

We acknowledge our state and local health colleagues for their partnership on the Legionnaires' disease outbreak investigations, especially Rebecca Greeley for her leadership and support. We also thank Sharon Greene and Alison Levin-Rector for their technical review and input in developing the SaTScan models and the drafting of this manuscript.

About the authors

Ms. Gleason received a master of science degree in public health from Emory University. She has worked as an environmental epidemiologist for the New Jersey Department of Health for 8 years, conducting research on emerging topics in drinking water, including perfluoroalkyl and polyfluoroalkyl substances (PFAS) and lead, and conducting private well outreach.

Ms. Ross received a master degree in public health from Drexel University. She has worked as an infectious disease epidemiologist for the NJDOH for 6 years and is responsible for legionellosis prevention, surveillance, and response efforts.

References

1. CDC. Legionella (Legionnaires' disease and Pontiac fever). History, burden, and trends [cited 2018 Dec 13] https://www.cdc.gov/legionella/about/history.html.
2. Fitzhenry R, Weiss D, Cimini D, Balter S, Boyd C, Alleyne L, et al. Legionnaires' disease outbreaks and cooling tow ers, New York City, New York, USA. Emerg Infect Dis. 2017;23:1769–76. https://doi.org/10.3201/eid2311.161584
3. Orkis LT, Harrison LH, Mertz KJ, Brooks MM, Bibby KJ, Stout JE. Environmental sources of community-acquired legionnaires' disease: a review. Int J Hyg Environ Health. 2018;221:764–74. https://doi.org/10.1016/j.ijheh.2018.04.013
4. Cohn PD, Gleason JA, Rudowski E, Tsai SM, Genese CA, Fagliano JA. Community outbreak of legionellosis and an environmental investigation into a community water system. Epidemiol Infect. 2015;143:1322–31. https://doi.org/10.1017/S0950268814001964
5. Zahran S, McElmurry SP, Kilgore PE, Mushinski D, Press J, Love NG, et al. Assessment of the Legionnaires' disease outbreak in Flint, Michigan. [Erratum in Proc Natl Acad Sci U S A. 2018;115:E5835.]. Proc Natl Acad Sci U S A. 2018;115:E1730–9. https://doi.org/10.1073/pnas.1718679115
6. O'Loughlin RE, Kightlinger L, Werpy MC, Brown E, Stevens V, Hepper C, et al. Restaurant outbreak of Legionnaires' disease associated with a decorative fountain: an environmental and case-control study. BMC Infect Dis. 2007;7:93. https://doi.org/10.1186/1471-2334-7-93
7. Carr R, Warren R, Towers L, Bartholomew A, Duggal HV, Rehman Y, et al.; Shropshire Outbreak Investigation Team. Investigating a cluster of Legionnaires' cases: public health implications. Public Health. 2010;124:326–31. https://doi.org/10.1016/j.puhe.2010.03.001
8. Edens C, Alden NB, Danila RN, Fill MA, Gacek P, Muse A, et al. Multistate analysis of prospective Legionnaires' disease cluster detection using SaTScan, 2011–2015. PLoS One. 2019;14:e0217632. https://doi.org/10.1371/journal.pone.0217632
9. Orkis LT, Peterson ER, Brooks MM, Mertz KJ, Harrison LH, Stout JE, et al. Simulation of Legionnaires' disease prospective spatiotemporal cluster detection, Allegheny County, Pennsylvania, USA. Epidemiol Infect. 2019;147:e29. https://doi.org/10.1017/S0950268818002789
10. Kulldorff M, Heffernan R, Hartman J, Assunção R, Mostashari F. A space-time permutation scan statistic for disease outbreak detection. PLoS Med. 2005;2:e59. https://doi.org/10.1371/journal.pmed.0020059
11. Kulldorff M, Kleinman K. Comments on 'a critical look at prospective surveillance using a scan statistic' by T. Correa, M. Costa, and R. Assunção. Stat Med. 2015;34:1094–5. https://doi.org/10.1002/sim.6430
12. Han J, Zhu L, Kulldorff M, Hostovich S, Stinchcomb DG, Tatalovich Z, et al. Using Gini coefficient to determining optimal cluster reporting sizes for spatial scan statistics. Int J Health Geogr. 2016;15:27. https://doi.org/10.1186/s12942-016-0056-6
13. Greene SK, Peterson ER, Kapell D, Fine AD, Kulldorff M. Daily reportable disease spatiotemporal cluster detection, New York City, New York, USA, 2014–2015. Emerg Infect Dis. 2016;22:1808–12. https://doi.org/10.3201/eid2210.160097
14. Kulldorf M. SaTScan™ user guide for version 9.6. 2018 [cited 2022 Jan 28]. https://www.satscan.org/cgi-bin/satscan/register.pl/SaTScan_Users_Guide.pdf
15. SAS. SAS software Version 9.4 [cited 2022 Jan 28]. https://support.sas.com
16. Gleason JA, Ross KM, Greeley RD. Analysis of population-level determinants of legionellosis: spatial and geovisual methods for enhancing classification of high-risk areas. Int J Health Geogr. 2017;16:45. https://doi.org/10.1186/s12942-017-0118-4
17. Cassell K, Gacek P, Rabatsky-Ehr T, Petit S, Cartter M, Weinberger DM. Estimating the true burden of Legionnaires' disease. Am J Epidemiol. 2019;188:1686–94. https://doi.org/10.1093/aje/kwz142

Address for correspondence: Kathleen M. Ross, New Jersey Department of Health, 135 East State Street, PO Box 369, Trenton, NJ, 08625, USA; email: kathleen.ross@doh.nj.gov

COVID-19 Vaccination Coverage, Behaviors, and Intentions among Adults with Previous Diagnosis, United States

Kimberly H. Nguyen, Jing Huang,[1] Kathrine Mansfield,[1] Laura Corlin, Jennifer D. Allen

To determine the extent of gaps in coronavirus disease (COVID-19) vaccine coverage among those in the United States with and without previous COVID-19 diagnoses, we used data from a large, nationally representative survey conducted during July 21–August 2, 2021. We analyzed vaccine receipt (≥1 dose and full vaccination) and intention to be vaccinated for 63,266 persons. Vaccination receipt was lower among those who had a prior diagnosis of COVID-19 compared to those without: >1 dose: 73% and 85%, respectively, p<0.001; full vaccination: 69% and 82%, respectively, p<0.001). Reluctance to be vaccinated was higher among those with a previous COVID-19 diagnosis (14%) than among those without (9%). These findings suggest the need to focus educational and confidence-building interventions on adults who receive a COVID-19 diagnosis during clinic visits, or at the time of discharge if hospitalized, and to better educate the public about the value of being vaccinated, regardless of previous COVID-19 infection.

The goal of the US coronavirus disease (COVID-19) vaccination campaign is to substantially reduce the overall burden of COVID-19 by preventing severe acute respiratory syndrome coronavirus (SARS-CoV-2) infections, reducing virus transmission, and reducing hospitalizations and deaths. Data from the Centers for Disease Control and Prevention (CDC) have demonstrated that the number of COVID-19 patients in intensive care units is higher in states with the lowest vaccination levels than in states with highest vaccination levels (*1*,*2*). However, as of September 10, 2021, ≈15% of US adults were not vaccinated, and 28% were not fully vaccinated (*3*).

Author affiliations: Tufts University School of Medicine, Boston, Massachusetts, USA (K.H. Nguyen, J. Huang, K. Mansfield, L. Corlin); Tufts University School of Engineering, Medford, Massachusetts, Massachusetts, USA (L. Corlin); Tufts University, Medford (J.D. Allen)

DOI: https://doi.org/10.3201/eid2803.211561

Whereas reasons for nonvaccination or undervaccination are multifactorial (*4*–*8*), studies suggest that persons with a previous diagnosis of COVID-19 are less likely to be vaccinated than are those who have not previously had COVID-19 (*9*). However, CDC recommends that persons previously infected with SARS-CoV-2 still get the vaccine (*10*). This recommendation reflects the knowledge that although the rate of reinfection among persons with previous COVID-19 illness is very low (*11*–*13*), natural immunity from infection may not provide a sufficient level of protection, particularly among the elderly (*14*). Persons who have had COVID-19 can still become severely ill if reinfected, and even those who were initially asymptomatic can have ongoing health problems several weeks or even longer after getting reinfected (long haulers) (*10*). Moreover, those who were previously infected with SARS-CoV-2 and became infected again can still transmit the infection to others (*10*). Vaccination not only protects persons who have not been previously infected but also provides a strong boost in protection for those who have recovered from COVID-19 (*10*); a growing body of evidence demonstrates added protection against reinfection for persons who were previously infected with SARS-CoV-2 when they have a higher titer of antibodies resulting from vaccination (*15*). It is vital that all persons be fully vaccinated, regardless of infection history. Without achieving this level of vaccination coverage, COVID-19 spikes and clusters will probably re-emerge in areas with low vaccination levels.

Vaccination coverage and intentions to be vaccinated among persons who had a previous diagnosis of COVID-19 is unknown. Our goals with this study were to 1) compare vaccination coverage (≥1 dose and receipt of all recommended doses) and intention to be vaccinated, by previous COVID-19 status; 2) examine

[1]These authors contributed equally to this article.

factors associated with vaccination coverage and intention to be vaccinated and reasons for nonvaccination, by previous COVID-19 status; and 3) assess the correlation between state-level prevalence of previous COVID-19 diagnoses and COVID-19 vaccination coverage, by using data from a large, nationally representative household survey. Knowing the extent of gaps in vaccination coverage among those with and without a history of COVID-19, as well as reasons for these gaps, is necessary for designing and targeting effective interventions to improve vaccine uptake at the population level.

Methods

Survey Design

To help elucidate household experiences during the COVID-19 pandemic, we examined data from the Household Pulse Survey (HPS), a large, nationally representative household survey that has been conducted by the US Census Bureau since April 2020 (*16*). The study design of the HPS has been published (*17*). We examined data collected during July 21–August 2, 2021; a total of 63,266 persons responded (response rate 6.1%) (*18*). This study was reviewed by Tufts University Health Sciences Institutional Review Board and was not considered human subjects research.

COVID-19 Questions

HPS questions cover COVID-19 diagnosis, vaccination coverage, vaccination intention, and reasons for not being vaccinated. COVID-19 diagnosis was assessed by the following question: "Has a doctor or other health care provider ever told you that you have COVID-19?" (yes/no/not sure). Because of the low numbers of responses in the not sure category (<1%), this study examined only responses for yes and no. COVID-19 vaccination receipt (≥1 dose) was assessed with the following question: "Have you received a COVID-19 vaccine?" (yes/no). Adults who reported having received ≥1 dose were asked: "Did you receive (or do you plan to receive) all required doses?" (Yes, received all required doses/Yes, plan to receive all required doses/No, don't plan to receive all required doses). Full vaccination coverage was defined as a response that all required doses have been received.

Among adults who did not receive any COVID-19 vaccinations, we assessed future vaccination intentions by asking, "Once a vaccine to prevent COVID-19 is available to you, would you... definitely, probably, be unsure about, probably not, or definitely not get(ting) a vaccine." Because the vaccination intention questions were asked only of those who were not vaccinated, assessing intention over time would show bias as more persons got vaccinated (reducing the sample size of those who are asked about intention). To reduce this potential for bias, the denominator for vaccination intention was everyone in the sample, including those who were vaccinated. We categorized unvaccinated respondents who did not definitely plan to be vaccinated as uncertain (those who probably will get vaccinated or are unsure about getting vaccinated) or reluctant (those who probably will not or definitely will not get vaccinated). Because of the low numbers of respondents who definitely would get vaccinated (<5%) and their similarities to the vaccinated group, we did not include them in this study.

Unvaccinated persons who did not report that they would definitely get vaccinated were asked about their reasons for not getting vaccinated: "Which of the following, if any, are reasons that you [probably will/are unsure about/probably won't/definitely won't] get a COVID-19 vaccine/did not receive all required doses." Response options, for which they could select all that applied: 1) "I am concerned about possible side effects of a COVID-19 vaccine," 2) "I don't know if a COVID-19 vaccine will protect me," 3) "I don't believe I need a COVID-19 vaccine," 4) "My doctor has not recommended it," 5) "I plan to wait and see if it is safe and may get it later," 6) "I am concerned about the cost of a COVID-19 vaccine," 7) "I don't trust COVID-19 vaccines," 8)" I don't trust the government," 9) "I don't think COVID-19 is that big of a threat," 10) "It's hard for me to get a COVID-19 vaccine," and 11) "Other (specify)." Respondents who reported that they were not fully vaccinated, despite already having received 1 dose, were given additional options: 1) "I believe one dose is enough to protect me," and 2) "I experienced side effects from the dose of COVID-19 vaccine received."

Sociodemographic Characteristics

We assessed the following sociodemographic characteristics:agegroup(18–49years/50–64years/≥65years, gender (male/female/transgender or other), race/ethnicity (non-Hispanic White/non-Hispanic Black/Hispanic/non-Hispanic Asian/non-Hispanic other or multiple races), educational attainment (less than high school/some college or college graduate/above college graduate), annual household income (<$35,000/$35,000–$49,999/$50,000–$74,999/≥$75,000/not reported), health insurance coverage (yes/no), number of persons in the household (1–2/3–5/≥6), and housing structure (single-family home/condominium or townhouse/multi-unit housing/other).

Analyses

We analyzed prevalence of previous COVID-19 infection overall and by sociodemographic characteristics. We determined the association between previous COVID-19 diagnosis and COVID-19 vaccination coverage (≥1 dose and receipt of all required doses) by using multivariable regression analyses adjusted for sociodemographic variables (age group, gender, race/ethnicity, educational status, annual household income, insurance status, household size, and housing structure). We also examined factors associated with COVID-19 vaccination coverage (≥1 dose and receipt of all required doses) stratified by previous COVID-19 disease status. Furthermore, intention to get vaccinated (uncertain/reluctant) was analyzed by previous COVID-19 disease status overall and by sociodemographic characteristics. We assessed factors associated with vaccination intention (uncertain/reluctant) stratified by previous COVID-19 disease status in multivariable analyses by using adjusted prevalence ratio (aPR). Reasons for not getting vaccinated were assessed by previous COVID-19 disease status. Proportions and 95% CIs for reasons for not getting vaccinated were examined by intention categories (uncertain/reluctant). We created a scatterplot of state-level prevalence of previous COVID-19 infection and vaccination coverage and determined R^2 for the correlation between the 2 variables. We conducted contrast tests for the differences in proportions, comparing each category to the referent category and comparing those who ever and never had a COVID-19 diagnosis with a 0.05 significance level ($\alpha = 0.05$). We used Stata 16.1 (*17*) to account for the survey design and weights to ensure a nationally representative sample. Unless otherwise noted, all results presented in this report are significant at $p<0.05$.

Results

Sample Characteristics

More than one half of the sample participants were 18–49 years of age, one quarter were 50–64 years, and 22% were ≥65 years (Table 1). Most (62%) were non-Hispanic White, 17% were Hispanic, 11% were non-Hispanic Black, 6% were non-Hispanic Asian, and 4% were non-Hispanic other/multiple race. More than 60% had at least some college education, 32% had annual household incomes of ≥$75,000, and most (92%) had health insurance. Half (50%) of the households had 3–5 persons living in the household, 39% had 1–2 persons, and 11% had ≥6 persons. Furthermore, 69% lived in single-family homes, 19% in a multi-unit home, 8% in a townhouse/condominium, and 5% in other settings (e.g., mobile homes, boats, vans, recreational vehicles).

COVID-19 Infection and Vaccine Receipt

Nationally, 15% of adults had a previous diagnosis of COVID-19 (Table 1). Prevalence of having a positive history of COVID-19 infection was highest among adults 18–49 years of age (17%), Hispanic adults (21%), and adults with high school education or less (16%) compared with their respective counterparts (Table 1). Moreover, respondents living in larger households were more likely to report having been infected with COVID-19 (20% among households with ≥6 persons) compared with those living in smaller households (12% among households with ≤2 persons).

Vaccination coverage (≥1 dose and full vaccination) was lower among those who ever had COVID-19 than those who had no history of COVID-19 infection (Table 2). For example, those with a history of COVID-19 were 0.88 (95% CI 0.86–0.91) times as likely to get ≥1 COVID-19 vaccination and 0.86 (95% CI 0.84–0.89) times as likely to be fully vaccinated. Across all sociodemographic characteristics, vaccination coverage (≥1 dose and full vaccination) was lower among those with a history of COVID-19 infection than among those who never had COVID-19 (Appendix Table 1, https://wwwnc.cdc.gov/EID/article/28/3/21-1561-App1.pdf). Among those with a history of COVID-19, factors associated with lower vaccination coverage (≥1 dose) were being male (aPR 0.93, 95% CI 0.88–0.99) and living in larger households (≥6 persons: aPR 0.87, 95% CI 0.77–0.99) compared with their respective counterparts. Being Hispanic (aPR 1.11, 95% CI 1.01–1.22), non-Hispanic Asian (aPR 1.21, 95% CI 1.10–1.32), having a high education level (above college degree: aPR 1.18, 95% CI 1.11–1.26), and high income (≥$75,000: aPR 1.14, 95% CI 1.05–1.25) were associated with higher vaccination coverage (≥1 dose) compared with their respective counterparts.

Across all states, prevalence of previous COVID-19 infection was inversely proportional to COVID-19 vaccination coverage ($R^2 = 0.4074$) (Figure). For example, in Mississippi, vaccination coverage was 75% and prevalence of previous COVID-19 infection was 22%, whereas in Vermont, vaccination coverage was 90% and prevalence of previous COVID-19 infection was 5%, and in Oregon, vaccination coverage was 88% and prevalence of previous COVID-19 infection was 7%.

Vaccination Intentions

Intention to get vaccinated and factors associated with vaccination also differed by previous COVID-19

Table 1. Prevalence of previous COVID-19 diagnosis among adults, by socioeconomic characteristics, United States, July 21–August 2, 2021*

Characteristic	Total, % (95% CI), N = 63,266	Ever had COVID-19 % (95% CI), n = 7,716	Never had COVID-19 % (95% CI), n = 55,186
All adults, ≥18 y		14.6 (14.1,15.2)	84.3 (83.7–84.9)
Age group, y			
18–49 (referent)	52.0 (51.7–52.3)	16.5 (15.4–17.6)	82.3 (81.2–83.4)
50–64	25.9 (25.5–26.2)	15.2 (14.2–16.2)	84.3 (83.3–85.2)
≥65	22.2 (21.9–22.4)	9.5 (8.5–10.6)†	89.1 (87.9–90.1)
Sex			
F (referent)	50.6 (50.3–50.8)	15.2 (14.5–15.9)	84.2 (83.5–84.9)
M	46.9 (46.6–47.3)	13.9 (13.0–14.9)	85.1 (84.0–86.0)
Transgender or other	2.5 (2.2–2.8)	15.3 (11.5–20.2)	73.9 (67.9–79.1)
Race/ethnicity			
Non-Hispanic White (referent)	62.4 (62,2–62.6)	13.1 (12.6–13.7)	86.4 (85.8–86.9)
Non-Hispanic Black	11.0 (10.8–11.2)	15.9 (14.2–17.8)†	82.8 (80.6–84.7)
Hispanic	17.2 (17.0–17.4)	20.8 (18.9–22.9)†	76.3 (74.1–78.4)
Non-Hispanic Asian	5.6 (5.4–5.9)	8.8 (7.2–10.6)†	90.5 (88.6–92.1)
Non-Hispanic other/multiple races	3.8 (3.5–4.0)	15.4 (12.7–18.5)	82.8 (79.6–85.6)
Education			
High school or less (referent)	38.5 (38.4–38.7)	15.9 (14.8–17.2)	82.3 (81.0–83.6)
Some college or college graduate	47.5 (47.2–47.8)	14.8 (14.1–15.4)	84.6 (83.9–85.3)
Above college graduate	14.0 (13.7–14.2)	10.3 (9.6–11.1)†	88.8 (88.0–89.5)
Annual household income			
<$35,000 (reference)	20.0 (19.3–20.7)	13.7 (12.4–15.1)	84.9 (83.4–86.2)
$35,000–$49,999	8.9 (8.5–9.3)	15.2 (13.6–16.9)	84.1 (82.4–85.7)
$50,000–$74,999	12.7 (12.2–13.2)	16.0 (14.3,18.0)†	83.1 (81.0–85.0)
≥$75,000	32.2 (31.6–32.7)	12.7 (11.9–13.4)	86.9 (86.1–87.6)
Did not report	26.3 (25.6–27.0)	16.8 (15.5–18.2)†	81.5 (79.9–82.9)
Insurance status			
Insured (reference)	91.8 (91.2–92.4)	13.6 (13.0–14.3)	85.6 (85.0–86.2)
Not insured	8.2 (7.6–8.8)	17.1 (14.0–20.6)†	79.9 (76.4–83.1)
No. persons in household			
1–2 (referent)	39.5 (38.6–40.4)	12.4 (11.8–13.0)	87.2 (86.6–87.8)
3–5	50.0 (49.2–50.7)	15.3 (14.4–16.1)†	83.9 (82.9–84.8)
≥6	10.6 (9.8–11.4)	19.8 (17.3–22.5)†	75.8 (72.9–78.5)
Housing structure			
Single-family home (referent)	68.8 (68.1–69.6)	14.0 (13.4–14.7)	85.3 (84.6–86.1)
Townhouse/condo	7.6 (7.1–8.1)	12.1 (9.6–15.1)	86.3 (83.1–89.0)
Multi-unit home	18.6 (18.0–19.3)	13.7 (12.1–15.5)	85.1 (83.2–86.8)
Other: e.g., mobile home, boat, van, RV	5.0 (4.6–5.4)	15.0 (12.8–17.4)	81.9 (79.5–84.1)

*All percentages are weighted. COVID-19, coronavirus disease; RV, recreational vehicle.
†Significant at p<0.05 comparing each group to the referent group for likelihood of having previously had COVID-19.

status (Appendix Table 2). The proportion of adults who were uncertain about vaccination was higher among those with a previous COVID-19 diagnosis (10%) than among those without (5%), and the proportion of adults who were reluctant about vaccination was higher among those with a previous COVID-19 diagnosis (14%) than among those without (9%). Across most socioeconomic characteristics, the proportion of uncertain and reluctant adults was also higher among those who ever had COVID-19 than among those who never had COVID-19. Furthermore, factors associated with being uncertain differed by COVID-19 case status. For example, being non-Hispanic Black was associated with being uncertain about getting vaccinated among those who never had COVID-19 (aPR 1.68, 95% CI 1.34–2.12) but not among those who ever had COVID-19. Furthermore, having high educational levels (above college graduate: aPR 0.29, 95% CI 0.22–0.38) and high income levels (≥$75,000: aPR 0.61, 95% CI 0.50–0.74) were associated with lower risk of being reluctant to get vaccinated, and living in larger households (≥6 persons: aPR 1.78, 95% CI 1.41–2.24) was associated with vaccination reluctance among those who never had COVID-19 but not among those who ever had

Table 2. Association between previous COVID-19 diagnosis and vaccination coverage, United States, July 21–August 2, 2021*

	Received ≥1 dose		Received all required doses	
Prior COVID-19 diagnosis†	% (95% CI)	aPR (95% CI)	% (95% CI)	aPR (95% CI)
Yes	73.3 (71.4–75.2)	0.88 (0.86–0.91)	68.9 (67.0–70.7)	0.86 (0.84–0.89)
No	84.6 (83.9–85.2)	Referent	81.6 (80.9–82.4)	Referent

*All percentages are weighted. aPR, adjusted prevalence ratio; COVID-19, coronavirus disease.
†Multivariable regression model adjusting for age group, gender, race/ethnicity, educational attainment, annual household income, insurance status, household size, and housing structure.

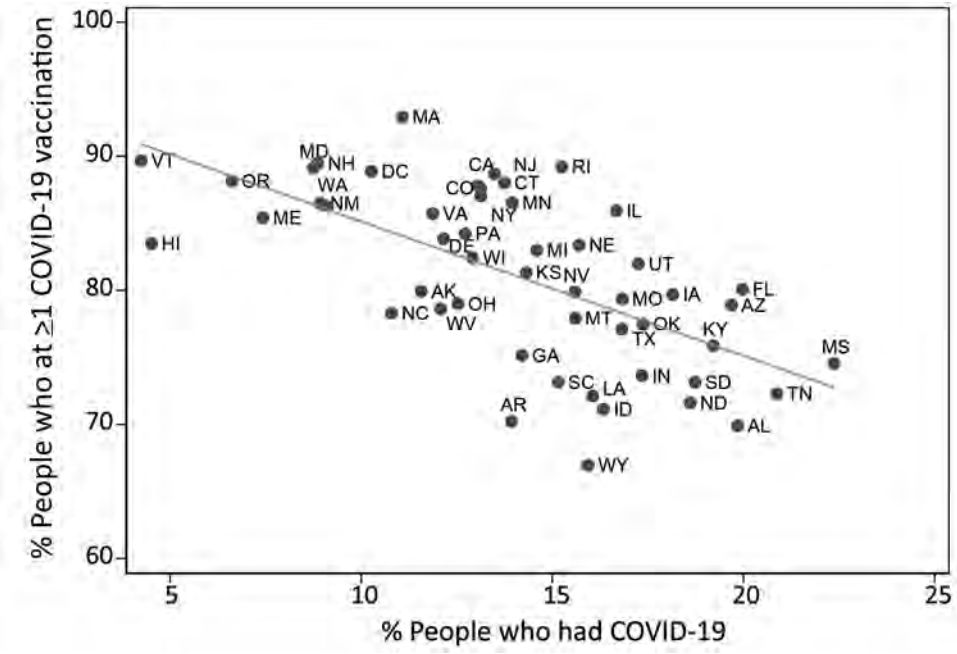

Figure. COVID-19 vaccination coverage estimates and prevalence of previous COVID-19 infection by state, United States, July 21–August 2, 2021. COVID-19, coronavirus disease.

COVID-19. Insurance status was associated with lower risk of being reluctant but did not differ by COVID-19 case history.

Reasons for not getting vaccinated differed among those with and without a previous COVID-19 diagnosis (Table 3). Among uncertain and reluctant adults, a higher percentage of respondents who ever had COVID-19, compared with those who never had COVID-19, reported concerns about possible side effects (71% vs. 57%), lack of doctor recommendation (15% vs. 9%), and other reasons (30% vs. 22%).

Discussion

Despite the availability of COVID-19 vaccines in the United States, vaccination coverage has plateaued since May 2021, and uptake remains suboptimal (*19*). Although the exact proportion of the population that must be vaccinated to attain herd immunity is debated (*20*,*21*), the current full vaccination coverage estimates found in this study (69% and 82% among those who ever or never had COVID-19, lower in some subpopulations) is probably insufficient to prevent ongoing community transmission (*20*,*21*). We found that those who have had COVID-19 were less likely to have been vaccinated with ≥1 dose or to be fully vaccinated and were more likely to be reluctant to get a future vaccination than were those who had not had the illness. This finding suggests a lack of understanding about the duration of immunity conferred by infection, as well as concerns about vaccine-associated side effects, general vaccine safety, and a lack of trust in the government. Addressing concerns about possible side effects as well as encouraging providers to have discussions about the safety and importance of vaccination may be critical for increasing coverage among this group. Regardless of sociodemographic characteristics, those who had a previous diagnosis of COVID-19 were also more likely to report uncertainty (probably/unsure) or reluctance (probably will not/definitely will not) toward vaccination. These results highlight the value of increasing vaccine uptake and confidence among those who have had the infection, particularly as new variants of SARS-CoV-2 emerge.

We found that prevalence of COVID-19 diagnoses and vaccination levels vary widely across states. In states with lowest vaccination coverage, prevalence of cases was highest. Previous studies have shown that persons in the South and Midwest were less likely to be vaccinated than were those in other areas of the United States (*9*) and that disparities in COVID-19 vaccination and intentions to be vaccinated persist among racial/ethnic groups, adults with lower incomes, and those living in rural areas (*22*–*24*). It is likely that states with low vaccination coverage have a higher proportion of persons who are hesitant toward vaccination, have higher social vulnerability, or have more access barriers (*22*–*24*). These findings point to the value of reaching these pockets of vulnerability, where the likelihood of future outbreaks is high (*25*), especially because new variants of SARS-CoV-2, such as the Delta variant, spread more easily and quickly than other variants, which may lead to increased cases, hospitalizations, and deaths from COVID-19 (*26*). CDC stated that

the 3 authorized vaccines (Pfizer-BioNTech, Moderna, and J&J/Janssen) effectively protect against the circulating variants (*10*,*27*). The public should be informed about the need for vaccination despite a history of COVID-19 infection because it remains uncertain whether infection confers immunity and, if so, the duration of protection.

Adding to the literature, we found that reluctance to get vaccinated (i.e., those who probably will not or definitely will not get vaccinated) was higher among all adults who ever had COVID-19 and by most socioeconomic characteristics. Reluctance to get vaccinated was highest among adults who were younger, identified as part of a non-Hispanic other racial/ethnic group, had lower educational attainment or lower household income, had no health insurance, lived in larger households, and lived in other transient settings (e.g., mobile homes, boats, vans, or recreational vehicles). These results suggest the need to focus interventions on groups already vulnerable to infection from COVID-19, including those living in larger households (which may be multigenerational) and adults living in transient homes.

The first limitation of our study involves representativeness of the sample. Although sampling methods and data weighting were designed to produce nationally representative results, respondents might not be fully representative of the general US adult population (*28*). Second, vaccination status and COVID-19 diagnosis were self-reported and subject to misclassification. Although prevalence of previous COVID-19 diagnosis for this sample was 15%, studies have found that >1 in 3 Americans had COVID-19 in 2020; this percentage is likely to be higher in August 2021, when the survey was conducted, suggesting that the survey responses may be underestimated (*29*). Third, because the HPS is a cross-sectional survey, temporal relationships between COVID-19 disease and vaccination cannot be assessed. Fourth, HPS data available to the public do not have information on county-level analyses, which would be useful for assessing vaccination coverage and intention at the local level. Fifth, the HPS response rate is low (<10%). However, nonresponse bias assessment conducted by the Census Bureau found that the survey weights adjusted for most of this bias. Although some bias may remain, we do not expect it to be sufficient to change the conclusions (*28*). Last, small sample sizes among adults who ever had COVID-19 may have contributed to lack of statistically significant results for some of the socioeconomic factors associated with being uncertain or reluctant.

Table 3. Reasons for not getting vaccinated, by vaccination intention and stratified by previous COVID-19 diagnosis, United States, July 21–August 2, 2021*

Reason	Ever had COVID-19, % (95% CI)	Never had COVID-19, % (95% CI), referent
Probably/unsure		
Concerned about possible side effects	70.6 (62.8–77.4)†	57.2 (52.1–62.2)
Don't know if a vaccine will protect me	20.7 (14.3–29.0)	20.5 (17.2–24.2)
Don't believe I need a vaccine	5.4 (3.0–9.5)	8.8 (6.6–11.5)
Doctor has not recommended it	5.1 (2.8–9.4)	5.9 (4.1–8.4)
Plan to wait and see if it is safe and may get it later	62.2 (54.0–69.8)	56.2 (51.3–60.9)
Concerned about the cost of the vaccine	‡	3.7 (2.5–5.4)
Don't trust COVID-19 vaccines	23.7 (17.5–31.2)	21.9 (18.9–25.2)
Don't trust the government	19.0 (11.1–30.7)	18.4 (15.1–22.2)
Don't think COVID-19 is that big of a threat	‡	5.2 (3.6–7.6)
It's hard for me to get a COVID-19 vaccine	‡	4.4 (2.7–7.1)
Other	12.5 (9.3–16.5)	11.8 (9.2–15.1)
Probably not/definitely not		
Concerned about possible side effects	51.2 (45.4–56.9)	54.9 (51.5–58.2)
Don't know if a vaccine will protect me	21.3 (17.0–26.4)	24.4 (21.7–27.2)
Don't believe I need a vaccine	36.6 (30.8–42.9)	31.0 (28.8–33.3)
Doctor has not recommended it	15.3 (11.2–20.4)†	9.4 (7.9–11.2)
Plan to wait and see if it is safe and may get it later	26.8 (22.6–31.5)	28.3 (25.7–31.0)
Concerned about the cost of the vaccine	‡	3.6 (2.3–5.4)
Don't trust COVID-19 vaccines	50.8 (45.1–56.5)	50.9 (48.0–53.7)
Don't trust the government	39.4 (33.8–45.3)	43.1 (40.4–45.9)
Don't think COVID-19 is that big of a threat	21.9 (17.4–27.2)	24.6 (22.6–26.7)
It's hard for me to get a COVID-19 vaccine	‡	2.5 (1.4–4.2)
Other	30.1 (25.0–35.8)†	21.7 (19.2–24.4)
Only received 1 of 2 doses		
I believe one dose is enough to protect me	‡	‡
I experienced side effects from the dose of COVID-19 vaccine I received	51.2 (32.6–69.4)	34.2 (24.0–46.0)

*All percentages are weighted. COVID-19, coronavirus disease.
†Significant at p<0.05 comparing ever and never had previous COVID-19 diagnosis.
‡Estimates suppressed if relative standard error >30%.

Despite COVID-19 vaccines being readily available to all Americans, many persons are still hesitant about getting vaccinated. Our finding that those with previous COVID-19 infection are less likely to be vaccinated or to complete all recommended doses suggests a strong need for direct messaging that infection does not confer reliable immunity. Although current health campaigns to improve COVID-19 vaccine uptake have successfully reached many Americans, additional efforts are needed to ensure that those with a COVID-19 history are well informed of the CDC COVID-19 vaccine recommendations. Studies have found that confidence in vaccines, weaker complacency, and collective responsibility were associated with higher likelihood of COVID-19 vaccination (*30*). The CDC strategy for reinforcing confidence in COVID-19 vaccines is to build trust in the safety and efficacy of vaccines, empower healthcare personnel to recommend vaccination to their patients, and engage communities around vaccine confidence by tailoring culturally appropriate messages and materials (*31*). This information could be emphasized to patients at the time of diagnosis, during clinical visits, and reinforced at time of hospital discharge among those who have been hospitalized. Messages should include the potential for reinfection, the role that nonvaccinated persons may play in continuing community transmission, and the potential for the emergence of additional variants of concern.

In summary, adults who have had COVID-19 are less likely to have been vaccinated than those who had not had the illness, suggesting the need to better educate the public about the importance of being vaccinated, regardless of previous COVID-19 diagnosis. Promising strategies to promote vaccination in localities with low vaccine uptake include door-to-door outreach, mobile vaccination units, vaccine offerings on public transportation and at public events, and incentives such as cash or other rewards (*32*,*33*). Studies have also shown that clear and consistent messages about the safety and effectiveness of vaccines; the protection they provide for families and communities; and the value of vaccines for returning to school, work, and social activities are needed to increase uptake and boost confidence (*5*,*9*). Building confidence in COVID-19 vaccines is critical for ensuring that communities are fully vaccinated and protected from the harmful effects of COVID-19. Reinforcing the message that the COVID-19 vaccine is needed, despite previous infection, will help protect communities against further spread of the disease, particularly as new variants emerge.

J.D.A. was supported by the Research and Scholarship Strategic Plan of the Tufts University Office of the Vice Provost for Research. L.C. was supported by Eunice Kennedy Shriver National Institute of Child Health & Human Development grant no. K12HD092535 and by the Tufts University/Tufts Medical Center COVID-19 Rapid Response Seed Funding Program.

About the Author

Dr. Nguyen is an assistant professor at Tufts University School of Medicine. Her main research areas are vaccine hesitancy and efforts to increase vaccine confidence in the United States.

References

1. Drillinger M. Here's who is being hospitalized for COVID-19 right now. Healthline [cited 2021 Dec 7]. https://www.healthline.com/health-news/heres-who-is-being-hospitalized-for-covid-19-right-now
2. US Government. COVID-19 reported patient impact and hospital capacity by state [cited 2021 Dec 7]. https://healthdata.gov/dataset/COVID-19-Reported-Patient-Impact-and-Hospital-Capa/6xf2-c3ie
3. Centers for Disease Control and Prevention. COVID-19 vaccinations in the United States [cited 2021 Dec 7]. https://covid.cdc.gov/covid-data-tracker/#vaccinations
4. Nguyen KH, Srivastav A, Razzaghi H, Williams W, Lindley MC, Jorgensen C, et al. COVID-19 vaccination intent, perceptions, and reasons for not vaccinating among groups prioritized for early vaccination—United States, September and December 2020. MMWR Morb Mortal Wkly Rep. 2021;70:217–22. https://doi.org/10.15585/mmwr.mm7006e3
5. Baack BN, Abad N, Yankey D, Kahn KE, Razzaghi H, Brookmeyer K, et al. COVID-19 vaccination coverage and intent among adults aged 18-39 years—United States, March–May 2021. MMWR Morb Mortal Wkly Rep. 2021;70:928–33. https://doi.org/10.15585/mmwr.mm7025e2
6. Dodd RH, Pickles K, Nickel B, Cvejic E, Ayre J, Batcup C, et al. Concerns and motivations about COVID-19 vaccination. Lancet Infect Dis. 2021;21:161–3. https://doi.org/10.1016/S1473-3099(20)30926-9
7. Allen JD, Feng W, Corlin L, Porteny T, Acevedo A, Schildkraut D, et al. Why are some people reluctant to be vaccinated for COVID-19? A cross-sectional survey among US adults in May–June 2020. Prev Med. 2020;24:101494.
8. Sherman SM, Smith LE, Sim J, Amlôt R, Cutts M, Dasch H, et al. COVID-19 vaccination intention in the UK: results from the COVID-19 vaccination acceptability study (CoVAccS), a nationally representative cross-sectional survey. Hum Vaccin Immunother. 2021;17:1612–21. https://doi.org/10.1080/21645515.2020.1846397
9. Nguyen KH, Nguyen KC, Corlin L, Allen J, Chung M. Changes in COVID-19 vaccination and intent, by socioeconomic characteristics and geographic area, adults ≥ 18 years, United States, January 6–March 29, 2021. Ann Med. 2021;53:1419–28.
10. Rubin R. As their numbers grow, COVID-19 "long haulers" stump experts. JAMA. 2020;324:1381–3.
11. Sheehan MM, Reddy AJ, Rothberg MB. reinfection rates among patients who previously tested positive for coronavirus disease 2019: a retrospective cohort study.

Clin Infect Dis. 2021;73:1882–6. https://doi.org/10.1093/cid/ciab234
12. Pilz S, Chakeri A, Ioannidis JP, Richter L, Theiler-Schwetz V, Trummer C, et al. SARS-CoV-2 re-infection risk in Austria. Eur J Clin Invest. 2021;51:e13520. https://doi.org/10.1111/eci.13520
13. Lumley SF, O'Donnell D, Stoesser NE, Matthews PC, Howarth A, Hatch SB, et al.; Oxford University Hospitals Staff Testing Group. Antibody status and incidence of SARS-CoV-2 infection in health care workers. N Engl J Med. 2021;384:533–40. https://doi.org/10.1056/NEJMoa2034545
14. Hansen CH, Michlmayr D, Gubbels SM, Mølbak K, Ethelberg S. Assessment of protection against reinfection with SARS-CoV-2 among 4 million PCR-tested individuals in Denmark in 2020: a population-level observational study. Lancet. 2021;397:1204–12. https://doi.org/10.1016/S0140-6736(21)00575-4
15. Ebinger JE, Fert-Bober J, Printsev I, Wu M, Sun N, Prostko JC, et al. Antibody responses to the BNT162b2 mRNA vaccine in individuals previously infected with SARS-CoV-2. Nat Med. 2021;27:981–4. https://doi.org/10.1038/s41591-021-01325-6
16. US Census Bureau. Household Pulse Survey [cited 2021 Dec 7]. https://www.census.gov/programs-surveys/household-pulse-survey.html
17. Fields JF, Hunter-Childs J, Tersine A, Sisson J, Parker E, Velkoff V, et al. Design and operation of the 2020 Household Pulse Survey, 2020 [cited 2021 Dec 7]. https://www2.census.gov/programs-surveys/demo/technical-documentation/hhp/2020_HPS_Background.pdf
18. US Census Bureau. Source of the data and accuracy of the estimate for the household pulse survey – phase 3.2 [cited 2021 Dec 7]. https://www2.census.gov/programs-surveys/demo/technical-documentation/hhp/Phase3-2_Source_and_Accuracy_Week%2034.pdf
19. Weixel N. Poll shows COVID-19 vaccine enthusiasm has reached a plateau. The Hill [cited 2021 Dec 7]. https://thehill.com/policy/healthcare/552129-poll-shows-covid-vaccine-enthusiasm-has-reached-a-plateau
20. Randolph HE, Barreiro LB. Herd immunity: understanding COVID-19. Immunity. 2020;52:737–41. https://doi.org/10.1016/j.immuni.2020.04.012
21. Fontanet A, Cauchemez S. COVID-19 herd immunity: where are we? Nat Rev Immunol. 2020;20:583–4. https://doi.org/10.1038/s41577-020-00451-5
22. Nguyen KH, Anneser E, Toppo A, Allen JD, Parott JS, Corlin L. 2021. Disparities in national and state estimates of COVID-19 vaccination receipt and intent to vaccinate by race/ethnicity, income, and age group among adults ≥18 years, United States. Vaccine. 2022;40:107–113.
23. Murthy BP, Sterrett N, Weller D, Zell E, Reynolds L, Toblin RL, et al. Disparities in COVID-19 vaccination coverage between urban and rural counties—United States, December 14, 2020–April 10, 2021. MMWR Morb Mortal Wkly Rep. 2021;70:759–64. https://doi.org/10.15585/mmwr.mm7020e3
24. Barry V, Dasgupta S, Weller DL, Kriss JL, Cadwell BL, Rose C, et al. Patterns in COVID-19 vaccination coverage, by social vulnerability and urbanicity—United States, December 14, 2020–May 1, 2021. MMWR Morb Mortal Wkly Rep. 2021;70:818–24. https://doi.org/10.15585/mmwr.mm7022e1
25. Office of the Assistant Secretary for Planning and Evaluation. Vaccine hesitancy for COVID-19: state, county, and local estimates [cited 2021 Dec 7]. https://aspe.hhs.gov/reports/vaccine-hesitancy-covid-19-state-county-local-estimates
26. Centers for Disease Control and Prevention. What you need to know about variants [cited 2021 Dec 7]. https://www.cdc.gov/coronavirus/2019-ncov/variants/variant.html
27. Sullivan P. Vaccinated people 'safe' from delta variant, do not need to wear masks. The Hill [cited 2021 Dec 7]. https://thehill.com/policy/healthcare/560871-cdc-director-vaccinated-people-safe-from-delta-variant-do-not-need-to-wear
28. US Census Bureau. Nonresponse bias report for the 2020 Household Pulse Survey [cited 2021 Dec 7]. https://www2.census.gov/programs-surveys/demo/technical-documentation/hhp/2020_HPS_NR_Bias_Report-final.pdf
29. Sen P, Yamana TK, Kandula S, Galanti M, Shaman J. Burden and characteristics of COVID-19 in the United States during 2020. Nature. 2021;598:338–41. https://doi.org/10.1038/s41586-021-03914-4
30. Kwok KO, Li KK, Tang A, Tsoi MTF, Chan EYY, Tang JWT, et al. Psychobehavioral responses and likelihood of receiving COVID-19 vaccines during the pandemic, Hong Kong. Emerg Infect Dis. 2021;27:1802–10. https://doi.org/10.3201/eid2707.210054
31. Centers for Disease Control and Prevention. Vaccinate with Confidence COVID-19 Vaccines Strategy for Adults [cited 2021 Dec 7]. https://www.cdc.gov/vaccines/covid-19/vaccinate-with-confidence/strategy.html
32. Bibbins-Domingo K, Petersen M, Havlir D. Taking vaccine to where the virus is—equity and effectiveness in coronavirus vaccinations. JAMA Health Forum 2021:2:e210213–e210213.
33. Volpp KG, Cannuscio CC. Incentives for immunity—strategies for increasing Covid-19 vaccine uptake. N Engl J Med. 2021;385:e1. https://doi.org/10.1056/NEJMp2107719

Address for correspondence: Kimberly H. Nguyen, Department of Public Health & Community Medicine, 145 Harrison Ave, Tufts University School of Medicine, Boston, MA 02111, USA; email: kimberly.nguyen@tufts.edu

Higher Viral Stability and Ethanol Resistance of Avian Influenza A(H5N1) Virus on Human Skin

Risa Bandou, Ryohei Hirose, Takaaki Nakaya, Hajime Miyazaki, Naoto Watanabe, Takuma Yoshida, Tomo Daidoji, Yoshito Itoh, Hiroshi Ikegaya

Evaluating the stability of highly pathogenic avian influenza viruses on human skin and measuring the effectiveness of disinfectants are crucial for preventing contact disease transmission. We constructed an evaluation model using autopsy skin samples and evaluated factors that affect the stability and disinfectant effectiveness for various subtypes. The survival time of the avian influenza A(H5N1) virus on plastic surfaces was ≈26 hours and on skin surfaces ≈4.5 hours, >2.5-fold longer than other subtypes. The effectiveness of a relatively low ethanol concentration (32%–36% wt/wt) against the H5N1 subtype was substantially reduced compared with other subtypes. Moreover, recombinant viruses with the neuraminidase gene of H5N1 survived longer on plastic and skin surfaces than other recombinant viruses and were resistant to ethanol. Our results imply that the H5N1 subtype poses a higher contact transmission risk because of its higher stability and ethanol resistance, which might depend on the neuraminidase protein.

Highly pathogenic subtypes of avian influenza virus (AIV) can infect humans and cause fatal respiratory failure (*1*–*3*). Since 2003, cases of avian influenza A(H5N1) and avian influenza A(H7N9) transmission from birds to humans have been confirmed in the Middle East, West Africa, Europe, and Asia. In >50% of these cases, the outcome was fatal (*4*,*5*). Recently, subtype H5N6, H5N8, and H9N2 AIVs have been confirmed to infect humans (*6*,*7*). The H5N9 subtype has also been reported to be highly transmissible (*8*). Most of these cases of AIV infection have been caused by contact transmission from infected birds (*9*–*14*). Therefore, preventing contact transmission is crucial for controlling the spread of AIV infection.

Author affiliation: Graduate School of Medical Science, Kyoto Prefectural University of Medicine, Kyoto, Japan

DOI: https://doi.org/10.3201/eid2803.211752

Knowledge of viral stability is vital to understanding contact transmission (*15*,*16*), and several studies have assessed the stability of AIVs under various conditions (*17*–*25*). Viral stability has been reported to decrease under conditions of high temperature, high salinity, or low pH (*17*,*19*,*21*–*25*). However, because contact transmission occurs when the virus enters the human body through the skin, evaluating the stability, or survival time, of AIV on human skin and the effectiveness of disinfectants against AIV on skin are essential to assess contact-transmission risks and develop more effective infection control methods (*26*–*29*). However, clinical research in this regard is limited because of the risks involved in applying highly pathogenic AIV directly to the skin of human study participants. Therefore, the stability of AIVs and the efficacy of related disinfectants remain unknown.

Moreover, although previous studies have suggested that the stability of different AIV subtypes might vary, these differences were not clearly defined (*20*–*22*,*25*). Current contact transmission control methods are based on the assumption that no great differences in stability among AIV subtypes or in the effectiveness of available disinfectants against them exist (*30*,*31*). If substantial differences exist in terms of stability and disinfectant effectiveness among subtypes, then the optimal infection control methods might differ for each subtype. Therefore, developing optimal methods for controlling the transmission of each subtype requires an accurate analysis of the differences among subtypes.

An ex vivo evaluation model using skin collected from autopsy specimens has been developed that accurately and safely assesses the stability of highly pathogenic pathogens and the effectiveness of different disinfectants (*26*–*28*). In this study, we aimed to elucidate the differences in the stability

of AIV subtypes and disinfectant efficacy against AIV on the surface of human skin by using this constructed model. Furthermore, we aimed to elucidate the genetic mechanisms responsible for stability differences among subtypes by using recombinant viruses.

Methods

Viruses

Recombinant H5N1 viruses with the neuraminidase (NA) or hemagglutinin (HA) gene of the H5N3 subtypes (rH5N1-H5N3-NA and rH5N1-H5N3-HA), or recombinant H5N3 viruses with the NA, HA, nonstructural protein (NS), or matrix protein (M) gene of the H5N1 subtypes (rH5N3-H5N1-NA, rH5N3-H5N1-NS, rH5N3-H5N1-M, and rH5N3-H5N1-HA) were generated as target viruses by using a reverse-genetics system. We evaluated the recombinant viruses A/crow/Kyoto/53/04(H5N1) (H5N1-Ky), A/chicken/Egypt/CL6/07(H5N1) (H5N1-Eg), A/Anhui/1/23(H7N9) (H7N9), A/duck/Hong Kong/820/80(H5N3) (H5N3), A/turkey/Ontario/7732/66(H5N9) (H5N9), a clinical H3N2 strain (H3N2), A/Puerto Rico/8/1934(H1N1) (H1N1-PR8), and A/Osaka/64/2009 (H1N1-Ok-pdm).

Constructing a Model to Evaluate Virus Stability and Disinfectant Effectiveness

Human skin was collected from forensic autopsy specimens obtained from the Department of Forensic Medicine, Kyoto Prefectural University of Medicine (Kyoto, Japan). Abdominal skin specimens from subjects from 20–70 years of age were cut into squares with approximate dimensions of 4 cm × 8 cm. Autopsy specimens in which the skin was considerably damaged by burning or drowning were excluded (*26*,*32*). Collected skin can reportedly be used for grafting even 24 hours after death, and within 36 hours of excision, the skin retains its physiologic function relatively well with no change in cell viability after 14 days in culture (*33*–*35*). Therefore, in this study, skin specimens were obtained at ≈1 day after death to preserve the physiologic function of the epidermis. By using the skin autopsy specimens, we developed an ex vivo model to evaluate the stability of different viruses on the surface of human skin and the effectiveness of different disinfectants against viruses on skin. Skin from which the panniculus adiposus had been removed was washed with phosphate-buffered saline (PBS) and placed in a culture insert (Corning Inc., https://www.corning.com) on a membrane with a pore size of 8.0 μm. The culture inserts were placed in six-well plates containing 1.0 mL of Dulbecco modified Eagle's medium (DMEM) (Sigma-Aldrich, https://www.sigmaaldrich.com) (*26*,*27*).

Evaluation of Viral Stability

We evaluated virus survival on plastic and human skin surfaces. Virus solutions (2.0×10^5 focus-forming units [FFUs] in 2 μL of PBS) were applied to the surface of plastic or human skin (the constructed evaluation model). Each sample was incubated in a controlled environment (25°C and 45%–55% relative humidity) for 0–24 h. The virus remaining on the surface was then collected in 1.0 mL of DMEM and titrated (*15*,*26*,*28*,*36*,*37*). The detection limit for the titer of the virus remaining on the surface was 10^1 FFUs. For each condition, we performed 3 independent experiments, and the titer values are expressed as mean ± SD of the mean. The elapsed time was used as the explanatory variable (x-axis) and the logarithmic virus titer was used as the explained variable (y-axis). Least-squares linear-regression analysis was performed by using a logarithmic link function to create regression curves for both viruses. Because the detection limit of each influenza virus titer was 10^1 FFUs, the X value (when the Y value of the regression curve was 1.0) was used as the survival time. The half-life of each virus was calculated from the slope of each regression curve when the amount of virus remaining on the surface was 2, 3, or 4 $\log_{10}$ FFUs (*26*,*28*).

Evaluation of Disinfectant Effectiveness

We evaluated the effectiveness of available disinfectants against influenza viruses. The disinfectants evaluated were 20%, 32%, 34%, 36%, 40%, 60%, and 80% (wt/wt) ethyl alcohol (EA); 70% (wt/wt) isopropanol (IPA); 0.05% and 0.2% (wt/vol) benzalkonium chloride (BAC); and 0.2% and 1.0% (wt/vol) chlorhexidine gluconate (CHG).

In a 1.5-mL tube, we mixed 5 μL of PBS containing either avian or human influenza virus (4.0×10^5 FFUs) with 95 μL of various disinfectants for 15 or 60 s. Subsequently, we neutralized the resulting solutions with 900 μL of Soybean–Casein Digest Broth prepared with Lecithin and Polysorbate 80 (SCLDP) medium. Thereafter, we added 3 mL of DMEM to the neutralized solution and measured the remaining viral titers (*27*,*38*–*40*). The detection limit for the virus titers was $10^{1.6}$ FFUs.

We used the same disinfectants for in vitro evaluations and ex vivo evaluations. We applied each virus solution (2 μL of PBS containing 2.0×10^5 FFUs of virus) to the skin specimens (the constructed evaluation model), then incubated each skin sample for 15 min at 25°C under 45%–55% relative humidity to completely

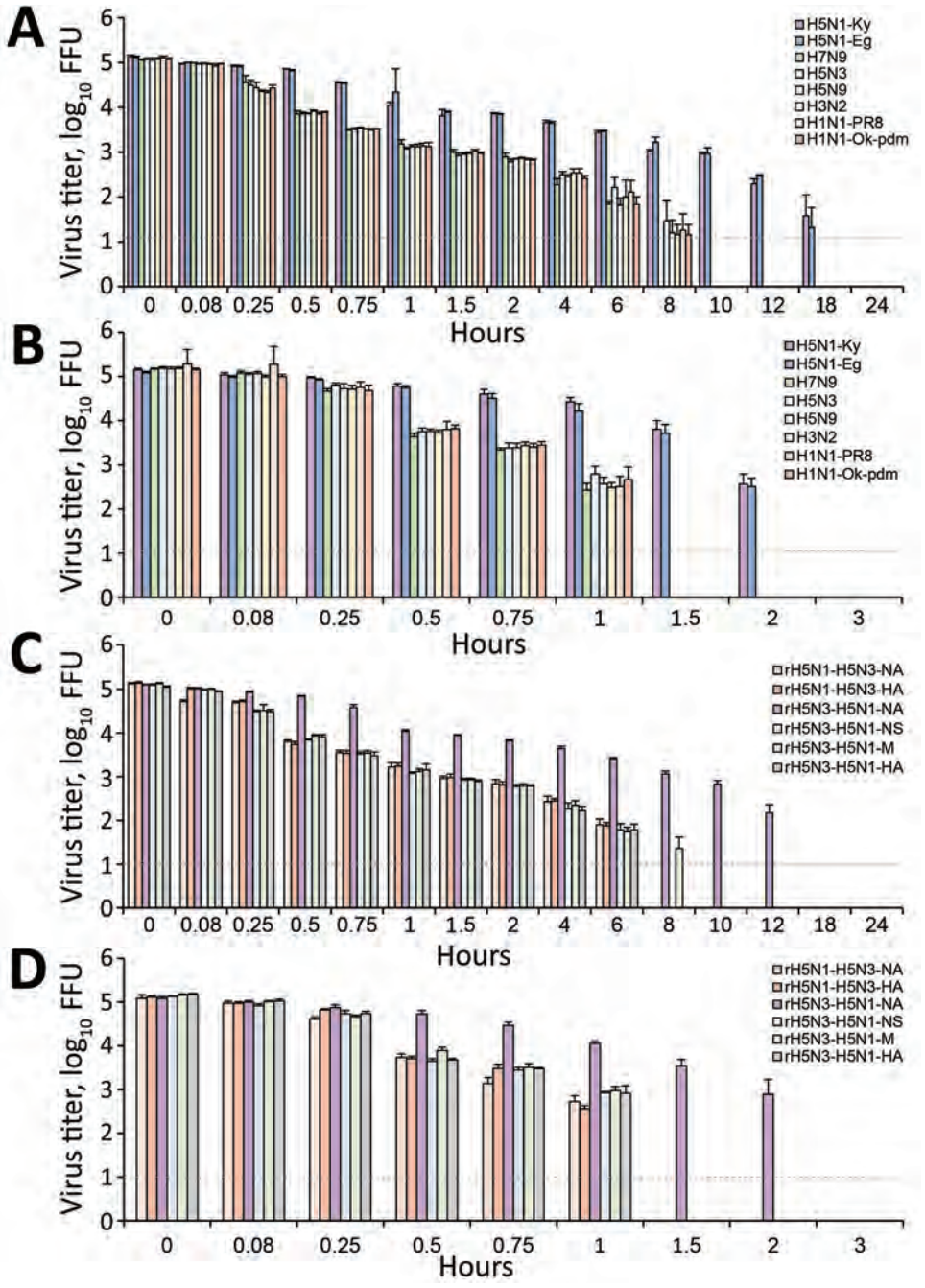

Figure 1. Decrease in titers of influenza virus on plastic (A, C) and the human skin (B, D) surfaces as a function of time. Various subtypes of influenza viruses (A, B) and recombinant viruses (C, D) were targeted. Each virus (2.0×10^5 FFUs) was mixed with 2 μL of phosphate-buffered saline and applied on each surface. Each surface was incubated in a controlled environment (temperature 25°C, humidity 45%–55%) for 0–24 h. The virus on the surface was then recovered in 1 mL of medium and titrated to calculate the titer of virus remaining on the surface. For each condition, 3 independent experiments were performed; results are expressed as mean ± SD of the mean. Dotted horizontal lines represent detection limit titers; data below this limit were omitted. Data are shown for H5N1-Ky, A/crow/Kyoto/53/04 (H5N1); H5N1-Eg, A/chicken/Egypt/CL6/07 (H5N1); H7N9, A/Anhui/1/23 (H7N9); H5N3, A/duck/Hong Kong/820/80 (H5N3); H5N9, A/turkey/Ontario/7732/66 (H5N9); H3N2, a clinical strain (H3N2); H1N1-PR8, A/Puerto Rico/8/1934 (H1N1); and H1N1-Ok-pdm, A/Osaka/64/2009 (H1N1). A/crow/Kyoto/53/04 (H5N1) was recombined with the neuraminidase or hemagglutinin gene of AdDuck/Hong Kong/820/80 (H5N3), and the recombinant viruses were designated as rH5N1-H5N3-NA or rH5N1-H5N3-HA, respectively. In addition, A/Duck/Hong Kong/820/80 (H5N3) was recombined with the neuraminidase, nonstructural protein, matrix protein, or hemagglutinin gene of A/crow/Kyoto/53/04 (H5N1), and the recombinant viruses were designated as rH5N3-H5N1-NA, rH5N3-H5N1-NS, rH5N3-H5N1-M, or rH5N3-H5N1-HA. FFU, focus-forming unit.

dry the viral mixture on the skin. Subsequently, we immersed each skin sample surface in 1 mL of the disinfectant for 15 or 60 s and then air-dried for 5 min. After drying, we recovered the remaining viruses on the skin with 250 μL of SCDLP and 750 μL of DMEM and measured the remaining viral load (*26*,*27*). The detection limit for the virus titers was 10^1 FFUs.

To determine the effectiveness of the disinfectants under each condition, we calculated logarithmic reductions of the virus titers with normalization to the PBS control. We performed 3 independent experiments for each condition, and the results are expressed as mean ± SD of the mean (Appendix, https://wwwnc.cdc.gov/EID/article/28/3/21-1752-App1.pdf). The research protocol,

including the sampling method, was reviewed and approved by the Institutional Review Board of Kyoto Prefectural University of Medicine (approval no. ERB-C-1593).

Results

Stability of Influenza Virus on Plastic

All influenza virus subtypes except for H5N1 were completely inactive within 10 hours. In contrast, the H5N1 subtype strains tested (H5N1-Ky and H5N1-Eg) remained infectious on the plastic surface after 10 hours but were completely inactive within 24 hours. In addition, the titers of H5N1-Ky and H5N1-Eg remaining on the plastic surface were significantly higher than those of other subtypes at most time points (Figure 1, panel A).

Next, we calculated the survival times and half-lives of the virus titers for the virus samples remaining on the surface. The survival times of all subtypes (except for the H5N1 subtype) were ≈8–10 hours. For example, the survival time of the H5N3 subtype was 10.01 (95% CI 8.35–11.91) hours. In contrast, the survival time of H5N1-Ky was 26.35 (95% CI 23.84–29.01) hours and survival time of H5N1-Eg was 26.30 (95% CI 23.64–29.14) hours, both significantly longer than those for other subtypes (Table 1; Figure 2, panel A). Moreover, the half-lives of the H5N1-Ky and H5N1-Eg strains were more than twice as long as those of other subtypes (Table 1; Figure 2, panel B).

Stability of Influenza Virus on Human Skin Surface

All subtypes (except H5N1) were completely inactive within 1.5 hours. In contrast, the H5N1-Ky and H5N1-Eg stains remained active on the skin even after 1.5 hours but were completely inactive within 3 hours. In addition, the titers of H5N1-Ky and H5N1-Eg remaining on the skin were substantially higher than those of other subtypes (Figure 1, panel B).

The survival times of all subtypes (except H5N1) were ≈2 hours. For example, the survival time of the H5N3 subtype was 2.10 (95% CI 1.94–2.26) hours. In contrast, the survival time of H5N1-Ky was 4.66 (95% CI 4.21–5.13) hours and survival time of H5N1-Eg was 4.54 (95% CI 4.16–4.97) hours, both of which were significantly longer than those of the other subtypes studied (Table 2; Figure 2, panel C). Furthermore, the half-life showed the same tendency as the survival time, and the half-lives of H5N1-Ky and H5N1-Eg were more than twice as long as those of other subtypes (Table 2; Figure 2, panel D).

Disinfectant Effectiveness against Influenza Virus (In Vitro Evaluations)

All influenza viruses were completely inactivated (below the detection limit) within 15 seconds by treatment with 40%, 60%, or 80% EA or 70% IPA (log reductions in titers were >4). However, all viruses were not inactivated by 20% EA (log reduction <1). Of note, although all subtypes except for H5N1 were completely inactivated within 15 seconds by 36% EA (log reduction >4), the disinfectant effectiveness of 36% EA against H5N1-Ky and H5N1-Eg was substantially low (log reduction <3) (Table 3; Appendix Table 1).

CHG and BAC were less effective than EA and IPA. The effectiveness of 0.2% GCH was low for all influenza viruses (log reduction <1), and 1.0% GCH was more effective than 0.2% GCH. BAC was more effective against all influenza viruses than CHG, and its effectiveness increased with increasing concentrations and disinfection times. In particular, treatment with 0.2% BAC for 15 seconds showed a log reduction value of >2.5, whereas the log reduction was >3.5 after a 60-second treatment (Table 3; Appendix Table 1).

Table 1. Survival times and half-lives of various subtypes of influenza viruses on a plastic surface*

Subtype	Median survival time (95% CI), h†	Median half-life (95% CI), h‡		
		4 (log_{10} FFU)	3 (log_{10} FFU)	2 (log_{10} FFU)
H5N1-Ky	26.35 (23.84–29.01)	1.28 (1.15–1.43)	1.71 (1.54–1.91)	2.56 (2.30–2.86)
H5N1-Eg	26.30 (23.64–29.14)	1.27 (1.13–1.43)	1.69 (1.51–1.90)	2.54 (2.27–2.85)
H7N9	7.97 (6.82–9.27)	0.40 (0.34–0.49)	0.54 (0.45–0.65)	0.81 (0.67–0.98)
H5N3	10.01 (8.35–11.91)	0.52 (0.42–0.65)	0.70 (0.57–0.87)	1.05 (0.85–1.30)
H5N9	8.88 (7.67–10.23)	0.46 (0.39–0.55)	0.61 (0.51–0.73)	0.92 (0.77–1.09)
H3N2	9.28 (7.94–10.79)	0.48 (0.40–0.58)	0.64 (0.54–0.77)	0.96 (0.80–1.16)
H1N1-PR8	9.70 (8.29–11.30)	0.51 (0.42–0.61)	0.68 (0.56–0.82)	1.01 (0.85–1.22)
H1N1-Ok-pdm	8.78 (7.60–10.10)	0.45 (0.38–0.54)	0.60 (0.51–0.72)	0.91 (0.76–1.08)

*FFU, focus-forming units; H5N1-Ky, A/crow/Kyoto/53/04 (H5N1); H5N1-Eg, A/chicken/Egypt/CL6/07 (H5N1); H7N9, A/Anhui/1/23 (H7N9); H5N3, A/Duck/Hong Kong/820/80 (H5N3); H5N9, A/Turkey/Ontario/7732/66 (H5N9); H3N2, Clinical strain (H3N2); H1N1-PR8, A/Puerto Rico /8/1934 (H1N1); H1N1-Ok-pdm, A/Osaka/64/2009 (H1N1).

†The elapsed time was used as the explanatory variable (x-axis), and the logarithmic virus titer was used as the explained variable (y-axis). A linear regression analysis with logarithmic link function was performed for each virus to create a curve of regression (Appendix Figure 1, https://wwwnc.cdc.gov/EID/article/28/3/21-1752-App1.pdf). Because the detection limit of each influenza virus titer was 10^1 FFUs, the X value (when the Y value of the regression curve was 1.0) was used as the survival times.

‡The half-life of each virus was calculated from the slope of each regression curve when the amount of virus remaining on the surface was 2, 3, or 4 log_{10} FFUs.

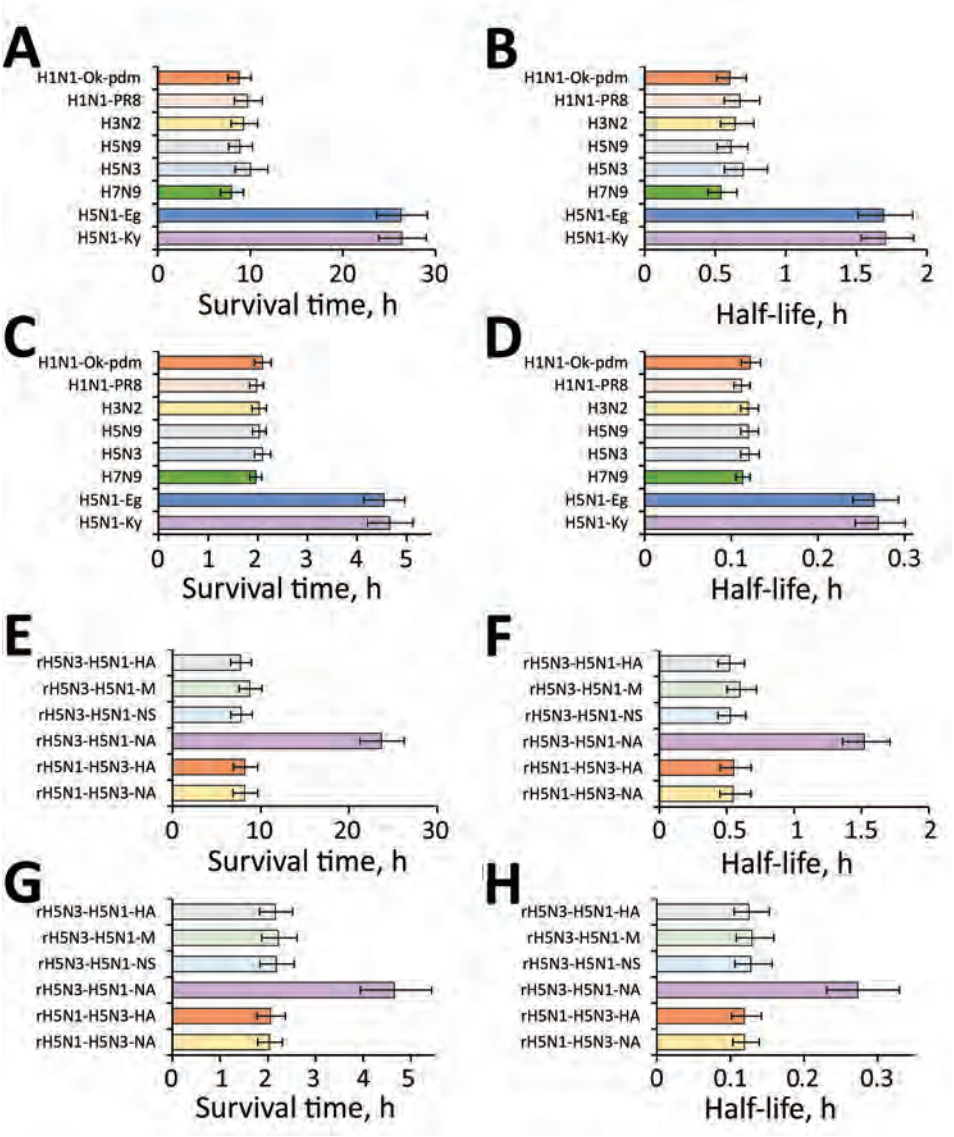

Figure 2. Survival times and half-lives of influenza viruses on plastic and human skin. A, B) Survival times (A) and half-lives (B) of various subtypes of influenza viruses on a plastic surface (Table 1). C, D) Survival times (C) and half-lives (D) of various subtypes of influenza viruses on the surface of human skin (Table 2). E, F) Survival times (E) and half-lives (F) of various recombinant viruses on plastic surfaces (Table 3). G, H) Survival times (G) and half-lives H) of various recombinant viruses on the surface of human skin (Table 4). Survival time is defined as the time until virus on the surface is no longer detected. All half-lives in the graphs refer to the half-life when 10^3 focus-forming units of virus remained on the skin surface. Data are expressed as median ± 95% CI. Data are presented for H5N1-Ky, A/crow/Kyoto/53/04 (H5N1); H5N1-Eg, A/chicken/Egypt/CL6/07 (H5N1); H7N9, A/Anhui/1/23 (H7N9); H5N3, A/duck/Hong Kong/820/80 (H5N3); H5N9, A/turkey/Ontario/7732/66 (H5N9); H3N2, a clinical strain (H3N2); H1N1-PR8, A/Puerto Rico/8/1934 (H1N1); and H1N1-Ok-pdm, A/Osaka/64/2009 (H1N1). A/crow/Kyoto/53/04 (H5N1) was recombined with the neuraminidase or hemagglutinin gene of A/Duck/Hong Kong/820/80 (H5N3), and the recombinant viruses were designated as rH5N1-H5N3-NA or rH5N1-H5N3-HA. In addition, A/Duck/Hong Kong/820/80 (H5N3) was recombined with the neuraminidase, nonstructural protein, matrix protein, or hemagglutinin gene of A/crow/Kyoto/53/04 (H5N1), and the recombinant viruses were designated as rH5N3-H5N1-NA, rH5N3-H5N1-NS, rH5N3-H5N1-M, or rH5N3-H5N1-HA.

Effectiveness of Disinfectants against Influenza Virus on Human Skin (Ex Vivo Evaluations)

All viruses were completely inactivated on the skin surface within 15 seconds after treatment with 40%, 60%, or 80% EA or 70% IPA (log reduction >4). However, all viruses were barely inactivated by 20% EA (log reduction <1). Of note, although all subtypes except H5N1 were completely inactivated within 15 seconds by 36% EA (log reduction >4), the disinfectant effectiveness of 36% EA against H5N1-Ky and H5N1-Eg was substantially lower (log reduction <2) (Table 4; Appendix Table 2).

CHG and BAC were less effective than EA and IPA. The effectiveness of CHG against all influenza viruses on human skin was higher than the in vitro disinfection effectiveness, and it increased as the CHG concentration and disinfection time increased. In particular, treatment with 1.0% CPG for 15 seconds showed log-reduction values of >2, and treatment with 1.0% CPG for 60 seconds showed log-reduction values of >2.5. In addition, BAC was more effective against all influenza viruses than CHG, and its effectiveness increased with increasing concentrations and disinfection times. Specifically, the log-reduction values after treatment with 0.2% BAC for 15 seconds and 60 seconds were >2.5 and >3.0 (Table 4; Appendix Table 2).

Table 2. Survival times and half-lives of various subtypes of influenza viruses on the surface of human skin*

Subtype	Median survival time (95% CI), h†	Median half-life (95% CI), h‡		
		4 (log_{10} FFU)	3 (log_{10} FFU)	2 (log_{10} FFU)
H5N1-Ky	4.66 (4.21–5.13)	0.20 (0.18–0.23)	0.27 (0.24–0.30)	0.40 (0.36–0.45)
H5N1-Eg	4.54 (4.14–4.97)	0.20 (0.18–0.22)	0.26 (0.24–0.29)	0.40 (0.36–0.44)
H7N9	1.96 (1.84–2.08)	0.08 (0.08–0.09)	0.11 (0.11–0.12)	0.17 (0.16–0.18)
H5N3	2.10 (1.94–2.26)	0.09 (0.08–0.10)	0.12 (0.11–0.13)	0.18 (0.17–0.20)
H5N9	2.03 (1.89–2.17)	0.09 (0.08–0.09)	0.12 (0.11–0.13)	0.18 (0.16–0.19)
H3N2	2.03 (1.89–2.17)	0.09 (0.08–0.10)	0.12 (0.11–0.13)	0.18 (0.16–0.19)
H1N1-PR8	1.97 (1.83–2.12)	0.08 (0.08–0.09)	0.11 (0.10–0.12)	0.17 (0.15–0.18)
H1N1-Ok-pdm	2.10 (1.93–2.27)	0.09 (0.08–0.10)	0.12 (0.11–0.13)	0.18 (0.17–0.20)

*FFU, focus-forming unit; H5N1-Ky, A/crow/Kyoto/53/04 (H5N1); H5N1-Eg, A/chicken/Egypt/CL6/07 (H5N1); H7N9, A/Anhui/1/23 (H7N9); H5N3, A/Duck/Hong Kong/820/80 (H5N3); H5N9, A/Turkey/Ontario/7732/66 (H5N9); H3N2, Clinical strain (H3N2); H1N1-PR8, A/Puerto Rico /8/1934 (H1N1); H1N1-Ok-pdm, A/Osaka/64/2009 (H1N1).
†The elapsed time was used as the explanatory variable (x-axis), and the logarithmic virus titer was used as the explained variable (y-axis). A linear regression analysis with logarithmic link function was performed for each virus to create a curve of regression (Appendix Figure 2, https://wwwnc.cdc.gov/EID/article/28/3/21-1752-App1.pdf). Because the detection limit of each influenza virus titer was 10^1 FFUs, the X value (when the Y value of the regression curve was 1.0) was used as the survival times.
‡The half-life of each virus was calculated from the slope of each regression curve when the amount of virus remaining on the surface was 2, 3, or 4 log_{10} FFUs.

Stability of Recombinant Viruses on Plastic and Human Skin Surfaces

Although all recombinant viruses (except rH5N3-H5N1-NA) became inactive on the plastic surface within 10 hours, rH5N3-H5N1-NA survived considerably longer than 10 hours. In addition, the titer of rH5N3-H5N1-NA remaining on the plastic surface was significantly higher than that of the other recombinant viruses at most time points (Figure 1, panel C). The survival times of the recombinant viruses (except for rH5N3-H5N1-NA) were ≈8 hours. For example, the survival time of rH5N1-H5N3NA was 8.15 (95% CI 6.86–9.62) hours. In contrast, the survival time of rH5N3-H5N1-NA was 23.68 (95% CI 21.68–26.25) hours, which was significantly longer than survival time of the other recombinant viruses tested (Table 5; Figure 2, panel E). Furthermore, half-lives showed the same tendency as survival times, and the half-life of rH5N3-H5N1-NA was more than twice that of other recombinant viruses (Table 5; Figure 2, panel F).

Although all recombinant viruses (except rH5N3-H5N1-NA) became inactive on the human skin within 1.5 hours, rH5N3-H5N1-NA remained infective for considerably longer. Moreover, the titer of rH5N3-H5N1-NA remaining on the skin was significantly higher than that of other recombinant viruses at most time points (Figure 1, panel D). The survival times of recombinant viruses (except rH5N3-H5N1-NA) was ≈2.2 hours. For example, the survival time of rH5N1-H5N3NA was 2.04 (95% CI 1.79–2.31) hours. In contrast, the survival time of rH5N3-H5N1-NA was 4.65 (95% CI 3.94–5.43) hours, which was significantly longer than other recombinant viruses (Table 6; Figure 2, panel G). In addition, half-lives showed the same tendency as survival times, and the half-life of rH5N3-H5N1-NA was more than twice that of other recombinant viruses (Table 6; Figure 2, panel H).

Disinfectant Effectiveness of a Relatively Low EA Concentration against Recombinant Viruses

Both in vitro and ex vivo evaluations demonstrated that all recombinant viruses were completely

Table 3. Results of in vitro evaluations of disinfectant effectiveness against various subtypes of influenza viruses*

Disinfectant	log reduction, mean							
	H5N1-Ky	H5N1-Eg	H7N9	H5N3	H5N9	H3N2	H1N1-PR8	H1N1-Ok-pdm
80% EA	>4.00	>4.00	>4.00	>4.00	>4.00	>4.00	>4.00	>4.00
60% EA	>4.00	>4.00	>4.00	>4.00	>4.00	>4.00	>4.00	>4.00
40% EA	>4.00	>4.00	>4.00	>4.00	>4.00	>4.00	>4.00	>4.00
36% EA	2.57	1.77	>4.00	>4.00	>4.00	>4.00	>4.00	>4.00
34% EA	0.29	0.28	1.60	1.54	1.54	1.46	1.53	1.48
32% EA	0.11	0.16	0.23	0.20	0.27	0.23	0.23	0.21
20% EA	0.03	0.04	0.10	0.10	0.13	0.04	0.09	0.04
70% IPA	>4.00	>4.00	>4.00	>4.00	>4.00	>4.00	>4.00	>4.00
0.2% CHG	0.43	0.42	0.58	0.54	0.66	0.52	0.55	0.65
1.0% CHG	1.05	1.35	1.17	1.54	1.59	1.47	1.52	1.53
0.05% BAC	1.66	1.63	1.70	2.03	2.48	1.88	2.00	2.15
0.2% BAC	3.13	3.11	2.97	3.35	3.50	3.27	2.95	3.42

*Reaction time with disinfectant was 15 seconds. Detailed data are presented in Appendix Table 1 (https://wwwnc.cdc.gov/EID/article/28/3/21-1752-App1.pdf). Log reduction value was calculated to evaluate disinfectant effectiveness under each condition and was expressed as mean. In addition, log reduction value of the condition wherein the virus was inactivated below the measurement limit ($10^{1.6}$ FFUs) was 4 or more and was expressed as >4.00. BAC, benzalkonium chloride; CHG, chlorhexidine gluconate; EA, ethyl alcohol; H5N1-Ky, A/crow/Kyoto/53/04 (H5N1); H5N1-Eg, A/chicken/Egypt/CL6/07 (H5N1); H7N9, A/Anhui/1/23 (H7N9); H5N3, A/Duck/Hong Kong/820/80 (H5N3); H5N9, A/Turkey/Ontario/7732/66 (H5N9); H3N2, Clinical strain (H3N2); H1N1-PR8, A/Puerto Rico /8/1934 (H1N1); H1N1-Ok-pdm, A/Osaka/64/2009 (H1N1); IPA, isopropanol.

Table 4. Results of ex vivo evaluations of disinfectant effectiveness of disinfectants against various subtypes of influenza viruses on the surface of human skin*

Disinfectant	log reduction, mean							
	H5N1-Ky	H5N1-Eg	H7N9	H5N3	H5N9	H3N2	H1N1-PR8	H1N1-Ok-pdm
80% EA	>4.00	>4.00	>4.00	>4.00	>4.00	>4.00	>4.00	>4.00
60% EA	>4.00	>4.00	>4.00	>4.00	>4.00	>4.00	>4.00	>4.00
40% EA	>4.00	>4.00	>4.00	>4.00	>4.00	>4.00	>4.00	>4.00
36% EA	1.71	1.61	>4.00	>4.00	>4.00	>4.00	>4.00	>4.00
34% EA	1.39	1.32	2.59	2.56	2.54	2.26	2.46	2.61
32% EA	1.17	1.14	2.20	2.18	2.18	2.31	2.21	2.18
20% EA	0.84	0.82	0.04	0.84	0.81	0.65	0.83	0.82
70% IPA	>4.00	>4.00	>4.00	>4.00	>4.00	>4.00	>4.00	>4.00
0.2% CHG	1.16	1.12	0.88	1.16	0.95	0.89	1.05	0.94
1.0% CHG	2.76	2.68	3.02	2.90	2.95	2.78	2.98	2.95
0.05% BAC	1.81	1.74	1.78	1.80	1.78	1.66	1.86	1.84
0.2% BAC	3.10	3.02	3.26	3.12	3.09	2.73	2.98	3.16

*Reaction time with disinfectant was 15 seconds. Detailed data are presented in Appendix Table 2 (https://wwwnc.cdc.gov/EID/article/28/3/21-1752-App1.pdf). Log reduction value was calculated to evaluate disinfectant effectiveness under each condition and was expressed as mean. In addition, the log reduction value of the condition wherein the virus was inactivated below the measurement limit (10^1 FFUs) was 4 or more and was expressed as >4.00. BAC, benzalkonium chloride; CHG, chlorhexidine gluconate; EA, ethyl alcohol; H5N1-Ky, A/crow/Kyoto/53/04 (H5N1); H5N1-Eg, A/chicken/Egypt/CL6/07 (H5N1); H7N9, A/Anhui/1/23 (H7N9); H5N3, A/Duck/Hong Kong/820/80 (H5N3); H5N9, A/Turkey/Ontario/7732/66 (H5N9); H3N2, Clinical strain (H3N2); H1N1-PR8, A/Puerto Rico /8/1934 (H1N1); H1N1-Ok-pdm, A/Osaka/64/2009 (H1N1); IPA, isopropanol.

inactivated within 15 seconds by treatment with ≥40% EA (log reduction >4). Furthermore, although all recombinant viruses (except rH5N3-H5N1-NA) were completely inactivated within 15 seconds by treatment with 36% EA (log reduction >4), 36% EA was substantially less effective against rH5N3-H5N1-NA (log reduction <2). Thus, rH5N3-H5N1-NA was resistant to relatively low EA concentrations (Figure 3; Appendix Table 3).

Discussion

Previous studies have suggested that the stability of AIVs might vary among subtypes, but the details remain unknown (*20*–*22*,*25*). In this study, we first evaluated the stability (survival time and half-life) of several influenza subtypes on plastic and human skin surfaces and clarified the differences in their stability. No significant differences were observed in the survival times and half-lives of most subtypes. However, the survival times and half-lives of 2 different H5N1 strains (H5N1-Ky and H5N1-Eg) on plastic and skin surfaces were approximately twice as long as those of the other subtypes tested, indicating that the H5N1 subtype had significantly higher stability. These findings suggest that the H5N1 subtype poses a higher risk for contact transmission than other subtypes. Specifically, the higher stability of the H5N1 subtype might be a reason that among AIVs, the H5N1 subtype is often transmitted from birds to humans. In addition, because the 4-hour survival time of the H5N1 subtype on human skin increases the risk for viral invasion into the body or for transmission from the skin to other surfaces, appropriate hand hygiene practices are especially vital (compared with other subtypes) for preventing contact transmission of this subtype. Furthermore, the survival times revealed in this study will help determine the interval during which contact transmission could occur and how contact transmission might be established.

Next, we evaluated the effectiveness of disinfectants against influenza viruses on the skin surface by using our ex vivo evaluation model that reproduced

Table 5. Survival times and half-lives of various recombinant viruses on a plastic surface*

Subtype†	Median survival time (95% CI), h‡	Median half-life (95% CI), h§		
		4 (log_{10} FFU)	3 (log_{10} FFU)	2 (log_{10} FFU)
rH5N1-H5N3-NA	8.15 (6.86–9.62)	0.41 (0.34–0.51)	0.55 (0.45–0.68)	0.82 (0.67–1.02)
rH5N1-H5N3-HA	8.17 (6.88–9.63)	0.41 (0.34–0.51)	0.55 (0.45–0.68)	0.83 (0.68–1.02)
rH5N3-H5N1-NA	23.68 (21.26–26.25)	1.14 (1.02–1.28)	1.52 (1.36–1.71)	2.28 (2.04–2.57)
rH5N3-H5N1-NS	7.74 (6.59–9.03)	0.39 (0.33–0.48)	0.53 (0.44–0.64)	0.79 (0.65–0.96)
rH5N3-H5N1-M	8.75 (7.52–10.11)	0.45 (0.38–0.54)	0.60 (0.50–0.72)	0.90 (0.75–1.08)
rH5N3-H5N1-HA	7.69 (6.59–8.93)	0.39 (0.33–0.47)	0.52 (0.44–0.63)	0.78 (0.65–0.95)

*FFU, focus-forming unit.
†A/crow/Kyoto/53/04 (H5N1) recombined with the NA and HA genes of A/Duck/Hong Kong/820/80 (H5N3) are defined as rH5N1-H5N3-NA and rH5N1-H5N3-HA. In addition, A/Duck/Hong Kong/820/80 (H5N3) recombined into the NA, NS, M, and HA genes of A/crow/Kyoto/53/04 (H5N1) was defined as rH5N3-H5N1-NA, rH5N3-H5N1-NS, rH5N3-H5N1-M, rH5N3-H5N1-HA.
‡The elapsed time was used as the explanatory variable (x-axis), and the logarithmic virus titer was used as the explained variable (y-axis). A linear regression analysis with logarithmic link function was performed for each virus to create a curve of regression (Appendix Figure 3, https://wwwnc.cdc.gov/EID/article/28/3/21-1752-App1.pdf). Because the detection limit of each influenza virus titer was 10^1 FFUs, the X value (when the Y value of the regression curve was 1.0) was used as the survival time.
§The half-life of each virus was calculated from the slope of each regression curve when the amount of virus remaining on the surface was 2, 3, or 4 log_{10} FFUs.

Table 6. Survival time and half-lives of various recombinant viruses on the surface of human skin*

Subtype†	Median survival time (95% CI), h‡	Median half-life (95% CI), h‡		
		4 (log_{10} FFU)	3 (log_{10} FFU)	2 (log_{10} FFU)
rH5N1-H5N3-NA	2.04 (1.79–2.31)	0.09 (0.08–0.10)	0.12 (0.10–0.14)	0.18 (0.15–0.21)
rH5N1-H5N3-HA	2.06 (1.77–2.37)	0.09 (0.08–0.11)	0.12 (0.10–0.14)	0.18 (0.15–0.21)
rH5N3-H5N1-NA	4.65 (3.94–5.43)	0.20 (0.17–0.25)	0.27 (0.23–0.33)	0.41 (0.35–0.49)
rH5N3-H5N1-NS	2.18 (1.83–2.55)	0.10 (0.08–0.12)	0.13 (0.11–0.16)	0.19 (0.16–0.23)
rH5N3-H5N1-M	2.22 (1.87–2.61)	0.10 (0.08–0.12)	0.13 (0.11–0.16)	0.19 (0.16–0.24)
rH5N3-H5N1-HA	2.16 (1.83–2.52)	0.09 (0.07–0.11)	0.13 (0.11–0.15)	0.19 (0.16–0.23)

*FFU, focus-forming unit.
†A/crow/Kyoto/53/04 (H5N1) recombined with the NA and HA genes of A/Duck/Hong Kong/820/80 (H5N3) are defined as rH5N1-H5N3-NA and rH5N1-H5N3-HA, respectively. In addition, A/Duck/Hong Kong/820/80 (H5N3) recombined into the NA, NS, M, and HA genes of A/crow/Kyoto/53/04 (H5N1) was defined as rH5N3-H5N1-NA, rH5N3-H5N1-NS, rH5N3-H5N1-M, rH5N3-H5N1-HA.
‡The elapsed time was used as the explanatory variable (x-axis), and the logarithmic virus titer was used as the explained variable (y-axis). A linear regression analysis with logarithmic link function was performed for each virus to create a curve of regression (Appendix Figure 4, https://wwwnc.cdc.gov/EID/article/28/3/21-1752-App1.pdf). Since the detection limit of each influenza virus titer was 10^1 FFUs, the X value (when the Y value of the regression curve was 1.0) was used as the survival time.
§The half-life of each virus was calculated from the slope of each regression curve when the amount of virus remaining on the surface was 2, 3, or 4 log_{10} FFUs.

actual hand hygiene condition and elucidated the differences in disinfectant efficacy against different subtypes (*26*–*28*). All viruses on the skin surface were completely inactivated by exposure to alcohol-based disinfectants (high concentrations of EA or IPA) for 15 seconds. In addition, most viruses on the skin surface were completely inactivated by exposure to 36% EA for 15 seconds, but the H5N1 subtype was not. These findings reveal that the H5N1 subtype was more resistant to EA than other subtypes and that the effectiveness of relatively low EA concentrations (36% wt/wt or 43% vol/vol) against the H5N1 subtype was lower. Therefore, to control contact transmission of the H5N1 subtype, disinfectants with appropriate EA concentrations, as proposed by the World Health Organization (>52% wt/wt or >60% vol/vol), should be used (*41*). Although low-level disinfectants such as BAC and CHG were much less effective than alcohol-based disinfectants, high concentrations of low-level disinfectants (i.e., 0.2% BAC or 1.0% CHG) were relatively effective against all influenza viruses on the skin surface. These results suggest that high concentrations of BAC-based and CHG-based disinfectants might

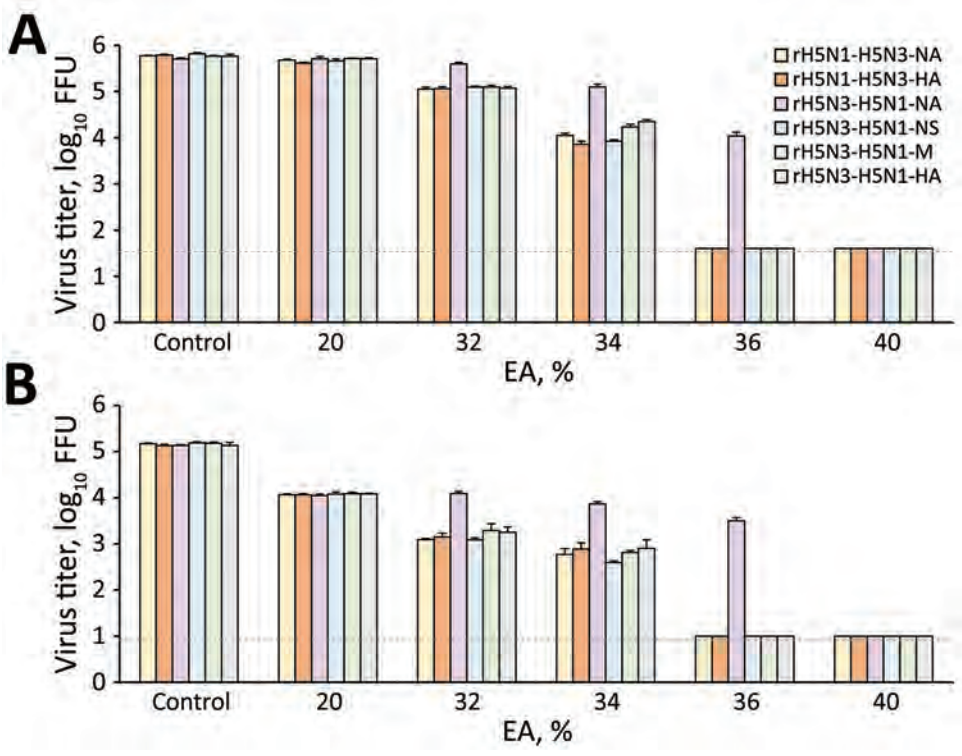

Figure 3. Effectiveness of disinfectants against various recombinant influenza viruses. A, B) In vitro (A) and ex vivo (B) evaluations were performed, and the residual viral titer after EA exposure is shown. The results are expressed as mean ± SD. Dotted horizontal lines represent the detection limit titers. A/crow/Kyoto/53/04 (H5N1) was recombined with the neuraminidase or hemagglutinin gene of A/Duck/Hong Kong/820/80 (H5N3), and the recombinant viruses were designated as rH5N1-H5N3-NA and rH5N1-H5N3-HA. In addition, A/Duck/Hong Kong/820/80 (H5N3) was recombined with the neuraminidase, nonstructural protein, matrix protein, or hemagglutinin gene of A/crow/Kyoto/53/04 (H5N1), and the recombinant viruses were designated as rH5N3-H5N1-NA, rH5N3-H5N1-NS, rH5N3-H5N1-M, or rH5N3-H5N1-HA. log reductions were calculated to evaluate the effectiveness of disinfectants under different conditions (Appendix Table 3, https://wwwnc.cdc.gov/EID/article/28/3/21-1752-App1.pdf). EA, ethyl alcohol.

be applicable for hand hygiene targeting influenza viruses as an alternative to alcohol-based disinfectants, although additional studies are needed to validate this possibility.

Finally, we tried to elucidate the genetic mechanisms responsible for differences in stability and disinfectant effectiveness among subtypes by using different recombinant viruses. The stability of all recombinant viruses tested (except rH5N3-H5N1-NA) on plastic and human skin surfaces was similar to that of all influenza viruses studied (except H5N1). Moreover, the survival time and half-life of rH5N3-H5N1-NA (a recombinant H5N3 virus with the NA gene of an H5N1 virus) on the plastic and human skin surfaces were approximately twice as long as other recombinant viruses, and it had the same stability as the H5N1 subtype (H5N1-Ky and H5N1-Eg). While evaluating the effectiveness of disinfectants, we found that although all recombinant viruses tested (except rH5N3-H5N1-NA) were completely inactivated by exposure to 36% EA for 15 seconds, only rH5N3-H5N1-NA was not significantly inactivated by exposure to 36% EA, and it had the same EA resistance as the H5N1 subtype. Those results strongly suggest that the higher stability and EA resistance of the H5N1 subtype might depend on NA, a spike protein. Although several studies have focused on the relationship between the NA segment and virulence (*42*,*43*), to the best of our knowledge, no study has focused on the relationship between the NA segment and stability. Future studies focusing on the NA segment are expected to elucidate factors that determine the stability and help identify subtypes with high stability and a high risk for contact transmission.

The first limitation of our study is that we used an ex vivo evaluation model in this study using human skin samples collected during forensic autopsies, because the application of highly pathogenic viruses (such as the H5N1 subtype) on the skin of humans is dangerous. At this stage, we tentatively conclude that virus survival time would not substantially differ between autopsy skin specimens and live human skin or between the different autopsy specimens. However, improving measurement accuracy, increasing the number of cumulative measurement samples, and more thorough evaluation of skin properties might elucidate the properties of skin samples and donor factors that affect virus survival. Second, we analyzed virus stability by mixing virus and PBS in this study. The use of solvents other than PBS (e.g., cell culture medium or human upper respiratory tract–derived mucus) might affect the residual virus titer on the surface and the analysis results. Furthermore, the evaluation was performed in a controlled environment (25°C and 45%–55% relative humidity); however, changes in temperature and humidity might have an effect on virus stability. Finally, this study revealed that the NA proteins in the influenza virus might contribute to the high stability of the H5N1 subtype, but the properties of the NA proteins that affect virus stability were not elucidated. In the future, preparing recombinant viruses with various NA proteins and clarifying the properties of NA that affect virus stability will be necessary.

In conclusion, we found that the H5N1 subtype had a higher risk for contact transmission because of its higher stability on plastic and skin surfaces and higher resistance to EA than other subtypes. Therefore, the optimal infection control methods may differ for each subtype. Our findings also suggest that these characteristics might depend on the NA protein.

Acknowledgments

We thank Shu Yuelong (Chinese Center for Disease Control and Prevention) and Eri Nobusawa, Masato Tashiro, and Takato Odagiri (National Institute of Infectious Diseases) for providing H7N9 viruses. We thank Editage (https://www.editage.com) for English language editing.

This research was supported by Adaptable and Seamless Technology Transfer Program through Target-driven R&D (ASTEP) from the Japan Science and Technology Agency (JST) (grant no. JPMJTR21UE and JPMJTM20PR); the AMED (grant no. JP 20fk0108077) and JSPS KAKENHI (grant no. 21K16326); and Takeda Science Foundation, and Mitsubishi Foundation.

Author contributions: R.S. conceived and designed the study; R.B., R.H., H.I., H.M., N.W., T.Y., and T.D. acquired the data; R.B., R.H., T.N., and H.I. analyzed and interpreted the data; R.H. secured funding and drafted the manuscript; R.B. and R.H. performed statistical analysis; R.B., R.H., T.N., and H.I. provided administrative, technical, and material support; R.H. and H.I. supervised the study.

All data included in this study are available from the corresponding author on request.

About the Author

Dr. Bandou is a project researcher in the Department of Forensics Medicine at Kyoto Prefectural University of Medicine, Kyoto, Japan.

References

1. Mathur MB, Patel RB, Gould M, Uyeki TM, Bhattacharya J, Xiao Y, et al. Seasonal patterns in human A (H5N1) virus infection: analysis of global cases. PLoS One. 2014;9:e106171. https://doi.org/10.1371/journal.pone.0106171
2. Tang J, Wang D. Research progress in human infection with avian influenza H7N9 virus. Sci China Life Sci. 2017;60:1299–306. https://doi.org/10.1007/s11427-017-9221-4
3. Kuiken T, Fouchier R, Rimmelzwaan G, van den Brand J, van Riel D, Osterhaus A. Pigs, poultry, and pandemic influenza: how zoonotic pathogens threaten human health. Adv Exp Med Biol. 2011;719:59–66. https://doi.org/10.1007/978-1-4614-0204-6_6
4. Chan KH, Sridhar S, Zhang RR, Chu H, Fung AY, Chan G, et al. Factors affecting stability and infectivity of SARS-CoV-2. J Hosp Infect. 2020;106:226–31. https://doi.org/10.1016/j.jhin.2020.07.009
5. Kampf G, Todt D, Pfaender S, Steinmann E. Persistence of coronaviruses on inanimate surfaces and their inactivation with biocidal agents. [Erratum in: J Hosp Infect. 2020; 105:587]. J Hosp Infect. 2020;104:246–51. https://doi.org/10.1016/j.jhin.2020.01.022
6. Kratzel A, Todt D, V'kovski P, Steiner S, Gultom M, Thao TTN, et al. Inactivation of severe acute respiratory syndrome coronavirus 2 by WHO-recommended hand rub formulations and alcohols. Emerg Infect Dis. 2020;26:1592–5. https://doi.org/10.3201/eid2607.200915
7. Leslie RA, Zhou SS, Macinga DR. Inactivation of SARS-CoV-2 by commercially available alcohol-based hand sanitizers. Am J Infect Control. 2020.
8. Nandy A, Basak SC. Prognosis of possible reassortments in recent H5N2 epidemic influenza in USA: implications for computer-assisted surveillance as well as drug/vaccine design. Curr Comput Aided Drug Des. 2015;11:110–6. https://doi.org/10.2174/1573409911666150722122034
9. Goubau P. Clinical aspects of human infection by the avian influenza virus [in French]. Bull Mem Acad R Med Belg. 2009;164:252–6.
10. Dinh PN, Long HT, Tien NT, Hien NT, Mai TQ, Phong H, et al.; World Health Organization/global outbreak alert and response network avian influenza investigation team in Vietnam. Risk factors for human infection with avian influenza A H5N1, Vietnam, 2004. Emerg Infect Dis. 2006;12:1841–7. https://doi.org/10.3201/eid1212.060829
11. Kim SM, Kim YI, Pascua PN, Choi YK. Avian influenza A viruses: evolution and zoonotic infection. Semin Respir Crit Care Med. 2016;37:501–11. https://doi.org/10.1055/s-0036-1584953
12. Somrongthong R, Beaudoin A, Bender J, Sasipreeyajan J, Laosee O, Pakinsee S, et al. Use of personal protective measures by Thai households in areas with avian influenza outbreaks. Zoonoses Public Health. 2012;59:339–46. https://doi.org/10.1111/j.1863-2378.2012.01460.x
13. Hayden F, Croisier A. Transmission of avian influenza viruses to and between humans. J Infect Dis. 2005;192:1311–4. https://doi.org/10.1086/444399
14. Rabinowitz P, Perdue M, Mumford E. Contact variables for exposure to avian influenza H5N1 virus at the human-animal interface. Zoonoses Public Health. 2010;57:227–38. https://doi.org/10.1111/j.1863-2378.2008.01223.x
15. Oxford J, Berezin EN, Courvalin P, Dwyer DE, Exner M, Jana LA, et al. The survival of influenza A(H1N1)pdm09 virus on 4 household surfaces. Am J Infect Control. 2014;42:423–5. https://doi.org/10.1016/j.ajic.2013.10.016
16. Otter JA, Donskey C, Yezli S, Douthwaite S, Goldenberg SD, Weber DJ. Transmission of SARS and MERS coronaviruses and influenza virus in healthcare settings: the possible role of dry surface contamination. J Hosp Infect. 2016;92:235–50. https://doi.org/10.1016/j.jhin.2015.08.027
17. Wood JP, Choi YW, Chappie DJ, Rogers JV, Kaye JZ. Environmental persistence of a highly pathogenic avian influenza (H5N1) virus. Environ Sci Technol. 2010;44:7515–20. https://doi.org/10.1021/es1016153
18. Tiwari A, Patnayak DP, Chander Y, Parsad M, Goyal SM. Survival of two avian respiratory viruses on porous and nonporous surfaces. Avian Dis. 2006;50:284–7. https://doi.org/10.1637/7453-101205R.1
19. Paek MR, Lee YJ, Yoon H, Kang HM, Kim MC, Choi JG, et al. Survival rate of H5N1 highly pathogenic avian influenza viruses at different temperatures. Poult Sci. 2010;89:1647–50. https://doi.org/10.3382/ps.2010-00800
20. Hauck R, Crossley B, Rejmanek D, Zhou H, Gallardo RA. Persistence of highly pathogenic and low pathogenic avian influenza viruses in footbaths and poultry manure. Avian Dis. 2017;61:64–9. https://doi.org/10.1637/11495-091916-Reg
21. Brown JD, Swayne DE, Cooper RJ, Burns RE, Stallknecht DE. Persistence of H5 and H7 avian influenza viruses in water. Avian Dis. 2007;51(Suppl):285–9. https://doi.org/10.1637/7636-042806R.1
22. Brown J, Stallknecht D, Lebarbenchon C, Swayne D. Survivability of Eurasian H5N1 highly pathogenic avian influenza viruses in water varies between strains. Avian Dis. 2014;58:453–7. https://doi.org/10.1637/10741-120513-ResNote.1
23. Brown JD, Goekjian G, Poulson R, Valeika S, Stallknecht DE. Avian influenza virus in water: infectivity is dependent on pH, salinity and temperature. Vet Microbiol. 2009;136:20–6. https://doi.org/10.1016/j.vetmic.2008.10.027
24. Yamamoto Y, Nakamura K, Mase M. Survival of highly pathogenic avian influenza H5N1 virus in tissues derived from experimentally infected chickens. Appl Environ Microbiol. 2017;83:e00604-17. https://doi.org/10.1128/AEM.00604-17
25. Beato MS, Mancin M, Bertoli E, Buratin A, Terregino C, Capua I. Infectivity of H7 LP and HP influenza viruses at different temperatures and pH and persistence of H7 HP virus in poultry meat at refrigeration temperature. Virology. 2012;433:522–7. https://doi.org/10.1016/j.virol.2012.08.009
26. Hirose R, Ikegaya H, Naito Y, Watanabe N, Yoshida T, Bandou R, et al. Survival of SARS-CoV-2 and influenza virus on the human skin: importance of hand hygiene in COVID-19. Clin Infect Dis. 2020 Oct 3 [Epub ahead of print]. https://doi.org/10.1093/cid/ciaa1517
27. Hirose R, Bandou R, Ikegaya H, Watanabe N, Yoshida T, Daidoji T, et al. Disinfectant effectiveness against SARS-CoV-2 and influenza viruses present on human skin: model-based evaluation. Clin Microbiol Infect. 2021; 27:1042.e1–4.
28. Hirose R, Ikegaya H, Naito Y, Watanabe N, Yoshida T, Bandou R, et al. Reply to Gracely. Clin Infect Dis. 2021;73:e854–6. https://doi.org/10.1093/cid/ciab023
29. Thomas Y, Boquete-Suter P, Koch D, Pittet D, Kaiser L. Survival of influenza virus on human fingers. Clin Microbiol Infect. 2014;20:O58–64. https://doi.org/10.1111/1469-0691.12324
30. Hansen S, Zimmerman PA, van de Mortel TF. Infectious illness prevention and control methods and their effectiveness in non-health workplaces: an integrated literature review. J Infect Prev. 2018;19:212–8. https://doi.org/10.1177/1757177418772184
31. Seet RC, Lim EC, Oh VM, Ong BK, Goh KT, Fisher DA, et al. Readiness exercise to combat avian influenza. QJM. 2009;102:133–7. https://doi.org/10.1093/qjmed/hcn159

32. Akutsu T, Ikegaya H, Watanabe K, Miyasaka S. Immunohistochemical staining of skin-expressed proteins to identify exfoliated epidermal cells for forensic purposes. Forensic Sci Int. 2019;303:109940. https://doi.org/10.1016/j.forsciint.2019.109940
33. Hirel B, Watier E, Chesne C, Patoux-Pibouin M, Guillouzo A. Culture and drug biotransformation capacity of adult human keratinocytes from post-mortem skin. Br J Dermatol. 1996;134:831–6. https://doi.org/10.1111/j.1365-2133.1996.tb06311.x
34. Boekema BK, Boekestijn B, Breederveld RS. Evaluation of saline, RPMI and DMEM/F12 for storage of split-thickness skin grafts. Burns. 2015;41:848–52. https://doi.org/10.1016/j.burns.2014.10.016
35. Corzo-León DE, Munro CA, MacCallum DM. An *ex vivo* human skin model to study superficial fungal infections. Front Microbiol. 2019;10:1172. https://doi.org/10.3389/fmicb.2019.01172
36. Chin AWH, Chu JTS, Perera MRA, Hui KPY, Yen HL, Chan MCW, et al. Stability of SARS-CoV-2 in different environmental conditions. Lancet Microbe. 2020;1:e10. https://doi.org/10.1016/S2666-5247(20)30003-3
37. van Doremalen N, Bushmaker T, Morris DH, Holbrook MG, Gamble A, Williamson BN, et al. Aerosol and surface stability of SARS-CoV-2 as compared with SARS-CoV-1. N Engl J Med. 2020;382:1564–7. https://doi.org/10.1056/NEJMc2004973
38. Gehrke C, Steinmann J, Goroncy-Bermes P. Inactivation of feline calicivirus, a surrogate of norovirus (formerly Norwalk-like viruses), by different types of alcohol in vitro and in vivo. J Hosp Infect. 2004;56:49–55. https://doi.org/10.1016/j.jhin.2003.08.019
39. Eggers M, Eickmann M, Kowalski K, Zorn J, Reimer K. Povidone-iodine hand wash and hand rub products demonstrated excellent in vitro virucidal efficacy against Ebola virus and modified vaccinia virus Ankara, the new European test virus for enveloped viruses. BMC Infect Dis. 2015;15:375. https://doi.org/10.1186/s12879-015-1111-9
40. Eggers M, Eickmann M, Zorn J. Rapid and effective virucidal activity of povidone-iodine products against Middle East respiratory syndrome coronavirus (MERS-CoV) and Modified Vaccinia Virus Ankara (MVA). Infect Dis Ther. 2015;4:491–501. https://doi.org/10.1007/s40121-015-0091-9
41. Golin AP, Choi D, Ghahary A. Hand sanitizers: a review of ingredients, mechanisms of action, modes of delivery, and efficacy against coronaviruses. Am J Infect Control. 2020;48:1062–7. https://doi.org/10.1016/j.ajic.2020.06.182
42. Li Y, Chen S, Zhang X, Fu Q, Zhang Z, Shi S, et al. A 20-amino-acid deletion in the neuraminidase stalk and a five-amino-acid deletion in the NS1 protein both contribute to the pathogenicity of H5N1 avian influenza viruses in mallard ducks. PLoS One. 2014;9:e95539. https://doi.org/10.1371/journal.pone.0095539
43. Chen S, Quan K, Wang D, Du Y, Qin T, Peng D, et al. Truncation or deglycosylation of the neuraminidase stalk enhances the pathogenicity of the H5N1 subtype avian influenza virus in mallard ducks. Front Microbiol. 2020;11:583588. https://doi.org/10.3389/fmicb.2020.583588

Address for correspondence: Ryohei Hirose, Department of Infectious Diseases, Graduate School of Medical Science, Kyoto Prefectural University of Medicine, 465 Kajii-cho, Kawaramachi-Hirokoji, Kamigyo-ku, Kyoto 602-8566, Japan; email: ryo-hiro@koto.kpu-m.ac.jp

Spatiotemporal Analyses of 2 Co-Circulating SARS-CoV-2 Variants, New York, USA

Alexis Russell,[1] Collin O'Connor,[1] Erica Lasek-Nesselquist,[1]
Jonathan Plitnick, John P. Kelly, Daryl M. Lamson, Kirsten St. George

The emergence of novel severe acute respiratory syndrome coronavirus 2 (SARS-CoV-2) variants in late 2020 and early 2021 raised alarm worldwide because of their potential for increased transmissibility and immune evasion. Elucidating the evolutionary and epidemiologic dynamics among novel SARS-CoV-2 variants is essential for understanding the trajectory of the coronavirus disease pandemic. We describe the interplay between B.1.1.7 (Alpha) and B.1.526 (Iota) variants in New York State, USA, during December 2020–April 2021 through phylogeographic analyses, space-time scan statistics, and cartographic visualization. Our results indicate that B.1.526 probably evolved in New York City, where it was displaced as the dominant lineage by B.1.1.7 months after its initial appearance. In contrast, B.1.1.7 became dominant earlier in regions with fewer B.1.526 infections. These results suggest that B.1.526 might have delayed the initial spread of B.1.1.7 in New York City. Our combined spatiotemporal methodologies can help disentangle the complexities of shifting SARS-CoV-2 variant landscapes.

The emergence of a novel severe acute respiratory syndrome coronavirus 2 (SARS-CoV-2) variant B.1.1.7 (Alpha) in the United Kingdom in late 2020 raised alarm worldwide and prompted major reassessment of the management, surveillance, and projected future of coronavirus disease (COVID-19) (*1*,*2*). Evidence of increased transmissibility and potential immune evasion prompted the World Health Organization to designate B.1.1.7 a variant of concern (VOC) in December 2020 (*3*–*5*; W.A. Haynes et al., unpub. data, https://doi.org/10.1101/2021.01.06.20248960). The emergence of B.1.1.7 and additional novel SARS-CoV-2 variants with competitive advantages has resulted in the localized dominance of single variants (E. Volz et al., unpub. data, https://doi.org/10.1101/2020.12.30.20249034) and raised concern for increases in COVID-19 incidence (*6*).

Novel variant B.1.526 (Iota) arose within New York State (NYS), USA, in late 2020 (E. Lasek-Nesselquist et al., unpub. data, https://doi.org/10.1101/2021.02.26.21251868) (*7*) and quickly increased in proportion throughout the state, leading to a noticeable shift in lineage distribution during early 2021 (E. Lasek-Nesselquist et al., unpub. data, https://doi.org/10.1101/2021.02.26.21251868) (*31*). The World Health Organization designated B.1.526 as a variant of interest (VOI) because of its increase in prevalence coupled with mutations associated with immune evasion (*8*). Despite these concerns, an epidemiologic assessment of B.1.526 in NYC during January–April 2021 found that the lineage did not cause more severe disease and was not associated with increased risk for reinfection or vaccine breakthrough (*9*). However, an epidemiologic study of NYS during late 2020–May 2021 concluded that B.1.526 was 35% more transmissible than non-VOC and non-VOI lineages circulating at the time (*10*).

Genomic surveillance of COVID-19 is a crucial tool to monitor and assess the physiologic and epidemiologic characteristics of SARS-CoV-2 variants as they emerge. The New York State Department of Health (NYSDOH) substantially expanded its genomic surveillance program in December 2020, with the aim of sequencing a more representative subset of COVID-19 cases across the state to track the spread and impact of novel variants. A robust genomic surveillance system enables assessment of changes in variant distribution over precise temporal and spatial scales.

Author affiliations: New York State Department of Health, Albany, New York, USA (A. Russell, C. O'Connor, E. Lasek-Nesselquist, J. Plitnick, J.P. Kelly, K. St. George); State University of New York at Buffalo, Buffalo, New York, USA (C. O'Connor); State University of New York at Albany, Albany (E. Lasek-Nesselquist, K. St. George)

DOI: https://doi.org/10.3201/eid2803.211972

[1]These authors contributed equally to this article.

This study employed spatial scan statistics paired with phylogeographic analyses to describe the shifting SARS-CoV-2 variant landscape in NYS during December 2020–April 2021, specifically the interplay between co-circulating B.1.526 and B.1.1.7 lineages. Our findings elucidate the dynamics of competing SARS-CoV-2 variants at a time when the highly transmissible VOC Delta had overtaken B.1.1.7 worldwide and future variant displacements were likely to occur.

Methods

Sample Acquisition and RNA Extraction

This study was approved by the NYSDOH Institutional Review Board, under study numbers 02-054 and 07-022. The NYSDOH Wadsworth Center coordinated with >30 clinical laboratories throughout NYS that routinely submitted respiratory swabs positive for SARS-CoV-2 for whole-genome sequencing (WGS). Specimens were required to have a real-time cycle threshold value <30. We performed nucleic acid extraction on a MagNAPure 96 with the Viral NA Small Volume Kit (Roche, https://www.roche.com) with 100 µL sample input and 100 µL eluate.

Sequencing and Bioinformatics Processing

We processed extracted RNA for WGS with a modified ARTIC V3 protocol (https://artic.network/ncov-2019) in the Applied Genomics Technology Core at the Wadsworth Center as previously described (*11*) (Appendix, https://wwwnc.cdc.gov/EID/article/28/3/21-1972-App1.pdf). We processed Illumina libraries with the ARTIC nextflow pipeline (https://github.com/connor-lab/ncov2019-artic-nf) as previously described (*14*) (Appendix).

Sample Inclusion Criteria

We included specimens with collection dates during December 2020–April 2021 with ZIP codes of patient addresses. We removed specimens that were prescreened for specific mutations or for clinical or epidemiologic criteria. For persons with multiple specimens collected, we included only the earliest specimen.

COVID Incidence Calculation

We obtained monthly COVID-19 case counts by ZIP code from online NYC COVID-19 data (https://github.com/nychealth/coronavirus-data) and from the NYSDOH Communicable Disease Electronic Surveillance System. We included reports with case status of confirmed or probable in the case count and assigned a month on the basis of diagnosis date. We converted ZIP code data to ZIP code tabulation area (ZCTA) and calculated incidence using population data from the 2019 1-year American Community Survey estimates (https://data.census.gov/cedsci).

Retrospective Multinomial Space-Time Scan Statistic

We used the retrospective multinomial space-time scan statistic in SaTScan version 9.6 and applied the nonordinal method (*12*,*13*). We calculated estimated SARS-CoV-2 variant data for each ZCTA-month aggregation by multiplying the proportion of either B.1.1.7, B.1.526, or other variants in our sample by the total number of COVID-19 cases.

We set the maximum cluster size parameter a priori to 10% of the population at risk (*14*) . Space-time cluster detection in SaTScan has a noted limitation where the size of clusters cannot change over time (*15*,*16*). Given that our data are aggregated to the temporal unit of months (December 2020–April 2021), we set the maximum temporal cluster size parameter to 1 month, to enable clusters to change their shape from month to month by being designated as new clusters (Appendix).

Inverse-Distance Weighted Interpolation and Spatial Average of SARS-CoV-2 Whole-Genome Sequencing

We used inverse-distance weighted (IDW) interpolation to visualize the spatiotemporal variation in the proportion of COVID-19 cases attributable to each SARS-CoV-2 variant in NYS and to provide estimates for these proportions in areas where we were missing data (*17*). We assigned the percentage of COVID-19 cases attributable to each variant per ZCTA to the ZCTA's centroid for the IDW calculation. IDW interpolation generated a continuous surface of values representing the percentage of total COVID-19 cases attributed to B.1.1.7 and B.1.526, which we then averaged over each ZCTA geometry.

We then multiplied the estimated percentage of each SARS-CoV-2 variant generated from IDW interpolation by the total number of COVID-19 cases for each ZCTA and month to estimate the total number of COVID-19 cases attributable to each variant. Estimated numbers of variant cases generated geographic mean centers for each month of the study period (*18*) (Appendix).

Phylogeographic Analyses

We incorporated into the analysis all NYS B.1.526 genomes generated by Wadsworth from the study period, barring a small fraction that did not pass quality control and those removed as redundant (Appendix). We downloaded all B.1.526 genomes from the United States and associated metadata (excluding NYS

sequences) from GISAID (https://www.gisaid.org) and randomly subsampled them proportionally to their overall frequency in the United States. The final dataset included B.1.526 genomes from domestic locations (Massachusetts, New Jersey, Pennsylvania, Connecticut, California, Florida, Maryland, Michigan, Minnesota, and North Carolina), the 5 boroughs of NYC (Bronx, Brooklyn, Queens, Staten Island, and Manhattan), Long Island, the Hudson Valley and upstate New York (Western NYS, the Finger Lakes, the Capital District, and Central NYS regions). We aligned genomes in mafft 7.475 (*19*), masking problematic sites (https://github.com/W-L/ProblematicSites_SARS-CoV2). We generated a maximum-likelihood phylogeny in IQTree 1.6.12 (*20*) with 1,000 ultrafast bootstrap replicates (*21*) and time-calibrated it in TreeTime 0.7.6 (*22*). This tree served as the fixed tree for ancestral state reconstruction in Beast 2.6.2 (*23*) to infer timing and source of B.1.526 introductions within NYS. We allowed the Bayesian analysis to run for >4 million generations and monitored it in Tracer 1.7.1 (*24*) until the effective sample size of all parameters ≥200 and the Markov chain Monte Carlo appeared to reach stationarity.

We conducted a B.1.1.7 phylogeographic analysis in the same manner with the states inferred for a fixed topology until all effective sample sizes reached ≥200. The final dataset included B.1.1.7 genomes from domestic locations (Massachusetts, New Jersey, Pennsylvania, Connecticut, California, and Florida) NYC, Long Island, Mid-Hudson, Finger Lakes, southwestern NYS (the Southern Tier and western regions of NYS) and Northern NYS (Capital District, Mohawk Valley, Central NYS, and the North Country).

We generated maximum clade credibility trees for B.1.526 and B.1.1.7 in TreeAnnotator 2.6.2 (*23*) with a 10% burn-in. We summarized the number of introductions between locations by using Baltic (https://github.com/evogytis/baltic), adopting the exploded tree script for Python 3. We considered only introductions with a posterior probability ≥0.7. We visualized and annotated trees in FigTree 1.5.5 (http://tree.bio.ed.ac.uk/software/figtree) and ggtree (*25*) for R 4.1.0 (http://www.R-project.org) (Appendix).

Results

Summary Statistics

We included in the study a total of 8,517 SARS-CoV-2 specimens sequenced by Wadsworth with collection dates during December 2020–April 2021. Among the included specimens, B.1.1.7 constituted 1,107 (13%) and B.1.526 constituted 904 (10.6%) of the samples.

The earliest B.1.1.7 samples sequenced by Wadsworth were collected on December 24, 2020, from a resident of Manhattan (Metro or NYC region) and a person in Saratoga County (Capital Region). B.1.1.7 remained relatively rare among all samples through the end of January. The Metro and Capital regions experienced the earliest increases in B.1.1.7, although the proportion of B.1.1.7 did not exceed 15% through February. The proportion of B.1.1.7 increased in March across all regions, most notably in the western region, where it constituted ≈75% of all samples by the end of March and continued to rise through April. The Metro Region experienced the most gradual increase in B.1.1.7; the proportion did not exceed 40% until the end of April.

The earliest B.1.526 sample sequenced by Wadsworth was collected on December 9, 2020, from a patient in the Bronx (Metro or NYC region). The proportion of B.1.526 increased in the Metro Region throughout December, reaching 10% of total samples by the end of the month. The proportion of B.1.526 in the Metro Region approached 40% by the end of January, peaked at ≈60% in mid-February to early March, and then plateaued at ≈50% through April. B.1.526 was not consistently detected in the other regions until February and its proportion generally remained <40%. The combined proportion of all lineages other than B.1.1.7 and B.1.526 dropped to <20% in all NYS regions by the end of April.

Cartographic Visualization

Maps of interpolated proportion of B.1.1.7 relative to all other lineages by ZCTA (Appendix Figure 1, panel A) show a general trend of spread through the southern portion of NYS in January, statewide distribution by February, diffuse increase in proportion in March, and a sustained high proportion throughout the state in April, with strong dominance in the western region. In contrast, maps of interpolated proportion of B.1.526 show more constricted initial spread focused around NYC and surrounding areas in January; statewide distribution was not achieved until March, and a moderate proportion was sustained mostly within the Metro Region (Appendix Figure 1, panel B).

Maps of geographic mean centers of estimated B.1.1.7 and B.1.526 cases (Figure 1) show that shifts in the SARS-CoV-2 variant landscape affected the spatial distribution of COVID-19 cases overall. In December 2020, the mean center of total COVID-19 cases and the mean center of the population of NYS were nearly spatially coincident, implying that COVID-19 cases were distributed in accordance with NYS's population. At the same time, the mean center of B.1.526 cases occurred near the NYC area, then gradually moved slightly northwest as

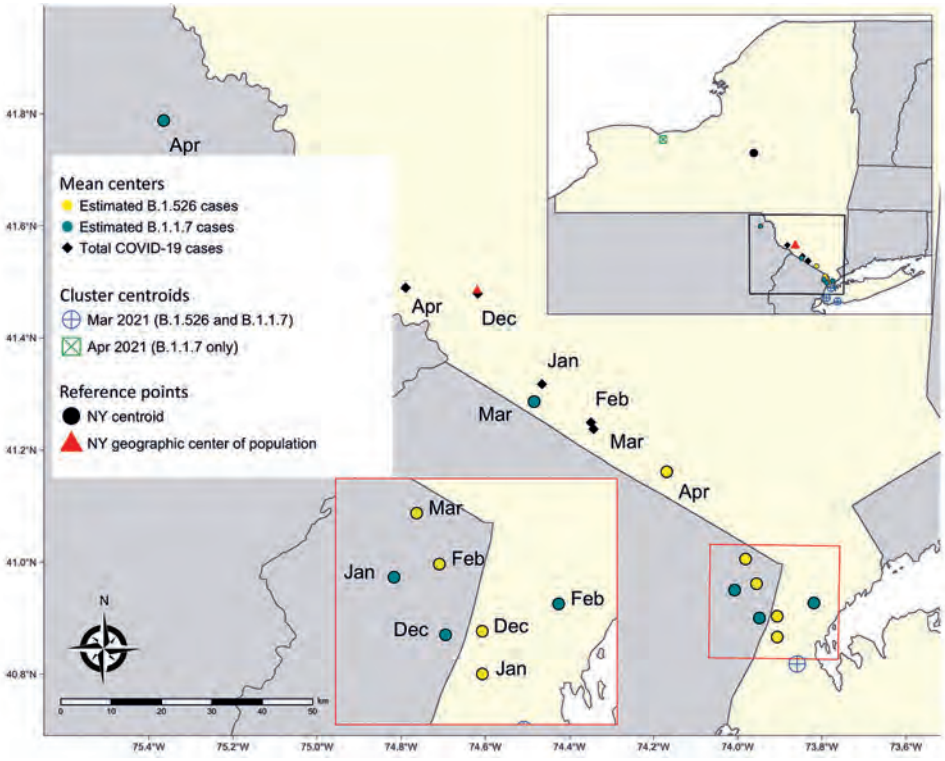

Figure 1. Geographically weighted mean centers of total and estimated coronavirus disease cases attributable to B.1.526 and B.1.1.7 variants, New York State, USA, December 2020–April 2021. Cluster centroids refer to the results of the multinomial space-time scan analysis (Figure 2). New York's centroid and geographic center of population are added as reference points.

B.1.526 expanded modestly into upstate regions. Similarly, the mean center of B.1.1.7 cases was located near NYC in December 2020, then moved northwest during March and April to a much greater degree than for B.1.526 cases, probably because of the B.1.1.7 cluster occurring in the Finger Lakes region. Consequently, the spread of B.1.1.7 in upstate NYS, especially within the western region, resulted in a northwesterly shift of the mean center of total COVID-19 cases by April 2021. The spatial shift pushed the mean center of COVID-19 cases northwest of NYS's population center, indicating that the April B.1.1.7 cluster had an outsized effect on the overall distribution of COVID-19 cases.

Retrospective Multinomial Space-Time Scan Statistic

Retrospective multinomial space-time scan analysis indicated 6 statistically significant clusters with elevated relative risk (RR) of COVID-19 attributable to specific variants (Figure 2; Appendix Table 1). Two clusters of elevated RR of other lineages were found in December, 2020 in the Metro and Capital regions as well as Long Island, reflecting the nearly nonexistent risk for B.1.1.7 and B.1.526 infection. Three clusters of elevated RR of multiple combinations of B.1.1.7, B.1.526, B.1.526.1, and B.1.526.2 were found in March 2021 in the NYC and Long Island regions. The sixth cluster exhibited an elevated RR of >7.0 for B.1.1.7, with a radius of 114.38 km centered in the Finger Lakes area (western and central regions) during April. In addition, the presence of B.1.1.7 and B.1.526 clusters in March and April coincide with a general statewide decrease in incidence of COVID-19 (Figure 2).

Phylogeographic Analyses

The final B.1.526 dataset for phylogenetic reconstruction contained 980 genomes from all regions of NYS and various domestic locations (Bronx, 222; Hudson Valley, 128; Brooklyn, 39; Long Island, 78; Manhattan, 49; Queens, 81; Staten Island, 12; upstate NYS, 81; domestic, 290). The final B.1.1.7 dataset contained 1,195 genomes from the NYC region (181), Finger Lakes (239), Hudson Valley (78), Long Island (130), Western NYS and the Southern Tier (southwestern NYS, 56), Capital District, Mohawk Valley, Central NYS, and the north country (Northern NYS, 149), as well as other states (domestic, 362). Results from the phylogeographic analysis indicated that B.1.526 emerged within the NYC area near the end of 2020 and that the Bronx was a major source of spread to other regions of NYS and the United States (domestic) (Figure 3). Although sampling biases could have influenced the number of introductions assigned to the Bronx, the domestic category had greater representation in the dataset but led to substantially fewer introductions (Appendix Table 2). Domestic genomes represented 29.5% of the dataset but this location was responsible

for only 6.7% of all B.1.526 introductions, whereas the Bronx represented 22.7% of the dataset and led to 63.8% of all introductions (Appendix Table 2). Excluding the Bronx, B.1.526 transmission between boroughs and from these boroughs to other locations was relatively infrequent. We used subsampling strategies to investigate the strength of our results from the full B.1.526 phylogeographic analysis. These strategies included evenly sampling each region or borough, sampling evenly across time (except for December, which had very few B.1.526 cases compared with other months), sampling proportionally to the total incidence of SARS-CoV-2 per region or borough, and downsampling high-incidence regions or boroughs to the mean of B.1.526 cases per month. We performed each subsampling analysis in triplicate. Despite the different subsampling strategies, the root of the tree consistently fell within NYC, and the Bronx continued to serve as a major source of B.1.526 (data not shown).

Multiple domestic introductions contributed to the initial presence of B.1.1.7 in NYS (*11*) (Figure 4), with transmission occurring most frequently in the Finger Lakes and Northern NYS (Figure 4). The Finger Lakes and Northern NYS were well-represented in the dataset (32% of genomes) but contributed substantially less to the distribution of B.1.1.7 (accounting for 13% of the total number of introductions) than domestic sites, which represented 20% of the data and were responsible for the highest percentage of introductions (≈39%) (Appendix Table 3). The Finger Lakes showed the lowest proportion of sequenced cases attributable to introductions but the largest sample size in NYS, suggesting more sustained transmission of B.1.1.7 in this region.

Discussion

The repeated emergence of novel variants of SARS-CoV-2 has largely defined the COVID-19 pandemic response in 2021. As vaccination rates, prior exposure levels, and behavioral public health measures continuously change, so too will selective pressures (*26*). Given that selective pressures likely vary across regions, it follows that the emergence and spread of SARS-CoV-2 variants are also regionally dynamic. We combined spatial statistical, phylogeographic, and cartographic visualization techniques to examine the spatiotemporal dynamics of the VOC B.1.1.7 (Alpha) and the VOI B.1.526 (Iota) in NYS during December 2020–April 2021.

The concurrent spread of B.1.1.7 and B.1.526 offers a unique opportunity to compare the dynamics of competing variants of SARS-CoV-2 within a population during a period of substantial fluctuations in statewide COVID-19 incidence and the implementation of a vaccination campaign in January 2021. Shortly after its appearance in the Bronx in late 2020, B.1.526 quickly became the most common lineage in NYC and the surrounding region. The rapid dominance of B.1.526 in NYC is corroborated by our phylogeographic results (Figure 3), which depict widespread initial transmission within the Bronx, periodic introductions to neighboring boroughs, and later introductions to the greater Metro Region and

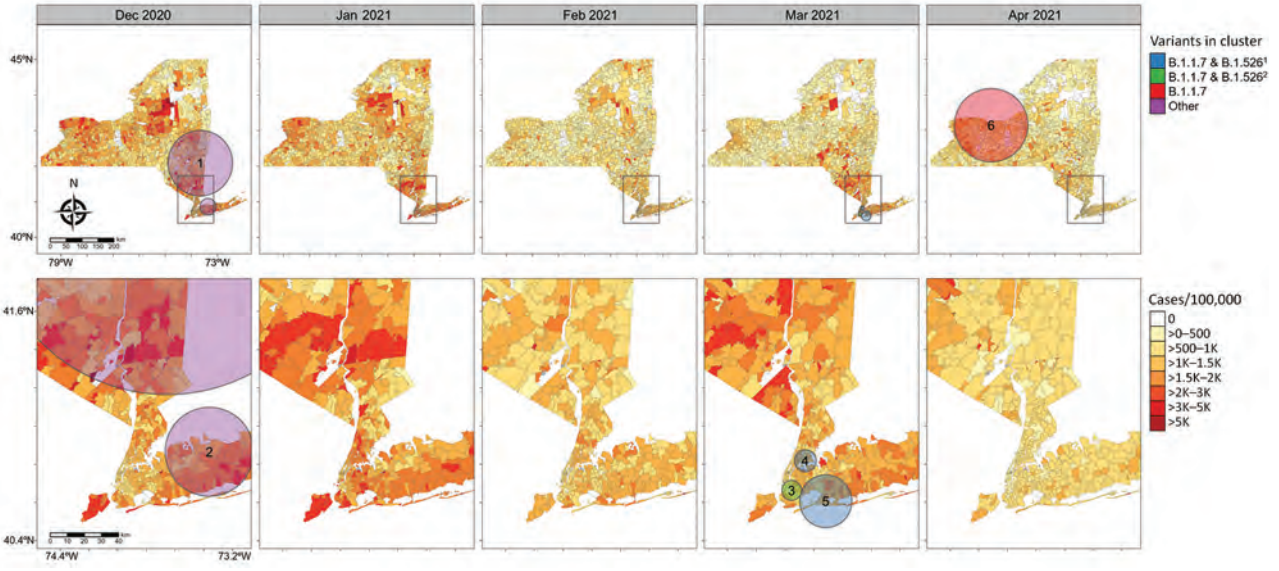

Figure 2. Severe acute respiratory syndrome coronavirus 2 variant clusters identified from retrospective multinomial space-time scan analysis and coronavirus disease incidence by ZIP code tabulation area, New York State, USA, December 2020–April 2021. Circles indicate clusters with relative risk >1. 1, variant includes B.1.526, B.1.526.1, and B.1.526.2; 2, variant includes B.1.526 and B.1.526.2.

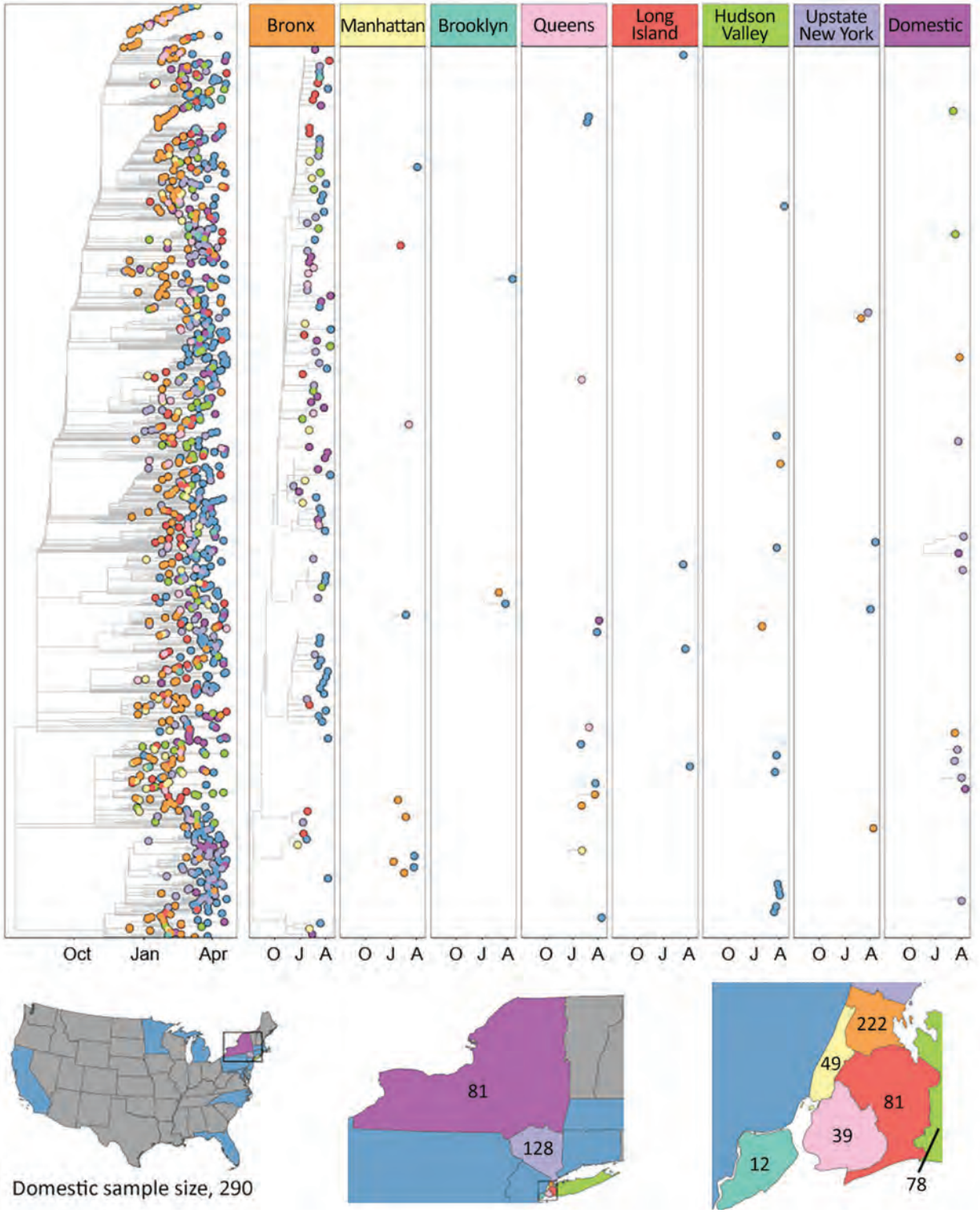

Figure 3. Time-calibrated phylogeny of severe acute respiratory syndrome coronavirus 2 variant B.1.526, New York and other states, USA, December 2020–April 2021. Left panel represents a maximum-likelihood phylogeny of 980 genomes from New York and other US states generated in IQTree 1.6.12 (*20*) with timescale inferred by TreeTime 0.7.6 (*22*) and ancestral state reconstruction performed in BEAST 2.6.2 (*23*). Faceted panels indicate the source of B.1.526 introductions into different regions of New York and other states (domestic). Only introductions supported by an ancestral state probability of ≥0.7 are shown. Bottom panel shows locations sampled and sample sizes. A, April; J, January; O, October.

other states. The spread of B.1.526 appears to have been spatially limited by the repeated introduction and transmission of B.1.1.7 outside NYC. However, behaviors such as differences in travel rates in NYC and between NYC and other regions probably contributed to the dynamics we observed. Similarly, the regional success of either variant may depend on the seroprevalence of the population. B.1.351 (Beta) was predicted to dominate in populations with a high degree of naturally acquired immunity because of immune evasion conferred by the E484K mutation in Spike (C.L. Althaus et al., unpub. data, https://doi.org/10.1101/2021.06.10.21258468), a mutation also observed in most NYS B.1.526 genomes. The spike mutations of B.1.526 (including the E484K mutation) were shown to reduce neutralization activity of convalescent-phase plasma and several antibodies (*10*). Thus, founder effects in an area of high transmission combined with high levels of prior exposure to SARS-CoV-2 might have provided B.1.526 its initial growth advantages in the NYC area, which was also the initial epicenter of the pandemic in the United States. Regions of NYS where B.1.526 had not yet established experienced rapid dominance of B.1.1.7 during March and April. This trend is most clearly seen in the near complete displacement of all other lineages by B.1.1.7 in Western NYS (Appendix Figure 2, panel A), resulting in a large cluster of elevated RR for B.1.1.7 cases in the Finger Lakes region during April (Figure 2). This finding is consistent with the enhanced transmissibility of B.1.1.7 in comparison to non-VOCs and non-VOIs and the conclusion that B.1.1.7 will dominate in populations with lower seroprevalence (C.L. Althaus et al., unpub. data, https://doi.org/10.1101/2021.06.10.21258468), such as those outside the NYC area.

The multinomial spatial scan detected 3 unique clusters in March 2021, all with increased RR for B.1.1.7 and B.1.526. The values for RR in each NYC cluster detail a distinct pattern: clusters centered within the Bronx, Brooklyn, and Manhattan had higher RR for B.1.526, whereas the cluster centered in east Queens and Long Island had a higher RR for B.1.1.7 (Appendix Table 1). During the months after B.1.526's initial advantage in NYC, B.1.1.7 trends toward becoming the major variant in the Metro Region. Given the elevated reproductive number of B.1.1.7 and B.1.526 in comparison to other non-VOC/VOIs lineages (*27*) and the delayed dominance of B.1.1.7 in the Bronx compared with Long Island and Queens, we hypothesize that B.1.526 was more difficult to displace than other lineages circulating at the time. Almost no difference can be observed in the average global reproductive number of B.1.526 compared with B.1.1.7, although differences exist on a country level (*27*). This finding supports the idea that B.1.526 was generally more competitive against B.1.1.7 than background lineages, but other factors, including the location examined, probably influence our results.

Similarly, maps of the geographic mean centers of the estimated number of COVID-19 cases attributable to each variant capture the rapid spread of B.1.1.7 out of NYC and the relative inability of B.1.526 to claim a foothold outside of the Metro Region. The northwesterly shift in the trajectory of overall COVID-19 cases in April indicates that the expansion of B.1.1.7, in particular clustering in western NYS, had a measurable influence on the spatial spread of COVID-19 cases overall.

There are some limitations to our study. A degree of selection bias exists within the dataset, given that specimens were screened by cycle threshold value and were submitted by a selected group of clinical and commercial laboratories that cannot perfectly represent all COVID-19 cases in NYS. We were unable to assess the demographic and clinical representativeness of our dataset because these data were not available to us. In addition, the number of specimens sequenced varied over the space and time of the study period, which created small sample sizes within many ZCTA-months. This limitation extended to the multinomial scan statistic, which was run with estimated values for COVID-19 cases attributable to B.1.1.7 and B.1.526, giving all ZCTAs with samples equal weight. However, the spatial scan assesses data according to their proximity to each other. In this context, ZCTAs are analyzed together rather than individually, which has the potential to reduce bias. Another consequence of our limited sampling was that our data exhibited zero samples from many ZCTAs for each month, which we addressed by using IDW interpolation of the proportion of B.1.1.7 and B.1.526 sequenced samples at the ZCTA-month level to visualize general patterns of variant proportions over geography. Phylogeographic analyses were hampered by similar limitations; uneven sampling among regions and the lack of global representation in our datasets could lead to incorrect trait assignments. Smaller sample sizes for some regions might have caused an underestimation of their contributions to variant transmission in NYS, whereas larger sample sizes might have inflated the number of introductions assigned. However, we believe our results largely capture the transmission dynamics of B.1.526 and B.1.1.7 in NYS, given that larger sample

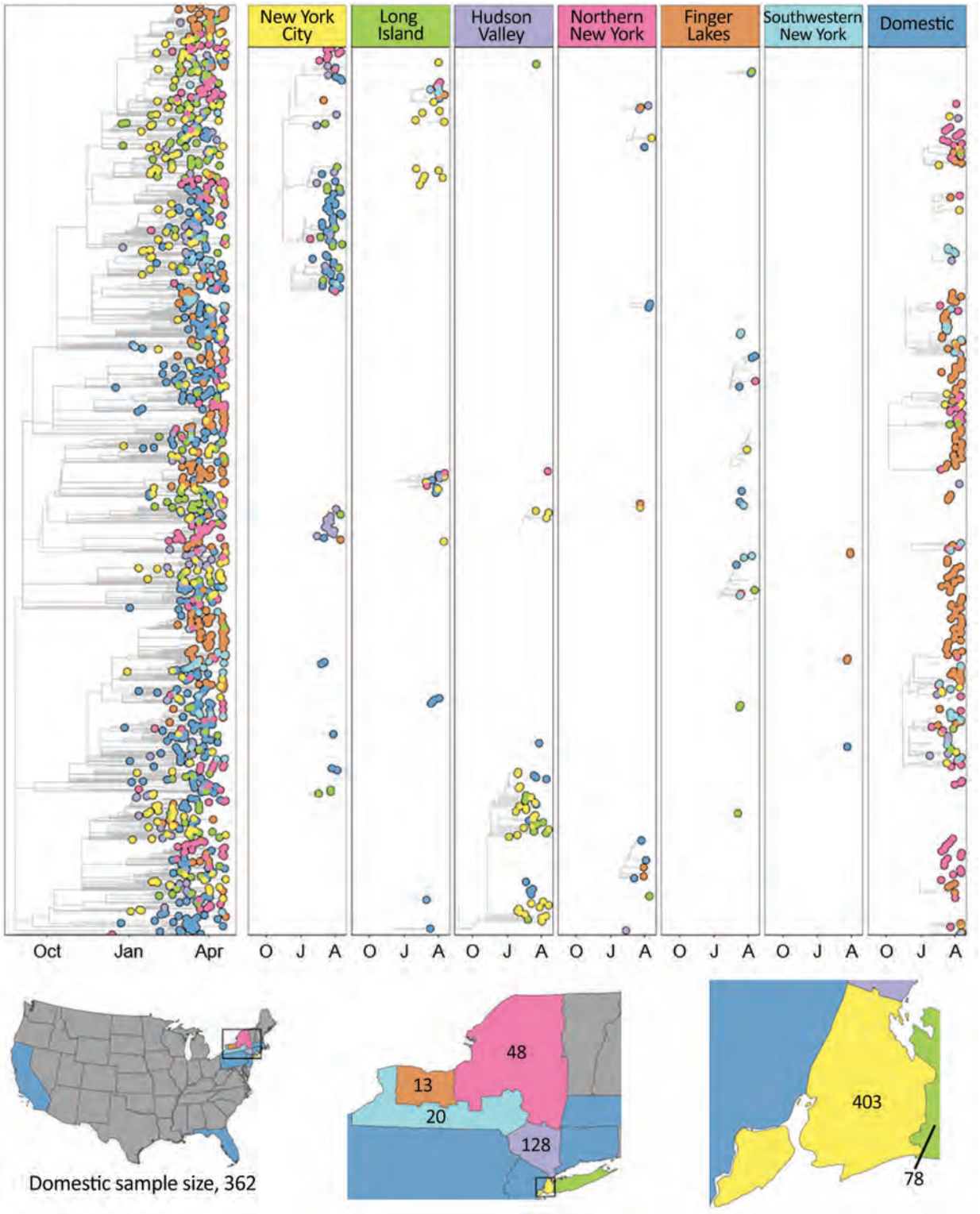

Figure 4. Time-calibrated phylogeny of severe acute respiratory syndrome coronavirus 2 variant B.1.1.7, New York and other states, USA, December 2020–April 2021. Left panel represents a maximum-likelihood phylogeny of 1,195 genomes from New York and other states generated in IQTree 1.6.12 (*20*) with timescale inferred by TreeTime 0.7.6 (*22*) and ancestral state reconstruction performed in BEAST 2.6.2 (*23*). The tree was rooted with a P.1 genome (not shown). Faceted panels indicate the source of B.1.1.7 introductions into different regions of New York and other states (domestic). Only introductions supported by an ancestral state probability of >0.7 are shown. Bottom panel shows locations sampled and sample sizes. A, April; J, January; O, October.

sizes did not always correspond to regions with outsized contributions to the spread of either variant, and subsampling the B.1.526 dataset consistently showed NYC as the dominant source of introductions.

Our phylogeographic and spatiotemporal analyses offer a method for evaluating the competitive advantages of co-circulating SARS-CoV-2 variants. We believe the emergence of VOI B.1.526 contributed to the slower rise of VOC B.1.1.7 as the dominant lineage in NYC compared with regions devoid of B.1.526. In this way, our study describes important dynamic interactions between variants with unequal transmissibility and is potentially generalizable to interactions between any known variants, including the highly transmissible Delta and Omicron variants and other variants to come.

Acknowledgments

The authors gratefully acknowledge the Advanced Genomic Technologies Core of the Wadsworth Center, where all next-generation sequencing was performed. We also graciously thank the New York State clinical laboratories that submitted SARS-CoV-2–positive specimens to Wadsworth for sequence analysis, all originating and submitting laboratories for their SARS-CoV-2 sequence contributions to the GISAID database, Wadsworth Center's Virology Laboratory for initial processing of specimens, and the Bioinformatics Core for sequence processing and analysis.

Initial funding for sequencing was generously provided by the New York Community Trust. The work for this publication was also funded by the Centers for Disease Control and Prevention (cooperative agreement no. NU50CK000516). Its contents are solely the responsibility of the authors and do not necessarily represent the official views of the Centers for Disease Control and Prevention or the Department of Health and Human Services.

A.R., C.O., E.L.-N., J.P., J.P.K., and D.M.L. declare no conflicts of interest. K.S.G. receives research support from ThermoFisher for the evaluation of new assays for the diagnosis and characterization of viruses, and has a royalty-generating collaborative agreement with Zeptometrix.

Author contributions: A.R. and C.O. conceived of the manuscript. A.R., C.O., and E.L.-N. analyzed data, interpreted results, and wrote and revised the manuscript. A.R., J.P., D.M.L., and K.S.G. contributed to the acquisition and processing of specimens. J.K. generated sequence data. D.M.L. and K.S.G. contributed conceptual insight and revised the manuscript. All authors approved of the final version.

About the Author

Ms. Russell is a research scientist in the Special Projects Unit of the Laboratory of Viral Diseases at the Wadsworth Center, New York State Department of Health, Albany, New York. Her primary research interests are in infectious disease epidemiology, with a particular focus on innovative applications of molecular surveillance methods.

References

1. Grubaugh ND, Hodcroft EB, Fauver JR, Phelan AL, Cevik M. Public health actions to control new SARS-CoV-2 variants. Cell. 2021;184:1127–32. https://doi.org/10.1016/j.cell.2021.01.044
2. Lauring AS, Hodcroft EB. Genetic variants of SARS-CoV-2—what do they mean? JAMA. 2021;325:529–31. https://doi.org/10.1001/jama.2020.27124
3. Frampton D, Rampling T, Cross A, Bailey H, Heaney J, Byott M, et al. Genomic characteristics and clinical effect of the emergent SARS-CoV-2 B.1.1.7 lineage in London, UK: a whole-genome sequencing and hospital-based cohort study. Lancet Infect Dis. 2021;21:1246–56. https://doi.org/10.1016/S1473-3099(21)00170-5
4. Kidd M, Richter A, Best A, Cumley N, Mirza J, Percival B, et al. S-variant SARS-CoV-2 lineage B1.1.7 is associated with significantly higher viral load in samples tested by TaqPath polymerase chain reaction. J Infect Dis. 2021;223:1666–70. https://doi.org/10.1093/infdis/jiab082
5. Planas D, Bruel T, Grzelak L, Guivel-Benhassine F, Staropoli I, Porrot F, et al. Sensitivity of infectious SARS-CoV-2 B.1.1.7 and B.1.351 variants to neutralizing antibodies. Nat Med. 2021;27:917–24. https://doi.org/10.1038/s41591-021-01318-5
6. Tegally H, Wilkinson E, Giovanetti M, Iranzadeh A, Fonseca V, Giandhari J, et al. Detection of a SARS-CoV-2 variant of concern in South Africa. Nature. 2021;592:438–43. https://doi.org/10.1038/s41586-021-03402-9
7. West AP Jr, Wertheim JO, Wang JC, Vasylyeva TI, Havens JL, Chowdhury MA, et al. Detection and characterization of the SARS-CoV-2 lineage B.1.526 in New York. Nat Commun. 2021;12:4886. https://doi.org/10.1038/s41467-021-25168-4
8. World Health Organization. Epidemiological update: variants of SARS-CoV-2 in the Americas. 2021 Mar [cited 2021 Dec 9]. https://iris.paho.org/handle/10665.2/53382
9. Thompson CN, Hughes S, Ngai S, Baumgartner J, Wang JC, McGibbon E, et al.; PhD1. PhD1. Rapid emergence and epidemiologic characteristics of the SARS-CoV-2 B.1.526 variant—New York City, New York, January 1–April 5, 2021. MMWR Morb Mortal Wkly Rep. 2021;70:712–6. https://doi.org/10.15585/mmwr.mm7019e1
10. Annavajhala MK, Mohri H, Wang P, Nair M, Zucker JE, Sheng Z, et al. Emergence and expansion of SARS-CoV-2 B.1.526 after identification in New York. Nature. 2021;597:703–8. https://doi.org/10.1038/s41586-021-03908-2
11. Alpert T, Brito AF, Lasek-Nesselquist E, Rothman J, Valesano AL, MacKay MJ, et al. Early introductions and transmission of SARS-CoV-2 variant B.1.1.7 in the United States. Cell. 2021;184:2595–2604.e13. https://doi.org/10.1016/j.cell.2021.03.061
12. Jung I, Kulldorff M, Richard OJ. A spatial scan statistic for multinomial data. Stat Med. 2010;29:1910–8. https://doi.org/10.1002/sim.3951

13. Kulldorff M. Software for the spatial and space-time scan statistics. 2018 [2021 Dec 9]. http://www.satscan.org
14. Desjardins MR, Hohl A, Delmelle EM. Rapid surveillance of COVID-19 in the United States using a prospective space-time scan statistic: Detecting and evaluating emerging clusters. Appl Geogr. 2020;118:102202. https://doi.org/10.1016/j.apgeog.2020.102202
15. Iyengar VS. Space-time clusters with flexible shapes. MMWR Suppl. 2005;54:71–6.
16. Takahashi K, Kulldorff M, Tango T, Yih K. A flexibly shaped space-time scan statistic for disease outbreak detection and monitoring. Int J Health Geogr. 2008;7:14. https://doi.org/10.1186/1476-072X-7-14
17. Shepard D. A two-dimensional interpolation function for irregularly-spaced data. 1968 Jan 1 [cited 2021 Jun 8]. http://portal.acm.org/citation.cfm?doid=800186.810616
18. Rogerson PA, Plane DA. Geographical analysis of population: with applications to planning and business. International edition. Hoboken (New Jersey): John Wiley and Sons Ltd; 1994.
19. Katoh K, Standley DM. MAFFT multiple sequence alignment software version 7: improvements in performance and usability. Mol Biol Evol. 2013;30:772–80. https://doi.org/10.1093/molbev/mst010
20. Nguyen L-T, Schmidt HA, von Haeseler A, Minh BQ. IQ-TREE: a fast and effective stochastic algorithm for estimating maximum-likelihood phylogenies. Mol Biol Evol. 2015;32:268–74. https://doi.org/10.1093/molbev/msu300
21. Minh BQ, Nguyen MAT, von Haeseler A. Ultrafast approximation for phylogenetic bootstrap. Mol Biol Evol. 2013;30:1188–95. https://doi.org/10.1093/molbev/mst024
22. Sagulenko P, Puller V, Neher RA. TreeTime: Maximum-likelihood phylodynamic analysis. Virus Evol. 2018;4:vex042. https://doi.org/10.1093/ve/vex042
23. Bouckaert R, Vaughan TG, Barido-Sottani J, Duchêne S, Fourment M, Gavryushkina A, et al. BEAST 2.5: an advanced software platform for Bayesian evolutionary analysis. PLOS Comput Biol. 2019;15:e1006650. https://doi.org/10.1371/journal.pcbi.1006650
24. Rambaut A, Drummond AJ, Xie D, Baele G, Suchard MA. Posterior summarization in Bayesian phylogenetics using Tracer 1.7. Syst Biol. 2018;67:901–4. https://doi.org/10.1093/sysbio/syy032
25. Yu G, Smith DK, Zhu H, Guan Y, Lam TT-Y. ggtree: an r package for visualization and annotation of phylogenetic trees with their covariates and other associated data. Methods Ecol Evol. 2017;8:28–36. https://doi.org/10.1111/2041-210X.12628
26. Neher R. The virus is under increasing selection pressure. Max-Planck-Gesellschaft. 2021 [cited 2021 Aug 10]. https://www.mpg.de/16371358/coronavirus-variants
27. Campbell F, Archer B, Laurenson-Schafer H, Jinnai Y, Konings F, Batra N, et al. Increased transmissibility and global spread of SARS-CoV-2 variants of concern as at June 2021. Euro Surveill. 2021;26:2100509. https://doi.org/10.2807/1560-7917.ES.2021.26.24.2100509

Address for correspondence: Kirsten St. George, Laboratory of Viral Diseases, Wadsworth Center, New York State Department of Health, David Axelrod Institute, 120 New Scotland Ave, Albany, New York, NY 12208, USA; email: Kirsten.St.George@health.ny.gov

Treatment Outcomes of Childhood Tuberculous Meningitis in a Real-World Retrospective Cohort, Bandung, Indonesia

Heda M. Nataprawira,[1] Fajri Gafar,[1] Nelly A. Risan, Diah A. Wulandari, Sri Sudarwati, Ben J. Marais, Jasper Stevens, Jan-Willem C. Alffenaar, Rovina Ruslami

We retrospectively evaluated clinical features and outcomes in children treated for tuberculous meningitis (TBM) at Hasan Sadikin Hospital, Bandung, Indonesia, during 2011–2020. Among 283 patients, 153 (54.1%) were <5 years of age, and 226 (79.9%) had stage II or III TBM. Predictors of in-hospital death (n = 44 [15.5%]) were stage III TBM, hydrocephalus, male sex, low-income parents, seizures at admission, and lack of bacillus Calmette-Guérin vaccination. Predictors of postdischarge death (n = 18 [6.4%]) were hydrocephalus, tuberculoma, and lack of bacillus Calmette-Guérin vaccination. At treatment completion, 91 (32.1%) patients were documented to have survived, of whom 33 (36.3%) had severe neurologic sequelae and 118 (41.7%) had unknown outcomes. Predictors of severe neurologic sequelae were baseline temperature ≥38°C, stage III TBM, and baseline motor deficit. Despite treatment, childhood TBM in Indonesia causes substantial neurologic sequelae and death, highlighting the importance of improved early diagnosis, better tuberculosis prevention, and optimized TBM management strategies.

Tuberculosis (TB) is a major global health problem, and an estimated 1.2 million new pediatric cases and 230,000 deaths occurred in children <15 years of age in 2019 (*1*). Tuberculous meningitis (TBM) is the most severe manifestation of TB, leading to high rates of childhood TBM mortality, at an average of 19%, and neurodisability in >50% of survivors, even when treatment is provided (*2*). After infection with *Mycobacterium tuberculosis*, children <2 years of age are at the highest risk for progression to miliary TB and TBM, most likely because of their immature immune systems (*3*). Childhood and adolescent TB has historically been neglected (*4*,*5*); however, recently this condition has begun to gain priority as a focus of global collaborative efforts toward ending TB in children and adolescents (*6*).

The most important predictors of favorable outcome in childhood TBM are early diagnosis and immediate initiation of treatment (*2*). However, incomplete understanding of the pathogenesis, nonspecific symptoms, suboptimal performance of diagnostic tests, and the paucibacillary nature of the disease often result in a lengthy process of obtaining a definite diagnosis (*7*–*9*). Moreover, antimicrobial therapy as currently recommended by the World Health Organization (WHO) for the management of childhood TBM remains suboptimal (*9*,*10*) and most likely contributes to poor outcomes. Summary estimates of neurologic sequelae and death associated with childhood TBM have been described in a meta-analysis, but predictors of these poor outcomes other than diagnosis in the most advanced disease stage were reported to have high heterogeneities across studies (*2*). Data on clinical features and treatment outcomes of childhood TBM from large cohorts of children outside of South Africa are limited (*11*–*13*). In settings in Indonesia, a few small studies have reported clinical outcomes of childhood TBM (*14*–*16*), but none have explored factors associated with the outcomes. This characterization is clinically relevant, enabling early and targeted interventions to optimize care

Author affiliations: Hasan Sadikin Hospital, Bandung, Indonesia (H.M. Nataprawira, N.A. Risan, D.A. Wulandari, S. Sudarwati); Universitas Padjadjaran, Bandung, Indonesia (H.M. Nataprawira, N.A. Risan, D.A. Wulandari, S. Sudarwati, R. Ruslami); University of Groningen, Groningen, the Netherlands (F. Gafar, J. Stevens); Children's Hospital at Westmead, Sydney, New South Wales, Australia (B.J. Marais); University of Sydney, Sydney (B.J. Marais, J.-W.C. Alffenaar); Westmead Hospital, Sydney (J.-W.C. Alffenaar)

DOI: https://doi.org/10.3201/eid2803.212230

[1]These first authors contributed equally to this article.

in this vulnerable population. In this context, our study aimed to assess clinical features of childhood TBM and to evaluate factors associated with poor outcomes, including in-hospital death, postdischarge death, and neurologic sequelae.

Methods

Patients and Setting

This real-world retrospective cohort study consecutively included children <15 years of age treated for TBM at the Department of Child Health of Hasan Sadikin Hospital, a national tertiary teaching hospital in Bandung, Indonesia, during January 2011–December 2020. The study was approved by the Independent Ethics Committee of Hasan Sadikin Hospital (approval no. LB.02.01/X.6.5/91/2021). Because of the retrospective nature of the study design, the Ethics Committee waived the need for written informed consent.

Diagnosis

We established TBM diagnosis on the basis of clinical, laboratory, and radiologic findings (*17*), combining medical history, physical and clinical examinations, tuberculin skin test, chest radiography, cerebrospinal fluid (CSF) analysis, and neuroimaging by using computed tomography (CT) scan. We performed microbiologic examination of CSF and non-CSF samples, including smear microscopy for acid-fast bacilli (AFB), culture for *M. tuberculosis*, and Xpert MTB/RIF assay, depending on sample availability. We assessed diagnostic certainty of definite, probable, or possible TBM by using uniform case definition criteria for TBM research (*18*) (Appendix Table 1, https://wwwnc.cdc.gov/EID/article/28/3/21-2230-App1.pdf). We presumed that patients had drug-susceptible TBM unless drug resistance was proven in Xpert MTB/RIF or drug-susceptibility testing. We excluded TBM patients with drug-resistant TB from the study.

Treatment

We based treatment regimens on the 2010 WHO guidelines in accordance with the Indonesian Paediatric Society guidelines for TBM treatment in children, consisting of daily isoniazid at 10 mg/kg (range 7–15 mg/kg), rifampin at 15 mg/kg (range 10–20 mg/kg), pyrazinamide at 35 mg/kg (range 30–40 mg/kg), and ethambutol at 20 mg/kg (range 15–25 mg/kg) for a 2-month intensive phase, followed by a 10-month continuation phase with isoniazid and rifampin at the same doses (*17*,*19*). We administered all anti-TB drugs orally as fixed-dose combination or single-drug formulation tablets, where available. Patients received facility-based directly observed therapy (DOT) during hospitalization. After discharge, patients received home-based DOT under the supervision of parents or other family members. Most patients received adjunctive oral prednisone (2–4 mg/kg/d) for the first 4–8 weeks, tapered according to the national guidelines (*17*). We treated patients with increased intracranial pressure with hypertonic saline or mannitol 20% (0.5–1 g/kg) every 8 hours. We performed ventriculoperitoneal shunt or extraventricular drain placements in patients with obstructive hydrocephalus, at the discretion of the neurosurgical team.

Data Collection

We collected individual patient data from hospital registry in a predefined form and appropriately deidentified the data before analysis. These data were demographic information (age, sex, parents' education and income, area of living, and length of hospital admission); medical history (HIV infection, bacillus Calmette-Guérin [BCG] vaccination, and TB contact history); clinical characteristics (symptoms of TBM, vital signs, nutritional status, physical and neurologic examinations, tuberculin skin test, Glasgow coma scale [GCS], and TBM staging); laboratory findings (CSF analysis, AFB microscopy, mycobacterial culture, and Xpert MTB/RIF test); radiographic findings (chest radiograph and neuroimaging); and other supporting data (corticosteroid therapy and in-hospital complications).

Definitions

We developed operational definitions for all variables (Appendix Table 2). We defined definite TBM as microbiologic confirmation of CSF and probable TBM as a total diagnostic score of ≥12 when neuroimaging was available or ≥10 when neuroimaging was unavailable. We defined possible TBM as a total score of 6–11 when neuroimaging was available or 6–9 when neuroimaging was unavailable (*18*). We classified TBM staging according to the modified British Medical Research Council grading system (*20*), as follows: stage I, GCS 15 without focal neurologic deficit; stage II, GCS 11–14, or 15 with focal neurologic deficit; and stage III, GCS ≤10. Patients with known BCG vaccination included those who had a documented vaccination history at hospital admission or had a BCG scar in the deltoid region of the upper arm. Motor deficits included hemiparesis, quadriparesis, and diplegia. Other neurologic deficits were signs of upper motor neuron lesion and cranial nerve palsies. We performed motor,

hearing, visual, and neurodevelopmental function assessments at treatment completion as indicated by the attending physicians (Appendix).

Outcomes

Outcomes of hospitalization were recovery (with or without disability), nonrecovery (persistent vegetative state and discharge against medical advice), and death. After 12 months of treatment, we reported the following outcomes: treatment completion, death, and lost to follow-up (LTFU; i.e., patients who stopped treatment for ≥2 consecutive months). "Not evaluated" or "unknown treatment outcome" categories were patients who were transferred back to regional public hospitals or community health clinics for follow-up after discharge. We defined survival as being alive at treatment completion and neurologic sequelae as any motor, hearing, visual, or neurodevelopmental impairment that appeared during the illness and persisted through treatment completion.

Data Analysis

We evaluated associations of patient characteristics with poor outcomes. First, we compared patients who died during hospitalization (in-hospital death) with those who had recovered at the time of discharge; this definition excluded persistent vegetative state and discharge against medical advice. Second, we compared patients who died after discharge (postdischarge death) with those who completed treatment, regardless of their sequelae status; this definition excluded LTFU and unknown outcomes. Third, we compared survivors with neurologic sequelae with those without sequelae; this definition excluded death, LTFU, and unknown outcomes.

We used Cox proportional-hazards regression analysis to assess predictors of in-hospital death. We calculated time to death on the basis of length of stay by subtracting day of admission from day of death. Most patients were discharged within 2 months of hospitalization; in this case, we assumed that recovering patients (with or without disability) discharged before 2 months were alive until the end of 2 months, and thus we censored these patients in the Cox regression analysis. Because the time to death after discharge was not recorded, we assessed associated factors with postdischarge death and neurologic sequelae by using logistic regression analysis. We adjusted our multivariate models for age, sex, and TBM staging, and completed the models with variables showing a trend toward association in univariate analysis. We selected these variables by using backward deletion, and the final models retained all additional variables with a p value <0.1. For logistic regression analysis, we evaluated the goodness-of-fit of the final models by using Hosmer-Lemeshow test and performance by the area under the receiver operating characteristic curve. For Cox regression analysis, we checked proportional hazards assumption using Kaplan-Meier curve before fitting the model, and using log-minus-log survival curve after fitting the model. We used adjusted hazard ratios (aHRs) for Cox regression models and adjusted odds ratios (aORs) for logistic regression models, as well as 95% CIs, to estimate the association between explanatory variables and outcomes. We defined statistical significance as $p<0.05$. We performed all analyses by using IBM SPSS Statistics 26.0 (https://www.ibm.com).

Results

Clinical Characteristics

During the study period (2011–2020), 286 children with TBM were treated at Hasan Sadikin Hospital; 3 patients with rifampin-resistant TB were excluded. No patients had concurrent bacterial meningitis. Among 283 included patients, 150 (53.0%) were boys, 153 (54.1%) were <5 years of age, 183 (64.7%) were malnourished, 226 (79.9%) had stage II or III TBM, and 51 (18.0%) had definite TBM. At admission, most patients had history of fever (88.3%), decreased consciousness (74.6%), and seizures (55.0%); the next most common signs and symptoms were weight loss (37.6%), persistent cough (33.7%), muscle weakness (26.3%), and severe headache (21.9%). These signs and symptoms had existed for >5 days before admission in 87.0% of patients (Table 1). We stratified manifestations by disease staging (Appendix Table 3).

In CSF analysis, most patients had pleocytosis (>10 cells/μL, 76.8%), and lymphocytic predominance (>50%, 81.8%), followed by a low CSF-to-plasma glucose ratio (<0.5, 54.8%), elevated protein level (>100 mg/dL, 51.8%), and hypoglycorrhachia (<40 mg/dL, 41.6%). *M. tuberculosis* susceptible to rifampin was identified by Xpert MTB/RIF assay in 48 (34.3%) of 140 CSF samples and in 76 (33.9%) of 224 non-CSF samples. In neuroimaging, most patients had basal meningeal enhancement (52.4%), followed by hydrocephalus (41.2%), tuberculoma (12.4%), and infarct (10.0%) (Table 2). Among 103 patients with hydrocephalus, 45 (43%) received neurosurgical intervention: 44 (97.8%) ventriculoperitoneal shunt and 1 (2.2%) extraventricular drain.

For in-hospital complications, 106 (37.5%) of the 283 patients had motor disorders, 37 (13.1%) had neurodevelopmental delay, 19 (6.7%) had epileptic

seizures, 17 (6.0%) had visual impairment, 12 (4.2%) had hearing impairment, and 27 (9.5%) had anti-TB drug-induced hepatotoxicity. Adjunctive oral corticosteroid was administered to 262 (92.6%) of patients. In addition, 1 of the patients (a 6-month-old boy with stage II TBM) had severe acute respiratory syndrome coronavirus 2 coinfection (Appendix).

In-Hospital Death

Upon discharge, 231 (81.6%) of 283 patients had recovered (with or without disability), 3 (1.1%) had a persistent vegetative state, and 5 (1.8%) were discharged against medical advice. The remaining 44 (15.5%) died; median time to death was 7 days (interquartile range 3–13 days) after admission (Table 3).

We performed univariate (Appendix Table 4) and multivariate (Table 4) analyses of risk for in-hospital death. In multivariate analysis, factors associated with increased risk were stage III TBM (aHR 5.96 [95% CI 1.39–25.58]), hydrocephalus (aHR 2.32 [95% CI 1.13–4.79]), male sex (aHR 2.10 [95% CI 1.09–4.05]), low-income parents (aHR 2.59

Table 1. Demographic and clinical characteristics at admission of children with TBM treated at Hasan Sadikin Hospital, Bandung, Indonesia, 2011–2020*

	Total patients		<5 y		5–14 y	
Characteristic	No.†	Value	No.†	Value	No.†	Value
Age, y , median (IQR)	283	4.0 (1.0; 10.0)	153	1.0 (0.7–2.4)	130	10.2 (8.0–12.2)
Sex						
M	283	150 (53.0)	153	74 (48.4)	130	76 (58.5)
F	283	133 (47.0)	153	79 (51.6)	130	54 (41.5)
Nutritional status‡						
WFAZ, median (IQR)	227	−2.2 (−3.0 to −1.0)	153	−1.9 (−2.9 to −0.7)	74	−2.5 (−3.2 to −1.7)
HFAZ, median (IQR)	283	−1.6 (−2.6 to −0.3)	153	−1.6 (−2.8 to −0.7)	130	−1.6 (−2.5 to −0.4)
BFAZ, median (IQR)	283	−2.1 (−3.2 to −0.4)	153	−1.7 (−2.8 to −0.2)	130	−2.6 (−3.7 to −0.5)
Moderately malnourished	283	74 (26.1)	153	44 (28.8)	130	30 (23.1)
Severely malnourished	283	109 (38.5)	153	47 (30.7)	130	62 (47.7)
Known BCG vaccination	283	223 (78.8)	153	120 (78.4)	130	103 (79.2)
Known TB contact history	283	73 (25.8)	153	36 (23.5)	130	37 (28.5)
Known HIV co-infection	283	4 (1.4)	153	0 (0.0)	130	4 (3.1)
Baseline temperature, °C, median (IQR)	282	37.0 (36.8–37.9)	153	37.2 (36.9–38.0)	129	37.0 (36.8–37.8)
Symptoms duration, d, median (IQR)§	269	8 (7–11)	145	8 (7–10)	124	9 (7–12)
Symptoms						
Fever	283	250 (88.3)	153	136 (88.9)	130	114 (87.7)
Severe headache	278	61 (21.9)	150	13 (8.7)	128	48 (37.5)
Muscle weakness	278	73 (26.3)	151	40 (26.5)	127	33 (26.0)
Altered consciousness	283	211 (74.6)	153	111 (72.5)	130	100 (76.9)
Seizures	282	155 (55.0)	153	84 (54.9)	129	71 (55.0)
Persistent cough	282	95 (33.7)	152	53 (34.9)	130	42 (32.3)
Poor weight gain or weight loss	279	105 (37.6)	151	51 (33.3)	128	54 (41.5)
Motor function						
Hemiparesis	263	51 (19.4)	142	27 (19.0)	121	24 (19.8)
Quadriparesis	263	95 (36.1)	142	59 (41.5)	121	36 (29.8)
Cranial nerve palsy	277	48 (17.3)	149	31 (20.8)	128	17 (13.3)
Signs of upper motor neuron lesion	264	188 (71.2)	143	93 (65.0)	121	95 (78.5
Signs of raised intracranial pressure	283	47 (16.6)	153	29 (19.0)	130	18 (13.8)
TBM category¶						
Definite	283	51 (18.0)	153	26 (17.0)	130	25 (19.2)
Probable	283	178 (62.9)	153	101 (66.0)	130	77 (59.2)
Possible	283	54 (19.1)	153	26 (17.0)	130	28 (21.5)
GCS, median (IQR)	283	12 (10–14)	153	12 (10–15)	130	12 (10–14)
TBM stage#						
Stage I	283	57 (20.1)	153	35 (22.9)	130	22 (16.9)
Stage II	283	131 (46.3)	153	60 (39.2)	130	71 (54.6)
Stage III	283	95 (33.6)	153	58 (37.9)	130	37 (28.5)

*Values are no. (%) or median (IQR) except as indicated. BCG, bacillus Calmette-Guérin; BFAZ, body mass index-for-age Z-score; GCS, Glasgow Coma Scale; HFAZ, height-for-age Z-score; IQR, interquartile rage; TB, tuberculosis; TBM, tuberculous meningitis; WFAZ, weight-for-age Z-score.
†Number of total patients for whom data were available (denominator).
‡In children <5 years of age, moderate malnutrition was defined as WFAZ or HFAZ ≥–3 but <–2 standard deviation (SD), and severe malnutrition as WFAZ or HFAZ <–3 SD. In children aged 5–14 y, moderate malnutrition was defined as HFAZ or BFAZ ≥–3 but <–2 SD, and severe malnutrition as HFAZ or BFAZ <–3 SD.
§Duration of symptoms before admission.
¶Diagnostic certainty was categorized as definite TBM (microbiologically proven from CSF examination), probable TBM (diagnostic score of ≥10 when neuroimaging was unavailable or ≥12 when neuroimaging was available), and possible TBM (diagnostic score of 6–9 when neuroimaging was unavailable or 6–11 when neuroimaging was available) (*18*).
#TBM staging was classified according to the modified British Medical Research Council grading system as stage I (GCS of 15 with no focal neurologic signs), stage II (GCS 11–14 or 15 with focal neurologic signs), or stage III (GCS ≤10) (*20*).

Table 2. Laboratory and radiographic findings at admission of children with tuberculous meningitis treated at Hasan Sadikin Hospital, Bandung, Indonesia, 2011–2020*

Characteristic	Total patients		Age <5 y		Age 5–14 y	
	No.†	Value	No.†	Value	No.†	Value
CSF analysis, median (IQR)						
Leukocytes, cells/μL	276	44 (11–109)	149	56 (14–117)	127	40 (8–95)
Protein, mg/dL	276	107 (60–239)	151	103 (68–234)	125	120 (46–248)
MN, %	275	83 (60–96)	151	81 (60–95)	124	86 (64–98)
PMN, %	275	15 (4–37)	151	18 (5–40)	124	12 (0.2–36)
Glucose, mg/dL	269	47 (25–66)	150	42 (20–67)	119	52 (34–66)
CSF-to-plasma glucose ratio, median (IQR)	241	0.4 (0.2–0.6)	140	0.4 (0.2–0.6)	101	0.5 (0.3–0.6)
Cerebral imaging‡						
Hydrocephalus	250	103 (41.2)	136	64 (47.1)	114	39 (34.2)
Basal meningeal enhancement	250	131 (52.4)	136	74 (54.4)	114	57 (50.0)
Infarct	250	25 (10.0)	136	12 (8.8)	114	13 (11.4)
Tuberculoma	250	31 (12.4)	136	17 (12.5)	114	14 (12.3)
Chest radiography						
Miliary TB	281	19 (6.8)	152	10 (6.6)	129	9 (7.0)
Other signs of active TB	281	128 (45.6)	152	66 (43.4)	129	62 (48.1)
TST positive§	283	64 (22.6)	153	37 (24.2)	130	27 (20.8)
M. tuberculosis cultured from any source¶	267	26 (9.7)	147	15 (10.2)	120	11 (9.2)
AFB smear microscopy						
Positive from CSF	272	6 (2.2)	149	4 (2.7)	123	2 (1.6)
Positive from any non-CSF sample#	282	49 (17.4)	152	23 (15.1)	130	26 (20.0)
Xpert MTB/RIF testing**						
Positive from CSF	140	48 (34.3)	77	24 (31.2)	63	24 (38.1)
Positive from gastric lavage	212	71 (33.5)	120	43 (35.8)	92	28 (30.4)
Positive from sputum	12	5 (41.7)	2	0	10	5 (50.0)

*Values are no. (%) or median (IQR) except as indicated. AFB, acid-fast bacilli; CSF, cerebrospinal fluid; IQR, interquartile rage; MN, mononuclear cells; PMN, polymorphonuclear cells; TB, tuberculosis; TST, tuberculin skin test.
†Number of total patients for whom data were available (denominator).
‡Cerebral imaging results were obtained mostly from noncontrast brain computed tomography scan, or from magnetic resonance imaging, where available.
§The median size of induration (minimum–maximum range) in patients with a positive TST result was 12 (10–30) mm and in patients with a negative TST result was 0 (0–8) mm.
¶Culture of *M. tuberculosis* from CSF is rarely performed in our setting, mostly because of the limited CSF volume available from lumbar puncture. From our experience, most of the non-CSF specimens were obtained from gastric lavage, and some specimens were obtained from sputum, but our data could not further specify the type of specimens used. Mycobacterial culture were mostly performed on solid media; the use of liquid culture media (MGIT, BACTEC) has only begun in recent years.
#We could not further specify the types of non-CSF specimens used for AFB smear microscopy.
**Data on Xpert MTB/RIF testing results have only been available since 2013.

[95% CI 1.06–6.31]), seizures on admission (aHR 1.96 [95% CI 1.01–3.82]), and unknown BCG vaccination (aHR 1.97 [95% CI 1.03–3.76]). Among children <5 years of age, known history of TB contact was associated with an increased risk for in-hospital death (aHR 2.42 [95% CI 1.06–5.50]), adjusted for age, sex, and TBM staging. We charted Kaplan-Meier curves for several risk groups for in-hospital death (Figure).

Postdischarge Death

After the 12-month follow-up, 272 (96.1%) of 283 patients were evaluated for treatment outcomes, and 11 (3.9%) in ongoing treatment who started taking anti-TB drugs in late 2020 were excluded from further analysis. Among the 272 patients, 91 (33.5%) completed treatment, 1 (0.4%) was LTFU, and 62 (22.8%) died, including 18 (6.6%) who died after discharge; 118 (43.4%) had unknown outcomes (Table 3).

We performed univariate (Appendix Table 5) and multivariate (Table 5) analyses of odds for postdischarge death. Multivariate analysis identified that patients with unknown BCG vaccination status (aOR 5.38 [95% CI 1.07–27.07]) and those with clinical findings during hospitalization such as hydrocephalus (aOR 18.97 [95% CI 2.68–134.38]) and tuberculoma (aOR 8.78 [95% CI 1.10–70.39]) had increased odds of postdischarge death. Among patients with hydrocephalus, the absence of neurosurgical intervention was associated with increased odds of postdischarge death (aOR 11.06 [95% CI 1.61–76.12]), adjusted for age, sex, and TBM staging.

Neurologic Sequelae

Among 91 survivors who completed treatment, 58 (63.7%) had good recovery without neurologic sequelae and 33 (36.3%) had severe neurologic sequelae (Table 3). Of patients with severe neurologic sequelae, 22 (66.7%) had motor disorders, 9 (27.3%) had epileptic seizures, 7 (21.2%) had neurodevelopmental delay, 3 (9.1%) had visual impairment, and 3 (9.1%) had hearing impairment. Neurologic sequelae were

observed in 23% of patients diagnosed with TBM at stage I, 31% at stage II, and 58% at stage III.

We performed univariate (Appendix Table 6) and multivariate (Table 6) analyses of odds for neurologic sequelae. In multivariate analysis, factors associated with higher odds of severe neurologic sequelae were baseline temperature ≥38°C (aOR 6.68 [95% CI 1.55–28.85]), stage III TBM (aOR 5.65 [95% CI 1.21–26.43]), and motor deficits at baseline (aOR 3.64 [95% CI 1.19–11.16]).

Discussion

We present important information from Indonesia about the high rates of neurologic sequelae and death in children with TBM, even when standard therapy has been provided. In TBM, treatment response is often judged by early morbidity, mortality, and relapse rates (*21*). Our overall case-fatality rate for childhood TBM (22.8%) is within the global estimates reported in a recent meta-analysis (19.3% [95% CI 14.0%–26.1%]) (*2*) but is lower than that reported in the same setting during 2007–2010 (34.4%) (*14*). The high proportion of unknown treatment outcomes in this study (43%) is unfortunate but comparable to a previous report in our hospital during 2007–2010 (45%), even after phone calls and home visits had been made (*14*). Considering the increased likelihood of death in patients with unknown outcomes after hospital discharge, the case-fatality rate recorded is probably an underestimate.

A diagnosis of TBM alone has been associated with an increased risk for childhood death compared with other types of TB (*22*), and this risk may be exacerbated by specific risk factors identified in this study. TBM diagnosis in stage II or III, hydrocephalus, and seizures are not surprising risk factors for death because they reflect more advanced disease. Neurosurgical complications (e.g., shunt blockage or infections) may have contributed to poor outcomes, but we believe the effect was minimal because the postdischarge death rate was significantly reduced with neurosurgery. The association of tuberculoma on baseline CT with postdischarge death might be related to a paradoxical worsening of tuberculomas during treatment (*23*). For male sex and low-income parents, their associations with in-hospital death are unclear but could be related to biologic factors (particularly for sex differences) or largely attributed to socioeconomic and cultural determinants (*24*).

This study confirms that TBM mainly affects young children (*8*), illustrated by 54% of our patients being <5 years of age. The high proportions of altered consciousness and seizures at admission suggest that these symptoms are the main reasons for clinicians to suspect childhood TBM. This finding raises important issues about training of healthcare

Table 3. Hospitalization and end of treatment outcome, stratified by disease staging, in children with tuberculous meningitis treated at Hasan Sadikin Hospital, Bandung, Indonesia, 2011–2020*

Variable	Total	Stage I†	Stage II†	Stage III†
Outcome of hospitalization‡				
Cases, no.	283	57	131	95
Recovered	231 (81.6)	54 (94.7)	111 (84.7)	66 (69.5)
Not recovered	8 (2.8)	1 (1.8)	5 (3.8)	2 (2.1)
Died	44 (15.5)	2 (3.5)§	15 (11.5)	27 (28.4)
Length of hospital stay, d, median (IQR)	10 (7–17)	9 (7–14)	10 (7–14)	15 (8–25)
Time to death, d, median (IQR)	7 (3–13)	(4–14)¶	6 (2–8)	8 (3–16)
Outcome at treatment completion‡#				
Cases, no.	272	56	122	94
Completed treatment	91 (33.5)	22 (39.3)	45 (36.9)	24 (25.5)
Without neurologic sequelae**	58 (63.7)	17 (77.3)	31 (68.9)	10 (41.7)
With neurologic sequelae**	33 (36.3)	5 (22.7)	14 (31.1)	14 (58.3)
Died	62 (22.8)	2 (3.6)	22 (18.0)	38 (40.4)
Died after hospital discharge	18 (6.6)	0 (0.0)	7 (5.7)	11 (11.7)
Lost to follow-up	1 (0.4)	0 (0.0)	1 (0.8)	0 (0.0)
Unknown treatment outcome	118 (43.4)	32 (57.1)	54 (44.3)	32 (34.0)

*Values are no. (%) except as indicated. IQR, interquartile rage.
†Stage I was defined as Glasgow Coma Scale (GCS) of 15 with no focal neurologic signs, stage II as GCS of 11–14 or 15 with focal neurologic signs, and stage III as GCS ≤10 (*20*).
‡On hospital discharge, recovering patients were those who had clinical improvement (with or without disability), whereas non-recovering patients were those who had persistent vegetative state or discharged against medical advice. Treatment completion included patients who completed 12 mo of TBM therapy. Lost to follow-up included patients who stopped treatment for two consecutive months or more. Unknown treatment outcome included patients who were transferred back to regional public hospitals or community health clinics for follow-up after discharge. Neurologic sequelae were defined as any motor, hearing, visual, or neurodevelopmental impairment that appeared during the illness and persisted through treatment completion.
§The causes of death in two patients with stage I TBM were hospital acquired pneumonia + thalassemia major (n = 1), and intracranial metastases of Burkitt lymphoma + increased intracranial pressure (n = 1).
¶Minimum–maximum range.
#Excluding 11 patients who were still in ongoing treatment.
**Percentages were calculated only in patients who completed 12 mo of treatment.

Table 4. Multivariate Cox proportional-hazards regression model for factors associated with in-hospital death in children treated for TBM at Hasan Sadikin Hospital, Bandung, Indonesia, 2011–2020*

Variable	Died†‡	Alive†	Crude HR (95% CI)	p value	aHR (95% CI)	p value
No. cases	44	231				
Age, y						
<2	13 (29.5)	78 (33.8)	0.78 (0.37–1.67)	0.527	0.78 (0.36–1.68)	0.522
2–4	11 (25.0)	47 (20.3)	1.04 (0.47–2.29)	0.992	0.93 (0.41–2.12)	0.867
5–9	6 (13.6)	43 (18.6)	0.65 (0.25–1.70)	0.384	0.41 (0.15–1.11)	0.079
10–14	14 (31.8)	63 (27.3)	Referent		Referent	
Sex						
M	29 (65.9)	118 (51.1)	1.72 (0.92–3.20)	0.089	2.10 (1.09–4.05)	0.027
F	15 (34.1)	113 (48.9)	Referent		Referent	
TBM stage§,¶						
Stage I	2 (4.5)	54 (23.4)	Referent		Referent	
Stage II	15 (34.1)	111 (48.1)	3.53 (0.81–15.44)	0.094	2.57 (0.58–11.41)	0.214
Stage III	27 (61.4)	66 (28.6)	9.16 (2.18–38.51)	0.003	5.96 (1.39–25.58)	0.016
Parents' monthly income#						
USD ≤140	33 (75.0)	136 (58.9)	2.79 (1.17–6.67)	0.021	2.59 (1.06–6.31)	0.036
USD >140	6 (13.6)	74 (32.0)	Referent		Referent	
Unknown	5 (11.4)	21 (9.1)	2.73 (0.83–8.95)	0.097	2.04 (0.59–7.02)	0.261
Known BCG vaccination						
No	15 (34.1)	44 (19.0)	2.01 (1.08–3.76)	0.028	1.97 (1.03–3.76)	0.040
Yes	29 (65.9)	187 (81.0)	Referent		Referent	
Hydrocephalus on CT¶						
No	12 (27.3)	133 (57.6)	Referent		Referent	
Yes**	22 (50.0)	76 (32.9)	3.00 (1.48–6.05)	0.002	2.32 (1.13–4.79)	0.022
Unknown	10 (22.7)	22 (9.5)	4.38 (1.89–10.13)	0.001	4.21 (1.77–10.01)	0.001
Seizures on admission¶						
No	13 (29.5)	112 (49.5)	Referent		Referent	
Yes	31 (70.5)	119 (51.5)	2.09 (1.09–3.99)	0.026	1.96 (1.01–3.82)	0.048

*Values are no. (%) except as indicated. aHR, adjusted hazard ratio; BCG, bacillus Calmette-Guérin; CT, computed tomography; GCS, Glasgow Coma Scale; IDR, Indonesian Rupiah; TBM, tuberculous meningitis.
†Including patients who died or had recovered (with or without disability) on hospital discharge, and excluding patients who had persistent vegetative state or discharged against medical advice.
‡Signs of upper motor neuron lesion was associated with an increased risk of in-hospital death in univariate analysis, but did not remain significant in multivariate analysis. Signs of raised intracranial pressure with hydrocephalus as well as GCS score with TBM stage had the likelihood of collinearity; therefore, only hydrocephalus and TBM staging were included in the final multivariate model. For HIV coinfection, although it was significantly associated with in-hospital death in univariate analysis, we did not include this variable in multivariate analysis due to the selective HIV testing and a very low number of patients with HIV positive (n = 4).
§Stage I TBM was defined as GCS of 15 with no focal neurologic signs, stage II TBM as GCS of 11–14 or 15 with focal neurologic signs, and stage III TBM as GCS ≤10 (*20*).
¶TBM staging might interact with hydrocephalus and seizures on admission; however, due to the low number of patients with stage I TBM who died during hospitalization (n = 2), these potential interactions could not be assessed in the Cox regression model.
#Parents' monthly income was estimated based on the current provincial minimum wage for West Java (IDR 1.810.350,00, rounded up to IDR 2.000.000,00, equal to approximately USD 140).
**In-hospital death among children with hydrocephalus was not significantly different between those who received neurosurgical intervention and who did not receive neurosurgical intervention (p = 0.604).

providers to improve their ability to recognize and diagnose the disease (*25*). In addition, increasing community awareness of the signs and symptoms of TBM by including enhanced messaging in existing TB advocacy materials has the potential to improve early recognition of childhood TBM (*25*).

The difficulty of early diagnosis is confirmed by the fact that nearly 80% of our patients had stage II or III TBM at admission. This high proportion of patients with advanced disease at admission is supported by various studies from high TB incidence countries in Asia and Africa (*11*,*14*,*26*,*27*), and only slightly reduced in low TB incidence countries in Europe, where 66% of the patients have stage II or III TBM at admission (*28*). In many cases, nonspecific symptoms such as fever, headache, and vomiting are often wrongly interpreted, and other systemic symptoms such as cough, weight loss, and night sweats may be suggestive of TB but are also nonspecific (*18*).

The high risk for death in patients with unknown BCG vaccination status highlights the importance of better TB prevention. In young children, BCG vaccination has consistently shown protection against miliary TB and TBM (*29*–*31*) for ≥10 years after vaccination (*29*). The global shortage of BCG vaccine since 2013, particularly in countries where it was procured through UNICEF (*32*), has led to an alarming increase in the number of hospital admissions for childhood TBM (*33*). In Indonesia, where BCG vaccine is recommended at birth for all infants and annual coverage has been an estimated ≈90% since 2011 (*34*), this shortage has also been experienced, although the vaccine supply depends largely on domestic production by Biofarma, a state-owned vaccine manufacturer

(*32*). In addition, among children with prolonged exposure to *M. tuberculosis*, protection with BCG vaccination alone is unlikely to be sufficient. Without early initiation of preventive therapy, the risk for TB disease development among exposed young children and infants is very high (*35*), but data on preventive treatment in our patients with known TB contact history were unavailable. Taken together, aside from improving BCG vaccination coverage, it is important to reduce TB transmission in children through contact investigation, coupled with preventive therapy among exposed children.

Neurologic sequelae occurred mostly in our patients who had stage III TBM at admission (58%), a higher rate than for those in stage I (23%) and II (31%). A meta-analysis in children with TBM confirms this upward trend with pooled estimates of 27% in stage I, 41% in stage II, and 70% in stage III (*2*). Recent studies also reported an increase in neurologic sequelae among children with stage II or III TBM (*36*,*37*). In children in South Africa with TBM, severe neurologic sequelae and death were significantly associated with cerebral infarctions (*11*); we did not find this association in our study. A high proportion of patients had hemiparesis or quadriparesis at admission in this study (55%), comparable to that reported in South Africa (62.1%) (*11*), but few patients had cerebral infarcts on brain CT (10%). This finding is difficult to explain but is likely attributable to the low sensitivity of early infarct detection with noncontrast CT as commonly used in the study.

Given the substantial levels of neurologic sequelae and death associated with childhood TBM, the current standard care for childhood TBM clearly remains suboptimal. New diagnostic strategies should be tested in future clinical trials because of the poor sensitivity, specificity, or both of available laboratory and clinical diagnostic tools (*38*). For TBM treatment, future research should explore the use of intensified antimicrobial therapy that contains high-dose

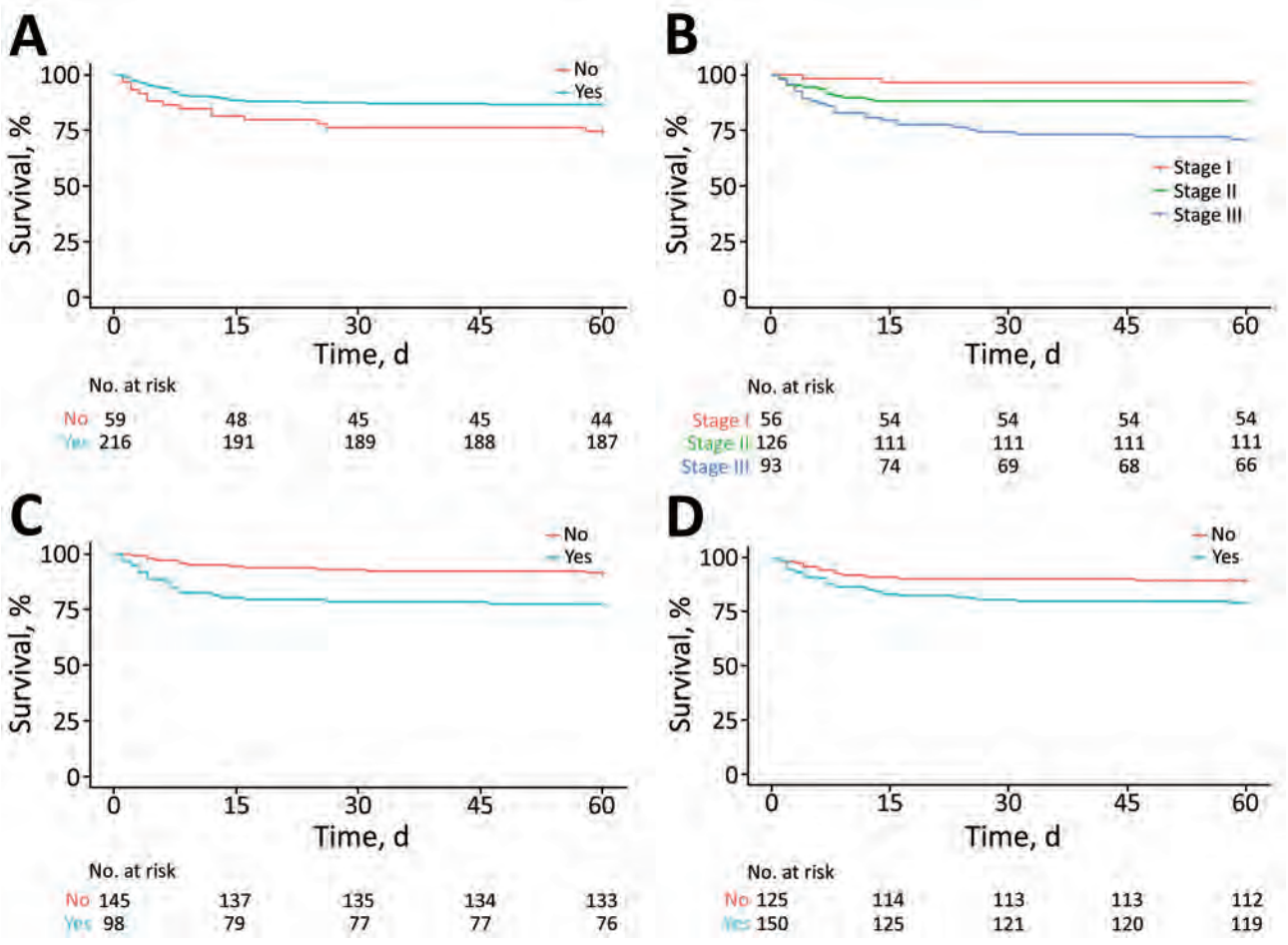

Figure. Survival curves for in-hospital death in children treated for tuberculous meningitis at Hasan Sadikin Hospital, Bandung, Indonesia, 2011–2020. A) Known bacillus Calmette-Guérin (BCG) vaccination status (yes/no); B) tuberculous meningitis stage (I–III); C) radiographic evidence of hydrocephalus (yes/no); D) presence of seizures at hospital admission (yes/no).

rifampin and other anti-TB drugs with better CSF penetration and bactericidal activity (*39*). On the basis of observational data among children in South Africa, a 6-month intensified TBM treatment regimen with isoniazid, rifampin, and ethionamide at 20 mg/kg/day and pyrazinamide at 40 mg/kg/day was reported to be safe and effective, with lower case-fatality rates ranging from 4%–14% (*11*,*12*,*40*). This short-course, high-dose therapy has recently been added by WHO as an alternative treatment option for childhood TBM (*41*). Suboptimal plasma and CSF concentrations with standard doses of oral rifampin at 10–20 mg/kg/day in children with TBM have also been reported in recent pharmacokinetic studies (*42*,*43*), advocating the use of higher rifampin doses with further efficacy and safety evaluations.

Minimizing damaging immunologic responses leading to neurologic complications by using anti-inflammatory drugs such as aspirin, thalidomide, and specific tumor necrosis factor α antibodies (e.g., infliximab) also warrants further investigations (*10*,*44*–*46*), particularly for paradoxical TBM reactions and potentially also for TBM in general. There is no evidence that corticosteroids (the mainstay of host-directed therapy) reduce neurologic sequelae although they do improve the TBM survival rate (*47*). Therefore, optimization of anti-TB drug dosing and consideration of immunomodulatory therapy beyond corticosteroids are required to improve childhood TBM treatment outcomes (*9*,*46*). Moreover, understanding the disease pathogenesis pathways of childhood TBM, particularly in the cerebral inflammatory response, is likely to offer valuable insights into potential targets for new treatment interventions (*48*,*49*).

The main limitation of our study is that, although most of the essential information recommended for TBM research was available (*50*), the retrospective nature of the study did not provide us with complete records on all key variables, especially longer-term outcome. Our dataset did not contain information on the drug-susceptibility pattern of the source case and was

Table 5. Multivariate logistic regression model for predictors of postdischarge death, tracked until the end of treatment in children treated for TBM at Hasan Sadikin Hospital, Bandung, Indonesia, 2011–2020*†

Variable	Died‡§	Alive‡	Crude OR (95% CI)	p value	aOR (95% CI)	p value
No. cases	18	91				
Age group, y						
<2	3 (16.7)	26 (28.6)	0.65 (0.15–2.86)	0.573	0.13 (0.01–1.12)	0.064
2–4	6 (33.3)	9 (9.9)	3.78 (0.98–14.56)	0.054	1.60 (0.26–9.86)	0.610
5–9	3 (16.7)	22 (24.2)	0.77 (0.17–3.41)	0.734	0.23 (0.03–1.75)	0.156
10–14	6 (33.3)	34 (37.4)	Referent		Referent	
Sex						
M	10 (55.6)	39 (42.9)	1.67 (0.60–4.61)	0.325	3.43 (0.76–15.45)	0.109
F	8 (44.4)	52 (57.1)	Referent		Referent	
TBM stage¶						
Stage I or II	7 (38.9)	67 (73.6)	Referent		Referent	
Stage III	11 (61.1)	24 (26.4)	4.39 (1.53–12.6)	0.006	2.31 (0.56–9.54)	0.247
Known BCG vaccination						
No	7 (38.9)	15 (16.5)	3.22 (1.08–9.66)	0.037	5.38 (1.07–27.07)	0.041
Yes	11 (61.1)	76 (83.5)	Referent		Referent	
Hydrocephalus on CT						
No	3 (16.7)	66 (72.5)	Referent		Referent	
Yes	13 (72.2)	23 (25.3)	12.43 (3.25–47.59)	<0.001	18.97 (2.68–134.38)	0.003
Unknown	2 (11.1)	2 (2.2)	22.00 (2.26–214.23)	0.008	17.85 (1.30–245.49)	0.031
Tuberculoma on CT#						
No	12 (66.7)	85 (93.4)	Referent		Referent	
Yes	4 (22.2)	4 (4.4)	7.08 (1.56–32.13)	0.011	8.78 (1.10–70.39)	0.041
Positive TST						
No	10 (55.6)	76 (83.5)	Referent		Referent	
Yes	8 (44.4)	15 (16.5)	4.05 (1.37–11.96)	0.011	4.79 (0.96–24.05)	0.057

*Data are no. (%) except as indicated. aOR, adjusted odds ratio; BCG, bacillus Calmette-Guérin; CT, computed tomography; GCS, Glasgow Coma Scale; TBM, tuberculous meningitis; TST, tuberculin skin test.
†The goodness-of-fit of the model using Hosmer-Lemeshow test was p = 0.877. The performance of the model using the area under the receiver operating characteristic curve was 0.91 (95% CI 0.85–0.97).
‡Including patients who were tracked until death or treatment completion, and excluding patients who were lost to follow-up and with unknown treatment outcomes.
§Positive TST and motor disorders were associated with higher odds of postdischarge death in univariate analysis but did not remain significant in multivariate analysis. Signs of raised intracranial pressure with hydrocephalus as well as GCS score with TBM staging had the likelihood of collinearity; therefore, only hydrocephalus and TBM staging were included in the final multivariate model. In our subgroup analysis among children aged <5 y, no additional independent predictors of postdischarge death were observed.
¶Stage I TBM was defined as GCS of 15 with no focal neurologic signs, stage II TBM as GCS of 11–14 or 15 with focal neurologic signs, and stage III TBM as GCS ≤10 (*20*). Patients with stages I and II TBM were combined in the analysis because there were no patients with TBM stage I died after hospital discharge.
#Because of the redundancy with the variable "unknown status of hydrocephalus," the degree of freedom for the variable "unknown status of tuberculoma" was reduced.

Table 6. Multivariate logistic regression model for predictors of severe neurologic sequelae at treatment completion in children treated for TBM at Hasan Sadikin Hospital, Bandung, Indonesia, 2011–2020*†

Variable	Neurologic sequelae		Crude OR (95% CI)	p value	aOR (95% CI)	p value
	Yes‡§	No‡				
Cases, no.	33	58				
Age group, y						
<2	13 (39.4)	13 (22.4)	2.78 (0.94–8.20)	0.064	2.59 (0.67–10.00)	0.166
2–4	2 (6.1)	7 (12.1)	0.79 (0.14–4.55)	0.795	0.97 (0.13–7.28)	0.974
5–9	9 (27.3)	13 (22.4)	1.92 (0.61–6.02)	0.261	1.32 (0.34–5.07)	0.684
10–14	9 (27.3)	25 (43.1)	Referent		Referent	
Sex						
M	12 (36.4)	27 (46.6)	0.66 (0.27–1.58)	0.346	0.48 (0.16–1.45)	0.191
F	21 (63.6)	31 (53.4)	Referent		Referent	
TBM stage¶						
Stage I	5 (15.2)	17 (29.3)	Referent		Referent	
Stage II	14 (42.4)	31 (53.4)	1.53 (0.47–5.00)	0.476	1.83 (0.43–7.75)	0.410
Stage III	14 (42.4)	10 (17.2)	4.76 (1.32–17.22)	0.017	5.65 (1.21–26.43)	0.028
Baseline temperature ≥38°C						
No	23 (69.7)	53 (91.4)	Referent		Referent	
Yes	10 (30.3)	5 (8.6)	4.61 (1.42–14.99)	0.011	6.68 (1.55–28.85)	0.011
Motor deficit at baseline						
No	8 (24.2)	27 (46.6)	Referent		Referent	
Yes	24 (72.7)	23 (39.7)	3.52 (1.33–9.33)	0.011	3.64 (1.19–11.16)	0.024
Unknown	1 (3.0)	8 (13.8)	0.42 (0.05–3.90)	0.447	0.39 (0.03–4.58)	0.452

*Values are no. (%) except as indicated. aOR, adjusted odds ratio; TB, tuberculosis; TBM, tuberculous meningitis.
†The goodness-of-fit of the model using Hosmer-Lemeshow test was p = 0.473. The performance of the model using the area under the receiver operating characteristic curve was 0.80 (95% CI 0.70–0.90).
‡Including patients who were tracked until treatment completion, and excluding those who died, who were lost to follow-up and with unknown treatment outcomes (which represents a large percentage of the cohort (n = 118, 43.3%). Neurologic sequelae were defined as any motor, hearing, visual or neurodevelopmental impairment that appeared during the illness and persisted through treatment completion.
§Suggestive TB through chest radiography was associated with an increased odd of neurologic sequelae in univariate analysis but did not remain significant in multivariate analysis. In our subgroup analysis among children aged <5 y, no additional independent predictors for neurologic sequelae were found.
¶Stage I TBM was defined as Glasgow Coma Scale (GCS) of 15 with no focal neurologic signs, stage II TBM as GCS of 11–14 or 15 with focal neurologic signs, and stage III TBM as GCS ≤10 (*20*).

unable to reliably distinguish a contact history with an infectious drug-susceptible or drug-resistant TB case. This limitation may have led to underdiagnosis of drug-resistant TB disease, resulting in inappropriate antimicrobial therapy that may have contributed to poor outcomes. However, drug-resistance rates are not known to be high in the study population, an estimated 2.4% of multidrug-resistant TB among new cases in Indonesia (*1*), limiting the likely effect of inappropriate treatment of drug-resistant disease. In addition, the frequency of total neurologic sequelae at treatment completion might be underestimated in this study, given that mild to moderate sequelae were not tested or recorded in the database. Despite its limitations, this study provides one of the largest child TBM cohorts ever described globally outside of South Africa (*11*), and includes a wide range of variables in the analysis.

In conclusion, childhood TBM in Indonesia causes substantial neurologic sequelae and death, despite standard treatment. Several predictors of in-hospital death, postdischarge death, and neurologic sequelae have been identified for further development of early and tailored interventions to optimize care in this population. This study emphasizes the importance of improved early diagnosis, better TB prevention beyond BCG vaccination, and optimizing TBM management strategies, including antimicrobial and supportive therapy.

Acknowledgments

We thank the director of Hasan Sadikin Hospital and head of the Department of Child Health of Hasan Sadikin Hospital for accommodating the study. We also thank Raisa Moeis for helping with data checking.

This work was supported by the Academic Leadership Grant of the Universitas Padjadjaran (grant no. 4851/UN6.C/LT/2018) awarded to H.M.N. The funding organization was in no way involved in study design or conception, writing or reviewing of the manuscript, and decision to submit the manuscript for publication.

H.M.N. was the principal investigator. H.M.N., R.R., N.A.R., and F.G. contributed to conception and design of the study. H.M.N. contributed to data collection, whereas H.M.N. and F.G. contributed to data cleaning. F.G. performed data analysis and created tables and figures. H.M.N., F.G., N.A.R., D.A.W., S.S., B.J.M., J.S., J.W.C.A., and R.R. interpreted the results. F.G. drafted the manuscript under the supervision of H.M.N. and J.W.C.A. All authors critically revised the manuscript for important intellectual content and approved the final version of the manuscript before submission for publication.

About the Author

Dr. Nataprawira is a professor of pediatrics at the Universitas Padjadjaran and Hasan Sadikin Hospital. Her primary research interests include pediatric respirology, particularly tuberculosis. Mr. Gafar is a PhD student at the University of Groningen. His primary research interests include the epidemiology and pharmacotherapy of pediatric tuberculosis.

References

1. World Health Organization. Global tuberculosis report 2020. 2020 [cited 2021 Dec 28]. https://www.who.int/publications/i/item/9789240013131
2. Chiang SS, Khan FA, Milstein MB, Tolman AW, Benedetti A, Starke JR, et al. Treatment outcomes of childhood tuberculous meningitis: a systematic review and meta-analysis. Lancet Infect Dis. 2014;14:947–57. https://doi.org/10.1016/S1473-3099(14)70852-7
3. Marais BJ, Gie RP, Schaaf HS, Hesseling AC, Obihara CC, Starke JJ, et al. The natural history of childhood intrathoracic tuberculosis—a critical review of the pre-chemotherapy literature. Int J Tuberc Lung Dis. 2004;8:392–402.
4. García-Basteiro AL, Schaaf HS, Diel R, Migliori GB. Adolescents and young adults: a neglected population group for tuberculosis surveillance. Eur Respir J. 2018;51:1800176. https://doi.org/10.1183/13993003.00176-2018
5. Marais BJ, Amanullah F, Gupta A, Becerra MC, Snow K, Ngadaya E, et al. Tuberculosis in children, adolescents, and women. Lancet Respir Med. 2020;8:335–7. https://doi.org/10.1016/S2213-2600(20)30077-1
6. World Health Organization. Roadmap towards ending TB in children and adolescents, second edition [cited 2021 Dec 28]. https://apps.who.int/iris/bitstream/handle/10665/274374/9789241514668-eng.pdf
7. Wilkinson RJ, Rohlwink U, Misra UK, van Crevel R, Mai NTH, Dooley KE, et al.; Tuberculous Meningitis International Research Consortium. Tuberculous meningitis. Nat Rev Neurol. 2017;13:581–98. https://doi.org/10.1038/nrneurol.2017.120
8. van Toorn R, Solomons R. Update on the diagnosis and management of tuberculous meningitis in children. Semin Pediatr Neurol. 2014;21:12–8. https://doi.org/10.1016/j.spen.2014.01.006
9. Hill J, Marais B. Improved treatment for children with tuberculous meningitis: acting on what we know. Arch Dis Child. 2022;107:68–9. https://doi.org/10.1136/archdischild-2021-322660
10. Huynh J, Thwaites G, Marais BJ, Schaaf HS. Tuberculosis treatment in children: the changing landscape. Paediatr Respir Rev. 2020;36:33–43.
11. van Well GTJ, Paes BF, Terwee CB, Springer P, Roord JJ, Donald PR, et al. Twenty years of pediatric tuberculous meningitis: a retrospective cohort study in the western cape of South Africa. Pediatrics. 2009;123:e1–8. https://doi.org/10.1542/peds.2008-1353
12. van Toorn R, Schaaf HS, Laubscher JA, van Elsland SL, Donald PR, Schoeman JF. Short intensified treatment in children with drug-susceptible tuberculous meningitis. Pediatr Infect Dis J. 2014;33:248–52. https://doi.org/10.1097/INF.0000000000000065
13. Yaramiş A, Gurkan F, Elevli M, Söker M, Haspolat K, Kirbaş G, et al. Central nervous system tuberculosis in children: a review of 214 cases. Pediatrics. 1998;102:E49. https://doi.org/10.1542/peds.102.5.e49
14. Nataprawira HM, Ruslianti V, Solek P, Hawani D, Milanti M, Anggraeni R, et al. Outcome of tuberculous meningitis in children: the first comprehensive retrospective cohort study in Indonesia. Int J Tuberc Lung Dis. 2016;20:909–14. https://doi.org/10.5588/ijtld.15.0555
15. Faried A, Ramdan A, Arifin MZ, Nataprawira HM. Characteristics and surgical outcomes of tuberculous meningitis and of tuberculous spondylitis in pediatric patients at Dr. Hasan Sadikin Hospital, Bandung: a single center experience. Interdiscip Neurosurg Adv Tech Case Manag. 2018;11:37–40. https://doi.org/10.1016/j.inat.2017.09.008
16. Faried A, Putra SPS, Suradji EW, Trianto, Akbar RR, Nugraheni NK, et al. Characteristics and outcomes of pediatric tuberculous meningitis patients with complicated by hydrocephalus with or without tuberculoma at Regional Public Hospital Teluk Bintuni, West Papua, Indonesia. Interdiscip Neurosurg. 2020;19:100609. https://doi.org/10.1016/j.inat.2019.100609
17. Rahajoe NN, Nawas A, Setyanto DB, Kaswandani N, Triasih R, Indawati W, et al. Buku petunjuk teknis manajemen dan tatalaksana TB anak [National guideline on the management of tuberculosis in children]. Ministry of Health of the Republic of Indonesia. Jakarta (Indonesia): Ministry of Health of the Republic of Indonesia; 2016.
18. Marais S, Thwaites G, Schoeman JF, Török ME, Misra UK, Prasad K, et al. Tuberculous meningitis: a uniform case definition for use in clinical research. Lancet Infect Dis. 2010;10:803–12. https://doi.org/10.1016/S1473-3099(10)70138-9
19. World Health Organization. Guidance for national tuberculosis programmes on the management of tuberculosis in children (2nd edition). World Health Organization; 2014 [cited 2022 Feb 5]. https://www.who.int/publications/i/item/9789241548748
20. Thwaites GE, Nguyen DB, Nguyen HD, Hoang TQ, Do TTO, Nguyen TCT, et al. Dexamethasone for the treatment of tuberculous meningitis in adolescents and adults. N Engl J Med. 2004;351:1741–51. https://doi.org/10.1056/NEJMoa040573
21. Donald PR. The chemotherapy of tuberculous meningitis in children and adults. Tuberculosis (Edinb). 2010;90:375–92. https://doi.org/10.1016/j.tube.2010.07.003
22. Gafar F, Van't Boveneind-Vrubleuskaya N, Akkerman OW, Wilffert B, Alffenaar JC. Nationwide analysis of treatment outcomes in children and adolescents routinely treated for tuberculosis in the Netherlands. Eur Respir J. 2019;54:1901402. https://doi.org/10.1183/13993003.01402-2019
23. Kalita J, Prasad S, Misra UK. Predictors of paradoxical tuberculoma in tuberculous meningitis. Int J Tuberc Lung Dis. 2014;18:486–91. https://doi.org/10.5588/ijtld.13.0556
24. Chidambaram V, Tun NL, Majella MG, Ruelas Castillo J, Ayeh SK, Kumar A, et al. Male sex is associated with worse microbiological and clinical outcomes following tuberculosis treatment: a retrospective cohort study, a systematic review of the literature, and meta-analysis. Clin Infect Dis. 2021;73:1580–8. https://doi.org/10.1093/cid/ciab527
25. Basu Roy R, Bakeera-Kitaka S, Chabala C, Gibb DM, Huynh J, Mujuru H, et al. Defeating paediatric tuberculous meningitis: applying the WHO "defeating meningitis by 2030: global roadmap." Microorganisms. 2021;9:857. https://doi.org/10.3390/microorganisms9040857
26. Maree F, Hesseling AC, Schaaf HS, Marais BJ, Beyers N, van Helden P, et al. Absence of an association between Mycobacterium tuberculosis genotype and clinical

features in children with tuberculous meningitis. Pediatr Infect Dis J. 2007;26:13–8. https://doi.org/10.1097/01.inf.0000247044.05140.c7
27. Rohlwink UK, Donald K, Gavine B, Padayachy L, Wilmshurst JM, Fieggen GA, et al. Clinical characteristics and neurodevelopmental outcomes of children with tuberculous meningitis and hydrocephalus. Dev Med Child Neurol. 2016;58:461–8. https://doi.org/10.1111/dmcn.13054
28. Basu Roy R, Thee S, Blázquez-Gamero D, Falcón-Neyra L, Neth O, Noguera-Julian A, et al.; ptbnet TB Meningitis Study Group. Performance of immune-based and microbiological tests in children with tuberculosis meningitis in Europe: a multicentre Paediatric Tuberculosis Network European Trials Group (ptbnet) study. Eur Respir J. 2020;56:1902004. https://doi.org/10.1183/13993003.02004-2019
29. Abubakar I, Pimpin L, Ariti C, Beynon R, Mangtani P, Sterne JA, et al. Systematic review and meta-analysis of the current evidence on the duration of protection by bacillus Calmette-Guérin vaccination against tuberculosis. [v–vi.]. Health Technol Assess. 2013;17:1–372, v–vi. https://doi.org/10.3310/hta17370
30. Gafar F, Ochi T, Van't Boveneind-Vrubleuskaya N, Akkerman OW, Erkens C, van den Hof S, et al. Towards elimination of childhood and adolescent tuberculosis in the Netherlands: an epidemiological time-series analysis of national surveillance data. Eur Respir J. 2020;56:2001086. https://doi.org/10.1183/13993003.01086-2020
31. Trunz BB, Fine P, Dye C. Effect of BCG vaccination on childhood tuberculous meningitis and miliary tuberculosis worldwide: a meta-analysis and assessment of cost-effectiveness. Lancet. 2006;367:1173–80. https://doi.org/10.1016/S0140-6736(06)68507-3
32. Cernuschi T, Malvolti S, Nickels E, Friede M. Bacillus Calmette-Guérin (BCG) vaccine: a global assessment of demand and supply balance. Vaccine. 2018;36:498–506. https://doi.org/10.1016/j.vaccine.2017.12.010
33. du Preez K, Seddon JA, Schaaf HS, Hesseling AC, Starke JR, Osman M, et al. Global shortages of BCG vaccine and tuberculous meningitis in children. Lancet Glob Health. 2019;7:e28–9. https://doi.org/10.1016/S2214-109X(18)30474-1
34. World Health Organization. Immunization Indonesia 2021 country profile. 2021 [cited 2021 Dec 28]. https://www.who.int/immunization/monitoring_surveillance/data/idn.pdf
35. Martinez L, Cords O, Horsburgh CR, Andrews JR, Acuna-Villaorduna C, Ahuja SD, et al.; Pediatric TB Contact Studies Consortium. The risk of tuberculosis in children after close exposure: a systematic review and individual-participant meta-analysis. Lancet. 2020;395:973–84. https://doi.org/10.1016/S0140-6736(20)30166-5
36. Bang ND, Caws M, Truc TT, Duong TN, Dung NH, Ha DTM, et al. Clinical presentations, diagnosis, mortality and prognostic markers of tuberculous meningitis in Vietnamese children: a prospective descriptive study. BMC Infect Dis. 2016;16:573. https://doi.org/10.1186/s12879-016-1923-2
37. Thee S, Roy RB, Blázquez-Gamero D, Falcón-Neyra L, Neth O, Noguera-Julian A, et al. Treatment and outcome in children with tuberculous meningitis—a multi-centre Paediatric Tuberculosis Network European Trials Group study. Clin Infect Dis. 2021 Nov 21 [Epub ahead of print]. https://doi.org/10.1093/cid/ciab982
38. Boyles TH, Lynen L, Seddon JA; Tuberculous Meningitis International Research Consortium. Decision-making in the diagnosis of tuberculous meningitis. Wellcome Open Res. 2020;5:11. https://doi.org/10.12688/wellcomeopenres.15611.1
39. Cresswell FV, Te Brake L, Atherton R, Ruslami R, Dooley KE, Aarnoutse R, et al. Intensified antibiotic treatment of tuberculosis meningitis. Expert Rev Clin Pharmacol. 2019;12:267–88. https://doi.org/10.1080/17512433.2019.1552831
40. Donald PR, Schoeman JF, Van Zyl LE, De Villiers JN, Pretorius M, Springer P. Intensive short course chemotherapy in the management of tuberculous meningitis. Int J Tuberc Lung Dis. 1998;2:704–11.
41. World Health Organization. Rapid communication on updated guidance on the management of tuberculosis in children and adolescents [cited 2021 Dec 28]. https://www.who.int/publications/i/item/9789240033450
42. Ruslami R, Gafar F, Yunivita V, Parwati I, Ganiem AR, Aarnoutse RE, et al. Pharmacokinetics and safety/tolerability of isoniazid, rifampicin and pyrazinamide in children and adolescents treated for tuberculous meningitis. Arch Dis Child. 2022;107:70–7. https://doi.org/10.1136/archdischild-2020-321426
43. Panjasawatwong N, Wattanakul T, Hoglund RM, Bang ND, Pouplin T, Nosoongnoen W, et al. Population pharmacokinetic properties of antituberculosis drugs in Vietnamese children with tuberculous meningitis. Antimicrob Agents Chemother. 2020;65:e00487–20. https://doi.org/10.1128/AAC.00487-20
44. van Toorn R, Zaharie S-D, Seddon JA, van der Kuip M, Marceline van Furth A, Schoeman JF, et al. The use of thalidomide to treat children with tuberculosis meningitis: a review. Tuberculosis (Edinb). 2021;130:102125. https://doi.org/10.1016/j.tube.2021.102125
45. Abo YN, Curtis N, Osowicki J, Haeusler G, Purcell R, Kadambari S, et al. Infliximab for paradoxical reactions in pediatric central nervous system tuberculosis. J Pediatric Infect Dis Soc. 2021 Oct 5;piab094. https://doi.org/10.1093/jpids/piab094
46. Gafar F, Marais BJ, Nataprawira HM, Alffenaar JC. Optimizing antimicrobial and host-directed therapies to improve clinical outcomes of childhood tuberculous meningitis. Clin Infect Dis. 2021 Dec 15 [Epub ahead of print]. https://doi.org/10.1093/cid/ciab1036
47. Schoeman JF, Van Zyl LE, Laubscher JA, Donald PR. Effect of corticosteroids on intracranial pressure, computed tomographic findings, and clinical outcome in young children with tuberculous meningitis. Pediatrics. 1997;99:226–31. https://doi.org/10.1542/peds.99.2.226
48. Rohlwink UK, Figaji A, Wilkinson KA, Horswell S, Sesay AK, Deffur A, et al. Tuberculous meningitis in children is characterized by compartmentalized immune responses and neural excitotoxicity. Nat Commun. 2019;10:3767. https://doi.org/10.1038/s41467-019-11783-9
49. Rohlwink UK, Mauff K, Wilkinson KA, Enslin N, Wegoye E, Wilkinson RJ, et al. Biomarkers of cerebral injury and inflammation in pediatric tuberculous meningitis. Clin Infect Dis. 2017;65:1298–307. https://doi.org/10.1093/cid/cix540
50. Marais BJ, Heemskerk AD, Marais SS, van Crevel R, Rohlwink U, Caws M, et al.; Tuberculous Meningitis International Research Consortium. Standardized methods for enhanced quality and comparability of tuberculous meningitis studies. Clin Infect Dis. 2017;64:501–9.

Address for correspondence: Fajri Gafar, University of Groningen, Groningen Research Institute of Pharmacy, Unit of PharmacoTherapy, Epidemiology and Economics, Antonius Deusinglaan 1 (Rm: 3214.0450), 9713 AV Groningen, The Netherlands; email: f.gafar@rug.nl, fajri.gafar@gmail.com

Evaluation of Commercially Available High-Throughput SARS-CoV-2 Serologic Assays for Serosurveillance and Related Applications

Mars Stone,[1] Eduard Grebe,[1] Hasan Sulaeman, Clara Di Germanio, Honey Dave, Kathleen Kelly, Brad J. Biggerstaff, Bridgit O. Crews, Nam Tran, Keith R. Jerome, Thomas N. Denny, Boris Hogema, Mark Destree, Jefferson M. Jones, Natalie Thornburg, Graham Simmons, Mel Krajden, Steve Kleinman, Larry J. Dumont, Michael P. Busch

Severe acute respiratory syndrome coronavirus 2 (SARS-CoV-2) serosurveys can estimate cumulative incidence for monitoring epidemics, requiring assessment of serologic assays to inform testing algorithm development and interpretation of results. We conducted a multilaboratory evaluation of 21 commercial high-throughput SARS-CoV-2 serologic assays using blinded panels of 1,000 highly characterized specimens. Assays demonstrated a range of sensitivities (96%–63%), specificities (99%–96%), and precision (intraclass correlation coefficient 0.55–0.99). Durability of antibody detection was dependent on antigen and immunoglobulin targets; antispike and total Ig assays demonstrated more stable longitudinal reactivity than antinucleocapsid and IgG assays. Assays with high sensitivity, specificity, and durable antibody detection are ideal for serosurveillance, but assays demonstrating waning reactivity are appropriate for other applications, including correlation with neutralizing activity and detection of anamnestic boosting by reinfections. Assay performance must be evaluated in context of intended use, particularly in the context of widespread vaccination and circulation of SARS-CoV-2 variants.

Serosurveillance for severe acute respiratory syndrome coronavirus 2 (SARS-CoV-2) infection is critical to monitor the course of the evolving pandemic and local outbreaks and can provide data on infection-fatality ratios, vaccine coverage, the effect of mitigation measures, and levels of population immunity. Serosurveillance should be conducted with representative population sampling using well-characterized serologic assays selected on the basis of their performance characteristics and optimized algorithms. Using assays and algorithms that detect mild or asymptomatic infections is critical for accurately estimating cumulative incidence, and case-to-infection and death-to-infection ratios.

More than 85 SARS-CoV-2 antibody assays had received US Food and Drug Administration Emergency Use Authorization as of August 19, 2021, ranging from point-of-care tests to fully automated high-throughput platforms (*1*). These assays target different immunoglobulins (total or selective IgG, IgM, or IgA) against viral antigens (full-length spike protein [S1/S2], subunit

Author affiliations: Vitalant Research Institute, San Francisco, California, USA (M. Stone, E. Grebe, H. Sulaeman, C. Di Germanio, H. Dave, K. Kelly, G. Simmons, L.J. Dumont, M.P. Busch); University of California–San Francisco, San Francisco (M. Stone, E. Grebe, G. Simmons, M.P. Busch); South African Centre for Epidemiological Modelling and Analysis, Stellenbosch University, Stellenbosch, South Africa (E. Grebe); Centers for Disease Control and Prevention, Fort Collins, Colorado, USA (B.J. Biggerstaff); University of California Irvine Medical Center, Orange, California, USA (B.O. Crews); University of California–Davis, Davis, California, USA (N. Tran); Fred Hutchinson Cancer Research Center, University of Washington, Seattle, Washington, USA (K.R. Jerome); Duke Human Vaccine Institute, Duke University, Durham, North Carolina, USA (T.N. Denny); Sanquin Research, Amsterdam, the Netherlands (B. Hogema); BloodWorks NorthWest, Seattle (M. Destree); Centers for Disease Control and Prevention, Atlanta, Georgia, USA (J.M. Jones, N. Thornburg); British Columbia Centre for Disease Control, Vancouver, British Columbia, Canada (M. Krajden); University of British Columbia, Vancouver (S. Kleinman); University of Colorado School of Medicine, Denver, Colorado, USA (L.J. Dumont)

DOI: https://doi.org/10.3201/eid2803.211885

[1]These first authors contributed equally to this article.

1 [S1], subunit 2 [S2] of spike, the receptor binding domain [RBD] of spike, or the nucleocapsid protein [NC]) (*1*). Limited head-to-head evaluation data are available for high-throughput SARS-CoV-2 serologic assays, and few large-scale studies have focused on performance for serosurveillance applications. Comprehensive characterization of assay performance must include sensitivity, specificity, and durability of antibody detection over time since infection.

To provide a comprehensive overview and direct comparison of assay characteristics and performance to inform assay selection and results interpretation for serosurveillance, we conducted a multilaboratory comparative assessment of 21 high-throughput, commercially available SARS-CoV-2 serologic assays by using blinded panels of 1,000 highly characterized specimens, including longitudinal and cross sectional coronavirus disease (COVID-19) convalescent plasma (CCP) and prepandemic control plasma specimens. We distributed panels to experienced testing laboratories that were deemed to be proficient by the manufacturers and selected assays to represent multiple formats and antigen targets. Data from this study can inform assay selection and development of testing algorithms to meet the optimal performance characteristics for primary screening and supplemental testing in US and global serosurveillance studies. The study also provides performance data relevant to other serologic testing contexts that will enable clinicians, public health organizations, laboratorians, and emergency response planners to develop optimal algorithms for infection detection and confirmation, including vaccine breakthrough and recurrent infections and correlations with neutralizing activity.

Methods

Assay Selection, Panel Development, and Testing

The study included assays from major manufacturers that were commercially available, were high-throughput, had received or were expected to receive Emergency Use Authorization, and were widely used for serosurveillance (*2*–*8*; S. Takahashi et al., unpub. data, https://doi.org/10.1101/2021.09.09.21263139) or other purposes. In some cases, we included additional assays from a manufacturer not necessarily ideal for serosurveillance applications but still informative to related applications. Key assay characteristics included format and configuration, antigen composition, and immunoglobulin target (Table 1). We distributed uniquely blinded panels consisting of 1,000 identical specimens to experienced testing laboratories to determine performance characteristics.

We obtained plasma or serum specimens from CCP donors from March–November 2020. Specimens were shipped, stored, and distributed frozen. All blood donors consented to use of deidentified, residual specimens for further research purposes. Consistent with the policies and guidance of the University of California–San Francisco Institutional Review Board, Vitalant Research Institute self-certified that use of the deidentified CCP donations in this study does not meet the criteria for human subjects research. Centers for Disease Control and Prevention (CDC) investigators reviewed and relied on this determination as consistent with applicable federal law and CDC policy (45 C.F.R. part 46, 21 C.F.R. part 56; 42 U.S.C. § 241[d]; 5 U.S.C. § 552a; 44 U.S.C. § 3501). Qualification for CCP donation required documentation of positive SARS-CoV-2 molecular (e.g., reverse-transcription PCR) or serologic test, complete resolution of symptoms 14–28 days before donation (*9*), and standard allogeneic blood donor qualification criteria (*10*). Samples were selected from CCP donors independent of reactivity on the primary blood donor SARS-CoV-2 screening Ortho VITROS SARS-CoV-2 S Total Ig (Ortho Clinical Diagnostics, https://www.orthoclinicaldiagnostics.com) assay.

To evaluate the waning of reactivity over time, we included longitudinal specimens from 24 CCP donors who continued to qualify for CCP donation at each of 4–14 donations (median 9 donation) over 79–126 days (median 95 days). A COVID-19 seroconversion panel consisted of 14 timepoints from a single-source plasma donor during the progression of a SARS-CoV-2 infection over 87 days (*11*). Fifteen CCP specimens were represented in 6 blinded replicates to evaluate precision. The dilution panel consisted of six 4-fold serial dilutions of specimens with a range of neat antibody titers (*12*). The panel also included 24 apparent serosilent specimens from donors who initially qualified for CCP donation as having a positive molecular test but without evidence of seroconversion by the Ortho S Total Ig assay (https://www.orthoclinicaldiagnostics.com).

Statistical Analysis

We performed all statistical analyses by using R 4.0.4 (*13*). We used various packages, including the binom package for 95% CIs on proportions (*14*), the glm2 package (*15*) for regression analysis, and the ggplot2 package (*16*) for plotting.

Sensitivity and Specificity

We assessed sensitivity in cross-sectional CCP specimens. Because data on symptoms, clinical severity,

Table 1. Key characteristics of assays evaluated in study of commercially available high-throughput SARS-CoV-2 assays for serosurveillance*

Manufacturer	Assay†	Ig target	Antigen	Assay format	Reported units	Testing laboratory
Ortho	VITROS Immunodiagnostic Products Anti-SARS-CoV-2 Total Ig	Total Ig	S1	Double-antigen sandwich CLIA	S/CO	Vitalant Research Institute
	VITROS Immunodiagnostic Products Anti-SARS-CoV-2 IgG	IgG	S1	Double-antigen sandwich CLIA	S/CO	CTS
EUROIMMUN	Anti-SARS-CoV-2 NCP ELISA	IgG	N	Indirect IgG EIA	S/CO	Advent Health
	Anti-SARS-CoV-2 ELISA	IgG	S1	Antigen sandwich ELISA	S/CO	
	Anti-SARS-CoV-2 QuantiVac ELISA	IgG	S1	Antigen sandwich ELISA	RU/mL	
	Anti-SARS-CoV-2 ELISA	IgA	S1	Antigen sandwich ELISA	S/CO	
Roche	Elecsys Anti-SARS-CoV-2 N on cobas	Total Ig	N	Double-antigen sandwich CLIA	COI	University of California–Davis
	Elecsys Anti-SARS-CoV-2 S on cobas	Total Ig	S1/S2/RBD	Double-antigen sandwich CLIA	U/mL	
DiaSorin	LIAISON 28 SARS-CoV-2 TrimericS IgG	IgG	TrimericS	IgG magnetic particle CLIA	AU/mL	British Columbia Centers for Disease Control and Prevention
Siemens	ADVIA Centaur SARS-CoV-2 Total Ig	Total Ig	S1/RBD	Ag sandwich CLIA	S/CO	
	ADVIA Centaur SARS-CoV-2 IgG	IgG	S1/RBD	Ag sandwich CLIA	Index	
Abbott	SARS-CoV-2 IgG N on ARCHITECT	IgG	N	CMIA	AU/mL	Duke Human Vaccine institute
	SARS-CoV-2 IgG S1 on ARCHITECT	IgG	S1	CMIA	S/CO	
	SARS-CoV-2 IgG N on Alinity	IgG	N	CMIA	S/CO	Fred Hutchinson Cancer Research Center
	SARS-CoV-2 IgG S1 on Alinity	IgG	S1	CMIA	AU/mL	
Bio-Rad	Platelia SARS-CoV-2 Total Ab (Evolis)	Total Ig	N	One-step antigen capture	S/CO	BloodWorks NorthWest
	BioPlex 2200 SARS-CoV-2 IgG Panel	IgG	RBD, S1, S2, N	Multiplexed microbeads two-step assay	S/CO	
Quotient	MosaiQ COVID-19 Antibody Microarray	IgM/IgG	S1/S2	Array	Qualitative only	
Diazyme	DZ-Lite SARS CoV-2	IgG	N & S1/S2	IgG microbead CLIA	S/CO	
Beckman Coulter	Access SARS-CoV-2 IgG	IgG	S1 RBD	IgG 2-step paramagnetic particle CLIA	S/CO	University of California–Irvine
Wantai	SARS-CoV-2 Total Ig	Total Ig	S1 RBD	Total Ig sandwich ELISA	S/CO	Sanquin

*Ab, antibody; Ag, antigen; AU, arbitrary units; CMIA, chemiluminescent microparticle immunoassay; CLIA, chemiluminescent immunoassay;.COVID-19, coronavirus disease; EIA, enzyme immunoassay; Ig, immunoglobulin; N, nucleocapsid; RBD, receptor binding domain; RU, relative units; S, spike protein; SARS-CoV-2, severe acute respiratory syndrome coronavirus 2; S/CO, signal to cutoff ratio;
†Current US regulatory status available at https://www.fda.gov/medical-devices/coronavirus-disease-2019-covid-19-emergency-use-authorizations-medical-devices/in-vitro-diagnostics-euas-serology-and-other-adaptive-immune-response-tests-sars-cov-2.

hospitalization, and diagnostic test results (molecular or antigen) were not available, we defined true positivity according to 3 sets of criteria: qualification as a CCP donor according to blood center policies, which required donors to provide evidence of a SARS-CoV-2 diagnosis, with resolved symptomatic infection (n = 191) (https://www.fda.gov/media/141477/download); confirmation of detectable neutralizing antibody by the Broad Institute plaque reduction neutralization test (PRNT) (*12*) (n = 154); or reactive on ≥3 evaluated binding antibody (bAb) tests (n = 188). Substantial overlap exists between the 3 definitions; 149 specimens were classified as positive by all 3 definitions, 34 by the first and third definitions, 3 by the second and third definitions, and only 12 by only 1 of the definitions. We excluded the 24 serosilent CCP specimens (Table 2) from the sensitivity analysis on the basis of the first criterion. We excluded longitudinal CCP donor cohort specimens from all sensitivity analyses as their continued CCP qualification may bias sensitivity estimates given they were required to have bAb reactivity for continued donation of CCP.

We assessed primary specificity with prepandemic blood donor specimens (n = 432) and included 27 seronegative donations from early 2020 (*12*) in a secondary specificity analysis (n = 459) (Appendix Figure 1,

https://wwwnc.cdc.gov/EID/article/28/3/21-1885-App1.pdf). Sensitivity and specificity estimates were based on reported qualitative interpretations of assay results. We excluded results reported as equivocal from primary sensitivity and specificity estimates, and conducted secondary analysis that included equivocal results as nonreactive (Appendix Figures 2, 3). All 95% CIs reported are Wilson score intervals.

Repeatability and Assay Precision

We computed coefficients of variation (CVs), defined as the ratio of the SD to the mean across 6 replicate specimen measurements expressed as a percentage, for each of the replicate specimens (n = 90). A limitation of this approach is that assays with narrower dynamic range produced very low or zero CVs at the upper limit of quantification. To adequately account for reactivity outside the measurement range, these results were excluded from the overall repeatability assessment, and intraclass correlation coefficients (ICCs) were used. The ICC expresses between-sample variance as a proportion of total variance in the tested replicate specimen. In the case of the Bio-Rad Bio-Plex assay (Bio-Rad, https://www.bio-rad.com), onboard dilutions were conducted by the testing laboratory and used to estimate reactivity in specimens with initial results above the assay's limit of quantitation.

Dilutional Performance

The dilution panel (n = 55 specimens) enables comparative assessment of the linearity of observed versus expected reactivity measurements above and below assay cutoffs. Expected reactivity is defined as the mean signal intensity measured over 6 replicates of the neat specimen divided by the dilution factor (Appendix).

Durability of Antibody Detection

We assessed qualitative and quantitative durability of bAb detection in longitudinal CCP specimens (n = 209 specimens from 24 donors). Documented dates of symptom onset, symptom resolution, or nucleic acid test–based diagnosis are not available for these donors, so all analyses are anchored to the index donation. These CCP donors first donated early in the pandemic, typically within 1 month of symptom resolution (*12*).

We assessed qualitative detection by estimating the proportion of specimens with detectable bAbs grouped in 30-day bins of time since index donations. To account for within-donor correlation, if a donor contributed >1 specimen in a particular time bin, the proportion of the donor's specimens that were reactive was added to the numerator for the bin and only 1 to the denominator, so that the proportion detected is the proportion of donors detected in each bin.

We assessed quantitative detection by fitting linear mixed effects regression models with time since index donation as the predictor. We estimated assay signal half-lives by transforming average (fixed) slopes obtained from these models (Appendix).

Results

When a true positive was defined by qualification as a CCP donor, the lowest assay sensitivity was 63.6% (95% CI 56.3%–70.4%) (EUROIMMUN IgA assay, https://www.euroimmun.com), and the highest was 95.8% (95% CI 92.0%–97.9%) (Ortho VITROS Total Ig S assay and Roche Elecsys Total Ig S and N [https://www.roche.com]) (Figure 1, panel A). When a true positive was defined by PRNT activity, the lowest assay sensitivity was 69.7% (95% CI 61.7%–76.7%)

Table 2. Composition of the assessment panel for evaluation of SARS-CoV-2 serologic assays in study of commercially available high-throughput SARS-CoV-2 assays for serosurveillance*

Group	Description	No. specimens
Sensitivity subpanels		
Qualification as CCP	191 CCP	191
Broad neutralization activity	152 CCP + 2 serosilent	154
Reactive on ≥3 assays	186 CCP + 2 serosilent	188
Specificity subpanel	Prepandemic blood donor specimens collected before 2020 and demonstrated to be anti–SARS-CoV-2 negative by RVP neutralization testing	459
Ab persistence subpanel	Longitudinal specimens from 24 donors with at ≥4 CCP donations 84–150 d after index donation	209
Seroconversion subpanel	Longitudinal specimens from a single-source plasma donor with acute SARS-CoV-2 infection	14
Dilutional performance subpanel	Serial dilutions of 5 specimens from sensitivity subpanel; neat (6 replicates), 1:40, 1:80, 1:160, 1:320, and 1:640 analogous to neutralizing antibody testing	55
Serosilent cases	Individual CCP donors nonreactive by S and N anti–SARS-CoV-2 total Ig	24
Repeatability subpanel	Six blinded replicates each of 15 CCP specimens	90

*CCP, coronavirus disease convalescent plasma; N, nucleocapsid; RBD, receptor binding domain; RVP, reporter viral particle; S, spike protein; SARS-CoV-2, severe acute respiratory syndrome coronavirus 2.

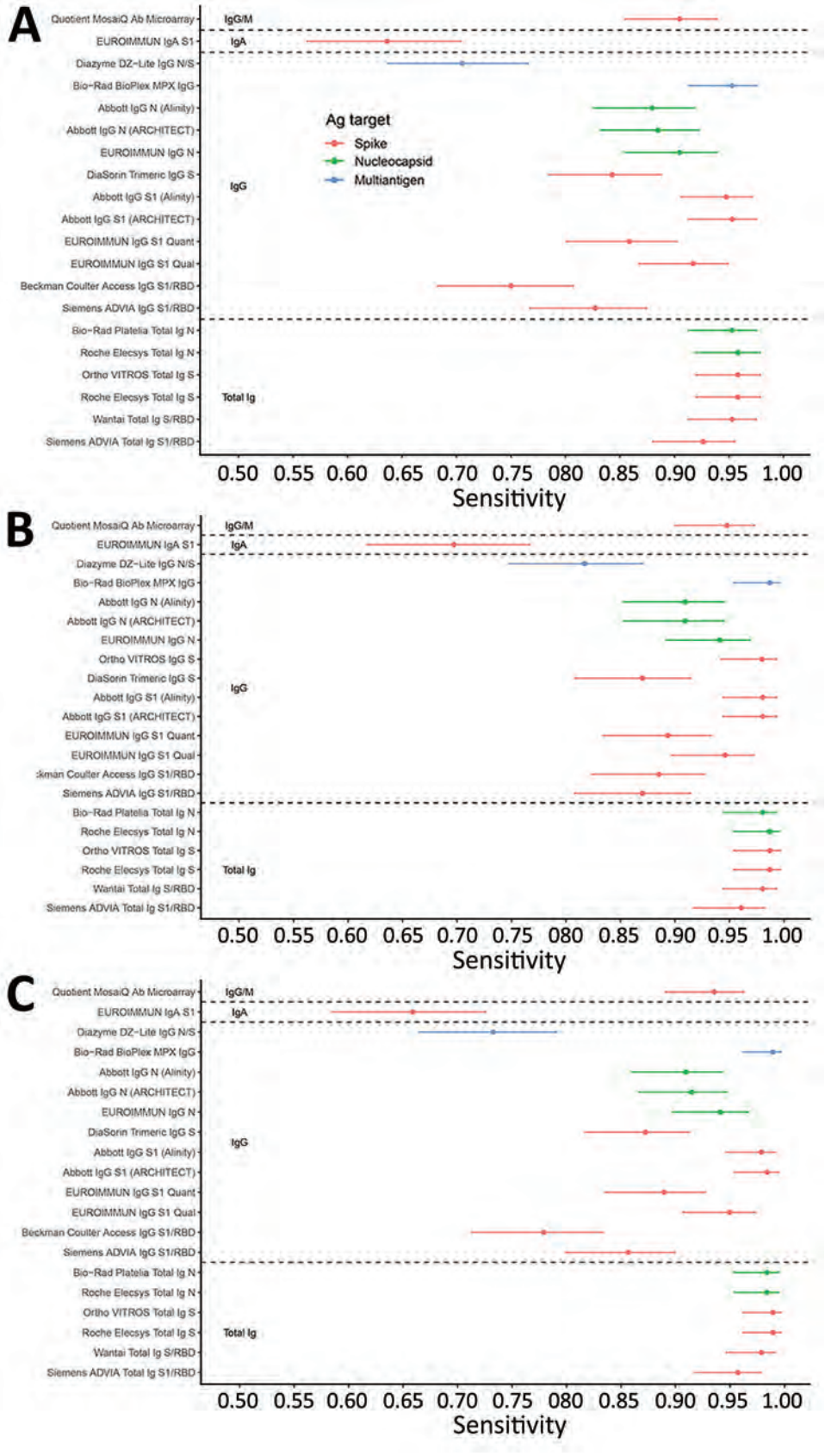

Figure 1. Sensitivity of severe acute respiratory syndrome coronavirus 2 serologic assays (descriptions in Table 1) using 3 definitions of a true positive in study of commercially available high-throughput assays for serosurveillance. A) Positivity defined by qualification as CCP, coronavirus disease convalescent plasma donor (excluding purposely selected serosilent specimens). B) Positivity defined by neutralizing activity measured by Broad plaque reduction neutralization test. C) Positivity defined by operational standard (≥3 binding antibody assays reactive). Dots indicate point estimates, and bars indicate Wilson score 95% CIs. Ortho VITROS IgG S assay is included only in panel B because the assay required use of serum for testing; thus, only specimens with available serum and neutralizing data were tested. Ab, antibody; Ag, antigen; N, nucleocapsid; RBD, receptor binding domain; PRNT, plaque reduction neutralization test; S, spike protein.

(EUROIMMUN IgA assay), and the highest was 98.7% (95% CI 95.4%–99.6%) (Ortho VITROS Total Ig S, Roche Elecsys Total Ig S and N, and Bio-Rad Bio-Plex MPX IgG assays) (Figure 1, panel B). Most assays (17/20) had sensitivities >80%, 12/20 had sensitivities >90%, and 7/20 had sensitivities >95%, by the first definition. None reached 96% by CCP qualification criteria or 99% by detectable neutralizing antibody criteria. Assays with the lowest sensitivity were the Beckman Coulter Access SARS-CoV-2 IgG (https://www.beckmancoulter.com), Diazyme DZ-Lite SARS-CoV-2 IgG (https://www.diazyme.com), and EUROIMMUN IgA assays, with estimates <80%. We observed similar patterns to the first and second definitions of true positivity when defined by bAb reactivity on ≥3 assays (Figure 1, panel C).

Specificities, based on testing 432 prepandemic specimens, were high, with estimates ranging from 96.1% (95% CI 93.8%–7.5%) (Diazyme DZ-Lite assay) to 100% (95% CI 99.1%–100%) (Abbott IgG N [https://www.abbott.com], Bio-Rad BioPlex IgG, Bio-Rad Platelia Total Ig N, and Ortho VITROS Total Ig S assays). Most assays (13/20) had specificities >99%, and 5/20 assays had specificities of 100% in this panel (Figure 2). Assays with poorer specificity tended to have poorer sensitivity, suggesting no tradeoff between sensitivity and specificity (Appendix Table 1, Appendix Figure 4). Specificity estimates including 27 specimens from 2020 (Appendix Figure 1) and secondary sensitivity and specificity analyses with equivocal results categorized as nonreactive (Appendix Figures 2, 3) had minimal impact on estimates of sensitivity and specificity.

Durability of bAb detection was highly variable, with some assays reactive at all timepoints, whereas others showed substantial declines in the proportion of reactive specimens over time (Figure 3). IgG assays and anti-N assays generally demonstrated more rapid seroreversion proportions compared with total Ig and anti-S assays. For example, the Abbott and EUROIMMUN IgG anti-N assays detected antibodies in <70% of specimens collected >90 days after index donation, whereas total Ig assays like the Ortho Vitros S total Ig and Roche Elecsys N total Ig assays detected antibodies in 100% of specimens at these timepoints. Given the relatively small number of donors in the cohort, the declining detection rates at later timepoints were generally not statistically distinguishable from sensitivity at earlier timepoints for these qualitative assays (χ^2 tests yielded large p values).

Regression models of quantitative signal intensity over time showed statistically significant declining reactivity in some assays. All anti-S total Ig (direct antigen sandwich format) assays showed stable or increasing reactivity, whereas all IgG assays showed declining reactivity over time (Figure 4, panel A). Anti-N assays showed more rapid waning than anti-S assays, with multivariable regression confirming that assay format and antigen target are important predictors of rate of waning. Among assays that showed statistically significant declining reactivity, estimated half-lives varied from 41 to 574 days (median 91 days) (Figure 4, panel B).

All assays included in the study showed good (ICCs ≥0.75) or excellent (ICCs ≥0.9) quantitative repeatability (*17*), with the exception of the Wantai assay (Wantai BioPharm, http://www.ystwt.cn), which had an ICC <0.6 (Figure 5; Appendix Table 2). CVs were generally <10% for low- and medium-titer blinded replicate specimens and somewhat higher for

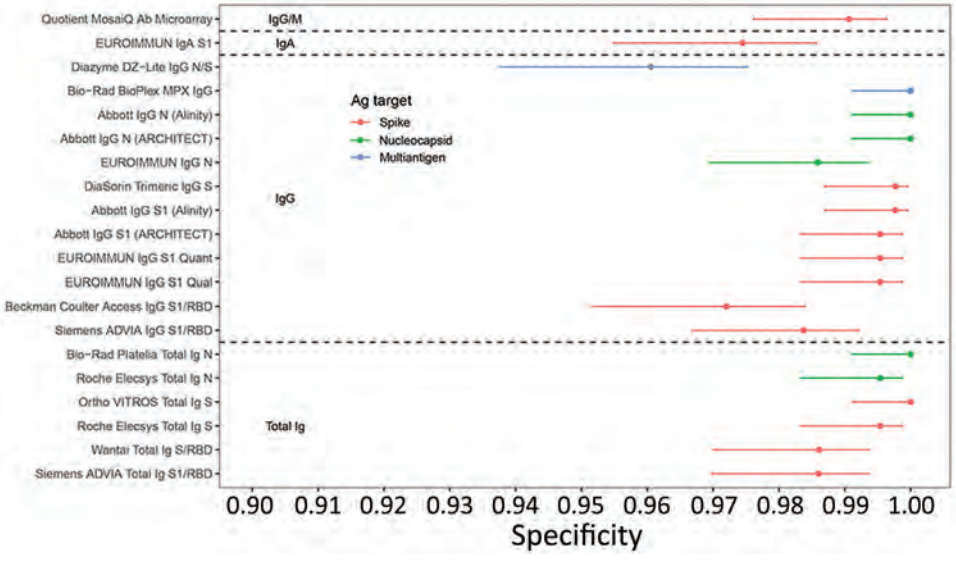

Figure 2. Specificity of severe acute respiratory syndrome coronavirus 2 serologic assays (descriptions in Table 1) in prepandemic negative control specimens in study of commercially available high-throughput assays for serosurveillance. Dots indicate point estimates and bars indicate Wilson score 95% CIs. Ab, antibody; Ag, antigen; N, nucleocapsid; RBD, receptor binding domain; S, spike protein.

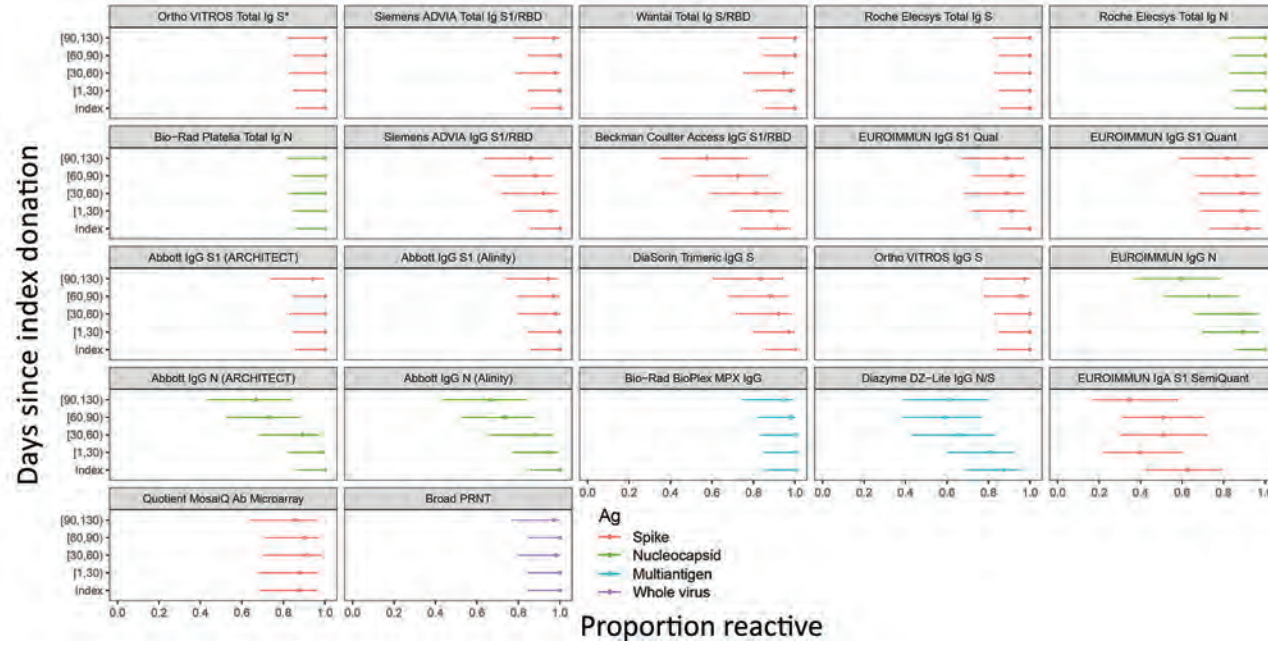

Figure 3. Proportion of donors with detectable severe acute respiratory syndrome coronavirus 2 antibodies in study of commercially available high-throughput assays for serosurveillance. In the longitudinal coronavirus disease convalescent plasma donor cohort, donations were sorted into time bins relative to index donation. Time bin labels on x-axis are denoted with brackets to indicate inclusive boundaries and parentheses to indicate exclusive boundaries. Donors who contributed >1 donation in a time bin contributed the fractional proportion reactive to the numerator and 1 to the denominator for estimation of proportion reactive in the time bin. Symbols indicate point estimates of proportion reactive, and bars indicate 95% CIs (Wilson score). Assays are described in Table 1. Each of the 24 donors had an index sample available. For time bins 1–29 days post index, n = 22 donors, n = 56 specimens; day 30–59, n = 19 donors, n = 45 specimens; day 60–89, n = 22 donors, n = 54 specimens; day 90+, n = 18 donors, n = 30 specimens. Ortho VITROS Total Ig anti-S reactivity was required for qualification of continued CCP donation and therefore shows 100% detection in all time bins by definition. Ab, antibody; Ag, antigen; N, nucleocapsid; PRNT, plaque reduction neutralization test; RBD, receptor binding domain; S, spike protein.

high-titer specimens, ranging from ≈20% to >100% (Appendix Table 3). The Ortho VITROS anti-S and Roche Elecsys anti-N total Ig assays had notably low CVs on most replicate specimens (generally <10%).

Dilutional performance was generally good, with most assays demonstrating reasonable linearity in the relationship between expected and observed reactivity above the assay cutoffs (Appendix Figure 5). Assays with greater dynamic ranges tended to show a linear dilutional response even below the cutoff. Most assays had a well-defined inflection point, representing a level of reactivity below which the dilutional response was not linear.

For most assays all 24 serosilent specimens were nonreactive, whereas 7 assays had 1/24 reactive and 2 assays had 2/24 reactive specimens (Appendix Figure 6). Two of these specimens were reactive on 3 assays, 1 of which was reactive on the 3 EURIMMUN IgG assays; the other had no clear pattern of reactivity (i.e., it was reactive on both IgG and total Ig and S and NC assays). For the single seroconversion series, most assays show seroconversion over the same 2-week timeframe, providing little evidence of variable sensitivity relative to time of infection (Appendix Figure 7). Reporter operator characteristic curve analysis indicated optimal thresholds and corresponding positive and negative percentage agreement for predicting neutralization titers of 1:20, 1:250, and 1:1,000 (Appendix Table 4).

Discussion

Comprehensive comparison of serologic assays with a broad range of formats, Ig class, and antigen targets are valuable for understanding their relative performance across a range of applications. We focused on application to cross-sectional serosurveillance, although our findings are also informative for other applications. The 3 most critical characteristics for assays used to conduct serosurveillance are sensitivity, including an assay's ability to detect antibodies after asymptomatic and mildly symptomatic infections, potentially resulting in weak antibody responses (*18*–*20*); specificity, to minimize the effect of false-positives on seroprevalence estimates; and the ability to durably detect antibody responses for accurate estimation of cumulative infections.

For serosurveillance in the context of widespread spike-based vaccine implementation, algorithms that combine S and NC assays with these characteristics can differentiate natural infection from vaccine-induced seroreactivity. In areas with high vaccine-induced anti-S reactivity, single-platform parallel testing is ideal, such as on the Ortho Vitros and Roche Elecsys platforms to maximize throughput and turnaround time. CDC's Nationwide Blood Donor Seroprevalence Study (https://covid.cdc.gov/covid-data-tracker/#nationwide-blood-donor-seroprevalence) initially screened for anti-S reactivity reflexing reactives to anti-NC testing, and subsequently initiated single-platform simultaneous parallel S and NC testing once anti-S reactivity mainly attributable to vaccination reached high levels to reduce cost and increase efficiency and turnaround time. However, testing algorithms should be context dependent; for example, in regions where whole-virus vaccines are used, alternative algorithms should be considered. The assay performance evaluation we describe informs algorithm development and implementation in different contexts.

Although not specifically applicable to serial cross-sectional serosurveys, the ability to detect breakthrough infections of anti-S–based vaccines in longitudinal datasets is important, requiring sensitive and specific assays to detect development of anti-N reactivity. Detection of reinfection by anamnestic Ab boosting requires quantitative assays with wide dynamic ranges, including the ability to extend the dynamic range through dilution, and assays that demonstrate waning reactivity over time and good quantitative repeatability, such as anti-S and anti-NC IgG.

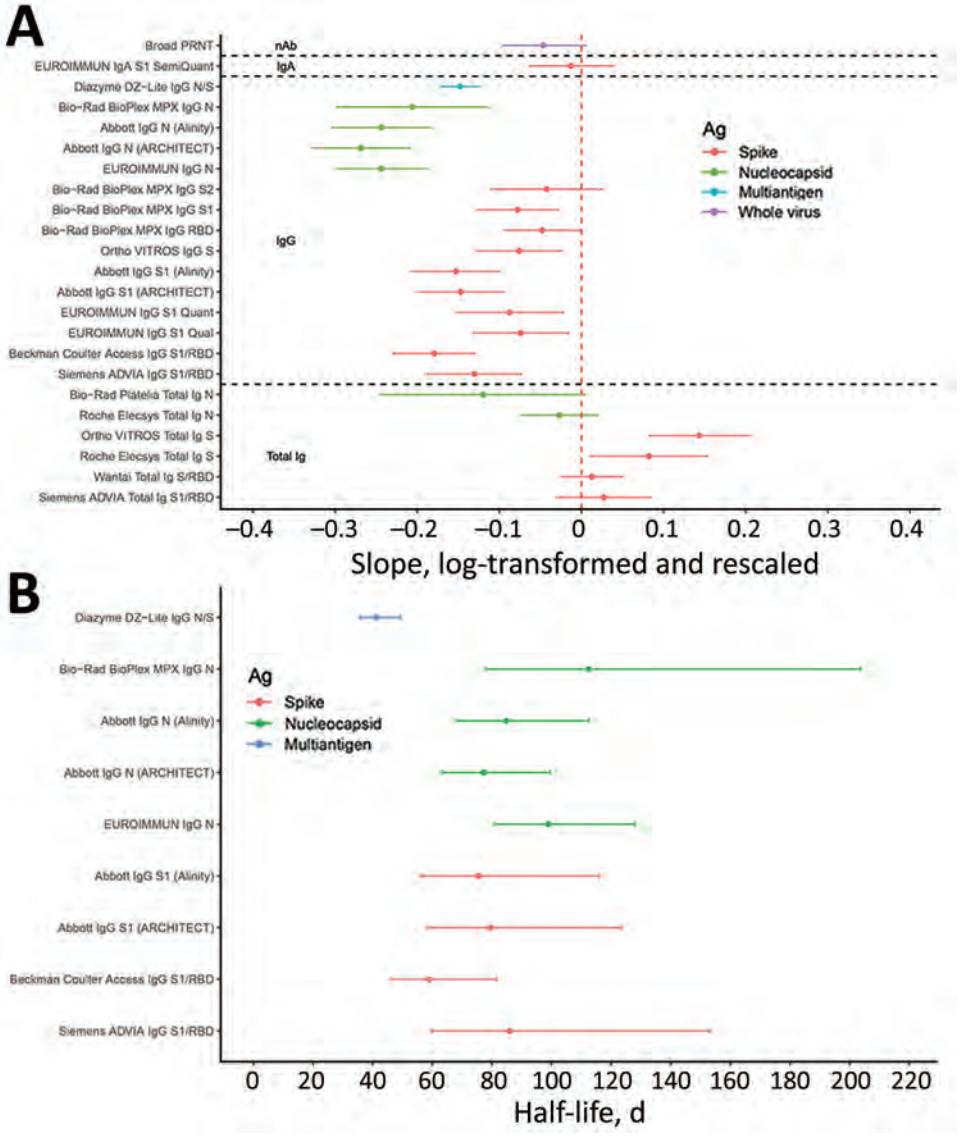

Figure 4. Durability of severe acute respiratory syndrome coronavirus 2 antibody detection as assessed by mixed effects regression modeling in study of commercially available high-throughput assays for serosurveillance. A) Average (fixed) slopes from linear mixed-effects regression models with donor random effects, fit to rescaled and log-transformed quantitative assay signal. B) Assay signal half-lives after index donation for assays demonstrating rapid waning of seroreactivity over time (upper bound on half-life <220 days), estimated on the basis of linear mixed-effects regression models. Assays are described in Table 1. Ab, antibody; Ag, antigen; N, nucleocapsid; RBD, receptor binding domain; S, spike protein.

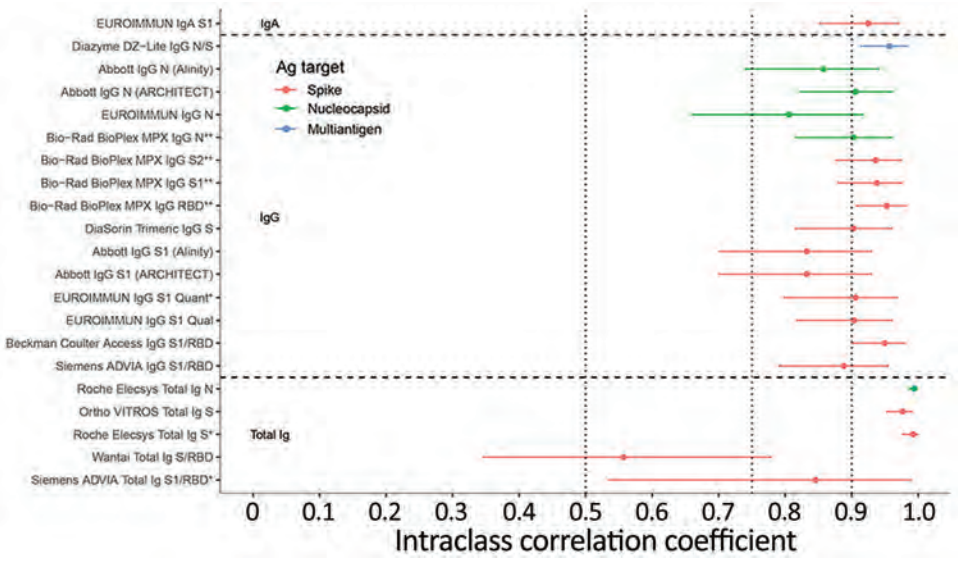

Figure 5. Intraclass correlation coefficients based on blinded replicate sample testing, reflecting the proportion of total variance that is between-sample rather than within-sample variability of severe acute respiratory syndrome coronavirus 2 antibody detection in study of commercially available high-throughput assays for serosurveillance. Results falling outside the primary measurement range were excluded. On-board dilutions were used to estimate reactivity in specimens where initial results fell outside the primary measurement range. Horizontal dotted lines show conventional (although arbitrary) thresholds for moderate (0.5), good (0.75), and excellent (0.9) repeatability (*17*). Assays are described in Table 1. Ab, antibody; Ag, antigen; N, nucleocapsid; PRNT, plaque reduction neutralization test; RBD, receptor binding domain; S, spike protein.

Ideal assays for serosurveillance applications may not be a viable option in all contexts, and other factors such as cost, logistics, and regulatory approval status may influence assay availability and selection, particularly in resource-constrained settings. However, with robustly characterized assay performance, statistical adjustments can be made in estimating of seroprevalence, such as adjustments for the rate of waning reactivity.

Assay manufacturers commonly determine sensitivity on the basis of timing of seroconversion relative to diagnostic testing or clinical disease, but this criterion may not be the most relevant where high rates of mildly symptomatic or asymptomatic infections exist; alternate definitions of true positivity should be considered. Thus, we used multiple definitions to assess sensitivity in practical serosurveillance contexts. Of particular note, including all CCP donors results in lower sensitivity estimates consequent to inclusion of serosilent infection cases, whereas the requirement for neutralization activity excludes those cases resulting in higher sensitivity estimates.

Detecting past infections long after symptom resolution is key to accurately estimating cumulative incidence of infections based on seroreactivity rates; otherwise, complex adjustments for seroreversion may be required (*3*,*4*,*21*; S. Takahashi et al., unpub. data). Rates of waning immunity are difficult to assess using assays with narrow dynamic ranges that constrain detection of declining reactivity and may plateau at the upper limit of quantitation. Diluting specimens, which many platforms can perform automatically, extends dynamic ranges, enabling quantitation of high-titer specimens, as demonstrated by the Bio-Rad BioPlex assay. Although qualitative seroreversion was observed in some assays, including ones with narrow dynamic ranges (Figure 3), further studies over longer timescales are required. Quantitation of very low-level reactivity is possible in assays demonstrating linearity of dilutional performance below the manufacturer-defined thresholds for reactivity, which are generally set to maintain high specificity. Stable detection of neutralizing activity up to 4 months after index donation demonstrates that in the cross-sectional samples used for sensitivity analysis, waning of neutralizing Ab titers was very unlikely by the time samples were collected and would therefore not have biased sensitivity analyses based on neutralizing activity.

Evaluating apparent serosilent cases with evidence of prior infection lacking detectable antibodies is important to confirm that this phenomenon is not assay-dependent. Although sporadic reactivity occurred in a few specimens from serosilent cases, most tested nonreactive on all samples, corroborating the findings of other studies (*18*,*22*) indicating some infected persons do not develop a detectable systemic humoral immune response after SARS-CoV-2 infection.

We observed that all anti-S total Ig (direct antigen sandwich format) assays showed stable or increasing reactivity presumably because of continued maturation of antibody affinity, avidity,

or both, resulting in increasing signal intensity in these assays (*23*–*25*), whereas all but 1 IgG assay showed declining reactivity over time. Anti-N assays showed more rapid waning than anti-S assays, with multivariable regression confirming that assay format and antigen target are important predictors of rate of waning, although assay format (i.e., Ig target) is a stronger predictor of antibody stability than antigen target. IgG assays demonstrating rapid waning are useful for longitudinal assessment of reactivity relative to neutralizing antibodies and for detecting anamnestic boosting of antibodies because of vaccination or reinfection. Among the IgG assays, the anti-NC assays demonstrated more rapid waning than anti-S assays, which is consistent with observed half-lives of these antibody classes (*26*). IgA assays are not suitable for primary serosurveillance screening; however, because IgA has different detection dynamics than total Ig or IgG assays included in the study, they are informative for detecting incident infections early in infection.

The best performing assays for serosurveillance applications in this evaluation were high-throughput total Ig antigen sandwich format assays, because they met the 3 key performance criteria of durable antibody detection, sensitivity, and specificity. The Ortho and Roche total Ig assays that target anti-S and anti-N antibodies performed well and are currently used in largescale serosurveillance studies including CDC's Nationwide Blood Donor Seroprevalence Study. The Wantai assay has been widely used in serosurveillance globally (*2*,*5*,*27*); although this assay demonstrated lower specificity and reproducibility than the best performing assays, it performs adequately for serosurveillance after accounting for those limitations. Several other assays, including the Abbott IgG anti-N and EUROIMMUN IgG anti-S assays, have been used in largescale serosurveillance, but require adjustments for rapid waning and seroreversion to estimate cumulative incidence or attack rates, especially over longer periods and multiple epidemic waves (S. Takahashi et al., unpub. data). Our study provides critical data that can be applied to adjust for waning in other studies.

Most assays showed strong correlations of signal intensity with neutralizing titers in cross-sectional specimens, although the IgG assays performed notably better than the rest, and among the IgG assays the anti-S assays showed the highest area under the reporter operator characteristic curve. These assays demonstrated high positive percentage agreement and relatively high negative percentage agreement even at 50% inhibitory dose (ID_{50}) >1:1,000. On the basis of these cross-sectional samples collected relatively early after infection, assays with stable or increasing antibody detection over time would show poorer correlation with neutralizing antibody titers, which wane at a similar rate to IgG anti-S assays (Figure 4) and may therefore be less appropriate for identifying correlates of protection.

Our study's first limitation is that asymptomatic cases are underrepresented in the panel because CCP donors had to qualify on the basis of recovery from symptomatic infection, potentially overestimating sensitivity. The assessment of durability of bAb detection is based on CCP donations from donors whose continued qualification required ongoing Ortho VITROS Total Ig anti-S1 reactivity. Although these CCP donors do not have documented dates of nucleic acid test positivity, symptom onset, or resolution, the first donations were generally within 1–2 months of symptom resolution (*12*). To address these limitations, we developed approaches to adequately characterize sensitivity and durability of reactivity. The study was executed at a time when available postvaccine samples were limited and before the emergence of variants of concern and is therefore constrained by the lack of these sample types (*21*,*28*–*31*). However, this evaluation provides an important foundation for understanding assay performance and their application as the pandemic progresses. The number of specimens included in the dilutional series subpanels are not sufficient for robust assessment of endpoint dilutional sensitivity. The single seroconversion series did not allow for robust assessment of time to seroconversion.

In summary, this study provides a standardized, comparative assessment of 21 SARS-CoV-2 antibody assays from major commercial manufacturers and enables identification of optimal assays and testing algorithms for serosurveillance applications in various contexts. These results also provide performance data applicable to other serologic testing use cases relevant to clinicians, public health organizations, laboratorians, and emergency response planners.

Acknowledgments

We thank the manufacturers for participating and providing reagents: Ortho Clinical Diagnostics, EuroImmun, Roche Diagnostics, DiaSorin, Siemens, Abbott, Bio-Rad, Quotient, Diazyme, Beckman Coulter, Wantai. We also thank the Vitalant Research Institute Research Operations Core Laboratory, the Vitalant Research Institute Core Immunology Laboratory, and the testing laboratories.

About the Author

Dr. Stone is senior scientist and senior director of Laboratory Cores at Vitalant Research Institute and associate adjunct professor of laboratory medicine at the University of California–San Francisco. Her primary research interests include epidemiology and transmission of infectious diseases.

References

1. US Food and Drug Administration. In vitro diagnostics EUAs [cited 2021 Aug 11]. https://www.fda.gov/medical-devices/coronavirus-disease-2019-covid-19-emergency-use-authorizations-medical-devices/vitro-diagnostics-euas
2. Jespersen S, Mikkelsen S, Greve T, et al. SARS-CoV-2 seroprevalence survey among 17,971 healthcare and administrative personnel at hospitals, pre-hospital services, and specialist practitioners in the Central Denmark Region. Clin Infect Dis. 2021;73:e2853–60. https://doi.org/10.1093/cid/ciaa1471
3. Pollán M, Pérez-Gómez B, Pastor-Barriuso R, Oteo J, Hernán MA, Pérez-Olmeda M, et al.; ENE-COVID Study Group. Prevalence of SARS-CoV-2 in Spain (ENE-COVID): a nationwide, population-based seroepidemiological study. Lancet. 2020;396:535–44. https://doi.org/10.1016/S0140-6736(20)31483-5
4. Shioda K, Lau MSY, Kraay ANM, Nelson KN, Siegler AJ, Sullivan PS, et al. Estimating the cumulative incidence of SARS-CoV-2 infection and the infection fatality ratio in light of waning antibodies. Epidemiology. 2021;32:518–24. https://doi.org/10.1097/EDE.0000000000001361
5. Slot E, Hogema BM, Reusken CBEM, Reimerink JH, Molier M, Karregat JHM, et al. Low SARS-CoV-2 seroprevalence in blood donors in the early COVID-19 epidemic in the Netherlands. Nat Commun. 2020;11:5744. https://doi.org/10.1038/s41467-020-19481-7
6. Mulenga LB, Hines JZ, Fwoloshi S, Chirwa L, Siwingwa M, Yingst S, et al. Prevalence of SARS-CoV-2 in six districts in Zambia in July, 2020: a cross-sectional cluster sample survey. Lancet Glob Health. 2021;9:e773–81. https://doi.org/10.1016/S2214-109X(21)00053-X
7. Hasan T, Pham TN, Nguyen TA, Le HTT, Van Le D, Dang TT, et al. Sero-prevalence of SARS-CoV-2 antibodies in high-risk populations in Vietnam. Int J Environ Res Public Health. 2021;18:6353. https://doi.org/10.3390/ijerph18126353
8. Anand S, Montez-Rath M, Han J, Bozeman J, Kerschmann R, Beyer P, et al. Prevalence of SARS-CoV-2 antibodies in a large nationwide sample of patients on dialysis in the USA: a cross-sectional study. Lancet. 2020;396:1335–44. https://doi.org/10.1016/S0140-6736(20)32009-2
9. Goodhue Meyer E, Simmons G, Grebe E, Gannett M, Franz S, Darst O, et al. Selecting COVID-19 convalescent plasma for neutralizing antibody potency using a high-capacity SARS-CoV-2 antibody assay. Transfusion. 2021;61:1160–70. https://doi.org/10.1111/trf.16321
10. US Food and Drug Administration. Investigational COVID-19 convalescent plasma: guidance for industry [cited 2021 Aug 11]. https://www.fda.gov/regulatory-information/search-fda-guidance-documents/investigational-covid-19-convalescent-plasma
11. Belda F, Lopez-Martinez M, Torres N, Cherenzia R, Crowley M. Available COVID-19 serial seroconversion panel for validation of SARS-CoV-2 antibody assays. Diagn Microbiol Infect Dis. 2021;100:115340. https://doi.org/10.1016/j.diagmicrobio.2021.115340
12. Di Germanio C, Simmons G, Kelly K, Martinelli R, Darst O, Azimpouran M, et al. SARS-CoV-2 antibody persistence in COVID-19 convalescent plasma donors: Dependency on assay format and applicability to serosurveillance. Transfusion. 2021;61:2677–87. https://doi.org/10.1111/trf.16555
13. R Core Team. R: a language and environment for statistical computing [cited 2021 Sep 1]. https://www.gbif.org/tool/81287/r-a-language-and-environment-for-statistical-computing
14. Dorai-Raj S. binom: binomial confidence intervals for several parameterizations [cited 2021 Sep 1]. https://rdrr.io/rforge/binom
15. Marschner IC. glm2: fitting generalized linear models with convergence problems. R J. 2011;3:12–5. https://doi.org/10.32614/RJ-2011-012
16. Wickham H. ggplot2: elegant graphics for data analysis: Springer-Verlag: New York; 2016.
17. Liljequist D, Elfving B, Skavberg Roaldsen K. Intraclass correlation—a discussion and demonstration of basic features. PLoS One. 2019;14:e0219854. https://doi.org/10.1371/journal.pone.0219854
18. Petersen LR, Sami S, Vuong N, et al. Lack of antibodies to SARS-CoV-2 in a large cohort of previously infected persons. Clin Infect Dis. 2021;73:e3066–73. https://doi.org/10.1093/cid/ciaa1685
19. Ibarrondo FJ, Fulcher JA, Goodman-Meza D, Elliott J, Hofmann C, Hausner MA, et al. Rapid decay of anti-SARS-CoV-2 antibodies in persons with mild Covid-19. N Engl J Med. 2020;383:1085–7. https://doi.org/10.1056/NEJMc2025179
20. Peluso MJ, Takahashi S, Hakim J, Kelly JD, Torres L, Iyer NS, et al. SARS-CoV-2 antibody magnitude and detectability are driven by disease severity, timing, and assay. Sci Adv. 2021;7:eabh3409. https://doi.org/10.1126/sciadv.abh3409
21. Sabino EC, Buss LF, Carvalho MPS, Prete CA Jr, Crispim MAE, Fraiji NA, et al. Resurgence of COVID-19 in Manaus, Brazil, despite high seroprevalence. Lancet. 2021;397:452–5. https://doi.org/10.1016/S0140-6736(21)00183-5
22. Gallais F, Velay A, Nazon C, Wendling MJ, Partisani M, Sibilia J, et al. Intrafamilial exposure to SARS-CoV-2 associated with cellular immune response without seroconversion, France. Emerg Infect Dis. 2021;27:113–21. https://doi.org/10.3201/eid2701.203611
23. Faria NR, Mellan TA, Whittaker C, Claro IM, Candido DDS, Mishra S, et al. Genomics and epidemiology of the P.1 SARS-CoV-2 lineage in Manaus, Brazil. Science. 2021;372:815–21. https://doi.org/10.1126/science.abh2644
24. Liu H, Wu NC, Yuan M, Bangaru S, Torres JL, Caniels TG, et al. Cross-neutralization of a SARS-CoV-2 antibody to a functionally conserved site is mediated by avidity. Immunity. 2020;53:1272–1280.e5. https://doi.org/10.1016/j.immuni.2020.10.023
25. Benner SE, Patel EU, Laeyendecker O, Pekosz A, Littlefield K, Eby Y, et al. SARS-CoV-2 antibody avidity responses in COVID-19 patients and convalescent plasma donors. J Infect Dis. 2020;222:1974–84. https://doi.org/10.1093/infdis/jiaa581
26. Lumley SF, Wei J, O'Donnell D, Stoesser NE, Matthews PC, Howarth A, et al.; Oxford University Hospitals Staff Testing Group. The Duration, dynamics, and determinants of severe acute respiratory syndrome coronavirus 2 (SARS-CoV-2)

antibody responses in individual healthcare workers. Clin Infect Dis. 2021;73:e699–709. https://doi.org/10.1093/cid/ciab004
27. Gudbjartsson DF, Norddahl GL, Melsted P, Gunnarsdottir K, Holm H, Eythorsson E, et al. Humoral immune response to SARS-CoV-2 in Iceland. N Engl J Med. 2020;383:1724–34. https://doi.org/10.1056/NEJMoa2026116
28. Garcia-Beltran WF, Lam EC, St Denis K, Nitido AD, Garcia ZH, Hauser BM, et al. Multiple SARS-CoV-2 variants escape neutralization by vaccine-induced humoral immunity. Cell. 2021;184:2372–2383.e9. https://doi.org/10.1016/j.cell.2021.03.013
29. Gundlapalli AV, Salerno RM, Brooks JT, Averhoff F, Petersen LR, McDonald LC, et al. SARS-CoV-2 serologic assay needs for the next phase of the US COVID-19 pandemic response. Open Forum Infect Dis 2021;8:ofaa555.
30. Moore JP, Offit PA. SARS-CoV-2 vaccines and the growing threat of viral variants. JAMA. 2021;325:821–2. https://doi.org/10.1001/jama.2021.1114
31. Babiker A, Marvil CE, Waggoner JJ, Collins MH, Piantadosi A. The importance and challenges of identifying SARS-CoV-2 reinfections. J Clin Microbiol. 2021;59:e02769–20. https://doi.org/10.1128/JCM.02769-20

Address for correspondence: Mars Stone, Vitalant Research Institute, 270 Masonic Ave, San Francisco, CA 94118, USA; email: mstone@vitalant.org

Retrospective Cohort Study of Effects of the COVID-19 Pandemic on Tuberculosis Notifications, Vietnam, 2020

Tasnim Hasan, Viet Nhung Nguyen, Hoa Binh Nguyen, Thu Anh Nguyen, Hien T.T. Le, Cuong D. Pham, Nam Hoang Do, Phuong T.M. Nguyen, Justin Beardsley, Guy B. Marks, Greg J. Fox

We evaluated the effects of the coronavirus disease pandemic on diagnosis of and treatment for tuberculosis (TB) in Vietnam. We obtained quarterly notifications for TB and multidrug-resistant/rifampin-resistant (MDR/RR) TB from 2015–2020 and evaluated changes in monthly TB case notifications. We used an interrupted time series to assess the change in notifications and treatment outcomes. Overall, TB case notifications were 8% lower in 2020 than in 2019; MDR/RR TB notifications were 1% lower. TB case notifications decreased by 364 (95% CI −1,236 to 508) notifications per quarter and MDR/RR TB by 1 (95% CI −129 to 132) notification per quarter. The proportion of successful TB treatment outcomes decreased by 0.1% per quarter (95% CI −1.1% to 0.8%) in 2020 compared with previous years. Our study suggests that Vietnam was able to maintain its TB response in 2020, despite the pandemic.

Since January 2020, severe acute respiratory syndrome coronavirus 2 (SARS-CoV-2) has been causing a global coronavirus disease (COVID-19) pandemic that has had wide-reaching effects on delivery of care for many other health conditions, including tuberculosis (TB). Each year, ≈10 million TB cases are diagnosed and ≈1.5 million TB deaths occur worldwide (*1*). The World Health Organization (WHO) has identified substantial effects of the COVID-19 pandemic on TB control efforts (*1*). By late 2020, substantial reductions in TB case notifications were evident in both high- and middle-income countries (*2*–*6*), including countries where COVID-19 had been well-controlled (*7*). Decreased TB notifications led to fears that delays in case detection and reduced treatment completion resulting from the COVID-19 pandemic might lead to increased *Mycobacterium tuberculosis* transmission and consequently higher mortality rates (*8*). Indeed, evidence suggests that the COVID-19 pandemic has resulted in reduced patient adherence to treatment (*9*), decreased access to medications (*10*,*11*), delayed access to services (*10*,*12*), and higher rates of loss to follow-up for patients with TB (*10*). Some of this disruption has been attributed to diversion of resources and interruptions to drug supply and delivery resulting from the COVID-19 pandemic (*13*). Furthermore, some persons with TB have avoided seeking healthcare because of fear of acquiring COVID-19 (*14*). In addition, evidence from South Africa suggests that outcomes for SARS-CoV-2 infection are worse for patients co-infected with TB (*15*).

Vietnam is a high-burden TB country and ranks among the top 30 high-burden countries for multidrug-resistant/rifampin-resistant (MDR/RR) TB (*16*). However, by the end of 2020, Vietnam had one of the lowest rates of reported COVID-19 cases in the region. Vietnam had its first confirmed COVID-19 case in January 2020; because of effective public health strategies, by the end of the year Vietnam had reported only ≈1,500 COVID-19 cases and 35 deaths (*17*,*18*). Early in 2020, localized outbreaks of COVID-19 occurred in Vietnam's 2 largest cities, Hanoi and Ho Chi Minh City; subsequent outbreaks occurred in central Vietnam. The effect of Vietnam's robust public health response against COVID-19 on TB case notifications is unknown. We aimed to

Author affiliations: The Woolcock Institute for Medical Research, Glebe, New South Wales, Australia (T. Hasan, T.A. Nguyen, H.T.T. Le, C.D. Pham, G.B. Marks, G.J. Fox); University of Sydney, Sydney, New South Wales, Australia (T. Hasan, J. Beardsley, G.B. Marks, G.J. Fox); National Lung Hospital, Hanoi, Vietnam (V.N. Nguyen, H.B. Nguyen, N.H. Do, P.T.M. Nguyen); University of New South Wales, Sydney (G.B. Marks)

DOI: https://doi.org/10.3201/eid2803.211919

evaluate the effect of the COVID-19 pandemic on TB case notifications and treatment outcomes during the first year of the pandemic in Vietnam by comparing programmatic data from 2020 to data for the preceding 5 years.

Methods

Study Design and Setting

We conducted a retrospective cohort study to compare national case notification and treatment outcomes for patients with TB and MDR/RR TB in Vietnam in 2020, the first year of the COVID-19 pandemic, with those from the preceding 5 years (2015–2019). Vietnam, located in Southeast Asia, has a population of 96 million and reports ≈100,000 TB cases and >11,000 TB deaths every year (*19*). Screening and treatment for TB are delivered by the National Tuberculosis Program (NTP) across all of Vietnam's 63 provinces. Standardized TB treatment is delivered free of charge through district TB units and continuous treatment generally is supervised at home by family members. Patients routinely collect medication from health facilities at intervals between once a week and once a month. Changes to the delivery of care for TB patients during periods of physical distancing for COVID-19 included longer intervals between medication dispensing and increased intervals between microbiological testing and clinical review.

Two primary COVID-19 outbreaks occurred in Vietnam during 2020. The first outbreak occurred in April, with epicenters in Hanoi and Ho Chi Minh City. The second outbreak occurred during July–September 2020 in central Vietnam, primarily in Da Nang and Quang Nam provinces. In response to the pandemic, the government of Vietnam implemented strict public health policies, including mandatory quarantine for travelers and those with confirmed COVID-19 cases; facility-based isolation and testing of first-generation case-contacts and self-isolation for second-generation case-contacts; closing of schools and business; physical distancing policies; and public health messaging (*17*). Between COVID-19 surges, the NTP provided mobile community screening clinics to improve case detection and access to TB services for patients. These policies were enforced nationally in April 2020, and more localized policies targeting provinces with increased COVID-19 case numbers were implemented during July–September 2020. Between outbreaks, Vietnam had long periods in which no COVID-19 cases were reported, at times going several months reporting zero SARS-CoV-2 community transmission (*20*). Furthermore, 17 provinces reported no COVID-19 cases in 2020.

Patient Eligibility and Data

TB Patients

We included patients of all ages who began TB treatment through the NTP during January 2015–December 2020. All persons with confirmed TB were recorded by district and by date of enrollment into TB treatment. Reported data include age, sex, prior treatment history, diagnostic test results, antimicrobial drug regimen, and treatment outcomes reported according to WHO standard definitions (*21*). We evaluated the number of quarterly TB notifications during 2015–2020 (Figure 1, panel A). WHO-defined treatment outcomes were reported for cases during 2016–2020. Cases notified outside the NTP, for example through private sector healthcare, comprised only a small portion (<10%) of all TB and MDR/RR TB cases and we did not include these cases in this study. However, cases reported outside NTP account for discrepancies between total notifications in this study compared with WHO reports.

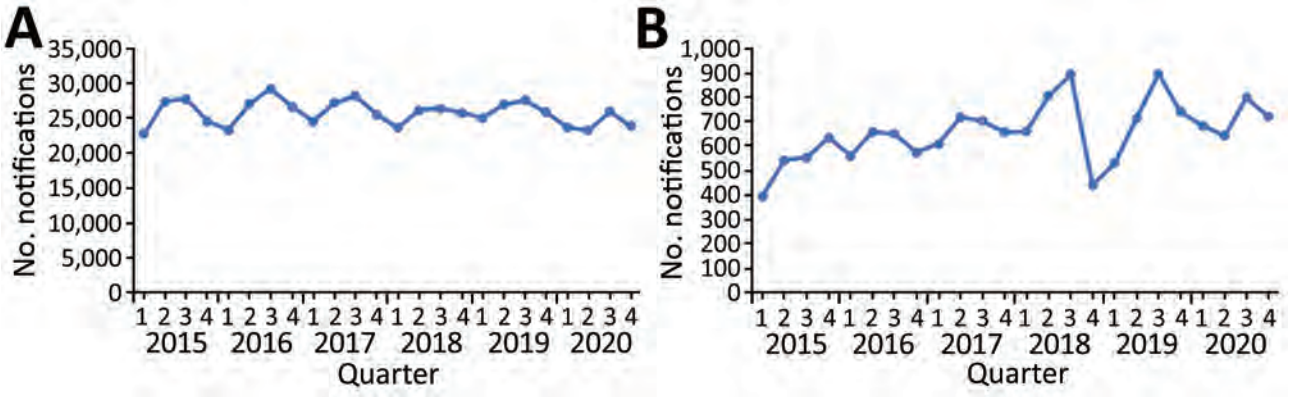

Figure 1. Quarterly tuberculosis notifications, Vietnam, 2015–2020. A) All tuberculosis notifications. B) Multidrug-resistant/rifampin-resistant tuberculosis notifications.

MDR/RR TB Patients

We identified patients who began treatment for MDR/RR TB (defined as TB with resistance to isoniazid and rifampin) through a separate national database. We included MDR/RR TB case notifications during January 2015–December 2020 (Figure 1, panel B). Reported data include underlying conditions, site of TB disease, smear and culture status at diagnosis, drug resistance, and adverse events. Patients with diagnosed MDR/RR TB underwent treatment according to WHO guidelines, comprising either 9-month or 20-month standardized antimicrobial drug regimens (*22*). NTP reported quarterly MDR/RR TB notifications during 2015–2020.

Data Analysis

Patient-level data were only available for 2019 and 2020. We summarized TB notifications by age, sex, history of previous treatment, and treatment outcome and reported proportions of missing data (Table 1), as well as monthly TB notifications for 2019 and 2020 (Figure 2), including the percentage change in monthly and yearly notifications (Appendix Table 1, https://wwwnc.cdc.gov/EID/article/28/3/21-1919-app1.pdf). We also calculated the monthly notifications and percentage change in notifications from cities and provinces where COVID-19 outbreaks occurred, Ho Chi Minh City and Hanoi in April 2020 and Da Nang and Quang Nam in July–August 2020 (Figure 2; Appendix Table 1). For comparison, we chose 2 provinces in South and Central Vietnam where no COVID-19 cases were detected during the study period, Can Tho and Nghe An (Appendix Figure).

For quarterly TB notifications during 2015–2020, we used an interrupted time series (*23*) to determine whether quarterly TB notifications decreased during January–June 2020, compared with quarterly notifications during 2015–2019. We used an interrupted time series because it enables a comparison of the change in the trend of an event before and after an interruption, in this case COVD-19. We also used an interrupted time series to determine whether the proportion of patients with treatment success changed for patients beginning treatment during July 2019–January 2020 compared with patients commencing treatment during January 2016–June 2019 (Table 2). Patients beginning first-line treatment for TB during July–December 2019 were scheduled to finish treatment during January–June 2020, after the onset of the COVID-19 pandemic.

For 2019 and 2020 data, we summarized MDR/RR TB notifications by age, sex, history of previous treatment, smear and culture results, and treatment outcome (Table 3). We noted proportions of missing data. We summarized monthly MDR/RR TB notifications made during 2019 and 2020, including the percentage change in monthly and yearly notifications, and separately calculated the difference in notifications for Ho Chi Minh City and Hanoi (Appendix Table 2). We used an interrupted time series to determine whether quarterly MDR/RR TB notifications decreased during 2020 compared with 2015–2019.

For MDR/RR TB, we calculated the relative risk for cases to have a positive smear diagnosis in 2020 compared with 2019. Similarly, we calculated the relative risk for a positive culture diagnosis in 2020 compared with 2019.

We calculated CIs and performed analyses by using SAS version 9.4 (SAS Institute, Inc., https://www.sas.com). The University of Sydney provided ethics approval for this study (approval no. HREC 2020/353). The study also was approved by the Vietnam National Lung Hospital.

Table 1. Characteristics of persons with diagnosed tuberculosis, Vietnam, 2019 and 2020*

Characteristics	2019	2020
Total no. cases notified	105,680	96,998
Age group, y		
<20	5,371 (5.1)	4,378 (4.5)
20–39	32,962 (31.2)	29,303 (30.2)
40–59	39,177 (37.1)	36,094 (37.2)
60–79	23,942 (22.7)	23,121 (23.8)
≥80	4,228 (4.0)	4,102 (4.2)
Sex†		
M	74,331 (70.3)	68,737 (70.9)
F	30,248 (28.6)	27,482 (28.3)
Region‡		
North	26,352 (24.9)	23,862 (24.6)
Central	18,969 (18.0)	16,329 (16.8)
South	59,256 (56.1)	56,027 (57.8)
Registration group§		
New diagnosis	96,445 (91.3)	89,048 (91.8)
Relapse	6,575 (6.2)	5,895 (6.1)
Retreatment	1941 (1.8)	1,812 (1.9)

*Values represent no. (%) except as indicated. Definitions for classification according to World Health Organization guidelines (https://www.who.int/tb/publications/definitions/en).
†Sex was not reported for 1,101 (1.0%) cases in 2019 and 779 (0.8%) cases in 2020.
‡District and region were not reported for 1,103 (1.0%) cases in 2019 and 780 (0.8%) cases in 2020.
§Registration group was not reported for 719 (0.7%) cases in 2019 and 243 (0.3%) cases in 2020.

Results

TB Notifications

NTP reported 105,680 TB cases in 2019 and 96,998 in 2020 (Table 1). Most cases were diagnosed among male persons, and most cases were notified in the south of the country.

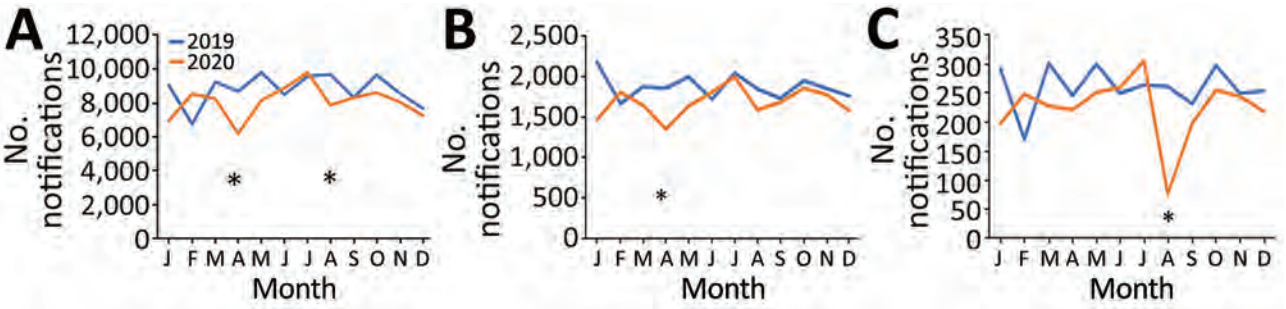

Figure 2. Change in number of monthly tuberculosis notifications during the COVID-19 pandemic, Vietnam, 2019–2020. A) Vietnam; B) Hanoi and Ho Chi Minh City; C) Da Nang and Quang Nam Provinces. Asterisks indicate timing of COVID-19 outbreaks. COVID-19, coronavirus disease.

Overall, national TB case notifications dropped by 8% during 2020 compared with 2019 (Appendix Table 1). In April 2020, during the first COVID-19 outbreak in Vietnam, we observed a 29% decrease in national TB notifications compared with April 2019 (Appendix Table 1). We also noted a decrease in case notifications during January 2020 compared with January 2019. This difference likely reflects the difference in the date of the Lunar New Year, which was earlier in 2020 than 2019, rather than an effect of the pandemic. In Hanoi and Ho Chi Minh City, areas most affected during this outbreak, the difference in TB notifications was 27% (Appendix Table 1). During the second major COVID-19 outbreak in August 2020, TB notifications declined by 19% nationally and 71% in the provinces most affected, Da Nang and Quang Nam, compared with August 2019 (Appendix Table 1). Although a pronounced decrease in TB notifications was not observed in the 2 provinces with no COVID-19 cases, Can Tho and Nghe An, we did note a 7%–16% decrease in annual TB notifications in these provinces for 2020 compared with 2019 (Appendix Table 1).

TB notifications decreased by 364 notifications per quarter (95% CI −1,236 to 508) during the year after the onset of the COVID-19 compared with the

Table 2. Tuberculosis treatment outcomes for patients receiving first-line therapy, stratified by date treatment began, Vietnam*

Treatment start date	Favorable outcome†	Failure	Lost to follow-up	Death	Transfer to MDR‡	Not evaluated	Total unfavorable outcome§
2016							
Q1	18,405 (92.9)	146 (0.7)	434 (2.2)	545 (2.8)	31 (0.2)	252 (1.3)	1,156 (5.8)
Q2	20,943 (93.3)	129 (0.6)	567 (2.5)	531 (2.4)	47 (0.2)	235 (1.0)	1,274 (5.7)
Q3	22,656 (93.5)	139 (0.6)	580 (2.4)	535 (2.2)	56 (0.2)	258 (1.1)	1,310 (5.4)
Q4	24,106 (91.6)	192 (0.7)	700 (2.7)	667 (2.5)	103 (0.4)	562 (2.1)	1,662 (6.3)
Total 2016	86,110 (92.8)	606 (0.7)	2,281 (2.5)	2,278 (2.5)	237 (0.3)	1,307 (1.4)	5,402 (5.8)
2017							
Q1	22,453 (91.0)	193 (0.8)	676 (2.7)	557 (2.3)	103 (0.4)	694 (2.8)	1,529 (6.2)
Q2	24,863 (91.5)	188 (0.7)	686 (2.5)	632 (2.3)	102 (0.4)	715 (2.6)	1,608 (5.9)
Q3	25,813 (92.3)	170 (0.6)	712 (2.5)	615 (2.2)	107 (0.4)	549 (2.0)	1,604 (5.7)
Q4	23,171 (91.6)	119 (0.5)	652 (2.6)	613 (2.4)	120 (0.5)	615 (2.4)	1,504 (5.9)
Total 2017	96,300 (91.6)	670 (0.6)	2,726 (2.6)	2,417 (2.3)	432 (0.4)	2,573 (2.4)	6,245 (5.9)
2018							
Q1	21,514 (90.9)	164 (0.7)	624 (2.6)	669 (2.8)	114 (0.5)	573 (2.4)	1,571 (6.6)
Q2	23,942 (91.4)	129 (0.5)	691 (2.6)	648 (2.5)	159 (0.6)	623 (2.4)	1,627 (6.2)
Q3	24,221 (91.6)	135 (0.5)	668 (2.5)	640 (2.4)	127 (0.5)	657 (2.5)	1,570 (5.9)
Q4	23,575 (91.1)	122 (0.5)	691 (2.7)	615 (2.4)	108 (0.4)	758 (2.9)	1,536 (5.9)
Total 2018	93,252 (91.3)	550 (0.5)	2,674 (2.6)	2,572 (2.5)	508 (0.5)	2,611 (2.6)	6,304 (6.2)
2019							
Q1	21,842 (90.4)	144 (0.6)	748 (3.1)	624 (2.6)	110 (0.5)	701 (2.9)	1,626 (6.7)
Q2	24,122 (90.7)	155 (0.6)	777 (2.9)	701 (2.6)	150 (0.6)	680 (2.6)	1,783 (6.7)
Q3	25,525 (91.3)	123 (0.4)	784 (2.8)	632 (2.3)	183 (0.7)	724 (2.6)	1,722 (6.2)
Q4	23,501 (91.0)	124 (0.5)	681 (2.6)	614 (2.4)	166 (0.6)	729 (2.8)	1,585 (6.1)
Total 2019	73,148 (91.0)	402 (0.5)	2,242 (2.8)	1,947 (2.4)	499 (0.6)	2,133 (2.7)	5,090 (6.3)
2020¶							
Q1	21,613 (91.2)	144 (0.6)	516 (2.2)	643 (2.7)	156 (0.7)	623 (2.6)	1,459 (6.2)

*Values are no. (%). MDR, multidrug-resistant; Q, quarter.
†Favorable outcomes include cure and treatment complete.
‡Cases were transferred to MDR status when resistance testing revealed MDR TB or treatment with first-line antimicrobial drugs failed.
§Unfavorable outcomes include failure, loss to follow-up, death, and transfer to MDR.
¶For 2020, only outcomes for Q1 were available.

Table 3. Characteristics of patients diagnosed with MDR/RR TB by the Vietnam National Tuberculosis Program, 2019 and 2020*

Characteristics	No. (%) cases notified	
	2019	2020
Total MDR/RR TB cases	2,889	2,851
Age group, y		
<20	124 (4.3)	71 (2.5)
20–39	1,083 (37.5)	1,072 (37.6)
40–59	1,237 (42.8)	1,221 (42.8)
60–79	414 (14.3)	455 (16.0)
≥80	31 (1.1)	32 (1.1)
Sex		
M	2,206 (76.4)	2,185 (76.6)
F	683 (23.6)	666 (23.4)
Registration group†		
New	1,059 (36.7)	1,258 (44.1)
Relapse	1,012 (35.0)	976 (34.2)
Failure	328 (11.4)	210 (7.4)
Transfer in	4 (0.1)	2 (0.0)
Transfer after default	154 (5.3)	125 (4.4)
Other	227 (7.9)	177 (6.2)
No. previous treatment episodes		
1	1,011 (35.0)	855 (30.0)
2	199 (6.9)	169 (5.9)
3	34 (1.1)	34 (1.2)
4	4 (0.1)	6 (0.2)
5	1 (0.0)	2 (0.0)
Smear status at diagnosis‡		
Negative	568 (19.7)	532 (18.7)
Scanty	289 (10.0)	244 (8.6)
1+	415 (14.4)	428 (15.0)
2+	308 (10.7)	261 (9.2)
3+	275 (9.5)	262 (9.2)
Culture status at diagnosis§		
Negative	132 (4.6)	91 (3.2)
Positive	675 (23.4)	564 (19.8)
Contaminated	14 (0.5)	12 (0.4)
Underlying conditions		
HIV	119 (4.1)	82 (2.9)
Diabetes	47 (1.6)	54 (1.9)
COPD	7 (0.2)	7 (0.2)
Chronic kidney disease	11 (0.4)	7 (0.2)
Cardiac disease	11 (0.4)	24 (0.8)
Baseline antimicrobial drug resistance¶		
Monoresistance#	301 (10.4)	260 (9.1)
Polydrug resistance	122 (4.2)	94 (3.3)
MDR TB	1,545 (53.5)	1,666 (58.4)
Pre-XDR TB	47 (1.6)	47 (1.6)
XDR TB	12 (0.4)	10 (0.4)
Site of disease**		
Extrapulmonary	119 (4.1)	131 (4.6)
Pulmonary††	2,619 (90.7)	2,592 (90.9)

*COPD, chronic obstructive pulmonary disease; MDR, multidrug-resistant; MDR/RR, multidrug-resistant/rifampin-resistant; TB, tuberculosis; XDR, extensively drug resistant.
†Registration group was not reported for 105 (3.6%) cases in 2019 and 103 (3.6%) cases in 2020.
‡Smear status was not reported for 1,034 (35.8%) cases in 2019 and 1,124(39.4%) cases in 2020.
§Culture status was not reported for 2,068 (71.6%) cases in 2019 and 2,184 (76.6%) cases in 2020.
¶Baseline resistance was not reported for 862 (29.8%) cases in 2019 and 774 (27.1%) cases in 2020.
#Site of disease was not reported for 151 (5.2%) cases in 2019 and 128 (4.5%) cases in 2020.
**Definitions for classification according to World Health Organization guidelines (https://www.who.int/tb/publications/definitions/en).
††Pulmonary TB includes patients with pulmonary TB alone and patients with pulmonary and extra-pulmonary TB.

previous 5 years. Successful TB treatment outcomes decreased by 0.1% per quarter (95% CI −1.1% to 0.8%) for patients completing treatment in 2020, compared with rates for 2016–2019 (Appendix Table 3).

MDR/RR TB Notifications

We noted all known MDR/RR TB cases reported in Vietnam during 2015–2020 (Appendix Table 4). In 2019, 2,889 MDR/RR TB cases were notified to the electronic TB manager; 2,851 cases were notified in 2020. We noted patient demographics, treatment history, and treatment outcomes between the 2 years (Table 3).

In April 2020, during the first major COVID-19 outbreak and the first nationally implemented social distancing efforts, MDR/RR TB notifications decreased by 27% compared with notifications during April 2019 (Figure 3; Appendix Table 3). Hanoi and Ho Chi Minh City, which were most affected during this outbreak, contributed >40% of national TB case notifications, but the combined number of notified MDR/RR TB cases in these 2 cities decreased by 47% (Appendix Table 3). However, overall MDR/RR TB notifications decreased by just 1% in 2020 compared with 2019. We observed no difference in the proportion of notified patients with smear-positive TB compared with smear-negative TB (risk ratio 1.00, 95% CI 0.96–1.05), or culture-positive TB compared with culture-negative TB (risk ratio 1.03, 95% CI 0.99–1.08) between 2020 and 2019 (Table 3). The difference in MDR/RR TB notifications decreased by 1 notification per quarter (95% CI −129 to 132) after the start of the COVID-19 pandemic compared with before the pandemic (Appendix Table 2).

Discussion

This retrospective cohort study compared the number of notified TB cases and treatment outcomes in Vietnam during the first year of the COVID-19 pandemic with those during the preceding 5 years. We found an 8% decrease in overall TB notifications and a 1% decrease in MDR/RR TB notifications in 2020 compared with the preceding year. We did not observe any difference in TB treatment outcomes in 2020 compared with the period 2016–2019. However, we did see noticeable decreases in TB and MDR/RR TB case notifications in the provinces affected most by COVID-19 in the months in which social distancing measures were enforced. This observation suggests a possible delay in the diagnosis of TB and MDR/RR TB cases. NTP and provincial TB programs in areas most affected by COVID-19 should develop strategies to reduce the delay in diagnosis and prevent community transmission.

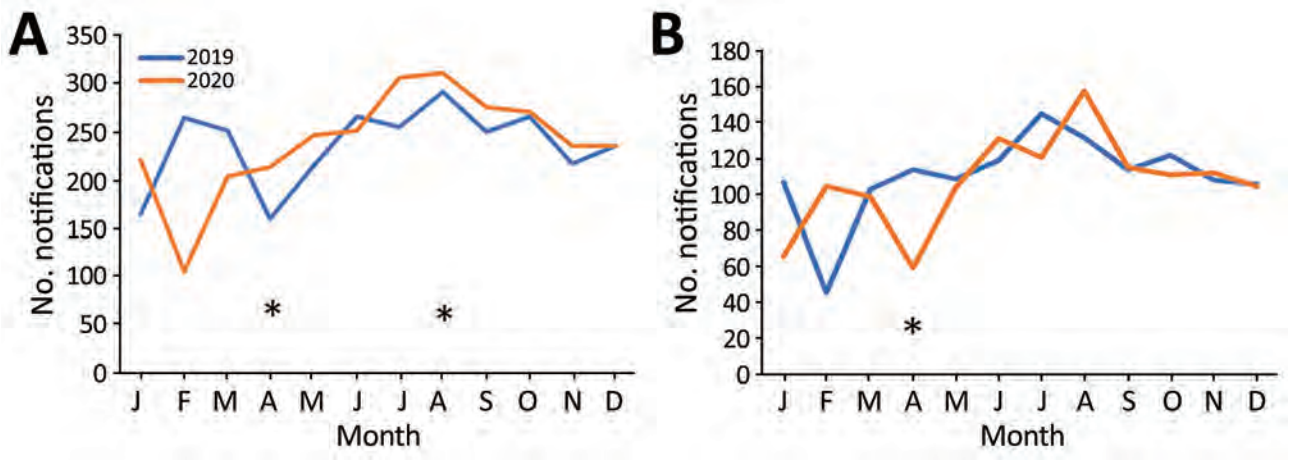

Figure 3. Change in number of monthly notifications for multidrug-resistant/rifampin-resistant tuberculosis during the COVID-19 pandemic, Vietnam, 2019–2020. A) Vietnam; B) Hanoi and Ho Chi Minh City. Asterisks indicate timing of COVID-19 outbreaks. COVID-19, coronavirus disease.

Our study starkly contrasts findings from other settings during the COVID-19 pandemic. Several countries reported ≤30% fewer TB notifications during the first half of 2020 than before COVID-19 (*2*,*4*,*7*,*9*,*24*,*25*). In Malawi, one province noted a 36% decrease in notifications, after which a subsequent rebound in notifications occurred by the end of the year, culminating in a 24% overall decrease in TB notifications in 2020 (*26*). Similarly, the United States reported an overall 20% decrease in TB notifications for 2020 compared with those for the previous year (*4*), although some of the reduction in low-prevalence settings might be due to reduced immigration from high-prevalence settings (*4*). The 8% decrease in TB notifications we observed in Vietnam was modest compared to these other settings. Effective control of the COVID-19 pandemic likely enabled health services to operate and compensate during non-lockdown periods. Although we found a decrease in TB notifications for most months in 2020 compared with those for 2019, the decrease in TB notifications was modest during months without surges in COVID-19 case numbers, including June, November, and December (Figure 2).

In 2020, during the first COVID-19 outbreak, Vietnam implemented nationwide physical distancing and public health policies. These restrictions lasted <2 months, after which daily life returned to normal for most of the population (*27*). Our study confirms that the largest decrease in case notifications for both TB and MDR/RR TB nationally was noted during this period. However, case notifications rebounded in subsequent months, resulting in the limited reduction observed in overall case notifications for the year. Nevertheless, substantial transient downturns in case notification were observed during these short periods of physical restrictions in hotspot areas, and we noted a 70% decrease in TB notifications in the 2 provinces most affected by the second outbreak. The findings overall confirm that TB notifications were adversely affected during COVID-19 outbreaks and periods in which lockdown was enforced to control the pandemic, even in the absence of COVID-19 cases. Factors contributing to the reduced TB notifications likely include difficulty accessing healthcare (*10*,*12*) and fear of catching COVID-19 at healthcare facilities (*14*).

Our findings mirror findings in neighboring China, where the incidence of COVID-19 remained low amidst a moderately high incidence of TB. Data from the first half of 2020 in China showed that TB notifications also rebounded in the months after the easing of initial COVID-19 restrictions (*28*). Our findings and those from China suggest that when COVID-19 outbreaks are relatively brief, losses in TB notifications can be compensated for in subsequent months. However, increased TB surveillance is required after periods of strict lockdown to identify transmission that can occur during delayed case finding. Delays in TB case finding also are suggested by observational studies that demonstrated fewer sputum samples submitted for TB smear and culture during 2020 than 2019 (*29*,*30*).

Furthermore, delayed case finding could result in more advanced TB disease before diagnosis. We found no difference in the proportion of patients being seen with more advanced TB disease in health facilities, measured by culture and smear status, after a period of social restrictions. Another study in South Korea also found no difference in smear status, culture results, or treatment adherence for TB patients between the first 6 months of 2020 and the year

preceding the pandemic (*31*). Both Vietnam and South Korea had smaller COVID-19 outbreaks, measured as total cases and per capita, in 2020 compared with other settings globally (*18*). However, a much smaller study in Spain, a country with a high COVID-19 burden, reported more advanced radiologic findings for TB notifications in 2020 (*32*). Further global data from settings with high COVID-19 burdens will be needed to appreciate the effects of the COVID-19 pandemic on delayed TB case finding.

We found no difference in treatment outcomes for TB patients who started treatment in the 6 months before the pandemic (July–December 2019) and completed treatment during the pandemic compared with TB patients beginning treatment during 2016–July 2019. In contrast, Italy, a country with low TB incidence, reported a substantial increase in the proportion of patients experiencing poor TB treatment outcomes during the pandemic, including loss to follow-up and death (*33*).

A strength of our study is that we used a comprehensive national database that can be generalizable at a national level for Vietnam. We evaluated TB notifications during the COVID-19 pandemic compared with TB notification data over a prolonged period (2016–2019) before the pandemic, which enabled us to account for trends over time; single comparisons might miss previously existing trends, including seasonal variation (*34*).

Our study is limited by using routinely collected programmatic data, which is limited to key information about patients and only includes the 2020 calendar year. Collection of smear status was missing for ≈30% of cases, and culture status at baseline was missing in ≈70%, limiting the ability to fully appreciate any change in smear or culture status between 2019 and 2020. Furthermore, because the duration of MDR/RR TB treatment is 9 or 20 months, we could only compare treatment outcomes for patients on standard first-line therapy. Finally, the effects on treatment outcomes can only be fully appreciated when all patients who commenced treatment in 2019 and 2020 receive an outcome.

Several policy implications arise from this study. Evidence suggests that countries with prolonged control of community transmission of SARS-CoV-2, such as China, Vietnam, and South Korea, have seen only modest impacts on overall TB notifications. Furthermore, evidence also suggests that TB notifications can rebound after COVID-19 has been controlled. Thus, involvement of national and international organizations in the care of TB patients is critical for monitoring and evaluating the interactions between COVID-19 and health priorities, preparing the healthcare sector, and limiting service disruptions. The COVID-19 pandemic is far from over and must be controlled before care to other infectious diseases such as TB can be restored.

Future studies could address the effect of a prolonged COVID-19 pandemic on delayed TB diagnosis, especially in settings with a high burden of COVID-19. The COVID-19 pandemic has taken a markedly different course from mid-2021, and Vietnam has experienced major outbreaks nationwide because of the Delta variant. Further research evaluating this period will enable us to contrast the effects of COVID-19 outbreaks on TB notifications over the course of the pandemic. Further evaluation also is needed to assess effects of COVID-19 on TB treatment outcomes, including changes in adverse TB outcomes, such as loss to follow-up due to decreased access to healthcare systems. Ultimately, the extent of the effects of the COVID-19 pandemic on TB care will take many years to fully appreciate, both in Vietnam and globally. Operational research is required to continue to identify these effects and to maintain resources for TB programs despite competing healthcare priorities. Finally, COVID-19–related restrictions, such as social distancing and the use of facemasks, might limit TB transmission; however, the adverse consequences of the COVID-19 pandemic likely are not adequately offset by these beneficial effects, and this requires further exploration.

In conclusion, our study demonstrated a very limited decrease in TB notifications in Vietnam during the first year of the COVID-19 pandemic, despite national physical distancing measures. Settings with high rates of community transmission of SARS-CoV-2 are likely to experience a surge in TB notifications when COVID-19 restrictions are eased. These settings should increase healthcare capacity to detect and treat TB cases missed during COVID-19 restrictions.

Acknowledgments

We thank all staff at the National Tuberculosis Program in Vietnam and staff involved in the care of tuberculosis patients in Vietnam for their contributions to this study. We also thank Alex Shaw for statistical advice.

About the Author

Dr. Hasan is an infectious disease physician at The University of Sydney Ringgold Standard Institution, Sydney, New South Wales, Australia. His research interests include drug-resistant tuberculosis and coronavirus disease (COVID-19) in endemic settings.

References

1. World Health Organization. Tuberculosis [cited 2021 Apr 5]. https://www.who.int/news-room/fact-sheets/detail/tuberculosis
2. Buonsenso D, Iodice F, Sorba Biala J, Goletti D. COVID-19 effects on tuberculosis care in Sierra Leone. Pulmonology. 2021;27:67–9. https://doi.org/10.1016/j.pulmoe.2020.05.013
3. Daw MA, Zgheel FA, El-Bouzedi A, Ahmed MO. Spatiotemporal distribution of tuberculosis and COVID-19 during the COVID-19 pandemic in Libya. Disaster Med Public Health Prep. 2021;15:e43–5. https://doi.org/0.1017/dmp.2020.458
4. Deutsch-Feldman M, Pratt RH, Price SF, Tsang CA, Self JL. Tuberculosis—United States, 2020. MMWR Morb Mortal Wkly Rep. 2021;70:409–14. https://doi.org/10.15585/mmwr.mm7012a1
5. Louie JK, Reid M, Stella J, Agraz-Lara R, Graves S, Chen L, et al. A decrease in tuberculosis evaluations and diagnoses during the COVID-19 pandemic. Int J Tuberc Lung Dis. 2020;24:860–2. https://doi.org/10.5588/ijtld.20.0364
6. Odume B, Falokun V, Chukwuogo O, Ogbudebe C, Useni S, Nwokoye N, et al. Impact of COVID-19 on TB active case finding in Nigeria. Public Health Action. 2020;10:157–62. https://doi.org/10.5588/pha.20.0037
7. Lai C-C, Yu W-L. The COVID-19 pandemic and tuberculosis in Taiwan. J Infect. 2020;81:e159–61. https://doi.org/10.1016/j.jinf.2020.06.014
8. Cilloni L, Fu H, Vesga JF, Dowdy D, Pretorius C, Ahmedov S, et al. The potential impact of the COVID-19 pandemic on the tuberculosis epidemic a modelling analysis. EClinicalMedicine. 2020;28:100603. https://doi.org/10.1016/j.eclinm.2020.100603
9. Ferrer JP, Suzuki S, Alvarez C, Berido C, Caballero M, Caraig B, et al. Experiences, challenges and looking to the future in a clinical tuberculosis cohort in the time of COVID-19 in the Philippines. Trans R Soc Trop Med Hyg. 2021;115:579–82. https://doi.org/10.1093/trstmh/trab025
10. Rai DK, Kumar R, Pandey SK. Problems faced by tuberculosis patients during COVID-19 pandemic: Urgent need to intervene. Indian J Tuberc. 2020;67(4S):S173–4. https://doi.org/10.1016/j.ijtb.2020.07.013
11. Udwadia ZF, Sharma S, Mullerpattan JB, Gajjar I, Pinto L. Effective use of telemedicine in Mumbai with a cohort of extensively drug-resistant "XDR" tuberculosis patients on bedaquiline during COVID-19 pandemic. Lung India. 2021;38:98–9. https://doi.org/10.4103/lungindia.lungindia_464_20
12. Cronin AM, Railey S, Fortune D, Wegener DH, Davis JB. Notes from the field: effects of the COVID-19 response on tuberculosis prevention and control efforts—United States, March–April 2020. MMWR Morb Mortal Wkly Rep. 2020;69:971–2. https://doi.org/10.15585/mmwr.mm6929a4
13. Jain VK, Iyengar KP, Samy DA, Vaishya R. Tuberculosis in the era of COVID-19 in India. Diabetes Metab Syndr. 2020;14:1439–43. https://doi.org/10.1016/j.dsx.2020.07.034
14. Ahmed SAKS, Ajisola M, Azeem K, Bakibinga P, Chen Y-F, Choudhury NN, et al.; Improving Health in Slums Collaborative. Impact of the societal response to COVID-19 on access to healthcare for non-COVID-19 health issues in slum communities of Bangladesh, Kenya, Nigeria and Pakistan: results of pre-COVID and COVID-19 lockdown stakeholder engagements. BMJ Glob Health. 2020;5:e003042. https://doi.org/10.1136/bmjgh-2020-003042
15. Boulle A, Davies M-A, Hussey H, Ismail M, Morden E, Vundle Z, et al. Risk factors for COVID-19 death in a population cohort study from the Western Cape Province, South Africa. Clin Infect Dis. 2021;73(7):e2005–e2015. https://doi.org/10.1093/cid/ciaa1198
16. World Health Organization. Use of high burden country lists for TB by WHO in the post-2015 era: summary [cited 2021 Apr 5]. https://www.who.int/tb/publications/global_report/high_tb_burdencountrylists2016-2020summary.pdf
17. Thanh HN, Van TN, Thu HNT, Van BN, Thanh BD, Thu HPT, et al. Outbreak investigation for COVID-19 in northern Vietnam. Lancet Infect Dis. 2020;20:535–6. https://doi.org/10.1016/S1473-3099(20)30159-6
18. John Hopkins University. COVID-19 dashboard by the Center for Systems Science and Engineering (CSSE) at Johns Hopkins University [cited 2021 Mar 1]. https://coronavirus.jhu.edu/map.html
19. Nguyen VN, Nguyen BH, Pham HK, Hennig C. Tuberculosis case notification data in Viet Nam, 2007 to 2012. Western Pac Surveill Response J. 2015;6:7–14. https://doi.org/10.5365/wpsar.2014.5.2.005
20. Nguyen TA, Nguyen BTC, Duong DT, Marks GB, Fox GJ. Experience in responding to COVID-19 outbreaks from Vietnam. Lancet Reg Health West Pac. 2021;7:100077. https://doi.org/10.1016/j.lanwpc.2020.100077
21. World Health Organization. Definitions and reporting framework for tuberculosis—2013 revision (updated December 2014 and January 2020). Geneva: The Organization; 2020.
22. World Health Organization. WHO consolidated guidelines on drug-resistant tuberculosis treatment. Geneva: The Organization; 2019.
23. Bernal JL, Cummins S, Gasparrini A. Interrupted time series regression for the evaluation of public health interventions: a tutorial. Int J Epidemiol. 2017;46:348–55. https://doi.org/10.1093/ije/dyw098
24. Shrinivasan R, Rane S, Pai M. India's syndemic of tuberculosis and COVID-19. BMJ Glob Health. 2020;5:e003979. https://doi.org/10.1136/bmjgh-2020-003979
25. Golandaj JA. Insight into the COVID-19 led slow-down in TB notifications in India. Indian J Tuberc. 2021;68:142–5. https://doi.org/10.1016/j.ijtb.2020.12.005
26. Soko RN, Burke RM, Feasey HRA, Sibande W, Nliwasa M, Henrion MYR, et al. Effects of coronavirus disease pandemic on tuberculosis notifications, Malawi. Emerg Infect Dis. 2021;27:1831–9. https://doi.org/10.3201/eid2707.210557
27. Thai PQ, Rabaa MA, Luong DH, Tan DQ, Quang TD, Quach H-L, et al.; OUCRU COVID-19 Research Group. The first 100 days of severe acute respiratory syndrome coronavirus 2 (SARS-CoV-2) control in Vietnam. Clin Infect Dis. 2021;72:e334–42. https://doi.org/10.1093/cid/ciaa1130
28. Chen H, Zhang K. Insight into the impact of the COVID-19 epidemic on tuberculosis burden in China. Eur Respir J. 2020;56:2002710. https://doi.org/10.1183/13993003.02710-2020
29. Komiya K, Yamasue M, Takahashi O, Hiramatsu K, Kadota J-I, Kato S. The COVID-19 pandemic and the true incidence of tuberculosis in Japan. J Infect. 2020;81:e24–5. https://doi.org/10.1016/j.jinf.2020.07.004
30. Nikolayevskyy V, Holicka Y, van Soolingen D, van der Werf MJ, Ködmön C, Surkova E, et al.; ERLTB-Net-2 study participants. Impact of the COVID-19 pandemic on tuberculosis laboratory services in Europe. Eur Respir J. 2021;57:2003890. https://doi.org/10.1183/13993003.03890-2020
31. Min J, Kim HW, Koo HK, Ko Y, Oh JY, Kim J, et al. Impact of COVID-19 pandemic on the national PPM tuberculosis control project in Korea: the Korean PPM a monitoring database between July 2019 and June 2020.

J Korean Med Sci. 2020;35:e388. https://doi.org/10.3346/jkms.2020.35.e388
32. Aznar ML, Espinosa-Pereiro J, Saborit N, Jové N, Sánchez Martinez F, Pérez-Recio S, et al. Impact of the COVID-19 pandemic on tuberculosis management in Spain. Int J Infect Dis. 2021;108:300–5. https://doi.org/10.1016/j.ijid.2021.04.075
33. Magro P, Formenti B, Marchese V, Gulletta M, Tomasoni LR, Caligaris S, et al. Impact of the SARS-CoV-2 epidemic on tuberculosis treatment outcome in Northern Italy. Eur Respir J. 2020;56:2002665. https://doi.org/10.1183/13993003.02665-2020
34. Bonell A, Contamin L, Thai PQ, Thuy HTT, van Doorn HR, White R, et al. Does sunlight drive seasonality of TB in Vietnam? A retrospective environmental ecological study of tuberculosis seasonality in Vietnam from 2010 to 2015. BMC Infect Dis. 2020;20:184. https://doi.org/10.1186/s12879-020-4908-0

Address for correspondence: Tasnim Hasan, The University of Sydney Ringgold Standard Institution, Faculty of Medicine and Health, Sydney, NSW 2006, Australia; email: tasnim.hn@gmail.com

Novel Hendra Virus Variant Detected by Sentinel Surveillance of Horses in Australia

Edward J. Annand,[1] Bethany A. Horsburgh,[1] Kai Xu, Peter A. Reid, Ben Poole, Maximillian C. de Kantzow, Nicole Brown, Alison Tweedie, Michelle Michie, John D. Grewar, Anne E. Jackson, Nagendrakumar B. Singanallur, Karren M. Plain, Karan Kim, Mary Tachedjian, Brenda van der Heide, Sandra Crameri, David T. Williams, Cristy Secombe, Eric D. Laing, Spencer Sterling, Lianying Yan, Louise Jackson, Cheryl Jones, Raina K. Plowright, Alison J. Peel, Andrew C. Breed, Ibrahim Diallo, Navneet K. Dhand, Philip N. Britton, Christopher C. Broder, Ina Smith,[2] John-Sebastian Eden[2]

We identified and isolated a novel Hendra virus (HeV) variant not detected by routine testing from a horse in Queensland, Australia, that died from acute illness with signs consistent with HeV infection. Using whole-genome sequencing and phylogenetic analysis, we determined the variant had ≈83% nt identity with prototypic HeV. In silico and in vitro comparisons of the receptor-binding protein with prototypic HeV support that the human monoclonal antibody m102.4 used for postexposure prophylaxis and current equine vaccine will be effective against this variant. An updated quantitative PCR developed for routine surveillance resulted in subsequent case detection. Genetic sequence consistency with virus detected in grey-headed flying foxes suggests the variant circulates at least among this species. Studies are needed to determine infection kinetics, pathogenicity, reservoir-species associations, viral-host coevolution, and spillover dynamics for this virus. Surveillance and biosecurity practices should be updated to acknowledge HeV spillover risk across all regions frequented by flying foxes.

Highly pathogenic zoonotic Hendra virus (HeV) and Nipah virus (NiV) are prototypic members of the genus *Henipavirus*, family *Paramyxoviridae*, that have natural reservoirs in pteropodid flying foxes (*1*). These viruses exhibit wide mammalian host tropism, cause severe acute respiratory and encephalitic disease mediated by endothelial vasculitis, have high case-fatality rates, and cause chronic encephalitis among survivors (*2*–*4*). By March 2021, a total of 63 natural HeV spillovers had been recognized in horses in Australia,

Author affiliations: EquiEpiVet, Equine Veterinary and One Health Epidemiology, Aireys Inlet, Victoria, Australia (E.J. Annand); Department of Agriculture, Water, and the Environment Epidemiology and One Health Section, Canberra (E.J. Annand, M.C. de Kantzow, A.C. Breed); University of Sydney School of Veterinary Science and Institute for Infectious Diseases, Sydney, New South Wales, Australia (E.J. Annand, N. Brown, A. Tweedie, A.E. Jackson, K.M. Plain, N.K. Dhand); CSIRO Health and Biosecurity Black Mountain Laboratories, Canberra, Australian Capital Territory, Australia (E.J. Annand, M. Michie, I. Smith); Westmead Institute for Medical Research, Sydney (B.A. Horsburgh, K. Kim, J.-S. Eden); University of Sydney School of Medicine, Sydney (B.A. Horsburgh, C. Jones, P.N. Britton, J.-S. Eden); Ohio State University College of Veterinary Medicine, Columbus, Ohio, USA (K. Xu); Private equine veterinary practice, Brisbane, Queensland, Australia (P.A. Reid); Cooroora Veterinary Clinic, Cooroy, Queensland, Australia (B. Poole); JData, Cape Town, South Africa (J.D. Grewar); University of Pretoria, Pretoria, South Africa (J.D. Grewar); CSIRO Australian Centre for Disease Preparedness, Geelong, Victoria, Australia (N.B. Singanallur, M. Tachedjian, B. van der Heide, S. Crameri, D.T. Williams); Murdoch University School of Veterinary Medicine and The Animal Hospital, Murdoch, Western Australia, Australia (C. Secombe); Uniformed Services University of the Health Sciences Microbiology and Immunology, Bethesda, Maryland, USA (E.D. Laing, S. Sterling, L. Yan, C.C. Broder); Queensland Department of Agriculture and Fisheries Biosecurity Sciences Laboratory, Brisbane (L. Jackson, I. Diallo); Children's Hospital at Westmead, Infectious Diseases, Sydney (C. Jones, P.N. Britton); Montana State University, Bozeman, Montana, USA (R.K. Plowright); Griffith University Centre for Planetary Health and Food Security, Brisbane (A.J. Peel); University of Queensland School of Veterinary Science, Gatton, Queensland, Australia (A.C. Breed)

DOI: https://doi.org/10.3201/eid2803.211245

[1]These authors contributed equally to this article.

[2]These senior authors contributed equally to this article.

resulting in 105 horse deaths (*5*,*6*) and 4 deaths among 7 confirmed human cases (*7*). In southern Asia, NiV has caused zoonotic outbreaks with 70%–91% case-fatality rates, resulting in >700 human deaths (*8*–*10*). In response to the fatal disease threat posed by henipaviruses to humans and domestic animals, vaccines and postexposure prophylaxis (PEP) have been developed (*11*). A subunit vaccine, Equivac HeV (Zoetis, https://www.zoetis.com.au), based on the soluble recombinant G-attachment glycoprotein (receptor-binding protein [RBP]) of HeV (HeV-sG), that has been used for horses in Australia since 2012 (*12*). The human monoclonal antibody (mAb) m102.4 has been administered as emergency PEP in 16 human cases and has demonstrated safety, tolerability, intended pharmacokinetics, and no immunogenicity in a phase 1 trial (*13*). Combinations of cross-reactive humanized fusion (F) protein and RBP mABS have also been described for clinical development as PEP (*14*–*16*), and a human vaccine using HeV-sG is now in phase 1 clinical trials (*17*).

Horses are the predominant species known to be infected with HeV by natural spillover from flying foxes; 2 canine (*18*) and all known human infections having resulted from close contact with infected horses. HeV transmission from *Pteropus* spp. (flying foxes) to horses is thought to occur primarily through contaminated urine (*19*). The spatial distribution of previously detected spillovers to horses and molecular HeV testing of flying fox urine suggested that transmission was predominantly from black flying foxes (BFF; *P. alecto*) and spectacled flying foxes (SFF; *P. conspicillatus*) (*19*,*20*). However, serologic testing has detected antibodies to HeV or related henipaviruses among all 4 flying fox species in Australia (*20*–*23*). Of note, seroprevalence of IgG targeting the HeV RBP has been reported in 43% of grey-headed flying foxes (GHFF; *P. poliocephalus*) in South Australia and Victoria (*22*) and 60% (169/284) in southeastern Queensland (*21*).

Australia hosts >1 million horses. Their grazing behavior, large respiratory tidal volume, and extensive highly vascularized upper respiratory epithelium may contribute to their vulnerability for HeV spillover (*23*). Detecting spillover to horses relies on attending veterinarians recognizing clinical manifestations consistent with HeV disease, sampling appropriately, and submitting samples for priority state laboratory testing (*24*). Passive surveillance using suspected disease testing is affected by a strong regional bias for areas where HeV has previously been detected and where domestic horse populations overlap with BFF distribution ranges, from eastern coastal Queensland to northern New South Wales (*25*). Testing for HeV is less commonly performed on horses with similar disease manifestations farther south in Australia because of a perception that spillover infection is less likely to occur in regions without BFF (*26*). Among >1,000 horses with manifestations consistent with HeV disease tested annually across regions of established risk, <1% are found to be positive (*25*,*27*).

Routine testing for equine HeV infection as part of priority disease investigation is specific for the matrix (M) gene (*28*). Additional nucleoprotein (N) gene–specific testing (*29*) is limited to HeV-positive samples that undergo confirmatory testing (*30*) or in the minority (<7% nationally) of suspected equine HeV cases submitted directly to the national reference laboratory from states where spillover is considered less likely (*25*) and state testing is unavailable. This distinction is notable because it means that most horse-disease cases found negative for HeV are not investigated further, despite evidence that other viruses with potential spillover risk to horses, including novel related batborne paramyxoviruses, circulate in Australia (*27*,*31*–*35*). Likewise, animal health surveillance worldwide prioritizes targeted testing to exclude pathogens of established importance over open-ended diagnostic approaches, which are inherently more challenging to put in place and interpret.

Employing a transdisciplinary, interagency approach combining clinical-syndromic analysis and molecular and serologic testing, we explored the hypothesis that some severe viral disease–like manifestations in horses that are consistent with HeV, despite the horse testing negative, could be caused by undetected spillover of novel paramyxoviruses from flying foxes that potentially pose similar zoonotic risk. Here we report the identification of a previously unrecognized variant of HeV (HeV-var), circulating as a second genotype lineage (HeV-g2), clinically indistinguishable from prototypic HeV infection, that resulted in severe neurologic and respiratory disease in a horse.

Materials and Methods

Study Cohort

A biobank of diagnostic specimens collected in Queensland during 2015–2018 was developed from horses that underwent quantitative reverse transcription PCR (RT-PCR) testing but were negative for HeV (*28*). We recorded clinical, epidemiologic, and sample-related data, including vaccination status and perceived exposure to flying foxes (inconsistently reported by submitting veterinarians). All samples were archived at –80°C. We applied a decision algorithm based on systematic interpretation of pathologic basis and syndromic analysis of clinical disease

descriptions to categorize each case by likelihood of infectious viral cause (Appendix Table, https://wwwnc.cdc.gov/EID/article/28/3/21-1245-App1.pdf). We plated samples (EDTA blood, serum, nasal swab, rectal swab) from cases assigned priority category 1 or 2 status, considered as having the highest likelihood of infectious cause, for serologic screening and high-throughput nucleic acid extraction using the MagMAX mirVANA and CORE pathogen kits (ThermoFisher, https://www.thermofisher.com).

Pan-paramyxovirus RT-PCR Screening

We prepared cDNA from extracted RNA using Invitrogen SuperScript IV VILO Master Mix with ezDNase (ThermoFisher). A nested RT-PCR assay targeting the paramyxovirus L protein gene was adapted using primers developed elsewhere (*36*) and an AllTaq PCR Core kit (QIAGEN, https://www.qiagen.com). We identified amplicons corresponding to the expected size (584 bp) by gel electrophoresis before purification with AMPure XP (Beckman Coulter, https://www.beckmancoulter.com). To capture any weak detections, we also prepared pools by equal-volume mixing all PCR products across plated rows. We performed next-generation sequencing using an Illumina iSeq with the Nextera XT DNA library preparation kit (Illumina, https://www.illumina.com). For analysis, we assembled reads with MEGAHIT (*37*) before identifying them by comparison to GenBank entries using BLAST (*38*).

HeV-var Whole-Genome Sequencing

We subjected samples positive for HeV-var by paramyxovirus RT-PCR to meta-transcriptomic sequencing to determine the complete genome sequence and identify any co-infecting agents. RNA was reverse transcribed with Invitrogen SSIV VILO Master Mix (ThermoFisher) and FastSelect reagent (QIAGEN). We performed second-strand synthesis with Sequenase 2.0 (ThermoFisher) before DNA library preparation with Nextera XT (Illumina) and unique dual indexes. We performed sequencing on an Illumina NextSeq system to generate 100 million paired reads (75 bp) per library.

Assembly and Comparative Genomic and Phylogenetic Analyses

For genome assembly, we trimmed RNA sequencing reads and mapped them to a horse reference genome (GenBank GCA_002863925.1) using STAR aligner to remove host sequences. We assembled nonhost reads de novo with MEGAHIT (*37*) and compared them with the GenBank nucleotide and protein databases using blastn and blastx (*38*). We extracted the putative virus contig and remapped reads to this draft genome using bbmap version 37.98 (https://sourceforge.net/projects/bbmap) to examine sequence coverage and identify misaligned reads. We extracted, aligned, and annotated the majority consensus sequence by reference to the prototype HeV strain using Geneious Prime version 2021.1.1 (https://www.geneious.com) and submitted it to GenBank (accession no. MZ318101).

For classification, we aligned the paramyxovirus polymerase (L) protein sequence according to International Committee on Taxonomy of Viruses (ICTV) guidelines (*39*). We prepared alignments of partial nucleocapsid (N) and phosphoprotein (P) nucleotide sequences with known HeV strains from the GenBank database. Phylogenies were prepared using a maximum likelihood approach in MEGA X (https://www.megasoftware.net) according to the best-fit substitution model and 500 bootstrap replicates.

Quantitative RT-PCR Development

We adapted quantitative RT-PCR targeting the HeV M gene (*28*) to target HeV-var. The duplex assay used the Applied Biosystems AgPath-ID One-Step RT-PCR kit (ThermoFisher), and distinguishes prototype and variant HeV strains. In brief, we combined 4 µL RNA with 10 µL 2× RT-PCR buffer, 0.8 µL 25× RT-PCR enzyme mix, 2 µL nuclease-free water, and 3.2 µL primer/probe mix (0.6 µL each primer, 0.3 µL each probe from 10 µmol stock; Table 1). We generated the reaction using 10 min at 50°C for cDNA synthesis, 10 min at 95°C for RT inactivation, and 50 cycles of 95°C for 15 s and 60°C for 30 s with FAM and HEX channels captured at the end of each cycle. As positive control, we synthesized

Table 1. Oligonucleotides used for duplex quantitative reverse transcription PCR targeting the matrix gene of novel Hendra virus variant from horse in Australia

Virus	Name	Sequence, 5′ → 3′*	Reference
Prototype	Mr_fwd_1	CTTCGACAAAGACGGAACCAA	(*34*)
	Mr_rev_1	CCAGCTCGTCGGACAAAATT	
	Mr_prb_1	FAM-TGGCATCTT-ZEN-TCATGCTCCATCTCGG-IABk	
Variant	Mv_fwd_1	TCTCGACAAGGACGGAGCTAA	Referent
	Mv_rev_1	CCGGCTCGTCGAACAAAATT	
	Mv_prb_1	HEX-TGGCATCCT-ZEN-TCATGCTTCACCTTGG-IABk	

*FAM and HEX 5′ reporter dyes were combined with ZEN Internal Quencher and the 3′ quencher Iowa Black, and supplied by Integrated DNA Technologies (https://www.idtdna.com).

gene fragments encoding a T7 promoter upstream of the partial M gene for both prototypic and variant HeV (Appendix Figure 1). We expressed RNA transcripts using the NEB HiScribe T7 High Yield RNA Synthesis kit (New England Biolabs, https://www.neb.com).

Virus Isolation, Confirmation, and Neutralization Studies

We attempted isolations in Vero cells (ATCC CCL-81) and primary kidney cells derived from black flying foxes (*40*). We confirmed them by cytopathogenic effect formation, quantitative RT-PCR, RNA sequencing, electron microscopy, and viral neutralization studies using HeV and isolated HeV-var mAb m102.4 (Appendix).

Serologic Analysis

We performed serologic analysis using multiplex microsphere immunoassays with a Luminex MAGPIX system (https://www.luminexcorp.com). We performed initial screening for IgG using an extensive panel of bacterial (*Leptospira*, *Brucella*) and viral antigens (paramyxovirus, filovirus, coronavirus, flavivirus, alphavirus) coupled to MagPlex beads (Bio-Rad, https://www.bio-rad.com) for multiplex screening. We added blood or serum diluted 1:100 to the beads, with binding detected following the addition of a combination of biotinylated-protein-G and -A and streptavidin-R-phycoerythrin. We read median fluorescence intensity on the MAGPIX system (Luminex) targeting 100 beads per antigen and used a Bayesian latent class model to assess test performance and determine appropriate cutoffs for positive test classification (*32*). We also applied an IgM assay in which biotinylated equine IgM was used in place of biotinylated proteins A and G.

In Silico Analysis of the RBP Homology and mAb Binding

We compared the translated protein sequence of the HeV-var RBP sequence with established x-ray crystallography-derived structures of the HeV RBP protein bound to mAb m102.4 (*41*) and to ephrin-B2 using SWISS-MODEL (https://swissmodel.expasy.org). We used the results to assess the ability of m102.4 to neutralize this variant and further establish the likelihood of antibodies produced by immunization with the HeV vaccine being protective against this variant.

Results

Case Report

In September 2015, veterinary care was sought for a 12-year-old Arabian gelding in southeastern Queensland for severe disease consistent with HeV infection. The horse had always resided on the same property. Disease onset was acute; rapid deterioration occurred over 24 hours. Clinical assessment determined depressed (obtunded) demeanor, darkened red-to-purple change of the gingival mucous membranes with darker periapical line and prolonged capillary refill time, tachycardia (heart rate 75 beats/min), tachypnoea (60 breaths/min), normal rectal temperature (38.0°C), muscle fasciculations, head pressing, and collapse.

HeV infection was suspected by the attending veterinarian, who had previously managed a confirmed case, on the basis of consistency with clinical disease manifestations and perception of plausible flying fox exposure. A nearby roost was known to host BFFs, GHFFs, and little red flying foxes (LRFF) of population sizes that varied seasonally and annually (*42*). Because of its moribund condition, the horse was humanely killed. We obtained postmortem nasal, oral, and rectal swab samples and combined them in 50 mL of sterile saline; we collected blood in an EDTA tube. Pooled swabs and blood samples were submitted to the Queensland Biosecurity Sciences Laboratory (Coopers Plains, Queensland, Australia) for priority HeV testing. Quantitative RT-PCR testing targeting the M gene did not detect viral RNA and ELISA testing did not detect HeV RBP IgG (*28*,*43*).

Identification of Novel HeV-var

Given the high assigned likelihood of a zoonotic infectious cause (Appendix Table), we screened both the EDTA blood and pooled swab samples using pan-paramyxovirus RT-PCR (*36*). This identified the partial polymerase sequence of a novel paramyxovirus, most closely related to HeV (≈89% nt identity). Deep sequencing (mean coverage depth: 46.9×) of blood RNA generated the near–full-length genome of a novel HeV (Figure 1, panel A). The virus was less abundant in the pooled swab sample; mean coverage depth was 0.6× reads, spanning only 9.9% of the genome (Figure 1, panel B). No other viruses were present in either sample, and other microbial reads assembled were from common microflora, including *Staphylococcus aureus* and *Aeromonas*, *Veillonella*, *Pseudarthrobacter*, *Streptococcus*, *Acinetobacter*, and *Psychrobacter* spp.

Confirmation of HeV Infection

A comparison of the primer and probe sequences used for the routine diagnostic PCR (*28*,*29*) revealed multiple mismatches in the binding sites, explaining the failure of routine surveillance to

detect this variant (Figure 2). A quantitative RT-PCR assay was designed to detect both prototype and variant HeV strains in duplex (Table 1; Appendix Figures 1, 2), which amplified the templates of each virus with similarly high efficiency (>94%) and sensitivity, capable of detecting <100 copies of target RNA (Appendix Figure 2). The assay quantified results from the EDTA blood and pooled swabs samples, confirming RNA sequencing; the virus was more abundant in the EDTA blood (quantification cycle 26.87) than in the pooled swab samples (quantification cycle 30.67). We rescreened the priority cohort (864 samples from 350 cases in Queensland) using this novel assay but identified no additional cases. We successfully isolated virus from the EDTA blood sample of the case-animal in Vero cells. Electron microscopy of infected cells revealed cytoplasmic inclusion bodies (nucleocapsid aggregations; Figure 3, panel A) and enveloped viral-particle budding (Figure 3, panel B), consistent with HeV (Figure 3, panels A–D) (*44*).

Blood was tested for IgM and IgG against a panel of 33 antigens representative of bacterial and viral zoonoses (*32*,*45*), including RBPs of paramyxoviruses: HeV, NiV, Cedar henipavirus (CedV), Mojiang henipavirus (MojV), Ghana bat henipavirus (GhV), Menangle, Grove, and Yeppoon and pararubula viruses. We observed no notable reactions for this animal-case blood in either the IgG or IgM assays, indicating a lack of detectable antibodies consistent with acute viremia.

Genomic Analysis of Novel HeV-var

We performed phylogenetic analyses of the novel HeV-var with other known paramyxoviruses (Figure 4, panels A–C). Comparison of the nucleotide similarity of the novel HeV-var to the HeV prototype strain (GenBank accession no. NC_001906) revealed an 83.5% pairwise identity across the genome (Figure 4, panel D). The L protein phylogeny revealed that the branch lengths of prototype and variant HeV to their common node did not exceed 0.03 substitutions/site (Figure 4, panels A, B). Therefore, the viruses were considered to be of the same species according to ICTV criteria (*39*). However, this HeV-var is clearly well outside known HeV diversity (Figure 4, panel C).

After this finding, comparison with a partial novel henipavirus M gene sequence derived from a GHFF from South Australia in 2013 (*46*) revealed 99% similarity to this HeV-var. This, along with additional subsequent flying fox detections (*47*), suggests that this HeV-var represents a previously undescribed lineage (HeV-g2), with reservoir-host infection across at least the range of this flying fox species.

Analysis of the RBP

Genomic sequencing showed greatest variability in the noncoding regions with mean pairwise genome identity higher (86.9%) across coding regions (Figure 4, panel D). At the protein level, this HeV-var shared 82.3%–95.7% (mean 92.5%) aa identity to the HeV prototype (Table 2). Of note, the HeV-var RBP shared 92.7% aa identity with prototypic HeV. Modeling of the novel HeV-var RBP structure based on the translated protein sequence using the x-ray crystal structure of the prototypic HeV RBP published elsewhere (*40*) supports that the epitopes for binding ephrin-B2 receptor and mAb m102.4 remain functionally unchanged because of consistency between key residues (Figure 5). Indeed, mAb m102.4 neutralization assays revealed equivalent neutralization potency of m102.4 (2.3 μg/mL of m102.4 neutralized 30 median tissue culture infectious dose of HeV-var and 4.6 μg/mL of m102.4 neutralized 300 median tissue culture infectious dose of HeV).

Discussion

We describe use of an innovative, syndromic risk-based targeted active sentinel surveillance activity for diagnostic investigation, extending from routine priority disease investigations, to identify a consequential virus. Based on ICTV criteria (*39*), this HeV-var is a novel genotypic variant of HeV, not a new *Henipavirus* species, but it evaded detection by routine diagnostic testing for HeV because of genomic divergence. Our findings highlight the potential of sentinel surveillance through One Health interagency and transdisciplinary syndromic infectious disease research to improve detection of emerging pathogens. We also describe a new assay for laboratory diagnosis and surveillance of this virus among humans and animals.

Comparing the translated amino acid sequences of this HeV-var and prototypic HeV RBP in silico revealed no change in the mAb m102.4 or ephrin-B2 entry receptor binding sites. Similarly, we confirmed equivalent m102.4 neutralization in vitro for this HeV-var and HeV. As such, it is expected that current PEP using mAb m102.4 will also be effective against this HeV-var. We emphasize that although the HeV RBP shares only 79% aa identity with NiV RBP, the HeV-sG subunit vaccine provided 100% protection against lethal challenge with both HeV and NiV in animal models (*11*). The high similarity between this HeV-var and HeV RBP (92.5% aa identity), structural consistency of

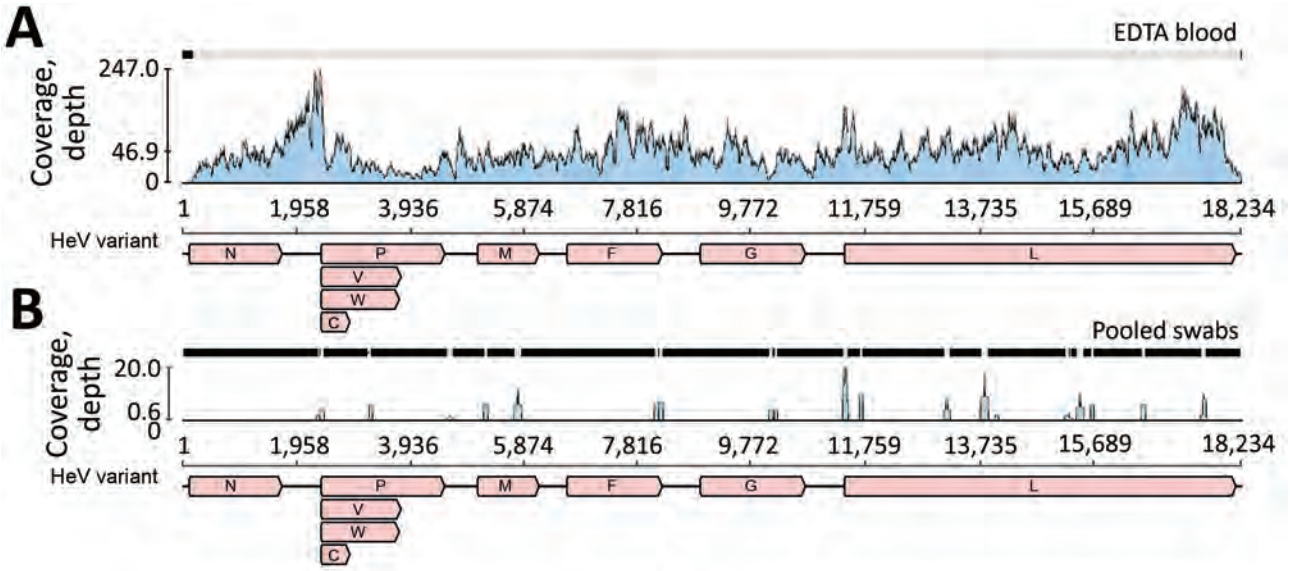

Figure 1. Sequence coverage of novel HeV variant from horse in Australia. The RNA sequencing reads were mapped to the novel HeV variant genome to examine coverage across the genome and depth for EDTA blood (A) and pooled swab samples (B). The x-axis shows the genome position with genes annotated and the y-axis shows the sequence read coverage (depth). Mean coverage depths were 46.9 for EDTA blood and 0.6 for pooled swab samples. V, W, and C indicate variably transcribed nonstructural proteins. F, fusion; G, glycoprotein; HeV, Hendra virus; M, matrix protein; N, nucleoprotein; P, phosphoprotein.

critical epitopes, and equivalent in vivo viral neutralization assays also support that current vaccination using the HEV RBP will elicit similarly protective antibodies against HeV-var.

The 99% similarity between HeV-var and a partial M-gene sequence detected in a GHFF from Adelaide in 2013 highlights that a greater diversity of HeV strains than previously recognized circulates among flying fox species in Australia and that this novel variant likely circulates as a relatively consistent sublineage (HeV-g2), at least across the range of GHFF. Subsequent identification of HeV-g2 in GHFF and LRFF from regions without previous molecular HeV detection further support this understanding (*47*).

Our findings indicate the urgent need for prompt reassessment of HeV spillover risk for horses and handlers living in southern New South Wales, Victoria, and South Australia, where risk for HeV infection has been perceived as substantially lower than that in regions within the range of BFF distribution. Our findings indicate a need to update current molecular assays, which are not expected to distinguish between HeV and HeV-var (HeV-g2), and increase surveillance testing in horses and screening of flying foxes for HeV-g2 in these areas. These might further resolve the previously reported anomaly of high seropositivity despite low HeV detection within these species reported elsewhere (*20*–*22*).

Despite relatively high genetic divergence, the phenotypic similarity of this variant to prototypic HeV, combined with the observed consistency of disease manifestations in horses, suggests that the 2 strains have equivalent pathogenicity and spillover potential. Further characterization of HeV genomic diversity and any host-species associations will increase our understanding of transmission dynamics as well as virus-host coevolution features, such as possible codivergence or founder effects. Indeed, as climate change and anthropogenic habitat loss alter the extent and nature of interspecies interactions, BFFs have rapidly expanded their range

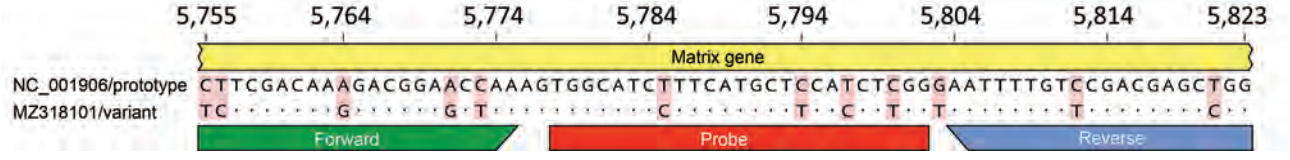

Figure 2. Genomic variation in the Hendra virus (HeV) matrix gene assay primer/probe binding sites for novel HeV variant from horse in Australia. The genomic region targeted by the commonly used HeV matrix gene quantitative RT-PCR assay (*28*) was aligned and compared for the prototype and variant HeV strains. The genomic positions relative to the prototype strain (GenBank accession no. NC_001906) are shown at the top. Primers (forward and reverse) and probe binding sites are indicated by the colored bars. Mismatches between the sequences are highlighted with red shading; dots indicate identical bases.

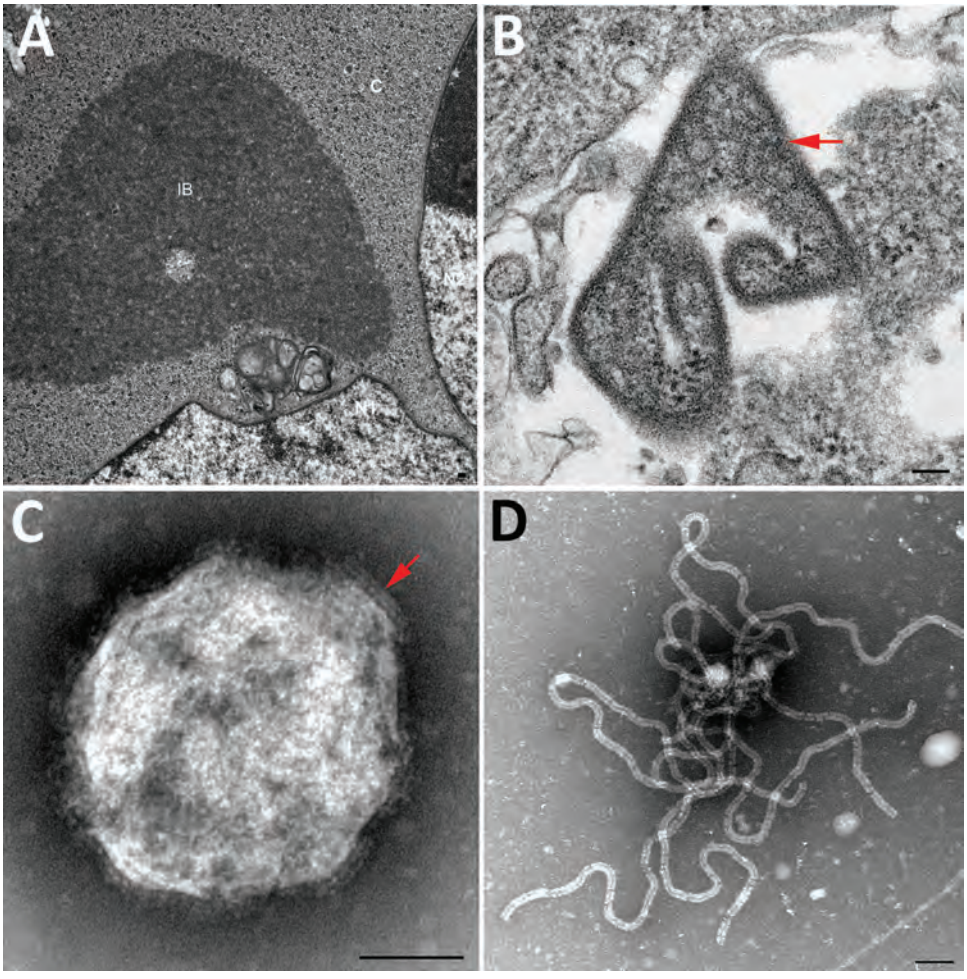

Figure 3. Transmission electron micrographs of Vero cells inoculated with the EDTA blood sample in study of novel Hendra virus variant from horse in Australia. A) Thin section showing inclusion body (IB) within the cytoplasm (C) of multinucleated (N1 and N2) syncytial cell. The nonmembrane bound IB consists of hollow nucleocapsids. B) Thin section showing virion (red arrow) with egress occurring at the plasma membrane. C) Negative contrast analysis shows a double-fringed envelope of the virion (red arrow). D) Negative contrast analysis shows strands of ribonucleic protein characteristic of the family *Paramyxoviridae*. Scale bars represent 100 nm.

southward, increasing their overlap with GHFFs (*48*). Sampling multiple species across time and space should inform how this variant strain circulates within and among flying fox species. Clearly, biosecurity practices should be updated to acknowledge spillover risk in all regions frequented by any species of flying fox.

Passive disease surveillance and biosecurity risk management for emerging diseases relies on recognition of suspected disease cases by clinical veterinarians, who play crucial roles relevant to animal and human health (*24*). Sporadic incidence of HeV and rare occurrence of Australian bat lyssavirus, yet high zoonotic consequence of both and lack of pathognomonic disease signs, inherently challenge surveillance of horses in Australia for these viruses. Critical and timely human postexposure management relies on confirmed animal-case diagnosis yet missed cases are inevitable, resulting in unmanaged risk of fatal zoonotic disease. Veterinarians are challenged in performing disease recognition by simultaneous obligations to serve both animals and animal owners, manage biosecurity risks, and meet Workplace Health and Safety Act and Biosecurity Act requirements (*24*,*49*,*50*). Veterinary description of disease manifestations most consistent with HeV led us to prioritize this case in our research testing pathway. This research detection of HeV-var highlights potential for improving emerging infectious disease surveillance through extending veterinarian-initiated risk-based suspect significant disease investigation, by selecting cases of highest likelihood of related viral cause and employing parallel serology and molecular testing pathways constructed to suit the available sample types and target diseases of highest clinical, species, and geographic relevance. These strategies build on the existing strength of systematic interpretation of clinical and field observations made by clinical veterinarians as part of existing submission and biosecurity protocols. This example serves as proof-of-concept for other disease contexts, highlighting the benefit of integrated transdisciplinary inquiry-based research approaches with routine biosecurity operations. Indeed, in

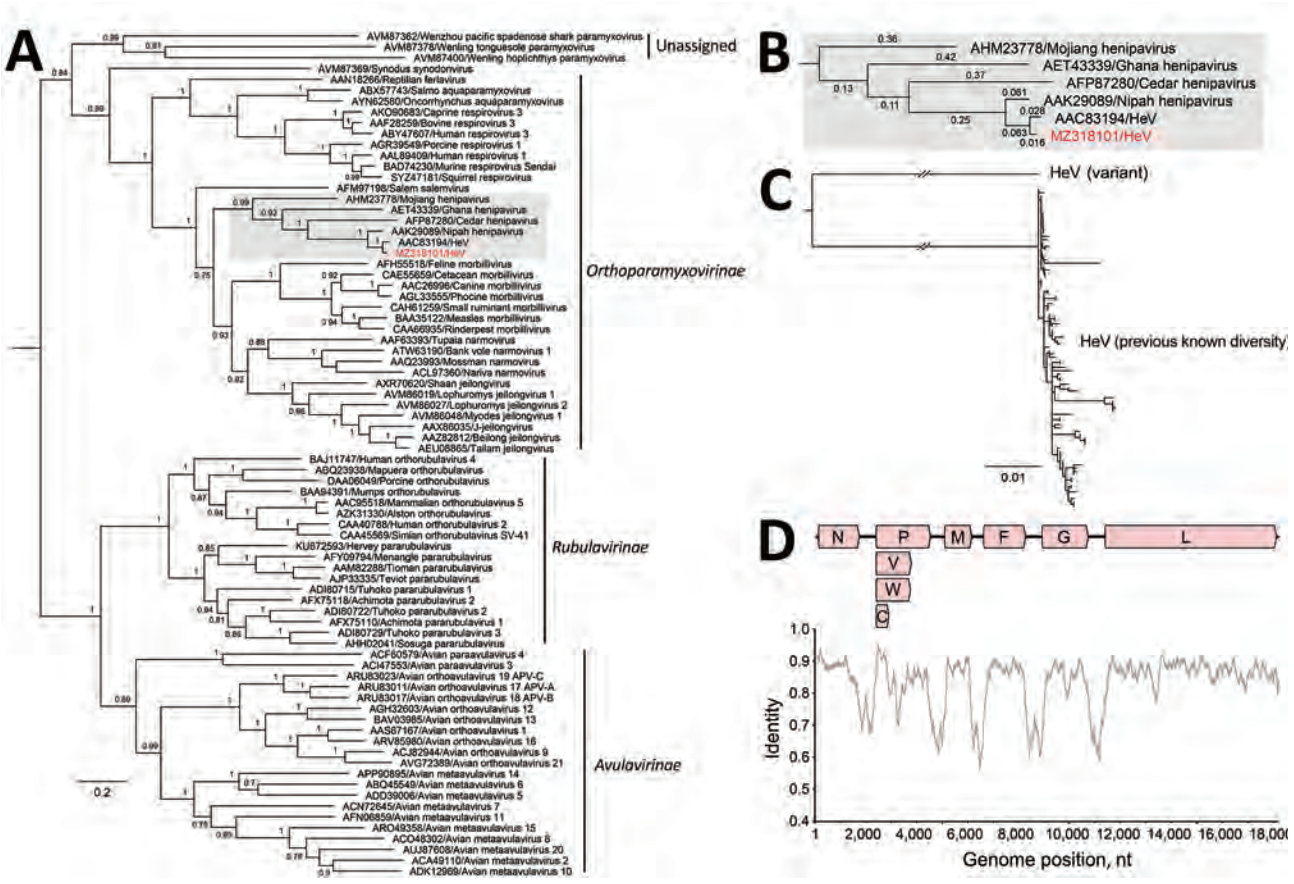

Figure 4. Phylogenomics of novel HeV variant from horse in Australia. A) Maximum-likelihood phylogeny of paramyxoviruses using complete L protein sequences. Gray shading indicates henipaviruses, and red text indicates the novel HeV variant, which groups with the prototypic HeV. Bootstrap support values as proportions of 500 replicates are shown at nodes; values <0.7 are hidden. Scale bar indicates substitutions per site. B) Enlarged gray area from panel A shows branch lengths for the henipavirus clade. The branch leading back to the common ancestor of all known HeVs and the novel HeV variant does not exceed 0.03; thus, they are considered variants of the same species. C) Maximum-likelihood phylogeny of partial N and P where deep branch lengths have been collapsed for visualization only to demonstrate that the variant is well outside the known diversity of HeV. Scale bar indicates substitutions per site. D) Nucleotide genomic similarity of the variant compared with the prototypic HeV strain. V, W, and C indicate variably transcribed nonstructural proteins. F, fusion; G, glycoprotein; HeV, Hendra virus; L, paramyxovirus polymerase; M, matrix protein; N, nucleoprotein; P, phosphoprotein.

October 2021, a fatal horse-case of HeV-g2 infection near Newcastle, New South Wales, was detected through an updated quantitative RT-PCR incorporated into routine priority disease testing.

Acknowledging the limitations of this single case, which lacked tissue for histopathology and immunohistochemistry, it is nonetheless appropriate that this HeV-var (Hev-g2) be considered equally pathogenic to prototype HeV based on coherent and consistent clinical signs of disease and pathology, evidence of viraemia, the phylogenetic analysis indicating that the variant belongs to the HeV species, and the modeling of the interactions of the functional RBP domain to the virus entry ephrin-B2 receptor. Moreover, this case fits the case definition for HeV infection in Australia's AUSVETPLAN, which is that an animal tests positive to HeV using ≥1 of PCR, virus isolation, or immunohistochemistry (*50*).

Updated PCR diagnostics suitable for routine priority detection of this HeV-var (Hev-g2) have been developed and are now used in many animal and human health laboratories in Australia. These findings demonstrate the limitation of exclusion-based testing

Table 2. Protein lengths of novel Hendra virus variant from horse in Australia and similarity to prototype strain*

Protein	Length, aa	Similarity, %
Nucleoprotein	532	96.6
Phosphoprotein	707	82.3
Matrix	352	95.7
Fusion	546	95.4
Glycoprotein	603	92.5
Large	2,244	95.7

*Prototype strain: GenBank accession no. NC_001906.

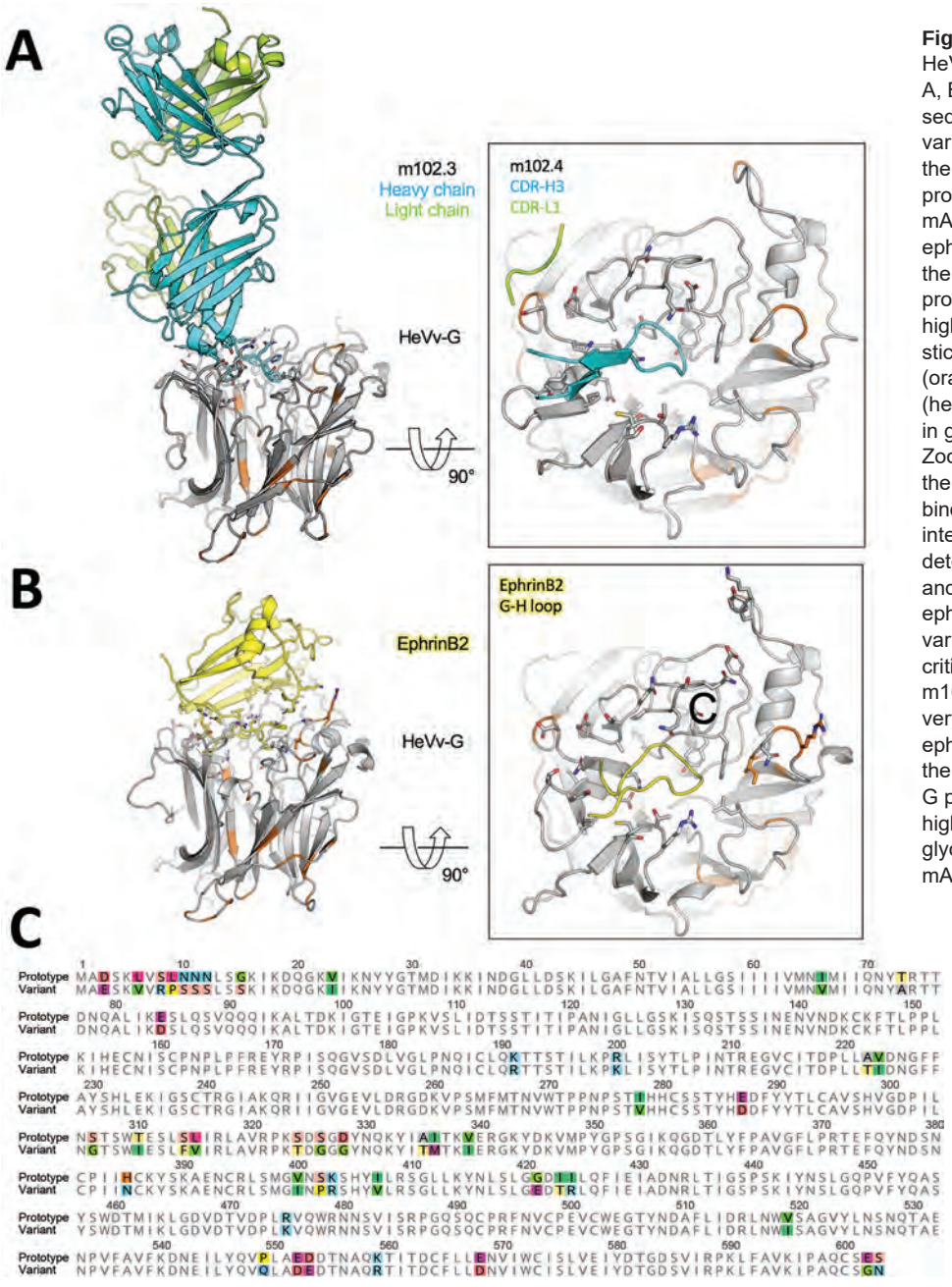

Figure 5. In silico modeling of HeV-var from a horse in Australia. A, B) The translated protein sequence encoded by the HeV variant G gene was modeled using the known protein structure of the prototype virus bound to the human mAb m102.4 (A) and the receptor ephrinB2 (B). Side views (at left) of the interactions between the HeV G protein and the 2 binding partners highlight key binding residues (as sticks) and the variant positions (orange) relative to the m102.4 (heavy chain in teal and light chain in green) and ephrinB2 (in yellow). Zoomed top views (at right) of the HeV G and m102.4/ephrinB2 binding interface highlight specific interactions by the complementarity-determining regions of the mAb and G-H loop of the receptor ephrinB2. These data show that variable positions do not occur at critical epitopes at the HeV G and m102.4 binding interface and have very minor effect on the receptor ephrinB2 binding. C) Alignment of the prototypic and variant HeV strain G proteins. Variable positions are highlighted in color. F, fusion; G, glycoprotein; HeV, Hendra virus; mAb, monoclonal antibody.

for emerging zoonoses and a gap in our understanding of how frequently detection of known zoonoses across a broad range of systems are missed because of the diagnostic tools used. Further investigations to determine the prevalence of HeV-g2 circulation among and excretion from all flying fox species in Australia should be prioritized. The risk of zoonotic HeV disease in horses and human contacts should be interpreted across all regions frequented by all species of flying foxes, particularly those areas previously considered to be at low risk for HeV spillover.

Acknowledgments

The authors thank the staff of Biosecurity Sciences Laboratory, Brisbane, for processing samples and submitting information for this case and others in the comparative cohort. We thank Jennifer Barr for processing samples, Andrea Certoma and Mel Hargreaves for technical assistance in isolating the virus, and Jianning Wang for assisting with sequence comparisons. We thank David Bath, Robyn Martin, William Wong, and others from the Department of Agriculture Water and the Environment for supporting

this project as part of the Biosecurity Innovation Program. We thank Jenny-Ann Toribio for PhD supervision. We thank Allan and Lyn Davies and the Dalara family foundation for their philanthropic financial support through the founding years of this research, without which this knowledge gap might not have been closed for much longer. We especially thank all veterinarians, owners, and caretakers who manage the health of horses and the public in relation to HeV.

Funding was provided by the Australian Government Department of Agriculture, Water, and the Environment Biosecurity Innovation Program 2020-21 Project ID 202043, Metagenomic Investigation of Horses as Sentinels research; Dalara Foundation, philanthropic donation for: Horses and Human Health; University of Sydney, Sydney Institute for Infectious Diseases: internal seed funding; CSIRO Health and Biosecurity: internal funding; Australian Government Research Training Program scholarship; C.C.B. was supported by grant AI142764, National Institute of Allergy and Infectious Diseases, National Institutes of Health; AJP was supported by an ARC DECRA fellowship (DE190100710).

C.C.B. is a United States federal employee and inventor on US and foreign patents pertaining to soluble forms of Hendra virus and Nipah virus G glycoproteins and monoclonal antibodies against Hendra and Nipah viruses, whose assignees are the US Department of Health and Human Services (Washington, DC, USA) and Henry M. Jackson Foundation for the Advancement of Military Medicine Inc. (Bethesda, Maryland, USA). Remaining authors declare no competing interests. Opinions or assertions contained herein are the private ones of the author(s) and are not to be construed as official or reflecting the views of any of the Australia or international affiliated government or research agencies or official policy or position of the Uniformed Services University, US Department of Defense, or Henry M. Jackson Foundation for the Advancement of Military Medicine, Inc.

About the Author

Dr. Annand is an equine veterinarian epidemiologist in private practice and a research associate at the University of Sydney, School of Veterinary Science and Sydney Institute for Infectious Diseases. His core research interests include One Health infectious disease surveillance, and culturally conscious biosecurity risk management. Dr. Horsburgh is an early-career researcher at the Westmead Institute for Medical Research. She is interested in using single-copy assays and high-throughput sequencing to characterize viral genomes and understand their effect on human health.

References

1. Eaton BT, Broder CC, Middleton D, Wang L-F. Hendra and Nipah viruses: different and dangerous. Nat Rev Microbiol. 2006;4:23–35. https://doi.org/10.1038/nrmicro1323
2. Selvey LA, Wells RM, McCormack JG, Ansford AJ, Murray K, Rogers RJ, et al. Infection of humans and horses by a newly described morbillivirus. Med J Aust. 1995;162:642–5. https://doi.org/10.5694/j.1326-5377.1995.tb126050.x
3. Wong KT, Tan CT. Clinical and pathological manifestations of human henipavirus infection. Curr Top Microbiol Immunol. 2012;359:95–104. https://doi.org/10.1007/82_2012_205
4. Playford EG, McCall B, Smith G, Slinko V, Allen G, Smith I, et al. Human Hendra virus encephalitis associated with equine outbreak, Australia, 2008. Emerg Infect Dis. 2010;16:219–23. https://doi.org/10.3201/eid1602.090552
5. Murray K, Rogers R, Selvey L, Selleck P, Hyatt A, Gould A, et al. A novel morbillivirus pneumonia of horses and its transmission to humans. Emerg Infect Dis. 1995;1:31–3. https://doi.org/10.3201/eid0101.950107
6. Business Queensland. Summary of Hendra virus incidents in horses. 2015 [cited 2020 Feb 14]. https://www.business.qld.gov.au/industries/service-industries-professionals/service-industries/veterinary-surgeons/guidelines-hendra/incident-summary
7. New South Wales Health. Summary of human cases of Hendra virus infection [cited 2021 Apr 23]. https://www.health.nsw.gov.au/Infectious/controlguideline/Pages/hendra-case-summary.aspx
8. Arunkumar G, Chandni R, Mourya DT, Singh SK, Sadanandan R, Sudan P, et al.; Nipah Investigators People and Health Study Group. Outbreak investigation of Nipah virus disease in Kerala, India, 2018. J Infect Dis. 2019;219:1867–78. https://doi.org/10.1093/infdis/jiy612
9. Ching PK, de los Reyes VC, Sucaldito MN, Tayag E, Columna-Vingno AB, Malbas FF Jr, et al. Outbreak of henipavirus infection, Philippines, 2014. Emerg Infect Dis. 2015;21:328–31. https://doi.org/10.3201/eid2102.141433
10. Nikolay B, Salje H, Hossain MJ, Khan AKMD, Sazzad HMS, Rahman M, et al. Transmission of Nipah virus—14 years of investigations in Bangladesh. N Engl J Med. 2019;380:1804–14. https://doi.org/10.1056/NEJMoa1805376
11. Amaya M, Broder CC. Vaccines to emerging viruses: Nipah and Hendra. Annu Rev Virol. 2020;7:447–73. https://doi.org/10.1146/annurev-virology-021920-113833
12. Middleton D, Pallister J, Klein R, Feng YR, Haining J, Arkinstall R, et al. Hendra virus vaccine, a One Health approach to protecting horse, human, and environmental health. Emerg Infect Dis. 2014;20:372–9. https://doi.org/10.3201/eid2003.131159
13. Playford EG, Munro T, Mahler SM, Elliott S, Gerometta M, Hoger KL, et al. Safety, tolerability, pharmacokinetics, and immunogenicity of a human monoclonal antibody targeting the G glycoprotein of henipaviruses in healthy adults: a first-in-human, randomised, controlled, phase 1 study. Lancet Infect Dis. 2020;20:445–54. https://doi.org/10.1016/S1473-3099(19)30634-6
14. Dong J, Cross RW, Doyle MP, Kose N, Mousa JJ, Annand EJ, et al. Potent henipavirus neutralization by antibodies recognizing diverse sites on Hendra and Nipah virus receptor binding protein. Cell. 2020;183:1536–50.e17. https://doi.org/10.1016/j.cell.2020.11.023
15. Doyle MP, Kose N, Borisevich V, Binshtein E, Amaya M, Nagel M, et al. Cooperativity mediated by rationally selected combinations of human monoclonal antibodies target-

ing the henipavirus receptor binding protein. Cell Rep. 2021;36:109628. https://doi.org/10.1016/j.celrep.2021.109628
16. Dang HV, Cross RW, Borisevich V, Bornholdt ZA, West BR, Chan Y-P, et al. Broadly neutralizing antibody cocktails targeting Nipah virus and Hendra virus fusion glycoproteins. Nat Struct Mol Biol. 2021;28:426–34. https://doi.org/10.1038/s41594-021-00584-8
17. Geisbert TW, Bobb K, Borisevich V, Geisbert JB, Agans KN, Cross RW, et al. A single dose investigational subunit vaccine for human use against Nipah virus and Hendra virus. NPJ Vaccines. 2021;6:23. https://doi.org/10.1038/s41541-021-00284-w
18. Kirkland PD, Gabor M, Poe I, Neale K, Chaffey K, Finlaison DS, et al. Hendra virus infection in dog, Australia, 2013. Emerg Infect Dis. 2015;21:2182–5. https://doi.org/10.3201/eid2112.151324
19. Edson D, Field H, McMichael L, Vidgen M, Goldspink L, Broos A, et al. Routes of Hendra virus excretion in naturally-infected flying-foxes: implications for viral transmission and spillover risk. PLoS One. 2015;10:e0140670. https://doi.org/10.1371/journal.pone.0140670
20. Burroughs AL, Durr PA, Boyd V, Graham K, White JR, Todd S, et al. Hendra virus infection dynamics in the grey-headed flying fox (*Pteropus poliocephalus*) at the southern-most extent of its range: further evidence this species does not readily transmit the virus to horses. PLoS One. 2016;11:e0155252. https://doi.org/10.1371/journal.pone.0155252
21. Edson D, Peel AJ, Huth L, Mayer DG, Vidgen ME, McMichael L, et al. Time of year, age class and body condition predict Hendra virus infection in Australian black flying foxes (*Pteropus alecto*). Epidemiol Infect. 2019;147:e240. https://doi.org/10.1017/S0950268819001237
22. Boardman WSJ, Baker ML, Boyd V, Crameri G, Peck GR, Reardon T, et al. Seroprevalence of three paramyxoviruses; Hendra virus, Tioman virus, Cedar virus and a rhabdovirus, Australian bat lyssavirus, in a range expanding fruit bat, the grey-headed flying fox (*Pteropus poliocephalus*). PLoS One. 2020;15:e0232339. https://doi.org/10.1371/journal.pone.0232339
23. Plowright RK, Eby P, Hudson PJ, Smith IL, Westcott D, Bryden WL, et al. Ecological dynamics of emerging bat virus spillover. Proc R Soc B. 2015;282:20142124.
24. Annand EJ, Reid PA, Johnson J, Gilbert GL, Taylor M, Walsh M, et al. Citizens' juries give verdict on whether private practice veterinarians should attend unvaccinated Hendra virus suspect horses. Aust Vet J. 2020;98:273–9. https://doi.org/10.1111/avj.12957
25. Animal Health Australia. Animal health surveillance quarterly [cited 2021 May 21]. file:///C:/Users/tkp3/Downloads/Animal%20Health%20Surveillance%20Quarterly%20Vol%2026%20Iss%201%20%20(2).pdf
26. Government of South Australia. Department of Primary Industries and Regions. Hendra virus in South Australia. 2018 [cited 2021 May 21]. https://pir.sa.gov.au/biosecurity/animal_health/horses/hendra_virus#toc1
27. Agnihotri K, Pease B, Oakey J, Campbell G. Confirmation of Elsey virus infection in a Queensland horse with mild neurologic signs. J Vet Diagn Invest. 2016;28:445–8. https://doi.org/10.1177/1040638716652652
28. Smith IL, Halpin K, Warrilow D, Smith GA. Development of a fluorogenic RT-PCR assay (TaqMan) for the detection of Hendra virus. J Virol Methods. 2001;98:33–40. https://doi.org/10.1016/S0166-0934(01)00354-8
29. Feldman KS, Foord A, Heine HG, Smith IL, Boyd V, Marsh GA, et al. Design and evaluation of consensus PCR assays for henipaviruses. J Virol Methods. 2009;161:52–7. https://doi.org/10.1016/j.jviromet.2009.05.014
30. Yuen KY, Fraser NS, Henning J, Halpin K, Gibson JS, Betzien L, et al. Hendra virus: epidemiology dynamics in relation to climate change, diagnostic tests and control measures. One Health. 2021;12:100207. https://doi.org/10.1016/j.onehlt.2020.100207
31. Annand EJ, Reid PA. Clinical review of two fatal equine cases of infection with the insectivorous bat strain of Australian bat lyssavirus. Aust Vet J. 2014;92:324–32. https://doi.org/10.1111/avj.12227
32. Annand E, Barr J, Singanallur Balasubramanian N, Reid P, Boyd V, Burneikienė-Petraitytė R, et al. Spillover of bat borne Rubulavirus in Australian horses—horses as sentinels for emerging infectious diseases. Int J Infect Dis. 2020;101:401–2. https://doi.org/10.1016/j.ijid.2020.09.1051
33. Barr J, Smith C, Smith I, de Jong C, Todd S, Melville D, et al. Isolation of multiple novel paramyxoviruses from pteropid bat urine. J Gen Virol. 2015;96:24–9. https://doi.org/10.1099/vir.0.068106-0
34. Marsh GA, de Jong C, Barr JA, Tachedjian M, Smith C, Middleton D, et al. Cedar virus: a novel henipavirus isolated from Australian bats. PLoS Pathog. 2012;8:e1002836. https://doi.org/10.1371/journal.ppat.1002836
35. Vidgen ME, de Jong C, Rose K, Hall J, Field HE, Smith CS. Novel paramyxoviruses in Australian flying-fox populations support host-virus co-evolution. J Gen Virol. 2015;96:1619–25. https://doi.org/10.1099/vir.0.000099
36. Tong S, Chern S-WW, Li Y, Pallansch MA, Anderson LJ. Sensitive and broadly reactive reverse transcription-PCR assays to detect novel paramyxoviruses. J Clin Microbiol. 2008;46:2652–8. https://doi.org/10.1128/JCM.00192-08
37. Li D, Liu C-M, Luo R, Sadakane K, Lam T-W. MEGAHIT: an ultra-fast single-node solution for large and complex metagenomics assembly via succinct de Bruijn graph. Bioinformatics. 2015;31:1674–6. https://doi.org/10.1093/bioinformatics/btv033
38. Altschul SF, Gish W, Miller W, Myers EW, Lipman DJ. Basic local alignment search tool. J Mol Biol. 1990;215:403–10. https://doi.org/10.1016/S0022-2836(05)80360-2
39. Rima B, Balkema-Buschmann A, Dundon WG, Duprex P, Easton A, Fouchier R, et al.; ICTV Report Consortium. ICTV virus taxonomy profile: *Paramyxoviridae*. J Gen Virol. 2019;100:1593–4. https://doi.org/10.1099/jgv.0.001328
40. Crameri G, Todd S, Grimley S, McEachern JA, Marsh GA, Smith C, et al. Establishment, immortalisation and characterisation of pteropid bat cell lines. PLoS One. 2009;4:e8266. https://doi.org/10.1371/journal.pone.0008266
41. Xu K, Rockx B, Xie Y, DeBuysscher BL, Fusco DL, Zhu Z, et al. Crystal structure of the Hendra virus attachment G glycoprotein bound to a potent cross-reactive neutralizing human monoclonal antibody. PLoS Pathog. 2013;9:e1003684. https://doi.org/10.1371/journal.ppat.1003684
42. Australian Government Department of Agriculture, Water and the Environment. Monitoring flying-fox populations [cited 2021 May 28]. https://www.environment.gov.au/biodiversity/threatened/species/flying-fox-monitoring
43. Colling A, Lunt R, Bergfeld J, McNabb L, Halpin K, Juzva S, et al. A network approach for provisional assay recognition of a Hendra virus antibody ELISA: test validation with low sample numbers from infected horses. J Vet Diagn Invest. 2018;30:362–9. https://doi.org/10.1177/1040638718760102
44. Hyatt AD, Zaki SR, Goldsmith CS, Wise TG, Hengstberger SG. Ultrastructure of Hendra virus and Nipah virus within cultured cells and host animals. Microbes Infect. 2001;3:297–306. https://doi.org/10.1016/S1286-4579(01)01383-1

45. Laing E, Yan L, Sterling S, Broder C. A Luminex-based multiplex assay for the simultaneous detection of glycoprotein specific antibodies to ebolaviruses, marburgviruses, and henipaviruses. Int J Infect Dis. 2016;53:108–9. https://doi.org/10.1016/j.ijid.2016.11.272
46. Wang J, Anderson D, Valdeter S, Chen H, Walker S, Meehan B, et al. A novel henipavirus in bats, Australia. In: Proceedings of the One Health EcoHealth Congress. One Health EcoHealth, 4–7 Dec 2016; Melbourne, Australia [cited 2021 Feb 18]. https://publications.csiro.au/rpr/pub?pid=csiro:EP173003
47. Wang J, Anderson DE, Halpin K, Hong X, Chen H, Walker S, et al. A new Hendra virus genotype found in Australian flying foxes. Virol J. 2021;18:197.
48. Roberts BJ, Catterall CP, Eby P, Kanowski J. Latitudinal range shifts in Australian flying-foxes: a re-evaluation. Austral Ecol. 2012;37:12–22. https://doi.org/10.1111/j.1442-9993.2011.02243.x
49. Mendez DH, Judd J, Speare R. Unexpected result of Hendra virus outbreaks for veterinarians, Queensland, Australia. Emerg Infect Dis. 2012;18:83–5. https://doi.org/10.3201/eid1801.111006
50. Animal Health Australia. Australia Veterinary Emergency Plan AUSVETPLAN, Response policy brief Hendra virus infection, version 4.0. Animal Health Australia; 2016 [cited 2021 May 5]. https://animalhealthaustralia.com.au/ausvetplan/download/5621

Address for correspondence: Edward Annand, Sydney School of Veterinary Science, University of Sydney, Camden, NSW 2570, Australia; email: ed.annand@sydney.edu.au

Encephalitozoon cuniculi and Extraintestinal Microsporidiosis in Bird Owners

Marta Kicia, Żaneta Zajączkowska, Martin Kváč, Kamil Cebulski, Nikola Holubová, Piotr Wencel, Leszek Mayer, Maria Wesołowska, Bohumil Sak

We identified *Encephalitozoon cuniculi* genotype II parasites as a cause of extraintestinal microsporidiosis in 2 owners of birds also infected with *E. cuniculi*. Patients experienced long-lasting nonspecific symptoms; the disease course was more progressive in a patient with diabetes. Our findings suggest direct bird-to-human transmission of this pathogen.

Microsporidia of the genus *Encephalitozoon* (*E. cuniculi*, *E. hellem*, and *E. intestinalis*) are intracellular pathogens infecting a wide range of animal species. Because spores can be released to the environment via hosts' feces, urine, and respiratory secretions, they can be ingested or inhaled, posing a risk for zoonotic infection in humans (*1*). The primary site of *Encephalitozoon* spp. infection is the small-intestine epithelium, but dissemination and systemic infections are also well known. Infection of a broad spectrum of cell types has been noted, especially for *E. cuniculi* (*1*); various pathological changes affecting the digestive, urinary, and respiratory tracts and the nervous system may occur. Because encephalitozoons are opportunistic pathogens, the extraintestinal and disseminated infections and severe symptoms they cause are of concern in immunocompromised hosts, such as transplant recipients or persons living with HIV (*2*,*3*). Microsporidiosis develops in patients whose immune response has been weakened by diabetes or malignant disease treated with chemotherapy (*2*,*4*).

Author affiliations: Wroclaw Medical University, Wroclaw, Poland (M. Kicia, Z. Zajączkowska, K. Cebulski, M. Wesołowska); Biology Centre of the Czech Academy of Sciences, České Budějovice, Czech Republic (M. Kváč, N. Holubová, B. Sak); University of South Bohemia, České Budějovice (M. Kváč, N. Holubová); Al Aseefa Falcon Clinic, Dubai, United Arab Emirates (P. Wencel); Medical University of Gdansk, Gdansk, Poland (L. Mayer)

DOI: https://doi.org/10.3201/eid2803.211556

We describe the case of 2 bird owners in Poland who acquired *E. cuniculi*–caused microsporidiosis from their infected pet birds. The Human Research Ethics Committee of Wroclaw Medical University (Wroclaw, Poland) approved this study in accordance with agreement no. KB-549/2012. Patients provided written informed consent before examination.

The Study

The 2 patients, a woman and a man, both 41 years of age, had nonspecific symptoms of fatigue, exhaustion, joint and muscle pain, frequent colds, and headaches, progressive and more severe in the woman. We observed fever reaching 38°C and lasting several months in both patients. Moreover, the woman had intense night palpitations, symptoms similar to bronchitis (occasionally treated with antimicrobial drugs), blurred vision, dizziness, and impaired concentration. She had had bipolar disorder and diabetes for years. Magnetic resonance imaging scans of her head revealed single minor demyelinating or vascular changes in the white matter of the frontal lobes. No information about diabetes treatment was available. No abnormalities were shown in abdominal ultrasound or chest radiograph. She tested seronegative for *Borrelia burgdorferi* and *Chlamydia psittaci* infection. Except for a low leukocyte count (3.00 cells/μL), the woman's basic laboratory tests of blood and urine and her electrocardiograms showed no abnormalities.

Symptoms emerged in the patients after 2 years of breeding exotic birds together. They had 30 birds of various species: budgerigars, canaries, diamond doves, tricolored parrotfinches, Gouldian finches, and diamond firetails. During the 2-year period, 17 birds died from infectious and metabolic diseases, trauma, and management-related issues.

As a part of standard flock management practice, we performed tentative postmortem diagnostic

cytology in 1 tricolored parrotfinch; we suspected disseminated microsporidial infection and conducted a detailed investigation of pooled feces collected from 8 aviaries at the patients' home and tissues from a dead budgerigar. All samples were delivered on ice to the Laboratory of Veterinary and Medical Protistology, Biology Centre of the Czech Academy of Sciences (České Budějovice, Czech Republic). We collected patients' urine and stool specimens every 2 days for 1 week, 3 samples from each, during diagnosis and follow-up and examined them at the Department of Biology and Medical Parasitology, Wroclaw Medical University.

We homogenized all samples by mechanical disruption before genomic DNA extraction as described previously (*5*). We performed nested PCR protocols amplifying a partial sequence of 16S rRNA gene (130 bp), the entire internal transcribed spacer region, and a partial sequence of 5.8S rRNA gene (137–139 bp) of *Encephalitozoon* spp. (*6*). In addition, we checked for the presence of *Enterocytozoon bieneusi* (*7*) and then performed a phylogenetic analysis of PCR products (*5*). We used standard light microscopy methods for spore detection (*8*). We deposited the sequences obtained in this study in GenBank (accession nos. OK356650–60).

We detected microsporidial DNA in the fecal specimens of all birds and in tissue samples from both tested birds. Genotyping revealed the presence of *E. hellem* genotype 1A in all tested specimens from the lung, liver, duodenum, and jejunum with ileum from the budgerigar, whereas *E. cuniculi* genotype II was found in pooled feces and in all sections from the liver, gizzard with proventriculus, and duodenum with jejunum and ileum from the tricolored parrotfinch.

E. cuniculi genotype II was present in 2 of the woman's urine samples and in 1 of the man's urine samples (Figure). Spores were confirmed in all samples. *E. bieneusi* was not found. We administered 400 mg albendazole daily for 10 days to both patients. In follow-up examination 3 months after treatment, the patients' urine repeatedly tested negative for *E. cuniculi* in all independent samplings, and the patients gradually improved. Patients' stools remained negative during the entire diagnostic process. No subsequent follow-up was conducted.

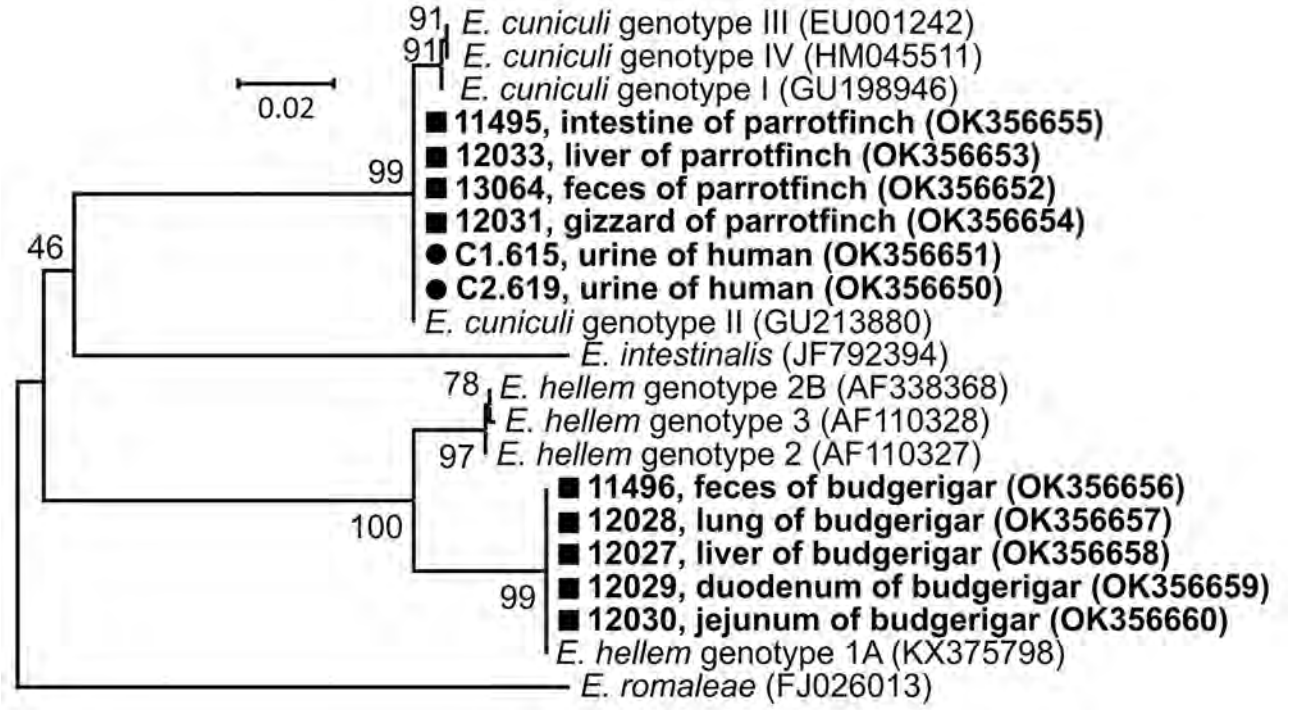

Figure. Phylogenetic relationships of *Encephalitozoon cuniculi* genotype II and *E. hellem* genotype 1A obtained from 2 exotic bird breeders and 2 of their birds compared with other *Encephalitozoon* species and genotypes. Bold type indicates sequences obtained in this study, identified by isolate number (e.g., C1.615); black circles indicate isolates from humans; squares indicate isolates from birds. We analyzed a partial sequence of 16S rRNA gene, the entire internal transcribed spacer region, and a partial sequence of 5.8S rRNA gene inferred by neighbor-joining analyses and computed using the Tamura 3-parameter method. We modeled the rate variation among sites with a gamma distribution. Percentages of replicate trees in which the associated taxa clustered together in the bootstrap test (1,000 replicates) are shown next to the branches. The final dataset contained a total of 220 positions. GenBank accession numbers are in parentheses. Scale bar indicates nucleotide substitutions per site.

Conclusions

Birds are a common source in the propagation of encephalitozoons in the environment (prevalence ≤15%), either acting as mechanical vectors or developing active infection (*9*–*11*). In both wild-living and captive birds, *E. hellem* is the most prevalent *Encephalitozoon* species, whereas *E. cuniculi* has been detected less frequently (*9*,*10*). Whether animal hosts indeed propagate microsporidia or serve as transmission vectors is debatable (*9*). However, the presence of pathogens in both feces and tissues of birds in our study confirms microsporidial proliferation in these animals rather than the passage of spores through the digestive tract; this finding suggests that encephalitozoons may have been circulating in this breeding group for some time. Although most earlier reports demonstrated asymptomatic infections and low infection intensity among birds, intermittent spore shedding in naturally infected birds contaminates the environment (*11*). Owners could be in constant contact with spores, which highly increases the risk for infection by ingestion or inhalation of spores. As a slow-growing pathogen, *E. cuniculi* can lead to chronic infection and microsporidiosis.

In immunocompetent hosts, an immune-controlled balance in the host–parasite relationship is established, and extraintestinal infections remain asymptomatic (*5*). Symptomatic cases of microsporidial infection usually manifest as self-limiting diarrhea (*2*). Symptomatic extraintestinal *Encephalitozoon* infections in immunocompetent humans are uncommon and usually present as keratoconjunctivitis (*2*). Of note, disseminated microsporidiosis caused by *E. cuniculi* genotype I with involvement of brain and urinary and intestinal tracts has been described in men with type 2 diabetes (*4*). However, diabetes is considered a risk factor for opportunistic infections. Experimental infection of diabetic mice with *E. cuniculi* resulted in more symptoms and a higher pathogen burden than in nondiabetic animals (*12*); indeed, the woman with diabetes in our study experienced more severe symptoms, which led to serious impairments in everyday functioning.

Even though we were able to test only urine and feces and confirmed *E. cuniculi* in the urinary tract, the symptoms we observed in our patients were complex, indicating disseminated infection. We cannot be confident in the extent to which *E. cuniculi* infection contributed to these symptoms. However, symptom relief coincided with pathogen clearance after albendazole treatment, which convinced us that microsporidia may have been at least partially involved in symptom development. The severity of symptoms despite the lack of lifelong immunosuppression is puzzling and may arise from high doses of spores acquired as a result of patients' everyday contact with birds.

In summary, our study documents the risk for bird-to-human transmission of *E. cuniculi* parasites. Exotic-bird breeders should be aware of the risk for infection with this opportunistic pathogen.

This work was supported by the Grant Agency of the Czech Republic [grant no. 20-10706S]. The funders had no role in study design, data collection and analysis, decision to publish, or preparation of the manuscript.

About the Author

Dr. Kicia is an associate professor in the Department of Biology and Medical Parasitology, Wroclaw Medical University, Wroclaw, Poland. Her research focuses on opportunistic pathogens, including the microsporidia *Pneumocystis jirovecii* and *Cryptosporidium* spp. in humans and animals.

References

1. Wasson K, Peper RL. Mammalian microsporidiosis. Vet Pathol. 2000;37:113–28. https://doi.org/10.1354/vp.37-2-113
2. Didier ES, Weiss LM. Microsporidiosis: not just in AIDS patients. Curr Opin Infect Dis. 2011;24:490–5. https://doi.org/10.1097/QCO.0b013e32834aa152
3. Kicia M, Szydłowicz M, Cebulski K, Jakuszko K, Piesiak P, Kowal A, et al. Symptomatic respiratory *Encephalitozoon cuniculi* infection in renal transplant recipients. Int J Infect Dis. 2019;79:21–5. https://doi.org/10.1016/j.ijid.2018.10.016
4. Ditrich O, Chrdle A, Sak B, Chmelík V, Kubále J, Dyková I, et al. *Encephalitozoon cuniculi* genotype I as a causative agent of brain abscess in an immunocompetent patient. J Clin Microbiol. 2011;49:2769–71. https://doi.org/10.1128/JCM.00620-11
5. Sak B, Kváč M, Kučerová Z, Květoňová D, Saková K. Latent microsporidial infection in immunocompetent individuals—a longitudinal study. PLoS Negl Trop Dis. 2011;5:e1162. https://doi.org/10.1371/journal.pntd.0001162
6. Katzwinkel-Wladarsch S, Lieb M, Heise W, Löscher T, Rinder H. Direct amplification and species determination of microsporidian DNA from stool specimens. Trop Med Int Health. 1996;1:373–8. https://doi.org/10.1046/j.1365-3156.1996.d01-51.x
7. Buckholt MA, Lee JH, Tzipori S. Prevalence of *Enterocytozoon bieneusi* in swine: an 18-month survey at a slaughterhouse in Massachusetts. Appl Environ Microbiol. 2002;68:2595–9. https://doi.org/10.1128/AEM.68.5.2595-2599.2002
8. Didier ES, Orenstein JM, Aldras A, Bertucci D, Rogers LB, Janney FA. Comparison of three staining methods for detecting microsporidia in fluids. J Clin Microbiol. 1995;33:3138–45. https://doi.org/10.1128/jcm.33.12.3138-3145.1995
9. Pekmezci D, Yetismis G, Esin C, Duzlu O, Colak ZN, Inci A, et al. Occurrence and molecular identification of zoonotic microsporidia in pet budgerigars (*Melopsittacus undulatus*) in Turkey. Med Mycol. 2020;59:85–91. https://doi.org/10.1093/mmy/myaa088
10. Hinney B, Sak B, Joachim A, Kváč M. More than a rabbit's tale—*Encephalitozoon* spp. in wild mammals and

birds. Int J Parasitol Parasites Wildl. 2016;5:76–87. https://doi.org/10.1016/j.ijppaw.2016.01.001
11. Sak B, Kasicková D, Kvác M, Kvetonová D, Ditrich O. Microsporidia in exotic birds: intermittent spore excretion of *Encephalitozoon* spp. in naturally infected budgerigars (*Melopsittacus undulatus*). Vet Parasitol. 2010;168:196–200. https://doi.org/10.1016/j.vetpar.2009.11.012
12. Francisco Neto A, Dell'Armelina Rocha PR, Perez EC, Xavier JG, Peres GB, Spadacci-Morena DD, et al. Diabetes mellitus increases the susceptibility to encephalitozoonosis in mice. PLoS One. 2017;12:e0186954. https://doi.org/10.1371/journal.pone.0186954

Address for correspondence: Marta Kicia, Department of Biology and Medical Parasitology, Wroclaw Medical University, ul. J. Mikulicza-Radeckiego 9, 50-367, Wroclaw, Poland; e-mail: marta.kicia@umw.edu.pl

Epidemiology of COVID-19 after Emergence of SARS-CoV-2 Gamma Variant, Brazilian Amazon, 2020–2021

Vanessa C. Nicolete, Priscila T. Rodrigues, Anderson R.J. Fernandes, Rodrigo M. Corder, Juliana Tonini, Lewis F. Buss, Flávia C. Sales, Nuno R. Faria, Ester C. Sabino, Marcia C. Castro, Marcelo U. Ferreira

The severe acute respiratory syndrome coronavirus 2 (SARS-CoV-2) Gamma variant has been hypothesized to cause more severe illness than previous variants, especially in children. Successive SARS-CoV-2 IgG serosurveys in the Brazilian Amazon showed that age-specific attack rates and proportions of symptomatic SARS-CoV-2 infections were similar before and after Gamma variant emergence.

The novel severe acute respiratory syndrome coronavirus 2 (SARS-CoV-2) Gamma (P.1) variant emerged in November 2020 and drove the second wave of coronavirus disease (COVID-19) in Brazil. Emergence of this variant in Manaus, the largest city in the Brazilian Amazon, was followed by a dramatic upsurge in deaths across the region in early 2021 (*1*,*2*). Gamma harbors amino acid substitutions in the angiotensin-converting enzyme 2 receptor–binding domain of the spike protein, which are thought to enhance host cell infectivity (*3*). This variant may be 1.7–2.4 times more transmissible than previously circulating variant lineages of SARS-CoV-2 (*3*) and can evade antibodies elicited by prior infection or vaccination (*4*,*5*).

During the first COVID-19 epidemic wave, symptoms were half as likely to develop in young children with SARS-CoV-2 infection than in adults >30 years of age, according to an ongoing population-based cohort study in the Brazilian Amazon (*6*). However, patients hospitalized for COVID-19 during the Gamma-dominated second wave in Brazil tended to be younger and more likely to die (*7*), suggesting that Gamma might cause more severe illness, especially in children (*8*). To determine the epidemiology of COVID-19 after emergence of SARS-CoV-2, we compared age-specific COVID-19 attack rates and proportions of symptomatic SARS-CoV-2 infections in the cohort before and after spread of the Gamma variant in the Amazon. The National Committee of Ethics in Research, Ministry of Health of Brazil (CAAE no. 30481820.3.0000.5467), approved the study protocol. Written informed consent was obtained from study participants or their parents/guardians.

The Study

Follow-up of the Mâncio Lima cohort in the Brazilian Amazon (https://www.niaid.nih.gov/research/amazonian-international-center-excellence-malaria-research), which accounts for 20% of the town's 9,000 residents, started in April 2018 (Figure 1; Appendix Methods, https://wwwnc.cdc.gov/EID/article/28/3/21-1993-App1.pdf). The first COVID-19 case in Mâncio Lima was notified on April 29, 2020; as of April 30, 2021, a total of 1,797 laboratory-confirmed infections and 24 deaths were recorded (Figure 2, panel A).

We estimated overall and age-specific SARS-CoV-2 attack rates and the proportion of infections leading to clinically apparent COVID-19 during the first and second epidemic waves in Mâncio Lima. We tested 1,215 cohort participants, <1 to 93 (median 29) years of age, for IgG to the subdomain S1 of the SARS-CoV-2 spike protein (Euroimmun ELISA, EI 2606–9601 G; PerkinElmer, https://www.perkinelmer) during October–November 2020 (*6*) and April–May

Author affiliations: University of São Paulo, São Paulo, Brazil (V.C. Nicolete, P.T. Rodrigues, A.R.J. Fernandes, R.M. Corder, J. Tonini, L.F. Buss, F.C. Sales, N.R. Faria, E.C. Sabino, M.U. Ferreira); Imperial College London, London, UK (N.R. Faria); University of Oxford, Oxford, UK (N.R. Faria); Harvard T.H. Chan School of Public Health, Boston, Massachusetts, USA (M.C. Castro)

DOI: https://doi.org/10.3201/eid2803.211993

2021 (Figure 2, panel A). We obtained information about sociodemographics, COVID-19 exposures, and history of recent illness and vaccination. As a simplifying assumption, we considered seropositive participants in 2020 to not be at risk for reinfection during the second wave, but we attempted to identify instances of antibody boosting, which might represent reinfection. We excluded IgG seroconversions in COVID-19–vaccinated participants because our serologic testing does not distinguish natural infection from vaccination (Figure 1; Appendix).

We collected nasopharyngeal specimens from patients seeking COVID-19 testing in August 2020 and April 2021 to genetically characterize local SARS-CoV-2 isolates (Appendix Methods) with nanopore sequencing on a MinION platform (Oxford Nanopore, https://nanoporetech.com), using the ARTIC V3 protocol (J.R. Tyson et al., unpub. data, https://www.biorxiv.org/content/10.1101/2020.09.04.283077v1). We used Pangolin version 3.1.5 (*9*) to classify SARS-CoV-2 lineages. The 14 isolates from August 2020 (*6*) were assigned to the B.1.1.33 lineage (*10*), and all 11 SARS-CoV-2 isolates from April 2021 were the Gamma variant (Appendix Table 1; GISAID accession nos. EPI_ISL_2987666–74, EPI_ISL_2988699, and EPI_ISL_2988700), which dominated the second wave.

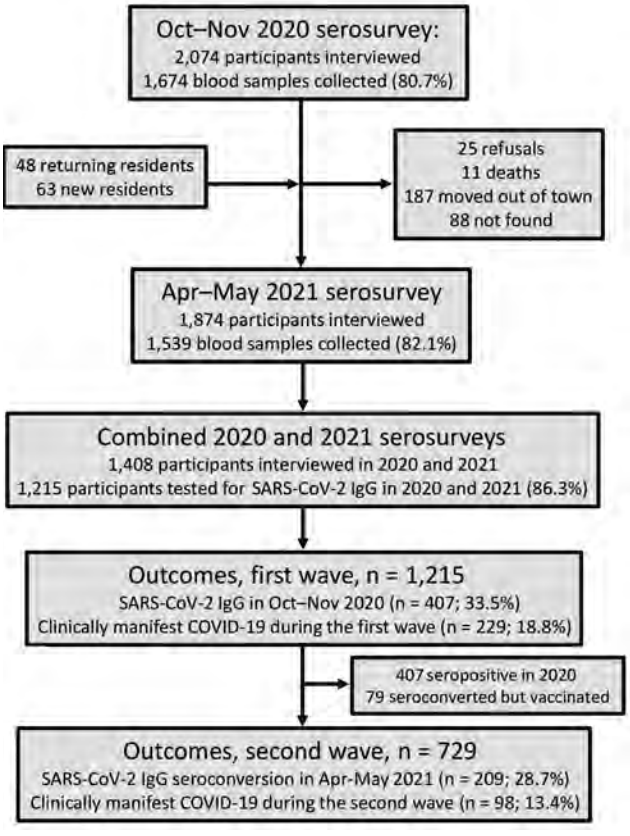

Figure 1. Study of epidemiology of COVID-19 after emergence of SARS-CoV-2 Gamma variant, Brazilian Amazon, 2020–2021. COVID-19, coronavirus disease; SARS-CoV-2, severe acute respiratory syndrome coronavirus 2.

Outcomes were 1) SARS-CoV-2 IgG positivity (2020 survey) or IgG seroconversion in the absence of COVID-19 vaccination (2021 survey), as proxies of SARS-CoV-2 infection, to estimate attack rates during the first and second waves, respectively; and 2) presence of ≥1 sign/symptom—new or increased fever, cough, shortness of breath, chills, muscle pain, loss of taste or smell, sore throat, diarrhea, or vomiting—within the past 6 months (*6*), self-reported by participants with serologic evidence of SARS-CoV-2 infection, as a proxy of clinically apparent COVID-19. We excluded 79 persons vaccinated for COVID-19 who seroconverted (Appendix Results, Figure 2). For each outcome, we used Stata 15.1 (StataCorp LLC, https://www.stata.com) to estimate adjusted relative risks, along with 95% CIs, and used mixed-effects Poisson regression models with random effects at the household level and robust variance (Appendix Methods). Statistical significance was defined at the 5% level.

Most Mâncio Lima residents (54.2%, 95% CI 51.3%–57.1%) demonstrated serologic evidence of SARS-CoV-2 infection at the end of the study (first and second waves combined); sensitivity/specificity-adjusted prevalence (Appendix) was 65.0% (95% highest density interval [95% HDI] 58.5%–73.9%). This finding is consistent with the high COVID-19 attack rates observed in population-based studies in the Amazon (*11*–*13*). One third of study participants (33.5%, 407/1,215) were seropositive at the end of the first wave, and adjusted seroprevalence was 38.9% (95% HDI 33.2%–44.8%). Ten (0.8%) participants reported having been hospitalized between April 2020 and the first survey (blood sampling and questionnaire administration; missing information for 4 study participants), but we did not explicitly ask whether the cause of hospital admission was COVID-19; only 4 of 10 patients who reported hospital admissions (28, 66, 58, and 68 years of age) were seropositive. Among 729 initially seronegative participants, 209 (28.7%) seroconverted (adjusted prevalence 32.7%, 95% HDI 26.7%–38.9%) by the second visit but were not vaccinated (Figure 2, panel B; Appendix Results, Figure 1). We specifically asked for COVID-19–associated hospitalizations, and 7 (0.6%) participants (32, 32, 67, 58, 71, 3, and 81 years of age) reported hospital admissions during the second wave.

Of the 407 participants who were seropositive at the time of the first survey, 60 (14.7%, 95% CI 11.4%–18.6%) became negative (seroreverted) by April–May

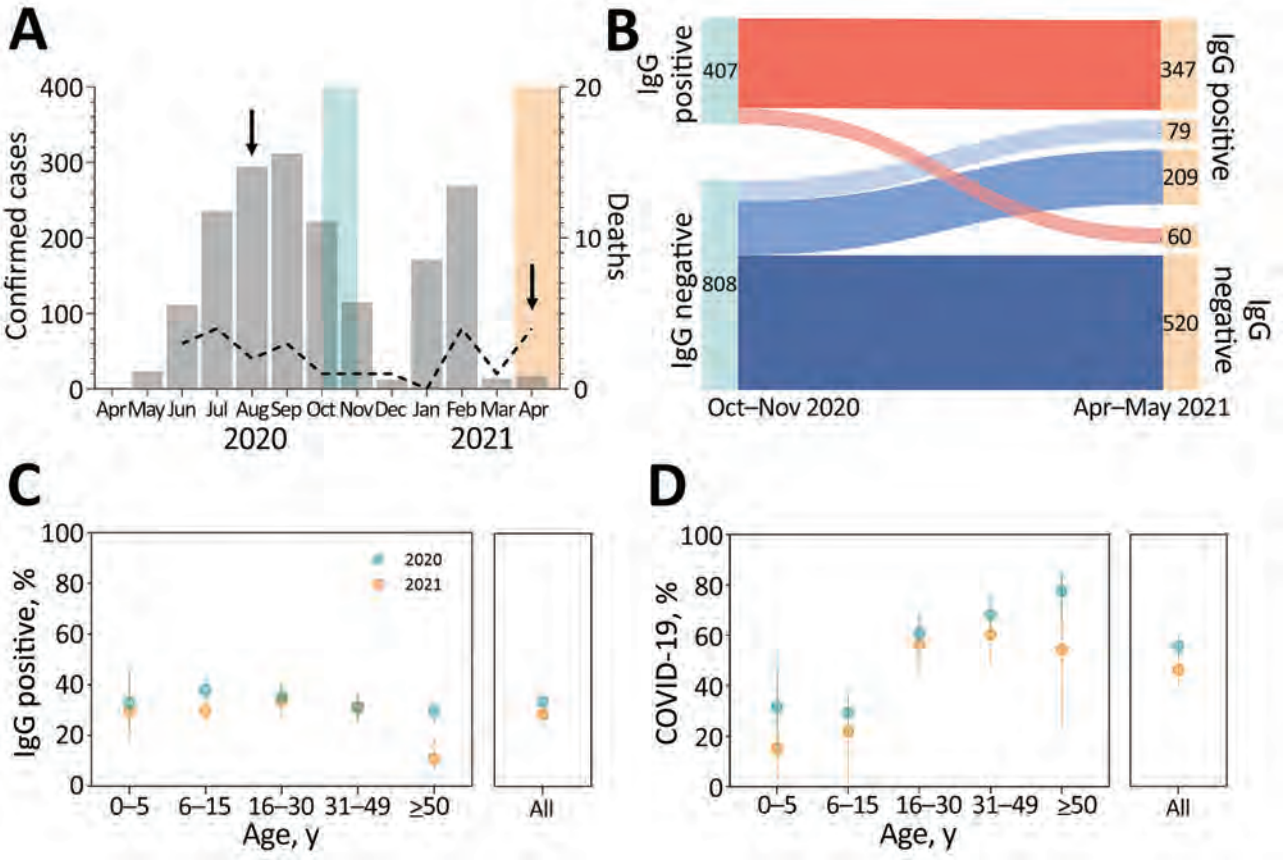

Figure 2. Severe acute respiratory syndrome coronavirus 2 (SARS-CoV-2) infection and clinically apparent coronavirus disease (COVID-19) during the first and second epidemic waves, Brazilian Amazon, 2020–2021. A) Monthly cases (bars) and COVID-19–associated deaths (dashed line) notified in the municipality of Mâncio Lima, Brazil, during April 2020–April 2021. Light blue shading represents serosurveys conducted during October–November 2020; light peach shading represents serosurveys conducted during April–May 2021; arrows indicate dates of SARS-CoV-2 isolate collection for genomic surveillance. B) Distribution of study participants (n = 1,215) according to SARS-CoV-2 IgG detected in each serosurvey. The 288 for whom IgG seroconverted during April–May 2021 includes 79 vaccinated persons (light blue), who were not considered when estimating rates of seroconversion resulting from natural SARS-CoV-2 infection. C) Age-specific percentages of persons positive for SARS-CoV-2 IgG at the end of the first wave (October–November 2020; light blue dots) and of IgG seroconversions among initially seronegative persons by the second wave (April–May 2021; light peach dots). Error bars indicate 95% CIs. D) Age-specific percentages of SARS-CoV-2 infections that led to clinically apparent COVID-19 during the first wave (light blue dots) and second wave (light peach dots). Denominators correspond to the number of participants with serologic evidence of SARS-CoV-2 infection during the period. Error bars indicate 95% CIs.

2021 (Figure 2, panel B). Of the 347 persistently seropositive participants, antibody reactivity index increased by >2-fold for 46 (13.3%) by April–May 2021 (Appendix Figure 3); 18 (5.2%) of the 347 were not vaccinated and therefore may have experienced reinfection during the second wave. Only 4 (22.2%) of the 18 participants with possible reinfection reported clinical manifestations (Appendix Results); the rest were asymptomatic.

At the end of the first and second epidemic waves, antibody positivity and seroconversion rates were similar across age groups, except for adults >50 years of age, among whom there were proportionally fewer infections in the second wave than in the first wave (Figure 2, panel C; Appendix Table 2). A smaller proportion of SARS-CoV-2–infected persons were symptomatic during the second wave (46.9% [95% CI 40.0%–53.9%]) than during the first wave (56.3% [95% CI, 51.3%–61.1%]; p = 0.034 by Yates-corrected χ^2 test) (Figure 2, panel D).

During the second wave, risk for SARS-CoV-2 infection was similar for young children and adults, but risk for symptomatic COVID-19 was lower for children than for adults. Similar trends were observed during the first wave (Appendix Tables 2, 3). After infection, clinical signs/symptoms were significantly less likely to develop in young children than in adults during both epidemic waves (Figure 2, panel D), even after we adjusted for potential confounders by using multiple Poisson regression (Appendix Table 3).

Conclusions

In this Brazilian Amazon cohort, we found no evidence that SARS-CoV-2 infections acquired during the second epidemic wave, dominated by the Gamma variant, produced more symptomatic illness than infections acquired during the first wave. Of note, symptomatic infections did not affect young children disproportionally more during the second wave. The explosive increase in illness and death in the Amazon during the second COVID-19 wave most likely reflects the rapid spread of a highly transmissible variant of concern, the regional and federal government's failure to enforce nonpharmaceutical interventions to curb community transmission of SARS-CoV-2, and limited availability of intensive care beds to cope with severe cases of COVID-19 (*14*).

Acknowledgments

We thank the 1,215 volunteers for participating in this study. We acknowledge Ajucilene (Joice) G. Mota, Francisco Melo, and their team at the Health Secretary of Mâncio Lima for providing overall logistics support and surveillance data and Igor C. Johansen and Bárbara Prado for conducting fieldwork.

This work was supported by the Fundação de Amparo à Pesquisa do Estado de São Paulo (FAPESP), Brazil (grant nos. 2016/18740-9 and 2020/04505-3 to M.U.F.), the US National Institutes of Health (grant no. U19 AI089681, subcontracts to M.U.F. and M.C.C.), and the Medical Research Council-FAPESP CADDE partnership award (grant nos. MR/S0195/1 and 2018/14389-0 to N.R.F. and E.C.S.). FAPESP provided postdoctoral or doctoral scholarships to V.C.N., P.T.R., and F.C.S.; M.U.F. and E.C.S. receive research scholarships from Conselho Nacional de Desenvolvimento Científico e Tecnológico, Brazil. The funders had no role in study design, data collection and interpretation, or the decision to submit the work for publication

About the Author

Dr. Nicolete holds a PhD degree in parasitology and is a |postdoctoral fellow at the Institute of Biomedical Sciences, University of São Paulo, Brazil. Her primary research interests include mechanisms of antibody-mediated immunity against infectious diseases such as malaria and COVID-19.

References

1. Sabino EC, Buss LF, Carvalho MPS, Prete CA Jr, Crispim MAE, Fraiji NA, et al. Resurgence of COVID-19 in Manaus, Brazil, despite high seroprevalence. Lancet. 2021;397:452–5. https://doi.org/10.1016/S0140-6736(21)00183-5
2. Naveca FG, Nascimento V, de Souza VC, Corado AL, Nascimento F, Silva G, et al. COVID-19 in Amazonas, Brazil, was driven by the persistence of endemic lineages and P.1 emergence. Nat Med. 2021;27:1230–8. https://doi.org/10.1038/s41591-021-01378-7
3. Faria NR, Mellan TA, Whittaker C, Claro IM, Candido DDS, Mishra S, et al. Genomics and epidemiology of the P.1 SARS-CoV-2 lineage in Manaus, Brazil. Science. 2021;372:815–21. https://doi.org/10.1126/science.abh2644
4. Souza WM, Amorim MR, Sesti-Costa R, Coimbra LD, Brunetti NS, Toledo-Teixeira DA, et al. Neutralisation of SARS-CoV-2 lineage P.1 by antibodies elicited through natural SARS-CoV-2 infection or vaccination with an inactivated SARS-CoV-2 vaccine: an immunological study. Lancet Microbe. 2021;2:e527–35. https://doi.org/10.1016/S2666-5247(21)00129-4
5. Vignier N, Bérot V, Bonnave N, Peugny S, Ballet M, Jacoud E, et al. Breakthrough infections of SARS-CoV-2 Gamma variant in fully vaccinated gold miners, French Guiana, 2021. Emerg Infect Dis. 2021;27:2673–6. https://doi.org/10.3201/eid2710.211427
6. Nicolete VC, Rodrigues PT, Johansen IC, et al. Interacting epidemics in Amazonian Brazil: prior dengue infection associated with increased COVID-19 risk in a population-based cohort study. Clin Infect Dis. 2021;73:2045–54. https://doi.org/10.1093/cid/ciab410
7. Bastos LS, Ranzani OT, Souza TML, Hamacher S, Bozza FA. COVID-19 hospital admissions: Brazil's first and second waves compared. Lancet Respir Med. 2021;9:e82–3. https://doi.org/10.1016/S2213-2600(21)00287-3
8. Freitas ARR, Beckedorff OA, Cavalcanti LPG, Siqueira AM, Castro DB, Costa CFD, et al. The emergence of novel SARS-CoV-2 variant P.1 in Amazonas (Brazil) was temporally associated with a change in the age and sex profile of COVID-19 mortality: a population based ecological study. Lancet Reg Health Am. 2021;1:100021. https://doi.org/10.1016/j.lana.2021.100021
9. Rambaut A, Holmes EC, O'Toole Á, Hill V, McCrone JT, Ruis C, et al. A dynamic nomenclature proposal for SARS-CoV-2 lineages to assist genomic epidemiology. Nat Microbiol. 2020;5:1403–7. https://doi.org/10.1038/s41564-020-0770-5
10. Resende PC, Delatorre E, Gräf T, Mir D, Motta FC, Appolinario LR, et al. Evolutionary dynamics and dissemination pattern of the SARS-CoV-2 lineage B.1.1.33 during the early pandemic phase in Brazil. Front Microbiol. 2021;11:615280. https://doi.org/10.3389/fmicb.2020.615280
11. Álvarez-Antonio C, Meza-Sánchez G, Calampa C, Casanova W, Carey C, Alava F, et al. Seroprevalence of anti-SARS-CoV-2 antibodies in Iquitos, Peru in July and August, 2020: a population-based study. Lancet Glob Health. 2021;9:e925–31. https://doi.org/10.1016/S2214-109X(21)00173-X
12. Buss LF, Prete CA Jr, Abrahim CMM, Mendrone A Jr, Salomon T, de Almeida-Neto C, et al. Three-quarters attack rate of SARS-CoV-2 in the Brazilian Amazon during a largely unmitigated epidemic. Science. 2021;371:288–92. https://doi.org/10.1126/science.abe9728
13. Lalwani P, Araujo-Castillo RV, Ganoza CA, Salgado BB, Pereira Filho IV, da Silva DSS, et al.; DETECTCoV-19 Study Team. High anti-SARS-CoV-2 antibody seroconversion rates before the second wave in Manaus, Brazil, and the protective effect of social behaviour measures: results from the prospective DETECTCoV-19 cohort. Lancet Glob Health. 2021;9:e1508–16. https://doi.org/10.1016/S2214-109X(21)00355-7
14. Hallal PC, Victora CG. Overcoming Brazil's monumental COVID-19 failure: an urgent call to action. Nat Med. 2021;27:933. https://doi.org/10.1038/s41591-021-01353-2

Address for correspondence: Marcelo U. Ferreira, Institute of Biomedical Sciences, University of São Paulo, Av. Prof. Lineu Prestes 1374, 05508-900 São Paulo, Brazil; email: muferrei@usp.br

Return of Norovirus and Rotavirus Activity in Winter 2020–21 in City with Strict COVID-19 Control Strategy, Hong Kong

Martin Chi-Wai Chan

A rapid decrease in viral gastroenteritis during winter 2019–20 and a return of norovirus and rotavirus activity during winter 2020–21 were observed while multiple nonpharmaceutical interventions for coronavirus disease were in effect in Hong Kong. The initial collateral benefit of coronavirus disease countermeasures that reduced the viral gastroenteritis burden is not sustainable.

The unfolding novel coronavirus disease (COVID-19) pandemic is an unprecedented public health crisis in the modern history of humankind. One collateral consequence of this pandemic is the concomitant rapid decrease in the incidence of viral gastroenteritis in the first year of the pandemic, as observed in many countries, such as China (*1*), the United States (*2*), England (*3*), Germany (*4*), Japan (*5*), and Australia (*6*). The most likely explanations were reduced testing capacity that led to underreporting and wide implementation of nonspecific nonpharmaceutical interventions for COVID-19, such as frequent handwashing and physical distancing, that reduced human-to-human transmission of different viruses.

Hong Kong is a metropolitan city in southern China and has been continuously implementing stringent and effective elimination (also known as zero COVID-19) strategy to suppress importation and local spread of COVID-19 since the start of the pandemic. Local routine laboratory syndromic surveillance for viral gastroenteritis remained largely unaffected during the pandemic, and testing capacity for common diarrheagenic viruses was only mildly reduced, providing a well-controlled setting to study the epidemiology of viral gastroenteritis in the COVID-19 era. This report compares the activity of norovirus and rotavirus in winters 2019–20 and 2020–21 in Hong Kong while stringent social distancing and continual zero COVID-19 control strategy were in effect in the city.

Author affiliations: Independent research scientist, Hong Kong, China.

DOI: https://doi.org/10.3201/eid2803.212117

The Study

Local territorywide monthly laboratory data on PCR-based detection of norovirus and rotavirus, the 2 leading causes of viral gastroenteritis (*7*), are publicly available since January 2013 from the Centre for Health Protection of Hong Kong (equivalent in function to other national public health agencies, such as the China Centers for Disease Control and Prevention) (*8*). Laboratory data for less common diarrheagenic viruses, including sapovirus, astrovirus, and enteric adenovirus, were available from May 2017 onward. During January 2013–September 2021, a total of 104,187 stool specimens collected from sporadic and outbreak case-patients who had acute gastroenteritis were tested (Figure, panel B). The median number of specimens tested each month was 1,008 (interquartile range [IQR] 912–1,114) before the COVID-19 pandemic and 872 (IQR 784–990) during the COVID-19 pandemic. Although an average of 13.5% fewer stool specimens were tested during the pandemic ($p<0.01$ by Mann-Whitney U test), the reduced sample sizes were still of sufficient power to detect ≥1 positive specimen under a virus prevalence as low as 0.5% (namely 1 in 200) at a 95% confidence level.

Monthly positive rates of the 5 common viral causes of acute gastroenteritis are provided (Figure, panel A). During winter 2019–20, the positive rate of rotavirus decreased abruptly from the peak by 70% during February 2020, shortly after the initial global spread of COVID-19, and remained at a much lower level of 0.1%–0.6% through September 2020,

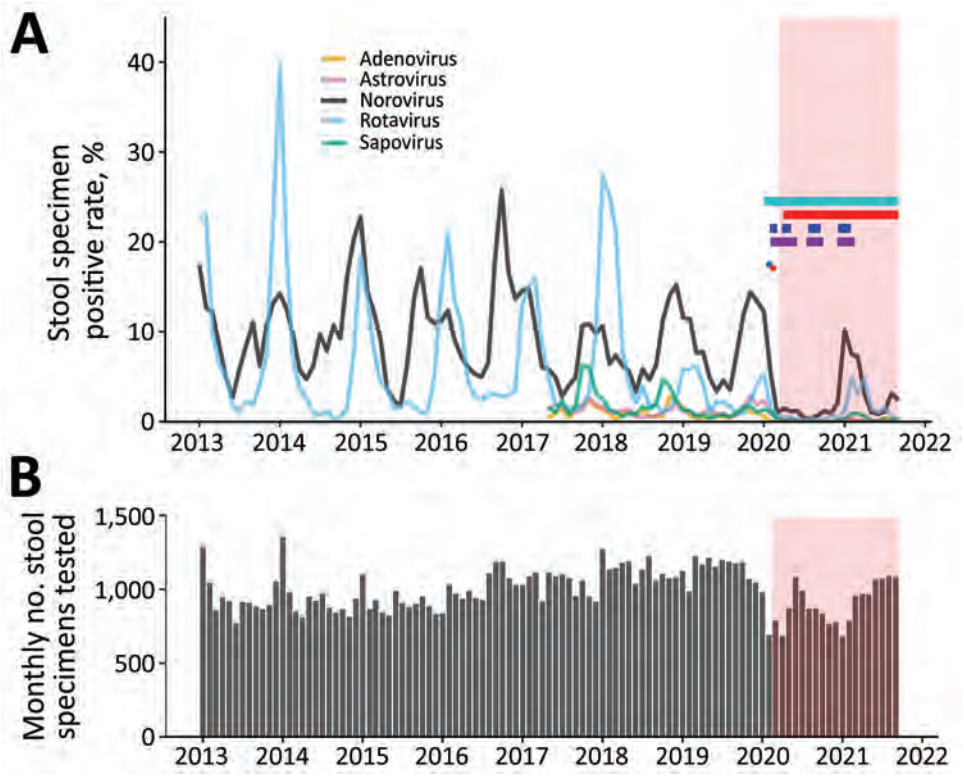

Figure. Positive rates for 5 common viral causes of acute gastroenteritis in stool specimens and total number of specimens tested from routine, territorywide, PCR-based laboratory syndromic surveillance data, Hong Kong, China, January 2013–September 2021. A) Monthly positive rates. Data for sapovirus, astrovirus, and enteric adenovirus were available for May 2017 onwards. The first imported COVID-19 case (blue dot) was reported on January 23, 2020, and the first locally acquired case (red dot) was reported on February 4, 2020. COVID-19 was declared pandemic by the World Health Organization on March 11, 2020. Colored horizontal bars indicate the periods of major nonpharmaceutical interventions for COVID-19 in the city, including universal mask-wearing outside homes (aqua), prohibition on group gatherings of >4 persons in public places (red), work-from-home arrangement for civil servants (blue), and school dismissal (purple). Pink indicates time of the COVID-19 pandemic. B) Monthly number of stool specimens tested. COVID-19, coronavirus disease.

compared with a median of 5.4% (IQR 2.8%–13.4%) during the same period in the previous 7 years. The winter 2019–20 rotavirus season ended ≈2 months earlier than usual.

The observed lower positive rate might be confounded by the decreasing trend in recent years with the availability of 2 rotavirus vaccines: RotaTeq (Merck and Co. Inc., https://www.merck.com) and Rotarix (GlaxoSmithKline, https://www.gsk.com), both licensed for use since 2006 in private clinics, but not yet included in the local childhood immunization program. Therefore, I examined data further for cases of norovirus, for which no effective antiviral drugs or vaccines are available. Likewise, norovirus positive rates decreased sharply from the peak by 56% during February 2020 and remained at a much lower level of 0.3%–1.5% through September 2020, compared with a median of 6.4% (IQR 5.2%–10.0%) during the same period in the previous 7 years. The winter 2019–20 season for norovirus ended almost 3 months earlier than usual.

I also reviewed data for sapovirus, astrovirus, and enteric adenovirus. These viruses became hardly detectable at the start of the COVID-19 pandemic, showing a positive rate of persistently <1% throughout 2020 and 2021.

In winter 2020–21, a typical seasonal peak of norovirus that had a positive rate of 10.3% was observed in January 2021, a rate comparable with the median of 14.4% during the previous 7 winter seasons. Likewise, a typical seasonal peak of rotavirus with a positive rate of 4.8% was observed in February 2021, highly comparable with the rates of 5.3% and 6.2% in the previous 2 winter seasons, albeit on a progressively decreasing trend in recent years. These data indicated active circulation of norovirus and rotavirus in the community during winter 2020–21 while strict nonpharmaceutical interventions for COVID-19 were in effect in the city, including work-from-home arrangement for civil servants, universal mask-wearing outside homes, school dismissal, and prohibition on group gatherings of >4 persons in public places (Figure, panel A).

Conclusions

An abrupt decrease in activities of multiple diarrheagenic viruses, in particular norovirus and rotavirus, and shortening of their seasons was observed soon

after the initial global spread of COVID-19 during early 2020. Hong Kong has adopted a multipronged elimination strategy to contain COVID-19 since the first imported case in late January 2020 (*9*) and maintained one of the world's lowest severe acute respiratory syndrome coronavirus 2 infection rates so far (<0.2% of the local population). If one considers that viral gastroenteritis was primarily transmitted through person-to-person contact, nonpharmaceutical interventions for COVID-19, such as social distancing, might have inadvertently stopped the spread of nonrespiratory pathogens.

Universal mask-wearing might have also reduced the transmission risk for norovirus, which can reportedly spread by the airborne route (*10*) and vomiting (*11*). The dramatic reduction in virus-positive rates to barely detectable levels in winter 2019–20 is not likely to be an artifact of underreporting because the corresponding number of stool specimens tested was only moderately reduced. Although the return of viral gastroenteritis is anticipated in countries implementing mitigation strategy accompanied with relaxation of infection control measures, the seasonal activities of norovirus and rotavirus observed in winter 2020–21 in Hong Kong were to some extent unexpected because major nonpharmaceutical interventions were still in force during that period, as in winter 2019–20. This finding is unlikely to be explained by pandemic fatigue because local seasonal influenza activity remained at an unprecedented virtually zero level during winter 2020–21 (*12*). Other factors, such as waning immunity and thus accumulation of susceptible population, might come to play.

This study is limited by the lack of virus characterization to determine whether the increase in viral gastroenteritis was a result of emergence of new strains, especially for norovirus, in which new immune-escaped strains emerged periodically (*13*). There were no reports of new and rapidly spreading norovirus variants detected during the COVID-19 pandemic. Additional analysis on the route of transmission of cases would be helpful because public health interventions for COVID-19 might be less effective for diarrheagenic viruses that can spread by foodborne or waterborne routes.

In conclusion, control measures for COVID-19 may have inadvertently reduced the activities of multiple diarrheagenic viruses to barely detectable levels in winter 2019–20. However, norovirus and rotavirus activity returned in winter 2020–21 to levels similar to that in the pre–COVID-19 period. The initial collateral benefit of nonpharmaceutical interventions for COVID-19 that reduced the burden of viral gastroenteritis is not sustainable even in a city with stringent social distancing and continual zero COVID-19 control strategy.

About the Author

Dr. Chan is an independent research scientist in Hong Kong, China. He was previously a senior scientific reviewer at the Research Office of the Food and Health Bureau of Hong Kong and an assistant professor in the Department of Microbiology and Stanley Ho Centre for Emerging Infectious Diseases of the Chinese University of Hong Kong. His primary research interests are molecular epidemiology and pathogenesis of intestinal and respiratory viral infections, especially those caused by noroviruses and influenza viruses.

References

1. Wang LP, Han JY, Zhou SX, Yu LJ, Lu QB, Zhang XA, et al.; Chinese Centers for Disease Control and Prevention (CDC) Etiology of Diarrhea Surveillance Study Team. The changing pattern of enteric pathogen infections in China during the COVID-19 pandemic: a nation-wide observational study. Lancet Reg Health West Pac. 2021;16:100268. https://doi.org/10.1016/j.lanwpc.2021.100268
2. Kraay AN, Han P, Kambhampati AK, Wikswo ME, Mirza SA, Lopman BA. Impact of nonpharmaceutical interventions for severe acute respiratory syndrome coronavirus 2 on norovirus outbreaks: an analysis of outbreaks reported by 9 US States. J Infect Dis. 2021;224:9–13. https://doi.org/10.1093/infdis/jiab093
3. Ondrikova N, Clough HE, Douglas A, Iturriza-Gomara M, Larkin L, Vivancos R, et al. Differential impact of the COVID-19 pandemic on laboratory reporting of norovirus and *Campylobacter* in England: A modelling approach. PLoS One. 2021;16:e0256638. https://doi.org/10.1371/journal.pone.0256638
4. Eigner U, Verstraeten T, Weil J. Decrease in norovirus infections in Germany following COVID-19 containment measures. J Infect. 2021;82:276–316. https://doi.org/10.1016/j.jinf.2021.02.012
5. Fukuda Y, Tsugawa T, Nagaoka Y, Ishii A, Nawa T, Togashi A, et al. Surveillance in hospitalized children with infectious diseases in Japan: pre- and post-coronavirus disease 2019. J Infect Chemother. 2021;27:1639–47. https://doi.org/10.1016/j.jiac.2021.07.024
6. Bruggink LD, Garcia-Clapes A, Tran T, Druce JD, Thorley BR. Decreased incidence of enterovirus and norovirus infections during the COVID-19 pandemic, Victoria, Australia, 2020. Commun Dis Intell (2018). 2021;45:45. https://doi.org/10.33321/cdi.2021.45.5
7. Bányai K, Estes MK, Martella V, Parashar UD. Viral gastroenteritis. Lancet. 2018;392:175–86. https://doi.org/10.1016/S0140-6736(18)31128-0
8. Centre for Health Protection. Detection of gastroenteritis viruses from faecal specimens [cited 2022 Jan 12]. https://www.chp.gov.hk/en/statistics/data/10/641/717/3957.html
9. Lam HY, Lam TS, Wong CH, Lam WH, Leung CM, Au KW, et al. The epidemiology of COVID-19 cases and the successful containment strategy in Hong Kong, January to

May 2020. Int J Infect Dis. 2020;98:51–8. https://doi.org/10.1016/j.ijid.2020.06.057
10. Bonifait L, Charlebois R, Vimont A, Turgeon N, Veillette M, Longtin Y, et al. Detection and quantification of airborne norovirus during outbreaks in healthcare facilities. Clin Infect Dis. 2015;61:299–304. https://doi.org/10.1093/cid/civ321
11. Kirby AE, Streby A, Moe CL. Vomiting as a symptom and transmission risk in norovirus illness: evidence from human challenge studies. PLoS One. 2016;11:e0143759. https://doi.org/10.1371/journal.pone.0143759
12. Centre for Health Protection. Detection of pathogens from respiratory specimens [cited 2022 Jan 12]. https://www.chp.gov.hk/en/statistics/data/10/641/642/2274.html
13. Parra GI. Emergence of norovirus strains: A tale of two genes. Virus Evol. 2019;5:vez048. https://doi.org/10.1093/ve/vez048

Address for correspondence: Martin Chi-Wai Chan, Hong Kong, China; email: martin.chan@link.cuhk.edu.hk

Relationship of SARS-CoV-2 Antigen and Reverse Transcription PCR Positivity for Viral Cultures

Dustin W. Currie, Melisa M. Shah, Phillip P. Salvatore, Laura Ford, Melissa J. Whaley, Jennifer Meece, Lynn Ivacic, Natalie J. Thornburg, Azaibi Tamin, Jennifer L. Harcourt, Jennifer Folster, Magdalena Medrzycki, Shilpi Jain, Phili Wong, Kimberly Goffard, Douglas Gieryn, Juliana Kahrs, Kimberly Langolf, Tara Zochert, Christopher H. Hsu, Hannah L. Kirking, Jacqueline E. Tate, for the CDC COVID-19 Response Epidemiology Field Studies Team[1]

We assessed the relationship between antigen and reverse transcription PCR (RT-PCR) test positivity and successful virus isolation.We found that antigen test results were more predictive of virus recovery than RT-PCR results. However, virus was isolated from some antigen-negative and RT-PCR–positive paired specimens, providing support for the Centers for Disease Control and Prevention antigen testing algorithm.

Antigen platforms for severe acute respiratory syndrome coronavirus 2 (SARS-CoV-2) diagnostic testing have rapid turnaround time, are easy to use, and are less expensive than real-time reverse transcription PCR (RT-PCR) diagnostic testing. Using RT-PCR as the reference test, performance evaluations of the Abbott BinaxNOW COVID-19 Antigen Card Test (https://www.abbott.com) reported a high specificity (>98%) (*1*–*4*) but lower sensitivity, ranging from 64.2% to 89.0% for symptomatic persons (*2*–*4*) and 35.8% to 70.2% for asymptomatic persons (*2*,*3*). However, other studies have demonstrated a period of prolonged positivity for RT-PCR testing beyond which virus has been isolated (*5*,*6*). Therefore, a comprehensive examination of antigen test performance characteristics in identifying infectious persons who have SARS-CoV-2 infections requires comparison with multiple data points, including RT-PCR test positivity and the ability to isolate the virus (a marker for infectiousness) (*5*–*7*). In this study, we expand on a previous report (*1*) that examined performance of antigen testing relative to RT-PCR by reporting virus isolation data for persons who had positive results by antigen test or RT-PCR.

The Study

The study population and testing methods have been described (*1*). Persons were recruited at a free, appointment-based, community antigen testing site in Winnebago County, Wisconsin, USA. Approximately 30 minutes after providing an initial nasal swab specimen for antigen testing, 2 additional self-collected specimens were collected under Centers of Disease Control and Prevention (CDC) staff supervision from the anterior nares simultaneously in an alternating fashion to maximize uniformity.

Of 2 simultaneous swab specimens, we used 1 specimen for rapid antigen testing by the Abbott BinaxNOW SARS-CoV-2 Antigen Card Test, a point-of-care lateral flow test with results available within 15 minutes of specimen collection. We placed the other specimen in viral transport medium and transported it on ice to the Marshfield Clinical Research Institute laboratory (Marshfield, Wisconsin, USA) for RT-PCR testing. Specimens with a cycle threshold (C_t) value ≤37 for at least 2 of 3 SARS-CoV-2 gene targets (open reading frame 1ab, spike gene, and nucleocapsid gene) were considered positive, according to the instructions of the manufacturer (TaqPath COVID-19 Combo Kit; Thermo Fisher Scientific, https://www.thermofisher.com).

Author affiliations: Centers for Disease Control and Prevention, Atlanta, Georgia, USA (D.W. Currie, M.M. Shah, P.P. Salvatore, L. Ford, M.J. Whaley, N.J. Thornburg, A. Tamin, J.L. Harcourt, J. Folster, M. Medrzycki, S. Jain, P. Wong, C.H. Hsu, H.L. Kirking, J.E. Tate); Marshfield Clinic Research Institute, Marshfield, Wisconsin, USA (J. Meece, L. Ivacic); Winnebago County Health Department, Oshkosh, Wisconsin, USA (K. Goffard, D. Gieryn); University of Wisconsin–Oshkosh, Oshkosh (J. Kahrs, K. Langolf, T. Zochert)

DOI: https://doi.org/10.3201/eid2803.211747

[1]Members of CDC COVID-19 Response Epidemiology Field Studies Team who collected data are listed at the end of this article.

We attempted viral culture at a CDC laboratory for all participants testing positive by RT-PCR or antigen test by using Vero-CCL81 cells, which were inoculated with clinical specimens, and observed daily for 7 days (*8*). All cultures that had a visible cytopathic effect were used for RNA extraction and SARS-CoV-2 RT-PCR confirmation. Any specimen that showed a cytopathic effect, was positive by RT-PCR, and had a $C_t \geq 2$ lower than that for the original clinical specimen was considered culture positive.

We collected symptoms at time of specimen collection, symptom onset date, and exposure history by using paper questionnaires and entered data into REDCap database version 11.0.3 (https://www.vumc.org/dbmi/redcap). Participants reporting ≥1 of 15 symptoms at the time of specimen collection were considered symptomatic. Possible symptoms were fever, rigors, nasal congestion, sore throat, shortness of breath, headache, diarrhea, loss of taste, loss of smell, chills, muscle aches, fatigue, cough, nausea, and abdominal pain.

We define known exposure as being within 6 feet of a person who tested positive for SARS-CoV-2 within the last 14 days for ≥15 minutes over a 24-hour period. We analyzed data by using SAS version 9.4 (https://www.sas.com). We made comparisons by using Kruskal–Wallis tests for continuous variables or χ^2 tests for categorical variables; statistical significance was defined as $\alpha<0.05$. This analysis was reviewed by CDC and was conducted consistent with applicable federal law and CDC policy.

During November 16–December 15, 2020, we collected 2,112 specimen pairs that had valid results for PCR and antigen tests; most (56.3%) participants were symptomatic (age range 5–95 years, median 42 years). Of 2,112 specimen pairs, 334 (15.8%) were positive by RT-PCR, 269 (12.7%) were positive by antigen test, and 200 (9.5%) had recoverable virus (culture positive). Of the 200 culture positive specimen pairs that had a positive RT-PCR result, 191 (95.5%) had a positive antigen test result. Positive predictive value (PPV) of antigen test for culture positivity (191/269, 71.0%) (Table 1) was higher than PPV for RT-PCR (200/334, 59.9%). Virus was successfully isolated from 191 (71.5%) of 267 specimen pairs with concordant positive antigen/RT-PCR results, 9 (13.4%) of 67 specimen pairs with positive RT-PCR and negative antigen test results, and 0 of 2 specimen pairs with positive antigen and negative RT-PCR test results.

All participants who had culture-positive specimens and false-negative antigen tests were symptomatic (7/9; 77.8%) or had a known exposure in the past 14 days (5/9; 55.6%). Among culture-positive symptomatic participants, those who had false-negative antigen and concordant positive antigen/RT-PCR results were tested a similar number of days after symptom onset (median 2 days vs. 3 days) (Table 2). The 2 persons who had recoverable virus and false-negative antigen test results and who were asymptomatic at the time of testing had known exposures the day before testing. For those who had recoverable virus, nucleocapsid gene C_t values were significantly lower in those with concordant positive results (median 19.1, interquartile range 17.1–21.3) than those who had false-negative antigen test results (median 26.6, interquartile range 25.6–31.0) ($p<0.0001$) (Table 2; Figure).

Conclusions

Consistent with previous studies assessing the relationship between antigen tests, RT-PCR, and ability to culture virus (*9*–*11*), we found that SARS-CoV-2 was more likely to be recovered among specimen pairs for which antigen test and RT-PCR results were positive than among pairs in which antigen test results were negative and RT-PCR results were positive. Although some studies have shown similar PPV for viral culture when comparing RT-PCR and antigen tests (*12*), we found higher PPV for the antigen test than for RT-PCR (*13*), suggesting that antigen test positivity might be a better marker of infectiousness than a positive RT-PCR result. However, a small but nontrivial proportion of samples that had negative antigen and positive RT-PCR results had recoverable virus, suggesting that antigen tests are misclassifying some infectious persons as SARS-CoV-2 negative. This finding, consistent with those of similar studies (*6*–*11*), suggests that lower sensitivity of antigen tests when compared with RT-PCR cannot be attributed exclusively to lingering positive RT-PCR results for persons who are no longer infectious.

Symptoms on the day of testing for most infectious persons who had false-negative antigen test results suggests that CDC's current antigen testing guidance, which recommends confirmatory RT-PCR testing after negative antigen test results for symptomatic persons in community settings (*14*), is appropriate. Both asymptomatic

Table 1. Positive predictive value of the BinaxNOW COVID-19 Antigen Card Test and RT-PCR relative to viral culture, Winnebago County, Wisconsin, USA, November–December 2020*

SARS-CoV-2 diagnostic test result	No. culture positive	No. culture negative	Total	Positive predictive value, %
BinaxNOW positive	191	78	269	71.0
RT-PCR positive	200	134	334	59.9

*BinaxNOW, https://www.abbott.com. RT-PCR, reverse transcription PCR; SARS-CoV-2, severe acute respiratory syndrome coronavirus 2.

Table 2: Symptoms and exposure history of persons testing positive for SARS-CoV-2, stratified by ability to culture virus and RT-PCR/antigen test concordance, Winnebago County, Wisconsin, USA, November-December 2020*

Characteristic	Culture positive			Culture negative		
	RT-PCR+/ antigen–, n = 9	RT-PCR+/ antigen+, n = 191	All, n = 200	RT-PCR+/ antigen–, n = 58	RT-PCR+/ antigen+, n = 76	All, n = 134†
Symptomatic						
Current symptoms	7 (77.8)	165 (88.2)	172 (87.8)	43 (73.7)	67 (88.2)	109 (82.0)
No current symptoms	2 (22.2)	22 (11.8)	24 (12.2)	15 (26.3)	9 (11.8)	24 (18.0)
Unknown/missing	0	4	4	1		1
Meets CSTE clinical criteria‡						
Yes	7 (77.8)	142 (74.3)	149 (74.5)	36 (62.1)	60 (78.9)	96 (71.6)
No	2 (22.2)	49 (25.7)	51 (25.5)	22 (37.9)	16 (21.1)	38 (28.4)
Days from symptom onset to specimen collection, median (IQR)	2 (1–6 d)	3 (1–4)	3 (1–5)	3 (1–10)	4 (2–7)	4 (2–7)
Known exposure in previous 14 d						
Yes	5 (55.6)	111 (58.7)	116 (58.6)	34 (59.7	39 (52.0)	73 (55.3)
No	1 (11.1)	42 (22.2)	43 (21.7)	19 (33.3)	22 (29.3)	41 (31.1)
Unknown	3 (33.3)	36 (19.1)	39 (19.7)	4 (7.0)	14 (18.7)	18 (13.6
Missing	0	2	2	1	1	2
Days since last known exposure, median (IQR)	2 (0.5–4)	4 (0–6)	4 (0–6)	2 (0–4 d)	3 (0–7)	2 (0–6)
N gene C_t value, median (IQR)	26.6 (25.6–31.0)	19.1 (17.1–21.3)	19.2 (17.2–21.7)	30.9 (29.3–33.4)	24.3 (21.1–27.7)	27.9 (23.8–30.9)

*Values are no. (%) except as indicated. CSTE, Council of State and Territorial Epidemiologists; C_t, cycle threshold; IQR, interquartile range; N, nucleocapsid; RT-PCR, reverse transcription PCR; SARS-CoV-2, severe acute respiratory syndrome coronavirus 2; +, positive; –, negative.
†All specimen pairs included tested positive by RT-PCR; the 2 participants who had false-positive antigen test results, both of whom were culture negative, were excluded.
‡CSTE clinical criteria are met if the case-patient has either cough, shortness of breath, loss of taste, or loss of smell, or ≥2 of the following symptoms: fever, chills, myalgia, headache, or sore throat.

participants who had false-negative antigen test results and recoverable virus had exposures within the previous 48 hours. Therefore, all participants who had false-negative antigen test results were unlikely to infect others if following CDC guidance because they would have been advised to quarantine because of exposure (asymptomatic close contacts) or while awaiting confirmatory RT-PCR results (symptomatic persons).

One limitation of this study was that although recoverable virus is indicative of infectiousness, lack of ability to isolate virus does not necessarily imply lack of infectiousness (*15*). Symptom status was only measured at the time of testing. Because we did not attempt virus isolation on antigen-negative and RT-PCR–negative specimens, PPV was the only reported measure of agreement between antigen test, RT-PCR, and recoverable virus in culture. Because RT-PCR testing was not performed with calibrators, we are not able to report values in copies/milliliter. Finally, this investigation assessed only the BinaxNOW antigen testing platform.

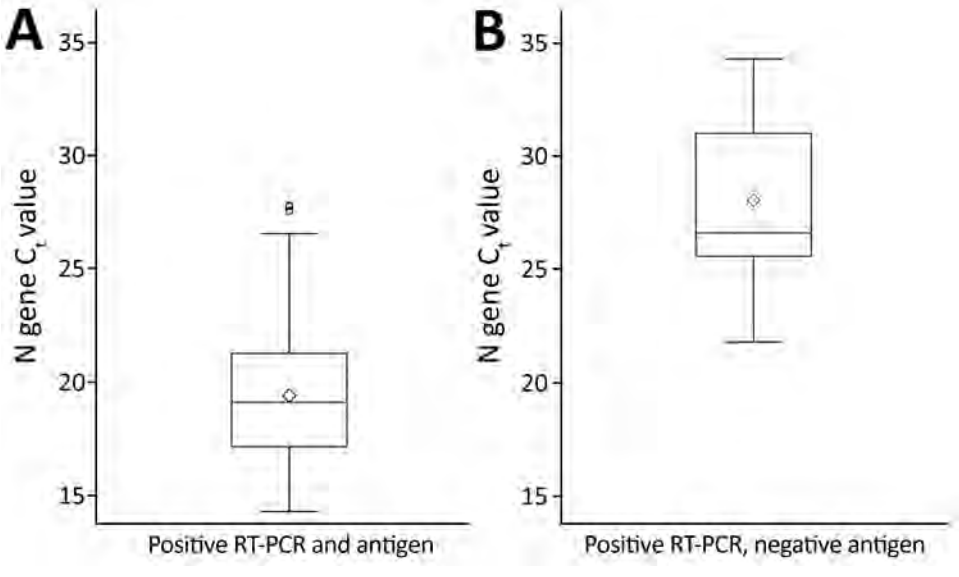

Figure. Box plots of Ct values among participants with recoverable virus who had concordant positive SARS-CoV-2 RT-PCR and antigen test results (A) compared with those who had positive RT-PCR and negative antigen test results (B), Winnebago County, Wisconsin, USA, November–December 2020. The difference between the 2 groups was significant (p<0.0001). Diamonds indicate means, boxes indicate the first quartile through the third quartile, horizontal bars in boxes indicate medians, and errors bars indicate minimum values to maximum values; outliers are plotted as individual circles. Ct, cycle threshold; RT-PCR, reverse transcription PCR; SARS-CoV-2, severe acute respiratory syndrome coronavirus 2.

This study suggests that antigen test positivity is more predictive of infectiousness than RT-PCR test positivity. However, false-negative antigen test results can be obtained for infectious persons, especially among those with symptoms, supporting CDC recommendations to follow negative antigen testing among symptomatic persons with RT-PCR confirmatory testing within 48 hours (*14*).

Members of the CDC COVID-19 Response Epidemiology Field Studies Team: Fatima Abdirizak (CDC), John Paul Bigouette (CDC), Lauren Boyle-Estheimer (CDC), Juliana DaSilva (CDC), Augustina Delaney (CDC), Emiko Kamitani (CDC), Shirley Lecher (CDC), Kaitlin Mitchell (CDC), Clint N. Morgan (CDC), Michelle O'Hegarty (CDC), Hannah E. Segaloff (CDC, Wisconsin Department of Health Services), Tarah Somers (*Agency for Toxic Substances and Disease Registry),* and Miriam E. Van Dyke (CDC).

Acknowledgments

We thank the participants in Wisconsin for contributing to this investigation, and the US Department of Health and Human Services community-based testing program for making this investigation possible.

About the Author

Dr. Currie is an Epidemic Intelligence Service Officer in the Division of Global HIV and Tuberculosis, Center for Global Health, Centers for Disease Control and Prevention, Atlanta, GA. His research interests include general population HIV surveillance, COVID-19 outbreak investigation, testing strategies for SARS-CoV-2 infection, and the relationship between behavioral science and communicable diseases.

References

1. Shah MM, Salvatore PP, Ford L, Kamitani E, Whaley MJ, Mitchell K, et al. Performance of repeat BinaxNOW SARS-CoV-2 antigen testing in a community setting, Wisconsin, November–December 2020. Clin Infect Dis. 2021;73(Suppl 1):S54–7. https://doi.org/10.1093/cid/ciab309
2. Prince-Guerra JL, Almendares O, Nolen LD, Gunn JKL, Dale AP, Buono SA, et al. Evaluation of Abbott BinaxNOW rapid antigen test for SARS-CoV-2 infection at two community-based testing sites—Pima County, Arizona, November 3–17, 2020. MMWR Morb Mortal Wkly Rep. 2021;70:100–5. https://doi.org/10.15585/mmwr.mm7003e3
3. Pollock NR, Jacobs JR, Tran K, Cranston AE, Smith S, O'Kane CY, et al. Performance and implementation evaluation of the Abbott BinaxNOW rapid antigen test in a high throughput drive-through community testing site in Massachusetts. J Clin Microbiol. 2021;59:e00083–21. https://doi.org/10.1128/JCM.00083-21
4. Pilarowski G, Marquez C, Rubio L, Peng J, Martinez J, Black D, et al. Field performance and public health response using the BinaxNOW™ rapid SARS-CoV-2 antigen detection assay during community-based testing. Clin Infect Dis. 2021; 73:e3098–1. https://doi.org/10.1093/cid/ciaa1890
5. Jefferson T, Spencer EA, Brassey J, Heneghan C. Viral cultures for COVID-19 infectious potential assessment: a systematic review. Clin Infect Dis. 2020 Dec 3 [Epub ahead of print]. https://doi.org/10.1093/cid/ciaa1764 PMID: 33270107
6. Doshi P, Powers JH. Determining the infectious potential of individuals with positive reverse transcription polymerase chain reaction severe acute respiratory syndrome 2 tests. Clin Infect Dis. 2020 Dec 4 [Epub ahead of print]. https://doi.org/10.1093/cid/ciaa1819 PMID: 33277652
7. Steinlin-Schopfer J, Barbani MT, Kamgang R, Zwahlen M, Suter-Riniker F, Dijkman R. Evaluation of the Roche antigen rapid test and a cell culture-based assay compared to rRT-PCR for the detection of SARS-CoV-2: a contribution to the discussion about SARS-CoV-2 diagnostic tests and contagiousness. J Clin Virol Plus. 2021;1:100020. https://doi.org/10.1016/j.jcvp.2021.100020
8. Harcourt J, Tamin A, Lu X, Kamili S, Sakthivel SK, Murray J, et al. Severe acute respiratory syndrome coronavirus 2 from patient with coronavirus disease, United States. Emerg Infect Dis. 2020;26:1266–73. https://doi.org/10.3201/eid2606.200516
9. Strömer A, Rose R, Schäfer M, Schön F, Vollersen A, Lorentz T, et al. Performance of a point-of-care test for the rapid detection of SARS-CoV-2 antigen. Microorganisms. 2020;9:58. https://doi.org/10.3390/microorganisms9010058
10. Kohmer N, Toptan T, Pallas C, Karaca O, Pfeiffer A, Westhaus S, et al. The comparative clinical performance of four SARS-CoV-2 rapid antigen tests and their correlation to infectivity in vitro. J Clin Med. 2021;10:328. https://doi.org/10.3390/jcm10020328
11. McKay SL, Tobolowsky FA, Moritz ED, Hatfield KM, Bhatnagar A, LaVoie SP, et al.; CDC Infection Prevention and Control Team and the CDC COVID-19 Surge Laboratory Group. Performance evaluation of serial SARS-CoV-2 rapid antigen testing during a nursing home outbreak. Ann Intern Med. 2021;174:945–51. https://doi.org/10.7326/M21-0422
12. Ford L, Lee C, Pray IW, Cole D, Bigouette JP, Abedi GR, et al. Epidemiologic characteristics associated with SARS-CoV-2 antigen-based test results, rRT-PCR cycle threshold values, subgenomic RNA, and viral culture results from university testing. Clin Infect Dis. 2021;73:e1345–55. https://doi.org/10.1093/cid/ciab303
13. Pekosz A, Parvu V, Li M, Andrews JC, Manabe YC, Kodsi S, et al. Antigen-based testing but not real-time polymerase chain reaction correlates with severe acute respiratory syndrome coronavirus 2 viral culture. Clin Infect Dis. 2021;73:e2861–6. https://doi.org/10.1093/cid/ciaa1706
14. Centers for Disease Control and Prevention. Using antigen tests for SARS-CoV-2 in community settings, 2021 [cited 201 Jun 5]. https://www.cdc.gov/coronavirus/2019-ncov/lab/resources/antigen-tests-guidelines.html#using-antigen-tests-community-settings
15. Gniazdowski V, Morris CP, Wohl S, Mehoke T, Ramakrishnan S, Thielen P, et al. Repeat COVID-19 molecular testing: correlation of SARS-CoV-2 culture with molecular assays and cycle thresholds. Clin Infect Dis. 2021;73:e860–9. https://doi.org/10.1093/cid/ciaa1616

Address for correspondence: Dustin W. Currie, Centers for Disease Control and Prevention, 1 Corporate Square Blvd NE, Mailstop US1-2, Atlanta, GA 30329-4027, USA; email: pif7@cdc.gov

Disseminated Histoplasmosis in Persons with HIV/AIDS, Southern Brazil, 2010–2019

Rossana Patricia Basso, Vanice Rodrigues Poester, Jéssica Louise Benelli, David A. Stevens, Melissa Orzechowski Xavier

We evaluated disseminated histoplasmosis (DH) in HIV patients over 10 years in southern Brazil. The incidence was 12 cases/1,000 hospitalizations (2010–2019); the mortality rate was 35%. Tuberculosis frequently obscured the diagnosis of DH. We emphasize the need in our region to suspect and investigate DH using more sensitive methods.

Disseminated histoplasmosis (DH) is an AIDS-defining disease and one of the major causes of death in persons living with HIV/AIDS (PLHIV) (mortality rate ranging from 13% to 48%) (*1*–*4*). DH is a neglected disease because of its nonspecific symptoms, frequent misdiagnosis as tuberculosis (TB), and limited access to sensitive diagnostic methods (*3*,*5*).

Worsening this scenario, an epidemic of AIDS is underway in Brazil; >800,000 new cases have been diagnosed in recent decades (*6*). Therefore, efforts are necessary to understand the epidemiology of DH/AIDS co-infection in the areas to which these diseases are endemic. We evaluated the clinical and epidemiologic profile of patients with DH/AIDS co-infection in a reference service for PLHIV over 10 years in southern Brazil and compared the incidence in periods before and after an internal hospital improvement of DH investigation.

The Study

We performed a retrospective study including all DH cases diagnosed in persons with HIV/AIDS at a regional reference service in University Hospital Dr. Miguel Riet Corrêa Jr. (UH-FURG-Ebserh), a 207-bed tertiary hospital in Rio Grande, Brazil, that serves as reference center for 21 cities in Brazil. The hospital has an average of 257 HIV/AIDS hospitalizations/year (*7*). DH cases were defined by 1) classical methods: growth of *H. capsulatum* in culture, presence of blastoconidia suggestive of *H. capsulatum* by Gomori-Grocott stain (direct mycological examination or histopathology), or both; 2) serologic method: positive immunodiffusion test (IMMY, https://www.immy.com); or 3) urinary antigen test: positive immunoenzymatic assay (IMMY). Patients with clinical suspicion of DH and ≥1 of these diagnostic criteria were included. The study was approved by our university ethics committee (CEP/FURG, approval no. 234/2018).

We analyzed databases from the hospital for clinical and epidemiologic evaluation. In cases in which HIV and AIDS were diagnosed simultaneously, DH was considered the AIDS-defining illness. We calculated the overall incidence rate of DH per 1,000 hospitalizations of persons with AIDS at UH-FURG-Ebserh (*8*); we then compared that with rates before improvement of DH investigation (2010–2016) and after improvement of DH investigation (2017–2019). These improvements consisted of health education and training of health professionals to improve clinical suspicion and implementing urinary antigen detection as another diagnostic method. Descriptive and frequencies analyses were performed in SPSS Statistics 25.0 (IBM, https://www.ibm.com).

Our study included 31 cases of DH, representing an overall incidence of 12 new cases/1,000 PLHIV hospitalized at UH-FURG-Ebserh. In the first period (2010–2016), 15 cases were diagnosed in 7 years, a rate of 8/1,000 hospitalizations. After more sensitive testing and enhanced physician training were im-

Author affiliations: Programa de Pós Graduação em Ciências da Saúde, Universidade Federal do Rio Grande, Rio Grande, Brazil (R.P. Basso, V.R. Poester, J.L. Benelli, M.O. Xavier); Hospital Universitário Dr. Miguel Riet Corrêa Jr., vinculado à Empresa Brasileira de Serviços Hospitalares, Rio Grande (R.P. Basso, J.L. Benelli); California Institute for Medical Research, San Jose, California, USA (D.A. Stevens); Stanford University Medical School, Stanford, California, USA (D.A. Stevens)

DOI: https://doi.org/10.3201/eid2803.212150

Table 1. Clinical-epidemiologic data of 31 disseminated histoplasmosis cases diagnosed in persons living with HIV/AIDS, University Hospital Dr. Miguel Riet Corrêa Jr., Rio Grande, Brazil, 2010–2019

Variable	Frequency, % (no./total no. participants)
M	74 (21/31)
F	26 (8/31)
Signs and symptoms	
Weight loss	100 (31/31)
Fever (>37.8°C)	100 (31/31)
Respiratory: cough and/or dyspnea	100 (31/31)
Cutaneous: papular and/or ulcerated	52 (16/31)
Neurologic: disorientation, focal deficit, paresthesia, confusion, headache and/or hemiplegia	52 (16/31)
Digestive: abdominal distension and pain, diarrhea and/or nausea	81 (25/31)
Hepatomegaly	55 (17/31)
Splenomegaly	81 (25/31)
Generalized lymph node enlargement	35 (11/31)
Image exams	
Interstitial lung pattern	55 (17/31)
Reticulonodular lung pattern	32 (10/31)
Pulmonary nodules	6 (2/31)
Mediastinal lymphadenopathy	26 (8/31)
Blood assays	
Anemia	100 (31/31)
Inflammatory marker*	100 (31/31)
Liver damage marker†	84 (26/31)
Tissue injury marker‡	87 (27/31)
Thrombocytopenia	74 (23/31)
HIV assays	
CD4+ lymphocytes ≤100/mm^3	71 (22/31)
CD4+ lymphocytes ≤50/mm^3	48 (15/31)
HIV Viral load ≥50,000 copies	90 (26/29)
First choice antifungal treatment	
None	3 (1/31)
Amphotericin B deoxycholate	81 (25/31)
Itraconazole	16 (5/31)
Outcome after 12 months	
Alive	65 (20/31)
Dead	35 (11/31)

*C-reactive protein increased.
†Alkaline phosphatase increased.
‡Lactate dehydrogenase increased.

plemented, 16 cases were diagnosed in only 3 years (2017–2019), a rate of 24/1,000 hospitalizations, a substantial increase.

Most patients were men; mean age was 41 (range 21–61) years (Table 1). Except for 3, all had co-infections diagnosed concomitantly (Table 2). The use of antiretroviral therapy at time of DH diagnosis was irregular or nonexistent in 90% (n = 28) of patients. Only 4 had >200 cells/mm^3 of CD4+ lymphocytes (mean 109 cells/mm^3; range 7–752 cells/mm^3). In 6 (19%), DH was the AIDS-defining illness. A total of 3 persons had DH associated with a systemic inflammatory response syndrome.

Table 2. Frequency of co-infections in 31 patients with disseminated histoplasmosis diagnosed in persons living with HIV/AIDS, University Hospital Dr. Miguel Riet Corrêa Jr., Rio Grande, Brazil, 2010–2019

Infectious disease	Frequency, % (no./total no. participants)
Oral candidiasis	61 (19/31)
Confirmed tuberculosis	29 (9/31)
Neurotoxoplasmosis	29 (9/31)
Pneumocystosis	23 (7/31)
Herpetic encephalitis	3 (1/31)
Herpes zoster	3 (1/31)
Syphilis	3 (1/31)
Medullary cytomegalovirus	3 (1/31)
Mycobacterium avium infection	3 (1/31)
Herpes simplex infection	3 (1/31)
Hepatitis C	3 (1/31)

Eight (26%) DH patients were empirically treated for TB (*9*); no cases were confirmed by GeneXpert MTB/RIF (Cepheid, https://www.cepheid.com). Up to 12 (mean 5) clinical samples/patient were submitted for TB investigations before suspicion of DH.

DH was diagnosed through classical mycologic exams in 14 (45%) patients, serologic tests in 9 (29%) patients, and urinary antigen assay in 4 (13%) patients. Four (13%) patients had ≥2 positive results by different methods (Figure). The diagnosis of histoplasmosis occurred after a mean of 10 (range 1–28) days from the beginning of hospitalization. This timing probably represents an underestimated delay,

because several patients reported symptoms that could have led to a diagnostic workup before the illness progressed to a point at which hospitalization was required.

The treatment of choice for 81% of patients was intravenous amphotericin deoxycholate (0.7–1 mg/kg/d, to a maximum 50 mg/d) for 14 days, followed by oral itraconazole (200 mg every 8 h for 3 days, then 200 mg every 12 h) for 12 months. A total of 5 (16%) patients were treated only with itraconazole (4 with early diagnosis of DH and 1 with renal dysfunction). Twelve months after the DH diagnosis, 35% of the patients had died (Table 1); 1 died before laboratory confirmation, and 4 died within an average of 25 (range 0–62) days after diagnosis of DH. Three patients died after 5–6 months while being treated with itraconazole, and 3 had recurrence of the disease after 6, 7, or 12 months because of antifungal interruption, which resulted in death (Table 1).

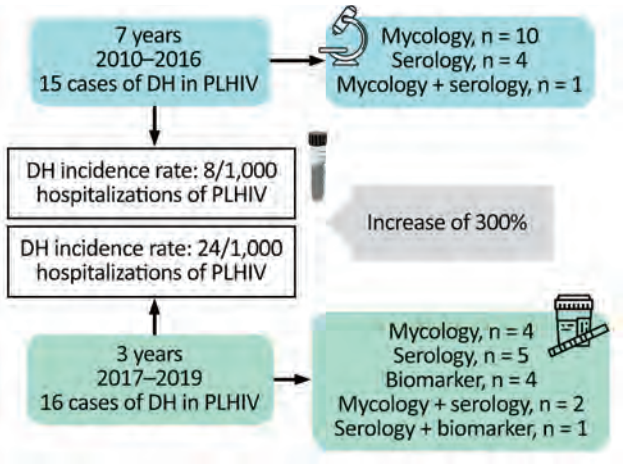

Figure. Approach used for the diagnosis of 31 cases of DH in PLHIV from a tertiary hospital in southern Brazil, 2010–2019. The incidence rate of DH between periods before (2010–2016) and after (2017–2019) implementation of the urinary antigen test shows an increase of 300%. DH, disseminated histoplasmosis; PLHIV, persons living with HIV.

Conclusions

DH causes severe clinical manifestations in PLHIV that can lead to death (*10*). Improved knowledge of the local epidemiology of DH and education of reference services for PLHIV are essential to reduce underdiagnosis and contribute to patient survival (*11*), especially in Rio Grande, a harbor city with the highest rate of HIV/AIDS among cities in Brazil with >100,000 inhabitants (*7*).

DH was the AIDS-defining illness in 21% of the patients in this study. Other co-infections (*12*,*13*) were noted. Respiratory signs, splenomegaly, and cutaneous lesions were more commonly described in our patients than in other studies, possibly because late diagnosis led to more severe extent of the disease (*12*,*13*). The high rate of neurologic impairment in our patients can be attributed to their co-infections; in 69% (9/13) of patients, this impairment was ascribed to neurotoxoplasmosis or herpetic encephalitis. In addition, neurologic signs were detected in 5 other patients without an ascribed neuropathogenic condition, meriting additional investigations.

Many of our patients were exhaustively investigated for TB, and 26% were empirically treated for TB despite negative results from the highly sensitive GeneXpert MTB/RIF assay (Cepheid). The long investigations for TB delayed the confirmation of the DH diagnosis despite descriptions of the concurrence of these 2 diseases (*14*). TB is a major opportunistic disease in PLHIV (*15*), evidenced by 29% of our DH patients with concomitant TB. Thus, the investigation of both diseases must occur simultaneously (*12*), and DH must be investigated in PLHIV with CD4+ lymphocytes <200 cells/mm^3 (*11*).

Tests to detect *Histoplasma* antibodies have poor sensitivity (30%–70%) in immunocompromised patients (*1*). Diagnostic methods with high rates of sensitivity and specificity are vital in areas where histoplasmosis is endemic and could improve the likelihood of early diagnosis and favorable outcomes for patients (*1*,*12*). An improvement in the investigation of DH in PLHIV with respiratory symptoms occurred in the UH-FURG-Ebserh in 2017, through a collaboration in a multicenter study (*12*). Subsequently, the results contributed to the acquisition of the urinary antigen assay by UH-FURG-Ebserh. In the last 3 years of our study, the urinary antigen test was the only method able to detect 25% (4/15) of our patients with DH. The detection of urinary antigens is the standard for DH diagnosis in immunosuppressed patients (*11*).

The mortality rate in our series (35%) was similar to the rate described in a systematic review from Brazil histoplasmosis cases (33%) (*10*). Therefore, the underdiagnosis of DH in PLHIV is a national problem in Brazil that must be urgently changed. In our hospital, DH was responsible for high rates of illness in PLHIV, up to 24 cases/1,000 hospitalizations, and high mortality rates (35%). In addition, we emphasize that 29% of patients were co-infected with TB, a disease with symptoms overlapping with histoplasmosis. Simultaneous investigation for the 2 diseases in all PLHIV patients living in areas in which histoplasmosis is endemic is mandatory.

Acknowledgments

We thank Coordenação de Aperfeiçoamento de Pessoal de Nível Superior (CAPES) and Conselho Nacional de Desenvolvimento Científico e Tecnológico (CNPQ).

About the Author

Dr. Basso is a PhD physician working in infectious diseases. Her research field is in medical mycology, mostly concerning opportunistic fungal diseases in HIV patients.

References

1. Cáceres DH, Samayoa BE, Medina NG, Tobón AM, Guzmán BJ, Mercado D, et al. Multicenter validation of commercial antigenuria reagents to diagnose progressive disseminated histoplasmosis in people living with HIV/AIDS in two Latin American countries. J Clin Microbiol. 2018;56:e01959–17. https://doi.org/10.1128/JCM.01959-17
2. Pasqualotto AC, Quieroz-Telles F. Histoplasmosis dethrones tuberculosis in Latin America. Lancet Infect Dis. 2018;18:1058–60. https://doi.org/10.1016/S1473-3099(18)30373-6
3. Centre d'Investigation Clinique Antilles Guyane C, Centre Hospitalier de Cayenne, Université de Guyane G. Disseminated histoplasmosis in Central and South America, the invisible elephant: the lethal blind spot of international health organizations. AIDS. 2016;30:167–70. https://doi.org/10.1097/QAD.0000000000000961
4. Samayoa B, Roy M, Cleveland AA, Medina N, Lau-Bonilla D, Scheel CM, et al. High mortality and coinfection in a prospective cohort of human immunodeficiency virus/acquired immune deficiency syndrome patients with histoplasmosis in Guatemala. Am J Trop Med Hyg. 2017;97:42–8. https://doi.org/10.4269/ajtmh.16-0009
5. Adenis AA, Valdes A, Cropet C, McCotter OZ, Derado G, Couppie P, et al. Burden of HIV-associated histoplasmosis compared with tuberculosis in Latin America: a modelling study. Lancet Infect Dis. 2018;18:1150–9. https://doi.org/10.1016/S1473-3099(18)30354-2
6. Traebert J, Traebert E, Schuelter-Trevisol F, Cortez Escalante JJ, Schneider IJC. The burden of AIDS: a time series analysis of thirty-five years of the epidemic in Brazil. AIDS Care. 2018;30:1413–20. https://doi.org/10.1080/09540121.2018.1456642
7. Ministry of Health, Brazil. National epidemiological bulletin HIV/AIDS, Brazil [in Portuguese]. 2020 [cited 2021 Oct 6]. https://www.gov.br/saude/pt-br/centrais-de-conteudo/publicacoes/boletins/boletins-epidemiologicos/especiais/2020/boletim-hiv_aids-2020-internet.pdf
8. Horta RL, da Costa JSD, Balbinot AD, Watte G, Teixeira VA, Poletto S. Hospitalizações psiquiátricas no Rio Grande do Sul de 2000 a 2011. Rev Bras Epidemiol. 2015;18:918–29. https://doi.org/10.1590/1980-5497201500040019
9. Ministry of Health, Brazil. Recommendations for TB-HIV co infection control in specialized facilities for people living with HIV [in Portuguese]. 2013 [cited 2021 Oct 6]. https://bvsms.saude.gov.br/bvs/publicacoes/recomendacoes_manejo_coinfeccao_tb_hiv.pdf
10. Almeida MA, Almeida-Silva F, Guimarães AJ, Almeida-Paes R, Zancopé-Oliveira RM. The occurrence of histoplasmosis in Brazil: A systematic review. Int J Infect Dis. 2019;86:147–56. https://doi.org/10.1016/j.ijid.2019.07.009
11. Pan American Health Organization/World Health Organization. Guidelines for diagnosing and managing disseminated histoplasmosis among people living with HIV. 2020 Apr 1 [cited 2021 Oct 6]. https://www.who.int/publications/i/item/9789240006430
12. Falci DR, Monteiro AA, Braz Caurio CF, Magalhães TCO, Xavier MO, Basso RP, et al. Histoplasmosis, an underdiagnosed disease affecting people living with HIV/AIDS in Brazil: results of a multicenter prospective cohort study using both classical mycology tests and *Histoplasma* urine antigen detection. Open Forum Infect Dis. 2019;6:ofz073. https://doi.org/10.1093/ofid/ofz073
13. Nacher M, Valdes A, Adenis A, Blaizot R, Abboud P, Demar M, et al. Disseminated histoplasmosis in HIV-infected patients: a description of 34 years of clinical and therapeutic practice. J Fungi (Basel). 2020;6:E164. https://doi.org/10.3390/jof6030164
14. Tucker RM, Hamilton JR, Stevens DA. Concurrent bloodstream infection with *Histoplasma capsulatum* and *Mycobacterium tuberculosis*. J Med Vet Mycol. 1991;29:343–5. https://doi.org/10.1080/02681219180000531
15. Boffo MMS, de Mattos IG, Ribeiro MO, Neto ICO. Tuberculosis associated to AIDS: demographic, clinical and laboratory characteristics of patients from a reference center in Southern Brazil [in Portuguese]. J Bras Pneumol. 2004;30:140–6. https://doi.org/10.1590/S1806-37132004000200011

Address for correspondence: Melissa Orzechowski Xavier, Laboratório de Micologia, Faculdade de Medicina, Universidade Federal do Rio Grande, Campus Saúde. Visconde de Paranaguá 102, Centro, 96201-900, Rio Grande, RS, Brazil; email: melissaxavierfurg@gmail.com

Schizophyllum commune [skiz-of′-ĭ-ləm kom′-yoon]

Monika Mahajan

Schizophyllum commune, or split-gill mushroom, is an environmental, wood-rotting basidiomycetous fungus. *Schizophyllum* is derived from "*Schíza*" meaning split because of the appearance of radial, centrally split, gill like folds; "*commune*" means common or shared ownership or ubiquitous. Swedish mycologist, Elias Magnus Fries (1794–1878), the Linnaeus of Mycology, assigned the scientific name in 1815. German mycologist Hans Kniep in 1930 discovered its sexual reproduction by consorting and recombining genomes with any one of numerous compatible mates (currently >2,800).

Figure 1. Colony of *Schizophyllum commune* on a culture plate. Numerous sexual reproductive structures, or fruiting bodies, called basidiocarps can be seen. Note the split gills. Source: https://phil.cdc.gov/Details.aspx?pid = 307

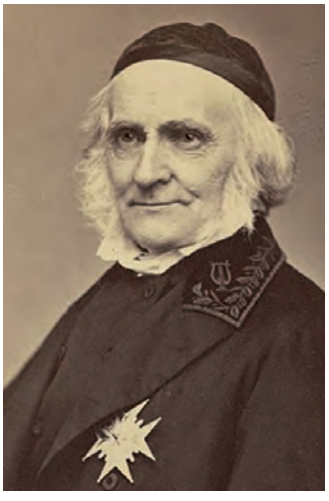

Figure 2. Swedish mycologist Elias Magnus Fries (1794–1878), who assigned the scientific name to *Schizophyllum commune.* Photograph by Emma Schenson, 1865. Source: Kungliga Biblioteket, Stockholm LIBRIS, Elias Fries, https://www.kb.se

Isolation by Kligman in 1950 of fleshy fungus that had fan-shaped sporophores from a case of onychomycosis was regarded as interesting. However, it was dismissed as improbable because mushrooms were not known to invade animal tissue. This emerging fungal pathogen is characterized by the presence of clamp connections, hyphal spicules, and formation of basidiocarps with basidiospores.

Sources

1. Chowdhary A, Kathuria S, Agarwal K, Meis JF. Recognizing filamentous basidiomycetes as agents of human disease: a review. Med Mycol. 2014;52:782–97. https://doi.org/10.1093/mmy/myu047
2. Cooke WB. The genus *Schizophyllum*. Mycologia. 1961;53:575–99. https://doi.org/10.1080/00275514.1961.12017987
3. Greer DL. Basidiomycetes as agents of human infections: a review. Mycopathologia. 1978;65:133–9. https://doi.org/10.1007/BF00447184
4. O'Reilly P. *Schizophyllum commune*, split gill fungus, 2016 [cited 2021 Aug 23]. https://www.first-nature.com/fungi/schizophyllum-commune.php
5. Raper CA, Fowler TJ. Why study *Schizophyllum*? Fungal Genet Rep. 2004;51:30–6. https://doi.org/10.4148/1941-4765.1142

Author affiliation: Postgraduate Institute of Medical Education and Research, Chandigarh, India

Address for correspondence: Monika Mahajan, Medical Microbiology, Postgraduate Institute of Medical Education and Research, Research Block A, Sector 12, Chandigarh 160012, India; email: monideepmj@yahoo.com

DOI: https://doi.org/10.3201/eid2703.211051

Transovarial Transmission of Heartland Virus by Invasive Asian Longhorned Ticks under Laboratory Conditions

Wilson R. Raney, Josiah B. Perry, Meghan E. Hermance

We demonstrated experimental acquisition and transmission of Heartland bandavirus by *Haemaphysalis longicornis* ticks. Virus was detected in tick salivary gland and midgut tissues. A total of 80% of mice exposed to 1 infected tick seroconverted, suggesting horizontal transmission. *H. longicornis* ticks can transmit the virus in the transovarial mode.

The Asian longhorned tick, *Haemaphysalis longicornis*, is an ixodid tick native to Southeast Asia that was reported in the United States during 2017 and has since been found in 17 states (*1*,*2*). In its native range, this tick is the main vector of Dabie bandavirus (*3*) (formerly severe fever with thrombocytopenia syndrome virus), the agent that causes severe human illnesses characterized by high fever, thrombocytopenia, leukopenia, and multiorgan dysfunction (*4*).

Dabie bandavirus is closely related genetically to Heartland bandavirus (HRTV) (*5*), an emerging North American virus reported during 2012 after 2 men in Missouri, USA, showed febrile illness with fatigue, thrombocytopenia, and leukopenia after exposure to ticks (*6*). Because the current geographic range and the predicted range expansion of invasive *H. longicornis* ticks overlap considerably with human cases of HRTV, including Missouri (*7*,*8*), this study was designed to assess the ability of this invasive tick species to maintain and transmit HRTV.

The Study

We selected 74 female *H. longicornis* ticks from an HRTV-free colony into experimental and control groups. We microinjected 50 ticks with 300 focus-forming units of HRTV into the anal pore and 24 ticks with an equivalent volume of Dulbecco modified Eagle medium into the anal pore (Appendix, https://wwwnc.cdc.gov/EID/article/28/3/21-0973-App1.pdf). We dissected *t*icks at 14, 21, 28, and 40 days postinjection (dpi) and collected the salivary glands, midgut, and carcass of each tick. We screened tick samples for HRTV RNA by using quantitative reverse transcription PCR (qRT-PCR) (Table 1; Figure 1). No samples taken from media-injected ticks screened positive for HRTV (Table 1). For virus-injected ticks, HRTV RNA titers followed a general trend across each organ, and titers peaked at 21 dpi (Figure 1).

To screen HRTV-microinjected ticks for infectious virions, we collected ticks at 14, 21, 28, and 40 dpi and individually homogenized them. We cultured tick homogenates in triplicate on Vero E6 cells, and titered infectious virus by using a focus-forming assay (FFA). All ticks from each time point produced foci, indicating the presence of infectious virions in the tick body at each interval (Table 1).

We selected an additional 26 female *H. longicornis* ticks to evaluate horizontal transmission of HRTV to BALB/c mice. We microinjected 16 ticks with HRTV and the remaining 10 with Dulbecco modified Eagle medium. At 40 dpi, mice were infested with the microinjected ticks at a ratio of 1 tick/mouse. Five of the HRTV-injected ticks and 5 medium-injected ticks attached and fed on the mice to repletion. After feeding was complete, we removed engorged ticks and housed them individually to aid oviposition. We monitored mice daily for clinical signs of disease. We collected blood from the mice at −1, 7, and 14 days after tick attachment. Mice were subjected to necropsy at 28 days after attachment, and we collected liver, spleen, kidney, brain, blood, and testis samples. We screened blood and organ samples for HRTV RNA by qRT-PCR. No HRTV RNA was detected in any blood or organs collected from the mice.

Author affiliation: University of South Alabama College of Medicine, Mobile, Alabama, USA

DOI: https://doi.org/10.3201/eid2803.210973

Table 1. Rate of detection of HRTV RNA by qRT-PCR and infectious HRTV by FFA in adult *Haemaphysalis longicornis* ticks at 14, 21, 28, and 40 dpi*

Procedure	Real-time qRT-PCR detection of HRTV RNA, no. positive/no. tested (%)			FFA titration of HRTV, whole tick
	Salivary glands	Midgut	Carcass	
Medium injected	0/15 (0)	0/15 (0)	0/15 (0)	0/9 (0)
HRTV-injected 14 dpi	4/8 (50)	8/8 (100)	8/8 (100)	5/5 (100)
HRTV-injected 21 dpi	7/8 (88)	8/8 (100)	8/8 (100)	5/5 (100)
HRTV-injected 28 dpi	6/8 (75)	8/8 (100)	8/8 (100)	5/5 (100)
HRTV-injected 40 dpi	3/6 (50)	6/6 (100)	6/6 (100)	4/5 (80)

*dpi, days postinjection; FFA, focus-forming assay; HRTV, Heartland virus; qRT-PCR, quantitative reverse transcription PCR.

We screened serum from the terminal blood samples to determine whether mice seroconverted relative to HRTV. We assayed each serum sample on 2 independent occasions. In brief, we assayed diluted serum samples by using HRTV-infected Vero E6 cells as antigens. Four of the 5 mice fed upon by a single HRTV-injected tick were positive for HRTV-specific antibodies. We detected antibodies up to a serum dilution of 1:1,600 for 3 mice and 1:800 for 1 mouse. None of the 5 mice fed upon by media-injected ticks were positive for HRTV-specific antibodies. Likewise, none of the age-matched, sex-matched, preimmune mouse serum demonstrated an antibody response to HRTV.

After each fed female tick completed oviposition, we removed the fed female carcass from the egg mass and homogenized the carcass. We screened the carcasses for HRTV RNA by qRT-PCR, and 5/5 HRTV-injected female carcasses were positive for HRTV RNA (Table 2; Figure 2). The media-injected fed female carcasses were negative for HRTV. We also removed 3 pools of 50 eggs/egg mass to screen for HRTV RNA. All 15 egg pools from HRTV-injected ticks were positive for HRTV RNA (Table 2; Figure 2). Egg pools from the media-injected ticks had no HRTV RNA.

We repeated this analysis for pools of larvae (4 pools of 50 larvae derived from each fed female) after hatching. All larvae clutches derived from HRTV-injected females were positive for HRTV RNA. To screen for infectious virions in larvae, we homogenized pools of 150 larvae from each clutch and cultured them on Vero E6 cells. We titered the infectious virus by using FFA, and all 5 clutches derived from HRTV-injected females were positive for infectious HRTV (Table 2).

Conclusions

We demonstrated experimental acquisition and transmission of HRTV by *H. longicornis* ticks after microinjection of the anal pore with HRTV. Although not a natural route of virus acquisition for ticks, microinjection of the anal pore is an established and reproducible procedure that delivers specific quantities of virus into the alimentary canal of the tick, the first organ system that virus contacts in naturally infected ticks (*9*). Microinjected ticks showed viral RNA titers peaking at 21 dpi in salivary glands, midguts, and carcasses, suggesting that HRTV replication took place within these organs between 14 and 21 dpi.

Maintenance of infectious HRTV virions for several weeks after microinjection suggests that an artificially infected tick is capable of transmitting HRTV to vertebrate hosts on which it feeds long after viral acquisition. Although the mice exposed to HRTV-infected ticks did not show clinical signs of disease and viral RNA was not detected in any mouse tissues, the absence of disease in these immunocompetent mice was expected; previously, only immunocompromised Ag129 mice have shown detectable viremia, clinical signs of HRTV infection, and death (*10*). Seroconversion of 4/5 mice exposed to an individual HRTV-infected *H. longicornis* tick suggests horizontal transmission of HRTV. Future studies should con-

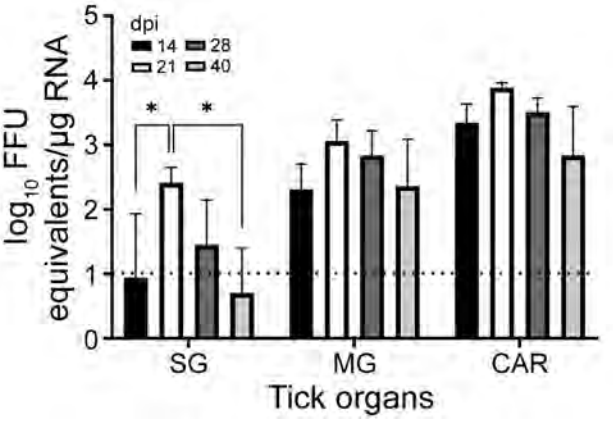

Figure 1. Detection of Heartland virus (HRTV) RNA by real-time, quantitative reverse transcription PCR reaction of HRTV-injected *Haemaphysalis longicornis* ticks. Ticks were dissected at 14, 21, 28, and 40 dpi. Tick organs were screened individually. Viral load data are expressed as FFU equivalents per microgram of RNA after normalization to a standard curve. Data were not normally distributed and are presented as medians with interquartile ranges. Statistical significance was determined by using Kruskal-Wallis tests followed by the Dunn test. Limit of detection was ≈10 FFU equivalents/µg RNA. *p<0.05. CAR, carcass; dpi, days postinjection; FFU, focus-forming units; MG, midgut; SG, salivary glands.

Table 2. Rate of detection of HRTV RNA by qRT-PCR and infectious HRTV by FFA in fed *Haemaphysalis longicornis* adult tick carcasses, tick eggs, and tick larvae*

Procedure	Real-time qRT-PCR detection of HRTV RNA, no. positive/no. tested (%)			FFA titration of HRTV, larvae pools‡
	Fed adult carcasses	Egg pools†	Larvae pools†	
Medium injected	0/5 (0)	0/15 (0)	0/20 (0)	0/5 (0)
HRTV-injected	5/5 (100)	15/15 (100)	20/20 (100)	5/5 (100)

*FFA, focus-forming assay; HRTV, Heartland virus; qRT-PCR, quantitative reverse transcription PCR.
† Egg and larvae pools contained 50 eggs or larvae/pool.
‡Larvae pools contained 150 larvae/pool.

firm the presence of infectious virions in tick saliva to eliminate the possibility of seroconversion caused by transmission of noninfectious HRTV antigens during tick feeding.

We also showed transovarial transmission of HRTV in *H. longicornis* ticks by detection of HRTV RNA in eggs and larvae derived from HRTV-infected mother ticks. Furthermore, we demonstrated the presence of infectious virions in larvae after hatching. The North American strain of the tick is parthenogenetic, a foremost public health concern because 1 female can reproduce asexually to establish and sustain local populations (*11*). Because *H. longicornis* ticks are a 3-host tick and a host generalist (*12*), the possibility of invasive *H. longicornis* ticks acquiring HRTV by cofeeding with infected ticks or by feeding on a viremic host further highlights the potential of the tick to efficiently disseminate the virus. This distinction becomes more crucial because the tick can withstand a wide range of climates (*7*,*13*). Further studies should be conducted to demonstrate whether the tick can transmit HRTV during co-feeding with other ticks because this would be a major factor in promoting the environmental spread of the virus.

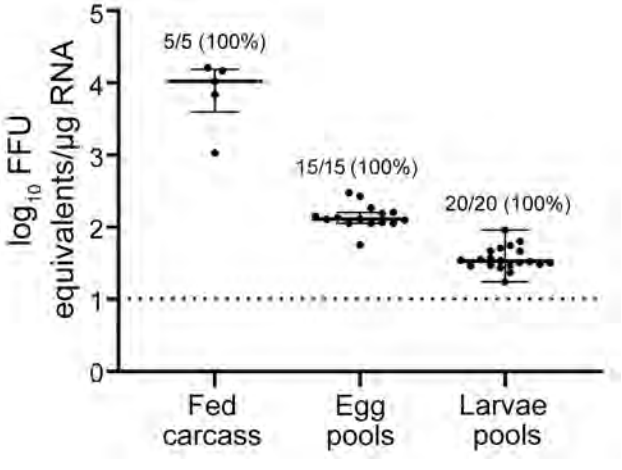

Figure 2. Scatter plot demonstrating detection of Heartland virus (HRTV) by real-time, quantitative reverse transcription PCR. Data were not normally distributed and are presented as medians with interquartile ranges. Fed female carcasses, egg pools, and larvae pools were screened for viral RNA. Egg pools and larvae pools were composed of 50 eggs or larvae per pool. Limit of detection was ≈10 FFU equivalents/µg RNA. FFU, focus-forming units.

The predicted spread of *H. longicornis* ticks in the United States shares a geographic range with states in which HRTV has already been reported in *Amblyomma americanum* ticks and wildlife (*7*,*8*,*14*). The introduction of a new vector species could amplify transmission in natural foci, resulting increased HRTV disease cases in humans.

Acknowledgments

We thank the Michele Schuler, Leigh Ann Wiggins, and Hannah Bryant for assistance with animal experiments and animal husbandry; and Michael Levin for providing the initial *H. longicornis* ticks (distributed by BEI Resources, https://www.beiresources.org) that seeded our in-house colony of ticks used in this study.

This study was supported by the University of South Alabama College of Medicine and the National Institute of Allergy and Infectious Diseases, National Institutes of Health (award no. R21AI163693).

About the Author

Mr. Raney is a research technologist in the Laboratory of Infectious Diseases at the College of Medicine, University of South Alabama, Mobile, AL. His research interests include tick-borne viruses and tick–host–virus interactions.

References

1. US Department of Agriculture. National *Haemaphysalis longicornis* (Asian longhorned tick) situation report as of September 10, 2021 [cited 2021 Dec 8]. https://www.aphis.usda.gov/animal_health/animal_diseases/tick/downloads/longhorned-tick-sitrep.pdf
2. Rainey T, Occi JL, Robbins RG, Egizi A. Discovery of Haemaphysalis longicornis (Ixodida: Ixodidae) parasitizing a Sseep in New Jersey, United States. J Med Entomol. 2018;55:757–9. https://doi.org/10.1093/jme/tjy006
3. Liu K, Zhou H, Sun RX, Yao HW, Li Y, Wang LP, et al. A national assessment of the epidemiology of severe fever with thrombocytopenia syndrome, China. Sci Rep. 2015;5:9679. https://doi.org/10.1038/srep09679
4. Yu XJ, Liang MF, Zhang SY, Liu Y, Li JD, Sun YL, et al. Fever with thrombocytopenia associated with a novel bunyavirus in China. N Engl J Med. 2011;364:1523–32. https://doi.org/10.1056/NEJMoa1010095
5. Matsuno K, Weisend C, Travassos da Rosa AP, Anzick SL, Dahlstrom E, Porcella SF, et al. Characterization of the Bhanja serogroup viruses (Bunyaviridae): a novel species of the genus Phlebovirus and its relationship with other

emerging tick-borne phleboviruses. J Virol. 2013;87:3719–28. https://doi.org/10.1128/JVI.02845-12
6. McMullan LK, Folk SM, Kelly AJ, MacNeil A, Goldsmith CS, Metcalfe MG, et al. A new phlebovirus associated with severe febrile illness in Missouri. N Engl J Med. 2012;367:834–41. https://doi.org/10.1056/NEJMoa1203378
7. Raghavan RK, Barker SC, Cobos ME, Barker D, Teo EJM, Foley DH, et al. Potential spatial distribution of the newly introduced long-horned tick, *Haemaphysalis longicornis*, in North America. Sci Rep. 2019;9:498. https://doi.org/10.1038/s41598-018-37205-2
8. Staples JE, Pastula DM, Panella AJ, Rabe IB, Kosoy OI, Walker WL, et al. Investigation of Heartland virus throughout the United States, 2013–2017. Open Forum Infect Dis. 2020;7:ofaa125.
9. Labuda M, Nuttall PA. Tick-borne viruses. Parasitology. 2004;129(Suppl):S221–45. https://doi.org/10.1017/S0031182004005220
10. Bosco-Lauth AM, Calvert AE, Root JJ, Gidlewski T, Bird BH, Bowen RA, et al. Vertebrate host susceptibility to Heartland virus. Emerg Infect Dis. 2016;22:2070–7. https://doi.org/10.3201/eid2212.160472
11. Egizi A, Bulaga-Seraphin L, Alt E, Bajwa WI, Bernick J, Bickerton M, et al. First glimpse into the origin and spread of the Asian longhorned tick, *Haemaphysalis longicornis*, in the United States. Zoonoses Public Health. 2020;67:637–50. https://doi.org/10.1111/zph.12743
12. Hoogstraal H, Roberts FH, Kohls GM, Tipton VJ. Review of *Haemaphysalis* (*kaiseriana*) *longicornis Neumann* (resurrected) of Australia, New Zealand, New Caledonia, Fiji, Japan, Korea, and Northeastern China and USSR, and its parthenogenetic and bisexual populations (Ixodoidea, Ixodidae). J Parasitol. 1968;54:1197–213. https://doi.org/10.2307/3276992
13. Heath A. Biology, ecology and distribution of the tick, *Haemaphysalis longicornis Neumann* (Acari: Ixodidae) in New Zealand. N Z Vet J. 2016;64:10–20. https://doi.org/10.1080/00480169.2015.1035769
14. Brault AC, Savage HM, Duggal NK, Eisen RJ, Staples JE. Heartland virus epidemiology, vector association, and disease potential. Viruses. 2018;10:E498. https://doi.org/10.3390/v10090498

Address for correspondence: Meghan E. Hermance, Department of Microbiology and Immunology, University of South Alabama College of Medicine, 610 Clinic Dr, Mobile, AL 36688, USA; email: mhermance@southalabama.edu

Long-Term Symptoms among COVID-19 Survivors in Prospective Cohort Study, Brazil

Lívia P. Bonifácio, Viviane N.F. Csizmar, Francisco Barbosa-Júnior, Ana P.S. Pereira, Marcel Koenigkam-Santos, Danilo T. Wada, Gilberto G. Gaspar, Felipe S. Carvalho, Valdes R. Bollela, Rodrigo C. Santana, João P. Souza, Fernando Bellissimo-Rodrigues

We conducted a prospective cohort study in a population with diverse ethnic backgrounds from Brazil to assess clinically meaningful symptoms after surviving coronavirus disease. For most of the 175 patients in the study, clinically meaningful symptoms, including fatigue, dyspnea, cough, headache, and muscle weakness, persisted for ≥120 days after disease onset.

Understanding is growing that coronavirus disease (COVID-19) can evolve and continue to cause prolonged symptoms, characterizing the post–COVID-19 condition (*1*–*3*). Potential implications go beyond effects on individual patients and might represent an additional burden on healthcare services and social security, which are both already affected by the pandemic. Therefore, learning more about the long-term repercussions of the disease among different populations is essential. This study aimed to describe the occurrence of long-term physical, psychological, and social consequences among patients who survived COVID-19 and received follow-up care at a post–COVID-19 outpatient clinic at a university hospital in Brazil.

The Study

This prospective cohort study (RECOVIDA) was performed among patients attending a post–COVID-19 outpatient clinic at Ribeirão Preto Medical School University Hospital, Ribeirão Preto, Brazil (*4*). The institutional review board approved the research protocol.

All adults with PCR-confirmed COVID-19 with symptom onset during February 1–December 31, 2020, who attended follow-up appointments at the study clinic were eligible. Most participants (85.7%) had been discharged after being hospitalized for COVID-19. The remaining participants (14.3%) were mostly healthcare workers from the study facility. No participants had been previously vaccinated against COVID-19. Patients were classified into 3 groups according to the World Health Organization (WHO) severity classification of COVID-19: mild/moderate, severe, and critical (*5*) (Appendix Table 1, https://wwwnc.cdc.gov/EID/article/28/3/21-2020-App1.pdf).

This study was exploratory, and sample size was established through convenience. We aimed to include all patients who attended the clinic during the study period and agreed to participate.

Participants were recruited just before the scheduled medical consultation. After the informed consent form was signed, we performed a structured interview and a brief physical examination. We obtained secondary data from patients' electronic health records. Laboratory and imaging tests were performed at the attending physician's clinical discretion. We collected study data by using the Research Electronic Data Capture platform (*6*).

We collected information on economic and demographic social profile, medical history, date of symptom onset, hospitalization data, laboratory and imaging test results, persistent symptoms, and quality of life. We assessed quality of life by using the WHO Quality of Life questionnaire (*7*–*9*) (Appendix). The date of symptom onset was used as the reference for follow-up.

Author affiliations: Ribeirão Preto Medical School Social Medicine Department, University of São Paulo, São Paulo, Brazil (L.P. Bonifácio, V.N.F. Csizmar, F. Barbosa-Júnior, A.P.S. Pereira, J.P. Souza, F. Bellissimo-Rodrigues); Ribeirão Preto Medical School Department of Medical Images, Hematology and Clinical Oncology, University of São Paulo, Ribeirão Preto, Brazil (M. Koenigkam-Santos, D.T. Wada); Ribeirão Preto Medical School Infectious and Tropical Diseases Division of Internal Medicine Department, University of São Paulo, Ribeirão Preto (G.G. Gaspar, F.S. Carvalho, V.R. Bollela, R.C. Santana)

DOI: https://doi.org/10.3201/eid2803.212020

We performed statistical procedures by using Minitab 19.2 (https://www.minitab.com) and Stata version 9 (https://www.stata.com). We used odds ratios, 95% CIs, and Fisher exact tests to verify the association between the persistence of symptoms and the severity of disease.

During the study period, 297 patients had a follow-up medical consultation scheduled at the outpatient clinic. We included 175 patients in this study (Table 1; Figure). In this sample, 20% of participants had illness that was considered mild/moderate, 45.7% were severe, and 34.3% were critical.

After COVID-19, 80% of the patients experienced persistent symptoms; the 5 most prevalent were fatigue, dyspnea, cough, headache, and loss of overall muscle strength. Compared with the mild/moderate group, patients from the critical group more frequently experienced headaches, change in skin sensitivity, hypogeusia, hyposmia, and loss of muscle strength (Table 2, https://wwwnc.cdc.gov/EID/article/28/3/21-2020-T2.htm).

Regarding quality of life after COVID-19, physical health was more severely affected than the other 3 domains evaluated by the WHO Quality of Life questionnaire (psychological, social relationships, and environmental). Moreover, the comparative evaluation before and after COVID-19 showed a decrease from 81.1% to 68.4% in the percentage of patients who believed that their quality of life was good or very good and an increase from 2.3% to 6.4% of those who believed that their quality of life was poor or very poor. Despite these changes, more than half of patients (56.7%) were satisfied with their current health status at the time of evaluation (Appendix).

Table 1. Baseline clinical and demographic characteristics among 175 patients surviving the acute phase of COVID-19, Ribeirão Preto, Brazil*

Characteristic	COVID-19 severity			
	Mild/moderate, n = 35 (20%)	Severe, n = 80 (45.7%)	Critical, n = 60 (34.3%)	Total, n = 175
Sex				
M	7 (20)	36 (45)	42 (70)	85 (48.6)
F	28 (80)	44 (55)	18 (30)	90 (51.4)
Mean age, y (SD)	44.9 (±10.3)	57.1 (±15.3)	54.2 (±13.2)	53.7 (±14.4)
Ethnic background†				
White (Caucasian or Latin)	19 (54.3)	36 (45)	25 (41.7)	80 (45.7)
Afro-American (Brown)	10 (28.6)	34 (42.5)	26 (43.3)	70 (40)
Afro-American (Black)	6 (17.1)	8 (10)	6 (10)	20 (11.4)
Asiatic	0	1 (1.3)	2 (3.3)	3 (1.7)
Brazilian Indigenous	0	1 (1.3)	1 (1.7)	2 (1.1)
Mean years of schooling (SD)	13.4 (±5.7)	8.1 (±5.5)	8.3 (±5.4)	9.2 (±5.9)
Mean income/person, USD (SD)‡	407.33 (±313.60)	273.01 (±295,85)	229.33 (±210.40)	285.57 (±279.56)
Median	364.01	200.21‡	182.01‡	216.77‡
Currently works as a health professional				
Yes	23 (65.7)	8 (10)	2 (3.3)	33 (18.9)
No	12 (34.3)	72 (90)	58 (96.7)	142 (81.1)
Mean BMI (SD)§	31.8 (±7.5)	32.1 (±7.3)§	31.1 (±7.5)	31.7 (±7.3)§
BMI ≥30§	17 (48.6)	44 (56.4)§	23 (38.3)	84 (48.6)§
Underlying conditions				
None	16 (45.7)	16 (20)	10 (16.7)	42 (24.0)
Hypertension	9 (25.7)	35 (43.8)	21 (35)	65 (37.1)
Diabetes	1 (2.9)	26 (32.5)	22 (36.7)	49 (28.0)
Dyslipidemia	2 (5.7)	12 (15)	12 (20)	26 (14.8)
Heart problems (other than hypertension)	1 (2.9)	10 (12.5)	8 (13.3)	19 (10.9)
Rhinitis or sinusitis	3 (8.6)	7 (8.8)	7 (11.7)	17 (9.7)
Cancer	1 (2.9)	9 (11.3)	1 (1.7)	11 (6.3)
Thyroid problems	0	4 (5)	6 (10)	10 (5.7)
Depression or anxiety	1 (2.9)	6 (7.5)	3 (5)	10 (5.7)
Smoking				
Current	0 (0)	2 (2.5)	0	2 (1.1)
Previous	2 (5.71)	18 (22.5)	19 (31.7)	39 (22.3)
Hospitalization				
Yes	10 (28.6)	80 (100)	60 (100)	150 (85.7)
No	25 (71.4)	0	0	25 (14.3)
Mean duration of hospitalization, d (SD)	5 (±4)	9.9 (±5.2)	24.1 (±11.1)	15.3 (±10.9)
Median	4	9	20.5	12

*Values are no. (%) except as indicated. BMI, body mass index; COVID-19, coronavirus disease.
†Ethnic background information was self-reported and consisted of Latin American, Caucasian, Afro-American, Asian, and Brazilian indigenous persons.
‡$1 US = R $5,49. Data on financial income by person were missing for 3 participants.
§BMI data were missing for 2 participants.

Conclusions

We describe the long-term repercussions of COVID-19 among a sample of patients in Brazil from diverse social and ethnic backgrounds who survived acute infection and attended a follow-up ambulatory clinic appointment. We identified that most patients experienced ≥1 symptom for ≥120 days after the onset of disease. This finding also applies to patients who had a mild or moderate form of COVID-19. These symptoms negatively affected the patients' quality of life; fatigue was the most common symptom, followed by dyspnea and cough.

The clinical picture we describe here, in a population with a mixed ethnic background consisting of Latin American, Caucasian, Afro-American, Asian, and Brazilian indigenous persons, is similar to those encountered in other parts of the world, mainly in Caucasian or Asian populations (*1*,*10*–*12*). Some persistent symptoms found in our study, such as altered skin sensitivity and muscle weakness, primarily affected the patients whose illness was critical, and this finding could be more related to their stay in the intensive care unit than to the COVID-19 itself (*13*).

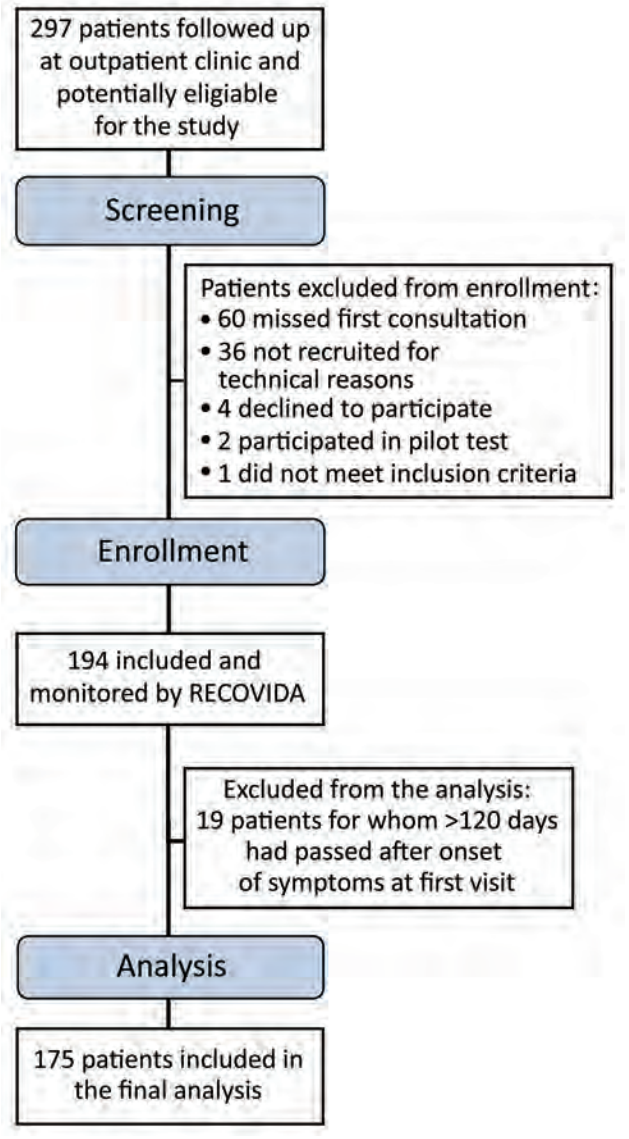

Figure. Flowchart of screening and inclusion of coronavirus disease survivors with long-term symptoms in prospective cohort study, Ribeirão Preto, Brazil.

Several possible pathophysiological explanations for the persistence of symptoms after COVID-19 have been proposed. The most commonly elicited in the literature are direct viral toxicity, endothelial damage, dysregulated immune response, hyperinflammation, hypercoagulability, and poor adaptation of the angiotensin-converting enzyme 2. So far, the actual mechanisms behind this scenario are not entirely understood and deserve further evaluation (*1*,*10*–*13*). Our sample identified that respiratory and heart rates were significantly higher in the patients whose illness was critical, possibly indicating impairment of autonomic function in these patients (*14*,*15*).

We highlight the need to study the persistent symptoms of patients with COVID-19, given the implications for the healthcare system and social security, both of which are already profoundly affected by the pandemic itself. From this perspective, most persons with COVID-19 requiring medical consultation would not be expected to recover fully or resume working immediately after the end of the disease's acute phase. Instead, they will require a prolonged interdisciplinary healthcare approach focused on physical, mental, and social rehabilitation (*1*,*10*–*15*).

We did not perform genetic sequencing of the severe acute respiratory syndrome coronavirus 2 detected in our patients. Therefore, we cannot evaluate whether different virus variants might affect the occurrence of long-term symptoms among survivors differently.

One of the strengths of our study was our systematic follow-up on participants with prespecified instruments, which ensured high-quality and consistent data. A novelty of the study was that we were able to recruit patients who had mild or moderate COVID-19, which is less common in other studies.

A limitation of our study was the small sample size; the results therefore cannot be generalized to the wider population. Another limitation is the lack of a control group for comparison and selection bias. Most likely, many patients who did not attend a medical consultation after being discharged from the hospital experienced only mild or no prolonged

symptoms at all. The same can be said for healthcare workers who were affected by COVID-19 but did not seek medical consultation. The actual prevalence of long-term symptoms among the reference population is unknown, and our data probably overestimate that prevalence.

In summary, it is likely that a substantial proportion of patients surviving COVID-19 will experience long-term symptoms requiring prolonged care, even after mild to moderate disease. These symptoms might negatively affect patients' quality of life and represent an additional burden for healthcare services and social security.

Acknowledgments

We thank the outpatient post–COVID-19 team (MINC) that gave us access to patients and offered the space for recruitment of study subjects and data collection; the surviving patients of COVID-19 who contributed to our work; and the research team of the Department of Social Medicine (Public Health) of the Ribeirão Preto Medical School, University of São Paulo (FMRP/USP). We would like to thank Editage (https://www.editage.com) for their excellent input on the English language editing.

This work was partially supported by the Fundação de Apoio ao Ensino, Pesquisa e Assistência do Hospital das Clínicas da Faculdade de Medicina de Ribeirão Preto da Universidade de São Paulo (FAEPA), and National Council for Scientific and Technological Development (CNPq). L.P.B. was granted a scholarship from CNPq to work on Covid-19 research activities (process no. 309098/2020-3).

About the Author

Dr. Bonifácio is a physiotherapist and current postdoctoral student at the Department of Social Medicine, Ribeirão Preto Medical School, University of São Paulo, Brazil. Her primary areas of interest are primary care, public health and epidemiology, reproductive health, women's and men's health and gender and masculinities, orthopedics, and traumatology.

References

1. Nalbandian A, Sehgal K, Gupta A, Madhavan MV, McGroder C, Stevens JS, et al. Post-acute COVID-19 syndrome. Nat Med. 2021;27:601–15. https://doi.org/10.1038/s41591-021-01283-z
2. World Health Organization. Emergency use ICD codes for COVID-19 disease outbreak [cited 2021 May 3]. https://www.who.int/standards/classifications/classification-of-diseases/emergency-use-icd-codes-for-covid-19-disease-outbreak
3. Havervall S, Rosell A, Phillipson M, Mangsbo SM, Nilsson P, Hober S, et al. Symptoms and functional impairment assessed 8 months after mild COVID-19 among health care workers. JAMA. 2021;325:2015–6. https://doi.org/10.1001/jama.2021.5612
4. Instituto Brasileiro de Geografia e Estatística. Geographic and statistical overview of Ribeirão Preto [in Portuguese] [cited 2021 Mar 29]. https://cidades.ibge.gov.br/brasil/sp/ribeirao-preto/panorama
5. World Health Organization. Global COVID-19 clinical platform case report form (CRF) for post COVID condition (Post COVID-19 CRF) [cited 2020 Oct 20]. https://cdn.who.int/media/docs/default-source/3rd-edl-submissions/who_crf_postcovid_feb9_2021.pdf
6. Harris PA, Taylor R, Thielke R, Payne J, Gonzalez N, Conde JG. Research electronic data capture (REDCap)—a metadata-driven methodology and workflow process for providing translational research informatics support. J Biomed Inform. 2009;42:377–81. https://doi.org/10.1016/j.jbi.2008.08.010
7. The WHOQOL Group. Development of the World Health Organization WHOQOL-BREF quality of life assessment. Psychol Med. 1998;28:551–8. https://doi.org/10.1017/S0033291798006667
8. Fleck MP, Louzada S, Xavier M, Chachamovich E, Vieira G, Santos L, et al. Application of the Portuguese version of the abbreviated instrument of quality of life WHOQOL-bref [in Portuguese]. Rev Saude Publica. 2000;34:178–83. https://doi.org/10.1590/S0034-89102000000200012
9. Pedroso B, Pilatti LA, Gutierrez GL, Picinin CT. Calculating WHOQOL-BREF scores and descriptive statistics through Microsoft Excel [in Portuguese]. Revista Brasileira de Qualidade de Vida. 2010;2:31–6. https://doi.org/10.3895/S2175-08582010000100004
10. Centers for Disease Control and Prevention. COVID-19: Long-term effects [cited 2021 May 3]. https://www.cdc.gov/coronavirus/2019-ncov/long-term-effects/index.html
11. Nature. Long COVID: let patients help define long-lasting COVID symptoms [editorial]. Nature. 2020;586:170. https://doi.org/10.1038/d41586-020-02796-2
12. Nehme M, Braillard O, Chappuis F, Courvoisier DS, Guessous I; CoviCare Study Team. Prevalence of symptoms more than seven months after diagnosis of symptomatic COVID-19 in an outpatient setting. Ann Intern Med. 2021;174:1252–60. https://doi.org/10.7326/M21-0878
13. Seeßle J, Waterboer T, Hippchen T, Simon J, Kirchner M, Lim A, et al. Persistent symptoms in adult patients one year after COVID-19: a prospective cohort study. Clin Infect Dis. 2021 Jul 5 [Epub ahead of print].
14. Antwi-Amoabeng D, Beutler BD, Singh S, Taha M, Ghuman J, Hanfy A, et al. Association between electrocardiographic features and mortality in COVID-19 patients. Ann Noninvasive Electrocardiol. 2021;26:e12833. https://doi.org/10.1111/anec.12833
15. Dixit NM, Churchill A, Nsair A, Hsu JJ. Post-acute COVID-19 Syndrome and the cardiovascular system: what is known? Am Heart J Plus. 2021;5:100025.

Address for correspondence: Fernando Bellissimo-Rodrigues or Lívia Pimenta Bonifácio, Social Medicine Department, Ribeirão Preto Medical School (USP), Campus Universitário, Monte Alegre 14048-900, Ribeirão Preto, São Paulo, Brazil; email: fbellissimo@usp.br or livia_pb@usp.br

Ebola Virus Glycoprotein IgG Seroprevalence in Community Previously Affected by Ebola, Sierra Leone

Daniela Manno, Philip Ayieko, David Ishola, Muhammed O. Afolabi, Baimba Rogers, Frank Baiden, Alimamy Serry-Bangura, Osman M. Bah, Brian Köhn, Ibrahim Swaray, Kwabena Owusu-Kyei, Godfrey T. Otieno, Dickens Kowuor, Daniel Tindanbil, Elizabeth Smout, Cynthia Robinson, Babajide Keshinro, Julie Foster, Katherine Gallagher, Brett Lowe, Macaya Douoguih, Bailah Leigh, Brian Greenwood, Deborah Watson-Jones

We explored the association of Ebola virus antibody seropositivity and concentration with potential risk factors for infection. Among 1,282 adults and children from a community affected by the 2014–2016 Ebola outbreak in Sierra Leone, 8% were seropositive for virus antibodies but never experienced disease symptoms. Antibody concentration increased with age.

Ebola virus (EBOV) antibodies have been found in populations that have never experienced documented Ebola outbreaks and in persons who reported no history of Ebola virus disease (EVD) (*1*). The clinical significance of these findings is unknown. We conducted a cross-sectional study in healthy adults and children from a population affected by the 2014–2016 EVD outbreak in Sierra Leone and explored the association of antibody seropositivity and concentration with potential risk factors for EBOV infection.

Author affiliations: London School of Hygiene and Tropical Medicine, London, UK (D. Manno, P. Ayieko, D. Ishola, M.O. Afolabi, F. Baiden, B. Köhn, K. Owusu-Kyei, G.T. Otieno, D. Kowuor, D. Tindanbil, E. Smout, J. Foster, K. Gallagher, B. Lowe, B. Greenwood, D. Watson-Jones); Mwanza Intervention Trials Unit, National Institute for Medical Research, Mwanza, Tanzania (P. Ayieko, D. Watson-Jones); University of Sierra Leone College of Medicine and Allied Health Sciences, Freetown, Sierra Leone (B. Rogers, A. Serry-Bangura, O.M. Bah, I. Swaray, B. Leigh); Janssen Vaccines and Prevention, Leiden, the Netherlands (C. Robinson, B. Keshinro, M. Douoguih)

DOI: https://doi.org/10.3201/eid2803.211496

The Study

We conducted a seroprevalence study in Kambia District, Sierra Leone, during March 2016–June 2018. We nested the study within the screening visit of the EBOVAC-Salone (https://www.ebovac.org) randomized controlled trial (RCT), which evaluated the safety and immunogenicity of the 2-dose Ad26.ZEBOV, MVA-BN-Filo Ebola vaccine regimen (ClinicalTrials.gov, no. NCT02509494) (*2*,*3*). Persons who reported having a previous EVD diagnosis and persons who previously received a candidate Ebola vaccine were ineligible for the RCT, and we excluded them from the seroprevalence study. We recruited adults first, then recruited children in 3 age cohorts: 12–17, 4–11, and 1–3 years of age.

We measured IgG to EBOV glycoprotein (GP) by using the Filovirus Animal Non-Clinical Group (FANG) ELISA (Q2 Solutions Vaccine Testing Laboratory, https://www.q2labsolutions.com). We determined seropositivity by using a cutoff of >607 ELISA units (EU)/mL, which was calculated previously in an EBOV-naive population in West Africa (*4*) (Appendix, https://wwwnc.cdc.gov/EID/article/28/3/21-1496-App1.pdf).

Among 1,282 study participants (Figure), 687 (53.6%) were <18 years of age (median 16 years, IQR 7–25 years), and 827 (64.5%) were male. Among 1,272 participants with antibody results, we considered 107 (8.4%, 95% CI 7.0%–10.0%) seropositive for EBOV GP IgG by using the prespecified cutoff.

Risk factor analysis showed that, after adjusting for age and sex, the only characteristic associated with seropositivity was living in a household compound with ≥1 pigs during the outbreak (adjusted odds ratio [OR] 4.5, 95% CI 1.6–13.0; p = 0.01) (Tables 1, 2; Appendix

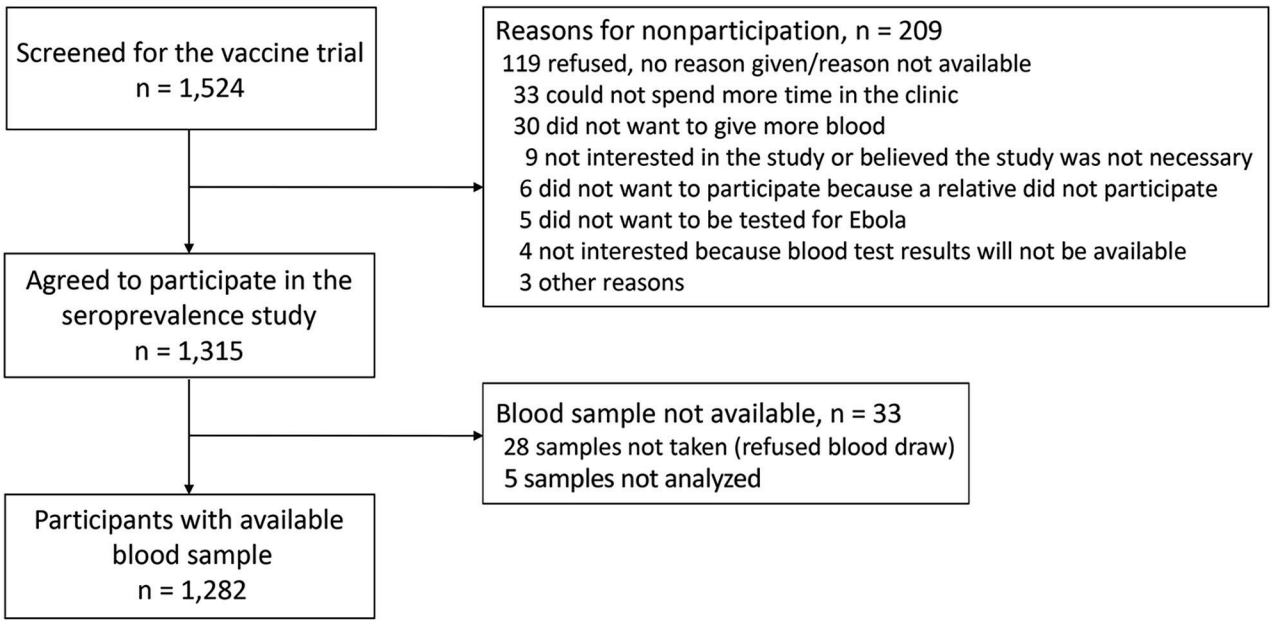

Figure. Flow chart of participants screened for the Ebola virus vaccine trial and seroprevalence study in a community affected by the 2014–2016 Ebola outbreak, Sierra Leone.

Table 1). The EBOV antibody geometric mean concetration (GMC) was higher in participants ≥5 years of age than in younger children (Appendix Table 1). After adjusting for age and sex, only pig ownership remained associated with antibody concentration (adjusted GMC ratio 3.0, 95% CI 1.5–5.9; p<0.01) (Table 2).

The 8.4% seroprevalence in our study is within the range of estimates (0%–24%) from prior studies; however, this range is large because of the use of different assays, different seroprevalence thresholds, different levels of exposure to EVD cases, and studies undertaken in different geographic areas and at different timepoints relative to reported outbreaks (*1*). Our estimate is similar to the baseline EBOV antibody seroprevalence (4.0%) measured in another Ebola vaccine trial conducted in Liberia during the 2014–2016 EVD outbreak that used the same assay and cutoff (*5*).

Similar to results from previous studies, our findings showed a statistically significant increase in EBOV antibody concentration with participants' age, possibly because of increased exposure of older age groups to EBOV or to other infections that could induce cross-reactive antibodies to the EBOV GP (*6*,*7*). Potential exposures to EVD, such as healthcare work, contact with EVD cases, and funeral attendance, which were associated with EBOV transmission in other studies (*8*), were not associated with EBOV antibody seropositivity or concentration in our study. However, few participants reporting those risk factors, and our study might have lacked the power to detect such associations.

We found an independent association of both EBOV antibody seropositivity and concentration with residence in a household compound that owned ≥1 pigs during the Ebola outbreak. Pigs can be experimentally infected with EBOV and can transmit the virus to nonhuman primates (*9*). EBOV-specific antibodies have been found in pigs in Sierra Leone and Guinea, suggesting that pigs can be naturally infected by EBOV (*10*,*11*). Pigs in the Philippines have been found to be naturally infected with Reston virus, an EBOV strain that is not known to cause disease in humans. Reston virus–specific antibodies were found in healthy farmers in contact with the infected pigs, suggesting potential transmission from pigs to humans (*12*). However, we found no association of EBOV antibody with having other domestic animals, in particular dogs, which also could be infected with EBOV (*13*,*14*).

One strength of our study is that we conducted our study in an area with prolonged EBOV transmission during the 2014–2016 EVD outbreak. Further, we explored a wide range of potential risk factors for EBOV acquisition, and we used the FANG ELISA, which has been proven to be more precise and accurate than a commercial alternative (*4*).

The first limitation of our study is that the parent RCT did not require random sampling of potential participants' households, which could have affected the generalizability of our results to the

general population. The RCT recruitment was age-staggered, and the youngest age cohort (1–3 years of age) was recruited >2 years after the EVD outbreak ended. However, a sensitivity analysis suggested that year of recruitment had a negligible confounding effect on the lower EBOV antibody concentrations observed in the youngest children (Appendix Table 2). Our study was conducted at the end of the 2014–2016 EVD outbreak in Sierra Leone, when public health measures to contain EBOV transmission had been in place for several months and the population had received messages about EVD prevention. This factor could have caused an underreporting of behaviors considered to put persons at risk for EVD. For example, hunting and consumption of bushmeat was rarely reported by our participants, in contrast with some reports that describe frequent hunting and bushmeat consumption in West Africa (*15*). The association of both antibody seropositivity and concentration with pig ownership is based on only 18 participants who reported keeping ≥1 pigs in their household compound at the time of the

Table 1. Potential EVD exposure in community or work during the 2014–2016 EVD outbreak and antibody seropositivity and GMC among participants in a study of EBOV GP–specific binding antibody seropositivity, Sierra Leone*

Risk factors	No. (%), n = 1,282	No. seropositive/ no. tested (%)	OR (95% CI)	Adjusted OR (95% CI)†	GMC, EU/mL (95% CI)	GMC ratio (95% CI)	Adjusted GMC ratio (95% CI)†
Living in a village or town with Ebola cases, n = 1,281							
N	199 (15.5)	10/198 (5.1)	Referent, p = 0.049	Referent, p = 0.125	49 (40–58)	Referent, p = 0.010	Referent, p = 0.882
Y	1,082 (84.5)	97/1,073 (9.0)	1.9 (1.0–3.6)	1.7 (0.8–3.3)	65 (60–71)	1.3 (1.1–1.6)	1.0 (0.8–1.3)
Knowing someone who had Ebola							
No, don't know	1,044 (81.4)	82/1,036 (7.9)	Referent, p = 0.193		61, 56–67)	Referent, p = 0.204	
Y	238 (18.6)	25/236 (10.6)	1.4 (0.9–2.2)		70 (57–85)	1.1 (0.92–1.4)	
No. EVD cases known by participant							
0	1,044 (81.4)	82/1,036 (7.9)	Referent, p = 0.55		61 (56–67)	Referent, p = 0.382	
1	125 (9.8)	13/125 (10.4)	1.4 (0.7–2.5)		64 (49–85)	1.1 (0.8–1.4)	
2–3	66 (5.2)	8/65 (12.3)	1.6 (0.8–3.5)		84 (57–124)	1.4 (0.9–2.0)	
>3	47 (3.7)	4/46 (8.7)	1.1 (0.4–3.2)		66 (44–99)	1.1 (0.7–1.6)	
Closest relationship with an EVD case, n = 1,280							
No relationship‡	1,044 (81.5)	82/1,036 (7.9)	Referent, p = 0.197		61, 56–67)	Referent, p = 0.259	
Close family§	27 (2.1)	1/27 (3.7)	0.5 (0.1–3.3)		52 (33–81)	0.9 (0.5–1.3)	
Other relative	52 (4.1)	6/51 (11.8)	1.6 (0.6–3.7)		64 (42–96)	1.0 (0.7–1.6)	
Friend	59 (4.6)	4/59 (6.8)	0.8 (0.3–2.4)		64 (45–91)	1.1 (0.7–1.5)	
Community member	98 (7.7)	14/97 (14.4)	2.0 (1.1–3.7)		86 (62–120)	1.4 (1.0–2.0)	
Living in the same household with an EVD case, n = 1,280							
N	1,269 (99.1)	107/1,260 (8.5)	–		63 (58–68)	Referent, p = 0.814	
Y	11 (0.9)	0/10 (0.0)	–		56 (31–102)	0.9 (0.5–1.6)	
Caring for an EVD case, n = 1,281							
N	1,272 (99.3)	107/1,262 (8.5)	–		63 (58–68)	Referent, p = 0.600	
Y	9 (0.7)	0/9 (0.0)	–		48 (24–98)	0.8 (0.4–1.6)	
Direct body contact with an EVD case, n = 1,281							
N	1,275 (99.5)	107/1,265 (8.5)	–		62 (57–67)	Referent, p = 0.640	
Y	6 (0.5)	0/6 (0.0)	–		83 (28–242)	1.3 (0.5–3.9)	
Attending a funeral of an EVD case							
N	1,263 (98.5)	105/1,254 (8.4)	Referent, p = 0.691		62 (57–67)	Referent, p = 0.346	
Y	19 (1.5)	2/18 (11.1)	1.4 (0.3–6.0)		87 (37–204)	1.4 (0.6–3.3)	
Healthcare frontline worker during EVD outbreak							
No, NA¶	1,254 (97.8)	105/1,244 (8.4)	Referent, p = 0.802		63 (58–69)	Referent, p = 0.798	
Y	28 (2.2)	2/28 (7.1)	0.8 (0.2–3.6)		58 (36–93)	0.9 (0.6–1.5)	

*Seropositivity defined as >607 EU/mL. EBOV GP–specific binding antibodies were indeterminate in 10 participants. p values calculated by using likelihood ratio test. EBOV GP, Ebola virus glycoprotein; EU, ELISA units; EVD, Ebola virus disease; GMC, geometric mean concentration; NA, not applicable; OR, odds ratio.
†Adjusted for age and sex.
‡Participant did not know anyone with Ebola.
§Participant was the parent or child or spouse or sibling of an EVD case.
¶Not applicable because participant was a child or did not have a job.

Table 2. Potential risk factors for transmission of Ebola virus from animals during the 2014–2016 EVD outbreak and antibody seropositivity and GMC among participants in a study of EBOV GP–specific binding antibody seropositivity, Sierra Leone*

Risk factors	No. (%), n = 1,282	No. seropositive/ no. tested (%)	OR (95% CI)	Adjusted OR (95% CI)†	GMC, EU/mL (95% CI)	GMC ratio (95% CI)	Adjusted GMC ratio (95% CI)†
Number of domestic animals in the participant's compound							
0	503 (39.2)	45/498 (9.0)	Referent, p = 0.558		59 (51–67)	Referent, p = 0.462	
1–5	374 (29.2)	33/371 (8.9)	1.0 (0.6–1.6)		65 (55–75)	1.1 (0.9–1.3)	
>5	405 (31.6)	29/403 (7.2)	0.8 (0.5–1.3)		66 (57–76)	1.1 (0.9–1.3)	
Having the following domestic animals in the compound‡							
Dog							
N	1,116 (87.1)	90/1,107 (8.1)	Referent, p = 0.349		66 (52–84)	Referent, p = 0.559	
Y	165 (12.9)	17/164 (10.4)	1.3 (0.8–2.3)		62 (57–67)	1.1 (0.8–1.4)	
Cat							
N	951 (74.2)	80/943 (8.5)	Referent, p = 0.887		61 (56–67)	Referent, p = 0.400	
Y	330 (25.8)	27/328 (8.2)	1.0 (0.6–1.5)		66 (56–78)	1.1 (0.9–1.3)	
Goat, sheep							
N	870 (67.9)	76/863 (8.8)	Referent, p = 0.465		62 (56–68)	Referent, p = 0.781	
Y	411 (32.1)	31/408 (7.6)	0.9 (0.6–1.3)		62 (57–67)	1.0 (0.9–1.2)	
Pig							
N	1,263 (98.6)	102/1,253 (8.1)	Referent, p = 0.015	Referent, p = 0.014	61 (57–67)	Referent, p<0.001	Referent, p = 0.001
Y	18 (1.4)	5/18 (27.8)	4.3 (1.5–12.4)	4.5 (1.6–13.0)	200 (93–431)	3.3 (1.5–7.1)	3.0 (1.5–5.9)
Other							
N	825 (64.4)	73/817 (8.9)	Referent, p = 0.370		61 (55–68)	Referent, p = 0.513	
Y	456 (35.6)	34/454 (7.5)	0.8 (0.5–1.3)		65 (57–74)	1.1 (0.9–1.3)	
Touching sick or dead domestic animals							
N	1,253 (97.7)	106/1,243(8.5)	Referent, p = 0.275		63 (58–68)	Referent, p = 0.824	
Y	29 (2.3)	1/29 (3.5)	0.4 (0.1–2.8)		59 (36–97)	0.9 (0.6–1.6)	
Hunting for wild animals§							
N	1,261 (99.3)	105/1,251(8.4)	Referent, p = 0.779		63 (58–68)	Referent, p = 0.859	
Y	9 (0.7)	1/9 (11.1)	1.4 (0.2–11.0)		57 (17–191)	0.9 (0.3–3.1)	
Touching sick or dead wild animals							
N	1,277 (99.6)	106/1,267 (8.4)	Referent, p = 0.419		62 (58–68)	Referent, p = 0.825	
Y	5 (0.4)	1/5 (20.0)	2.7 (0.3–24.7)		54 (8–369)	0.9 (0.1–5.9)	
Consuming bushmeat							
N	1,275 (99.4)	106/1,265 (8.4)	Referent, p = 0.606		62 (58–68)	Referent, p = 0.962	
Y	7 (0.6)	1/7(14.3)	1.8 (0.2–15.3)		61 (14–274)	1.0 (0.2–4.4)	

*Seropositivity defined as >607 EU/mL. EBOV GP–specific binding antibodies were indeterminate in 10 participants. p values calculated by using likelihood ratio test. EBOV, Ebola virus; EU, ELISA units; GMC, geometric mean concentration; GP, glycoprotein; OR, odds ratio.
†Adjusted for age and sex.
‡Participants could indicate >1 type of domestic animal.
§Types of wild animals hunted by participants who answered yes included monkeys, duiker antelopes, bats, and rodents.

outbreak. This association could have occurred by chance, although the evidence of an association is quite strong. The observed association also could be confounded by unrecorded risk factors among participants who also kept pigs, such as EBOV transmission clustering in participants from a household that also owned pigs. However, that possibility seems unlikely because none of the seropositive participants who owned pigs reported contact with an EVD case, and these participants all came from different households. Finally, we are not able to determine whether EBOV antibody seropositivity in this setting reflects true asymptomatic infection because we cannot exclude underreporting of earlier EVD symptoms and we have not yet investigated cross-reactivity with other viral infections. Whether EBOV seropositivity reflects acquired immunity that might provide some protection against future EBOV infections also is unclear.

Our findings suggest that the role of pigs as potential, occasional reservoirs of EBOV needs to be investigated further. The presence of antibodies binding the EBOV GP could also suggest circulation of other infectious agents, probably viruses, inducing cross-reactivity with the EBOV GP, but this possibility needs further investigation.

Conclusions

The incidence of EBOV infection during the 2014–2016 EVD outbreak in Sierra Leone could have been higher than previously reported; 8.4% of adults and children from a community affected by the outbreak who never experienced symptoms of EVD had serologic responses to EBOV above a cutoff threshold. Our study suggests that EBOV might cause asymptomatic infection, but whether underreporting of symptoms, FANG assay specificity, or exposure to other viral infections that could generate cross-reactive antibodies also contributed to the results is unclear. These questions would benefit from further investigation to help define the extent of future EVD outbreaks. Countries at high risk for EVD outbreaks should be aware of the risk of asymptomatic or paucisyntomatic infections.

Acknowledgments

We thank Christian Hansen for support in the sample size calculation for the study protocol and Kathy Baisley for advice on the statistical analysis. We thank Viki Bockstal and Kerstin Luhn for advice on the interpretation of FANG ELISA results. We thank the site study team, including study physicians and other clinicians; the data management team; the quality assurance, social science, community engagement teams, the laboratory team, the College of Medicine and Allied Health Sciences (COMAHS) and the London School of Hygiene & Tropical Medicine (LSHTM) project management and administrative teams; and colleagues from World Vision, GOAL, and the Ebola Vaccine Deployment, Acceptance and Compliance (EBODAC) project. We thank all the study participants and their families. We also thank the other EBOVAC 1 Consortium partners, the University of Oxford, and Institut National de la Santé et de la Recherche Médicale (INSERM) in France for their support for this study.

This study was funded by the Innovative Medicines Initiative 2 Joint Undertaking (grant no. 115854, EBOVAC 1 project).

About the Author

Dr. Manno is a clinical epidemiologist and assistant professor at the London School of Hygiene and Tropical Medicine. Her primary research interests include epidemiological studies and clinical trials in infectious diseases.

References

1. Bower H, Glynn JR. A systematic review and meta-analysis of seroprevalence surveys of ebolavirus infection. Sci Data. 2017;4:160133. https://doi.org/10.1038/sdata.2016.133
2. Ishola D, Manno D, Afolabi MO, Keshinro B, Bockstal V, Rogers B, et al. Safety and long-term immunogenicity of the two-dose heterologous Ad26.ZEBOV and MVA-BN-Filo Ebola vaccine regimen in adults in Sierra Leone: a combined open-label, non-randomised stage 1, and a randomised, double-blind, controlled stage 2 trial. Lancet Infect Dis. 2022;22:97–109. https://doi.org/10.1016/S1473-3099(21)00125-0
3. Afolabi MO, Ishola D, Manno D, Keshinro B, Bockstal V, Rogers B, et al. Safety and immunogenicity of the two-dose heterologous Ad26.ZEBOV and MVA-BN-Filo Ebola vaccine regimen in children in Sierra Leone: a randomised, double-blind, controlled trial. Lancet Infect Dis. 2022;22:110–22. https://doi.org/10.1016/S1473-3099(21)00128-6
4. Logue J, Tuznik K, Follmann D, Grandits G, Marchand J, Reilly C, et al. Use of the Filovirus Animal Non-Clinical Group (FANG) Ebola virus immuno-assay requires fewer study participants to power a study than the Alpha Diagnostic International assay. J Virol Methods. 2018;255:84–90. https://doi.org/10.1016/j.jviromet.2018.02.018
5. Kennedy SB, Bolay F, Kieh M, Grandits G, Badio M, Ballou R, et al.; PREVAIL I Study Group. Phase 2 placebo-controlled trial of two vaccines to prevent ebola in Liberia. N Engl J Med. 2017;377:1438–47. https://doi.org/10.1056/NEJMoa1614067
6. Mulangu S, Borchert M, Paweska J, Tshomba A, Afounde A, Kulidri A, et al. High prevalence of IgG antibodies to Ebola virus in the Efé pygmy population in the Watsa region, Democratic Republic of the Congo. BMC Infect Dis. 2016;16:263. https://doi.org/10.1186/s12879-016-1607-y
7. Bouree P, Bergmann JF. Ebola virus infection in man: a serological and epidemiological survey in the Cameroons. Am J Trop Med Hyg. 1983;32:1465–6. https://doi.org/10.4269/ajtmh.1983.32.1465
8. Brainard J, Hooper L, Pond K, Edmunds K, Hunter PR. Risk factors for transmission of Ebola or Marburg virus disease: a systematic review and meta-analysis. Int J Epidemiol. 2016;45:102–16. https://doi.org/10.1093/ije/dyv307
9. Weingartl HM, Embury-Hyatt C, Nfon C, Leung A, Smith G, Kobinger G. Transmission of Ebola virus from pigs to non-human primates. Sci Rep. 2012;2:811. https://doi.org/10.1038/srep00811
10. Fischer K, Jabaty J, Suluku R, Strecker T, Groseth A, Fehling SK, et al. Serological evidence for the circulation of ebolaviruses in pigs from Sierra Leone. J Infect Dis. 2018;218(suppl_5):S305–11. PubMed https://www.doi.org/10.1093/infdis/jiy330
11. Fischer K, Camara A, Troupin C, Fehling SK, Strecker T, Groschup MH, et al. Serological evidence of exposure to ebolaviruses in domestic pigs from Guinea. Transbound Emerg Dis. 2020;67:724–32. https://doi.org/10.1111/tbed.13391
12. Barrette RW, Metwally SA, Rowland JM, Xu L, Zaki SR, Nichol ST, et al. Discovery of swine as a host for the Reston ebolavirus. Science. 2009;325:204–6. https://doi.org/10.1126/science.1172705
13. Haun BK, Kamara V, Dweh AS, Garalde-Machida K, Forkay SSE, Takaaze M, et al. Serological evidence of Ebola virus exposure in dogs from affected communities in Liberia: A preliminary report. PLoS Negl Trop Dis. 2019;13(7):e0007614. PubMed https://doi.org/10.1371/journal.pntd.0007614
14. Fischer K, Suluku R, Fehling SK, Jabaty J, Koroma B, Strecker T, et al. Ebola virus neutralizing antibodies in dogs from Sierra Leone, 2017. Emerg Infect Dis. 2020;26:760–3. https://doi.org/10.3201/eid2604.190802
15. Luiselli L, Hema E, Segniagbeto G, Ouattara V, Eniang EA, Parfait G, et al. Bushmeat consumption in large urban centres in West Africa. Oryx. 2020;54:731–4.

Address for Correspondence: Daniela Manno, London School of Hygiene & Tropical Medicine, Keppel Street, London WC1E 7HT, UK; email: daniela.manno@lshtm.ac.uk

Effects of COVID-19 Pandemic Response on Service Provision for Sexually Transmitted Infections, HIV, and Viral Hepatitis, England

Holly D. Mitchell, Tatiana Garcia Vilaplana, Sema Mandal, Natasha Ratna, Megan Glancy, Ammi Shah, Ruth Simmons, Celia Penman, Freja Kirsebom, Annastella Costella, Alison E. Brown, Hamish Mohammed, Valerie Delpech, Katy Sinka,[1] Gwenda Hughes,[1] on behalf of the UK Health Security Agency National STI, HIV and Viral Hepatitis Surveillance Group[2]

Since the coronavirus disease pandemic response began in March 2020, tests, vaccinations, diagnoses, and treatment initiations for sexual health, HIV, and viral hepatitis in England have declined. The shift towards online and outreach services happened rapidly during 2020 and highlights the need to evaluate the effects of these strategies on health inequalities.

Beginning March 23, 2020, the UK government introduced social and physical distancing (SPD) measures to reduce transmission of severe acute respiratory syndrome 2 (SARS-CoV-2), and health staff were redeployed to the coronavirus disease (COVID-19) pandemic response. The staffing shift and SPD measures affected clinical services for sexually transmitted infections (STIs), HIV, and hepatitis A, B, and C (HAV, HBV, and HCV) provided through the National Health Service (*1*,*2*). We assessed the effects of COVID-19 measures in England on service provision in this area and on health outcomes for persons with STIs, HIV, or hepatitis.

The Study

In England, surveillance of STIs, HIV, and hepatitis relies on patient-level data on consultations, tests, diagnoses, vaccinations, treatment, and outcomes from sexual health services (SHS), general practitioners, hospital outpatient clinics, and drug treatment centers (*3*). Laboratories also submit patient-level reports of tests and diagnoses for hepatitis and chlamydia. Given the disruption in routine reporting in 2020 (only 71%–98% complete for STI and HIV data), when possible, we analyzed data from clinics and laboratories who provided complete reports for January–September in both 2019 and 2020.

Testing at SHS declined by 77%, from 95,455 to 22,332, for HIV and by 71%, from 391,006 to 112,441, for STIs during January–April 2020, and although there was a modest increase beginning in May, testing remained far lower than in 2019 (Figure 1). For January–September 2020 compared with the same period in 2019, overall numbers of tests were lower by 36% (768,216 vs. 494,433) for HIV and 28% (3,137,537 vs. 2,244,153) for STIs (Appendix, https://wwwnc.cdc.gov/EID/article/28/3/21-1998-App1.pdf). However, the proportion of tests accessed through internet services (self-sampling kits returned directly to the laboratory with results provided by text message, email, letter, or online) increased substantially beginning in April 2020 (Appendix). Internet services accounted for ≥63% of HIV and ≥51% of STI tests during April–September 2020, compared with 25% for HIV and 22% for STIs in 2019.

During January–April 2020, the largest proportional declines in testing occurred among persons 15–19 years of age (79% for HIV, 75% for STIs) and ≥45 years of age (80% for HIV, 76% for STIs); for persons 20–44 years of age, testing for HIV declined by 76% and for STIs by 70%. The 15–19- and ≥45-year age groups also showed the slowest relative recovery towards prepandemic levels of testing during June–September 2020. Over the same period, we observed larger proportional declines in testing among

Author affiliation: UK Health Security Agency, London, UK

DOI: https://doi.org/10.3201/eid2803.211998

[1]These senior authors contributed equally to this article.

[2]Additional group members who contributed are listed at the end of this article.

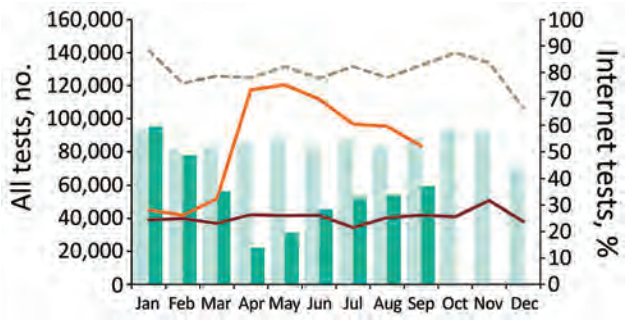

Figure 1. Total number of HIV tests provided through sexual health services (SHS) and proportion of those accessed through internet services, England, January 2019–September 2020. Bars compare HIV test data from SHS that reported complete data for January–September in both 2019 (light green) and 2020 (dark green). Dashed line represents the total number of HIV tests from all SHS reported in each month in 2019. Solid lines indicate the percentages of total tests accessed through the internet for 2019 (red) and 2020 (orange). Data are from routine specialist and nonspecialist SHS reporting to the GUMCAD STI Surveillance System.

heterosexual men (81% for HIV, 79% for STIs) and heterosexual or bisexual women (women who have sex with men or women; 76% for HIV, 75% for STIs) compared with gay, bisexual, and other men who have sex with men (MSM) (67% for HIV, 71% for STIs) and lesbian and other women who have sex exclusively with women (66% for HIV, 65% for STIs); recovery was slowest among heterosexual men. We observed the largest declines among persons of Asian (81% for HIV, 77% for STIs), Black (81% for HIV, 76% for STIs), and other (81% for HIV, 76% for STIs) races; persons of Black race showed the slowest recovery.

We also observed a sharp decline in the number of persons tested for hepatitis during January–April 2020: by 63% (from 4,295 to 1,610) for HAV, 61% (from 57,392 to 22,224) for HBV, and 74% (from 43,238 to 11,250) for HCV (Appendix). The number of persons tested for HCV in community drug treatment facilities showed the greatest decline (98%, from 3,324 to 74) and a slow recovery to prepandemic levels; testing was 58% lower in September 2020 than for 2019 (*3*).

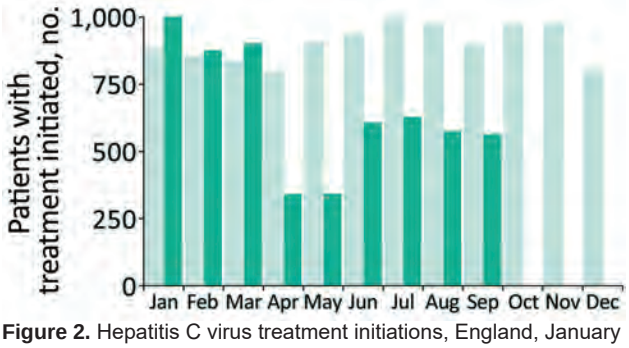

Figure 2. Hepatitis C virus treatment initiations, England, January 2019–September 2020. Data are from the National Health Service England Hepatitis C Patient Registry and Treatment Outcome system. Bars indicate the number of persons having treatment initiated by month for 2019 (light green) and 2020 (dark green).

Consistent with testing patterns, the number of diagnoses for HIV, STIs, and hepatitis declined during January–April 2020, followed by a partial recovery (Appendix Figure 1). Bacterial STI positivity (Appendix) increased during March and April 2020 (12% in January 2020 vs. 17% in April 2020) then returned to 2019 and early 2020 levels, whereas HIV test positivity peaked in April 2020 (0.20%) and remained at a higher level until September 2020 (0.09% vs 0.10% in September 2019). By contrast, HBV and HCV positivity declined during January–April 2020 (from 0.8% to 0.4% for HBV surface antigen and from 2.8% to 1.4% for HCV antibody); although there was a slight increase thereafter, positivity remained lower for the rest of 2020 than in 2019.

The number of first-dose vaccinations administered to MSM at SHS during January–April 2020 fell by 97% for HAV (from 841 to 22) and human papillomavirus (from 1,507 to 47) and by 96% (from 757 to 34) for HBV (Appendix Figure 2). A slight increase was reported beginning in May 2020, but rates for HAV, HBV, and HPV vaccinations were >50% lower in September 2020 than in September 2019.

HCV treatment initiations declined by 66% (from 1,004 to 341) during January–April 2020; although recovering slightly, the overall number of treatment initiations during January–September 2020 was 27% lower than in the same period in 2019 (Figure 2). We saw the largest relative declines for referrals from drug services and prisons, with some recovery during June–September 2020. Delays commonly occur between HCV diagnoses and treatment, so reductions in treatment initiations likely reflected reduced access to services rather than new diagnoses alone.

Conclusions

The COVID-19 pandemic response in England, including the introduction of SPD measures, coincided with a decline in the provision of, and access to, health services for STIs, HIV, and hepatitis. We observed the greatest decline in services that cannot be provided remotely, such as vaccination.

These findings are supported by staff and peer-support surveys in SHS and community drug treatment services (*4*,*5*). Some reduction in infections and need for services might be a consequence of reduced exposure because of compliance with SPD measures, leading to fewer opportunities for socializing and meeting sexual partners. The partial rebound in the summer of 2020 might indicate some recovery in

service provision and demand, with increased demand also influenced by changes in risk perception and behaviors. However, these levels remained below prepandemic levels.

Declines in the numbers of STI, HIV, and hepatitis tests (*6*–*8*) and diagnoses (*8*–*11*) after COVID-19 restrictions began have also been reported across Europe and elsewhere. Disruption in HCV treatment provision is of concern as direct-acting antivirals clear the virus, minimizing long-term harms. HCV treatment disruptions have also been reported in Spain (*12*) and Germany (*13*); in Germany, a minority of treatment providers also reported an increase in delayed diagnoses of liver decompensation and hepatocellular carcinoma (*13*).

During the early stages of the pandemic, there was a rapid shift in service delivery toward online, remote, and outreach provision in England; similar shifts were reported in the United States and Croatia (*14*,*15*). While enabling service access during the pandemic, it will be important to evaluate the effects on health inequalities of changing to remote services, because hepatitis, HIV, and STIs already disproportionately affect socially disadvantaged and excluded groups. Whereas our findings suggest SHS were accessed by some populations of need, such as MSM, the decline in access by young adults and persons of Asian, Black, or other races requires further investigation. Furthermore, early indications of adverse effects on access to harm reduction and bloodborne virus testing services for people who inject drugs is concerning and requires mitigating actions. The full effects of the COVID-19 pandemic response on STI, HIV, and hepatitis infection control, including efforts to eliminate HIV and hepatitis, and longer-term health outcomes will take time to emerge. These effects warrant close monitoring and assessment to ensure services are accessible and used by all who need them.

Additional members of the UK Health Security Agency National STI, HIV and Viral Hepatitis Surveillance Group who contributed to data collection, analysis and interpretation: Ana Harb, Galena Kuyumdzhieva, Tamilore Sonubi, Alireza Talebi, Stephen Duffell, Mateo Prochazka, Louise Thorn, Hannah Charles, Koye Balogun, Rebecca Wilkinson, Sara Croxford, Claire Edmundson, Mark McCall, Louise Logan, Adam Winter, Helen Harris, Kate Folkard, and Emily Phipps.

This work was conducted by the UK Health Security Agency (formerly Public Health England) as part of routine public health surveillance. No additional funds were received for this analysis.

No specific consent was required from the patients whose data were used in these analyses. The UK Health Security Agency has authority to handle patient data for public health monitoring and infection control under Regulation 3 of the Health Service (Control of Patient Information) Regulations 2002.

About the Author

Dr. Mitchell is an epidemiologist at the UK Health Security Agency. Her work focuses on surveillance and prevention of STIs and HIV.

References

1. Association of Directors of Public Health (UK). COVID-19 prioritisation of sexual and reproductive health service [cited 2020 Jul 21]. https://www.adph.org.uk/2020/04/covid-19-prioritisation-of-sexual-reproductive-health-services
2. Public Health England. People who inject drugs: HIV and viral hepatitis monitoring [cited 2020 July 28]. https://www.gov.uk/government/publications/people-who-inject-drugs-hiv-and-viral-hepatitis-monitoring.
3. Public Health England. COVID-19: impact on STIs, HIV and viral hepatitis [cited 2020 Dec 15]. https://www.gov.uk/government/publications/covid-19-impact-on-stis-hiv-and-viral-hepatitis
4. British Association for Sexual Health and HIV. BASHH COVID-19 survey finds over half of services have been closed [cited 2020 Jul 21]. https://www.bashh.org/news/news/bashh-covid-19-survey-finds-over-half-of-services-have-been-closed
5. Action HCV; Public Health England. The impact of lockdown on hepatitis C services in England. June 2020 [cited 2020 Nov 27]. http://www.hcvaction.org.uk/sites/default/files/HCV%20Action%20e-update%20July%202020.pdf
6. Pinto CN, Niles JK, Kaufman HW, Marlowe EM, Alagia DP, Chi G, et al. Impact of the COVID-19 pandemic on chlamydia and gonorrhea screening in the U.S. Am J Prev Med. 2021;61:386–93. https://doi.org/10.1016/j.amepre.2021.03.009
7. Simoes D, Stengaard AR, Combs L, Raben D. EuroTEST COVID-19 impact assessment consortium of partners. Impact of the COVID-19 pandemic on testing services for HIV, viral hepatitis and sexually transmitted infections in the WHO European region, March to August 2020. Euro Surveill. 2020;25:2001943. https://doi.org/10.2807/1560-7917.ES.2020.25.47.2001943
8. Darcis G, Vaira D, Moutschen M. Impact of coronavirus pandemic and containment measures on HIV diagnosis. Epidemiol Infect. 2020;148:e185. https://doi.org/10.1017/S0950268820001867
9. Crane MA, Popovic A, Stolbach AI, Ghanem KG. Reporting of sexually transmitted infections during the COVID-19 pandemic. Sex Transm Infect. 2021;97:101–2. https://doi.org/10.1136/sextrans-2020-054805
10. Apalla Z, Lallas A, Mastraftsi S, Giannoukos A, Noukari D, Goula M, et al. Impact of COVID-19 pandemic on STIs in Greece. Sex Transm Infect. 2022;98:70. https://doi.org/10.1136/sextrans-2021-054965
11. Chia CC, Chao CM, Lai CC. Diagnoses of syphilis and HIV infection during the COVID-19 pandemic in Taiwan. Sex Transm Infect. 2021;97:319. https://doi.org/10.1136/sextrans-2020-054802

12. Picchio CA, Valencia J, Doran J, Swan T, Pastor M, Martró E, et al. The impact of the COVID-19 pandemic on harm reduction services in Spain. Harm Reduct J. 2020;17:87. https://doi.org/10.1186/s12954-020-00432-w
13. Hüppe D, Niederau C, Serfert Y, Hartmann H, Wedemeyer H; für das DHC-R. Problems in treating patients with chronic HCV infection due to the COVID-19 pandemic and during the lockdown phase in Germany [in German]. Z Gastroenterol. 2020;58:1182–5.
14. Bogdanic N, Javoric I, Skugor SB, Zekan S, Lukas D, Benkovic I, et al. Initial impact of COVID-19 epidemic on HIV services in Croatia. Infektol Glas. 2020;40:79–80.
15. Melendez JH, Hamill MM, Armington GS, Gaydos CA, Manabe YC. Home-based testing for sexually transmitted infections: leveraging online resources during the COVID-19 pandemic. Sex Transm Dis. 2021;48:e8–10. https://doi.org/10.1097/OLQ.0000000000001309

Address for correspondence: Holly D. Mitchell, Blood Safety, Hepatitis, STI and HIV Division, Clinical and Public Health Group, UK Health Security Agency, 61 Colindale Ave, London NW9 5EQ, UK; email: holly.mitchell@phe.gov.uk

Who is this person?

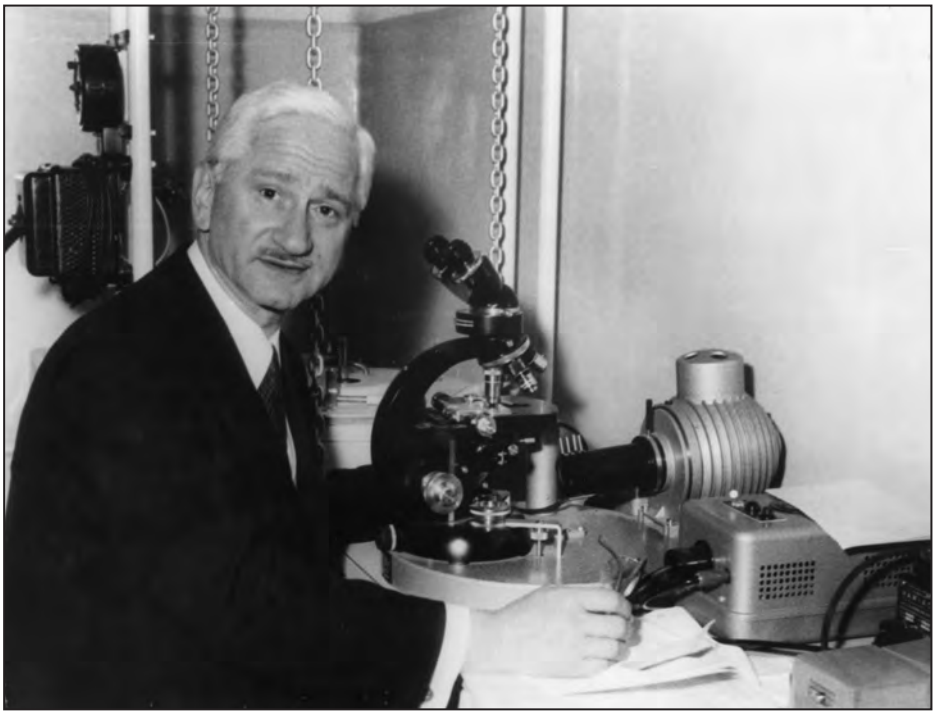

Here is a clue: he made the oral polio vaccine.

Who is he?

A) Edward Jenner

B) Albert Bruce Sabin

C) Robert Koch

D) Jonas Edward Salk

Decide first.
Then see next page for the answer.

Albert Bruce Sabin: The Man Who Made the Oral Polio Vaccine

Davide Orsini, Mariano Martini

This is a photograph of Albert Bruce Sabin (1906–1993), the man who made the oral polio vaccine. Sabin's name will always be associated with poliomyelitis, a disease that claimed millions of victims in the 20th century, particularly among children. At the beginning of the polio eradication initiative in 1988, the World Health Organization (WHO) estimated that ≈350,000 cases of paralytic polio were still occurring each year and that in the prevaccine era ≈650,000 cases occurred each year.

It was his mentor, William Hallock Park, famous for his research into a diphtheria vaccine, who in 1931 first urged Sabin to study poliomyelitis. In that year, Sabin had just finished his medical studies and polio was again raging in the United States, causing ≈17,000 cases of disease annually.

Indeed, in the first half of the 20th century, recurrent epidemics of poliovirus broke out during the hot season, striking thousands of children ≥2 years of age and also several adults. The most severely affected persons died or were left paralyzed, deformed, and unable to breathe outside an iron lung. Although a relatively low percentage of those affected died, millions of survivors carried the marks of the disease for the rest of their lives.

As the number of cases continued to grow, reaching a peak of ≈3,100 deaths and ≈21,000 cases of paralysis in 1952 in the United States, terror spread through a whole generation. According to the virologists, the only hope was to produce a vaccine. However, the first 2 attempts, in 1934 and 1935, failed dismally, resulting in a large number of victims.

In the middle of the 1930s, Sabin continued his studies on poliovirus, the etiologic agent of poliomyelitis, and in 1939 he realized that it was not a

respiratory virus but an enteric virus that lived and multiplied in the intestine. Moreover, he was able to demonstrate that contagion occurred through both the respiratory route from coughing and sneezing and the enteric route from fecal contamination.

Starting from this important discovery, Sabin set out to create a vaccine against poliovirus. The pathway was not simple, and he ran into numerous obstacles, not all of which were of a scientific nature. Moreover, his work led him to clash with Jonas Salk in one of the most celebrated scientific challenges of the 20th century.

Salk, a researcher at the University of Pittsburgh, created his inactivated polio vaccine (IPV) during 1952–1953. The vaccine contained wild polioviruses of all 3 serotypes that had been killed by means of

Author affiliation: University of Siena, Siena, Italy (D. Orsini); University of Genoa, Genoa, Italy (M. Martini)

DOI: https://doi.org/10.3201/eid2803.204699

formaldehyde; when injected intramuscularly, the vaccine elicited the production of antibodies, rendering recipients immune to the disease. On April 12, 1955, it was proclaimed that the battle against poliomyelitis had potentially been won thanks to Salk's vaccine. Unfortunately, however, 2 defective lots of the vaccine produced by Cutter Laboratories, a pharmaceutical company in Berkeley, California, contained residual live polioviruses, causing the so-called Cutter incident. In total, 192 paralytic polio cases occurred among vaccinated children and their family and community contacts, of whom 11 died. The government temporarily suspended the vaccination program until it was determined that Cutter vaccine should be permanently withdrawn and IPV from other manufacturers could be reinitiated safely.

Meanwhile, at the University of Cincinnati, Sabin was also at work on his vaccine. His approach, however, was completely different; he aimed to create a live attenuated vaccine for oral administration. This process marked the advent of the oral polio vaccine (OPV).

Sabin created his vaccine at the Children's Hospital in Cincinnati, where he subsequently tested it on 10,000 monkeys and 160 chimpanzees, as well as on himself, on his daughters, and on young volunteers recruited from among the inmates of the federal prison of Chillichote in Ohio. However, because the painful memory of the Cutter incident was still fresh and especially because the commercial stakes were high, the US government did not consent to large-scale field testing.

Subsequent testing of Sabin's vaccine was therefore carried out in the Soviet Union. During 1959–1961, millions of children received Sabin's vaccine (77 million in the Soviet Union alone). These early vaccination campaigns yielded very good results, just as the 1958 campaign had done in the Belgian Congo, a region that had been severely afflicted by the virus.

The mass vaccination campaign in the Soviet Union demonstrated high vaccine effectiveness and resulted in licensure of OPV in the United States in 1961. Subsequently, in the United States, OPV rapidly replaced IPV during the 1960s as the vaccine of choice. OPV was preferred over IPV because it induced both systemic and intestinal immunity, was easier to administer, and was less expensive than IPV. The main drawback of OPV is that, very rarely (in 1 case out of ≈750,000), Sabin viruses can mutate back to a more neurovirulent form and cause vaccine-associated paralytic polio.

In any case, Sabin's vaccine, which was economical to produce and very easy to administer on a sugar lump to children, came to be used worldwide in the 1960s. The method of administration of the Sabin vaccine inspired the popular song written by the Sherman brothers, featured in the film *Mary Poppins* whose refrain states, "Just a spoonful of sugar helps the medicine go down in a most delightful way." In 1961, OPV was adopted in the United States, where, in the meantime, thanks to Salk's vaccine, the spread of poliomyelitis had been markedly curbed.

Like Salk, Sabin did not patent his vaccine because he wanted it to be used as broadly as possible. "A lot of people insisted that I should patent the vaccine, but I didn't want to do that," he said. "It's my gift to all the world's children." Thus, he refused to exploit the vaccine commercially, so that its price could be kept as low as possible.

Sabin's preparation was subsequently adopted by WHO, becoming the mainstay of the worldwide vaccination campaign that enabled poliomyelitis to be eradicated from many countries. The last case in the United States was reported in 1979. In 1994, WHO certified the eradication of polio from the Americas, and in 2000 from 36 countries in the Western Pacific Region, including China and Australia. In 2002, Europe was certified polio-free, followed by the entire South-East Asia Region of WHO in 2014. After 2014, polio remained endemic in only 3 countries, Nigeria, Pakistan, and Afghanistan, until August 25, 2020, when Africa was declared totally polio-free.

Albert Bruce Sabin died in the hospital of Georgetown University in Washington on March 3, 1993, at the age of 86 years. Among the many accolades that he received, in 1970 he was awarded the National Medal of Science "for numerous fundamental contributions to the understanding of viruses and viral diseases, culminating in the development of the vaccine which has eliminated poliomyelitis as a major threat to human health."

About the Author

Dr. Orsini is director of the University Museum System of Siena and professor of history of medicine at the University of Siena, Siena, Italy. His research interests include history of medicine, hygiene, and epidemiology.

Dr. Martini is professor of medical history, medical humanities, public health ethics, and hygiene at the University of Genoa, Genoa, Italy, and section chief of StopTB Italia for the Leguria Region. His research interests include epidemiology, infectious diseases (especially tropical diseases), hygiene, medical history, public health, ethics, and vaccines.

Bibliography

1. Cosmacini G. Storia della medicina e della sanità nell'Italia contemporanea. Rome: Laterza; 1994.
2. Global Polio Eradication Initiative. Endemic countries [cited 2021 Dec 29]. http://polioeradication.org/where-we-work/polio-endemic-countries
3. Lashkevich VA. History of development of the live poliomyelitis vaccine from Sabin attenuated strains in 1959 and idea of poliomyelitis eradication [in Russian]. Vopr Virusol. 2013;58:4–10.
4. Nathanson N, Langmuir AD. The Cutter incident. Poliomyelitis following formaldehyde-inactivated poliovirus vaccination in the United States during the Spring of 1955. II. Relationship of poliomyelitis to Cutter vaccine. 1963. Am J Epidemiol. 1995;142:109–40, discussion 107–8. https://doi.org/10.1093/oxfordjournals.aje.a117611
5. National Science Foundation. National Medal of Science Albert B. Sabin (1906–1993) [cited 2021 Dec 27]. https://www.nsf.gov/news/special_reports/medalofscience50/sabin.jsp
6. Okayasu H, Sein C, Hamidi A, Bakker WA, Sutter RW. Development of inactivated poliovirus vaccine from Sabin strains: a progress report. Biologicals. 2016;44:581–7. https://doi.org/10.1016/j.biologicals.2016.08.005
7. World Health Organization. Global polio eradication initiative applauds WHO African region for wild polio-free certification [cited 2021 Dec 29]. https://www.who.int/news-room/detail/25-08-2020-global-polio-eradication-initiative-applauds-who-african-region-for-wild-polio-free-certification
8. World Health Organization. Poliomyelitis (polio) [cited 2021 Dec 29]. https://www.who.int/health-topics/poliomyelitis

Address for correspondence: Mariano Martini, University of Genoa, Department of Health Sciences (DISSAL), San Martino Polyclinc Hospital, Genoa, Largo R. Benzi, 10 Padiglione 3, 16132 Genoa, Italy; email: mariano.yy@gmail.comw

Mycobacterium leprae Infection in a Wild Nine-Banded Armadillo, Nuevo León, Mexico

Lucio Vera-Cabrera, Cesar J. Ramos-Cavazos, Nathan A. Youssef, Camron M. Pearce, Carmen A. Molina-Torres, Ramiro Avalos-Ramirez, Sebastien Gagneux, Jorge Ocampo-Candiani, Mercedes Gonzalez-Juarrero, Jorge A. Mayorga-Rodriguez, Leonardo Mayorga-Garibaldi, John S. Spencer, Mary Jackson, Charlotte Avanzi

Author affiliations: Servicio de Dermatología, Hospital Universitario "José E. González," Universidad Autónoma de Nuevo León, Monterrey, Mexico (L. Vera-Cabrera, C.J. Ramos-Cavazos, C.A. Molina-Torres, R. Avalos-Ramirez, J. Ocampo-Candiani); Mycobacteria Research Laboratories, Colorado State University, Fort Collins, Colorado, USA (N.A. Youssef, J.S. Spencer, C.M. Pearce, M. Gonzalez-Juarrero, M. Jackson, C. Avanzi); Swiss Tropical and Public Health Institute, Basel, Switzerland (S. Gagneux, C. Avanzi); University of Basel, Basel (S. Gagneux, C. Avanzi); Instituto Dermatológico de Jalisco "Dr. José Barba Rubio," Guadalajara, Mexico (J.A. Mayorga-Rodriguez, L. Mayorga-Garibaldi)

DOI: https://doi.org/10.3201/eid2803.211295

Nine-banded armadillos (*Dasypus novemcinctus*) are naturally infected with *Mycobacterium leprae* and are implicated in the zoonotic transmission of leprosy in the United States. In Mexico, the existence of such a reservoir remains to be characterized. We describe a wild armadillo infected by *M. leprae* in the state of Nuevo León, Mexico.

Nine-banded armadillos (*Dasypus novemcinctus*) can be naturally infected with *Mycobacterium leprae* and have been implicated in the zoonotic transmission of leprosy in the US states of Texas, Louisiana, Alabama, Georgia, and Florida (*1*,*2*). Despite Mexico falling within the armadillos' natural geographic habitat and the report of 182 new human leprosy cases in Mexico in 2019 (*3*), only 1 report of an armadillo infected with acid-fast bacilli has occurred since 1984, and the bacterial species in that case was never fully characterized (*4*).

In 2019, a nine-banded armadillo with ataxia, dyspnea, and adynamia was captured along the Pilon River in Montemorelos in the state of Nuevo León, Mexico. The animal was euthanized, and necropsy revealed granulomatous lesions in diverse organs and tissues (Appendix Figure 1, https://wwwnc.cdc.gov/EID/article/28/3/21-1295-App1.pdf). Histopathologic examination identified acid-fast bacilli in the liver, lung, heart, striated muscle, and ear; the bacilli were especially abundant in the spleen (Figure; Appendix Figure 2). We confirmed the presence of M. leprae in tissue by PCR testing of DNA extracted from the ear, liver, and lung by using the specific repetitive element RLEP (5) (Appendix). We used bacterial DNA extracted from the liver of the infected armadillo (strain A1), harboring the highest bacilli number by microscopy, for library preparation, followed by targeted enrichment using hybridization capture and whole-genome sequencing using NextSeq 500 (Illumina, https://www.illumina.com) (Appendix).After targeted enrichment using hybridization capture, we extracted bacterial DNA from the liver of the infected armadillo (strain A1), harboring the highest bacilli number by microscopy, and conducted sequencing by using NextSeq 500 (Illumina, https://www.illumina.com) (Appendix). The mean read coverage of 87× was sufficient for further comparative analysis at the single nucleotide level with other *M. leprae* isolates (Appendix Table 1). The armadillo-derived A1 strain belongs to genotype 3I-2, similar to other *M. leprae* isolates from the United States, Venezuela, Brazil, and Mexico (*1*).

Phylogenetically, A1 branches between the US human (NHDP-98) and animal–human (I30, NHDP-63, NHDP-55) *M. leprae* strains and closely clusters with EGG (*6*), a strain isolated in 2014 from a 70 year-old man with leprosy living in Nuevo León, Mexico (Appendix Figures 4, 5). Strains A1 and EGG share 9 polymorphisms when compared with the whole-genome sequences from 295 other *M. leprae* isolates and differed from each other by only 5 single-nucleotide polymorphisms (SNPs) (Appendix Figure 6).

We submitted DNA from *M. leprae* isolates recovered from the biopsies of additional leprosy patients from the states of Nuevo León (n = 9) and Jalisco (n = 2), Mexico, to partial whole-genome sequencing (n = 4) and PCR genotyping (n = 7) (Appendix Table 2, Figure 5.), We deciphered their clustering from previously described positions specific to genotypes 3I-1 and 3I-2 (*1*) as well as new informative SNPs specific to EGG and A1 (Appendix Table 2, Figure 6). Partial genome reconstruction for all 11 isolates revealed that 4 of them belong to genotype 3I-1, whereas 7 belong to genotype 3I-2. Within genotype 3I-1, isolates F2, F6, and F11 belong to a similar cluster, named 3I-1-c2 (Appendix Figure 4, 5). Within genotype 3I-2, 4 isolates (F1, F8, F14, and F23) belong to the same cluster, named 3I-2-c3, which also encompasses A1 and EGG. Of these isolates, only F1 shared an additional common SNP with A1 but differed >1 SNP (genome position 3232319) from it

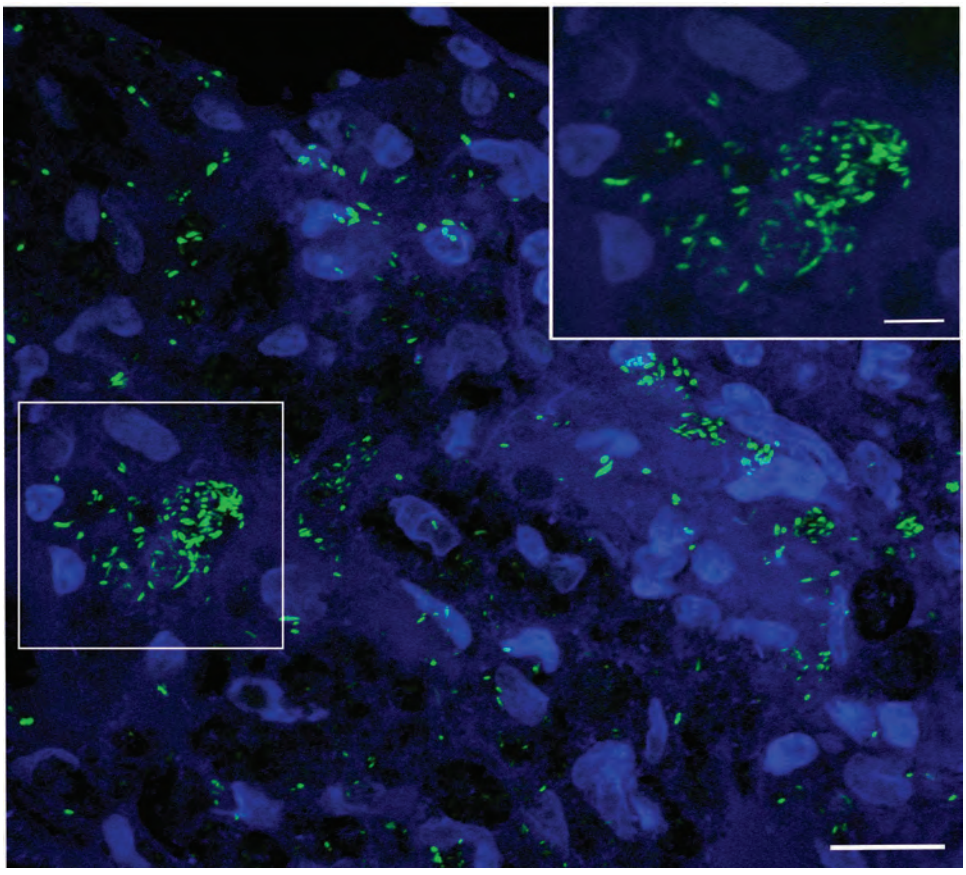

Figure. Identification and characterization of leprosy and *Mycobacterium leprae* acid-fast bacilli in the tissue in the wild nine-banded armadillo (*Dasypus novemcinctus*), Nuevo León, Mexico. SYBR gold staining shows a high density of bacilli in the spleen tissue organized in globi (boxed area at left and inset at right). Image is a merger of 16 images, 0.33 μm apart, in a z-stack taken with a 100× objective lens. Scale bars represent 20 μm (main image) and 5 μm (inset).

(Appendix Figures 4, 6). All patients infected with an *M. leprae* isolate from cluster 3I-2-c3 live in close vicinity (radius of ≈100 km) to the city of Montemorelos, where the infected armadillo was captured (Appendix Figure 5).

We describe the identification and genetic characterization of *Mycobacterium leprae* in a wild nine-banded armadillo in Mexico. In addition, we show that *M. leprae* strains belonging to different clusters are circulating in patients in Mexico. The state of Nuevo León, Mexico, shares a border with the US state of Texas, where a high density of leprosy-infected nine-banded armadillos have been reported (*4*,*7*). Nine-banded armadillos expanded their range into the United States in the mid-1800s from Mexico (*8*).

The *M. leprae* armadillo isolate from Mexico we describe belongs to the same genotype as patients and armadillo isolates from the United States but clusters separately. Isolate A1 further clusters with human isolates exclusively identified in Mexico thus far, with which it displays similar low genetic variation as observed between animal and human isolates in the United States (*1*). Therefore, our results raise concerns that wild-banded armadillos may, similarly to the situation in the United States, serve as reservoirs for the leprosy bacillus in the state of Nuevo León and call for additional surveillance across Mexico to assess the spread of the disease in the animal population and evaluate zoonosis risks associated with human contact with armadillos.

The existence of an animal reservoir hosting the leprosy bacillus in Mexico threatens the goal of leprosy elimination. In light of our results, we propose that interventions based on a One Health approach may be more efficient in achieving eradication of the disease.

Acknowledgments

We are grateful to all the patients and clinical staff who participated in the study. We thank Mark Stenglein, Marylee Kapuscinski, Mikaela Samsel for Illumina sequencing and technical support, and Dan Sloan for facilitating access to his laboratory.

This work was supported by the Fondation Raoul Follereau (grants to M.J. and C.A.), the Heiser Program of the New York Community Trust for Research in Leprosy (grant no. P18-000250 to J.S.S. and C.A.), a Fulbright Scholar to Brazil award 2019–2020 (grant to J.S.S.), the Association de Chimiothérapie Anti-Infectieuse of the Société Française de Microbiologie, the European Union's Horizon 2020 Research and Innovation Program (Marie

Sklodowska-Curie grant no. 845479 to C.A.), the National Institutes of Health (grant no. 1 S10 RR023735 [Zeiss LSM 510 Laser Scanning Microscope] to M.G.J.), and the Programa de Apoyo a la Investigación Científica y Tecnológica of the Universidad Autonoma de Nuevo León (grant no. SA-1900-21).

About the Author

Dr. Vera-Cabrera is a professor of dermatology at the Faculty of Medicine in University of Nuevo León, Monterrey, Mexico. His research interests include immune response against intracellular infectious agents and pathogenic mechanisms of bacteria of the genus *Mycobacterium* and *Nocardia*.

References

1. Truman RW, Singh P, Sharma R, Busso P, Rougemont J, Paniz-Mondolfi A, et al. Probable zoonotic leprosy in the southern United States. N Engl J Med. 2011;364:1626–33. https://doi.org/10.1056/NEJMoa1010536
2. Sharma R, Singh P, Loughry WJ, Lockhart JM, Inman WB, Duthie MS, et al. Zoonotic leprosy in the southeastern United States. Emerg Infect Dis. 2015;21:2127–34. https://doi.org/10.3201/eid2112.150501
3. World Health Organization. Global leprosy (Hansen disease) update, 2019: time to step-up prevention initiatives. Wkly Epidemiol Rec. 2020;36:417–40.
4. Ploemacher T, Faber WR, Menke H, Rutten V, Pieters T. Reservoirs and transmission routes of leprosy; a systematic review. PLoS Negl Trop Dis. 2020;14:e0008276. https://doi.org/10.1371/journal.pntd.0008276
5. Braet S, Vandelannoote K, Meehan CJ, Brum Fontes AN, Hasker E, Rosa PS, et al. The repetitive element RLEP is a highly specific target for detection of *Mycobacterium leprae*. J Clin Microbiol. 2018;56:e01924–17. https://doi.org/10.1128/JCM.01924-17
6. Benjak A, Avanzi C, Singh P, Loiseau C, Girma S, Busso P, et al. Phylogenomics and antimicrobial resistance of the leprosy bacillus *Mycobacterium leprae*. Nat Commun. 2018;9:352. https://doi.org/10.1038/s41467-017-02576-z
7. Feng X, Papeş M. Ecological niche modelling confirms potential north-east range expansion of the nine-banded armadillo (*Dasypus novemcinctus*) in the USA. J Biogeogr. 2015;42:803–7. https://doi.org/10.1111/jbi.12427
8. Taulman JF, Robbins LW. Range expansion and distributional limits of the nine-banded armadillo in the United States: an update of Taulman & Robbins (1996). J Biogeogr. 2014;41:1626–30. https://doi.org/10.1111/jbi.12319

Address for correspondence: Charlotte Avanzi, Department of Microbiology, Immunology and Pathology, Mycobacteria Research Laboratories, Colorado State University, 1682 Campus Delivery, Fort Collins, CO 80523-1682, USA; email: charlotte.avanzi@colostate.edu; Lucio Vera-Cabrera, Servicio de Dermatologia, Hospital Universitario, UANL, Madero y Gonzalitos s/n, Colonia Mitras Centro, Monterrey, Nuevo León, Mexico CP64460; email: luvera_99@yahoo.com

Sensitivity of *Mycobacterium leprae* to Telacebec

Ramanuj Lahiri, Linda B. Adams, Sangeeta Susan Thomas, Kevin Pethe

Author affiliations: US Department of Health and Human Services, Health Resources and Services Administration, Health Systems Bureau, National Hansen's Disease Program, Baton Rouge, Louisiana, USA (R. Lahiri, L.B. Adams); Lee Kong Chian School of Medicine, Nanyang Technological University, Singapore (S.S. Thomas, K. Pethe)

DOI: https://doi.org/10.3201/eid2803.210394

The treatment of leprosy is long and complex, benefiting from the development of sterilizing, rapidly-acting drugs. Reductive evolution made *Mycobacterium leprae* exquisitely sensitive to Telacebec, a phase 2 drug candidate for tuberculosis. The unprecedented potency of Telacebec against *M. leprae* warrants further validation in clinical trials.

Leprosy, also known as Hansen disease, is a chronic infectious disease caused primarily by *Mycobacterium leprae* and to a lesser extent by *M. lepromatosis* bacteria. Both species have a strong tropism for the Schwann cells; infection causes peripheral neuropathy, which leads to the characteristic deformities and disabilities. Despite successful implementation of multidrug therapies for the treatment of leprosy, >200,000 new cases were reported globally in 2019. Drug-resistant *M. leprae* strains, although rare, are emerging in several parts of the world (*1*). Therefore, newer rapidly acting bactericidal, orally bioavailable drugs are required to shorten treatment time and reduce transmission.

The high potency of drugs targeting the cytochrome *bcc:aa*$_3$ terminal oxidase (also known as QcrB inhibitors) against *M. ulcerans* has been reported (*3*). Of particular importance is the finding that a single dose of the drug candidate, Telacebec (Q203) (*3*), eradicates infection in a mouse model of Buruli ulcer (*4*). The potency of drugs targeting the cytochrome *bcc:aa*$_3$ terminal oxidase against *M. ulcerans* is explained by the absence of a functional cytochrome *bd* oxidase, an alternate terminal oxidase that limits the potency of telacebec in *M. tuberculosis* (*5*,*6*). Like *M. ulcerans*, *M. leprae* has lost the genes encoding the cytochrome *bd* oxidase and any other alternate terminal electron acceptors (*7*). Because *M. leprae* relies exclusively on the cytochrome *bcc:aa*$_3$ terminal oxidase for respiration, Scherr et al. hypothesized that telacebec and related QcrB

inhibitors could represent a new class of bactericidal drugs for leprosy (*2*).

The potency of telacebec was initially tested against extracellular *M. leprae* using a radio-respirometry assay to determine bacterial β-oxidation rate. This assay is used to assess viability of noncultivable *M. leprae* and measures cumulative production of CO_2 by the bacilli when palmitic acid is the sole carbon source (*8*). Telacebec at a concentration of 0.2 nM inhibited ≈90% ($p<0.001$) and 2 nM inhibited ≈99.9% ($p<0.0001$) of *M. leprae* metabolic activity after 3 days of incubation (Figure, panel A). In comparison, rifampin used at 2.0 μM inhibited only ≈45% ($p = 0.020$) of the metabolic activity compared with untreated control in the same time frame (Figure, panel A). We observed a similar trend after 7 days of incubation (Figure, panel A); 0.2 nM of telacebec was significantly more potent than 2 μM of rifampin at all tested concentrations in this assay. Telacebec was also active against intracellular *M. leprae* maintained in murine bone marrow–derived macrophages (*9*). Telacebec at 2.0 nM inhibited ≈97% ($p<0.001$ vs. untreated) of the metabolic activity of intracellular *M. leprae* in 3 days. Telacebec was also marginally potent against intracellular *M. leprae* at 0.2 nM but required longer incubation; we observed a statistically nonsignificant reduction of ≈33% ($p = 0.069$) after 3 days' incubation and a significant reduction of ≈40% ($p = 0.034$) after 7 days. Under similar experimental conditions, rifampin at 2.0 μM inhibited metabolic activity of intracellular *M. leprae* by ≈44% ($p = 0.025$) at day 3 and ≈72% ($p<0.001$) at day 7 compared with the untreated control group (Figure, panel B). Telacebec at 2 or 20 nM was more potent than rifampin in this assay as well.

The high nanomolar potency of telacebec against both intracellular and extracellular *M. leprae* prompted us to evaluate its efficacy in a mouse foot pad model of infection. We inoculated groups of 5 athymic nude mice with 3×10^7 viable *M. leprae* in both hind foot pads. At 8 weeks postinfection, we administered telacebec (2 mg/kg) or rifampin (10 mg/kg) by gavage as 1 dose, 5 consecutive daily doses, or 20 doses (5 days × 4 weeks). We harvested foot pads 4 weeks after completion of the drug treatment. Because *M. leprae* is noncultivable, we measured mycobacterial load using an established molecular method (*10*). We determined *M. leprae hsp18* and *esxA* expression levels as a surrogate measure of viability (*10*). Bacterial *hsp18* and *esxA* expression were significantly lower in mice receiving 1 ($p<0.001$) or 5 ($p<0.001$) consecutive doses of telacebec compared with rifampin or to the vehicle-treated control group, indicating a faster in vivo bactericidal efficacy of telacebec (Figure, panels C, D). Although ≥5 consecutive doses of rifampin were needed to detect a bactericidal efficacy, 1 dose of telacebec at a low dose of 2 mg/kg was sufficient to reduce the bacterial viability substantially (Figure, panels C, D).

This study demonstrates the exquisite sensitivity of *M. leprae* to telacebec and the potential of a shorter treatment regimen. Dose-finding studies in animals will help to determine an optimum dosing regimen for rapid bacterial eradication. Combination

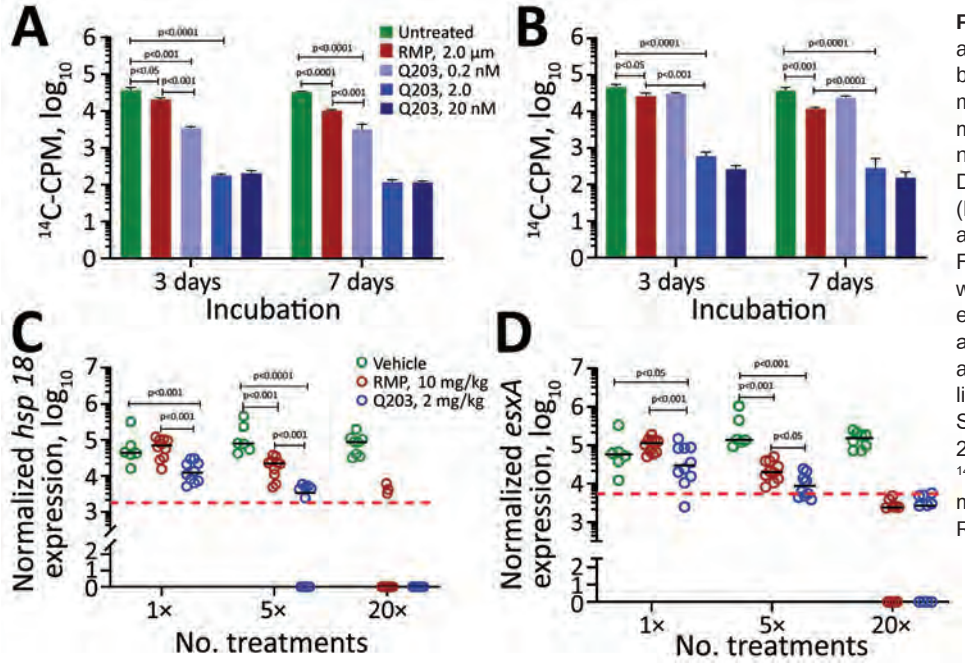

Figure. Efficacy of telacebec against *Mycobacterium leprae* bacteria in axenic culture (A), in murine bone marrow–derived macrophages (B), and in athymic nude mouse foot pad model (C, D). *M. leprae hsp18* (C) and *esxA* (D) expression levels were used as a surrogate measure of viability. For panels A and B, the assays were performed in triplicate for each condition. For panels C and D, each foot pad is taken as a data point, and the red dotted lines indicate ≈99% *M. leprae* kill. Significance was determined by 2-tailed unpaired Student *t*-test. ^{14}C, carbon 14; CPM, counts per minute; Q203, telacebec; RMP, rifampin.

therapies between telacebec and first- or second-line drugs such as rifampin, clofazimine, or minocycline should be evaluated in preclinical animal models to guide the development of a potent, fast-acting, sterilizing drug combination for humans that has a low propensity for resistance development for humans. The curative promise of telacebec or other advanced QcrB inhibitors should be validated in human clinical trials.

Acknowledgments

This work was supported in part by the Lee Kong Chian School of Medicine, Nanyang Technological University Start-Up Grant (K.P.), the National Research Foundation, Singapore, under its Investigatorship Programme (grant no. NRF-NRFI06-2020-0004), and the New York Community Trust Heiser Program (grant no. P18-000248). US National Institute of Allergy and Infectious Diseases funded the provision of viable *M. leprae* through an interagency agreement with Health Resources and Services Administration, Healthcare Systems Bureau, National Hansen's Disease Program (no. AAI20009-001-00000).

The views expressed in this article are solely the opinions of the authors and do not necessarily reflect the official policies of the U.S. Department of Health and Human Services or the Health Resources and Services Administration, nor does mention of the department or agency names imply endorsement by the US Government.

About the Author

Dr. Lahiri is a principal investigator at the Laboratory Research Branch, National Hansen's Disease Program, Baton Rouge, Louisiana, USA. His research focuses on understanding host pathogen relationship, developing animal models and evaluating novel therapeutic interventions in Hansen disease.

References

1. Mahajan NP, Lavania M, Singh I, Nashi S, Preethish-Kumar V, Vengalil S, et al. Evidence for *Mycobacterium leprae* drug resistance in a large cohort of leprous neuropathy patients from India. Am J Trop Med Hyg. 2020;102:547–52. https://doi.org/10.4269/ajtmh.19-0390
2. Pethe K, Bifani P, Jang J, Kang S, Park S, Ahn S, et al. Discovery of Q203, a potent clinical candidate for the treatment of tuberculosis. Nature Medicine. 2013;19:1157. https://doi.org/10.1038/nm.3262
3. Scherr N, Bieri R, Thomas SS, Chauffour A, Kalia NP, Schneide P, et al. Targeting the *Mycobacterium ulcerans* cytochrome *bc1:aa3* for the treatment of Buruli ulcer. Nat Commun. 2018;9:5370. https://doi.org/10.1038/s41467-018-07804-8
4. Thomas SS, Kalia NP, Ruf MT, Pluschke G, Pethe K. Toward a single-dose cure for Buruli ulcer. Antimicrob Agents Chemother. 2020;64:e00727-20. https://doi.org/10.1128/AAC.00727-20
5. Kalia NP, Hasenoehrl EJ, Ab Rahman NB, Koh VH, Ang MLT, Sajorda DR, et al. Exploiting the synthetic lethality between terminal respiratory oxidases to kill *Mycobacterium tuberculosis* and clear host infection. Proc Natl Acad Sci U S A. 2017;114:7426–31. https://doi.org/10.1073/pnas.1706139114
6. Moosa A, Lamprecht DA, Arora K, Barry CE III, Boshoff HIM, Ioerger TR, et al. Susceptibility of *Mycobacterium tuberculosis* cytochrome *bd* oxidase mutants to compounds targeting the terminal respiratory oxidase, cytochrome *c*. Antimicrob Agents Chemother. 2017;61:e01338-17. https://doi.org/10.1128/AAC.01338-17
7. Cole ST, Eiglmeier K, Parkhill J, James KD, Thomson NR, Wheeler PR, et al. Massive gene decay in the leprosy bacillus. Nature. 2001;409:1007–11. https://doi.org/10.1038/35059006
8. Franzblau SG, Hastings RC. Rapid in vitro metabolic screen for antileprosy compounds. Antimicrob Agents Chemother. 1987;31:780–3. https://doi.org/10.1128/AAC.31.5.780
9. Bailey MA, Na H, Duthie MS, Gillis TP, Lahiri R, Parish T. Nitazoxanide is active against *Mycobacterium leprae*. PLoS One. 2017;12:e0184107. https://doi.org/10.1371/journal.pone.0184107
10. Davis GL, Ray NA, Lahiri R, Gillis TP, Krahenbuhl JL, Williams DL, et al. Molecular assays for determining *Mycobacterium leprae* viability in tissues of experimentally infected mice. PLoS Negl Trop Dis. 2013;7:e2404. https://doi.org/10.1371/journal.pntd.0002404

Address for correspondence: Kevin Pethe, Lee Kong Chian School of Medicine, Experimental Medicine Building, 59 Nanyang Dr, 636921, Singapore; email: kevin.pethe@ntu.edu.sg; Ramanuj Lahiri, Department of Health and Human Services, Health Resources and Services Administration, Healthcare Systems Bureau, National Hansen's Disease Program, 9181 Interline Ave, Baton Rouge, LA 70809, USA; email: rlahiri@hrsa.gov

Mycobacterium mageritense Lymphadenitis in Child

Miguel García-Boyano, Fernando Baquero-Artigao, Carlos Toro, Marina Alguacil-Guillén, Fernando Lázaro-Perona, Cristina Calvo

Author affiliation: Hospital Universitario La Paz, Madrid, Spain (M. García-Boyano, F. Baquero-Artigao, C. Toro, M. Alguacil-Guillén, A. Lázaro-Perona, C. Calvo); Translational Research Network of Pediatric Infectious Diseases, Madrid (F. Baquero-Artigao, C. Calvo); CIBERINFEC, Instituto de Salud Carlos III, Madrid (F. Baquero-Artigao, C. Calvo)

DOI: https://doi.org/10.320/eid2803.211486

Although human infections caused by *Mycobacterium mageritense* are rare, there are some case reports involving sinusitis, pneumonia, and hospital-acquired infections in adults. We report a case of lymphadenitis caused by *M. mageritense* in a child in Spain.

Mycobacterium mageritense was identified as a novel distinct species in 1997. Its name is derived from Magerit, the old Arabic name of Madrid, Spain, the source of most of the human sputum specimens from which it was first isolated (*1*). Five years later, cases of clinical disease caused by *M. mageritense* were reported in adults (*2*). We report a case of lymphadenitis caused by *M. mageritense* in a child in Spain.

A previously healthy boy, 2 years and 9 months of age, came to a pediatric clinic because of a 1-week history of swelling of the right submandibular lymph node. Physical examination showed lymph node swelling in the right submandibular region with red–violet discolored skin. He did not had a fever, pain, or any other signs and symptoms. An ultrasound examination showed an enlarged submandibular lymph node 18 mm in diameter. Laboratory studies showed a leukocyte count of 9,220 cells/mm^3 (reference range 4,800–15,000 cells/mm^3), a differential count of 42% neutrophils (reference range 55%–70%), and a C-reactive protein level of <0.05 mg/dL (reference range <1–0.5 mg/dL).

Three days later, he underwent fine-needle aspiration of the involved lymph node. Histopathologic analysis showed necrotizing granulomatous lymphadenitis. Acid-fast bacillus staining was negative. Therefore, a nontuberculous mycobacterial lymphadenitis was suspected and treatment with oral clarithromycin (7.5 mg/kg every 12 h) and ciprofloxacin (15 mg/kg every 12 h) was started.

A rapidly growing mycobacterium was isolated from the lymph node specimen after 6 days of incubation in liquid culture medium (BBL Mycobacteria Growth Indicator Tube; Becton Dickinson, https://www.bd.com). It was identified as *M. mageritense* by using GenoType Mycobacterium CM version 2.0 (Hain Lifescience, https://www.hain-lifescience.de). Matrix-assisted laser desorption/ionization time-of-flight mass spectrometry (Bruker Daltonics, https://www.bruker.com) yielded a score of 2.4 for *M. mageritense*. Whole-genome sequencing was performed to confirm these findings (GenBank accession no. JAJJNE010000000).

Susceptibility testing using a microdilution technique showed a susceptible MIC for linezolid (8 μg/mL); an intermediate MIC for moxifloxacin (2 μg/mL), imipenem (8 μg/mL), and cefoxitin (32 μg/mL); and a resistant MIC for trimethoprim/sulfamethoxazole (>8/152 μg/mL), ciprofloxacin (>4 μg/mL), amikacin (>64 μg/mL), clarithromycin (>16 μg/mL), doxycycline (>16 μg/mL), and tobramycin (>16 μg/mL). Breakpoints were those suggested by the Clinical and Laboratory Standards Institute for rapidly growing mycobacteria (*3*).

Accordingly, 3 weeks after fine-needle aspiration was performed, clarithromycin was replaced by oral linezolid (10 mg/kg every 8 h). However, this change was promptly stopped because of intolerance to linezolid, and clarithromycin was given again. The enlarged lymph node gradually improved, and antimicrobial drug treatment was discontinued 11 weeks after initial prescription. The lymph node was reduced to <50% of its initial size. Complete excision of residual lymph node and scar tissue was performed 2 months later, leading to total resolution of the lymphadenitis.

The biochemical and drug susceptibility patterns of *M. mageritense* are relatively similar to the formerly known *M. fortuitum* third biovariant complex (*1*,*2*). It is not surprising that they also seem to have the same clinical spectrum (*2*). Although human infections caused by *M. mageritense* are rare, there are case reports involving sinusitis, pneumonia, and hospital-acquired infections, including catheter-related bloodstream infections, implantable cardioverter defibrillator-related infections, prosthetic valve endocarditis, and intrathecal catheter-related meningitis (*2*,*4*,*5*). Skin and soft tissue infections, including parotitis, furunculosis, and surgical site infections, have also been reported (*4*).

Mycobacteria are widespread in nature (*1*) and rapidly growing mycobacteria, such as *M. mageritense*, are ubiquitous in most municipal water supplies (*6*).

Although *M. mageritense* has been isolated from cutaneous lesions of a tsunami survivor (*7*) and from 2 patients who received footbaths at the same nail salon (*6*), in most of these case reports, such as for our case, the source of contamination was unknown. Thus, *M. mageritense* is a rapidly growing mycobacteria that can cause granulomatous lymphadenitis in children. Clinicians should be aware of this bacteria during differential diagnoses.

Acknowledgment

We thank Jaime Esteban for providing assistance with antimicrobial drug susceptibility testing.

About the Author

Dr. García-Boyano is a doctoral candidate in pediatric infectious diseases at the Hospital Universitario La Paz, Madrid. His primary research interests are tropical medicine, HIV, and healthcare-associated infections.

References

1. Domenech P, Jimenez MS, Menendez MC, Bull TJ, Samper S, Manrique A, et al. *Mycobacterium mageritense* sp. nov. Int J Syst Bacteriol. 1997;47:535–40. https://doi.org/10.1099/00207713-47-2-535
2. Wallace RJ Jr, Brown-Elliott BA, Hall L, Roberts G, Wilson RW, Mann LB, et al. Clinical and laboratory features of *Mycobacterium mageritense*. J Clin Microbiol. 2002;40:2930–5. https://doi.org/10.1128/JCM.40.8.2930-2935.2002
3. Clinical and Laboratory Standards Institute. Performance standards for susceptibility testing of *Mycobacteria*, *Nocardia* spp, and other aerobic Actonomycetes. CLSI supplement M62. Wayne (PA): The Institute; 2018.
4. Okabe T, Sasahara T, Suzuki J, Onishi T, Komura M, Hagiwara S, et al. *Mycobacterium mageritense* parotitis in an immunocompetent adult. Indian J Microbiol. 2018;58:28–32. https://doi.org/10.1007/s12088-017-0692-y
5. Kim J, Seong MW, Kim EC, Han SK, Yim JJ. Frequency and clinical implications of the isolation of rare nontuberculous mycobacteria. BMC Infect Dis. 2015;15:9. https://doi.org/10.1186/s12879-014-0741-7
6. Gira AK, Reisenauer AH, Hammock L, Nadiminti U, Macy JT, Reeves A, et al. Furunculosis due to *Mycobacterium mageritense* associated with footbaths at a nail salon. J Clin Microbiol. 2004;42:1813–7. https://doi.org/10.1128/JCM.42.4.1813-1817.2004
7. Appelgren P, Farnebo F, Dotevall L, Studahl M, Jönsson B, Petrini B. Late-onset posttraumatic skin and soft-tissue infections caused by rapid-growing mycobacteria in tsunami survivors. Clin Infect Dis. 2008;47:e11–6. https://doi.org/10.1086/589300

Address for correspondence: Miguel García-Boyano, C/ Ginzo de Limia 55, 9°C, Madrid 28034, Spain; email: miguelgarciaboyano@gmail.com

SARS-CoV-2 Breakthrough Infections after Introduction of 4 COVID-19 Vaccines, South Korea, 2021

Seonju Yi,[1] Young June Choe,[1] Jia Kim, Yoo-Yeon Kim, Ryu Kyung Kim, Eun Jung Jang, Do Sang Lim, Hye Ryeon Byeon, Sangwon Lee, Eonjoo Park, Seung-Jin Kim, Young-Joon Park

Author affiliations: Korea Disease Control and Prevention Agency, Cheongju, South Korea (S. Yi, J. Kim, Y.-Y. Kim, R.K. Kim, E.J. Jang, D.S .Lim, H.R. Byeon, S. Lee, E. Park, S.-J. Kim, Y.-J. Park); Korea University Anam Hospital, Seoul, South Korea (Y.J. Choe)

DOI: https://doi.org/10.3201/eid2803.212210

We conducted a nationwide retrospective cohort study to estimate severe acute respiratory syndrome coronavirus 2 (SARS-CoV-2) breakthrough infection among recipients of 4 different vaccines in South Korea. Age-adjusted breakthrough infection rate per month was highest for Janssen (42.6/100,000 population), followed by AstraZeneca (21.7/100,000 population), Pfizer-BioNTech (8.5/100,000 population), and Moderna (1.8/100,000 population).

Since their rollout, vaccines have been highly effective globally in controlling coronavirus disease (COVID-19), caused by severe acute respiratory syndrome coronavirus 2 (SARS-CoV-2) (*1*). Breakthrough infections have been reported in some vaccine recipients, suggesting the need for public health assessment and monitoring (*2*). To date, the vaccine-specific data on breakthrough infections are limited. In early 2021, the national immunization program of South Korea introduced 4 COVID-19 vaccines: ChAdOx1 nCov-19 (AstraZeneca, https://www.astrazeneca.com), BNT162b2 (Pfizer-BioNTech, https://www.pfizer.com), Ad26.COV2.S (Johnson & Johnson/Janssen [hereafter Janssen], https://www.janssen.com), and mRNA-1273 (Moderna, https://www.moderna.com). As of October 10, 2021, a total of 70% of the country's population have received ≥1 dose of vaccine (*3*). Introduction of the vaccines provided an opportunity to study breakthrough infections by different vaccine types. We describe a snapshot of SARS-CoV-2 breakthrough infections in South Korea and aim to identify risk by age group that might influence the observed pattern.

We conducted a nationwide retrospective cohort study to estimate SARS-CoV-2 breakthrough

[1]These authors contributed equally to this article.

infection rates among AstraZeneca, Pfizer-BioNTech, Janssen, and Moderna vaccine recipients in South Korea. We included fully vaccinated persons (2 weeks past 2-dose vaccination for AstraZeneca, Pfizer-BioNTech, and Moderna vaccines; 2 weeks past 1-dose vaccination for Janssen vaccine) without history of SARS-CoV-2 infection (Appendix Figure 1, https://wwwnc.cdc.gov/EID/article/28/3/21-2210-App1.pdf). A Pfizer-BioNTech booster vaccination was offered to AstraZeneca vaccine–primed persons (2 doses of AstraZeneca vaccine, then a third dose of Pfizer-BioNTech vaccine), who were thereafter included in the analysis. Observed periods were April 7–October 10, 2021, for AstraZeneca vaccine; April 3–October 10, 2021, for Pfizer-BioNTech vaccine; June 24–October 10, 2021, for Janssen vaccine; July 30–October 10, 2021, for Moderna vaccine; and July 19–October 10, 2021, for AstraZeneca/Pfizer-BioNTech prime/booster recipients.

We estimated breakthrough infection rate by vaccine, number of serious outcomes (cases treated with high-flow oxygen therapy, mechanical ventilator, extracorporeal membrane oxygenation, continuous renal replacement therapy, or death), and number of secondary transmissions originated from the breakthrough infection case. We identified the presence of serious outcomes through the case reporting form collected under the Infectious Disease Control and Prevention Act, which mandates epidemiologic investigation on all confirmed SARS-CoV-2 cases in South Korea. In all close contacts of laboratory-confirmed SARS-CoV-2 case-patients, we conducted epidemiologic investigations to search for the preceding link and potential onward transmission cases. We calculated age-adjusted and age-specific breakthrough infection rates as well as age-adjusted rates for serious outcomes and deaths. We randomly tested ≈20% of samples for full-length genome and spike protein sequencing to identify the presence of variant of concern.

The number of vaccinations by vaccine type are as follows: AstraZeneca (prime/booster), 8,737,343 persons; Pfizer-BioNTech (prime/booster), 10,235,891 persons; Janssen (single), 1,408,921 persons; Moderna (prime/booster), 1,190,973 persons; and AstraZeneca/Pfizer-BioNTech (prime/booster), 1,600,998 persons (Table). Age-adjusted breakthrough infection rate per month was highest among Ad26.COV2.S recipients (42.6/100,000 population), followed by AstraZeneca (prime/booster) recipients (21.7/100,000 population), AstraZeneca/Pfizer-BioNTech (prime/booster) recipients (21.3/100,000 population), Pfizer-BioNTech (prime/booster) recipients (8.5/100,000 population), and Moderna (prime/booster) recipients (1.8/100,000 population). Serious outcome (0–0.9/100,000 population) and death (0–0.2/100,000 population) after breakthrough infection were rare for all vaccine types. Secondary transmission rate was highest among Janssen recipients (19.2/100,000 population), followed by AstraZeneca (prime/booster) recipients (4.9/100,000 population).

The highest breakthrough infection rates we observed in younger age groups were in AstraZeneca (prime/booster), Janssen (single), Moderna (prime/booster), and AstraZeneca/Pfizer-BioNTech (prime/booster) recipients (Figure). Among the Pfizer-BioNTech (prime/booster) recipients, breakthrough infection rate was highest among elderly persons 70–79 years and ≥80 years of age (Appendix Figure 2).

We identified the variants of concern found in AstraZeneca (prime/booster) recipients as 1,285 Delta and 4 Alpha variants; in Pfizer-BioNTech (prime/booster) as 888 Delta, 14 Alpha, and 1 Beta variants; in Janssen (single), 789 Delta, 12 Alpha, and 2 Gamma variants; in Moderna (prime/booster), 13 Delta variants; and in AstraZeneca/Pfizer-BioNTech (prime/booster), 188 Delta variants.

Our findings of a higher breakthrough infection in adenovirus DNA vector vaccine recipients and lower risk among mRNA vaccine recipients are consistent with other studies. In clinical trials, 0.5% of AstraZeneca recipients (*4*) and 0.3% of Janssen recipients (*5*) had SARS-CoV-2 infections, whereas 0.05% of Pfizer-BioNTech recipients (*6*) and 0.08% of Moderna recipients (*7*) had infections. The AstraZeneca/Pfizer-BioNTech (prime/booster) recipients had breakthrough infection rate in between that of

Table. Severe acute respiratory syndrome coronavirus 2 breakthrough infections by vaccine type, South Korea, 2021

Variable	ChAdOx1 nCov-19, AstraZeneca, prime/booster	BNT162b2, Pfizer-BioNTech, prime/booster	Ad26.COV2.S, Johnson & Johnson/Janssen, single dose	mRNA-1273, Moderna, prime/booster	ChAdOx1 nCov-19/BNT162b2, AstraZeneca/Pfizer-BioNTech, prime/booster
Observed period	Apr 7–Oct 10	Apr 3–Oct 10	Jun 24–Oct 1	Jul 30–Oct 10	Jul 19–Oct 10
Total vaccinations, no.	8,737,343	10,235,891	1,408,921	1,190,973	1,600,998
Breakthrough infections*	21.7	8.5	42.6	1.8	21.3
Serious outcomes*	0.3	0.2	0.9	0.0	0.1
Deaths*	0.2	0.0	0.0	0.0	0.1
Secondary transmission*	4.9	2.1	19.2	0.4	2.0

*Monthly age-adjusted rate per 100,000 population.

AstraZeneca (prime/booster) and Pfizer-BioNTech (prime/booster) recipients, suggesting a potential benefit from mix-and-match vaccination as observed in previous studies (*8*).

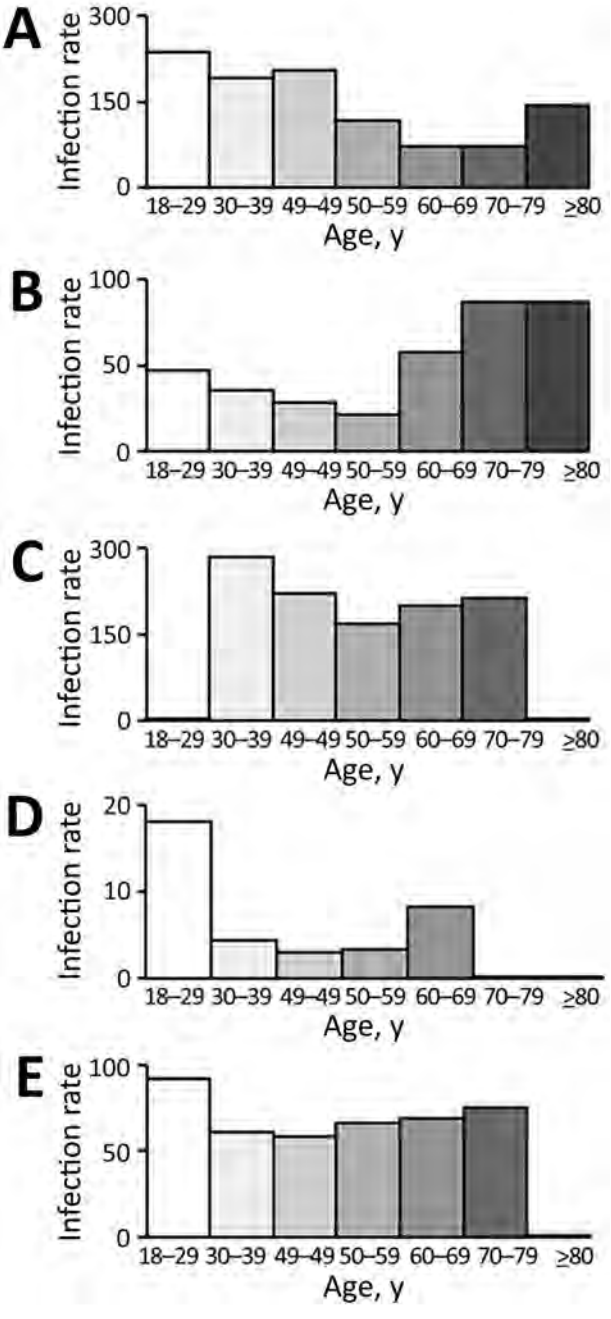

Figure. Age-specific breakthrough infection rates (cases/100,000 population) of severe acute respiratory syndrome coronavirus 2 for 4 vaccines by vaccine type, South Korea. A) ChAdOx1 nCov-19 (AstraZeneca prime/booster), April–October 2021. B) BNT162b2 (Pfizer-BioNTech prime/booster), April–October 2021. C) Ad26. COV2.S (Johnson & Johnson/Janssen, single dose), June–October 2021. D) mRNA-1273 (Moderna, prime/booster), July–October 2021. E) ChAdOx1 nCov-19/BNT162b2(AstraZeneca prime/Pfizer-BioNTech booster), July–October 2021

A limitation of this study is that the observed period between the vaccines were different: AstraZeneca and Pfizer-BioNTech were available for nearly 6 months, whereas Janssen and Moderna were introduced 2–3 months later. We conducted monthly adjustments of daily data; however, unidentified confounders may have affected the observed result. In addition, emergence of new variants may also affect the risk for breakthrough infection (*9*). Since mid-June 2021, Delta variant has become the dominant strain in South Korea, which may have affected vaccine effectiveness and postinfection health outcomes. Despite these limitations, our findings demonstrate uniformly low numbers of serious disease cases in recipients of all 4 vaccine types, consistent with previous findings (*10*).

In conclusion, breakthrough infection was more common among adenovirus DNA vector vaccine recipients than among mRNA vaccine recipients. Booster vaccination with mRNA vaccines in adenovirus DNA vector vaccine–primed individuals may confer additional protection against SARS-CoV-2 breakthrough infections.

Acknowledgments

We thank the relevant ministries, including the Ministry of Interior and Safety, Si/Do and Si/Gun/Gu, medical staffs in health centers, and medical facilities for their efforts in responding to COVID-19 outbreak.

About the Author

Dr. Yi is a public health officer at Korea Disease Control and Prevention Agency. Her main research interest is in epidemiologic investigation and surveillance measures of infectious diseases. Dr. Choe is a clinical assistant professor of pediatrics at Korea University Anam Hospital. His main research addresses quantification of and understanding the mechanisms of immunization program's impact on public health.

References

1. Thompson MG, Stenehjem E, Grannis S, Ball SW, Naleway AL, Ong TC, et al. Effectiveness of Covid-19 Vaccines in Ambulatory and Inpatient Care Settings. N Engl J Med. 2021;385:1355–71. 10.1056/NEJMoa2110362 https://doi.org/10.1056/NEJMoa2110362
2. Scobie HM, Johnson AG, Suthar AB, Severson R, Alden NB, Balter S, et al. Monitoring Incidence of COVID-19 Cases, Hospitalizations, and Deaths, by Vaccination Status — 13 U.S. Jurisdictions, April 4–July 17, 2021. MMWR Morb Mortal Wkly Rep. 2021;70:1284–90. 10.15585/mmwr.mm7037e1 https://doi.org/10.15585/mmwr.mm7037e1
3. Korea Disease Control and Prevention Agency. COVID-19 vaccination dashboard [cited 2021 Oct 25]. https://ncv.kdca.go.kr/eng/

4. Voysey M, Clemens SAC, Madhi SA, Weckx LY, Folegatti PM, Aley PK, et al. Safety and efficacy of the ChAdOx1 nCoV-19 vaccine (AZD1222) against SARS-CoV-2: an interim analysis of four randomised controlled trials in Brazil, South Africa, and the UK. Lancet. 2021;397:99–111. 10.1016/S0140-6736(20)32661-1 https://doi.org/10.1016/S0140-6736(20)32661-1
5. Sadoff J, Gray G, Vandebosch A, Cárdenas V, Shukarev G, Grinsztejn B, et al. Safety and Efficacy of Single-Dose Ad26.COV2.S Vaccine against Covid-19. N Engl J Med. 2021;384:2187–201. 10.1056/NEJMoa2101544 https://doi.org/10.1056/NEJMoa2101544
6. Polack FP, Thomas SJ, Kitchin N, Absalon J, Gurtman A, Lockhart S, et al. Safety and Efficacy of the BNT162b2 mRNA Covid-19 Vaccine. N Engl J Med. 2020;383:2603–15. 10.1056/NEJMoa2034577 https://doi.org/10.1056/NEJMoa2034577
7. Baden LR, El Sahly HM, Essink B, Kotloff K, Frey S, Novak R, et al. Efficacy and Safety of the mRNA-1273 SARS-CoV-2 Vaccine. N Engl J Med. 2021;384:403–16. 10.1056/NEJMoa2035389 https://doi.org/10.1056/NEJMoa2035389
8. Tenbusch M, Schumacher S, Vogel E, Priller A, Held J, Steininger P, et al. Heterologous prime–boost vaccination with ChAdOx1 nCoV-19 and BNT162b2. Lancet Infect Dis. 2021;21:1212–3. 10.1016/S1473-3099(21)00420-5 https://doi.org/10.1016/S1473-3099(21)00420-5
9. Blanquart F, Abad C, Ambroise J, Bernard M, Cosentino G, Giannoli J-M, et al. Characterisation of vaccine breakthrough infections of SARS-CoV-2 Delta and Alpha variants and within-host viral load dynamics in the community, France, June to July 2021. Euro Surveill. 2021;26. 10.2807/1560-7917.ES.2021.26.37.2100824 https://doi.org/10.2807/1560-7917.ES.2021.26.37.2100824
10. Butt AA, Yan P, Shaikh OS, Mayr FB. Outcomes among patients with breakthrough SARS-CoV-2 infection after vaccination in a high-risk national population. EClinicalMedicine. 2021;40:101117. 10.1016/j.eclinm.2021.101117 https://doi.org/10.1016/j.eclinm.2021.101117

Address for correspondence: Young-Joon Park, Director of Epidemiologic Investigation. Korea Disease Control and Prevention Agency, Cheongju, South Korea; email: pahmun@korea.kr

Serial Intervals and Household Transmission of SARS-CoV-2 Omicron Variant, South Korea, 2021

Jin Su Song,[1] Jihee Lee,[1] Miyoung Kim, Hyeong Seop Jeong, Moon Su Kim, Seong Gon Kim, Han Na Yoo, Ji Joo Lee, Hye Young Lee, Sang-Eun Lee, Eun Jin Kim, Jee Eun Rhee, Il Hwan Kim, Young-Joon Park

Author affiliations: Capital Regional Center for Disease Control and Prevention, Seoul, South Korea (J.S. Song, J. Lee, M. Kim); Incheon Metropolitan Government, Incheon, South Korea (H.S. Jeong, M.S. Kim, S.G. Kim, H.N. Yoo); Korea Disease Control and Prevention Agency, Cheongju, South Korea (J.J. Lee, H.Y. Lee, S.-E. Lee, E.J. Kim, J.E. Rhee, I.H. Kim, Y.-J. Park)

DOI: https://doi.org/10.3201/eid2803.212607

To clarify transmissibility of the severe acute respiratory syndrome coronavirus 2 Omicron variant, we determined serial intervals and secondary attack rates among household contacts in South Korea. Mean serial interval for 12 transmission pairs was 2.9 days, and secondary attack rate among 25 households was 50.0%, raising concern about a rapid surge in cases.

The severe acute respiratory syndrome coronavirus 2 (SARS-CoV-2) Omicron (B.1.1.529) variant of concern has been confirmed on all continents and has spread through communities around the world at unprecedented speed (*1*). Given uncertainties about current estimates of virus transmissibility, we analyzed real-life data on serial intervals for transmission pairs (time from infector symptom onset to infectee symptom onset) and secondary attack rate among household contacts, offering metrics essential for predicting epidemic size, forecasting healthcare demand, and devising effective public health interventions. Details of the epidemiologic situation with regard to importation and transmission of the Omicron variant in South Korea have been described elsewhere (*2*). We further traced a total of 76 case-patients with Omicron infection that originated from 2 persons with imported cases (75 confirmed cases and 1 suspected case) and their contacts, focusing on infector-infectee relationships and household transmission during November–December 2021.

Because of the possibility of their being exposed to other potential sources of infection at church on

[1]These authors contributed equally to this article.

November 28, 2021, we excluded infectees who had visited church on that date from transmission pairs. As for the time of infection in households, we assumed that the earliest exposure occurred 2 days before symptom onset of an infector and the last exposure before isolation of the infector. To calculate serial intervals, we did not include case-patients without a clear date of symptom onset. We defined a household as a group of persons living in the same residence with a shared space. This study was conducted as a legally mandated public health investigation under the authority of the Korean Infectious Diseases Control and Prevention Act (no. 12444 and no. 13392). The study was not research that was subject to institutional review board approval; therefore, written informed consent was not required.

We identified 25 households, comprising 55 household members. Only 1 household comprised South Korea nationals; the others, foreign nationals. Of the 55 household members, 36 were confirmed to be Omicron-positive, among which secondary attack rate was 0.65 (95% CI 0.48–0.81). After we

Table. Characteristics of SARS-CoV-2 Omicron (B.1.1.529) variant of concern of index case-patients and household members, South Korea, 2021*

	Index case-patient				Household members†	
Household	Age, y/sex	Transmission route	Signs/symptoms at diagnosis	COVID-19 vaccination status (vaccine)‡	No. members, n = 36	No. confirmed cases, n = 18
1	44/M	Imported case	Cough, sputum, sore throat	Fully (mRNA-1273)	2	1
2	38/M	Contact with a confirmed case at the airport	Fever, cough, myalgia	Unvaccinated	2	1
3	33/M	Contact at church and restaurant	Fever, cough, myalgia, headache	Unvaccinated	1	1
4	39/F	Contact at church	Fever, myalgia	Partially (BNT162b)	1	0
5	31/F	Contact at church	Myalgia	Unvaccinated	0	0
6	27/F	Contact at church	Fever, sore throat	Unvaccinated	1	1
7	33/F	Contact at church	Fever, chill, cough, myalgia, headache	Unvaccinated	2	2
8	34/F	Contact at church	Sore throat	Unvaccinated	2	1
9	50/F	Contact at church	Cough, sore throat, headache	Fully (Ad26.COV2.S)	1	1
10	56/F	Contact with a friend	Cough, fatigue	Fully (Ad26.COV2.S)	0	0
11	46/M	Contact at church	Asymptomatic	Fully (mRNA-1273)	0	0
12	39/F	Contact at a restaurant	Sore throat	Unvaccinated	2	2
13	77/F	Contact at church	Cough, sore throat	Fully (BNT162b)	2	0
14	44/F	Contact at church	Sputum, sore throat	Fully (mRNA-1273)	1	1
15	6/M	Contact at a childcare center	Asymptomatic	Unvaccinated	2	0
16	31/F	Contact at church	Fever, sputum, sore throat	Unvaccinated	1	0
17	23/F	Contact with a friend	Fever, chill, cough, sputum, sore throat, myalgia, headache	Fully (mRNA-1273)	1	0
18	4/M	Contact at street	Asymptomatic	Unvaccinated	3	0
19	64/F	Contact at church	Asymptomatic	Fully (mRNA-1273)	0	0
20	67/F	Contact at church	Asymptomatic	Unvaccinated	1	1
21	34/F	Contact at church	Fever, myalgia	Unvaccinated	1	1
22	33/F	Contact at church	Sore throat, rhinorrhea	Fully (BNT162b)	2	0
23	45/F	Contact with a family member	Asymptomatic	Fully (Ad26.COV2.S)	2	1
24	2/F	Contact at playground	Fever, rhinorrhea	Unvaccinated	4	3
25	3/M	Contact at a childcare center	Asymptomatic	Unvaccinated	2	1
Total		NA	NA	NA	36	18
Attack rate		NA	NA	NA	NA	0.50

*COVID-19, coronavirus disease; SARS-CoV-2, severe acute respiratory syndrome coronavirus 2.
†Household members who participated in church service on November 28, 2021, were excluded.
‡An unvaccinated person had received no COVID-19 vaccine. A partially vaccinated person had received a COVID-19 vaccine but had not completed the primary series ≥14 d before illness onset. A fully vaccinated person had completed the primary series of COVID-19 vaccine ≥14 d before illness onset; vaccinated index case-patients received BNT162b, n = 3; mRNA-1273, n = 5; or Ad26.COV2.S, n = 3.

excluded the 19 household members who had visited church on November 28, 2021, the remaining 36 were confirmed to be Omicron case-patients; secondary attack rate among the 18 was 0.50 (95% CI 0.35–0.72) (Table).

We used 12 transmission pairs for the calculation, including 12 infectors and 19 infectees. Mean (± SD) ages were 34.2 (± 18.2) years for infectors and 32.5 (± 21.7) years for infectees. The mean incubation period of the transmission pairs was 2.5–4.3 days, and the median incubation period was 3–4 days. The mean (± SD) serial interval for the pairs was 2.9 (± 1.6) days; the median serial interval was 3.0 days (Appendix, https://wwwnc.cdc.gov/EID/article/28/3/21-2607-App1.xlsx).

The estimated mean serial interval of 2.9 days for Omicron was shorter than that determined for wild-type virus and the Delta variant found in other studies conducted in South Korea (*3*,*4*). Enhanced nonpharmaceutical interventions such as rapid isolation of case-patients, as revealed by the mean time of 0.75 (range 0–4) days from symptom onset to isolation among infectors, and meticulous contact tracing during the study period may have shortened the serial interval and reduced superspreading potential, as evidenced in other research (*5*). Thus, further studies in other places or at other periods, are needed, using larger sample sizes to more accurately estimate transmission dynamics and effects of public health measures.

The household secondary attack rate that we found, factoring in vaccination status and prior infections, was substantially higher than rates for wild type virus and the Delta variant of concern previously reported in South Korea and other countries (*6*). This finding is in line with earlier reports that suggested increased household risk for transmission of Omicron variant (*7*,*8*), although enhanced isolation in conjunction with a comprehensive testing strategy for contacts of case-patients may partially inflate secondary attack rate in our study. Of note, in our study, the secondary attack rate among fully vaccinated persons is high (62.5%, 10/16), thus heightening concerns over immune escape and the possibility that Omicron may be associated with considerably reduced vaccine effectiveness. However, further studies are needed to accurately assess the relative roles of increased intrinsic transmissibility and immune escape.

Our findings with regard to Omicron transmissibility by symptomatic index case-patients supports that of a meta-analysis reporting that that secondary attack rates were higher in households with symptomatic rather than asymptomatic index case-patients (*6*). However, caution is warranted when interpreting our results because other social and demographic factors could not be properly adjusted and sample size was too small to ensure adequate statistical power. Our findings of a short serial interval among transmission pairs and a high secondary attack rate among household members adds timely real-life evidence of increased transmissibility of the Omicron variant of concern along with the potential for immune escape, thus necessitating a package of effective public health measures to mitigate the spread of Omicron in each country.

Acknowledgments

We thank the relevant ministries, including the Ministry of Interior and Safety, Si/Do and Si/Gun/Gu, medical staff in health centers, and medical facilities for their efforts in responding to the coronavirus disease outbreak.

The opinions expressed by authors contributing to this article do not necessarily reflect the opinions of the Korea Disease Control and Prevention Agency or the institutions with which the authors are affiliated. The authors declare that there is neither conflict of interest nor financial support for this work.

About the Author

Dr. Song is an infectious disease specialist at the Korea Disease Control and Prevention Agency and an adjunct professor of global health at Handong Global University. His research interests focus on design, implementation, and evaluation of infectious diseases program in low-income countries. Dr. J. Lee is a public health officer at the Korea Disease Control and Prevention Agency, whose main research addresses epidemiologic investigation and surveillance measures of infectious diseases and strengthening health systems.

Reference

1. World Health Organization. Enhancing response to SARS-CoV-2 Omicron variant [cited 2021 Dec 23]. https://www.who.int/publications/m/item/enhancing-readiness-for-omicron-(b.1.1.529)-technical-brief-and-priority-actions-for-member-states
2. Lee JJ, Choe YJ, Jeong H, Kim M, Kim S, Yoo H, et al. Importation and transmission of SARS-CoV-2 B.1.1.529 (Omicron) variant of concern in Korea, November 2021. J Korean Med Sci. 2021;36:e346. https://doi.org/10.3346/jkms.2021.36.e346
3. Hong K, Yum S, Kim J, Chun BC. The serial interval of COVID-19 in Korea: 1,567 pairs of symptomatic cases from contact tracing. J Korean Med Sci. 2020;35:e435. https://doi.org/10.3346/jkms.2020.35.e435
4. Ryu S, Kim D, Lim JS, Ali ST, Cowling BJ. Serial interval and transmission dynamics during SARS-CoV-2 Delta

variant predominance, South Korea. Emerg Infect Dis. 2022 Feb [cited 2021 Dec 22]. https://wwwnc.cdc.gov/eid/article/28/2/21-1774_article
5. Ali ST, Wang L, Lau EHY, Xu XK, Du Z, Wu Y, et al. Serial interval of SARS-CoV-2 was shortened over time by nonpharmaceutical interventions. Science. 2020;369:1106–9. https://doi.org/10.1126/science.abc9004
6. Madewell ZJ, Yang Y, Longini IM Jr, Halloran ME, Dean NE. Household transmission of SARS-CoV-2: a systematic review and meta-analysis. JAMA Netw Open. 2020;3:e2031756. https://doi.org/10.1001/jamanetworkopen.2020.31756
7. European Centre for Disease Prevention and Control. Assessment of the future emergence and potential impact of the SARS-CoV-2 Omicron variant of concern in the context of ongoing transmission of the Delta variant of concern in the EU/EEA, 18th update [cited 2021 Dec 23]. https://www.ecdc.europa.eu/en/publications-data/covid-19-assessment-further-emergence-omicron-18th-risk-assessment
8. UK Health Security Agency. SARS-CoV-2 variants of concern and variants under investigation in England: technical briefing 32 [cited 2021 Dec 22]. https://assets.publishing.service.gov.uk/government/uploads/system/uploads/attachment_data/file/1042688/RA_Technical_Briefing_32_DRAFT_17_December_2021_2021_12_17.pdf

Address for correspondence: Young-Joon Park, Director of Epidemiologic Investigation, Korea Disease Control and Prevention Agency, 187 Osongsaengmyeong2-ro, Osong-eup, Heungdeok-gu, Cheongju-si, Chungcheongbuk-do 28159, South Korea; email: pahmun@korea.kr

Restaurant-Based Measures to Control Community Transmission of COVID-19, Hong Kong

Faith Ho, Tim K. Tsang, Huizhi Gao, Jingyi Xiao, Eric H.Y. Lau, Jessica Y. Wong, Peng Wu, Gabriel M. Leung, Benjamin J. Cowling

Author affiliations: World Health Organization Collaborating Centre for Infectious Disease Epidemiology and Control, University of Hong Kong, Hong Kong, China (F. Ho, T.K. Tsang, H. Gao, J. Xiao, E.H.Y. Lau, J.Y. Wong, P. Wu, G.M. Leung, B.J. Cowling); Hong Kong Science and Technology Park, Hong Kong (E.H.Y. Lau, P. Wu, G.M. Leung, B.J. Cowling)

DOI: https://doi.org/10.3201/eid2803.211015

Controlling transmission in restaurants is an important component of public health and social measures for coronavirus disease. We examined the effects of restaurant measures in Hong Kong. Our findings indicate that shortening operating hours did not have an effect on time-varying effective reproduction number when capacity was already reduced.

As of April 14, 2021, a total of 11,608 cases and 207 deaths from coronavirus disease (COVID-19) had been reported in Hong Kong (*1*). A series of community epidemics have occurred, the largest of which have been the third wave in June–October 2020, which had 3,978 cases, and the fourth wave in November 2020–March 2021, which had 6,048 cases. To suppress local transmission of COVID-19, the government implemented a combination of public health and social measures (PHSMs): bar closures, restaurant capacity restrictions and opening hour restrictions, bans on live music performances and dancing, and work-from-home advisories (*2*). Ongoing assessment of the effect of these measures on transmission can guide evidence-based policy. One type of location in which COVID-19 transmission is known to occur is restaurants (*3*). Earlier studies have evaluated the impact of PHSMs, including restrictions on large group gatherings (*4*–*6*), but the specific effect of restaurant measures was not studied. Here we focus on the effect of restaurant measures on transmission in Hong Kong.

We collected details and time of implementation of each intervention of all the PHSMs applied during the third and fourth waves from the official reports of the Hong Kong government (*7*) (Appendix Table 1, https://wwwnc.cdc.gov/EID/article/28/3/21-1015-App1.pdf). In wave 3, a ban on dine-in service after 6:00 PM was in force during July 15–August 27, 2020 (Figure, panel A). Other PHSMs were implemented on the same day and kept in place for longer. Wave 4 was initiated by multiple superspreading events in a network of dancing venues. A ban on dine-in service after 6:00 PM was implemented on December 10, 2020, which was a week to a month later than the implementation of other PHSMs (Figure, panel B). Hence, we could disentangle the effect of shortened dine-in hours from other measures. No other PHSMs were implemented before the study period.

To determine the effect of the ban on dine-in services after 6:00 PM, we applied a previous approach to estimate time-varying reproduction number (R_t) (*8*,*9*). Then, we fitted LASSO regression models to

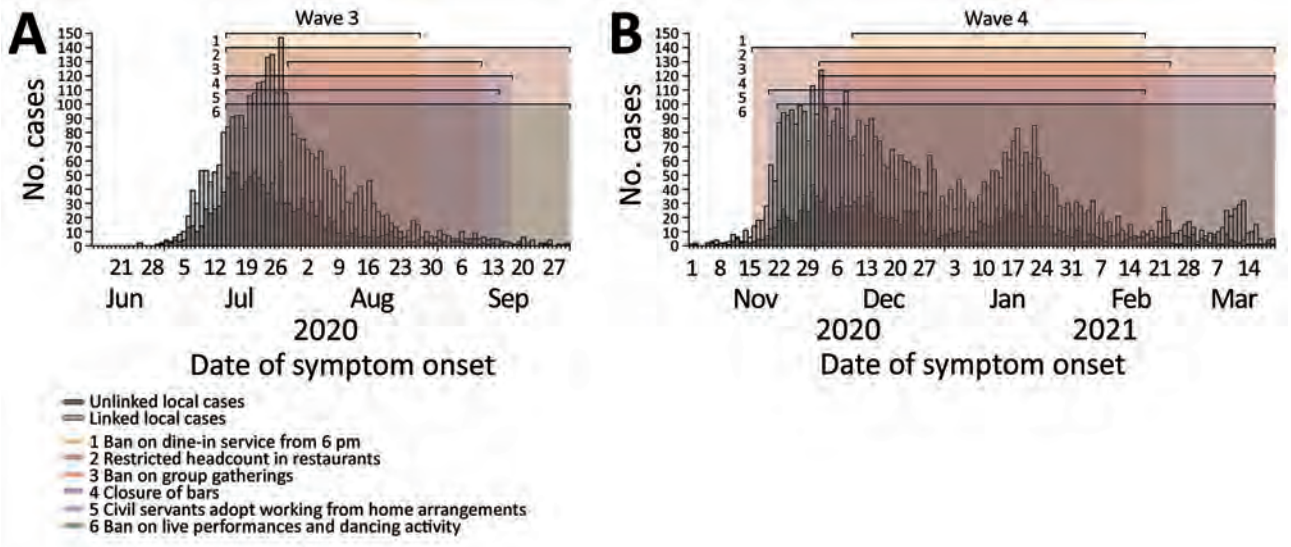

Figure. Use of public health and social measures (PHSMs) to reduce transmission of coronavirus disease in 2 waves of the epidemic, Hong Kong, 2020–2021. A) Incidence and implementation of PHSMs during wave 3, June 15–September 30, 2020. B) Incidence and implementation of PHSMs during wave 4, November 1, 2020–March 20, 2021. Dark and light gray bars represent the incidence of unlinked local cases and linked local cases of coronavirus disease in Hong Kong. Linked local cases are cases that are linked initially or after epidemiological investigation. Effective periods of PHSMs related to restaurants are shown in shaded areas in different colors.

log(R_t) to assess the effect of the ban on dine-in services after 6:00 PM on R_t, accounting for the effect from other PHSMs (*10*). We allowed for a 7-day lag between implementation of a measure and its effect on incidence, to account for the incubation period. In both waves, we grouped the PHSMs other than ban on dine-in services after 6:00 PM into a single variable to indicate the period when ≥3 of these other PHSMs were in place.

Table. Effect on time-varying reproduction number of public health and social measures in waves 3 and 4 of COVID-19, Hong Kong, 2020–2021

PHSM	% Change in R_t (95% CI)
Model 1	
Wave 3	
Ban on dine-in service after 6:00 PM†	0
≥3 other PHSMs‡	−53 (−59 to −44)
Wave 4	
Ban on dine-in service after 6:00 PM	0
≥3 other PHSMs	−40 (−47 to −28)
Model 2	
Wave 3	
Ban on dine-in service after 6:00 PM	0
≥3 other PHSMs, excluding basic civil service arrangement	−51 (−57 to −43)
Wave 4	
Ban on dine-in service after 6:00 PM	0
≥3 other PHSMs, excluding basic civil service arrangement	−38 (−46 to −27)

*Wave 3 was June 15–September 30, 2020; wave 4 was November 1, 2020–March 15, 2021. COVID-19, coronavirus disease; PHSM, public health and social measure; R_t, reproduction number.
†Because of variable selection and regularization in LASSO regression, the regression coefficient was shrunk to 0 in the model.
‡Other PHSMs include restricted headcount in restaurants, ban on group gatherings, bar closure, flexible civil service arrangement, and ban on live performances and dancing activity.

We estimated that the ban on dine-in services after 6:00 PM did not reduce R_t in both waves, but other PHSMs were associated with substantial reductions in R_t. In wave 3, R_t rose rapidly to 4.5 on June 27, 2020, but ≈1 week after measures were applied it was <1.0 (Appendix Figure, panel A). Implementation of ≥3 other PHSMs was associated with a 53% (95% CI 44%–59%) decrease in R_t (Table).

In wave 4, R_t increased to 3.1 on November 16, 2020, and then decreased to ≈1.0 after PHSMs began (Appendix Figure, panel B). Implementation of ≥3 other PHSMs was associated with a 40% (95% CI 28%–47%) decrease in R_t. Another model that excluded basic civil service arrangement in other PHSMs showed that a ban on dine-in service beginning at 6:00 PM did not have an effect (Table). We performed sensitivity analysis to remove the effect of superspreading in wave 3 by changing the start date to July 1, 2020; we found the ban on dine-in service from 6:00 PM did not have an effect (Appendix Table 2).

Our analysis suggested that the PHSMs were critical for suppressing the third and fourth waves of COVID-19 in Hong Kong. However, we found that a ban on dine-in hours after 6:00 PM might not have had an effect in both waves when capacity was already reduced. A complete closure of restaurants in Hong Kong would have considerable social impact because dining out is very common. We

hypothesize that encouraging restaurants to extend dine-in hours, but with capacity restrictions to reduce crowding, could be a reasonable approach to reduce transmission.

A limitation of our analysis is that we cannot distinguish the effect of some PHSMs because they began simultaneously. We cannot rule out that a ban on dine-in service after 6:00 PM might have an effect if it began earlier than other PHSMs or in regions with high incidences. In addition, changes in R_t are a consequence of individual behavioral changes such as avoiding crowded areas; increasing incidence and implementation of multiple PHSMs could raise the public's perception of risk. Determining the effectiveness of alternative PHSMs would provide evidence-based guidance on control strategies.

This project was supported by the Health and Medical Research Fund, Food and Health Bureau, Government of the Hong Kong Special Administrative Region (grant no. COVID190118) and the Collaborative Research Fund (project no. C7123-20G), and by the general research fund (project no. 17110221) of the Research Grants Council of the Hong Kong SAR Government. B.J.C. and P.W. are supported by the AIR@innoHK program of the Innovation and Technology Commission of the Hong Kong SAR Government.

About the Author

Ms. Ho is a research postgraduate student at the School of Public Health, University of Hong Kong. Her research interest is the transmission and control of emerging infections.

References

1. The Centre for Health Protection (CHP) of the Department of Health (DH) of Hong Kong. CHP investigates 13 additional confirmed cases of COVID-19. 2021 [cited 2021 Apr 15]. https://www.info.gov.hk/gia/general/202104/13/P2021041300746.htm
2. The Government of the Hong Kong Special Administrative Region. Government further tightens social distancing measures. 2020 [cited 2021 Mar 29]. https://www.info.gov.hk/gia/general/202007/14/P2020071400010.htm
3. Lu J, Gu J, Li K, Xu C, Su W, Lai Z, et al. COVID-19 outbreak associated with air conditioning in restaurant, Guangzhou, China, 2020. Emerg Infect Dis. 2020;26:1628–31. https://doi.org/10.3201/eid2607.200764
4. Flaxman S, Mishra S, Gandy A, Unwin HJT, Mellan TA, Coupland H, et al.; Imperial College COVID-19 Response Team. Estimating the effects of non-pharmaceutical interventions on COVID-19 in Europe. Nature. 2020;584:257–61. https://doi.org/10.1038/s41586-020-2405-7
5. Islam N, Sharp SJ, Chowell G, Shabnam S, Kawachi I, Lacey B, et al. Physical distancing interventions and incidence of coronavirus disease 2019: natural experiment in 149 countries. BMJ. 2020;370:m2743. https://doi.org/10.1136/bmj.m2743
6. Brauner JM, Mindermann S, Sharma M, Johnston D, Salvatier J, Gavenciak T, et al.; Inferring the effectiveness of government interventions against COVID-19. Science. 2021;371:6531
7. The Government of the Hong Kong Special Administrative Region. Press releases. 2020 [cited 2021 Mar 21]. https://www.info.gov.hk/gia/general/today.htm
8. Cori A, Ferguson NM, Fraser C, Cauchemez S. A new framework and software to estimate time-varying reproduction numbers during epidemics. Am J Epidemiol. 2013;178:1505–12. https://doi.org/10.1093/aje/kwt133
9. Tsang T, Wu P, Lau E, Cowling BJ. Accounting for imported cases in estimating the time-varying reproductive number of coronavirus disease 2019 in Hong Kong. J Infect Dis. 2021;224:783–87. https://doi.org/10.1093/infdis/jiab299
10. Friedman J, Hastie T, Tibshirani R. Regularization paths for generalized linear models via coordinate descent. J Stat Softw. 2010;33:1–22. https://doi.org/10.18637/jss.v033.i01

Address for correspondence: Tim K. Tsang, University of Hong Kong—WHO Collaborating Centre for Infectious Disease Epidemiology and Control, School of Public Health, Li Ka Shing Faculty of Medicine, Patrick Manson Building, 7 Sassoon Rd, Pokfulam, Hong Kong School of Public Health, Hong Kong; email: timtsang@connect.hku.hk

Subcutaneous Nodules Caused by *Tropheryma whipplei* Infection

Lili Wang, Peng Su, Li Song, Lintao Sai

Author affiliation: Shandong University Qilu Hospital, Shandong, China

DOI: https://doi.org/10.3201/eid2803.211989

To help clarify the clinical manifestations, diagnosis, and treatment for Whipple disease, we report a case of a man in China infected with *Tropheryma whipplei.* The patient had multiple subcutaneous nodules as the only manifestation, which was not consistent with the typical symptoms of *T. whipplei* infection.

Whipple disease was reported in 1907 and is a chronic infectious disease caused by the bacterium *Tropheryma whipplei* (*1*). This disease can involve

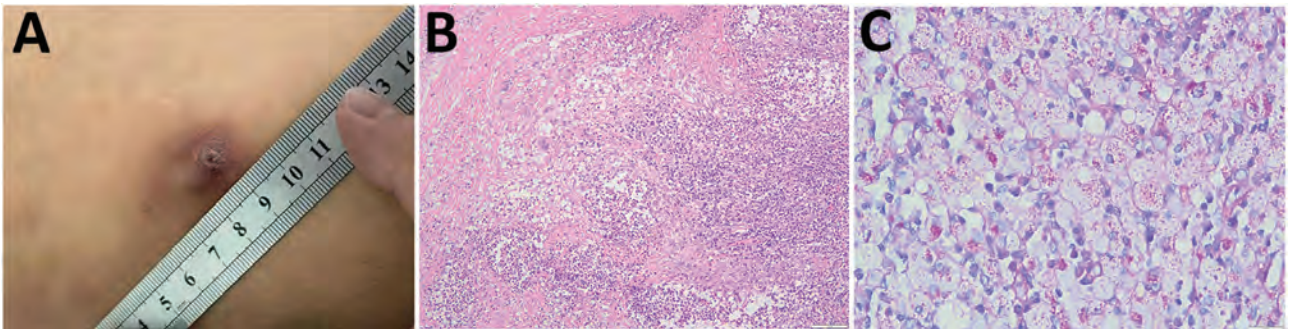

Figure. Analysis of subcutaneous nodules caused by *Tropheryma whipplei* infection in a patient in China, 2020. A) Surface of subcutaneous nodule on the left thigh showing ulceration. B) Histopathologic analysis showing granulomatous inflammation with massive necrosis and small abscesses formation. Periodic acid-Schiff stain. Scale bar indicates 100 μm. C) Inclusions inside cytoplasms of foamy macrophages. Periodic acid-Schiff stain. Scale bar indicates 20 μm.

multiple organs and systems and has a variety of clinical manifestations, in which arthralgia and digestive disorders are the most common first symptoms. Because of the variety and confusion of symptoms, the average time to diagnosis is >6 years (2). We report an elderly man given a diagnosis of *T. whipplei* skin infection and aim to increase awareness of diagnosis and treatment for Whipple disease.

A 62-year-old man (farmer) came to a dermatology clinic in Shandong, China, during November 2020 because of multiple subcutaneous nodules. The patient was otherwise healthy. These nodules were the only manifestation; the patient had no fever, arthralgia, diarrhea, malabsorption, or emaciation. The subcutaneous nodules first appeared on the left waist during January 2020. Nodules were ≈0.3 cm × 0.3 cm and gradually increased to ≈2.0 cm × 2.0 cm before treatment. Nodules then appeared successively on the right axilla, back, left thigh, and waist. These subcutaneous nodules were 0.8 cm × 2.5 cm, firm, and painless. The surfaces of 2 nodules on the left thigh were ulcerated.

The nodules were removed surgically at a local hospital during March and August 2020 (Figure, panel A). However, pathologic examination was not performed, and treatment was not given.

When the patient visited our hospital, a series of examinations were given. Laboratory results included a leukocyte count of 6.76 × 10^9 cells/L (reference range 3.5 × 10^9–9.5 × 10^9 cells/L) with 58.3% neutrophils (reference range 50%–70%), a C-reactive protein level of 24.35 mg/L (reference value <8.0 mg/L), and an erythrocyte sedimentation rate of 89 mm/h (reference range <1–12 mm/h).

The subcutaneous nodule on the right axilla was surgically removed and tested by using pathologic examination. The result showed granulomatous inflammation with massive necrosis and small abscesses (Figure, panel B). The other subcutaneous nodules, except for the small nodules that reappeared on the waist, were then removed and tested by using pathologic examination, routine culture (aerobic and anaerobic culture for 7 days), and shotgun metagenomic sequencing (CapitalBio MedLab, https://www.bionity.com).

Pathologic examination showed granulomatous inflammation and formation of small abscesses. Routine cultures of nodules were negative, but the metagenomic sequencing result was positive for *T. whipplei* (Appendix, https://wwwnc.cdc.gov/EID/article/28/3/21-1989-App1.pdf).

To verify the result of metagenomic sequencing, we performed PCR to amplify a partial nucleotide sequence for *T. whipplei* and examined pathologic sections by using periodic acid–Schiff stain. We sequenced the positive PCR product to further confirm the infection (Appendix). Staining results showed PAS-positive inclusions inside the cytoplasm of foamy macrophages, which was the typical pathologic feature of *T. whipplei* infection (Figure, panel C).

On the basis of the diagnosis of *T. whipplei* infection, the patient was given doxycycline (100 mg 2×/d) and hydroxychloroquine (200 mg 2×/d) orally for ≥1 year starting in January 2021. Six months later, the subcutaneous nodules on the waist were not palpated, and no other new subcutaneous nodules were observed. The patient remains free of relapse.

Whipple disease is a rare infectious disease. Nearly 80% of patients had arthralgia and digestive disorders before they were given a diagnosis (3). Skin lesions in this disease are infrequent. Erythema nodosum–like lesions are specific manifestations in patients with *T. whipplei* infection because of the response to the immune reconstitution inflammatory reaction after initial of antimicrobial drug therapy (4). Our patient had multiple subcutaneous nodules and was not given any antimicrobial drugs before

diagnosis. Therefore, the multiple subcutaneous nodules were considered to be primary skin lesions.

To further evaluate whether the infection affected the intestine, the patient underwent enteroscopy. Results of enteroscopy showed that there was no infection in the intestine. Symptoms was not consistent with the typical symptoms of *T. whipplei* infection and complicated the diagnosis.

Although metagenome sequencing results positive for *T. whipplei* infection are not the standard for diagnosis, this technology provided clues and improved the diagnosis. Specific PAS staining for *T. whipplei* further confirmed the result of metagenome sequencing.

On the basis of the diagnosis, we discontinued treatment with doxycycline and trimethoprim/sulfamethoxazole because of inactivity of trimethoprim and acquired resistance to sulfamethoxazole for *T. whipplei* infection (*5*). The patient was then given doxycycline and hydroxychloroquine and showed satisfactory results. However, a long-term therapeutic course and close follow-up are essential to avoid relapses and reinfection.

Whipple disease has been rarely reported in China. The few reports involved the central nervous system and respiratory system (*6*,*7*). Our report demonstrates a patient who had *T. whipplei* infection and multiple subcutaneous nodules as the initial and single symptom. Currently, treatment and follow-up are ongoing, and the therapeutic effect is satisfactory. However, lifetime susceptibility and high relapse rate pose a challenge to treatment. We hope to increase the understanding of Whipple disease through the diagnosis and treatment for this case-patient.

About the Author

Dr. Wang is a clinical laboratory technician at Shandong University, Shandong, China. Her primary research interest is etiologic diagnosis of infectious diseases.

References

1. Fenollar F, Puéchal X, Raoult D. Whipple's disease. N Engl J Med. 2007;356:55–66. https://doi.org/10.1056/NEJMra062477
2. Lagier JC, Lepidi H, Raoult D, Fenollar F. Systemic *Tropheryma whipplei*: clinical presentation of 142 patients with infections diagnosed or confirmed in a reference center. Medicine (Baltimore). 2010;89:337–45. https://doi.org/10.1097/MD.0b013e3181f204a8
3. Lagier JC, Raoult D. Whipple's disease and *Tropheryma whipplei* infections: when to suspect them and how to diagnose and treat them. Curr Opin Infect Dis. 2018;31:463–70. https://doi.org/10.1097/QCO.0000000000000489
4. Schaller J, Carlson JA. Erythema nodosum-like lesions in treated Whipple's disease: signs of immune reconstitution inflammatory syndrome. J Am Acad Dermatol. 2009;60:277–88. https://doi.org/10.1016/j.jaad.2008.09.024
5. Lagier JC, Fenollar F, Lepidi H, Giorgi R, Million M, Raoult D. Treatment of classic Whipple's disease: from in vitro results to clinical outcome. J Antimicrob Chemother. 2014;69:219–27. https://doi.org/10.1093/jac/dkt310
6. Yu C, Jiang A, Yu Y. Serial imaging changes of cerebral Whipple's disease: from onset to the end. J Neuroimaging. 2007;17:81–3. https://doi.org/10.1111/j.1552-6569.2006.00072.x
7. Wang S, Xia D, Wu J, Jia D, Li L, Xu S. Severe pneumonia caused by infection with *Tropheryma whipplei* complicated with *Acinetobacter baumannii* infection: a case report involving a young woman. Front Public Health. 2021;9:729595. https://doi.org/10.3389/fpubh.2021.729595

Address for correspondence: Lintao Sai, Department of Infectious Diseases, Qilu Hospital, Cheeloo College of Medicine, Shandong University, Wenhua Xi Rd 107, Ji'nan, Shandong 250012, China; email: sailintao@sdu.edu.cn

Addendum to Proposal for Human Respiratory Syncytial Virus Nomenclature below the Species Level

Ian G. Barr, Thomas C. Williams, Vahid Salimi, Ursula J. Buchholz

Author affiliations: WHO Collaborating Centre for Reference and Research on Influenza, VIDRL, Doherty Institute, Melbourne, Victoria, Australia (I.G. Barr); University of Edinburgh, Edinburgh, Scotland, UK (T.C. Williams); Tehran University of Medical Sciences, Tehran, Iran (V. Salimi); National Institute of Allergy and Infectious Diseases, National Institutes of Health, Maryland, USA (U. Buchholz)

DOI: https://doi.org/10.3201/eid2803.212438

To the Editor: We previously proposed a nomenclature for human respiratory syncytial virus (HRSV) to standardize the sharing of viral isolates and sequences (*1*). This nomenclature was adopted by the World Health Organization's Global RSV surveillance program and incorporated into the GISAID EpiRS platform (https://www.gisaid.org). One situation not covered in our proposal was when subtypes HRSV A and HRSV B coexist in the same clinical sample. Although this situation appears relatively infrequently, usually in <1% of HRSV-positive respiratory samples (*2*,*3*), some sources describe higher levels of codetection (e.g., 3.4% in a study from Senegal [*4*]). Dual infections may also be more frequently identified when subtype-specific PCR is introduced, as they have been in phase 2 of the World Health Organization RSV program (*5*,*6*). We offer an approach to clarify nomenclature in such instances of codetection.

We recommend that the designations in the style of HRSV/A-B/Iran/1234/2021 be used in laboratory databases. However, the most important output from these samples is likely to be the genetic sequences. We recommend separate database submissions of the consensus sequences from HRSV A and HRSV B be designated, for example, HRSV/A/Iran/1234/2021 and HRSV/B/Iran/1234/2021, each having the same metadata and noting that both sequences came from the same clinical sample. Clearly identifying dual HRSV A and B infections will enable closer monitoring and, therefore, better understanding of the true frequency of these co-occurrences, of importance because dual infections raise interesting questions about illness severity compared with infection with HRSV A or B alone, duration of protection from reinfection, and factors modulating the frequency of dual infections.

We also note that dual infections may raise technical difficulties, such as assignment of sequence reads to the correct subgroup. However, algorithms such as IRMA (image registration meta-algorithm) (*7*) that appear effective for sequencing approaches (e.g., Illumina, https://www.illumina.com) and long-read approaches (e.g., Oxford Nanopore, https://nanoporetech.com) might also be employed to ensure correct generation and assignment of HRSV A and B sequences from dual infections. Whereas co-infections with other respiratory pathogens are clearly recognized and well-studied, dual infections with HRSV A and B remain less so, but we are now well-positioned to identify these infections.

U.J.B. was supported by the Intramural Program of the National Institute of Allergy and Infectious Diseases of the National Institutes of Health.

References

1. Salimi V, Viegas M, Trento A, Agoti CN, Anderson LJ, Avadhanula V, et al. Proposal for human respiratory syncytial virus nomenclature below the species level. Emerg Infect Dis. 2021;27:1–9. PubMed https://doi.org/10.3201/eid2706.204608
2. Mlinaric-Galinovic G, Tabain I, Kukovec T, Vojnovic G, Bozikov J, Bogovic-Cepin J, et al. Analysis of biennial outbreak pattern of respiratory syncytial virus according to subtype (A and B) in the Zagreb region. Pediatr Int. 2012;54:331–5. PubMed https://doi.org/10.1111/j.1442-200X.2011.03557.x
3. Zhang Y, Yuan L, Zhang Y, Zhang X, Zheng M, Kyaw MH. Burden of respiratory syncytial virus infections in China: systematic review and meta-analysis. J Glob Health. 2015;5:020417. PubMed https://doi.org/10.7189/jogh.05.020417
4. Fall A, Dia N, Cisse HA, Kiori DE, Sarr FD, Sy S, et al. Epidemiology and molecular characterization of human respiratory syncytial virus in Senegal after four consecutive years of surveillance, 2012–2015. PLoS One. 2016;11:e0157163. PubMed https://doi.org/10.1371/journal.pone.0157163
5. Todd AK, Costa AM, Waller G, Daley AJ, Barr IG, Deng YM. Rapid detection of human respiratory syncytial virus A and B by duplex real-time RT-PCR. J Virol Methods. 2021;294:114171. PubMed https://doi.org/10.1016/j.jviromet.2021.114171
6. Wang L, Piedra PA, Avadhanula V, Durigon EL, Machablishvili A, López MR, et al. Duplex real-time RT-PCR assay for detection and subgroup-specific identification of human respiratory syncytial virus. J Virol Methods. 2019;271:113676. https://doi.org/10.1016/j.jviromet.2019.113676
7. Shepard SS, Meno S, Bahl J, Wilson MM, Barnes J, Neuhaus E. Viral deep sequencing needs an adaptive approach: IRMA, the iterative refinement meta-assembler. BMC Genomics. 2016;17:708. [Erratum in BMC Genomics. 2016;17:801.] https://doi.org/10.1186/s12864-016-3030-6

Address for correspondence: Ian Barr, WHO Collaborating Centre for Reference and Research on Influenza, Doherty Institute, Melbourne, VIC 3000, Australia; email: Ian.Barr@influenzacentre.org

Angel (Coin) of the Second Reign (1471–1483) of Edward IV. Gold, 29 mm, 5.1 g, 1473–1477. British Museum, London, UK.

When a Touch of Gold Was Used to Heal the King's Evil

Jean Krugman and Terence Chorba

"'Tis called the evil.
A most miraculous work in this good king,
Which often since my here-remain in England
I have seen him do. How he solicits heaven,
Himself best knows, but strangely visited people,
All swoll'n and ulcerous, pitiful to the eye,
The mere despair of surgery, he cures,
Hanging a golden stamp about their necks,
Put on with holy prayers."

–Malcolm, Act 4, Scene 3, in
William Shakespeare's Macbeth

Author affiliations: Atlanta, Georgia, USA (J. Krugman); Centers for Disease Control and Prevention, Atlanta (T. Chorba)

DOI: https://doi.org/10.3201/eid2803.AC2803

Throughout history, divine approval has been claimed by many rulers in establishing legitimacy of their monarchy and has been integral to governance in the development of many cultures. In ancient and Imperial China, a tradition of a mandate of heaven, as the will of the universe or natural law, was used to justify the position of the ruler. In the Inca Empire, the traditional ruler was considered the progeny of the sun god and in that capacity had to be accorded absolute power over the people, such as the sun itself has. European history is replete with similar traditions of monarchical claims for legitimacy. In Britain and in France, the evolution of the concept of "the divine right of kings" and the resultant philosophic traditions favoring or opposing such a concept shaped much of the history of the past millennium. Both monarchies claimed to rule by divine will, and to this day, the British Coronation service includes a sacred anointing of the new king or queen.

Figure. Artist unknown. Magnification of portion of page from Flemish manuscript "Romance of Alexander," fol. 001r. 15th century. https://digital.bodleian.ox.ac.uk/objects/8d17bc13-14b6-4a56-b3b5-d2e1a935c60d/surfaces/6fb21473-8721-4b74-8916-8519575b90cc/

Many religious traditions have had thaumaturgic (relating to supernatural powers) touch as a tradition. In Britain, reference to the monarch as having divine power in "the royal touch" dates to the 11th century, when it was believed that Edward the Confessor, last of the Anglo-Saxon kings, possessed powers to heal the sick through some form of laying on of hands. In official ceremonies in his and subsequent reigns, subjects could approach the monarch to seek the imperial touch, hoping to cure their ailments or diseases. For centuries, the disease that most readily lent itself to the occasional appearance of success in this regard was scrofula (i.e., lymphadenitis—most commonly tuberculous cervical lymphadenitis), which would manifest itself with painful and visible sores that could go into remission and even go into resolution, giving the impression of a royally induced cure. Scrofula is a term that has fallen into disuse like many other medical terms in English (e.g., catarrh, ague, quinsy, dropsy, and grippe), principally because of diagnostic advances and more precise disease characterization. However, because of the association of its spontaneous remission with the royal touch, tuberculous lymphadenitis was also called "the king's evil," and throughout most of the past millennium, its presence in European populations was very common.

In well-orchestrated ceremonies in which a monarch would come into contact with crowds of infected people, the laying on of hands benefited both ruler and subject; it underlined the divinely legitimized authority and power of the monarch and demonstrated accessibility to poor mortals. Common petitioners received hope for a cure of their disease by virtue of the imperial touch. Frequently, from the 15th through the 17th centuries, such supplicants were also given a hammered gold coin, known as an Angel, as a gift. This denomination of coin was introduced to England by King Edward IV in 1465, patterned after a similar coin minted in France, called an *ange* or *angelot*.

An example of a gold Angel is featured on this month's cover. On the obverse (front) of the coin, there is a winged standing figure of the Archangel Michael slaying a dragon (evil) with a spear, a figure with a mythology dating from the 4th century BCE. On the reverse, a central shield is depicted within the ship of state with a thick mast and thick main spar, flanked by the King's initial (E) and a rose; the stays of the mast emanate from the ship's masthead below the crow's nest. A depiction of three ships with similar masts and rigging, found in a Flemish 15th century manuscript, is presented in the Figure. Unlike most other coinage that was hammered by hand as the production method that dominated until 1662, the basic design of the Angel remained constant over two centuries. Commonly, these coins were pierced with a hole at the top through which a cloth or chain could be passed for the coin to be worn around the neck. Touching the coin, which the king himself had touched, was thought to be healing as well. Tales of success and demand for physical contact with the king by persons with scrofula became so great that distribution and receipt of such coins gradually became a substitute for the regal touch itself.

In March 1882, Robert Koch demonstrated that the tubercle bacillus was the causative organism of the clinical manifestations associated with pulmonary tuberculosis (TB). In 1896, the organism was assigned to a new genus, *Mycobacterium*. At the time, TB was a leading cause of death in Europe; discovery of an infectious etiology led to preventive approaches that resulted in dramatic decreases in cases of illness and death from TB, even in the 19th

century. Although lymphadenitis is one of the clinical manifestations of infection with *Mycobacterium tuberculosis*, either as the result of hematogenous or lymphatic spread, cervical lymphadenitis is also often observed when the primary focus of disease is the tonsils or pharynx, as was common in the time of Edward IV, as the result of drinking milk or eating milk products contaminated with bovine tubercle bacilli (i.e., *M. bovis*). Although pasteurization of milk and screening and care of cattle have greatly limited exposure to *M. bovis* since the late 19th century, cervical lymphadenitis remains an extrapulmonary feature of *M. tuberculosis* disease; in 2020, ≈8% of US TB patients had lymphatic TB. Cervical lymphadenitis may also result from receipt of *M. bovis*–derived Bacillus Calmette-Guérin (BCG) vaccine, which is given to infants in high-risk countries to reduce the risk for TB disease and disseminated TB, as well as from nontuberculous (environmental) mycobacterial infections, usually *M. avium intracellulare* or *M. scrofulaceum*. Fortunately for all, the contributions of Koch, his contemporaries, and his successors to our understanding of the infectious etiologies of scrofula have obviated the need to pursue the royal touch of gold to cure the king's evil.

Bibliography

1. Barberis I, Bragazzi NL, Galluzzo L, Martini M. The history of tuberculosis: from the first historical records to the isolation of Koch's bacillus. J Prev Med Hyg. 2017;58:E9–12.
2. Bloch M. The Royal Touch. New York, NY: Dorset Press; 1989.
3. Centers for Disease Control and Prevention. Reported tuberculosis in the United States, 2020 [cited 2022 Feb 4]. https://www.cdc.gov/tb/statistics/reports/2020/default.htm
4. Favorov M, Ali M, Tursunbayeva A, Aitmagambetova I, Kilgore P, Ismailov S, et al. Comparative tuberculosis (TB) prevention effectiveness in children of Bacillus Calmette-Guérin (BCG) vaccines from different sources, Kazakhstan. PLoS One. 2012;7:e32567. https://doi.org/10.1371/journal.pone.0032567
5. Fontanilla J-M, Barnes A, von Reyn CF. Current diagnosis and management of peripheral tuberculous lymphadenitis. Clin Infect Dis. 2011;53:555–62. https://doi.org/10.1093/cid/cir454
6. Grzybowski S, Allen EA. History and importance of scrofula. Lancet. 1995;346:1472–4. https://doi.org/10.1016/S0140-6736(95)92478-7
7. Sturdy DJ. The Royal Touch in England. In: Heinz D, Jackson RA, Sturdy D, editors. European Monarchy: Its Evolution and Practice from Roman Antiquity to Modern Times. Stuttgart, Germany: Franz Steiner Verlag; 1992. p. 171–84.

Address for correspondence: Terence Chorba, Centers for Disease Control and Prevention, 1600 Clifton Rd NE, Mailstop US12-4, Atlanta, GA 30329-4027, USA; email: tlc2@cdc.gov

EMERGING INFECTIOUS DISEASES®

Upcoming Issue • April 2022 • Zoonotic Infections

- Shewanella Species Bloodstream Infections in Queensland, Australia
- Increasing Antimicrobial-Drug Resistance in the World Health Organization Eastern Mediterranean Region, 2017–2019
- Diminishing Immune Responses against Variants of Concern in Dialysis Patients 4 Months after SARS-CoV-2 mRNA Vaccination
- Infection Attack Rate and Reporting of Deaths in the First 6 Months of the COVID-19 Epidemic, Delhi, India
- Detection of Infectious Toscana Virus in Seminal Fluid of Young Man Returning from Elba Island, Italy
- Fatal Human Alphaherpesvirus 1 Infection in Free-Ranging Black-Tufted Marmosets in Anthropized Environments, Brazil, 2012–2019
- Mapping the Risk for West Nile Virus Transmission, Africa
- Decrease in Tuberculosis Cases during COVID-19 Pandemic as Reflected by Outpatient Pharmacy Data, United States, 2020
- Genomic Epidemiology of Early SARS-CoV-2 Transmission Dynamics, Gujarat, India
- Increased Attack Rates and Decreased Incubation Periods of Chronic Wasting Disease in Raccoons after Passage through Meadow Voles
- SARS-CoV-2 IgG Seroprevalence among Blood Donors as a Monitor of the COVID-19 Epidemic, Brazil
- Autochthonous *Leishmania infantum* in Dogs, Zambia, 2021
- Durability of Antibody Response and Frequency of SARS-CoV-2 Infection 6 Months after COVID-19 Vaccination in Healthcare Workers
- Vehicle Windshield Wiper Fluid as Potential Source of Sporadic Legionnaires' Disease in Commercial Truck Drivers
- Isolation of Heartland Virus from Lone Star Ticks, Georgia, USA, 2019
- In Vitro Confirmation of Artemisinin Resistance in *Plasmodium falciparum* from Patient Isolates, Southern Rwanda, 2019
- *Bordetella hinzii* Pneumonia in Patient with SARS-CoV-2 Superinfection
- Zoonotic Pathogens in Wildlife Traded in Markets for Human Consumption, Laos
- *Streptobacillus notomytis* Bacteremia after Exposure to Rats and Rat Feces
- Hantavirus Pulmonary Syndrome in a COVID-19 Patient, Argentina, 2020
- High Prevalence and Low Diversity of *Rickettsia* in *Dermacentor reticulatus* Ticks, Central Europe
- Amplification Artifact in SARS-CoV-2 Omicron Sequences Carrying P681R Mutation, New York, USA
- Recurrent SARS-CoV-2 RNA Detection after COVID-19 Illness Onset During Pregnancy
- Time from Exposure to Diagnosis among Quarantined Close Contacts of SARS-CoV-2 Omicron Variant Index Case-Patients, South Korea

Complete list of articles in the April issue at https://wwwnc.cdc.gov/eid/#issue-287

Earning CME Credit

To obtain credit, you should first read the journal article. After reading the article, you should be able to answer the following, related, multiple-choice questions. To complete the questions (with a minimum 75% passing score) and earn continuing medical education (CME) credit, please go to http://www.medscape.org/journal/eid. Credit cannot be obtained for tests completed on paper, although you may use the worksheet below to keep a record of your answers.

You must be a registered user on http://www.medscape.org. If you are not registered on http://www.medscape.org, please click on the "Register" link on the right hand side of the website.

Only one answer is correct for each question. Once you successfully answer all post-test questions, you will be able to view and/or print your certificate. For questions regarding this activity, contact the accredited provider, CME@medscape.net. For technical assistance, contact CME@medscape.net. American Medical Association's Physician's Recognition Award (AMA PRA) credits are accepted in the US as evidence of participation in CME activities. For further information on this award, please go to https://www.ama-assn.org. The AMA has determined that physicians not licensed in the US who participate in this CME activity are eligible for AMA PRA Category 1 Credits™. Through agreements that the AMA has made with agencies in some countries, AMA PRA credit may be acceptable as evidence of participation in CME activities. If you are not licensed in the US, please complete the questions online, print the AMA PRA CME credit certificate, and present it to your national medical association for review.

Article Title

Rising Incidence of Legionnaires' Disease and Associated Epidemiologic Patterns, United States, 1992–2018

CME Questions

1. What did the current study find regarding trends in Legionnaires' disease (LD) incidence according to age?

A. The incidence of LD increased to a similar degree across all age groups
B. There was a trend toward increasing incidence of LD among adults as age increased
C. The incidence of LD increased only among adults at age ≥65 years
D. The incidence of LD declined among persons aged <30 years but increased among older adults

2. Which of the following trends was noted in the incidence of LD according to sex in the current study?

A. The incidence of LD was consistently higher among men compared with women over time
B. The incidence of LD was higher among men vs women until 2011, when this trend reversed
C. The incidence of LD rose only among men during the study period
D. There were no sex-based differences in the incidence of LD during the study period

3. Which of the following trends in the incidence of LD according to race was noted in the current study?

A. Most cases of LD occurred among White individuals, who had a larger increase in age-standardized incidence rates of LD over time compared with Black individuals
B. Most cases of LD occurred among White individuals, who had a smaller increase in age-standardized incidence rates of LD over time compared with Black individuals
C. Most cases of LD occurred among Black individuals, who had a smaller increase in age-standardized incidence rates of LD over time compared with White individuals
D. Most cases of LD occurred among Black individuals, who had a larger increase in age-standardized incidence rates of LD over time compared with White individuals

4. What were the most common regions and seasons for LD in the current study?

A. Northeast; summer
B. Midwest; winter
C. West; spring
D. Southeast; fall

Earning CME Credit

To obtain credit, you should first read the journal article. After reading the article, you should be able to answer the following, related, multiple-choice questions. To complete the questions (with a minimum 75% passing score) and earn continuing medical education (CME) credit, please go to http://www.medscape.org/journal/eid. Credit cannot be obtained for tests completed on paper, although you may use the worksheet below to keep a record of your answers.

You must be a registered user on http://www.medscape.org. If you are not registered on http://www.medscape.org, please click on the "Register" link on the right hand side of the website.

Only one answer is correct for each question. Once you successfully answer all post-test questions, you will be able to view and/or print your certificate. For questions regarding this activity, contact the accredited provider, CME@medscape.net. For technical assistance, contact CME@medscape.net. American Medical Association's Physician's Recognition Award (AMA PRA) credits are accepted in the US as evidence of participation in CME activities. For further information on this award, please go to https://www.ama-assn.org. The AMA has determined that physicians not licensed in the US who participate in this CME activity are eligible for AMA PRA Category 1 Credits™. Through agreements that the AMA has made with agencies in some countries, AMA PRA credit may be acceptable as evidence of participation in CME activities. If you are not licensed in the US, please complete the questions online, print the AMA PRA CME credit certificate, and present it to your national medical association for review.

Article Title

Neutralizing Enterovirus D68 Antibodies in Children after 2014 Outbreak, Kansas City, Missouri, USA

CME Questions

1. Your patient is a 6-year-old boy thought to have enterovirus (EV) infection. According to the serologic study in Kansas City, Missouri, by Livingston and colleagues, which of the following statements about neutralizing EV-D68 antibodies to the 2014 B1, 2014 B2, and 2014 D clade virus in pediatric sera salvaged during 2017 from patients aged 6 months to 18 years, including persons born after the 2014 outbreak, is correct?

A. Neutralizing antibodies to B1 were not detected in children born after 2014
B. Neutralizing antibodies to B2 and D were detected in approximately half of samples
C. Serum titers from 2017 samples were similar to those in sera obtained in 2012 to 2013 from comparably aged children
D. Seronegative rate was highest (15.3%) for the B2 virus

2. According to the serologic study in Kansas City, Missouri, by Livingston and colleagues, which of the following statements about associations of neutralizing EV-D68 antibody titers with demographic and medical history factors is correct?

A. Median neutralizing titers rose with advancing age groups ($P<0.001$), except that titers were similar in age groups 11 to 15 years and >15 years
B. On multivariate analysis, titers against B1 virus were significantly higher in people with asthma
C. Family size was significantly associated with neutralizing EV-D68 antibody titers
D. Children born in 2016 had lower titers than those born in 2014 or 2015

3. According to the serologic study in Kansas City, Missouri, by Livingston and colleagues, which of the following statements about clinical and public health implications of neutralizing EV-D68 antibodies to the 2014 B1, 2014 B2, and 2014 D clade virus in pediatric sera salvaged during 2017 from patients aged 6 months to 18 years, including persons born after the 2014 outbreak, and of associations of antibody titers with demographic and medical history factors is correct?

A. This study determined protective thresholds for serum-neutralizing antibodies
B. EV-D68 causes severe pediatric respiratory illness outbreaks, particularly affecting persons with asthma, and is associated with acute flaccid myelitis
C. The study findings suggest that EV-D68 no longer circulated in Kansas City once the 2014 outbreak concluded
D. Increasing titers with increasing age resulted solely from increasing EV-D68 antibody specificity over time after the initial infection